

## **Verification of the DIF3D Software to Support Fast Reactor Analysis**

---

**Nuclear Science and Engineering Division**

### **About Argonne National Laboratory**

Argonne is a U.S. Department of Energy laboratory managed by UChicago Argonne, LLC under contract DE-AC02-06CH11357. The Laboratory's main facility is outside Chicago, at 9700 South Cass Avenue, Argonne, Illinois 60439. For information about Argonne and its pioneering science and technology programs, see [www.anl.gov](http://www.anl.gov).

### **DOCUMENT AVAILABILITY**

**Online Access:** U.S. Department of Energy (DOE) reports produced after 1991 and a growing number of pre-1991 documents are available free at OSTI.GOV (<http://www.osti.gov/>), a service of the US Dept. of Energy's Office of Scientific and Technical Information.

### **Reports not in digital format may be purchased by the public from the National Technical Information Service (NTIS):**

U.S. Department of Commerce  
National Technical Information  
Service 5301 Shawnee Rd  
Alexandria, VA 22312  
**[www.ntis.gov](http://www.ntis.gov)**  
Phone: (800) 553-NTIS (6847) or (703) 605-6000  
Fax: (703) 605-6900  
Email: [orders@ntis.gov](mailto:orders@ntis.gov)

### **Reports not in digital format are available to DOE and DOE contractors from the Office of Scientific and Technical Information (OSTI):**

U.S. Department of Energy  
Office of Scientific and Technical Information  
P.O. Box 62  
Oak Ridge, TN 37831-0062  
**[www.osti.gov](http://www.osti.gov)**  
Phone: (865) 576-8401  
Fax: (865) 576-5728  
Email: [reports@osti.gov](mailto:reports@osti.gov)

### **Disclaimer**

This report was prepared as an account of work sponsored by an agency of the United States Government. Neither the United States Government nor any agency thereof, nor UChicago Argonne, LLC, nor any of their employees or officers, makes any warranty, express or implied, or assumes any legal liability or responsibility for the accuracy, completeness, or usefulness of any information, apparatus, product, or process disclosed, or represents that its use would not infringe privately owned rights. Reference herein to any specific commercial product, process, or service by trade name, trademark, manufacturer, or otherwise, does not necessarily constitute or imply its endorsement, recommendation, or favoring by the United States Government or any agency thereof. The views and opinions of document authors expressed herein do not necessarily state or reflect those of the United States Government or any agency thereof, Argonne National Laboratory, or UChicago Argonne, LLC.

## **Verification of the DIF3D Software to Support Fast Reactor Analysis**

---

**Adam G. Nelson, Micheal A. Smith**

Nuclear Science and Engineering Division

Argonne National Laboratory

February 13, 2020

## ABSTRACT

Ongoing design activities at Argonne National Laboratory are requiring a thorough verification of the Argonne Reactor Computation codes be performed. DIF3D is central to this system. The driver for this effort requires the 3D Cartesian, triangular-Z, and hexagonal-Z core geometry options of DIF3D be verified.

Previous work identified the DIF3D features required to be verified to support current design activities, features of which are generally applicable to hexagonal-Z fast reactor designs. The scope of this verification effort includes verifying DIF3D's ability to correctly translate the user's model in to DIF3D's preferred format, verifying that options planned for use have the desired effect, and verifying the correctness of the eigenvalue, fixed-source, forward, and adjoint solvers in DIF3D-FD and DIF3D-VARIANT. This manuscript provides the verification tasks and their results with respect to the features needed for current design activities.

Since analytic solutions of the neutron diffusion and transport equations are either limited in scope or not possible, multiple tiers of problems unique to each solver and geometry type were implemented. Each of these tiers tests features independent and complementary arguments for why the separate testing of functionalities is acceptable. Finally, this separate testing was also supplemented with a high-level integral check of each the diffusion and transport capabilities and applicable geometries.

To accommodate cases which an analytic solution is not feasible, MCNP6.2 was relied upon to provide a higher-order reference solution. This therefore required that the capabilities within MCNP6.2 which were relied upon for this work are also verified in this work. No MCNP discrepancies were noted in this effort. Note that the MCNP6.2 verification included in this work does not stand as a full verification of MCNP6.2, but merely verifies the features used in verifying DIF3D.

The verification effort identified no issues that are debilitating or otherwise impactful to design usage of DIF3D, and thus DIF3D version 11.0, release 3012 is considered verified. The types of issues that were identified were predominantly in the areas of: unclear documentation, software bugs which were inconsequential to final results, editing options which were ignored in favor of printing more information than requested, bugs in the outputs of intermediate results, or secondary output binary file information which was not present. While not a bug, this verification report also identified that the algorithm used to evaluate the peak fast flux in a nodal transport solution can be quite unreliable due to the polynomial order used and the location of the peak within the mesh. The authors of the report therefore recommend the usage of the EvaluateFlux software (distributed with ARC) as a more robust alternative.



## TABLE OF CONTENTS

Table of Contents .....	ii
List of Figures .....	iv
List of Tables.....	ix
1 Introduction .....	15
2 Verification Strategy.....	17
3 DIF3D Verification Tasks .....	23
3.1 DIF3D-FD 3D Cartesian Verification.....	23
3.1.1 Model Building Verification .....	23
3.1.2 Multigroup Infinite Homogeneous Eigenvalue Verification.....	102
3.1.3 Multi-group Infinite Homogeneous Fixed Source Verification .....	104
3.1.4 One-Region Analytic Spatial Eigenvalue Solution .....	105
3.1.5 One-Region Analytic Spatial Fixed-Source Verification.....	114
3.1.6 Inhomogeneous Diffusion Equation Verification.....	120
3.1.7 Power and Flux Peaking Verification.....	125
3.1.8 Radial Periodic Boundary Conditions Verification.....	143
3.1.9 Extrapolated and Reflected Boundary Conditions Verification .....	144
3.1.10 Iteration and Convergence Control Verification .....	145
3.1.11 Solution Edit Verification.....	150
3.1.12 A.SUMMAR Output .....	156
3.1.13 Integral Verification .....	158
3.2 Triangular-Z Diffusion Verification .....	161
3.2.1 Model Building Verification .....	161
3.2.2 One-Region Spatial Eigenvalue Verification .....	202
3.2.3 Extrapolated and Reflected Boundary Conditions Verification .....	220
3.2.4 Radial Periodic Boundary Conditions Verification.....	223
3.2.5 Iteration and Convergence Control Verification .....	224
3.2.6 Solution Edit Verification.....	229
3.2.7 Integral Verification .....	236
3.3 3D Cartesian Transport Verification.....	239
3.3.1 Model Building Verification .....	239
3.3.2 Multigroup Fixed Source Verification .....	255

3.3.3	Multigroup Eigenvalue Verification.....	265
3.3.4	Reflective Boundary Conditions Verification .....	277
3.3.5	Iteration and Convergence Control Verification .....	278
3.3.6	Solution Edit Verification.....	284
3.3.7	Integral Verification .....	286
3.4	Hexagonal-Z Transport Verification.....	301
3.4.1	Model Building Verification .....	301
3.4.2	Multigroup Fixed Source Verification .....	320
3.4.3	Multigroup Eigenvalue Verification.....	329
3.4.4	Radial Periodic Boundary Conditions Verification.....	341
3.4.5	Iteration and Convergence Control Verification .....	343
3.4.6	Solution Edit Verification.....	348
3.4.7	Integral Verification .....	351
4	Monte Carlo Verification.....	368
4.1	MCNP6.2 Capabilities to Verify.....	368
4.2	MCNP6.2 Verification Cases.....	371
4.2.1	Criticality Case 6 .....	371
4.2.2	Criticality Case 31 .....	373
4.2.3	Criticality Case 32 .....	373
4.2.4	Criticality Case 54 .....	374
4.2.5	Criticality Case 64 .....	375
4.2.6	Criticality Case 72 .....	375
4.2.7	Criticality Case 74 .....	376
4.2.8	Criticality Case 75 .....	376
4.2.9	Fixed Source Case .....	377
4.2.10	Fixed Cell Source Case.....	378
4.2.11	Fixed Isotropic Source Case .....	379
5	Conclusion.....	381
6	References .....	385

## LIST OF FIGURES

Figure 1. 3D Cartesian Model Geometry .....	24
Figure 2. A.NIP3 3D Cartesian Model Geometry Definition .....	26
Figure 3. A.NIP3 3D Cartesian Model Composition Definition .....	27
Figure 4. ISOBCD Formatted Microscopic Cross Section Data .....	31
Figure 5. ISOBCD Formatted Macroscopic Cross Section Data .....	32
Figure 6. ISOBCD Formatted Photon Transport Cross Section Data .....	33
Figure 7. ISOBCD Formatted User Style 1 Cross Section Data .....	34
Figure 8. ISOBCD Formatted User Style 2 Cross Section Data .....	35
Figure 9. Remaining DIF3D Input Options .....	38
Figure 10. ASCII-Formatted GEODST File .....	57
Figure 11. ASCII-Formatted NDXSFR File .....	60
Figure 12. ASCII-Formatted ZNATDN File .....	62
Figure 13. ASCII-Formatted COMPS File .....	64
Figure 14. ASCII-Formatted LABELS File .....	71
Figure 15. Condensed LABELS Output From CCCC_PrintTables .....	71
Figure 16. Python-Extracted LABELS Information .....	72
Figure 17. Modified A.HMG4C Option for Chi Processing Option 1 .....	81
Figure 18. Modified A.HMG4C Option for Chi Processing Option 2 .....	83
Figure 19. Perturbed Case 1 ISOTXS .....	85
Figure 20. Perturbed Case 2 ISOTXS .....	86
Figure 21. Perturbed Case 3 ISOTXS .....	87
Figure 22. Control Rod Bank Problem Regions and Areas .....	99
Figure 23. Control Rod Bank Problem Bank Assignments .....	99
Figure 24. Control Rod Bank Problem A.NIP3 Input Block .....	101
Figure 25. Snippet of Relevant Standard Output for Control Rod Bank Problem .....	102
Figure 26. DIF3D Forward and Adjoint Input and Output Samples for the Infinite Homogeneous Fixed Source Test Case .....	105
Figure 27. DIF3D-FD Flux Solution for 3D Domain in Lowest Z Plane .....	109
Figure 28. The DIF3D-FD Flux Error Distribution for the Fixed Source Diffusion Benchmark .....	117
Figure 29. The DIF3D-VARIANT Error Distribution for the Fixed Source Diffusion Benchmark .....	118
Figure 30. The DIF3D-FD Flux Error Distribution for the Inhomogeneous Diffusion Benchmark .....	122
Figure 31. The DIF3D Example Power Peaking Table of Output .....	127

---

Figure 32. The DIF3D Example Flux Peaking Table of Output.....	128
Figure 33. The Flux Distribution for the Diffusion Theory Peaking Problem .....	129
Figure 34. The Power Distribution for the Diffusion Theory Peaking Problem.....	130
Figure 35. DIF3D-VARIANT Spatial Flux Convergence for the Diffusion Peaking Problem .....	132
Figure 36. DIF3D-FD Spatial Flux Convergence for the Diffusion Theory Peaking Problem .....	133
Figure 37. The DIF3D-VARIANT 20x20x20 Mesh Result for the Peaking Output Tables .....	141
Figure 38. 3D Cartesian Periodic Input and Core Map.....	143
Figure 39. XYZ Diffusion Edit Table Model.....	151
Figure 40. SUMMAR Verification Model A.NIP3 Block.....	157
Figure 41. SUMMAR Verification Model A.SUMMAR Block .....	157
Figure 42. SUMMAR Module Output .....	158
Figure 43. IAEA Benchmark Model and Average Assembly Power Map .....	159
Figure 44. Triangular-Z Reference Geometry axially between 0 - 10cm (left) and 10 - 30 cm (right).....	164
Figure 45 A.NIP3 Triangular-Z Model Geometry Definition .....	165
Figure 46. GNIP4C Model Description Edit.....	168
Figure 47. Rectangular Boundary Domain Triangular-Z Grid Sketch .....	169
Figure 48. Region and Zone Specifications Output .....	169
Figure 49. DIF3D Region/Composition Map for Triangular-Z Geometry Model; the lower plane is on the left, and the upper plane is on the right.....	170
Figure 50. DIF3D Reactor Region by Mesh Point Comparison to Triangular-Z Geometry Reference.....	172
Figure 51. Region Number to Name Assignments .....	172
Figure 52. Triangular-Z Base Case GEODST File .....	176
Figure 53. GEODST File Coarse-Mesh Interval Region Assignments .....	177
Figure 54. A.NIP3 Changes for Sixth-Core Geometry .....	179
Figure 55. Sixth-Core Geometry Mesh Sketch.....	180
Figure 56. DIF3D Region/Composition Map for the Sixth-Core Triangular-Z Geometry Model; the lower plane is on the left, and the upper plane is on the right .....	181
Figure 57. Sixth-Core Reactor Region Map for the Lower Plane.....	181
Figure 58. Sixth-Core Geometry GEODST File Region to Mesh Assignments .....	182
Figure 59. A.NIP3 Changes for Third-Core Geometry.....	183
Figure 60. Third-Core Geometry Mesh Sketch.....	183

---

Figure 61. DIF3D Region/Composition Map for the Third-Core Triangular-Z Geometry Model; the lower plane is on the left, and the upper plane is on the right .....	184
Figure 62. Third-Core Reactor Region Map for the Lower Plane .....	185
Figure 63. Third-Core Geometry GEODST File Region to Mesh Assignments .....	186
Figure 64. Sketch of the Full-Core Mesh with Type 29 Card 4 Set to 2 .....	188
Figure 65. DIF3D Region to Mesh Interval Map for Plane 1 of Full-Core Model.....	188
Figure 66. DIF3D GEODST File 6D Record for Plane 1 of Full-Core Model.....	189
Figure 67. DIF3D GEODST File 6D Record for Plane 2 of Full-Core Model.....	190
Figure 68. Sketch of the Sixth-Core Mesh with Type 29 Card 4 Set to 2 .....	192
Figure 69. Region Map for Sixth-Core Model.....	192
Figure 70. DIF3D GEODST File 6D Record for both Planes of the Sixth-Core Model	192
Figure 71. Sketch of the Third-Core Mesh with Type 29 Card 4 Set to 2 .....	194
Figure 72. Region Map for Third-Core Model .....	194
Figure 73. DIF3D GEODST File 6D Record for both Planes of the Third-Core Model	195
Figure 74. Control Rod Bank Problem Areas (Left) and Bank Assignments (Right) ....	201
Figure 75. Snippet of Relevant Standard Output for Control Rod Bank Problem.....	202
Figure 76. Triangular-Z Example Sub-meshing of Hex Geometry Input.....	203
Figure 77. One, Two, and Three Ring Hexagonal Geometries.....	204
Figure 78. Four Ring Hexagonal Geometry Boundary Condition Based Flux Profile...	207
Figure 79. Flux Profile for the Three Ring Test Problem .....	208
Figure 80. DIF3D-FD Flux and Error Profile for Two Meshes of the Three Ring Test Problem .....	210
Figure 81. DIF3D-FD Absolute Error Profiles for the Three Ring Test Problem .....	211
Figure 82. DIF3D-VARIANT Low Order Polynomial Flux and Relative Error Profiles for Five Ring Test Problem .....	213
Figure 83. DIF3D-VARIANT High Order Polynomial Flux and Relative Error Profiles for a Five Ring Test Problem.....	215
Figure 84. Sixth-Core Periodic Triangular-Z Input and Core Map .....	224
Figure 85. Third-Core Periodic Triangular-Z Input and Core Map .....	224
Figure 86. Triangular-Z Diffusion Edit Table Model.....	230
Figure 87. VVER-440 Benchmark Model .....	237
Figure 88. Remaining DIF3D Input Options .....	240
Figure 89. Variational Nodal Option Output .....	243
Figure 90. P <sub>2</sub> Modified User-Defined Style 2 ISOTXS File.....	251
Figure 91. XYZ MG Fixed Source MCNP Reference Flux in Group 1 .....	257
Figure 92. XYZ MG Fixed Source MCNP Reference Flux in Group 2 .....	258

Figure 93. XYZ MG DIF3D to MCNP Flux Ratios in Group 1 .....	262
Figure 94. XYZ MG DIF3D to MCNP Flux Ratios in Group 2 .....	263
Figure 95. XYZ MG Isotropic to Anisotropic DIF3D Flux Ratios in Group 1 .....	264
Figure 96. XYZ MG Isotropic to Anisotropic DIF3D Flux Ratios in Group 2 .....	264
Figure 97. XYZ MG Eigenvalue MCNP Flux Rel. Err. Distribution .....	268
Figure 98. XYZ MG Eigenvalue MCNP Reference Flux in Group 1 .....	269
Figure 99. XYZ MG Eigenvalue MCNP Reference Flux in Group 2 .....	269
Figure 100. XYZ MG Eigenvalue MCNP Reference Flux in Group 3 .....	270
Figure 101. XYZ MG DIF3D to MCNP Flux Ratios in Group 1 .....	274
Figure 102. XYZ MG DIF3D to MCNP Flux Ratios in Group 2 .....	275
Figure 103. XYZ MG DIF3D to MCNP Flux Ratios in Group 3 .....	275
Figure 104. XYZ MG Isotropic to Anisotropic DIF3D Flux Ratios in Group 1 .....	276
Figure 105. XYZ MG Isotropic to Anisotropic DIF3D Flux Ratios in Group 2 .....	277
Figure 106. XYZ MG Isotropic to Anisotropic DIF3D Flux Ratios in Group 3 .....	277
Figure 107. XYZ Transport Edit Table Model .....	284
Figure 108. XYZ Transport Neutron Leakage Edit Table Model .....	286
Figure 109. Takeda 3 Benchmark Model Configurations .....	287
Figure 110. MCNP Relative Error Distribution for Rods-In Case .....	288
Figure 111. Ratio of DIF3D to MCNP Fluxes in Group 1 .....	293
Figure 112. MCNP Relative Error Distribution for Rods-Half Case .....	294
Figure 113. Ratio of DIF3D to MCNP Fluxes in Group 1 .....	297
Figure 114. MCNP Relative Error Distribution for Core Case .....	298
Figure 115. Ratio of DIF3D to MCNP Fluxes in Group 1 .....	301
Figure 116. Hexagonal-Z Base Case Input .....	304
Figure 117. Hexagonal-Z Base Case GEODST File .....	309
Figure 118. GEODST File Coarse-Mesh Interval Region Assignments .....	309
Figure 119. Sixth-Core Geometry GEODST File Region to Mesh Assignments .....	312
Figure 120. Third-Core Geometry GEODST File Region to Mesh Assignments .....	314
Figure 121. Snippet of Relevant Standard Output for Control Rod Bank Problem .....	320
Figure 122. Hexagonal-Z MG Fixed Source MCNP Reference Flux in Group 1 .....	322
Figure 123. Hexagonal-Z MG Fixed Source MCNP Reference Flux in Group 2 .....	323
Figure 124. Hexagonal-Z MG DIF3D to MCNP Flux Ratios in Group 1 .....	327
Figure 125. Hexagonal-Z MG DIF3D to MCNP Flux Ratios in Group 2 .....	327
Figure 126. Hexagonal-Z MG Isotropic to Anisotropic DIF3D Flux Ratios in Group 1 .....	328
Figure 127. Hexagonal-Z MG Isotropic to Anisotropic DIF3D Flux Ratios in Group 2 .....	328
Figure 128. Hexagonal-Z MG Eigenvalue MCNP Flux Rel. Err. Distribution .....	331

---

Figure 129. Hexagonal-Z MG Eigenvalue MCNP Reference Flux in Group 1.....	332
Figure 130. Hexagonal-Z MG Eigenvalue MCNP Reference Flux in Group 2.....	332
Figure 131. Hexagonal-Z MG Eigenvalue MCNP Reference Flux in Group 3.....	333
Figure 132. Hexagonal-Z MG DIF3D to MCNP Flux Ratios in Group 1 .....	338
Figure 133. Hexagonal-Z MG DIF3D to MCNP Flux Ratios in Group 2 .....	338
Figure 134. Hexagonal-Z MG DIF3D to MCNP Flux Ratios in Group 3 .....	338
Figure 135. Hexagonal-Z MG Isotropic to Anisotropic DIF3D Flux Ratios in Group 1	339
Figure 136. Hexagonal-Z MG Isotropic to Anisotropic DIF3D Flux Ratios in Group 2	340
Figure 137. Hexagonal-Z MG Isotropic to Anisotropic DIF3D Flux Ratios in Group 3	340
Figure 138. Sixth-Core Periodic Hexagonal-Z Input and Core Map .....	342
Figure 139. Third-Core Periodic Hexagonal-Z Input and Core Map .....	342
Figure 140. Hexagonal-Z Diffusion Edit Table Model.....	349
Figure 141. Hexagonal-Z Transport Neutron Leakage Edit Table Model.....	350
Figure 142. Full-Core Hexagonal-Z Transport Neutron Leakage with Group-Wise Albedos .....	351
Figure 143. Takeda Benchmark Model Series 4.....	351
Figure 144. MCNP Relative Error Distribution for Rods-In Case .....	352
Figure 145. Ratio of DIF3D to MCNP Fluxes in Group 1 .....	356
Figure 146. Ratio of DIF3D to MCNP Fluxes in Group 2 .....	356
Figure 147. Ratio of DIF3D to MCNP Fluxes in Group 3 .....	357
Figure 148. Ratio of DIF3D to MCNP Fluxes in Group 4 .....	357
Figure 149. MCNP Relative Error Distribution for Rods-Half Case.....	358
Figure 150. Ratio of DIF3D to MCNP Fluxes in Group 1 .....	361
Figure 151. Ratio of DIF3D to MCNP Fluxes in Group 2 .....	361
Figure 152. Ratio of DIF3D to MCNP Fluxes in Group 3 .....	361
Figure 153. Ratio of DIF3D to MCNP Fluxes in Group 4 .....	362
Figure 154. MCNP Relative Error Distribution for Rods-Out Case.....	362
Figure 155. Ratio of DIF3D to MCNP Fluxes in Group 1 .....	366
Figure 156. Ratio of DIF3D to MCNP Fluxes in Group 2 .....	366
Figure 157. Ratio of DIF3D to MCNP Fluxes in Group 3 .....	366
Figure 158. Ratio of DIF3D to MCNP Fluxes in Group 4 .....	367
Figure 159. Criticality Case 6 Flux Distribution.....	372
Figure 160. Criticality Case 54 Flux Distributions .....	374
Figure 161. Fixed Source Case Flux Distributions .....	378
Figure 162. Fixed Cell Source Case Flux Distributions .....	379



## LIST OF TABLES

Table 1. DIF3D Identifiable Sub-Programs with Auxiliary Input Controls .....	16
Table 2. DIF3D Nomenclature.....	16
Table 3. A.NIP3 Verification Case Matrix .....	18
Table 4. A.HMG4C Verification Case Matrix.....	19
Table 5. A.DIF3D Verification Case Matrix .....	19
Table 6. DIF3D Standard Output Verification Case Matrix .....	21
Table 7: A.SUMMAR Verification Case Matrix.....	22
Table 8. Binary File Verification Case Matrix.....	22
Table 9. 3D Cartesian Region Dimensions and Area Assignments.....	24
Table 10. 3D Cartesian Variable Mesh Structure .....	25
Table 11. 3D Cartesian Region Mesh Indices.....	25
Table 12. Isotopic Metadata .....	28
Table 13. Base Isotopic Cross Section Values.....	28
Table 14. Base Scattering Matrix Data .....	29
Table 15. ISOTXS File Styles.....	30
Table 16. DIF3D Control Options and Their Perturbations.....	39
Table 17. Variable Mesh Structure Verification .....	41
Table 18. Region Assignments and Volumes Verification.....	41
Table 19. Reactor Region Map for Z-Planes 1-8 .....	43
Table 20. Reactor Region Map for Z-Planes 9-17 .....	44
Table 21. Reactor Composition Map for Z-Planes 1-8 (Left) and 9-17 (Right).....	45
Table 22. Composition Number Densities .....	48
Table 23. Hand-Calculated Composition Cross Sections .....	49
Table 24. HMG4C Standard Output Cross Sections.....	49
Table 25. HMG4C and Hand-Calculated Cross Section Differences .....	50
Table 26. Hand-Calculated Scattering Matrices .....	50
Table 27. HMG4C Standard Output Scattering Matrices .....	51
Table 28. HMG4C and Hand-Calculated Scattering Matrices Differences .....	51
Table 29. Mesh Midpoint Comparisons.....	52
Table 30. Additional Hand Calculated Composition Cross Sections .....	53
Table 31. DIF3D-Outputted Composition Cross Sections.....	53
Table 32. DIF3D-Outputted Composition Cross Section Errors .....	54
Table 33. DIF3D-Outputted Scattering Matrices.....	55
Table 34. DIF3D-Outputted Scattering Matrix Errors.....	55



---

Table 35. Comparison of GEODST Values .....	59
Table 36. Comparison of NDXSRF Values .....	61
Table 37. Comparison of ZNATDN Values .....	63
Table 38. Comparison of COMPXS Type 01, Type 02, and Type 05 Cards .....	65
Table 39. Comparison of COMP1 from the COMPXS File .....	66
Table 40. Comparison of COMP2 from the COMPXS File .....	67
Table 41. Comparison of COMP3 from the COMPXS File .....	68
Table 42. Comparison of COMP4 from the COMPXS File .....	69
Table 43. Comparison of LABELS Values .....	73
Table 44. Comparison of Hand-Calculated Cross Sections for Base and GAMISO Cases .....	77
Table 45. Comparison of Hand-Calculated Cross Sections for Base and User 1 Cases...	78
Table 46. Hand-Calculated Chi Vectors for User-Defined Style 1 Chi Option 1 Case ....	82
Table 47. Hand-Calculated Chi Vectors for Chi Option 2 Case .....	83
Table 48. Isotope Classification Case Summary.....	84
Table 49. Edit Control Perturbations .....	89
Table 50. Macroscopic Multigroup Cross Sections for Infinite Homogeneous Test.....	102
Table 51. DIF3D eigenvalue results for the Infinite Homogeneous Test Problem.....	103
Table 52. DIF3D-FD Eigenvalue for the Cartesian Analytic Diffusion Benchmark.....	108
Table 53. DIF3D-FD Peak and RMS Errors on the Lowest Plane .....	110
Table 54. DIF3D-VARIANT Eigenvalue for the Cartesian Analytic Diffusion Benchmark .....	111
Table 55. DIF3D-VARIANT Peak and RMS Errors on the Lowest Planer Flux Distribution .....	111
Table 56. DIF3D-VARIANT P-refinement for the Cartesian Analytic Diffusion Benchmark .....	112
Table 57. DIF3D Eigenvalue Results for the Modified Analytic Diffusion Benchmark	113
Table 58. DIF3D-FD Forward and Adjoint Flux Comparison for the Diffusion Benchmark .....	114
Table 59. DIF3D-VARIANT Forward and Adjoint Flux Comparison for the Diffusion Benchmark .....	114
Table 60. DIF3D-FD Flux Error Results for the Fixed Source Analytic Diffusion Benchmark .....	116
Table 61. DIF3D-VARIANT Flux Error Results for the Fixed Source Diffusion Benchmark .....	118
Table 62. DIF3D-VARIANT P-Refinement Error for the Fixed Source Diffusion Benchmark .....	119

---

Table 63. DIF3D-FD Forward and Adjoint Flux Comparison for the Fixed Source Benchmark .....	119
Table 64. VARIANT Forward and Adjoint Flux Comparison for the Fixed Source Benchmark .....	120
Table 65. DIF3D-FD Flux Error Results for the Inhomogeneous Diffusion Benchmark .....	122
Table 66. DIF3D-VARIANT Flux Error Results for the Inhomogeneous Diffusion Benchmark .....	123
Table 67. DIF3D-VARIANT P-Refinement Error for the Inhomogeneous Diffusion Benchmark .....	123
Table 68. DIF3D-FD Forward and Adjoint Flux Comparison for the Fixed Source Benchmark .....	124
Table 69. VARIANT Forward and Adjoint Flux Comparison for the Fixed Source Benchmark .....	124
Table 70. Cross Sections for the Diffusion Theory Peaking Problem .....	125
Table 71. Region and Area Definitions for the Diffusion Theory Peaking Problem.....	130
Table 72. Region Errors for the Total Flux in the Diffusion Theory Peaking Problem .	134
Table 73. Region Errors for the Peak of the Total Flux in the Diffusion Theory Peaking Problem .....	134
Table 74. Region Errors for the Total Fast Flux in the Diffusion Theory Peaking Problem .....	135
Table 75. Region Errors for the Peak Fast Flux in the Diffusion Theory Peaking Problem .....	135
Table 76. Peak of the Total Flux Positions and DIF3D-VARIANT Error .....	136
Table 77. Peak of the Fast Flux Positions and DIF3D-VARIANT Error .....	137
Table 78. Peak of the Power Density Positions and the DIF3D-VARIANT Error.....	138
Table 79. Region Errors for the Power Density in the Diffusion Theory Peaking Problem .....	140
Table 80. Region Errors for the Peak Power Density in the Diffusion Theory Peaking Problem .....	140
Table 81. Region Errors for the Total Fast Flux and Peak Fast Flux in the Diffusion Theory Peaking Problem .....	142
Table 82. Cartesian DIF3D-FD Extrapolated Boundary Condition Results.....	145
Table 83. Iteration Control Options for the Diffusion Solver.....	146
Table 84. XYZ Diffusion Edit Table Perturbations .....	151
Table 85. DIF3D Neutron Balance Table Set 1 .....	152
Table 86. DIF3D Neutron Balance Table Set 2 .....	153
Table 87. DIF3D Neutron Balance Table Set 3 .....	153

---

Table 88. Reference Neutron Balance Table Set 1 .....	155
Table 89. Reference Neutron Balance Table Set 2 .....	155
Table 90. Reference Neutron Balance Table Set 3 .....	156
Table 91. DIF3D keff and Power Distribution Errors for the IAEA Benchmark .....	160
Table 92. External keff and Power Distribution Errors for the IAEA Benchmark.....	161
Table 93. Triangular-Z Geometry Hand-Calculated Volumes .....	166
Table 94. Diffusion Theory Triangular-Z Perturbation Cases .....	166
Table 95. Triangular-Z NDXSFR Volumes.....	174
Table 96. Comparison of GEODST Values for Triangular-Z Problem .....	178
Table 97. Volumes for REG1 in Background.....	196
Table 98. Diffusion Theory Triangular-Z Perturbation Cases .....	197
Table 99. Peak Flux Predictions of DIF3D-FD .....	216
Table 100. Peak Flux Predictions of DIF3D-VARIANT reported by DIF3D.....	217
Table 101. Peak Flux (left) and Zero Flux (right) Predictions of DIF3D-VARIANT reported by the EvaluateFlux Utility.....	219
Table 102. Full-Core Triangular-Z DIF3D-FD Extrapolated Boundary Condition Results.....	221
Table 103. Sixth-Core Triangular-Z DIF3D-FD Extrapolated Boundary Condition Results .....	222
Table 104. Third-Core Triangular-Z DIF3D-FD Extrapolated Boundary Condition Results .....	223
Table 105. Iteration Control Options for the Diffusion Solver.....	225
Table 106. DIF3D Neutron Balance Table Set 1 .....	231
Table 107. DIF3D Neutron Balance Table Set 2 .....	232
Table 108. DIF3D Neutron Balance Table Set 3 .....	233
Table 109. Reference Neutron Balance Table Set 1 .....	234
Table 110. Reference Neutron Balance Table Set 2 .....	235
Table 111. Reference Neutron Balance Table Set 3 .....	236
Table 112. DIF3D-FD VVER-440 Eigenvalue Results.....	238
Table 113. DIF3D-FD VVER 440 Power Distribution Errors .....	239
Table 114. DIF3D Transport Control Options and Their Perturbations .....	241
Table 115. Transport Case Total and Transport Cross Sections.....	244
Table 116. Transport Case P <sub>0</sub> Total Scattering Matrices .....	244
Table 117. Edit Control Perturbations .....	246
Table 118. Composition Cross Sections for P <sub>2</sub> ISOTXS File Data .....	252
Table 119. Card 12 Option 10, Case 5 Reference Solution .....	254

---

Table 120. 3D Cartesian Transport Multigroup Fixed Source Macroscopic Cross Sections; units of cross sections are 1/cm.....	256
Table 121. XYZ MG DIF3D Peak Flux Errors in units of percent.....	259
Table 122. XYZ MG DIF3D Flux Root-Mean-Squared-Errors .....	261
Table 123. Modified Multigroup Macroscopic Cross Sections for Inhomogeneous Case; units of cross sections are 1/cm.....	265
Table 124. 3D Cartesian Transport Multigroup Eigenvalue Cross Sections; units of cross sections are 1/cm .....	267
Table 125. XYZ MG DIF3D Eigenvalue Errors in units of pcm.....	271
Table 126. XYZ MG DIF3D Peak Flux Errors in units of percent.....	272
Table 127. XYZ MG DIF3D Flux Root-Mean-Squared-Errors .....	273
Table 128. Cartesian DIF3D-VARIANT Extrapolated Boundary Condition Results....	278
Table 129. Iteration Control Options for Cartesian Transport.....	279
Table 130. Takeda 3, Rods-In, Eigenvalue Errors with Standard Functions [pcm] .....	289
Table 131. Takeda 3, Rods-In, Eigenvalue Errors with Yang Functions [pcm].....	290
Table 132. Takeda 3, Rods-In, Peak Flux Errors [%].....	291
Table 133. Takeda 3, Rods-In, Root-Mean-Squared Flux Errors .....	292
Table 134. Takeda 3, Rods-Out, Eigenvalue Errors [pcm].....	294
Table 135. Takeda 3, Rods-Out, Peak Flux Errors [%] .....	295
Table 136. Takeda 3, Rods-Out, Root-Mean-Squared Flux Errors .....	296
Table 137. Takeda 3, Core, Eigenvalue Errors [pcm].....	298
Table 138. Takeda 3, Core, Peak Flux Errors [%] .....	299
Table 139. Takeda 3, Core, Root-Mean-Squared Flux Errors .....	300
Table 140. Transport Theory Hexagonal-Z Perturbation Cases .....	302
Table 141. Comparison of GEODST Values for Hexagonal-Z Problem.....	310
Table 142. Volumes for REG1 in Background.....	315
Table 143. Transport Theory Hexagonal-Z Perturbation Cases .....	316
Table 144. 3D Cartesian Transport Multigroup Fixed Source Macroscopic Cross Sections; units of cross sections are 1/cm.....	321
Table 145. Hexagonal-Z MG DIF3D Peak Flux Errors in units of percent.....	324
Table 146. Hexagonal-Z MG DIF3D Flux Root-Mean-Squared-Errors .....	326
Table 147. Modified Multigroup Macroscopic Cross Sections for Inhomogeneous Case; units of cross sections are 1/cm.....	329
Table 148. Hexagonal-Z MG DIF3D Eigenvalue Errors in units of pcm.....	334
Table 149. Hexagonal-Z MG DIF3D Peak Flux Errors in units of percent.....	336
Table 150. Hexagonal-Z MG DIF3D Flux Root-Mean-Squared-Errors .....	337
Table 151. Hexagonal-Z MG DIF3D Eigenvalue Errors in units of pcm.....	341

Table 152. Iteration Control Options for Hexagonal Transport.....	343
Table 153. Takeda 4, Rods-In, Eigenvalue Errors [pcm] .....	353
Table 154. Takeda 4, Rods-In, Peak Flux Errors [%].....	354
Table 155. Takeda 4, Rods-In, Root-Mean-Squared Flux Errors .....	355
Table 156. Takeda 4, Rods-Half, Eigenvalue Errors [pcm].....	358
Table 157. Takeda 4, Rods-Half, Peak Flux Errors [%] .....	359
Table 158. Takeda 4, Rods-Half, Root-Mean-Squared Flux Errors .....	360
Table 159. Takeda 4, Rods-Out, Eigenvalue Errors [pcm].....	363
Table 160. Takeda 4, Rods-Out, Peak Flux Errors [%] .....	364
Table 161. Takeda 4, Rods-Out, Root-Mean-Squared Flux Errors .....	365
Table 162. MCNP Capability Verification List .....	371
Table 163. Criticality Case 72 Fluxes .....	375
Table 164. Criticality Case 74 Normalized Fluxes .....	376
Table 165. Criticality Case 75 Normalized Fluxes .....	377
Table 166. Fixed Isotropic Source Case Fluxes.....	380

## 1 Introduction

The DIF3D code (DIffusion 3D) was primarily built as a three-dimensional solver of the multigroup diffusion equation for semi-structured grid geometries using a finite difference spatial differencing methodology [1]. This capability still exists and is commonly referred to as DIF3D-FD. Later, in the early 1980s, a transverse integrated nodal methodology, referred to as DIF3D-Nodal [2], was built into DIF3D to improve the performance on large scale reactor problems. Later work, motivated by the research and development to support fast spectrum reactors that promote non-proliferation by eliminating blanket assemblies, the DIF3D-VARIANT solver [3] was added to DIF3D in the mid 1990s, and later updated [4], that extends the nodal concept to transport via a variational three-dimensional transport method applying spherical harmonic expansions in angle.

The present DIF3D capability can treat slab and cylindrical 1D domains, Cartesian, hexagonal, and R-Z 2D domains, and Cartesian, hexagonal-Z, triangular-Z, and R-Z- $\theta$  3D domains. The DIF3D-FD diffusion solver can be applied to every geometry type in DIF3D except for hexagonal and hexagonal-Z geometries, where a triangular-Z mesh geometry is instead used to represent hexagonal reactor designs. The DIF3D-Nodal diffusion and DIF3D-VARIANT solvers only support 2D and 3D dimensional Cartesian and hexagonal geometries.

Current Argonne National Laboratory design activities are require that a thorough verification of the Argonne Reactor Computation (ARC) [5] codes be performed. DIF3D is central to the entire ARC system. The driver for this effort requires the 3D Cartesian, triangular-Z, and hexagonal-Z core geometry options of DIF3D be verified.

The DIF3D features required to be verified to support these design activities are documented in [6], which is generally applicable to hexagonal-Z fast reactor designs; this reference also includes the tasks that were anticipated to be used to perform the verification. The scope of this verification defined in [6] includes verifying DIF3D's ability to correctly translate the user's model in to DIF3D's preferred format, verifying that options planned for use have the desired effect, and verifying the correctness of the eigenvalue, fixed-source, forward, and adjoint solvers in DIF3D-FD and DIF3D-VARIANT. Note that this work did not verify the DIF3D-Nodal capability.

This manuscript summarizes the verification tasks performed to verify the forward and adjoint forms of the steady state fixed source, inhomogeneous fixed source, and eigenvalue forms of the transport and diffusion equation as implemented for Cartesian, hexagonal-Z and triangular-Z geometries in DIF3D.

Before progressing to the verification, this report will frequently reference the sub-modules within DIF3D. Therefore, DIF3D is composed of several sub-modules with features that can be controlled by the user. The modules used for fast reactor design work are provided in [6] with a summary of their function in the DIF3D execution. The RODPOS module will not be verified as part of DIF3D, instead it will be verified as part of REBUS, the only ARC component that uses it.

The SCAN and STUFF modules are input pre-processors and will be exercised by most fast reactor design use cases, however the user has no control over their functionality. No further discussion or specific verification efforts will be required for these modules as their verification is implicit in the other verification tasks.

**Table 1. DIF3D Identifiable Sub-Programs with Auxiliary Input Controls**

<b>Module</b>	<b>Description</b>
SCAN	Separates user input into ARC components or identified binary data file
STUFF	Generates the associated ASCII or binary file from user input
GNIP4C	Defines the case geometry and assigns materials
HMG4C	Generates macroscopic cross-sections for each composition
DIF3D	Solves the diffusion or transport equation
SUMMAR	Composes summary outputs after solver execution
RODPOS	Used in the search procedure to move designated control rods

Before detailing the above functionality, the ARC-specific concepts of zones, regions, meshes, and areas are defined in Table 2 for clarity.

**Table 2. DIF3D Nomenclature**

<b>Term</b>	<b>Definition</b>
Zone	A set of isotopes at a given temperature with stated atom densities. A zone can be assigned to multiple regions.
Composition	Equivalent to a zone.
Region	A Volume of space filled with a zone. Every region contains only one zone.
Mesh	The computational mesh used for the numerical determination of the flux and/or eigenvalue. There is at least one mesh per region.
Area	A collection of regions that are assigned a consistent label for analyst convenience and downstream usage by other ARC software such as REBUS.

Multiple versions of DIF3D have been created over the software's 40-year history. The verification plan discussed in this document is generated based on the capabilities of DIF3D version 11.0, release 3012 (more specifically, the executable named dif3d\_v11.0\_r3012\_d2019\_03\_14\_512GB.x installed on the KOOKIE cluster within the Nuclear Science and Engineering Division at Argonne National Laboratory).

The remainder of this report will progress through a re-hash of the verification strategy from [6], followed by the discussion of the verification cases as well as the results and any findings. Finally, these findings will be summarized and any concluding remarks made.



## 2 Verification Strategy

No non-trivial analytic solution of the neutron diffusion and transport equations can be generated for the geometries of interest for multigroup, multi-region, fixed source and eigenvalue reference solutions. The verification of DIF3D therefore requires multiple tiers of problems unique to each solver and geometry type, each testing features independently and present complementary arguments for why that separate testing of functionality is acceptable. The parameters in the verification tests are chosen so the reference solution is only reasonably obtained through a correct implementation of the governing equations and algorithms in DIF3D. For example, problems with anisotropic scattering will use cross sections for which the expected solution is significantly different if the anisotropic scattering data is ignored. To add confidence in the separate testing as well as to provide confidence that the chosen problems did not fortuitously yield a correct solution, a final integral check of each the diffusion and transport capabilities and applicable geometries are also incorporated in the plan. These final integral problems utilize previously published benchmark problems with externally published solutions.

Due to the different strategies required for the solver and geometry combinations, the following sub-sections separately discuss the diffusion and transport solver verification efforts for the geometries of interest. Table 3 through Table 8 summarize how these verification cases are used to verify the inputs and the most important options identified in [6]. For conciseness, these tables do not highlight which cases simply exercise each feature, instead they only identify the cases that are relied upon to show verification of that feature. Table 8 provides a similar matrix for the output binary file verification. Note that this table does not include the files that are implicitly verified by virtue the fact that DIF3D writes and reads these files internally in addition to being a potential user input (e.g., FIXSRC, VARSRC, and ISOTXS).

These tables, and the remainder of the report, split the verification across categories specific to 3D Cartesian diffusion, Triangular-Z diffusion, 3D Cartesian transport, and Hexagonal-Z transport. The individual functionalities may not need to be repeated for each solver as the functionality may be completely independent of the solver and/or geometry type. Therefore the cases identified in Table 3 through Table 8 may apply to multiple solver/geometry combinations. For example this is observed with the Section 3.1.1 (3D Cartesian diffusion Model Building) work also applying to 3D Cartesian transport or Section 3.1.12 (SUMMAR Verification) applying to every geometry/solver combination though it was only performed with a 3D diffusion model. Regardless, the general progression of each of the geometry and solver type combination evaluations is to first evaluate the model definition (geometry, materials, etc.), then the correctness of the solver, then evaluating the various options that affect the solver (boundary conditions, iteration control), and finally verifying the post-processing.



Table 3. A.NIP3 Verification Case Matrix

Card Type	Summary	Applicable Verification Cases			
		Diffusion Solver		Transport Solver	
		3D Cartesian	Triangular-Z	3D Cartesian	Hexagonal-Z
1	Problem Title	3.1.1	3.2.1	3.3.1	3.4.1
2.3	Geometry Processing Edit	3.1.1	3.2.1	3.1.1	3.4.1
2.9	Cross-Section Processing Edit	3.1.1	3.2.1	3.1.1	3.2.1
2.10	Region/Mesh Interval Map Edit	3.1.1	3.2.1	3.1.1	3.4.1
2.11	Zone/Mesh Interval Map Edit	3.1.1	3.2.1	3.1.1	3.4.1
3	<i>Problem Geometry:</i>	-			
	3D Cartesian	3.1.2	N/A	3.3.2	N/A
	Triangular-Z sixth-core	N/A	3.2.1	N/A	N/A
	Triangular-Z third-core	N/A	3.2.1	N/A	N/A
	Triangular-Z full-core	N/A	3.2.1	N/A	N/A
	Hexagonal-Z sixth-core	N/A	N/A	N/A	3.4.1
	Hexagonal-Z third-core	N/A	N/A	N/A	3.4.1
	Hexagonal-Z full-core	N/A	N/A	N/A	3.4.1
4	<i>External Boundary Conditions:</i>	-			
	Z-Plane Zero Flux	3.1.4	3.2.2	N/A	N/A
	Z-Plane Extrapolated Flux	3.1.9	3.2.3	N/A	N/A
	Z-Plane Vacuum	N/A	N/A	3.3.2, 3.3.3, 3.3.4	3.4.2, 3.4.3
	X-Y Plane or Radial Zero Flux	3.1.4	3.2.2	N/A	N/A
	X-Y Plane or Radial Extrap. Flux	3.1.9	3.2.3	N/A	N/A
	X-Y Plane or Radial Vacuum	N/A	N/A	3.3.2, 3.3.3, 3.3.4	3.4.2, 3.4.3
	Radial Reflective Symmetry	3.1.2	3.2.3	3.3.2, 3.3.3, 3.3.4	N/A
	Radial Periodic Symmetry	3.1.8	3.2.4	N/A	3.4.2, 3.4.3, 3.4.4
5	External Boundary Condition Constants	3.1.9	3.2.3	N/A	N/A
6	Region Boundaries for Ortho. Geom.	3.1.1	N/A	3.3.1	N/A
7	Area Specifications	3.1.1	3.2.1	3.3.1	3.4.1
9	Variable-Mesh Structure	3.1.1	3.2.1	3.3.1	3.4.1
13	Material Specifications	3.1.1	3.2.1	3.3.1	3.4.1
14	Composition (Zone) Specifications	3.1.1	3.2.1	3.3.1	3.4.1
15	Region/Composition Correspondence	3.1.1	3.2.1	3.3.1	3.4.1

February 13, 2020

**Table 3. A.NIP3 Verification Case Matrix, Continued**

19	Region Or Mesh Distrib. Inhomog. Source	3.1.3, 3.1.4	3.1.3, 3.1.4, 3.2.2	3.3.2	3.4.2
29	Hexagon Dimension	N/A	3.2.1	N/A	3.4.1
30	Region Def. for Arrays of Hexagons	N/A	3.2.1	N/A	3.4.1
31	Bkgd. Region for Arrays of Hexagons	N/A	3.2.1	N/A	3.4.1
40	Source Edit, Synthesis Trial Function Source	Verified with PERSENT Verification			
42	Source Spectra	3.3.2	3.4.2	3.3.2	3.4.2
44	Region Assignment to Control Rod Bank	3.1.1	3.2.1	3.1.1	3.4.1

**Table 4. A.HMG4C Verification Case Matrix**

Card Type	Summary	Applicable Verification Cases			
		Diffusion Solver		Transport Solver	
		3D Cartesian	Triangular-Z	3D Cartesian	Hexagonal-Z
1	Problem Title	3.1.1	3.2.1	3.3.1	3.4.1
2.3	Print File Master Control Flag	3.1.1	3.2.1	3.3.1	3.4.1
2.4	COMPXS Edit Flag	3.1.1			
2.5	ISOTXS Edit Flag	3.1.1			
2.7	Prompt Fission Spectrum Options	3.1.1	3.2.1	3.3.1	3.4.1
2.8	Auxiliary Output File Control	3.1.1	3.2.1	3.3.1	3.4.1
2.9	Edit of Supplied COMPXS	3.1.1			

**Table 5. A.DIF3D Verification Case Matrix**

Card Type	Summary	Applicable Verification Cases			
		Diffusion Solver		Transport Solver	
		3D Cartesian	Triangular-Z	3D Cartesian	Hexagonal-Z
1	Problem Title	3.1.1	3.2.1	3.3.1	3.4.1
3.2	<i>Problem Type:</i>	-			
	K-Effective	3.1.2, 3.1.4	3.1.2, 3.2.2	3.1.2, 3.3.3	3.1.2, 3.4.3
	Fixed Source	3.1.3, 3.1.5, 3.1.6	3.2.2	3.3.2	3.4.2
3.3	<i>Solution Type:</i>	-			
	Real Solution	3.1.2, 3.1.3	3.1.2, 3.2.2	3.1.2, 3.3.2, 3.3.3	3.1.2, 3.4.2, 3.4.3
	Adjoint Solution	3.1.2, 3.1.3	3.1.2	3.1.2	3.1.2
	Both Real and Adjoint Solution	3.1.2, 3.1.3	3.1.2	3.1.2	3.1.2

February 13, 2020

**Table 5. A.DIF3D Verification Case Matrix, Continued**

3.4	Tchebyshev Acceleration	3.1.10	3.2.5	3.3.5	3.4.5
3.6	Outer Iteration Control	3.1.10	3.2.5	3.3.5	3.4.5
3.7	Restart Flag	3.1.10	3.2.5	3.3.5	3.4.5
3.9	Upscatter Iterations per Outer Iteration	3.1.10	3.2.5	3.3.5	3.4.5
3.10	Concurrent Iteration Efficiency	3.1.10	3.2.5	3.3.5	3.4.5
3.11	Acceleration of Optimum Overrelaxation	3.1.10	3.2.5	3.3.5	3.4.5
3.12	Optimum Overrelaxation Factor Calculation Control	3.1.10	3.2.5	3.3.5	3.4.5
4.2	Problem Description Edit	3.1.1	3.2.1	3.3.1	3.4.1
4.3	Region to Mesh Interval Map Edit	3.1.1	3.2.1	3.3.1	3.4.1
4.4	Zone to Mesh Interval Map Edit	3.1.1	3.2.1	3.3.1	3.4.1
4.5	Macroscopic Cross-Section Edit	3.1.1		3.3.1	
4.6	Balance Edits	3.1.11	3.1.11	3.3.6	3.4.6
4.7	Power Edits	3.1.7, 3.1.11	3.2.2, 3.1.11	3.1.7, 3.3.6	3.2.2, 3.4.6
4.8	Flux Edits	3.1.7, 3.1.11	3.2.23.1.11	3.1.7, 3.3.6	3.2.2, 3.4.6
4.9	Zone Averaged Edits	3.1.11	3.1.11	3.3.6	3.4.6
4.10	Region Averaged Flux Edits	3.1.11	3.1.11	3.3.6	3.4.6
4.11	Interface Files	3.1.11	3.1.11	3.3.6	3.4.6
5.2	Eigenvalue Criterion	3.1.10	3.2.5	3.3.5	3.4.5
5.3	Pointwise Fiss. Source Criterion	3.1.10	3.2.5	3.3.5	3.4.5
5.4	Average Fission Source Criterion	3.1.10	3.2.5	3.3.5	3.4.5
6.2	Restart k-effective	3.1.10	3.2.5	3.3.5	3.4.5
6.6	Restart Dominance Ratio	3.1.10	3.2.5	3.3.5	3.4.5
12.2	Nodal Spatial Approximation	N/A	N/A	3.3.2, 3.3.3	3.4.2, 3.4.3
12.3	Angular Approximation	N/A	N/A	3.3.2, 3.3.3, 3.3.7	3.4.2, 3.4.3
12.5	Num. of X-Y Plane Partial Current Sweeps	N/A	N/A	3.3.5	3.4.5
12.6	Num. of Axial Partial Current Sweeps	N/A	N/A	3.3.5	3.4.5
12.9	Anisotropic Scattering Order	N/A	N/A	3.3.1	
12.10	Extended Transport Approx on Total Cross-Section	N/A	N/A	3.3.1	
12.11	Omega Transformation Acceleration	N/A	N/A	3.3.5	3.4.5
12.14	NHFLUX Content	N/A	N/A	3.3.6	3.4.6

Table 6. DIF3D Standard Output Verification Case Matrix

Standard Outputs	Summary	Applicable Verification Cases			
		Diffusion Solver		Transport Solver	
		3D Cartesian	Triangular-Z	3D Cartesian	Hexagonal-Z
1	Model Description Tables	3.1.1	3.2.1	3.3.1	3.4.1
2	Mesh Interval Tables	3.1.1	3.2.1	3.3.1	3.4.1
3	K-effective Convergence	3.1.2	3.2.2	3.3.3	3.4.3
4	Power Density Table by Mesh	3.1.11	3.1.11	3.3.6	3.4.6
5	Power Density Table by Region and Area	3.1.7	3.2.2	3.1.7	3.2.2
5	Peak Flux and Power	3.1.7	3.2.2	3.1.7	3.2.2
6	Real Flux Table by Mesh by Group	3.1.7	3.2.2	3.1.7	3.2.2
7	Real Flux Table by Mesh Integrated over Groups	3.1.7	3.2.2	3.1.7	3.2.2
8	Region and Area Balance Tables by Group	3.1.11	3.1.11	3.3.6	3.4.6
9	Region and Area Balance Tables Integrated over Groups	3.1.11	3.1.11	3.3.6	3.4.6

February 13, 2020

Table 7: A.SUMMAR Verification Case Matrix

Card Type	Summary	Applicable Verification Cases			
		Diffusion Solver		Transport Solver	
		3D Cartesian	Triangular-Z	3D Cartesian	Hexagonal-Z
2	Plot Specifications	3.1.12			
6	Core Region Specification	3.1.12			

Table 8. Binary File Verification Case Matrix

File	Summary	Applicable Verification Cases			
		Diffusion Solver		Transport Solver	
		3D Cartesian	Triangular-Z	3D Cartesian	Hexagonal-Z
GEODST	Geometry Description	3.1.1	3.2.1	3.3.1	3.4.1
NDXSRF	Nuc. Density, Data, XS Referencing	3.1.1	3.2.1	3.3.1	3.4.1
ZNATDN	Zone Atomic Densities	3.1.1	3.2.1	3.3.1	3.4.1
COMPXS	Composition XS	3.1.1	3.2.1	3.3.1	3.4.1
LABELS	Misc. Labels and Info	3.1.1	3.2.1	3.3.1	3.4.1
RTFLUX	Forward Fluxes	3.1.2	3.1.2	3.1.2, 3.3.3	3.1.2, 3.3.3
ATFLUX	Adjoint Fluxes	3.1.2	3.1.2	3.1.2	3.1.2
RZFLUX	Zone Fluxes	3.1.11	3.1.11	3.3.6	3.4.6
PWDINT	Power Density by Interval	3.1.11	3.1.11	3.3.6	3.4.6

### 3 DIF3D Verification Tasks

This section contains the verification tasks, the models used for verification, the presentation of results, and identification of any verification issues. Section 3.1 will present the cases relevant primarily to the DIF3D-FD 3D Cartesian solver; Section 3.2 will do the same for DIF3D-FD Triangular-Z, Section 3.3 for DIF3D-VARIANT 3D Cartesian, and finally Section 3.4 for DIF3D-VARIANT Hexagonal-Z. Some of these sections and tasks apply to the verification of other geometry types or solvers; where applicable it will be noted. As discussed, the general progression of each of the geometry and solver type combination evaluations is to first evaluate the model definition (geometry, materials, etc.), then the correctness of the solver, then evaluating the various options that affect the solver (boundary conditions, iteration control), verifying the post-processing, and finally using an integral verification problem to wrap it all up through comparisons with more realistic models. The reader is also referred to Tables 2 through 7 for a reference regarding which sections cover which features.

#### 3.1 DIF3D-FD 3D Cartesian Verification

##### 3.1.1 Model Building Verification

A “Model Building” case will be used to verify the ability of the BCDINP and HMG4C modules to create the user-specified 3D Cartesian diffusion model from the input by creating a simple two-group, multi-isotope, multi-composition, multi-region 3D Cartesian model. This case will specifically be used to verify the following card types and options consistent with Tables 7 through 9 of [6]: card Types 1, 2 (options 3, 9, 10, and 11), 6, 7, 9, 13, 14, 15, and 44 of the NIP3 data set; card Types 1, 2 (options 3, 4, 5, 7, and 8) of the HMG4C module; and card Types 1, 4 (Options 2, 3, 4, and 5) of the DIF3D module.

The verification of these options will be exercised through a base model and perturbations thereof to test various features. This section will begin by discussing the base model, the sub-sections that follow will show the verification of each of the card types and their options from Tables 7 of [6] with the perturbations to the model introduced as required.

##### 3.1.1.1 Model Definition

###### 3.1.1.1.1 Geometry

To verify DIF3D’s ability to create a fine-meshed representation of the input geometry, the verification model will include at least two regions in each of the X, Y, and Z directions with misaligned coarse-mesh boundaries. The two unique axial planes of this model are shown in Figure 1. The dimensions of each region are provided in the figure, and more explicitly provided in Table 9, with all values provided in units of centimeters. Importantly, these figures were generated without the use of DIF3D, enabling their usage as a reference to compare the DIF3D region sketches. The model’s eight regions are assigned to three unique and non-contiguous areas such that REG1 and REG8 are assigned to AREA1, REG2 and REG7 to AREA2, etc., as is shown in the last column of Table 9. REG4 and REG5 are not assigned so that composition assignments can

be tested using both areas and regions. At this stage of the verification process, all six sides of the model geometry have reflective boundary conditions imposed on them.

**Table 9. 3D Cartesian Region Dimensions and Area Assignments**

Label	X <sub>low</sub>	X <sub>high</sub>	Y <sub>low</sub>	Y <sub>high</sub>	Z <sub>low</sub>	Z <sub>high</sub>	Area Assignment
REG1	0.0	1.0	0.0	6.0	0.0	3.0	AREA1
REG2	1.0	3.5	0.0	6.0	0.0	3.0	AREA2
REG3	3.5	10.0	0.0	12.0	0.0	3.0	AREA3
REG4	0.0	3.5	6.0	20.0	0.0	30.0	Not Assigned
REG5	3.5	10.0	12.0	20.0	0.0	3.0	Not Assigned
REG6	0.0	10.0	0.0	6.0	3.0	30.0	AREA3
REG7	3.5	10.0	6.0	10.0	3.0	30.0	AREA2
REG8	3.5	10.0	10.0	20.0	3.0	30.0	AREA1

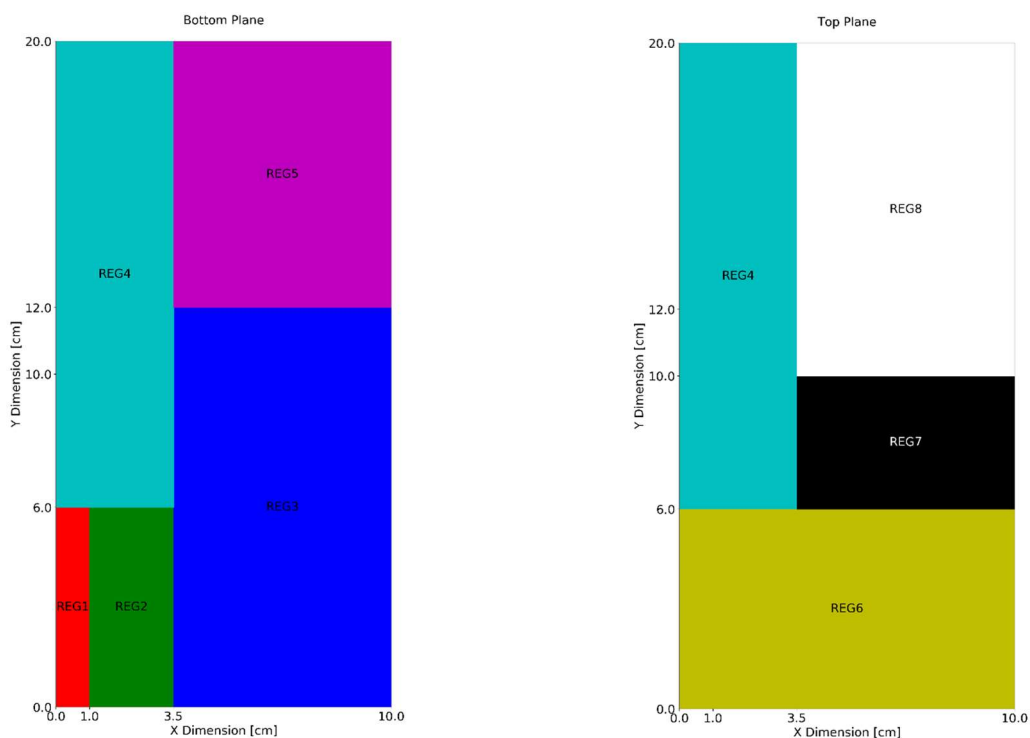


**Figure 1. 3D Cartesian Model Geometry**

DIF3D uses a variable-mesh structure that can be defined in each dimension of the 3D Cartesian model. To test this functionality, the above model will be meshed as shown in Table 10. Note that the number of mesh elements per domain was given a unique number so that if DIF3D uses an incorrect number of mesh elements and spacing, it will be obvious.

**Table 10. 3D Cartesian Variable Mesh Structure**

	Domain	Number of Elements	Mesh Spacing [cm]
<b>X</b>	0.0 – 1.0	1	1
	1.0 – 3.5	2	1.25
	3.5 – 10.0	3	2.16666 $\bar{6}$
<b>Y</b>	0.0 – 6.0	4	1.5
	6.0 – 10.0	5	0.8
	10.0 – 12.0	6	0.333333 $\bar{3}$
	12.0 – 20.0	7	1.142857...
<b>Z</b>	0.0 – 3.0	8	0.375
	3.0 – 30.0	9	3

The above region dimensions and mesh structure can be converted to the region extents in terms of the fine mesh indices in each of the X, Y, and Z dimensions as shown in Table 11.

**Table 11. 3D Cartesian Region Mesh Indices**

Label	X Mesh Indices	Y Mesh Indices	Z Mesh Indices
<b>REG1</b>	1	1-4	1-3
<b>REG2</b>	2,3	1-4	1-3
<b>REG3</b>	4-6	1-15	1-3
<b>REG4</b>	1-3	5-22	1-17
<b>REG5</b>	4-6	16-22	1-3
<b>REG6</b>	1-6	1-4	4-17
<b>REG7</b>	4-6	5-9	4-17
<b>REG8</b>	4-6	10-22	4-17

This geometry is set by the user with the A.NIP3 input block; the specific input used for to describe the geometry in this section is shown in Figure 2. This figure provides the line numbers on the left and the cards on the right. Note that lines that start with “c” are effectively comments as they are ignored by DIF3D. This figure shows specifically how line 4 (card Type 03) sets the geometry to be a 3D Cartesian geometry, line 6 (a Type 04 card) sets reflective boundary conditions on all six



February 13, 2020

surfaces, lines 8 through 15 (all Type 06 cards) define the region extents consistent with the geometry shown in Figure 1, lines 17 through 20 (all Type 09 cards) establish the variable mesh structure as defined in Table 10, and finally lines 22 through 25 (all Type 07 cards) set the area assignments consistent with Table 9. This geometric definition will be used in all follow-on cases except where otherwise noted.

```

1  UNIFORM=A.NIP3
2  ...
3  c Set to 3D Cartesian Geometry
4  03 44
5  c Define Boundary Conditions
6  04 3 3 3 3 3
7  c Define the Regions
8  06 REG1 0.0 1.0 0 8 0.0 6.0
9  06 REG2 1.0 3.5 0 8 0.0 6.0
10 06 REG3 3.5 10.0 0 8 0.0 12.0
11 06 REG4 0.0 3.5 0 17 6.0 20.0
12 06 REG5 3.5 10.0 0 8 12.0 20.0
13 06 REG6 0.0 10.0 8 17 0.0 6.0
14 06 REG7 3.5 10.0 8 17 6.0 10.0
15 06 REG8 3.5 10.0 8 17 10.0 20.0
16 c Define the variable mesh structure
17 09 X 1 1.0 2 3.5 3 10.0
18 09 Y 4 6.0 5 10.0 6 12.0
19 09 Y 7 20.0
20 09 Z 8 3.0 9 30.0
21 c Define the Areas
22 07 AREA1 REG1 REG8
23 07 AREA2 REG2 REG7
24 07 AREA3 REG3 REG6
25 ...

```

**Figure 2. A.NIP3 3D Cartesian Model Geometry Definition**

### 3.1.1.1.2 Compositions

DIF3D provides multiple methods for defining the compositions that are to be assigned to regions: isotopes can be directly assigned to a composition via the Type 14 card, a material defined via the Type 13 card and combined with an isotope to create a composition via the Type 14 card, multiple materials combined into a composition via the Type 14 card, and multiple compositions combined into a composition mixture via the Type 14 card. These four approaches can be tested by defining four unique compositions. The definitions of these four compositions are provided in Figure 3. This A.NIP3 input contains four sets of Type 13, 14, and 15 cards.

Lines 5 and 6 define the first composition; here, a single isotope from the isotopic cross section file (ISOTXS) is assigned to the composition named COMP1 with an atom density of 1.0. This composition is then assigned to the regions within AREA1 (defined previously).

Lines 8-11 define the second composition. Here, a material is defined in Type 13 card as MISO3 composed of the ISO3 isotope from the ISOTXS file with an atom density of 2.0. We next assign the material MISO3, scaled by a factor of 0.25 + 0.20, and the isotope ISO1 from the ISOTXS file, scaled by a factor of 0.1, together to create the composition named COMP2. The composition definition for MISO3 is split across two Type 14 cards to test the statement in the A.NIP3 specification that the atom densities/volume fractions for multiple instances of an isotope or material are summed.

Lines 13-17 define the third composition as a combination of a multi-isotope material (MAT31) and a multi-isotope composition (COMP32). MAT31 and COMP32 are combined on lines 15 and 16 to form COMP3, again ensuring that the atom densities/volume fractions for multiple instances of a composition are summed. COMP3 is then assigned to AREA3 in the Type 15 card of line 17.

The fourth and final composition is defined in Lines 19-26. This composition, COMP4, is a combination of two compositions, COMP41, and COMP42, each being defined by single isotopes from the ISOTXS file. This composition is assigned to the regions named REG4 and REG5 in lines 25 and 26. The A.NIP3 listing states that when a region/area is referenced on more than one Type 15 card, the last reference sets the composition assignment; therefore COMP1 is first assigned to REG4 before the permanent assignment of COMP4 to REG4 is made.

```

1  UNFORM=A.NIP3
2  ...
3  c Define Compositions
4  c Composition 1
5  14 COMP1 ISO1 1.0
6  15 COMP1 AREA1
7  c Composition 2
8  13 MISO3 ISO3 2.0
9  14 COMP2 MISO3 0.25 ISO1 0.1
10 14 COMP2 MISO3 0.2
11 15 COMP2 AREA2
12 c Composition 3
13 13 MAT31 ISO4 0.4 ISO1 0.6
14 14 COMP32 ISO3 0.6 ISO2 0.4
15 14 COMP3 MAT31 0.4 COMP32 0.4
16 14 COMP3 COMP32 0.2
17 15 COMP3 AREA3
18 c Composition 4
19 14 COMP41 ISO4 2.0
20 14 COMP42 ISO1 2.0
21 14 COMP4 COMP41 0.5 COMP42 0.5
22 15 COMP1 REG4
23 c Test overlay of composition assignments
24 c by overwriting COMP1 assignment to REG4
25 15 COMP4 REG4
26 15 COMP4 REG5
27 ...

```

**Figure 3. A.NIP3 3D Cartesian Model Composition Definition**

### 3.1.1.1.3 Isotopic Cross Sections

To verify the A.HMG4C module computation of homogenized cross sections, four unique isotopes, named ISO1, ISO2, ISO3, and ISO4, are defined in a two-group cross section library. The cross sections and associated values for these isotopes are provided in Table 12, Table 13, and Table 14. All significant digits are shown for each value. The units of the microscopic cross section quantities of Table 13 are barns,  $v_{\text{total}}$  has units of neutrons per fission, and  $\chi_{\text{total}}$  is unitless. The value of  $\chi_{\text{total}}$  is shown as a blank (“-”) for ISO1 and ISO2 since they are not fissionable. Finally, the scattering data in Table 13 are also in units of barns, with the exception that the (n,2n) scattering matrix is production-based and is thus twice the cross section in barns. These values are provided

with up to six significant figures, the same as are allowed as input in an ISOTXS file, to ensure that any loss of significant figures during DIF3D cross section processing is evident.

Table 12. Isotopic Metadata

	Gram Atomic Weight [g]	Tot. Thermal Energy Yield per Fission [J/fiss]	Tot. Thermal Energy Yield per Capture [J/cap]	Iso. Temp. [K]	Avg. Eff. Potential Scattering [b/atom]	Iso. Density when Generating XS [a/b-cm]	Iso. Classification
ISO1	1.0	1.1E-11	2.2E-12	294.0	1.1	1.2	Undefined
ISO2	2.0	2.2E-11	4.4E-12	394.0	2.1	2.2	Coolant
ISO3	3.0	3.3E-11	6.6E-12	494.0	3.1	3.2	Fissile
ISO4	4.0	4.4E-11	8.8E-12	594.0	4.1	4.2	Fissile

Table 13. Base Isotopic Cross Section Values

	ISO1		ISO2		ISO3		ISO4	
	Group 1	Group 2	Group 1	Group 2	Group 1	Group 2	Group 1	Group 2
$\sigma_{\text{transport}}$	0.110683	0.36355	1.33152	4.3735	0.374796	1.68707	0.269337	0.49189
$\sigma_{\text{total},0}$	0.110683	0.36355	1.33152	4.3735	0.65696	2.52025	0.33588	0.54628
$\sigma_{\text{total},1}$	0.0110683	0.036355	0.133152	0.43735	0.065696	0.252025	0.033588	0.054628
$\sigma_{(n,g)}$	8.48029E-06	0.00016	0.000248615	0.0094	0.0005023	0.012894	0.0087078	0.02518
$\sigma_{(n,fiss)}$	0	0	0	0	0.0010484	0.050632	0.002817	0.097
$\nu_{\text{total}}$	0	0	0	0	2	2.5	2.1	2.4
$\chi_{\text{total}}$	-	-	-	-	0.95	0.05	1	0
$\sigma_{(n,\alpha)}$	0	0	9.94458E-05	0.00376	0.00020092	0.0051576	0	0
$\sigma_{(n,p)}$	0	0	7.45844E-05	0.00282	0.00015069	0.0038682	0	0
$\sigma_{(n,2n)}$	0	0	0.025	0	0.0015	0	0.0015	0
$\sigma_{(n,d)}$	0	0	4.97229E-05	0.00188	0.00010046	0.0025788	0	0
$\sigma_{(n,t)}$	0	0	2.48615E-05	0.00094	0.00005023	0.0012894	0	0

Table 14. Base Scattering Matrix Data

			ISO1		ISO2		ISO3		ISO4	
			<i>To</i>		<i>To</i>		<i>To</i>		<i>To</i>	
			<i>1</i>	<i>2</i>	<i>1</i>	<i>2</i>	<i>1</i>	<i>2</i>	<i>1</i>	<i>2</i>
$\sigma_{\text{elastic},0}$	<i>From</i>	<i>1</i>	0.109674	0.0010006	1.15138	0.10464	0.61968	0.029227	0.3183	0.004555
		<i>2</i>	0	0.36339	0	4.3547	0	2.44383	0.0001	0.424
$\sigma_{\text{elastic},1}$	<i>From</i>	<i>1</i>	0	0	0	0	0.27459	0.0075737	0.06694	-0.0003972
		<i>2</i>	0	0	0	0	0	0.83318	0.00001	0.05438
$\sigma_{\text{inelastic},0}$	<i>From</i>	<i>1</i>	0	0	0	0	0.0015	0	0	0
		<i>2</i>	0	0	0	0	0	0	0	0
$\sigma_{(n,2n),0}$	<i>From</i>	<i>1</i>	0	0	0.05	0	0.003	0	0.003	0
		<i>2</i>	0	0	0	0	0	0	0	0

The isotopic cross sections used by DIF3D are provided by an ISOTXS file whose format was set by the Committee on Computer Code Coordination [8]. The ISOTXS format is flexible in that a file-wide fission spectrum vector or matrix can be specified, isotopic fission spectrum vectors or matrices can be provided, not all cross section reaction channels need to be provided, and scattering data can be defined in multiple formats. For the scattering data the following options are provided: the user can specify the number of blocks to represent that scattering data (to reduce the maximum record size); whether the scattering data represents the total scatter or if there are blocks to represent elastic, inelastic, and/or (n,2n) reactions; and how many Legendre expansion orders are present in each scattering block.

This verification work can reduce the possible set of ISOTXS options under consideration by first recognizing that DIF3D does not support fission spectrum matrices, whether they be file-wide or isotopic. Finally, consistent with [6], this verification work will not include direction-dependent diffusion cross sections; therefore the ISTRPD flag in the “Isotope Control and Group Independent Data” record of the ISOTXS file will always be provided with a value of 0, indicating that no coordinate dependent transport cross sections (in the STRPD parameter) will be present.

Since the ISOTXS files used by modern fast reactor analyses are generated by the MC2-3 software [9], the ISOTXS options tested must represent the options exercised by MC2-3. A review of the MC2-3 source code revealed that there are three unique representations that must be considered. These representations are summarized in Table 15. In this table, N refers to the scattering expansion order; for the cross sections described in Table 13 and Table 13, N = 1. Further, the “SN2N Present” column refers to if the group-wise (n,2n) is present or not, independent of the

February 13, 2020

scattering matrix for this (n,2n) reaction is present. This table also includes two user types; these are useful formats for creating ISOTXS by hand as frequently used within this verification.

Table 15. ISOTXS File Styles

Type	File-Wide Chi	Num. of Total XS Moments	Num. of Transport XS Moments	Scattering Sub-Block Control	Scatter Orders per Block	Scatter Types	SN2N Present?
<b>Micro. XS</b>	No	N	N-1	1	1	Elastic, Inelastic, (n,2n)	Yes
<b>Macro. XS</b>	No	1	1	1	1	Elastic, (n,2n)	Yes
<b>Photon Transport</b>	No	N	N-1	1	1	Elastic	No
<b>User 1</b>	Yes	1	1	1	1	Total	Yes
<b>User 2</b>	Yes	1	1	1	N	Total	Yes

For ease of use, the cross section data is inputted into DIF3D using the A.ISO input block of the regular DIF3D input stream. The A.ISO input block takes an ASCII version of the ISOTXS data set, termed ISOBCD, and creates a binary file when DIF3D processes the A.NIP3 data set in to the NDXSRF, GEODST, LABELS, and ZNATDN files. The HMG4C component of DIF3D only handles a binary ISOTXS. This approach to providing cross section data is not typical of design work; however, it is used for this work because it is required to allow a manual creation of the ISOTXS data. Internal to DIF3D, this approach verifies the additional functionality of the A.ISO input block and does not skip any section that is part of the typical input path for design work.

The cross section data provided in Table 12 through Table 13 is included in A.ISO blocks with modifications made as necessary to accommodate limited precision input format. Figure 4 through Figure 8 provide the ISOBCD files in the same order as presented in Table 15. From this point, both A.ISO, ISOBCD, and ISOTXS will all be referred to as ISOTXS data for simplicity. It should be noted that the HMG4C cross section homogenization module within DIF3D executes different code to calculate the removal cross section, depending on if the  $\sigma(n,2n)$  principal cross section is present in the ISOTXS file or not. To test both execution paths, the data for isotope “ISO3” includes the  $\sigma(n,2n)$  reaction while the data for isotope “ISO4” does not. This is still consistent with the data in Table 13 for the Microscopic and Macroscopic ISOTXS formats that include an explicit (n,2n) scattering matrix. The base case model will use the Microscopic XS ISOTXS data of Figure 4.

February 13, 2020

```

1 0V ISOTXS *2G * 1
2 1D 2 4 2 2 1 0 5 1
3 2D * Custom *
4 * * ISO1 ISO2 ISO3 ISO4
5 7.73210E+01 4.37393E+05 2.00000E+07 1.00000E+00 0.00000E+00
6 0 7 14 21
7 4D ISO1 BYHAND NONE
8 1.00000E+00 1.10000E-11 2.20000E-12 2.94000E+02 1.10000E+00 1.20000E+00
9 0 0 0 0 0 0 0 2 1 0 100
10 101 200 201 300 1 1 1 1 1 1 2 1
11 2 1 2 1 2 1 2 1 1 1 1 1
12 1 1 1 1 1
13 5D 1.10683E-01 3.63550E-01 1.10683E-01 3.63550E-01 1.10683E-02
14 3.63550E-02 8.48029E-06 1.60000E-04
15 7D 1.09674E-01 3.63390E-01 1.00060E-03
16 7D 0.00000E+00 0.00000E+00 0.00000E+00
17 7D 0.00000E+00 0.00000E+00 0.00000E+00
18 7D 0.00000E+00 0.00000E+00 0.00000E+00
19 7D 0.00000E+00 0.00000E+00 0.00000E+00
20 4D ISO2 BYHAND NONE
21 2.00000E+00 2.20000E-11 4.40000E-12 3.94000E+02 2.10000E+00 2.20000E+00
22 6 0 0 1 1 1 1 1 2 1 0 100
23 101 200 201 300 1 1 1 1 1 1 2 1
24 2 1 2 1 2 1 2 1 1 1 1 1
25 1 1 1 1 1
26 5D 1.33152E+00 4.37350E+00 1.33152E+00 4.37350E+00 1.33152E-01
27 4.37350E-01 2.48615E-04 9.40000E-03 9.94458E-05 3.76000E-03 7.45844E-05
28 2.82000E-03 2.50000E-02 0.00000E+00 4.97229E-05 1.88000E-03 2.48615E-05
29 9.40000E-04
30 7D 1.15138E+00 4.35470E+00 1.04640E-01
31 7D 0.00000E+00 0.00000E+00 0.00000E+00
32 7D 0.00000E+00 0.00000E+00 0.00000E+00
33 7D 0.00000E+00 0.00000E+00 0.00000E+00
34 7D 5.00000E-02 0.00000E+00 0.00000E+00
35 4D ISO3 BYHAND NONE
36 3.00000E+00 3.30000E-11 6.60000E-12 4.94000E+02 3.10000E+00 3.20000E+00
37 1 1 1 1 1 1 1 1 2 1 0 100
38 101 200 201 300 1 1 1 1 1 1 2 1
39 2 1 2 1 2 1 2 1 1 1 1 1
40 1 1 1 1 1
41 5D 3.74796E-01 1.68707E+00 6.56960E-01 2.52025E+00 6.56960E-02
42 2.52025E-01 5.02300E-04 1.28940E-02 1.04840E-03 5.06320E-02 2.00000E+00
43 2.50000E+00 9.50000E-01 5.00000E-02 2.00920E-04 5.15760E-03 1.50690E-04
44 3.86820E-03 1.50000E-03 0.00000E+00 1.00460E-04 2.57880E-03 5.02300E-05
45 1.28940E-03
46 7D 6.19680E-01 2.44383E+00 2.92270E-02
47 7D 2.74590E-01 8.33180E-01 7.57370E-03
48 7D 1.50000E-03 0.00000E+00 0.00000E+00
49 7D 0.00000E+00 0.00000E+00 0.00000E+00
50 7D 3.00000E-03 0.00000E+00 0.00000E+00
51 4D ISO4 BYHAND NONE
52 4.00000E+00 4.40000E-11 8.80000E-12 5.94000E+02 4.10000E+00 4.20000E+00
53 1 1 1 0 0 0 0 2 1 0 100
54 101 200 201 300 1 1 1 1 1 2 2 2
55 2 2 2 2 2 2 2 2 1 2 1 2
56 1 2 1 2 1
57 5D 2.69337E-01 4.91890E-01 3.35880E-01 5.46280E-01 3.35880E-02
58 5.46280E-02 8.70780E-03 2.51800E-02 2.81700E-03 9.70000E-02 2.10000E+00
59 2.40000E+00 1.00000E+00 0.00000E+00
60 7D 1.00000E-04 3.18300E-01 4.24000E-01 4.55500E-03
61 7D 1.00000E-05 6.69400E-02 5.43800E-02 3.97200E-04
62 7D 0.00000E+00 0.00000E+00 0.00000E+00 0.00000E+00
63 7D 0.00000E+00 0.00000E+00 0.00000E+00 0.00000E+00
64 7D 3.00000E-03 0.00000E+00 0.00000E+00 0.00000E+00

```

Figure 4. ISOBCD Formatted Microscopic Cross Section Data

February 13, 2020

```

1 0V ISOTXS *2G          *      1
2 1D      2      4      2      2      1      0      3      1
3 2D * Custom *
4 *      *      IS01      IS02      IS03      IS04
5 7.73210E+01 4.37393E+05 2.00000E+07 1.00000E+00 0.00000E+00
6      0      5      10      15
7 4D IS01 BYHAND NONE
8 1.00000E+00 1.10000E-11 2.20000E-12 2.94000E+02 1.10000E+00 1.20000E+00
9      0      0      0      0      0      0      0      1      1      0      100
10 101      300      1      1      1      1      2      1      2      1      2      1
11      1      1      1      1      1
12 5D 1.10683E-01 3.63550E-01 1.10683E-01 3.63550E-01 8.48029E-06
13 1.60000E-04
14 7D 1.09674E-01 3.63390E-01 1.00060E-03
15 7D 0.00000E+00 0.00000E+00 0.00000E+00
16 7D 0.00000E+00 0.00000E+00 0.00000E+00
17 4D IS02 BYHAND NONE
18 2.00000E+00 2.20000E-11 4.40000E-12 3.94000E+02 2.10000E+00 2.20000E+00
19      6      0      0      1      1      1      1      1      1      1      0      100
20 101      300      1      1      1      1      2      1      2      1      2      1
21      1      1      1      1      1
22 5D 1.33152E+00 4.37350E+00 1.33152E+00 4.37350E+00 2.48615E-04
23 9.40000E-03 9.94458E-05 3.76000E-03 7.45844E-05 2.82000E-03 2.50000E-02
24 0.00000E+00 4.97229E-05 1.88000E-03 2.48615E-05 9.40000E-04
25 7D 1.15138E+00 4.35470E+00 1.04640E-01
26 7D 0.00000E+00 0.00000E+00 0.00000E+00
27 7D 5.00000E-02 0.00000E+00 0.00000E+00
28 4D IS03 BYHAND NONE
29 3.00000E+00 3.30000E-11 6.60000E-12 4.94000E+02 3.10000E+00 3.20000E+00
30      1      1      1      1      1      1      1      1      1      1      0      100
31 101      300      1      1      1      1      2      1      2      1      2      1
32      1      1      1      1      1
33 5D 3.74796E-01 1.68707E+00 6.56960E-01 2.52025E+00 5.02300E-04
34 1.28940E-02 1.04840E-03 5.06320E-02 2.00000E+00 2.50000E+00 9.50000E-01
35 5.00000E-02 2.00920E-04 5.15760E-03 1.50690E-04 3.86820E-03 1.50000E-03
36 0.00000E+00 1.00460E-04 2.57880E-03 5.02300E-05 1.28940E-03
37 7D 6.21180E-01 2.44383E+00 2.92270E-02
38 7D 2.74590E-01 8.33180E-01 7.57370E-03
39 7D 3.00000E-03 0.00000E+00 0.00000E+00
40 4D IS04 BYHAND NONE
41 4.00000E+00 4.40000E-11 8.80000E-12 5.94000E+02 4.10000E+00 4.20000E+00
42      1      1      1      0      0      0      0      1      1      0      100
43 101      300      1      1      1      2      2      2      2      2      2      2
44      1      2      1      2      1
45 5D 2.69337E-01 4.91890E-01 3.35880E-01 5.46280E-01 8.70780E-03
46 2.51800E-02 2.81700E-03 9.70000E-02 2.10000E+00 2.40000E+00 1.00000E+00
47 0.00000E+00
48 7D 1.00000E-04 3.18300E-01 4.24000E-01 4.55500E-03
49 7D 1.00000E-05 6.69400E-02 5.43800E-02 3.97200E-04
50 7D 3.00000E-03 0.00000E+00 0.00000E+00 0.00000E+00

```

Figure 5. ISOBCD Formatted Macroscopic Cross Section Data

February 13, 2020

```

1  0V ISOTXS *2G          *      1
2  1D      2      4      2      2      1      0      2      1
3  2D * Custom *
4  *      *      ISO1      ISO2      ISO3      ISO4
5  7.73210E+01 4.37393E+05 2.00000E+07 1.00000E+00 0.00000E+00
6      0      3      6      10
7  4D ISO1 BYHAND NONE
8  1.00000E+00 1.10000E-11 2.20000E-12 2.94000E+02 1.10000E+00 1.20000E+00
9      0      0      0      0      0      0      0      2      1      0      100
10 101      1      0      1      2      0      0      1      1      0      0
11 5D 1.10683E-01 3.63550E-01 1.10683E-01 3.63550E-01 1.10683E-02
12 3.63550E-02 8.48029E-06 1.60000E-04
13 7D 1.09674E-01 3.63390E-01 1.00060E-03
14 4D ISO2 BYHAND NONE
15 2.00000E+00 2.20000E-11 4.40000E-12 3.94000E+02 2.10000E+00 2.20000E+00
16      6      0      0      1      1      0      1      1      2      1      0      100
17 101      1      0      1      2      0      0      1      1      0      0
18 5D 1.33152E+00 4.37350E+00 1.33152E+00 4.37350E+00 1.33152E-01
19 4.37350E-01 2.48615E-04 9.40000E-03 9.94458E-05 3.76000E-03 7.45844E-05
20 2.82000E-03 4.97229E-05 1.88000E-03 2.48615E-05 9.40000E-04
21 7D 1.17638E+00 4.35470E+00 1.04640E-01
22 4D ISO3 BYHAND NONE
23 3.00000E+00 3.30000E-11 6.60000E-12 4.94000E+02 3.10000E+00 3.20000E+00
24      1      1      1      1      1      0      1      1      2      1      0      100
25 101      1      1      1      2      1      2      1      1      1      1
26 5D 3.74796E-01 1.68707E+00 6.56960E-01 2.52025E+00 6.56960E-02
27 2.52025E-01 5.02300E-04 1.28940E-02 1.04840E-03 5.06320E-02 2.00000E+00
28 2.50000E+00 9.50000E-01 5.00000E-02 2.00920E-04 5.15760E-03 1.50690E-04
29 3.86820E-03 1.00460E-04 2.57880E-03 5.02300E-05 1.28940E-03
30 7D 6.22680E-01 2.44383E+00 2.92270E-02
31 7D 2.74590E-01 8.33180E-01 7.57370E-03
32 4D ISO4 BYHAND NONE
33 4.00000E+00 4.40000E-11 8.80000E-12 5.94000E+02 4.10000E+00 4.20000E+00
34      1      1      1      0      0      0      0      0      2      1      0      100
35 101      1      1      2      2      2      2      2      1      2      1
36 5D 2.69337E-01 4.91890E-01 3.35880E-01 5.46280E-01 3.35880E-01
37 5.46280E-01 8.70780E-03 2.51800E-02 2.81700E-03 9.70000E-02 2.10000E+00
38 2.40000E+00 1.00000E+00 0.00000E+00
39 7D 1.00000E-04 3.19800E-01 4.24000E-01 4.55500E-03
40 7D 1.00000E-05 6.69400E-02 5.43800E-02 3.97200E-04

```

Figure 6. ISOBCD Formatted Photon Transport Cross Section Data



February 13, 2020

```

1 0V ISOTXS *2G      *      1
2 1D      2      4      2      2      1      1      2      1
3 2D * Custom *
4 *      *      IS01      IS02      IS03      IS04
5 9.50000E-01 5.00000E-02
6 7.73210E+01 4.37393E+05 2.00000E+07 1.00000E+00 0.00000E+00
7      0      3      6      10
8 4D IS01 BYHAND NONE
9 1.00000E+00 1.10000E-11 2.20000E-12 2.94000E+02 1.10000E+00 1.20000E+00
10      0      0      0      0      0      0      0      1      1      0      0
11      1      1      0      1      2      0      0      1      1      0      0
12 5D 1.10683E-01 3.63550E-01 1.10683E-01 3.63550E-01 8.48029E-06
13 1.60000E-04
14 7D 1.09674E-01 3.63390E-01 1.00060E-03
15 4D IS02 BYHAND NONE
16 2.00000E+00 2.20000E-11 4.40000E-12 3.94000E+02 2.10000E+00 2.20000E+00
17      6      0      0      1      1      1      1      1      1      1      0      0
18      1      1      0      1      2      0      0      1      1      0      0
19 5D 1.33152E+00 4.37350E+00 1.33152E+00 4.37350E+00 2.48615E-04
20 9.40000E-03 9.94458E-05 3.76000E-03 7.45844E-05 2.82000E-03 2.50000E-02
21 0.00000E+00 4.97229E-05 1.88000E-03 2.48615E-05 9.40000E-04
22 7D 1.17638E+00 4.35470E+00 1.04640E-01
23 4D IS03 BYHAND NONE
24 3.00000E+00 3.30000E-11 6.60000E-12 4.94000E+02 3.10000E+00 3.20000E+00
25      1      0      1      1      1      1      1      1      1      1      0      0
26      1      1      1      1      2      1      2      1      1      1      1
27 5D 3.74796E-01 1.68707E+00 6.56960E-01 2.52025E+00 5.02300E-04
28 1.28940E-02 1.04840E-03 5.06320E-02 2.00000E+00 2.50000E+00 2.00920E-04
29 5.15760E-03 1.50690E-04 3.86820E-03 1.50000E-03 0.00000E+00 1.00460E-04
30 2.57880E-03 5.02300E-05 1.28940E-03
31 7D 6.21180E-01 2.44383E+00 2.92270E-02
32 7D 2.74590E-01 8.33180E-01 7.57370E-03
33 4D IS04 BYHAND NONE
34 4.00000E+00 4.40000E-11 8.80000E-12 5.94000E+02 4.10000E+00 4.20000E+00
35      1      1      1      0      0      0      0      0      1      1      0      0
36      1      1      1      2      2      2      2      1      2      1
37 5D 2.69337E-01 4.91890E-01 3.35880E-01 5.46280E-01 8.70780E-03
38 2.51800E-02 2.81700E-03 9.70000E-02 2.10000E+00 2.40000E+00 1.00000E+00
39 0.00000E+00
40 7D 1.00000E-04 3.19800E-01 4.24000E-01 4.55500E-03
41 7D 1.00000E-05 6.69400E-02 5.43800E-02 3.97200E-04

```

Figure 7. ISOB CD Formatted User Style 1 Cross Section Data

February 13, 2020

```

1 0V ISOTXS *2G      *      1
2 1D      2      4      2      2      1      1      1      1
3 2D * Custom *
4 *      *      IS01      IS02      IS03      IS04
5 9.50000E-01 5.00000E-02
6 7.73210E+01 4.37393E+05 2.00000E+07 1.00000E+00 0.00000E+00
7      0      3      6      9
8 4D IS01 BYHAND NONE
9 1.00000E+00 1.10000E-11 2.20000E-12 2.94000E+02 1.10000E+00 1.20000E+00
10      0      0      0      0      0      0      0      0      1      1      0      0
11      1      1      2      1      1
12 5D 1.10683E-01 3.63550E-01 1.10683E-01 3.63550E-01 8.48029E-06
13 1.60000E-04
14 7D 1.09674E-01 3.63390E-01 1.00060E-03
15 4D IS02 BYHAND NONE
16 2.00000E+00 2.20000E-11 4.40000E-12 3.94000E+02 2.10000E+00 2.20000E+00
17      6      0      0      1      1      1      1      1      1      1      0      0
18      1      1      2      1      1
19 5D 1.33152E+00 4.37350E+00 1.33152E+00 4.37350E+00 2.48615E-04
20 9.40000E-03 9.94458E-05 3.76000E-03 7.45844E-05 2.82000E-03 2.50000E-02
21 0.00000E+00 4.97229E-05 1.88000E-03 2.48615E-05 9.40000E-04
22 7D 1.17638E+00 4.35470E+00 1.04640E-01
23 4D IS03 BYHAND NONE
24 3.00000E+00 3.30000E-11 6.60000E-12 4.94000E+02 3.10000E+00 3.20000E+00
25      1      0      1      1      1      1      1      1      1      1      0      0
26      2      1      2      1      1
27 5D 3.74796E-01 1.68707E+00 6.56960E-01 2.52025E+00 5.02300E-04
28 1.28940E-02 1.04840E-03 5.06320E-02 2.00000E+00 2.50000E+00 2.00920E-04
29 5.15760E-03 1.50690E-04 3.86820E-03 1.50000E-03 0.00000E+00 1.00460E-04
30 2.57880E-03 5.02300E-05 1.28940E-03
31 7D 6.21180E-01 2.44383E+00 2.92270E-02 2.74590E-01 8.33180E-01
32 7.57370E-03
33 4D IS04 BYHAND NONE
34 4.00000E+00 4.40000E-11 8.80000E-12 5.94000E+02 4.10000E+00 4.20000E+00
35      1      1      1      0      0      0      0      0      1      1      0      0
36      2      2      2      2      1
37 5D 2.69337E-01 4.91890E-01 3.35880E-01 5.46280E-01 8.70780E-03
38 2.51800E-02 2.81700E-03 9.70000E-02 2.10000E+00 2.40000E+00 1.00000E+00
39 0.00000E+00
40 7D 1.00000E-04 3.19800E-01 4.24000E-01 4.55500E-03 1.00000E-05
41 6.69400E-02 5.43800E-02 3.97200E-04

```

Figure 8. ISOBCD Formatted User Style 2 Cross Section Data

### 3.1.1.1.4 Remaining Options

Figure 9 provides an excerpt of DIF3D input options used to verify DIF3D’s model building capabilities that have not yet been discussed. Line 1, “BLOCK=STP021”, states that this model will utilize the “Standard Path 21” module execution of ARC which refers to DIF3D. That is, if the REBUS executable is provided input using the STP021 block keyword, it will only process the A.NIP3 inputs and not go into the REBUS execution. There are several block associated input options (MODIFY, REMOVE, DELETE, SUBBLOCK) that allow other execution options that are not used in current design activities and therefore will not be verified. One can also specify the version numbering for each data set or block that allows the input to be treated differently. As an example, one can use “BLOCK=STP021,3” and “DATASET=RTFLUX,1” as alternative inputs to DIF3D. For the first example, user controlled sections of the reiterated DIF3D input can be removed from the regular output stream and many regular ancillary DIF3D input processing outputs are also removed. For the second example, the DIF3D software understands that the RTFLUX data file format is of type 1 instead and thus the correct import routine will be called for this format which is different from version 2. All of these additional options, none of which are used by current design activities, are best described in the DIF3D manual [1].

Lines 3, 6, and 14 are the title cards for the A.HMG4C, A.NIP3, and A.DIF3D blocks, respectively. Line 4 defines the problem options that are specific to the HMG4C module. The eight values that are set are as follows:

1. 900000: The size of the main core container array. Consistent with [6], this will not be verified by this process and so no further perturbations to this value will be pursued.
2. 0: Print file master control flag. This is set to the value of 0, which prints the general run information and requested edits. Later cases will explicitly verify that setting this to the other option, 1, in fact does suppress the printing of everything except the diagnostics.
3. 3: COMPXS edit flag. The base case has this set to a value of 3 which prints a COMPXS edit both to the standard output as well as the auxiliary output files. Later cases in this section will explicitly verify that the other options (no printing, only printing to standard output or only to the auxiliary output) are obeyed.
4. 3: ISOTXS edit flag. The base case has this set to a value of 3 which prints the edit of ISOTXS to both the standard output as well as the auxiliary output files. Later cases in this section will explicitly verify that the other options (no printing, only printing to standard output or only to the auxiliary output) are obeyed.
5. 0: Pointer debugging edit flag. This value states that no debugging printout is provided. This option will not be verified and so there will be no later perturbations of this option.
6. 0: Prompt fission spectrum option flag. This value states that isotopic fission spectrum vectors will be ignored, and the file-wide fission spectrum will be used instead, if provided. If the file-wide data is not provided, then the composition fission spectrum will be computed with fission source weighting of the isotopic fission spectra. Later cases in this section will verify that the remaining two options relating to how isotopic fission spectra are to be weighted to determine a composition-specific fission spectrum.
7. 0: Auxiliary output file master control flag. This value requests DIF3D to write general run information and requested edits to an auxiliary output file. The other option, suppression of all output to an auxiliary file, will be verified explicitly by a later case in this section.
8. 3: Edit flag for a supplied COMPXS file. This value sets an edit of the COMPXS file to be written to both standard and auxiliary outputs. The case will not utilize a supplied COMPXS file; later cases in this section will therefore explicitly verify that this and the other options (no printing, only printing to standard output or only to the auxiliary output) are obeyed.

Line 5 begins the A.NIP3 module input and line 7 contains the A.NIP3 input processing specifications card. The ten values that are set are as follows:

1. 0: Flag for geometry pointer debugging. This value states that no debugging printout is provided. This option will not be verified and so there will be no later perturbations of this option.

2. 3: Geometry processing module edit. The base case has this set to a value of 3 which prints the geometry edits to both the standard output as well as the auxiliary output files. Later cases in this section will explicitly verify that the other options (no printing, only printing to standard output or only to the auxiliary output) are obeyed.
3. Four instances of 40000000: Storage array sizes. Consistent with [6], these will not be verified by this process and so no further perturbations to this value will be pursued.
4. 0: Flag for cross section pointer debugging. This value states that no debugging printout is provided. This option will not be verified and so there will be no later perturbations of this option.
5. 3: Cross section processing module edit. The base case has this set to a value of 3 which prints the cross section edits to both the standard output as well as the auxiliary output files. Later cases in this section will explicitly verify that the other options (no printing, only printing to standard output or only to the auxiliary output) are obeyed.
6. 3: Region/mesh interval printer-plotter map edit during geometry processing. The base case has this set to a value of 3 which writes the region map to both standard and auxiliary output. Later cases in this section will explicitly verify the other options (no printing, only printing to standard output or only to the auxiliary output) are obeyed.
7. 3: Zone (composition)/mesh interval printer-plotter map edit during geometry processing. The base case has this set to a value of 3 which writes the zone map to both standard and auxiliary output. Later cases in this section will explicitly verify that the other options (no printing, only printing to standard output or only to the auxiliary output) are obeyed.

The content of lines 8 through 13 was previously provided in Figure 2 and Figure 3. Lines 14, 15, and 16 enter the A.DIF3D block, provide a title, and set the storage array sizes, respectively. Similar to the card types in the A.NIP3 and A.HMG4C blocks, these features will not be explicitly tested by this work. Line 17 is the DIF3D problem control parameter card; the functionality of this card type will be tested as applicable in other sections of this work and thus will not be verified in this section. Line 19 provides the A.DIF3D Type 04 card which sets the DIF3D edit options. The first four of these parameters are related to the edits of the problem as defined and so will be verified in this section. The remaining parameters related to the output of solution results and will be explicitly tested in later sections. The four parameters to verify in this block are:

1. 3: Problem description edit. The base case has this set to a value of 3 which writes the edits to both standard and auxiliary output. Later cases in this section will explicitly verify that the other options (no printing, only printing to standard output or only to the auxiliary output) are obeyed.
2. 3: Geometry (region to mesh interval) map edit. The base case has this set to a value of 3 which writes the edits to both standard and auxiliary output. Later cases in this section will explicitly verify that the other options (no printing, only printing to standard output or only to the auxiliary output) are obeyed.

3. 3: Geometry (zone to mesh interval) map edit. The base case has this set to a value of 3 which writes the edits to both standard and auxiliary output. Later cases in this section will explicitly verify that the other options (no printing, only printing to standard output or only to the auxiliary output) are obeyed.
4. 33: Macroscopic cross section edit. The base case has this set to a value of 33. For this parameter, the first digit controls scattering and principal cross section edits while the second controls the principal cross section edits only. Values of three for each of these two digits writes the edits to both standard and auxiliary output. Later cases in this section will explicitly verify that the other options (no printing, only printing to standard output or only to the auxiliary output) are obeyed for each of the two digits.

Finally, line 20 provides the A.ISO data block where the ISOTXS is provided. The ISOBCD inputs were provided in Figure 4 through Figure 8.

```

1 BLOCK=STP021
2 DATASET=A.HMG4C
3 01 3D XYZ - MCC Micro XS ISOTXS
4 02 900000 0 3 3 0 0 0 3
5 UNFORM=A.NIP3
6 01 3D XYZ - MCC Micro XS ISOTXS
7 02 0 3 40000000 40000000 40000000 40000000 0 3 3 3
8 ...
9 ... See A.NIP3 Model Geometry Definition Listing
10 ...
11 ... See A.NIP3 Model Composition Definition Listing
12 ...
13 C
14 UNFORM=A.DIF3D
15 01 3D XYZ - MCC Micro XS ISOTXS
16 02 30000000 15000000 0
17 03 0 2 0 4500 200
18 04 3 3 3 33 000 00 000 0 0 0000 -1
19 05 1.0E-06 1.0E-07 1.0E-08
20 NOSORT=A.ISO
21 ...
22 ... See Micro XS ISOTXS Listing
23 ...

```

**Figure 9. Remaining DIF3D Input Options**

The edit options discussed yields multiple follow-on cases to evaluate in addition to the base case.

### 3.1.1.2 Verification

The previous section defined the base case of the model to examine. This section will compare the DIF3D processing of this base case and show that DIF3D correctly handles the inputs provided to it. The verification will begin by examining the above base case with the Microscopic XS ISOTXS format of Figure 4. Then, the ISOTXS format cases will each be verified. Finally, the perturbations to this base case will be performed and verified to be implemented correctly.

These perturbations were discussed immediately before Figure 9. The summary of options applied in the base case to support this model building verification are provided in Table 16. In this table,

the perturbations to the base case that must be performed with respect to these control parameters are specifically identified and the subsections where they are tested are noted.

**Table 16. DIF3D Control Options and Their Perturbations**

<b>A.HMG4C</b>				
<b>Card Type &amp; Option</b>	<b>Description</b>	<b>Option in Base Case</b>	<b>Perturbations to Base</b>	<b>Evaluated in Sections</b>
<b>2.3</b>	Print file master control flag	0	1	3.1.1.2.10.1
<b>2.4</b>	COMPXS edit flag	3	0, 1, 2	3.1.1.2.10.2
<b>2.5</b>	ISOTXS edit flag	3	0, 1, 2, 3	3.1.1.2.10.3
<b>2.7</b>	Prompt Fission Spectrum Options	0	1, 2	3.1.1.2.7, 3.1.1.2.8
<b>2.8</b>	Aux output file master control flag	0	1	3.1.1.2.10.4
<b>2.9</b>	Edit for supplied COMPXS	3	0, 1, 2	3.1.1.2.10.5
<b>A.NIP3</b>				
<b>Card Type &amp; Option</b>	<b>Description</b>	<b>Option in Base Case</b>	<b>Perturbations to Base</b>	<b>Evaluated in Sections</b>
<b>2.3</b>	Geometry processing edits	3	0, 1, 2	3.1.1.2.10.6
<b>2.9</b>	Cross section processing edits	3	0, 1, 2	3.1.1.2.10.7
<b>2.10</b>	Region/mesh interval plotter edits	3	0, 1, 2	3.1.1.2.10.8
<b>2.11</b>	Zone/mesh interval plotter edits	3	0, 1, 2	3.1.1.2.10.9
<b>A.DIF3D</b>				
<b>Card Type &amp; Option</b>	<b>Description</b>	<b>Option in Base Case</b>	<b>Perturbations to Base</b>	<b>Evaluated in Sections</b>
<b>4.2</b>	Problem description edit	3	0, 1, 2	3.1.1.2.10.10
<b>4.3</b>	Geometry (region to mesh interval) map edit	3	0, 1, 2	3.1.1.2.10.11
<b>4.4</b>	Geometry (zone to mesh interval) map edit	3	0, 1, 2	3.1.1.2.10.12
<b>4.5</b>	Macroscopic cross section edit	33	00, 01, 02, 03, 10, 11, 12, 13, 20, 21, 22, 23, 30, 31, 32	3.1.1.2.10.13

### 3.1.1.2.1 Microscopic XS ISOTXS Base Case

The DIF3D input for the Microscopic XS ISOTXS base case is the same as defined in Figure 2, Figure 3, Figure 4, and Figure 9. The output to the screen (i.e., standard output) was redirected to a text file; this and all other output files from this run are stored in an isolated directory.

The remainder of this section will progress by first traversing the standard output and the edited information compared to the independently computed values (e.g., mesh spacing and macroscopic cross sections). Next, the auxiliary output file (fort.10) will be evaluated to ensure that all of the expected output edits are present and correct. The evaluation will then progress to the binary output files relating to the model definition (i.e., GEODST, NDXSRF, ZNATDN, COMPTS, and LABELS) are correct. Intermediate files (e.g., ADIF3D, ISOTXS, and ARC) and those related to the solution of the given model (e.g., RTFLUX) will not be evaluated as they are either not directly used by current design activities or will be verified in later sections of this work.

#### *3.1.1.2.2 Standard Output Edit Verification*

This section will progress through the DIF3D standard output file and evaluate the correctness of the outputted data, based upon the model description provided previously. These outputs are 2,000 lines long and therefore, the information replicated within the main body of this document will be minimized.

Aside from an echo of the input file and the separation of inputs into the individual module's components, the first edit encountered that requires verification is the general GNIP4C module parameter echo and outputs related to defining the problem geometry. This begins on line 288 of the output. This provides an echo of the input information, including the geometry type, the number of regions, compositions, coarse and fine mesh intervals. These were explicitly compared with the input file utilized and all were found to match. Additionally, line 22 of Figure 3 produced a warning stating that the composition assignment to REG4 is ignored; this behavior is as expected since line 25 overwrote this composition assignment specifically in order to test this.

The next output table encountered contains the fine mesh interval boundaries for each of the X-, Y-, and Z-directions. This can be found on line 341 of the output. The expected mesh boundaries, based upon the data provided in Table 10, were calculated by-hand and are provided in the upper portion of Table 17 and are displayed at the same precision as DIF3D uses for its' output. The outputted mesh boundaries from DIF3D are provided in the lower portion of Table 17. As can be seen, all of the values match to the displayed precision.

### Expected Mesh Boundaries

X	0.00000E+00	1.00000E+00	2.25000E+00	3.50000E+00	5.66667E+00	7.83333E+00	1.00000E+01
	0.00000E+00	1.50000E+00	3.00000E+00	4.50000E+00	6.00000E+00	6.80000E+00	7.60000E+00
Y	8.40000E+00	9.20000E+00	1.00000E+01	1.03333E+01	1.06667E+01	1.10000E+01	1.13333E+01
	1.16667E+01	1.20000E+01	1.31429E+01	1.42857E+01	1.54286E+01	1.65714E+01	1.77143E+01
Z	1.88571E+01	2.00000E+01					
	0.00000E+00	3.75000E-01	7.50000E-01	1.12500E+00	1.50000E+00	1.87500E+00	2.25000E+00
	2.62500E+00	3.00000E+00	6.00000E+00	9.00000E+00	1.20000E+01	1.50000E+01	1.80000E+01
	2.10000E+01	2.40000E+01	2.70000E+01	3.00000E+01			
	DIF3D Mesh Boundaries						
X	0.00000E+00	1.00000E+00	2.25000E+00	3.50000E+00	5.66667E+00	7.83333E+00	1.00000E+01
	0.00000E+00	1.50000E+00	3.00000E+00	4.50000E+00	6.00000E+00	6.80000E+00	7.60000E+00
Y	8.40000E+00	9.20000E+00	1.00000E+01	1.03333E+01	1.06667E+01	1.10000E+01	1.13333E+01
	1.16667E+01	1.20000E+01	1.31429E+01	1.42857E+01	1.54286E+01	1.65714E+01	1.77143E+01
Z	1.88571E+01	2.00000E+01					
	0.00000E+00	3.75000E-01	7.50000E-01	1.12500E+00	1.50000E+00	1.87500E+00	2.25000E+00
	2.62500E+00	3.00000E+00	6.00000E+00	9.00000E+00	1.20000E+01	1.50000E+01	1.80000E+01
	2.10000E+01	2.40000E+01	2.70000E+01	3.00000E+01			

### Table 18. Region Assignments and Volumes Verification

DIF3D Output					Computed
Region name	Region volume [cm <sup>3</sup> ]	Zone number	Zone name	Assigned Area	Region volume [cm <sup>3</sup> ]
REG1	1.800E+01	1	COMP1	AREA1	1.800E+01
REG2	4.500E+01	2	COMP2	AREA2	4.500E+01
REG3	2.340E+02	3	COMP3	AREA3	2.340E+02
REG4	1.470E+03	4	COMP4	-	1.470E+03
REG5	1.560E+02	4	COMP4	-	1.560E+02
REG6	1.620E+03	3	COMP3	AREA3	1.620E+03
REG7	7.020E+02	2	COMP2	AREA2	7.020E+02
REG8	1.755E+03	1	COMP1	AREA1	1.755E+03



February 13, 2020

---

Immediately following the region/zone and area specifications is the reactor region and composition maps. Since these outputs are visual representations of the geometry, these tables are replicated here nearly directly from the output files themselves.

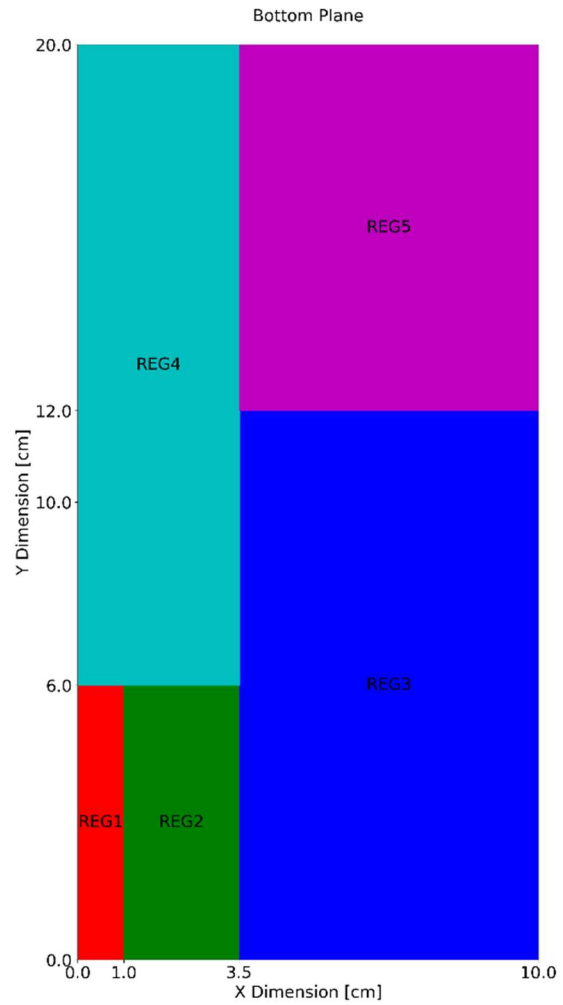
Specifically, Table 19 contains the region map for the lower (in Z) of the two portions of the core and Table 20 contains the region map for the upper portion. The right side of each of these tables provides the geometry for that portion of the core from Figure 1. Table 21 provides the reactor composition map for the lower and upper portions on the left and right sides, respectively. These tables are copied directly from the standard output file with that lines removed that do not contain information, allowing the map to fit on one page. Line numbers are included and still reference the lines of the original input file despite the removal of lines. In these tables, the numbers outside the asterisk are the fine mesh element indices along the appropriate axis. The numbers within the axes are either the region number (Table 19 and Table 20) or composition number (Table 21).

Upon inspection it is clear that the general geometric laydown and the region/composition assignments are as expected. The mesh element assignments in these maps were then compared with the mesh index extents provided earlier in Table 11. This comparison confirms that the region and composition maps were generated correctly.

February 13, 2020

Table 19. Reactor Region Map for Z-Planes 1-8

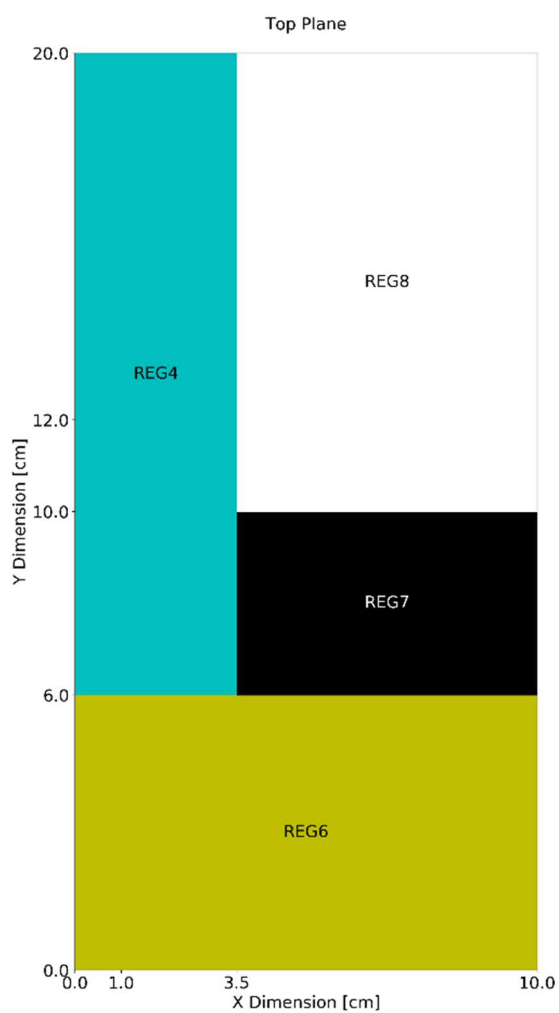
393	0	Z-DIM	MAP FOR PLANES				1 - 8
394	0	-DIM /X	-DIM				
395	0	1 2 3 4 5 6					
396		*****					
397		22 * 4 4 4 5 5 5	22				
398	+						
399		* * *					
401		21 * 4 4 4 5 5 5	21				
402	+						
403		* * *					
405		20 * 4 4 4 5 5 5	20				
406	+						
407		* * *					
409		19 * 4 4 4 5 5 5	19				
410	+						
411		* * *					
413		18 * 4 4 4 5 5 5	18				
414	+						
415		* * *					
417		17 * 4 4 4 5 5 5	17				
418	+						
419		* * *					
421		16 * 4 4 4 5 5 5	16				
422	+						
423		* * *					
424	+						
425		15 * 4 4 4 3 3 3	15				
426	+						
427		* * *					
429		14 * 4 4 4 3 3 3	14				
430	+						
431		* * *					
433		13 * 4 4 4 3 3 3	13				
434	+						
435		* * *					
437		12 * 4 4 4 3 3 3	12				
438	+						
439		* * *					
441		11 * 4 4 4 3 3 3	11				
442	+						
443		* * *					
445		10 * 4 4 4 3 3 3	10				
446	+						
447		* * *					
449		9 * 4 4 4 3 3 3	9				
450	+						
451		* * *					
453		8 * 4 4 4 3 3 3	8				
454	+						
455		* * *					
457		7 * 4 4 4 3 3 3	7				
458	+						
459		* * *					
461		6 * 4 4 4 3 3 3	6				
462	+						
463		* * *					
465		5 * 4 4 4 3 3 3	5				
466	+						
467		* * *					
468	+	*****					
469		4 * 1 2 2 3 3 3	4				
470	+						
471		* * *					
473		3 * 1 2 2 3 3 3	3				
474	+						
475		* * *					
477		2 * 1 2 2 3 3 3	2				
478	+						
479		* * *					
481		1 * 1 2 2 3 3 3	1				
482	+						
483		* * *					
484	+	*****					
485		1 2 3 4 5 6					



February 13, 2020

Table 20. Reactor Region Map for Z-Planes 9-17

488	0	Z-DIM	MAP FOR PLANES	9 - 17
489	0	-DIM /X	-DIM	
490	0	1 2 3 4 5 6		
491		*****		
492	22	* 4 4 4 8 8 8	22	
493	+			
494		* 4 4 4 8 8 8		
496	21	* 4 4 4 8 8 8	21	
497	+			
498		* 4 4 4 8 8 8		
500	20	* 4 4 4 8 8 8	20	
501	+			
502		* 4 4 4 8 8 8		
504	19	* 4 4 4 8 8 8	19	
505	+			
506		* 4 4 4 8 8 8		
508	18	* 4 4 4 8 8 8	18	
509	+			
510		* 4 4 4 8 8 8		
512	17	* 4 4 4 8 8 8	17	
513	+			
514		* 4 4 4 8 8 8		
516	16	* 4 4 4 8 8 8	16	
517	+			
518		* 4 4 4 8 8 8		
520	15	* 4 4 4 8 8 8	15	
521	+			
522		* 4 4 4 8 8 8		
524	14	* 4 4 4 8 8 8	14	
525	+			
526		* 4 4 4 8 8 8		
528	13	* 4 4 4 8 8 8	13	
529	+			
530		* 4 4 4 8 8 8		
532	12	* 4 4 4 8 8 8	12	
533	+			
534		* 4 4 4 8 8 8		
536	11	* 4 4 4 8 8 8	11	
537	+			
538		* 4 4 4 8 8 8		
540	10	* 4 4 4 8 8 8	10	
541	+			
542		* 4 4 4 8 8 8		
543	+			
544	9	* 4 4 4 7 7 7	9	
545	+			
546		* 4 4 4 7 7 7		
548	8	* 4 4 4 7 7 7	8	
549	+			
550		* 4 4 4 7 7 7		
552	7	* 4 4 4 7 7 7	7	
553	+			
554		* 4 4 4 7 7 7		
556	6	* 4 4 4 7 7 7	6	
557	+			
558		* 4 4 4 7 7 7		
560	5	* 4 4 4 7 7 7	5	
561	+			
562		* 4 4 4 7 7 7		
563	+			
564	4	* 6 6 6 6 6 6	4	
565	+			
566		* 6 6 6 6 6 6		
568	3	* 6 6 6 6 6 6	3	
569	+			
570		* 6 6 6 6 6 6		
572	2	* 6 6 6 6 6 6	2	
573	+			
574		* 6 6 6 6 6 6		
576	1	* 6 6 6 6 6 6	1	
577	+			
578		* 6 6 6 6 6 6		
579	+			
580		1 2 3 4 5 6		



February 13, 2020

Table 21. Reactor Composition Map for Z-Planes 1-8 (Left) and 9-17 (Right)

583	0	Z-DIM	MAP FOR PLANES	1 - 8
584	0	-DIM /X	-DIM	
585	0	1 2 3 4 5 6		
586		*****		
587		22 * 4 4 4 4 4 4 22		
588	+	*		*
589		21 * 4 4 4 4 4 4 21		
591	+	*		*
592		20 * 4 4 4 4 4 4 20		
593	+	*		*
595		19 * 4 4 4 4 4 4 19		
596	+	*		*
597		18 * 4 4 4 4 4 4 18		
599	+	*		*
600		17 * 4 4 4 4 4 4 17		
601	+	*		*
602		16 * 4 4 4 4 4 4 16		
603	+	*		*
604		15 * 4 4 4 3 3 3 15		
605	+	*		*
607		14 * 4 4 4 3 3 3 14		
608	+	*		*
609		13 * 4 4 4 3 3 3 13		
611	+	*		*
612		12 * 4 4 4 3 3 3 12		
613	+	*		*
614		11 * 4 4 4 3 3 3 11		
615	+	*		*
616		10 * 4 4 4 3 3 3 10		
617	+	*		*
619		9 * 4 4 4 3 3 3 9		
620	+	*		*
621		8 * 4 4 4 3 3 3 8		
622	+	*		*
623		7 * 4 4 4 3 3 3 7		
624	+	*		*
625		6 * 4 4 4 3 3 3 6		
627	+	*		*
628		5 * 4 4 4 3 3 3 5		
629	+	*		*
631		4 * 1 2 2 3 3 3 4		
632	+	*		*
633		3 * 1 2 2 3 3 3 3		
635	+	*		*
636		2 * 1 2 2 3 3 3 2		
637	+	*		*
638		1 * 1 2 2 3 3 3 1		
639	+	*		*
640		*****		
641	+	1 2 3 4 5 6		
643				
644	+			
645				
647	+			
648				
649	+			
651				
652	+			
653				
655	+			
656				
657	+			
658				
659	+			
660				
661	+			
663				
664	+			
665				
667	+			
668				
669	+			
671				
672	+			
673				
674	+			
675				

678	0	Z-DIM	MAP FOR PLANES	9 - 17
679	0	-DIM /X	-DIM	
680	0	1 2 3 4 5 6		
681		*****		
682		22 * 4 4 4 1 1 1 22		
683	+	*		*
684		21 * 4 4 4 1 1 1 21		
686	+	*		*
687		20 * 4 4 4 1 1 1 20		
688	+	*		*
690		19 * 4 4 4 1 1 1 19		
691	+	*		*
692		18 * 4 4 4 1 1 1 18		
694	+	*		*
695		17 * 4 4 4 1 1 1 17		
696	+	*		*
698		16 * 4 4 4 1 1 1 16		
699	+	*		*
700		15 * 4 4 4 1 1 1 15		
702	+	*		*
703		14 * 4 4 4 1 1 1 14		
704	+	*		*
706		13 * 4 4 4 1 1 1 13		
707	+	*		*
708		12 * 4 4 4 1 1 1 12		
710	+	*		*
711		11 * 4 4 4 1 1 1 11		
712	+	*		*
714		10 * 4 4 4 1 1 1 10		
715	+	*		*
716		9 * 4 4 4 2 2 2 9		
718	+	*		*
719		8 * 4 4 4 2 2 2 8		
720	+	*		*
722		7 * 4 4 4 2 2 2 7		
723	+	*		*
724		6 * 4 4 4 2 2 2 6		
726	+	*		*
727		5 * 4 4 4 2 2 2 5		
728	+	*		*
730		4 * 3 3 3 3 3 3 4		
731	+	*		*
732		3 * 3 3 3 3 3 3 3		
733	+	*		*
734		2 * 3 3 3 3 3 3 2		
735	+	*		*
736		1 * 3 3 3 3 3 3 1		
738	+	*		*
739		*****		
740	+	1 2 3 4 5 6		
742				
743	+			
744				
746	+			
747				
748	+			
750				
751	+			
752				
753	+			
754				
755	+			
756				
758	+			
759				
760	+			
762				
763	+			
764				
766	+			
767				
768	+			
769				
770	+			

The next information printed in the standard output is a summary of the ISOTXS file, beginning on line 774 of the output. This section of output includes information such as the number of groups, the number of isotopes, the scattering orders, fission spectrum flags, and the composition assignments of that isotope. This information is repeated details from the A.ISO input and was verified, parameter by parameter, and is as expected.

Line 792 begins the NDXSRF file description, including the number of nuclides, zones, subzones, etc., and the assignments of the nuclide set 1 to the different zones and subzones. The values and arrays of set assignments match expectations.

Similarly, line 819 provides the contents of the ZNATDN specification, including the assignment of isotopes to compositions and their respective atom densities in each composition. These values were explicitly compared with the expectations from Table 22 and found to match.

The macroscopic cross section homogenization (via the HMG4C module) output begins on line 867. This begins with a repeat of some metadata, including the number of groups, energy group structure, etc. and then continues with edits of each isotope's group-independent and group-dependent data. For brevity, this information will not be included here, but each of these isotopic edits were compared with that provided in Table 12 through Table 13; no differences were noted.

The next output type encountered is the edit of macroscopic cross sections from the COMPXS file. These are found beginning on line 1327. This data begins with COMPXS metadata: the number of compositions, groups, prompt fission spectrum flag, number of fissionable compositions, maximum up and down-scattering groups, scattering order, mean neutron velocities and the group structure. All of this metadata match the expected values based upon the data provided in the input.

Before explicitly comparing the homogenized cross section values that were computed by DIF3D and written to the COMPXS file, this report will present the equations used to create the reference solutions. The quantities that need to be computed are the group-wise absorption, total, removal, transport, fission, nu-fission, and (n,2n) cross sections, fission spectra, scattering matrices, power conversion factors, and directional diffusion coefficients. These group-wise equations are presented below. In these equations,  $i$  is the isotopic index,  $c$  is the composition number, and  $g$  is the group.

$$\Sigma_{absorption,g,c} = \sum_{i \in I} N_{i,c} (\sigma_{fission,g,i} + \sigma_{capture,g,i}), \quad (1)$$

$$\Sigma_{total,g,c} = \sum_{i \in I} N_{i,c} \sigma_{total,g,i}, \quad (2)$$

$$\Sigma_{removal,g,c} = \sum_{i \in I} N_{i,c} (\sigma_{fission,g,i} + \sigma_{capture,g,i} + \sigma_{out-scatter,g,i}), \quad (3)$$

$$\sigma_{scatter,g' \rightarrow g,i,l} = \begin{cases} \sigma_{total\ scatter,g' \rightarrow g,i,l}; & \text{if total scatter matrix present} \\ \sigma_{elastic,g' \rightarrow g,i,l} + \sigma_{inelastic,g' \rightarrow g,i,l} + \frac{1}{2} \sigma_{(n,2n),g' \rightarrow g,i,l}; & \text{otherwise} \end{cases}, \quad (4)$$

$$\sigma_{scatter-production,g' \rightarrow g,i,l} = \begin{cases} \sigma_{total\ scatter,g' \rightarrow g,i,l}; & \text{if total scatter matrix present} \\ \sigma_{elastic,g' \rightarrow g,i,l} + \sigma_{inelastic,g' \rightarrow g,i,l} + \sigma_{(n,2n),g' \rightarrow g,i,l}; & \text{otherwise} \end{cases}, \quad (5)$$

$$\sigma_{out-scatter,g,i} = \sum_{g' \in G, g' \neq g} [\sigma_{scatter,g' \rightarrow g,i,0}] - \begin{cases} \sigma_{(n,2n),g,i}; & \text{if } \sigma_{(n,2n),g,i} \text{ present} \\ \frac{1}{2} \sum_{g' \in G} \sigma_{(n,2n),g' \rightarrow g,i,0}; & \text{otherwise} \end{cases}, \quad (6)$$

$$\Sigma_{transport,g,c} = \sum_{i \in I} N_{i,c} \sigma_{transport,g,i}, \quad (7)$$

$$\Sigma_{fission,g,c} = \sum_{i \in I} N_{i,c} \sigma_{fission,g,i}, \quad (8)$$

$$\text{Production}_{g,c} = \sum_{i \in I} N_{i,c} v_{g,i} \sigma_{fission,g,i}, \quad (9)$$

$$\chi_{g,c} = \begin{cases} \begin{cases} \chi_{g,file-wide}; & \text{if present} \\ \frac{\sum_{i \in I} N_{i,c} (\chi_{g,i} \sum_{g' \in G} v_{g',c} \Sigma_{fission,g',c})}{\sum_{i \in I} N_{i,c} (\sum_{g' \in G} v_{g',c} \Sigma_{fission,g',c})}; & \text{otherwise} \end{cases} & ; \text{ Chi calc option is 0} \\ \begin{cases} \frac{\sum_{i \in I} N_{i,c} (\chi_{g,i} \sum_{g' \in G} v_{g',c} \Sigma_{fission,g',c})}{\sum_{i \in I} N_{i,c} (\sum_{g' \in G} v_{g',c} \Sigma_{fission,g',c})}; & \chi_{g,i} \text{ present} \\ \chi_{g,file-wide}; & \text{otherwise} \end{cases} & ; \text{ Chi calc option is 1} \\ \begin{cases} \frac{\sum_{i \in I} N_{i,c} (\chi_{g,i} v_{g,c} \Sigma_{fission,g,c})}{\sum_{i \in I} N_{i,c} v_{g,c} \Sigma_{fission,g,c}}; & \chi_{g,i} \text{ present} \\ \chi_{g,file-wide}; & \text{otherwise} \end{cases} & ; \text{ Chi calc option is 2} \end{cases}, \quad (10)$$

$$PCF_{g,c} = \sum_{i \in I} N_{i,c} (E_{fission,i} \sigma_{fission,g,i} + E_{capture,i} \sigma_{capture,g,i}), \quad (11)$$

$$\Sigma_{(n,2n),g,c} = \sum_{i \in I} N_{i,c} \sigma_{(n,2n),g,i}, \quad (12)$$

$$\Sigma_{total\ scatter,g' \rightarrow g,c,l} = \sum_{i \in I} N_{i,c} \sigma_{total\ scatter,g' \rightarrow g,i,l}, \quad (13)$$

$$D_{g,c} = \frac{1}{3 \Sigma_{transport,g,c}}, \quad (14)$$

$$v_{g,c} = \frac{\text{Production}_{g,c}}{\Sigma_{fission,g,c}}, \quad (15)$$

The number densities,  $N_{i,c}$ , in the equations above are simply the scalar numbers present in the material and compositions defined as shown in Figure 3. For clarity, these are repeated in Table 22 for each of the four compositions.

**Table 22. Composition Number Densities**

	$N_{c,I} [atoms/cm^3]$			
	ISO1	ISO2	ISO3	ISO4
<b>COMP1</b>	1.00	0.00	0.00	0.00
<b>COMP2</b>	0.10	0.00	0.90	0.00
<b>COMP3</b>	0.24	0.24	0.36	0.16
<b>COMP4</b>	1.00	0.00	0.00	1.00

The number densities of Table 22 and the isotopic data provided in Table 12 through Table 14 were used in the above equations in a spreadsheet to produce the composition cross sections (except for scattering matrices, discussed later) that are shown in Table 23. Table 24 contains the equivalent data in standard output produced by the HMG4C module. Table 25 shows the differences between these values. These differences are the absolute value of the fractional differences (compared to the hand calculations), unless the hand calculated value is zero, then the value is an absolute difference. Differences less than  $10^{-6}$  can only be attributed to rounding errors in the DIF3D output and differences greater than this value are real. Table 25 clearly shows that the composition cross sections for all four compositions match the computed values.

Table 26 provides the  $P_0$  and  $P_1$  total scattering matrices computed by hand. Table 27 shows the  $P_0$  values output by HMG4C in the standard output, and Table 28 shows the differences. No significant differences are noted as the differences on the order of  $10^{-16}$  are attributable to the double precision floating point approximation errors.

The HMG4C output in this block includes additional information that is not included in the tables below. These are the number of up- and down-scatter groups as well as the directional diffusion coefficient multipliers and additive terms. The number of up- and down-scatter groups were manually checked for consistency with the scattering matrices; they are consistent. The diffusion coefficient multipliers and additive terms have values of 1.0 and 0.0, respectively, for every entry. This is expected since directional diffusion coefficients were not used (and are not tested) by this work. The final HMG4C output is the edit of the fissions per watt-second and captures per watt-second; these are outputted as the default value of  $-1.0E+20$ , indicating that the ISOTXS data will be used, as intended.

February 13, 2020

**Table 23. Hand-Calculated Composition Cross Sections**

Comp #	Grp	Absorption	Total	Removal	Transport	Fission	Nu*Fission	Chi	PCF	N2N
1	1	8.480290E-06	1.106830E-01	1.009080E-03	1.106830E-01	0.000000E+00	0.000000E+00	N/A	1.865664E-17	0.000000E+00
	2	1.600000E-04	3.635500E-01	1.600000E-04	3.635500E-01	0.000000E+00	0.000000E+00	N/A	3.520000E-16	0.000000E+00
2	1	1.848548E-03	6.023323E-01	2.690291E-02	3.483847E-01	9.435600E-04	1.887120E-03	9.500000E-01	3.710667E-14	1.350000E-03
	2	6.879400E-02	2.304580E+00	6.879400E-02	1.554718E+00	4.556880E-02	1.139220E-01	5.000000E-02	1.656986E-12	0.000000E+00
3	1	2.704418E-03	6.363751E-01	3.252868E-02	5.241492E-01	8.281440E-04	1.701360E-03	9.725954E-01	4.746374E-14	6.540000E-03
	2	5.161040E-02	2.131587E+00	5.162640E-02	1.822940E+00	3.374752E-02	8.281680E-02	2.740455E-02	1.401051E-12	0.000000E+00
4	1	1.153328E-02	4.465630E-01	1.558888E-02	3.800200E-01	2.817000E-03	5.915700E-03	1.000000E+00	2.005953E-13	0.000000E+00
	2	1.223400E-01	9.098300E-01	1.224400E-01	8.554400E-01	9.700000E-02	2.328000E-01	0.000000E+00	4.489936E-12	0.000000E+00

**Table 24. HMG4C Standard Output Cross Sections**

Comp #	Grp	Absorption	Total	Removal	Transport	Fission	Nu*Fission	Chi	PCF	N2N
1	1	8.480290E-06	1.106830E-01	1.009080E-03	1.106830E-01	N/A	N/A	N/A	1.865664E-17	0.000000E+00
	2	1.600000E-04	3.635500E-01	1.600000E-04	3.635500E-01	N/A	N/A	N/A	3.520000E-16	0.000000E+00
2	1	1.848548E-03	6.023323E-01	2.690291E-02	3.483847E-01	9.435599E-04	1.887120E-03	9.500000E-01	3.710667E-14	1.350000E-03
	2	6.879400E-02	2.304580E+00	6.879400E-02	1.554718E+00	4.556880E-02	1.139220E-01	5.000000E-02	1.656986E-12	0.000000E+00
3	1	2.704418E-03	6.363751E-01	3.252868E-02	5.241492E-01	8.281440E-04	1.701360E-03	9.725954E-01	4.746374E-14	6.540000E-03
	2	5.161040E-02	2.131587E+00	5.162640E-02	1.822940E+00	3.374752E-02	8.281680E-02	2.740455E-02	1.401051E-12	0.000000E+00
4	1	1.153328E-02	4.465630E-01	1.558888E-02	3.800200E-01	2.817000E-03	5.915700E-03	1.000000E+00	2.005953E-13	0.000000E+00
	2	1.223400E-01	9.098300E-01	1.224400E-01	8.554400E-01	9.700000E-02	2.328000E-01	0.000000E+00	4.489936E-12	0.000000E+00



**Table 25. HMG4C and Hand-Calculated Cross Section Differences**

Comp #	Grp	Absorption	Total	Removal	Transport	Fission	Nu*Fission	Chi	PCF	N2N
1	1	0.0E+00	0.0E+00	2.9E-07	0.0E+00	N/A	N/A	N/A	1.1E-07	0.0E+00
	2	0.0E+00	0.0E+00	0.0E+00	0.0E+00	N/A	N/A	N/A	2.8E-16	0.0E+00
2	1	1.6E-08	0.0E+00	7.3E-08	0.0E+00	1.1E-07	0.0E+00	1.2E-16	9.1E-09	0.0E+00
	2	2.0E-16	0.0E+00	2.0E-16	1.4E-16	1.5E-16	2.4E-16	0.0E+00	1.9E-07	0.0E+00
3	1	1.4E-07	3.1E-08	7.3E-08	0.0E+00	1.3E-16	1.3E-16	4.8E-08	8.3E-08	0.0E+00
	2	1.3E-16	9.4E-08	1.3E-16	2.2E-07	0.0E+00	1.7E-16	1.1E-07	1.2E-07	0.0E+00
4	1	2.5E-08	1.2E-16	1.9E-08	0.0E+00	0.0E+00	0.0E+00	0.0E+00	1.7E-08	0.0E+00
	2	0.0E+00	1.2E-16	1.1E-16	0.0E+00	0.0E+00	0.0E+00	0.0E+00	1.8E-16	0.0E+00

**Table 26. Hand-Calculated Scattering Matrices**

Comp #	To Grp	P <sub>0</sub> , From Group		P <sub>1</sub> , From Group	
		1	2	1	2
1	1	1.096740E-01	0.000000E+00	0.000000E+00	0.000000E+00
	2	1.000600E-03	3.633900E-01	0.000000E+00	0.000000E+00
2	1	5.727294E-01	0.000000E+00	2.471310E-01	0.000000E+00
	2	2.640436E-02	2.235786E+00	6.816330E-03	7.498620E-01
3	1	5.907658E-01	1.600000E-05	1.095628E-01	1.600000E-06
	2	3.660426E-02	2.079960E+00	2.662980E-03	3.086456E-01
4	1	4.309740E-01	1.000000E-04	6.694000E-02	1.000000E-05
	2	5.555600E-03	7.873900E-01	-3.972000E-04	5.438000E-02

**Table 27. HMG4C Standard Output Scattering Matrices**

Comp #	To Grp	P <sub>0</sub> , From Group	
		1	2
1	1	1.096740E-01	
	2	1.000600E-03	3.633900E-01
2	1	5.727294E-01	
	2	2.640436E-02	2.235786E+00
3	1	5.907658E-01	1.600000E-05
	2	3.660427E-02	2.079961E+00
4	1	4.309740E-01	1.000000E-04
	2	5.555600E-03	7.873900E-01

**Table 28. HMG4C and Hand-Calculated Scattering Matrices Differences**

Comp #	To Grp	P <sub>0</sub> , From Group	
		1	2
1	1	0.0E+00	0.0E+00
	2	0.0E+00	0.0E+00
2	1	1.9E-16	0.0E+00
	2	1.3E-16	0.0E+00
3	1	6.8E-08	2.1E-16
	2	1.6E-07	2.9E-07
4	1	0.0E+00	0.0E+00
	2	0.0E+00	0.0E+00

February 13, 2020

The first relevant output of the DIF3D block is found on line 1515, which repeats the user input specifications. These specific parameters match the inputted values and are omitted for brevity.

The problem geometry is repeated, first with the mesh intervals and boundaries on line 1582. The mesh interval boundaries were compared with a tool that uses the commonly used diffliB package in Python's standard library; the only differences present are the number of significant figures printed (NIP3 prints 5 while DIF3D prints six). The mesh midpoints were calculated by hand and compared with the DIF3D results. These are both provided in Table 29; all values match to the six significant digits.

**Table 29. Mesh Midpoint Comparisons**

Expected Mesh Midpoints							
X	5.000000E-01	1.625000E+00	2.875000E+00	4.583334E+00	6.750001E+00	8.916668E+00	
	7.500000E-01	2.250000E+00	3.750000E+00	5.250000E+00	6.400000E+00	7.200000E+00	8.000000E+00
Y	8.800000E+00	9.600000E+00	1.016667E+01	1.050000E+01	1.083333E+01	1.116667E+01	1.150000E+01
	1.183333E+01	1.257143E+01	1.371428E+01	1.485714E+01	1.600000E+01	1.714285E+01	1.828571E+01
	1.942857E+01						
	1.875000E-01	5.625000E-01	9.375000E-01	1.312500E+00	1.687500E+00	2.062500E+00	2.437500E+00
Z	2.812500E+00	4.500000E+00	7.500000E+00	1.050000E+01	1.350000E+01	1.650000E+01	1.950000E+01
	2.250000E+01	2.550000E+01	2.850000E+01				
DIF3D Mesh Midpoints							
X	5.000000E-01	1.625000E+00	2.875000E+00	4.583333E+00	6.750000E+00	8.916667E+00	
	7.500000E-01	2.250000E+00	3.750000E+00	5.250000E+00	6.400000E+00	7.200000E+00	8.000000E+00
Y	8.800000E+00	9.600000E+00	1.016667E+01	1.050000E+01	1.083333E+01	1.116667E+01	1.150000E+01
	1.183333E+01	1.257143E+01	1.371429E+01	1.485714E+01	1.600000E+01	1.714286E+01	1.828571E+01
	1.942857E+01						
	1.875000E-01	5.625000E-01	9.375000E-01	1.312500E+00	1.687500E+00	2.062500E+00	2.437500E+00
Z	2.812500E+00	4.500000E+00	7.500000E+00	1.050000E+01	1.350000E+01	1.650000E+01	1.950000E+01
	2.250000E+01	2.550000E+01	2.850000E+01				

The next output in the DIF3D standard output file are the boundary conditions, internal black boundary condition constants, and the region/composition assignment table. These were all manually verified to match the expected output.

Line 1647 begins the DIF3D reactor region (and zone) by mesh point plots. The information in these plots is intended to be the same as previously shown in Table 19 through Table 21. Another diffliB comparison of these plots reveals that the information is the same, though the plot style

chosen by the DIF3D module is slightly different than by the NIP3 module. Specifically, the DIF3D plots are slightly more compressed with the removal of the “+” characters at the start of the NIP3 map’s lines. These are the same lines/characters that were removed in the Table 19 and Table 20 plots to fit the data on one page. The content is otherwise exactly the same.

The final standard output table to be verified in this section is the DIF3D module’s output of the composition cross sections. This data includes the diffusion coefficient and the neutron emission rate for fission (labelled Nu), in addition to a subset of the output shown earlier. The hand-calculated diffusion coefficients and neutron emission rates are provided in Table 30. The DIF3D output for the non-scattering matrix quantities are provided in Table 31, and the deviations from the hand-calculated values (from Table 23 and Table 30) are provided in Table 32.

Table 30 uses the same strategy as before wherein the relative difference from the hand-calculated values are used, unless the hand-calculated value is zero, then the absolute difference is shown. This table shows that the DIF3D output is correct to within the number of significant figures provided by DIF3D’s ASCII output.

**Table 30. Additional Hand Calculated Composition Cross Sections**

Comp #	Grp	Diff. Coeff.	Nu
1	1	3.011604E+00	N/A
	2	9.168844E-01	N/A
2	1	9.567967E-01	2.000000E+00
	2	2.144012E-01	2.500000E+00
3	1	6.359512E-01	2.054425E+00
	2	1.828548E-01	2.454011E+00
4	1	8.771468E-01	2.100000E+00
	2	3.896630E-01	2.400000E+00

**Table 31. DIF3D-Outputted Composition Cross Sections**

Comp #	Grp	Absorption	Diff. Coeff.	Removal	Fission	Chi	Nu	PCF
1	1	8.480290E-06	3.011604E+00	1.009080E-03				1.865664E-17
	2	1.600000E-04	9.168844E-01	1.600000E-04				3.520000E-16
2	1	1.848548E-03	9.567967E-01	2.690291E-02	9.435599E-04	9.500000E-01	2.000000E+00	3.710667E-14
	2	6.879400E-02	2.144012E-01	6.879400E-02	4.556880E-02	5.000000E-02	2.500000E+00	1.656986E-12
3	1	2.704418E-03	6.359512E-01	3.252868E-02	8.281440E-04	9.725954E-01	2.054425E+00	4.746374E-14
	2	5.161040E-02	1.828548E-01	5.162640E-02	3.374752E-02	2.740455E-02	2.454011E+00	1.401051E-12
4	1	1.153328E-02	8.771468E-01	1.558888E-02	2.817000E-03	1.000000E+00	2.100000E+00	2.005953E-13
	2	1.223400E-01	3.896630E-01	1.224400E-01	9.700000E-02	0.000000E+00	2.400000E+00	4.489936E-12

**Table 32. DIF3D-Outputted Composition Cross Section Errors**

Comp #	Grp	Absorption	Diff. Coeff.	Removal	Fission	Chi	Nu	PCF
1	1	0.0E+00	9.7E-08	2.9E-07	N/A	N/A	N/A	1.1E-07
	2	0.0E+00	2.9E-08	0.0E+00	N/A	N/A	N/A	2.8E-16
2	1	1.6E-08	6.1E-09	7.3E-08	1.1E-07	1.2E-16	0.0E+00	9.1E-09
	2	2.0E-16	2.1E-07	2.0E-16	1.5E-16	0.0E+00	0.0E+00	1.9E-07
3	1	1.4E-07	6.2E-08	7.3E-08	1.3E-16	4.8E-08	1.5E-07	8.3E-08
	2	1.3E-16	2.3E-07	1.3E-16	0.0E+00	1.1E-07	1.8E-07	1.2E-07
4	1	2.5E-08	1.9E-08	1.9E-08	0.0E+00	0.0E+00	0.0E+00	1.7E-08
	2	0.0E+00	5.0E-08	1.1E-16	0.0E+00	0.0E+00	0.0E+00	1.8E-16

Immediately after the principal cross sections for each composition, DIF3D prints the  $P_0$  scattering matrices. The hand-calculated values for these are the same as shown in Table 26. Table 33 provides the equivalent output from DIF3D. Blanks indicate that DIF3D did not print that value, whereas zeros were printed by DIF3D. It is evident that DIF3D is not printing the diagonals (i.e., self-scatter components) of the scattering matrix for the group 2 self-scatter entry, but it does print zeros or a value for the group 1 self-scatter entry. The heading of this table, “SCATTERING CROSS SECTION (TOTAL)”, provides no further information as to why, nor is there any user-facing documentation for this output table. While not conclusive, the only compositions with non-zero group 1 self-scatter values printed are those that contain the ISO4 isotope. This is the same isotope that utilized an (n,2n) matrix but no (n,2n) principal cross section. It may be that DIF3D is handling this situation erroneously when creating the data that is outputted to this table. If this is the source of the discrepancy, then it is unlikely to impact design work as the MC<sup>2</sup>-3 cross sections are not expected to output a nuclide with an (n,2n) matrix without an (n,2n) principal cross section.

Since the removal cross section is correct, then this issue is likely isolated to simply a cross section editing issue. To verify, three infinite homogeneous material models were created with COMP2, COMP3, and COMP4 as the lone material (COMP1 is not fissionable). The relevant cross section edit tables displayed the same misrepresented scattering matrix from the DIF3D module as shown in Table 33. The eigenvalues from these three models were compared with their analytic solution and all DIF3D eigenvalues matched the analytic solution to all reported significant digits. To ensure that the effect of missing those out-scatter cross sections is not because their particular value may have no effect on the computations, and thus the errors may not be observable, the analytical solution was also repeated with the scattering matrices as stated by DIF3D provided in Table 33. These analytic eigenvalues changed by at least a factor of 2.25 indicating that the out-scatter terms are important and their exclusion in DIF3D would be obvious. Therefore, this error is simply an edit issue and not an error that propagates to the DIF3D solution.

Table 34 is the relative error of the DIF3D output from the Table 26 reference values, with significant differences in red. Unsurprisingly, the differences are the self-scatter entries that were just discussed. All other values match.

The remaining outputs are related to the solution of the model. These are therefore not verified as part of this case, but will be handled by others.

**Table 33. DIF3D-Outputted Scattering Matrices**

Comp #	To Grp	P0, From Group	
		1	2
1	1	0.000000E+00	0.000000E+00
	2	1.000600E-03	
2	1	0.000000E+00	0.000000E+00
	2	2.640436E-02	
3	1	5.907658E-01	1.600000E-05
	2	3.660427E-02	
4	1	4.309740E-01	1.000000E-04
	2	5.555600E-03	

**Table 34. DIF3D-Outputted Scattering Matrix Errors**

Comp #	To Grp	P0, From Group	
		1	2
1	1	1.0E+00	0.0E+00
	2	0.0E+00	1.0E+00
2	1	1.0E+00	0.0E+00
	2	1.3E-16	1.0E+00
3	1	6.8E-08	2.1E-16
	2	1.6E-07	1.0E+00
4	1	0.0E+00	0.0E+00
	2	0.0E+00	1.0E+00

#### 3.1.1.2.2.1 Auxiliary Output Verification

This base case requested every output table be printed to both the standard and auxiliary outputs. This section will examine the auxiliary output (i.e., the “fort.10” file) to ensure the content there is correct and consistent with the expectations. This evaluation will utilize the previous standard output verification heavily, and primarily focus on comparing to the already-verified standard outputs as opposed to comparing to hand-calculations.

This comparison (again with the `diff` Python package) revealed that the only differences between the standard and auxiliary outputs are:

1. The page breaks are inconsistent between the two outputs and so page numbers may be different.
2. The standard output includes additional information that was not verified by the standard output work (output file number assignments, memory storage sizes, and runtime warnings about over-relaxation factors reaching the iteration threshold).
3. The auxiliary output is apparently using non-ASCII characters to print composition names whereas the standard output was using ASCII (note it may be possible that the GNU/Linux shell, `bash`, was converting these behind the scenes). Specifically, the standard output says: “EDIT OF (NONFISSIONABLE COMPOSITION COMP1” while the auxiliary output says “EDIT OF (NONFISSIONABLE COMPOSITION”. This is only seen in the composition edits. Note that both are missing closing parentheses. This could be indicative of a memory access error, however as the importance of this is minor, it was not pursued further.

These differences are not important to this verification work, and since the content of the files match, the auxiliary output file is considered verified.

#### *3.1.1.2.2.2 Binary Output Verification*

The final set of outputs to verify are the CCCC-formatted [8] and ANL-specific binary output files relating to the model definition (i.e., GEODST, NDXSRF, ZNATDN, COMPXS, and LABELS) binary files. As stated earlier, intermediate files such (e.g., ADIF3D, ISOTXS, and ARC) and those related to the solution of the given model (e.g., RTFLUX) will not be evaluated as they are either not directly used by designers or will be verified in later sections of this work. The binary files that will be evaluated will be first converted to an ASCII format with the “/software/ARC/CCCC\_convert\_v11.0\_r3012\_d2019\_03\_14.x” executable that is distributed with ARC.

The verification of these files is presented in the sub-sections that follow. To verify that the binary files are written correctly, this work will compare the ASCII interpretation of the binary files to the applicable format to ensure the correct values are there as well as ensuring that the values are as expected. To this end, each of the binary file verifications will include a table that has the data that should be present (from the standard), the expected values, and the actual values. Note that these tables will not include the file identification record (the “0V Record”) as this table only identifies the type of file and the version number, and thus how to read it; if this table was incorrect then all later values would also be incorrect.

##### *3.1.1.2.2.2.1 GEODST Verification*

The GEODST file is a binary representation of the model geometry specification. Figure 10 provides the ASCII-formatted version of the GEODST file.

February 13, 2020

```

1 0V GEODST*          *      1
2 1D      14      4      8      1      3      4      2      6      22      17      1
3      1      1      1      1      1      1      1      1      0      0      0      0
4      44      0      0      0
5 4D 0.00000E+00 1.00000E+00 3.50000E+00 1.00000E+01 0.00000E+00
6 6.00000E+00 1.00000E+01 1.20000E+01 2.00000E+01 0.00000E+00 3.00000E+00
7 3.00000E+01
8      1      2      3      4      5      6      7      8      9
9 5D 1.80000E+01 4.50000E+01 2.34000E+02 1.47000E+03 1.56000E+02
10 1.62000E+03 7.02000E+02 1.75500E+03 0.00000E+00 4.69200E-01 0.00000E+00
11      0      0      0      0      1      2      3      4      4      3      2      1
12 6D      1      2      3      4      4      3      4      4      3      4      4
13      5
14 6D      6      6      6      4      4      7      4      4      8      4      4
15      8

```

**Figure 10. ASCII-Formatted GEODST File**

Table 35 shows the variables within the GEODST file with the expected values and the reported value in the Figure 10 data. The expected values provided in Table 35 were obtained from the model definition information provided in Figure 1 through Figure 3 and Table 9 through Table 11.

The values in Table 35 highlighted in red indicate that there is a difference between the expected values and DIF3D values in a few cases. These, and their dispositions, are discussed separately below:

1. NZCL (number of zone classifications): this quantity is not well defined in the DIF3D manuals, GEODST format, or the CCCC format specification document. For that reason a reference value was not readily determined. However, the GEODST file has a value of one here, and by context, this value likely refers to the number of zone types in the problem, whether it be standard, internal black boundary, or a rodDED region. As this model has no internal black boundaries or rodDED regions, a value of 1 for NZCL is reasonable, given this interpretation. No further work is necessary.
2. NBS (number of buckling specifications), NBCS (number of constants for external boundaries), and NIBCS (number of constants for internal boundaries): These parameters are either related to the application of internal or external boundary conditions. Since only reflective boundaries and no buckling or internal boundaries were modeled in the problem, the expected value for each of these is 0. However, the GEODST file contains values of 1 here, indicating there is a single value for each that applies everywhere. Since a value of 0 was only allowed in the CCCC format in version 4 [8], and there is no functional difference between no value and a single value everywhere if that value is a zero or ignored; the maintainers of the ARC suite chose to continue applying a single value everywhere instead of using the new 0 value feature of the standard. No further work is necessary.



3. BSQ(N) (buckling values): The expected value is that this value is not present because it is expected that NBS would be 0. However, the GEODST file does contain a value of 1 for NBS and thus a value for BSQ(N) of 0.0. This is equivalent to no buckling, and therefore is correct.
4. BNDC(N) (boundary constants): This value is the boundary constant derived from  $D\phi' + A\phi = 0$  per the A.NIP3 input format specification (and equivalently  $D\phi' + C\phi = 0$  in the GEODST format guide). The expectation is that since a reflective boundary condition is used,  $A$  (or  $C$ ) are either not supplied or are zero. However, the value in the GEODST file is 0.4692. This is listed as the default value in the A.NIP3 manual, if extrapolated boundary conditions are specified but no A.NIP3 Type 05 card (external boundary condition constants) is provided. Therefore DIF3D must populate this value as the default even if it is never needed. Later problems verifying the treatment of boundary conditions will confirm that this value truly is ignored by the solver with boundary conditions where it is not relevant.
5. BNCI(N) (internal black boundary constants): The expected value is that this value is not present because it is expected that NIBCS would be 0. However, the GEODST file does contain a value of 1 for NIBCS and thus a value for BNCI(N) of 0.0. This is equivalent to no internal black boundary constant, and therefore is correct.
6. NZC(N) (zone classification assignments): Similar to NZCL, since it is unclear what a zone classification is, expected values are difficult to identify. Given the contextual understanding discussed above with NZCL, the GEODST file's four values of 0 (for each of the four zones) are reasonable and no further work is needed.

Based on the above, the GEODST file contents are considered verified for this problem; later cases with reference flux and eigenvalue solutions will examine the impact of the boundary condition constant value of 0.4692 that is in the GEODST file.

February 13, 2020

Table 35. Comparison of GEODST Values

Variable	Expected Value	DIF3D Value	Variable	Expected Value	DIF3D Value	Variable	Expected Value	DIF3D Value
<b>Specifications (1D Record)</b>			<b>1D Mesh Boundaries (2D Record)</b>			<b>Geometry Data (5D Record)</b>		
<i>IGOM</i>	14 (XYZ)	14	<i>Not present since 3D</i>			<i>VOLR(N)</i>	NREG Values: 18, 45, 234, 1470, 156, 1620, 702, 1755	18, 45, 234, 1470, 156, 1620, 705, 1755
<i>NZONE</i>	4	4	<b>2D Mesh Boundaries (3D Record)</b>			<i>BSQ(N)</i>	NBS Values: Not Present	0
<i>NREG</i>	8	8	<i>Not present since 3D</i>			<i>BNDC(N)</i>	NBCS Values: Not Present	0.4692
<i>NZCL</i>	?	1	<b>3D Mesh Boundaries (4D Record)</b>			<i>BNCI(N)</i>	NIBCS Values: Not Present	0
<i>NCINTI</i>	3	3	<i>XMESH(I)</i>	NCINTI+1 Values: 0, 1, 3.5, 10	0, 1, 3.5, 10	<i>NZHBB(N)</i>	NZWBB Values: Not Present	Not Present
<i>NCINTJ</i>	4	4	<i>YMESH(J)</i>	NCINTJ+1 Values: 0, 6, 10, 12, 20	0, 6, 10, 12, 20	<i>NZC(N)</i>	NZONE Values: ?	0,0,0,0
<i>NCINTK</i>	2	2	<i>ZMESH(K)</i>	NCINTK+1 Values: 0, 3, 30	0, 3, 30	<i>NZNR</i>	NREG Values: 1,2,3,4,4,3,2,1	1,2,3,4,4,3,2,1
<i>NINTI</i>	6	6	<i>IFINTS(I)</i>	NCINTI Values 1, 2, 3	1, 2, 3	<b>Region Assignments to Coarse Mesh (6D Record)</b>		
<i>NINTJ</i>	22	22	<i>JFINTS(J)</i>	NCINTJ Values 4, 5, 6, 7	4, 5, 6, 7	<i>MR(I,J,K=1)</i>	NCINTI $\times$ NCINTJ Values: 1,2,3,4,4,3,4,4,3,4,4,5	1,2,3,4,4,3,4,4,3,4,4,5
<i>NINTK</i>	17	17	<i>KFINTS(K)</i>	NCINTK Values 8, 9	8, 9	<i>MR(I,J,K=2)</i>	NCINTI $\times$ NCINTJ Values: 6,6,6,4,4,7,4,4,8,4,4,8	6,6,6,4,4,7,4,4,8,4,4,8
<i>IMB1</i>	1 (Refl)	1				<b>Region Assignments to Fine Mesh (7D Record)</b>		
<i>IMB2</i>	1 (Refl)	1				<i>Not present since NRASS=0</i>		
<i>JMB1</i>	1 (Refl)	1						
<i>JMB2</i>	1 (Refl)	1						
<i>KMB1</i>	1 (Refl)	1						
<i>KMB2</i>	1 (Refl)	1						
<i>NBS</i>	0	1						
<i>NBCS</i>	0	1						
<i>NIBCS</i>	0	1						
<i>NZWBB</i>	0	0						
<i>NTRIAG</i>	N/A	0						
<i>NRASS</i>	0	0						
<i>NTHPT</i>	N/A	0						
<i>NGOP</i>	Reserved	44						

February 13, 2020

### 3.1.1.2.2.2 NDXSRF Verification

The NDXSRF file is a binary representation of the model's nuclide densities and cross section referencing data. Figure 11 shows the ASCII-formatted version of the NDXSRF file.

```

1 0V NDXSRF*          *      1
2 1D      4      1      4      4      4      3
3 2D ISO1  ISO2  ISO3  ISO4  ISO1  ISO2  ISO3  ISO4
4 0.00000E+00 0.00000E+00 0.00000E+00 0.00000E+00 1.00000E+00 2.00000E+00
5 3.00000E+00 4.00000E+00
6      0      6      1      1      4      0      0      0      1      2      3      4
7      1      2      3      4
8 3D 1.77300E+03 7.47000E+02 1.85400E+03 1.62600E+03 1.00000E+00
9 1.00000E+00 1.00000E+00 1.00000E+00 1.11240E+03 8.13000E+02 8.13000E+02
10      1      1      1      0      1      1      1      3      4      4

```

**Figure 11. ASCII-Formatted NDXSRF File**

Table 36 shows the variables within the NDXSRF file with the expected values and the reported value in the Figure 11 data. The expected values provided in Table 36 were obtained from the model definition information provided in Figure 3 (for the number of zones and subzones), and Table 9 for the volumes. This model information tells us that there are four total zones (COMP1 through COMP4), and three subzones (COMP32, COMP41, and COMP42). The NDXSRF file contains data for the volumes of subzones. Based on lines 15 and 16 of Figure 3, the ratio of the subzone volume to the zone volume should be  $(0.4 + 0.2)$ , or 0.6. Thus, given the volume of COMP 3 is 1854, the COMP32 subzone will have 60% of that volume, or 1112.4 cm<sup>3</sup>. Similarly, COMP41 and COMP42 are both half of COMP4 and thus they should half the volume of COMP4, or 813 cm<sup>3</sup>. These values are included in Table 36.

There is one discrepant value in Table 36 in red text. This is a value for NCL(N) (the nuclide classification). The NDXSRF listing and standard state that the value of NCL(N) will be 1 for fissile, 2 for fertile, 3 for other actinide, 4 for fission product, 5 for structural, 6 for coolant, 7 for control rod, and greater than 7 if undefined. However, the KBR value (isotope classification) of the ISOTXS file uses a value of 0 for an undefined isotope with all others consistent. ISO1 is provided in the ISOTXS file as an “undefined” isotope classification (i.e. a value of 0) as defined in Table 12. This “0” is passed on by DIF3D when writing the NDXSRF file instead of being converted to a value greater than 7, per the standard. The DIF3D code relies upon the user and any upstream data processing software to correctly identify isotopes and therefore DIF3D performs no sanity check on these values. Therefore this is not considered an issue with DIF3D but is noted here for completeness. However, for additional confidence, the values of isotope/nuclide classifiers that have not been tested will be tested explicitly by a later perturbation to this base case.

February 13, 2020

Table 36. Comparison of NDXSFR Values

Variable	Expected Value	DIF3D Value	Variable	Expected Value	DIF3D Value
<b>Specifications (1D Record)</b>			<b>Nucl. Conc. Assignments (3D Record)</b>		
<i>NON</i>	4	4	<i>VOLZ(N)</i>	NZONE Values: 1773, 747, 1854, 1626	1773, 747, 1854, 1626
<i>NSN</i>	1	1	<i>VFPA(N)</i>	NZONE Values: 1, 1, 1, 1	1, 1, 1, 1
<i>NNS</i>	4	4	<i>VLSA(M)</i>	NSZ Values: 1112.4, 813, 813	1112.4, 813, 813
<i>NAN</i>	4	4	<i>NSPA(N)</i>	NZONE Values: 1, 1, 1, 0	1, 1, 1, 0
<i>NZONE</i>	4	4	<i>NSSA(M)</i>	NSZ Values: 1, 1, 1	1, 1, 1
<i>NSZ</i>	3	3	<i>NZSZ(M)</i>	NSZ Values: 3, 4, 4	3, 4, 4
<b>Nucl. Referencing (2D Record)</b>					
<i>HNNAME(N)</i>	NON Values: ISO1, ISO2, ISO3, ISO4	ISO1, ISO2, ISO3, ISO4			
<i>HANAME(N)</i>	NON Values: ISO1, ISO2, ISO3, ISO4	ISO1, ISO2, ISO3, ISO4			
<i>WPF(N)</i>	NON Values: Reserved	0, 0, 0, 0			
<i>ATWT(J)</i>	NAN Values: 1., 2., 3., 4.	1., 2., 3., 4.			
<i>NCLN(N)</i>	NON Values: >7, 6, 1, 1	0, 6, 1, 1			
<i>NDXS(K=1,L)</i>	NSN Values: 4	4			
<i>NDXS(K=2:4,L)</i>	NSN Values: Reserved (3x) NNSxNSN Values:	0, 0, 0			
<i>NOS(I,L)</i>	1, 2, 3, 4 NONxNSN Values:	1, 2, 3, 4			
<i>NOR(N,L)</i>	1, 2, 3, 4	1, 2, 3, 4			

### 3.1.1.2.2.3 ZNATDN Verification

The ZNATDN file is a binary representation of the model's zone and subzone nuclide atomic densities. Figure 12 shows the ASCII-formatted version of the ZNATDN file.

```

1  0V ZNATDN*          *      1
2  1D  0.00000E+00      0      7      4      1
3  2D  1.00000E+00 0.00000E+00 0.00000E+00 0.00000E+00 1.00000E-01
4  0.00000E+00 9.00000E-01 0.00000E+00 2.40000E-01 0.00000E+00 0.00000E+00
5  1.60000E-01 0.00000E+00 0.00000E+00 0.00000E+00 0.00000E+00 0.00000E+00
6  4.00000E-01 6.00000E-01 0.00000E+00 0.00000E+00 0.00000E+00 0.00000E+00
7  2.00000E+00 2.00000E+00 0.00000E+00 0.00000E+00 0.00000E+00

```

**Figure 12. ASCII-Formatted ZNATDN File**

Table 37 shows the variables within the ZNATDN file with the expected values and the reported value in the Figure 12 data. The expected values provided in Table 37 were obtained from the model definition information provided in Figure 3 for the number of zones and subzones and the constituents of each.

The ZNATDN file contains a blocking data structure to compress data as needed. Therefore when creating the expected values for ADEN(N,J), the value of NBLKAD was used from the ZNATDN file to structure the output. This value of NBLKAD is 1, effectively meaning that all zone atomic density data is provided in a flattened 2-D array. Since the subzones will be combined with zones to yield the final primary zones, the ZNATDN file's atomic densities should be the isotopic/material constituents of each zone without any subzone information. This strategy was used to generate the reference values provided in Table 37.

Finally, since this is a DIF3D calculation without REBUS, there is no depletion and thus the reference real time and cycle number are both 0.

As can be seen in Table 37, the ZNATDN file contains no deviations from expectations. Therefore, the ZNATDN file contents are considered verified for this problem.

**Table 37. Comparison of ZNATDN Values**

Variable	Expected Value	DIF3D Value
<b>Specifications (1D Record)</b>		
<i>TIME</i>	0.0	0.0
<i>NCY</i>	0	0
<i>NTZSZ</i>	7	7
<i>NNS</i>	4	4
<i>NBLKAD</i>	?	1
<b>Zone Atomic Densities (2D Record)</b>		
<i>ADEN(N,J=1)</i>	NNS Values: 1.0, 0.0, 0.0, 0.0	1.0, 0.0, 0.0, 0.0
<i>ADEN(N,J=2)</i>	NNS Values: 0.1, 0.0, 0.9, 0.0	0.1, 0.0, 0.9, 0.0
<i>ADEN(N,J=3)</i>	NNS Values: 0.24, 0.0, 0.0, 0.16	0.24, 0.0, 0.0, 0.16
<i>ADEN(N,J=4)</i>	NNS Values: 0.0, 0.0, 0.0, 0.0	0.0, 0.0, 0.0, 0.0
<i>ADEN(N,J=5)</i>	NNS Values: 0.0, 0.4, 0.6, 0.0	0.0, 0.4, 0.6, 0.0
<i>ADEN(N,J=6)</i>	NNS Values: 0.0, 0.0, 0.0, 2.0	0.0, 0.0, 0.0, 2.0
<i>ADEN(N,J=7)</i>	NNS Values: 2.0, 0.0, 0.0, 0.0	2.0, 0.0, 0.0, 0.0

#### 3.1.1.2.2.2.4 COMPXS Verification

The COMPXS file is a binary representation of the model's macroscopic cross sections. Figure 13 shows the ASCII-formatted version of the COMPXS file. The values in this file were directly used to produce the "DIF3D Values" column Table 38 through Table 42. The expected values in these tables are taken directly from Table 23 and Table 26.

February 13, 2020

```

1      4      2      0      3      1      1      0      1      0      0
2  7.73209991455E+01 4.37393000000E+05 2.00000000000E+07 1.00000000000E+00
3  0.00000000000E+00
4      0      0      0      0
5      0      0      0      0      1
6  8.48028957989E-06 1.10683001578E-01 1.00908034165E-03 1.10683001578E-01
7  1.09673999250E-01 1.86566366334E-17 1.00000000000E+00 0.00000000000E+00
8  1.00000000000E+00 0.00000000000E+00 1.00000000000E+00 0.00000000000E+00
9  0.00000000000E+00 0.00000000000E+00
10 1.59999995958E-04 3.63550007343E-01 1.59999995958E-04 3.63550007343E-01
11 3.63389998674E-01 1.00060005207E-03 3.51999982762E-16 1.00000000000E+00
12 0.00000000000E+00 1.00000000000E+00 0.00000000000E+00 1.00000000000E+00
13 0.00000000000E+00 0.00000000000E+00 0.00000000000E+00 0.00000000000E+00
14      1      0      0      0      1
15 1.84854790486E-03 6.02332294135E-01 2.69029076243E-02 3.48384694180E-01
16 9.43559930344E-04 1.88711986069E-03 9.49999988079E-01 5.72729373930E-01
17 3.71066657082E-14 1.00000000000E+00 0.00000000000E+00 1.00000000000E+00
18 0.00000000000E+00 1.00000000000E+00 0.00000000000E+00 1.34999997597E-03
19 2.47130980501E-01
20 6.87939980185E-02 2.30458001500E+00 6.87939980185E-02 1.55471797194E+00
21 4.55687987654E-02 1.13921996913E-01 5.00000007451E-02 2.23578595409E+00
22 2.64043590668E-02 1.65698621043E-12 1.00000000000E+00 0.00000000000E+00
23 1.00000000000E+00 0.00000000000E+00 1.00000000000E+00 0.00000000000E+00
24 0.00000000000E+00 7.49861989422E-01 6.81632985930E-03
25      1      1      0      0      1
26 2.70441834018E-03 6.36375138657E-01 3.25286839077E-02 5.24149210128E-01
27 8.28143991796E-04 1.70135994008E-03 9.72595440483E-01 1.59999992382E-05
28 5.90765763474E-01 4.74637353225E-14 1.00000000000E+00 0.00000000000E+00
29 1.00000000000E+00 0.00000000000E+00 1.00000000000E+00 0.00000000000E+00
30 6.54000035398E-03 1.59999992382E-06 1.09562798851E-01
31 5.16104012949E-02 2.13158688366E+00 5.16264012942E-02 1.82293964465E+00
32 3.37475208242E-02 8.28168035295E-02 2.74045533920E-02 2.07996050334E+00
33 3.66042652197E-02 1.40105119668E-12 1.00000000000E+00 0.00000000000E+00
34 1.00000000000E+00 0.00000000000E+00 1.00000000000E+00 0.00000000000E+00
35 0.00000000000E+00 3.08645615381E-01 2.66298012608E-03
36      1      1      0      0      1
37 1.15332802679E-02 4.46563012898E-01 1.55888802992E-02 3.80020000041E-01
38 2.81700002961E-03 5.91569979353E-03 1.00000000000E+00 9.99999974738E-05
39 4.30974008050E-01 2.00595300063E-13 1.00000000000E+00 0.00000000000E+00
40 1.00000000000E+00 0.00000000000E+00 1.00000000000E+00 0.00000000000E+00
41 0.00000000000E+00 9.99999974738E-06 6.69400021434E-02
42 1.22340003669E-01 9.09830033779E-01 1.22440003666E-01 8.55440020561E-01
43 9.70000028610E-02 2.32800016117E-01 0.00000000000E+00 7.87389993668E-01
44 5.55560004432E-03 4.48993627897E-12 1.00000000000E+00 0.00000000000E+00
45 1.00000000000E+00 0.00000000000E+00 1.00000000000E+00 0.00000000000E+00
46 0.00000000000E+00 5.43799996376E-02-3.97199997678E-04
47 -1.00000000000E+20-1.00000000000E+20-1.00000000000E+20-1.00000000000E+20
48 -1.00000000000E+20-1.00000000000E+20-1.00000000000E+20-1.00000000000E+20

```

Figure 13. ASCII-Formatted COMPXS File

Table 38 provides the comparison data from the COMPXS file strictly for the file's metadata: the overall specifications, the composition-independent data, and the power conversion factors. No deviations were identified.

**Table 38. Comparison of COMPTS Type 01, Type 02, and Type 05 Cards**

Variable	Expected Value	DIF3D Value
<b>Specifications (Type 1)</b>		
<i>NCMP</i>	4	4
<i>NGROUP</i>	2	2
<i>ISCHI</i>	0	0
<i>NFCMP</i>	3	3
<i>MAXUP</i>	1	1
<i>MAXDN</i>	1	1
<i>NFAM</i>	0	0
<i>MAXORD</i>	1	1
<i>NDUM2</i>	Reserved	0
<i>NDUM3</i>	Reserved	0
<b>Composition Indep. Data (Type 2)</b>		
<i>CHI(I, J=:)</i>	Not Present	Not Present
<i>VEL(J)</i>	77.321, 4.37393E5	77.321, 4.37393E5
<i>EMAX(J)</i>	20.0E7, 1.0	20.0E7, 1.0
<i>EMIN</i>	0	0
<i>CHID(J,K=:)</i>	Not Present	Not Present
<i>FLAM(K)</i>	Not Present	Not Present
<i>NKFAM(J)</i>	NCMP Values 0, 0, 0, 0	0, 0, 0, 0
<b>Power Conversion Factors (Type 5)</b>		
<i>FPWS(I)</i>	-1E20, -1E20, -1E20, -1E20	-1E20, -1E20, -1E20, -1E20
<i>CPWS(I)</i>	-1E20, -1E20, -1E20, -1E20	-1E20, -1E20, -1E20, -1E20

The remaining data in the COMPTS file are the composition-specific information. This comparison is provided in Table 39 through Table 42 for compositions COMP1, COMP2, COMP3, and COMP4, respectively. This comparison also includes the relative difference from the expected value for floating point values. All DIF3D values are consistent with expectations.

These tables include an additional XSCADP variable that is not included in the COMPTS listing. This value is the down-scatter; in the COMPTS listing this down-scatter information is included in XSCAJP. For consistency with the naming used in the isotropic component, we rename this XSCADP here instead of including a vector of XSCAJP.



February 13, 2020

Table 39. Comparison of COMP1 from the COMPXS File

Variable	Expected Value	DIF3D Value	Error	Variable	Expected Value	DIF3D Value	Error
<b>COMP1 Specs (Type 4)</b>				<b>COMP1 Group 2 MGXS (Type 4)</b>			
<i>ICHI</i>	0	0		<i>XA</i>	1.60000E-04	1.60000E-04	2.52625E-08
<i>NUP</i>	0, 0	0, 0		<i>XTOT</i>	3.63550E-01	3.63550E-01	2.01980E-08
<i>NDN</i>	0, 1	0, 1		<i>XREM</i>	1.60000E-04	1.60000E-04	2.52625E-08
<i>NUMFAM(I)</i>	Not Present	Not Present		<i>XTR</i>	3.63550E-01	3.63550E-01	2.01980E-08
<b>COMP1 Group 1 MGXS (Type 4)</b>				<i>XF</i>	Not Present	Not Present	
<i>XA</i>	8.48029E-06	8.48029E-06	4.95396E-08	<i>XNF</i>	Not Present	Not Present	
<i>XTOT</i>	1.10683E-01	1.10683E-01	1.42569E-08	<i>CHI(I)</i>	Not Present	Not Present	
<i>XREM</i>	1.00908E-03	1.00908E-03	3.38576E-07	<i>XSCATU</i>	Not Present	Not Present	
<i>XTR</i>	1.10683E-01	1.10683E-01	1.42569E-08	<i>XSCATJ</i>	3.63390E-01	3.63390E-01	3.64897E-09
<i>XF</i>	Not Present	Not Present		<i>XSCATD</i>	1.00060E-03	1.00060E-03	5.20388E-08
<i>XNF</i>	Not Present	Not Present		<i>PC</i>	3.52000E-16	3.52000E-16	4.89716E-08
<i>CHI(I)</i>	Not Present	Not Present		<i>A1 to A3</i>	1.00000E+00	1.00000E+00	0.00000E+00
<i>XSCATU</i>	Not Present	Not Present		<i>B1 to B3</i>	0.00000E+00	0.00000E+00	0.00000E+00
<i>XSCATJ</i>	1.09674E-01	1.09674E-01	6.83845E-09	<i>SNUDEL</i>	Not Present	Not Present	
<i>XSCATD</i>	Not Present	Not Present		<i>XN2N</i>	0.00000E+00	0.00000E+00	0.00000E+00
<i>PC</i>	1.86566E-17	1.86566E-17	1.80450E-07	<i>XSCAUP(I,L)</i>	Not Present	Not Present	
<i>A1 to A3</i>	1.00000E+00	1.00000E+00	0.00000E+00	<i>XSCAJP(L)</i>	0.00000E+00	0.00000E+00	0.00000E+00
<i>B1 to B3</i>	0.00000E+00	0.00000E+00	0.00000E+00	<i>XSCADP(I,L)</i>	0.00000E+00	0.00000E+00	0.00000E+00
<i>SNUDEL</i>	Not Present	Not Present					
<i>XN2N</i>	0.00000E+00	0.00000E+00	0.00000E+00				
<i>XSCAUP(I,L)</i>	Not Present	Not Present					
<i>XSCAJP(L)</i>	0.00000E+00	0.00000E+00	0.00000E+00				
<i>XSCADP(I,L)</i>	Not Present	Not Present					

February 13, 2020

Table 40. Comparison of COMP2 from the COMPXS File

Variable	Expected Value	DIF3D Value	Error	Variable	Expected Value	DIF3D Value	Error
<b>COMP2 Specs (Type 3)</b>				<b>COMP2 Group 2 MGXS (3D Record)</b>			
<i>ICHI</i>	1	1		<i>XA</i>	6.87940E-02	6.87940E-02	2.88034E-08
<i>NUP</i>	0, 0	0, 0		<i>XTOT</i>	2.30458E+00	2.30458E+00	6.50878E-09
<i>NDN</i>	0, 1	0, 1		<i>XREM</i>	6.87940E-02	6.87940E-02	2.88034E-08
<i>NUMFAM(I)</i>	Not Present	Not Present		<i>XTR</i>	1.55472E+00	1.55472E+00	1.80483E-08
<b>COMP2 Group 1 MGXS (3D Record)</b>				<i>XF</i>	4.55688E-02	4.55688E-02	2.70931E-08
<i>XA</i>	1.84855E-03	1.84855E-03	5.14674E-08	<i>XNF</i>	1.13922E-01	1.13922E-01	2.70975E-08
<i>XTOT</i>	6.02332E-01	6.02332E-01	9.73715E-09	<i>CHI(I)</i>	5.00000E-02	5.00000E-02	1.49020E-08
<i>XREM</i>	2.69029E-02	2.69029E-02	8.83064E-08	<i>XSCATU</i>	Not Present	Not Present	
<i>XTR</i>	3.48385E-01	3.48385E-01	1.67057E-08	<i>XSCATJ</i>	2.23579E+00	2.23579E+00	2.05342E-08
<i>XF</i>	9.43560E-04	9.43560E-04	7.38225E-08	<i>XSCATD</i>	2.64044E-02	2.64044E-02	3.53426E-08
<i>XNF</i>	1.88712E-03	1.88712E-03	7.38215E-08	<i>PC</i>	1.65699E-12	1.65699E-12	1.26996E-07
<i>CHI(I)</i>	9.50000E-01	9.50000E-01	1.25484E-08	<i>A1 to A3</i>	1.00000E+00	1.00000E+00	0.00000E+00
<i>XSCATU</i>	Not Present	Not Present		<i>B1 to B3</i>	0.00000E+00	0.00000E+00	0.00000E+00
<i>XSCATJ</i>	5.72729E-01	5.72729E-01	4.55189E-08	<i>SNUDEL</i>	Not Present	Not Present	
<i>XSCATD</i>	Not Present	Not Present		<i>XN2N</i>	0.00000E+00	0.00000E+00	0.00000E+00
<i>PC</i>	3.71067E-14	3.71067E-14	1.15661E-07	<i>XSCAUP(I,L)</i>	Not Present	Not Present	
<i>A1 to A3</i>	1	1.00E+00	0.00000E+00	<i>XSCAJP(L)</i>	7.49862E-01	7.49862E-01	1.41066E-08
<i>B1 to B3</i>	0	0.00E+00	0.00000E+00	<i>XSCADP(I,L)</i>	6.81633E-03	6.81633E-03	2.06416E-08
<i>SNUDEL</i>	Not Present	Not Present					
<i>XN2N</i>	1.35000E-03	1.35000E-03	1.78000E-08				
<i>XSCAUP(I,L)</i>	Not Present	Not Present					
<i>XSCAJP(L)</i>	2.47131E-01	2.47131E-01	7.89015E-08				
<i>XSCADP(I,L)</i>	Not Present	Not Present					

February 13, 2020

Table 41. Comparison of COMP3 from the COMPXS File

Variable	Expected Value	DIF3D Value	Error	Variable	Expected Value	DIF3D Value	Error
<b>COMP3 Specs (Type 3)</b>				<b>COMP3 Group 2 MGXS (Type 4)</b>			
<i>ICHI</i>	1	1		<i>XA</i>	5.16104E-02	5.16104E-02	2.50899E-08
<i>NUP</i>	1, 0	1, 0		<i>XTOT</i>	2.13159E+00	2.13159E+00	5.45791E-08
<i>NDN</i>	0, 1	0, 1		<i>XREM</i>	5.16264E-02	5.16264E-02	2.50686E-08
<i>NUMFAM(I)</i>	Not Present	Not Present		<i>XTR</i>	1.82294E+00	1.82294E+00	1.94932E-07
<b>COMP3 Group 1 MGXS (Type 4)</b>				<i>XF</i>	3.37475E-02	3.37475E-02	2.44225E-08
<i>XA</i>	2.70442E-03	2.70442E-03	1.25787E-07	<i>XNF</i>	8.28168E-02	8.28168E-02	4.26182E-08
<i>XTOT</i>	6.36375E-01	6.36375E-01	6.07456E-08	<i>CHI(I)</i>	2.74046E-02	2.74046E-02	1.23775E-07
<i>XREM</i>	3.25287E-02	3.25287E-02	1.20131E-07	<i>XSCATU</i>	Not Present	Not Present	
<i>XTR</i>	5.24149E-01	5.24149E-01	1.93227E-08	<i>XSCATJ</i>	2.07996E+00	2.07996E+00	2.41995E-07
<i>XF</i>	8.28144E-04	8.28144E-04	9.90649E-09	<i>XSCATD</i>	3.66043E-02	3.66043E-02	1.42598E-07
<i>XNF</i>	1.70136E-03	1.70136E-03	3.52189E-08	<i>PC</i>	1.40105E-12	1.40105E-12	1.40380E-07
<i>CHI(I)</i>	9.72595E-01	9.72595E-01	4.16237E-08	<i>A1 to A3</i>	1.00000E+00	1.00000E+00	0.00000E+00
<i>XSCATU</i>	1.60000E-05	1.60000E-05	4.76125E-08	<i>B1 to B3</i>	0.00000E+00	0.00000E+00	0.00000E+00
<i>XSCATJ</i>	5.90766E-01	5.90766E-01	6.18282E-08	<i>SNUDEL</i>	Not Present	Not Present	
<i>XSCATD</i>	Not Present	Not Present		<i>XN2N</i>	0.00000E+00	0.00000E+00	0.00000E+00
<i>PC</i>	4.74637E-14	4.74637E-14	9.85489E-08	<i>XSCAUP(I,L)</i>	Not Present	Not Present	
<i>A1 to A3</i>	1.00000E+00	1.00000E+00	0.00000E+00	<i>XSCAJP(L)</i>	3.08646E-01	3.08646E-01	4.98339E-08
<i>B1 to B3</i>	0.00000E+00	0.00000E+00	0.00000E+00	<i>XSCADP(I,L)</i>	2.66298E-03	2.66298E-03	4.73455E-08
<i>SNUDEL</i>	Not Present	Not Present					
<i>XN2N</i>	6.54000E-03	6.54000E-03	5.41254E-08				
<i>XSCAUP(I,L)</i>	1.60000E-06	1.60000E-06	4.76125E-08				
<i>XSCAJP(L)</i>	1.09563E-01	1.09563E-01	1.04871E-08				
<i>XSCADP(I,L)</i>	Not Present	Not Present					

February 13, 2020

Table 42. Comparison of COMP4 from the COMPXS File

Variable	Expected Value	DIF3D Value	Error	Variable	Expected Value	DIF3D Value	Error
<b>COMP4 Specs (Type 3)</b>				<b>COMP4 Group 2 MGXS (Type 4)</b>			
<i>ICHI</i>	1	1		<i>XA</i>	1.22340E-01	1.22340E-01	2.99902E-08
<i>NUP</i>	1, 0	1, 0		<i>XTOT</i>	9.09830E-01	9.09830E-01	3.71267E-08
<i>NDN</i>	0, 1	0, 1		<i>XREM</i>	1.22440E-01	1.22440E-01	2.99412E-08
<i>NUMFAM(I)</i>	Not Present	Not Present		<i>XTR</i>	8.55440E-01	8.55440E-01	2.40356E-08
<b>COMP4 Group 1 MGXS (Type 4)</b>				<i>XF</i>	9.70000E-02	9.70000E-02	2.94948E-08
<i>XA</i>	1.15333E-02	1.15333E-02	2.32284E-08	<i>XNF</i>	2.32800E-01	2.32800E-01	6.92311E-08
<i>XTOT</i>	4.46563E-01	4.46563E-01	2.88828E-08	<i>CHI(I)</i>	0.00000E+00	0.00000E+00	0.00000E+00
<i>XREM</i>	1.55889E-02	1.55889E-02	1.91932E-08	<i>XSCATU</i>	Not Present	Not Present	
<i>XTR</i>	3.80020E-01	3.80020E-01	1.07889E-10	<i>XSCATJ</i>	7.87390E-01	7.87390E-01	8.04176E-09
<i>XF</i>	2.81700E-03	2.81700E-03	1.05112E-08	<i>XSCATD</i>	5.55560E-03	5.55560E-03	7.97754E-09
<i>XNF</i>	5.91570E-03	5.91570E-03	3.49020E-08	<i>PC</i>	4.48994E-12	4.48994E-12	6.21323E-08
<i>CHI(I)</i>	1.00000E+00	1.00000E+00	0.00000E+00	<i>A1 to A3</i>	1.00000E+00	1.00000E+00	0.00000E+00
<i>XSCATU</i>	1.00000E-04	1.00000E-04	2.52620E-08	<i>B1 to B3</i>	0.00000E+00	0.00000E+00	0.00000E+00
<i>XSCATJ</i>	4.30974E-01	4.30974E-01	1.86786E-08	<i>SNUDEL</i>	Not Present	Not Present	
<i>XSCATD</i>	Not Present	Not Present		<i>XN2N</i>	0.00000E+00	0.00000E+00	0.00000E+00
<i>PC</i>	2.00595E-13	2.00595E-13	3.14065E-10	<i>XSCAUP(I,L)</i>	Not Present	Not Present	
<i>A1 to A3</i>	1.00000E+00	1.00000E+00	0.00000E+00	<i>XSCAJP(L)</i>	5.43800E-02	5.43800E-02	6.66421E-09
<i>B1 to B3</i>	0.00000E+00	0.00000E+00	0.00000E+00	<i>XSCADP(I,L)</i>	-3.97200E-04	-3.97200E-04	2.32200E-12
<i>SNUDEL</i>	Not Present	Not Present					
<i>XN2N</i>	0.00000E+00	0.00000E+00	0.00000E+00				
<i>XSCAUP(I,L)</i>	1.00000E-05	1.00000E-05	2.52620E-08				
<i>XSCAJP(L)</i>	6.69400E-02	6.69400E-02	3.20197E-08				
<i>XSCADP(I,L)</i>	Not Present	Not Present					

### 3.1.1.2.2.2.5 LABELS Verification

The LABELS file is a binary representation of the model's region and composition labels, area data, half heights, nuclide set labels, alias zone labels, control rod model data, and burnup-dependent cross section data. Figure 14 shows the ASCII-formatted version of the LABELS file. It should be noted that modern text readers claim that not all characters in the file outputted from the CCCC\_convert.x program are representable in Hexadecimal, and thus they need to be viewed with UTF-8 formatting. This was done to create the image in Figure 14. This seems to be coming from the Hollerith user identification (HUSE(I)) entry in the file identification record. In addition to this relatively minor error, some remaining errors are evident based upon comparing Figure 14 to the listing of LABELS distributed with the ARC software source code:

1. The file outputted by CCCC\_convert.x raises an error in modern graphical text editors stating that not all characters “are representable in hexadecimal” and thus they need to be viewed with UTF-8 formatting. This seems to be isolated to the Hollerith user identification value on line 1, which is displayed as “^@^@^@^@^@^@^@^@” on older editors such as VIM and Nano.
2. The file identification card on line 1 should begin with “ 0V LABELS” versus “ 1D LABELS”
3. The 1D record on line 2 is not part of the standard
4. The 2D record beginning on line 3 should be a 1D record
5. The 3D record beginning on line 6 should be a 2D record
6. The 3D record beginning on line 8 should be a continuation of the line 6 2D record.

While none of these errors seem to affect the values in the record (the main product to be verified), the ASCII version of the LABELS file in Figure 14 produced by CCCC\_convert.x cannot be relied upon for verification. Instead, a minimal python program will be written which aims to pull out the expected information from the LABELS file. Further, another ARC utility program, “CCCC\_PrintTables\_v11.0\_r3012\_d2019\_03\_14.x” will be used to output the LABELS file into a human-readable format to add confidence in the python script.

The output from CCCC\_PrintTables is shown in Figure 15; note that extra whitespace and generic header output information were removed from this snippet as well as line breaks inserted in three locations to ensure the output was still readable. The locations where line breaks were inserted are highlighted with the text “[! line break inserted]”. The custom python script is named “read\_LABELs.py”. The output from this script is shown in Figure 16.

Based on the above, the LABELS file contents are considered verified for this problem; a later case will explore more of the LABELS file as control rods are modeled.

February 13, 2020

```

1 1D LABELS
2 1D      1
3 2D      7      8      3      9      0      0      0      0      6      0
4      0      0      0      0      0      0      0      0      0      0
5      0      0      0      0
6 3D COMP1 COMP2 COMP3 COMP4 COMP32 COMP41 COMP42 REG1 REG2 REG3
7 REG4 REG5 REG6 REG7 REG8 AREA1 AREA2 AREA3
8 3D      2      1      8      2      2      7      2      3      6

```

Figure 14. ASCII-Formatted LABELS File

```

12 [LABELS]...NUMBER OF ZONES AND SUBZONES..... 7
13 [LABELS]...NUMBER OF REGIONS..... 8
14 [LABELS]...NUMBER OF AREAS..... 3
15 [LABELS]...LENGTH OF NRA ARRAY..... 9
16 [LABELS]...NUMBER OF HALF-HEIGHT AND EXTPOL. DIST. SPECS D=1..... 0
17 [LABELS]...NUMBER OF HALF-HEIGHT AND EXTPOL. DIST. SPECS D=2..... 0
18 [LABELS]...NUMBER OF NUCLIDE SETS..... 0
19 [LABELS]...LENGTH OF ALIAS ARRAY..... 0
20 [LABELS]...NO. OF TRIANGLES PER HEX FOR TRIANGULAR GEOMETRIES..... 6
21 [LABELS]...MAX. NO. OF RINGS OF HEXAGONS FOR TRIANGULAR GEOMETRIES... 0
22 [LABELS]...NO. OF CONTROL-ROD CHANNELS IN THE MODEL..... 0
23 [LABELS]...NO. OF CONTROL-ROD BANKS..... 0
24 [LABELS]...ORIGINAL NO. OF FINE MESH INTERVALS IN AXIAL DIMENSION.... 0
25 [LABELS]...MAXIMUM TIME..... 0
26 [LABELS]...MAXIMUM NUMBER OF CONTROL RODS..... 0
27 [LABELS]...MAXIMUM NUMBER OF MESHES..... 0
28 [LABELS]...MAXIMUM NUMBER OF CONTROL ROD PIECES..... 0
29 [LABELS]...MAXIMUM NUMBER OF CONTROL ROD CHANNELS?..... 0
30 [LABELS]...NUMBER OF BURNUP DEPENDENT ISOTOPES..... 0
31 [LABELS]...MAXIMUM NUMBER OF BURNUP DEPENDENT GROUPS..... 0
32 [LABELS]...HIGHEST ORDER POLYNOMIAL FIT..... 0
33 [LABELS]...DIMENSIONS? 1 OR 2..... 0
34 [LABELS]...COMPOSITION NAMES.....
35 [LABELS]...[ 1,COMP1 ][ 2,COMP2 ][ 3,COMP3 ][ 4,COMP4 ]
36 [! line break inserted] [ 5,COMP32 ][ 6,COMP41 ][ 7,COMP42 ]
37 [LABELS]...REGION NAMES.....
38 [LABELS]...[ 1,REG1 ][ 2,REG2 ][ 3,REG3 ][ 4,REG4 ]
39 [! line break inserted] [ 5,REG5 ][ 6,REG6 ][ 7,REG7 ]
40 [LABELS]...[ 8,REG8 ][
41 [LABELS]...AREA NAMES.....
42 [LABELS]...[ 1,AREA1 ][ 2,AREA2 ][ 3,AREA3 ][
43 [LABELS]...REGIONS FOR AREA..... 1
44 [LABELS]...[ 1,REG1 ][ 2,REG8 ][
45 [LABELS]...REGIONS FOR AREA..... 2
46 [LABELS]...[ 1,REG2 ][ 2,REG7 ][
47 [LABELS]...REGIONS FOR AREA..... 3
48 [LABELS]...[ 1,REG3 ][ 2,REG6 ][

```

Figure 15. Condensed LABELS Output From CCCC\_PrintTables

February 13, 2020

```

1
2 Record Padding: b''\x00\x00\x00\xb4\x00\x00\x00'
3
4 1D RECORD
5 *****
6 NTZSZ  NREG  NAREA  LREGA  NHTS1  NHTS2  NSETS  NALIAS  NTRI  NRING
7 7      8      3      9      0      0      0      0      6      0
8 NCHAN  NBANKS LINTAX MAXTIM MAXROD MAXMSH MAXLRD MAXLCH NVARY  MAXBRN
9 0      0      0      0      0      0      0      0      0      0
10 MAXORD ND      IDUM1  IDUM2
11 0      0      0      0
12 1D END
13 *****
14
15 2D RECORD
16 *****
17 CMPNAM ['COMP1', 'COMP2', 'COMP3', 'COMP4', 'COMP32', 'COMP41', 'COMP42']
18 REGNAM [2, 1, 8, 2, 2, 7, 2, 3, 6]
19 ARANAM ['AREA1', 'AREA2', 'AREA3']
20 NRA [2, 1, 8, 2, 2, 7, 2, 3, 6]
21 2D END
22 *****
23
24 Remaining data in the file: b'\xb4\x00\x00\x00'

```

**Figure 16. Python-Extracted LABELS Information**

Since a comparison of Figure 15 and Figure 16 shows the same values for the same physical items, it can be said that the Python script is confidently extracting the correct information from the LABELS file.

Table 43 shows the variables within the LABELS file with the expected values and the reported value in the Figure 11 data. The expected values provided in Table 43 were obtained from the model definition information provided earlier in Figure 2 and Figure 3. The DIF3D data was obtained from the outputted Python script's outputted data shown in Figure 16.

Like other data comparison tables, the values highlighted in red are those with discrepancies that require explanation, if not identification as a problem. These discrepancies are as follows:

1. NTRI (number of triangles per hex): The expected value of this value is listed as “not applicable” simply because the LABELS specification does not state what the default value is. The DIF3D value, 6, is derived from the default inputted value on card 29 in A.NIP3. Since this is not a hexagonal geometry problem, no card type 29 data is provided, yet the auto-initialization internal to DIF3D fills the value with 6. This difference is not important.
2. LINTAX (original number of fine mesh intervals in the axial dimension): This is a minor discrepancy included here only to highlight a weakness in the documentation of the LABELS file. Specifically, the LINTAX parameter is explained as the “original number of fine mesh intervals in the axial dimension” in the LABELS listing distributed with the ARC suite. The number of fine mesh intervals in the axial dimension is 17 per Table 11 so this

February 13, 2020

is the source of the expected value in Table 43. However, the value reported by DIF3D is 0. When inspecting the GNIP4C module source code (src\_G4CH4C/gnip4c.F), it was identified that the function which populated the LINTAX variable, “wrrods”, is not called unless a moveable control device is specified in the Type 44 card of the A.NIP3 input block. Therefore, this LINTAX description should more accurately refer to the original number of fine mesh intervals for a moving control rod model. This again is not a bug, just a failure in the LABELS specification.

Table 43. Comparison of LABELS Values

Variable	Expected Value	DIF3D Value	Variable	Expected Value	DIF3D Value
<b>Specifications (1D Record)</b>			<b>Label and Area Data (2D Record)</b>		
NTZSZ	7	7	CMPNAM(I)	NTZSZ Values: COMP1, COMP2, COMP3, COMP4, COMP32, COMP41, COMP42	COMP1, COMP2, COMP3, COMP4, COMP32, COMP41, COMP42
NREG	8	8	REGNAM(I)	NREG Values: REG1, REG2, REG3, REG4, REG5, REG6, REG7, REG8	REG1, REG2, REG3, REG4, REG5, REG6, REG7, REG8
NAREA	3	3	ARANAM(I)	NAREA Values: AREA1, AREA2, AREA2	AREA1, AREA2, AREA2
LREGA	9	9	NRA(I)	LREGA Values: 2, 1, 8, 2, 2, 7, 2, 3, 6	2, 1, 8, 2, 2, 7, 2, 3, 6
NHTS1	0	0	<b>Finite-Geom. Transv. Dist. (3D Record)</b>		
NHTS2	0	0	Not present since NHST1 and NHST2 are 0		
NSETS	1	0	<b>Nuclide Set Labels (4D Record)</b>		
NALLAS	0	0	Not present since NSETS is 1		
NTRI	N/A	6	<b>Alias Zone Labels (5D Record)</b>		
NRING	0	0	Not present since NALLAS is 0		
NCHAN	0	0	<b>General CR Model Data (6D Record)</b>		
NBANKS	0	0	Not present since NBANKS is 0		
LINTAX	17	0	<b>CR Bank Data (7D Record)</b>		
MAXTIM	0	0	Not present since NBANKS is 0		
MAXROD	0	0	<b>CR Channel Data (8D Record)</b>		
MAXMSH	0	0	Not present since NBANKS is 0		
MAXLRD	0	0	<b>Burnup-Dependent XS (9D Record)</b>		
MAXLCH	0	0	Not present since NVARY is 0		
NVARY	0	0	<b>Burnup-Dependent Groups (10D Record)</b>		
MAXBRN	0	0	Not present since MAXBRN is 0		
MAXORD	0	0			
ND	2	0			
IDUM(1)	Reserved	0			
IDUM(2)	Reserved	0			



### 3.1.1.2.3 Macroscopic XS ISOTXS Case

The DIF3D input for the Macroscopic XS ISOTXS case is the same as defined in the previous base case (the Microscopic XS ISOTXS case) except here the ISOBCD data set from Figure 4 is replaced with the ISOBCD data set from Figure 5. Per Table 15, the differences between the Macroscopic XS ISOTXS file and the Microscopic XS ISOTXS file are limited to the number of total and transport moments and that the elastic and inelastic data are combined into the same scattering matrix in the Macroscopic XS ISOTXS format. Since the Macroscopic ISOTXS file of Figure 5 contains the same total scattering matrix as that of the Microscopic ISOTXS in Figure 4, the vast majority of the standard output, auxiliary output, and binary files should be the same. The verification evaluation for this case will therefore be limited to using a tool wrapping the Python diffliib package to highlight any differences and to ensure those differences are expected.

This input was executed on the KOOKIE cluster with the DIF3D executable located at /software/ARC/dif3d\_v11.0\_r3012\_d2019\_03\_14\_512GB.x. The output to screen (i.e., standard output) was redirected to a text file; this and all other output files from this run are stored in an isolated directory. The binary files are converted to ASCII as was performed above before utilizing the diffliib package.

#### 3.1.1.2.3.1 Standard Output Edit Verification

This section will progress through the differences in the DIF3D standard output file compared to the base case discussed in the previous section. The differences will be discussed with the goal of showing that the change in the ISOTXS format type does not introduce any additional issues in the execution of DIF3D.

The majority of differences in the input are limited to the differences in the repeat of the input file, the title prints, and prints of the words used for processing data. Since the input file changed, the title (from type 01 cards of the A.HMG4C, A.NIP3, and A.DIF3D blocks), and the ISOTXS file sizes changed, these are all to be expected.

The first and only meaningful difference to discuss is on line 1097 of the standard output. Here, the elastic scattering cross section for the ISO3 nuclide's isotropic self-scattering in group 1 is listed as 6.21180E-01 barns. The same value for the reference base case is 6.19680E-01 b. The remaining elastic scattering cross section values are the same. However, as shown in Table 15, the Macroscopic XS format merges the elastic and inelastic scattering data. When the  $1.5 \times 10^{-3}$  b from the base case inelastic scattering cross section, the value of 0.621180 is produced as expected. No inelastic data is present in the Macroscopic XS format, which is also to be expected as this data is not present in the ISOTXS file.

The change to the cross section file format type had no impact upon the geometry and macroscopic composition outputs.

#### *3.1.1.2.3.2 Auxiliary Output Verification*

The differences in the auxiliary output are the same as those discussed for the standard output, including the ISO3 self-scattering cross section in group 1.

#### *3.1.1.2.3.3 Binary Output Verification*

The final set of outputs to verify are the CCCC-formatted [8] and ANL-specific binary output files relating to the model definition (i.e., GEODST, NDXSRF, ZNATDN, COMPXS, and LABELS). Like the previous case, the binary files that will be evaluated will be first converted to an ASCII format with the “/software/ARC/CCCC\_convert\_v11.0\_r3012\_d2019\_03\_14.x” executable that is distributed with the ARC suite.

These binary files will only be inspected for differences with their equivalent files from the base case. Finally, the GEODST, NDXSRF, ZNATDN, COMPXS, and LABELS outputs will be verified to be consistent with expectations compared to the values from the base case already discussed.

The GEODST, NDXSRF, ZNATDN, and LABELS files contain no differences from the reference case, as expected, since no geometry or atom density information was changed by simply modifying the ISOTXS file. Further, since the COMPXS file only contains the total scattering matrix and does not discriminate between elastic and inelastic data, the COMPXS has also not changed.

#### *3.1.1.2.4 GAMISO XS ISOTXS Case*

The DIF3D input for the GAMISO XS ISOTXS case is the same as defined in the previous base case (the Microscopic XS ISOTXS case) except here the ISOTXS data from Figure 4 is replaced with the data from Figure 6. Per Table 15, the differences between the GAMISO XS ISOTXS file and the Microscopic XS ISOTXS file is that there is neither an inelastic scattering matrix or (n,2n) reaction channel (principal or matrix) in the GAMISO XS ISOTXS file. Therefore, it is expected that the differences between the base case and the GAMISO XS ISOTXS case should be limited to the reported scattering matrices, removal cross section, and (n,2n) principal cross section in the standard output, auxiliary output and COMPXS binary output. Additionally, since the cross section values are changing, the actual calculated eigenvalue and flux distributions will also be different; however those quantities will not be verified in this section and so those differences will not be explored rigorously.

The verification evaluation for this case will therefore be limited to using a tool wrapping the Python diffliB package to highlight any differences and to ensure those differences match the previously discussed expectations.

This input was executed on the KOOKIE cluster with the DIF3D executable located at /software/ARC/dif3d\_v11.0\_r3012\_d2019\_03\_14\_512GB.x. The output to screen (i.e., standard output) was redirected to a text file; this and all other output files from this run are stored in an

isolated directory. The binary files will be first converted to ASCII as was performed above before utilizing the difflib package.

#### *3.1.1.2.4.1 Standard Output Edit Verification*

This section will progress through the differences in the DIF3D standard output file from this case compared to the base case discussed in the previous section. The differences will be discussed with the goal of showing that the change in ISOTXS format type does not introduce any additional issues in the execution of DIF3D.

The majority of differences in the input are limited to the differences in the repeat of the input file, the title prints, and prints of the words used for processing data. Since the input file changed, the title (from type 01 cards of the A.HMG4C, A.NIP3, and A.DIF3D blocks), and the ISOTXS file sizes changed, these are all to be expected.

The isotopic cross section edits begin in line 860 of the standard output file. The GAMISO file lacks a printing of data for any scattering aside from the elastic scattering, as expected. The first numerical difference between the GAMISO and base cases is found in the edit of the ISO2 data where the (n,2n) principal cross section has a value of 0.0. This again is expected since the GAMISO format specifically excludes (n,2n) data as shown in Table 15. Additionally, the ISO2 group 1 elastic self-scattering value is 1.17638 b whereas in the base case it is 1.15138 b. This is exactly as expected based upon the ISOTXS file shown in Figure 6. Here the 1.17638 b value is used for the (n,2n) reaction to maintain the same total scattering matrix as the base case when (n,2n) data is not available. The same is true for the ISO3 and ISO4 data with each manually verified to contain the same scattering data as provided in Figure 6.

Line 1101 of the GAMISO case standard output file begins the composition cross section edits. Before discussing any differences, Table 44 provides a comparison of the fast group removal, (n,2n) and total scattering fast group self-scattering macroscopic cross sections for both the base case (from Table 23 and Table 26) and the GAMISO case using the data in Figure 6. Since the (n,2n) and inelastic scattering channels contained no data for group 2, the base case and GAMISO ISOTXS cases are the same for group 2 and thus no group 2 values are provided in Table 44. The data are computed with the macroscopic cross section equations provided during the base case discussion.

**Table 44. Comparison of Hand-Calculated Cross Sections for Base and GAMISO Cases**

Composition	Value [1/cm]	Base Case	GAMISO	Composition	Value [1/cm]	Base Case	GAMISO
COMP1	$\Sigma_{\text{removal},1}$	1.009080E-03	1.009080E-03	COMP3	$\Sigma_{\text{removal},1}$	3.252868E-02	3.930868E-02
	$\Sigma_{(n,2n),1}$	0.000000E+00	0.000000E+00		$\Sigma_{(n,2n),1}$	6.540000E-03	0.000000E+00
	$\Sigma_{\text{scatter}, 1 \rightarrow 1}$	1.096740E-01	1.096740E-01		$\Sigma_{\text{scatter}, 1 \rightarrow 1}$	5.907658E-01	5.839858E-01
COMP2	$\Sigma_{\text{removal},1}$	2.690291E-02	2.825291E-02	COMP4	$\Sigma_{\text{removal},1}$	1.558888E-02	1.708888E-02
	$\Sigma_{(n,2n),1}$	1.350000E-03	0.000000E+00		$\Sigma_{(n,2n),1}$	0.000000E+00	0.000000E+00
	$\Sigma_{\text{scatter}, 1 \rightarrow 1}$	5.727294E-01	5.713794E-01		$\Sigma_{\text{scatter}, 1 \rightarrow 1}$	4.309740E-01	4.294740E-01

These composition cross section edits are reported in lines 1101 through 1195 of the GAMISO case's standard output file. In this block it was verified that 1) only the values above changed when comparing the base case to the GAMISO case, and 2) the values in the GAMISO case were consistent (to all digits shown) with the data in Table 44.

The next block of output with significant differences is the edit of the COMPXS file provided in lines 1624 through 1682 of the GAMISO case's standard output file. The values in these lines contain the removal and scattering matrix data within Table 44 and therefore those differences, and only those differences, are expected. In this block it was also verified that 1) only the values above changed when comparing the base case to the GAMISO case, and 2) the values in the GAMISO case were consistent (to all digits shown) with the data in Table 44.

The output after line 1682 is related to the DIF3D solution of the given problem. While the accuracy of the solution is not the focus of this section for the verification, it is noted that the GAMISO solution is different than the base case where as the Microscopic XS case had the same solution. This is as expected since the GAMISO case has a different removal cross section and total scattering matrix, whereas the Microscopic XS case did not.

#### 3.1.1.2.4.2 Auxiliary Output Verification

The differences in the auxiliary output are the same as those discussed for the standard output, the values shown in Table 44.

#### 3.1.1.2.4.3 Binary Output Verification

This subsection will evaluate the GEODST, NDXSRF, ZNATDN, COMPXS, and LABELS binary files for accuracy. Similar to the previous files, the differences between the GAMISO case outputs and the base case outputs will be evaluated.

The GEODST, NDXSRF, ZNATDN, and LABELS files contains no differences from the reference case, as expected since no geometry or atom density information was changed by simply modifying the ISOTXS file. The COMPXS file contains differences; every single difference was a difference consistent with the expected differences found in Table 44.

### 3.1.1.2.5 User-Defined Style 1 XS ISOTXS Case

The DIF3D input for the User-Defined Style 1 XS case (referred to hereafter as the User 1 case) is the same as the base case except the ISOTXS data from Figure 4 is replaced with the data from Figure 7. Per Table 15, the differences between the User 1 ISOTXS file and the Microscopic XS ISOTXS file are that there are only isotropic total and transport cross sections in the User 1 style, only a total scattering matrix is provided, and the ISO3 isotope uses a file-wide chi vector.

It is therefore expected that the reported scattering matrices and Chi values should vary in the output. In addition to expecting these values with the isotopic output, the user file includes (n,2n) principal cross sections but no (n,2n) matrix; per the  $\sigma_{out-scatter,g,i}$  equation provided in the base case section, the calculation methodology depends on the presence of this matrix or not. Using the equations from the base case section, the values that will change are shown in Table 45. Finally, it is expected that all values for the fission energy spectrum (chi) should be 0.95 for the fast group and 0.05 for the thermal group, consistent with the set-wide chi vector used for all fissionable compositions. This is because this case (and the base case) use the default value for the “prompt fission spectrum option flag” in the Type 02 card of the A.HMG4C block; this option will use the set fission vector instead of computing one based upon the isotopic data.

**Table 45. Comparison of Hand-Calculated Cross Sections for Base and User 1 Cases**

Composition	Value [1/cm]	Base Case	User 1	Composition	Value [1/cm]	Base Case	User 1
COMP1	$\Sigma_{removal,1}$	1.009080E-03	1.009080E-03	COMP3	$\Sigma_{removal,1}$	3.252868E-02	3.276868E-02
	$\Sigma_{(n,2n),1}$	0.000000E+00	0.000000E+00		$\Sigma_{(n,2n),1}$	6.540000E-03	6.540000E-03
	$\Sigma_{scatter, 1 \rightarrow 1}$	1.096740E-01	1.096740E-01		$\Sigma_{scatter, 1 \rightarrow 1}$	5.907658E-01	5.834458E-01
COMP2	$\Sigma_{removal,1}$	2.690291E-02	2.690291E-02	COMP4	$\Sigma_{removal,1}$	1.558888E-02	1.708888E-02
	$\Sigma_{(n,2n),1}$	1.350000E-03	1.350000E-03		$\Sigma_{(n,2n),1}$	0.000000E+00	0.000000E+00
	$\Sigma_{scatter, 1 \rightarrow 1}$	5.727294E-01	5.700294E-01		$\Sigma_{scatter, 1 \rightarrow 1}$	4.309740E-01	4.294740E-01

Like the previous cases, the verification evaluation for this case will therefore be limited to using a tool wrapping the Python diffliB package to highlight any differences and to ensure those differences match the previously discussed expectations.

During execution, the output to screen (i.e., standard output) was redirected to a text file; this and all other output files from this run are stored in an isolated directory. The binary files will be first converted to ASCII as was performed above before utilizing the diffliB package.

#### 3.1.1.2.5.1 Standard Output Edit Verification

This section will progress through the differences in the DIF3D standard output file from this case compared to the base case discussed in the previous section. The differences will be discussed with the goal of showing that the change in ISOTXS format type does not introduce any additional issues in the execution of DIF3D.

February 13, 2020

---

The majority of differences in the input are limited to the differences in the repeat of the input file, the title prints, and prints of the words used for processing data. Since the input file changed, the title (from Type 01 cards of the A.HMG4C, A.NIP3, and A.DIF3D blocks), and the ISOTXS file sizes changed, these are all to be expected.

The isotopic cross section edits begin in line 889 of the standard output file. The User 1 output file lacks a printing of data for any scattering aside from the total scattering, as expected. The first numerical difference between the User 1 and base cases is found in the edit of the ISO2 data. Here, the total scattering cross section for the ISO2 nuclide's isotropic self-scattering in group 1 is listed as 1.17638 barns. The same value for the reference base case is 1.15138 barns. The remaining scattering cross section values are the same. This difference is because the base case contains an additional (n,2n) scattering matrix; including the 2.5E-2 b from the base case's (n,2n) scattering cross section, the value of 1.17638 b is as expected.

Next, line 1003 begins the reporting of data for ISO3; the differences in this area are limited to the value of the fission energy spectra ("Chi") and the total scattering matrix cross section.

The value of chi for the User 1 case is reported as zeroes in the fast and thermal energy groups as opposed to a value of 0.95 and 0.05, respectively, for the base case. Since the User 1 cases applies a file-wide Chi value for ISO3 (and only ISO3), this explains why no Chi value is present for this and only this isotope.

The total scattering data for ISO3 is similar to that observed for ISO2: when incorporating the inelastic and (n,2n) contributions in the base case, both the base case and User 1 values match.

The data for isotope ISO4 is reported beginning on line 1063 of the User 1 standard output file. The only differences here are related again to the total scattering data; like the previous two isotopes, when including the inelastic and (n,2n) data from the base case, the values match.

Before leaving the isotopic data edits, the User 1 output has an additional output not present in the base case: an edit of the "Prompt Fission Spectrum (Set Chi Vector)" with values of 0.95 and 0.05 for the fast and thermal groups, respectively. These values are the same as used in the Figure 7 ISOTXS file and since the base case did not use a set-wide chi vector, it is expected that the User 1 output would include this data and the base case would not.

The next set of data is the edit of the COMPXS file. This set begins with the prompt fission spectrum again being printed in the User 1 case output but not the base case output. The set chi values are the ones expected. The remaining COMPXS edited data should be consistent with the base case unless explicitly pre-computed in Table 45 or the values of chi for fissionable compositions. This was verified for every reported value to all reported digits and it was found that all values are as expected.



The same data is repeated again beginning on line 1628 of the user 1 standard output. Like before, all values were verified to match Table 45, the set values of chi, or the base case to all digits. All values are as expected.

The output after line 1687 is related to the DIF3D solution of the given problem. While the accuracy of the solution is not the focus of this section for the verification, it is noted that the User 1 solution is different than the base case where the Microscopic XS test case had the same solution. This is as expected since the GAMISO case has a different removal cross section and total scattering matrix, whereas the Microscopic XS case did not.

#### *3.1.1.2.5.2 Auxiliary Output Verification*

The differences in the auxiliary output are the same as those discussed for the standard output.

#### *3.1.1.2.5.3 Binary Output Verification*

This subsection will evaluate the GEODST, NDXSRF, ZNATDN, COMPXS, and LABELS binary files for accuracy. Similar to the previous files, the differences between the GAMISO case outputs and the base case outputs will be evaluated.

The GEODST, NDXSRF, ZNATDN, and LABELS files contains no differences from the reference case, as expected since no geometry or atom density information was changed with the modification of the ISOTXS data.

The COMPXS file contains differences; each was consistent with the expected differences found in Table 45 or to use the expected set wide chi values.

#### *3.1.1.2.6 User-Defined Style 2 XS ISOTXS Case*

The second user-defined style (referred to as the User 2 case) is the same as the first except all Legendre orders of the scattering matrix are combined into one block as stated in Table 15. This difference is purely semantical and therefore the output from the User 2 case should be the exact same as for the User 1 case except for the repeat of the ISOTXS file in the initial input echo.

This was explicitly verified to be true for the standard and auxiliary outputs as well as the binary files. No deficiencies were noted. However, one difference was noted: the ISOTXS edits in the standard and auxiliary output files provided for the User 2 case only printed the first order scattering matrix even though it had data for the higher order terms. The User 1 case, with the same data, did print these higher order matrices. This discrepancy did not propagate to the solution and therefore has no impact on the accuracy of DIF3D.

#### *3.1.1.2.7 A.HMG4C Chi Processing Option 1 Verification*

The Type 02 card (Problem Options) in the A.HMG4C block provides the user with the ability to compute the composition prompt fission energy spectrum (chi) with three possible values of the 7<sup>th</sup> parameter. The first option is denoted with a value of 0; with this option, if a set chi is present in the ISOTXS file then that will be applied for all fissile compositions. If no set chi vector is

present, then the composition chi vector will be computed by HMG4C using total fission source weighting. The second option is denoted with a value of 1; with this option, if an isotopic chi vector is present, it will be used to compute the composition chi vectors using total fission source weighting. If no isotopic fission chi vector is present, then the set chi vector will be used in its place. The third option is denoted with a value of 2; this option is similar to option 1 except that  $v\Sigma_{\text{fission}}$  weighting will be applied instead of the total fission source method. These three options are provided mathematically using the previously provided equations.

The execution of the default option, 0, was already verified in the both the base case (with no set-wide chi vector) and the User-Defined Styles cases (with a set-wide chi vector). This section will verify the execution of option 1 to this Type 02 card of the A.HMG4C block. This will be performed by changing the parameter in question of the Type 02 card of the A.HMG4C block to a value of 1 in two cases: the base case and the User-Defined Style 1 case. These two cases are used to handle the cases of when a set-wide chi vector is or is not provided. These are discussed separately below.

#### 3.1.1.2.7.1 A.HMG4C Chi Procession Option 1 Verification: Base Case

To test this option, the fourth line of the base case input file from Figure 9 was modified as shown in the highlighted sections of Figure 17. Here we see that the title was changed (in this line and also for the A.NIP3 and A.DIF3D blocks; these other changes are not shown) as well as the parameter of question.

```

1 BLOCK=STP021
2 DATASET=A.HMG4C
3 01 3D XYZ - MCC Micro XS ISOTXS & Chi Opt = 1
4 02 900000 0 3 3 0 1 0 3

```

**Figure 17. Modified A.HMG4C Option for Chi Processing Option 1**

For the base case, no set-wide chi vector was provided in the ISOTXS file. Therefore the chi processing options 0 and 1 are expected to perform the same computations and thus the change of the chi processing option is not expected to yield any changes to the output for this case.

This was explicitly verified by first executing DIF3D exactly as in all other cases discussed thus far. After execution, the standard, auxiliary outputs, and the COMPTS binary output file were compared to the base case equivalents using a tool wrapping the Python difflib package to highlight any differences and to ensure those differences match the previously discussed expectations. The COMPTS binary output file was converted to ASCII text in a similar fashion to all other cases within this section thus far. This comparison found that the only differences in outputs were in the repeated outputs of the new title cards and in the input echo. There are no changes in the computed chi values, as expected.



### 3.1.1.2.7.2 A.HMG4C Chi Procession Option 1 Verification: User-Defined Style 1 Case

This option was tested in a completely analogous fashion to the base case described above, including changing the parameter on line 4 of Figure 17 from the User-Defined Style 1 case to a value of 1 in this evaluation.

Unlike the base case, the User-Defined Style 1 case does include a set-wide chi vector in the ISOTXS file. Therefore the chi processing options 0 and 1 are expected to yield different values of composition chi vectors that will also propagate to the final solution. The expected values of chi, computed using the previously provided equations, composition data from Table 22, and the nuclear data provided in Table 13, are provided for each of the four compositions in Table 46.

**Table 46. Hand-Calculated Chi Vectors for User-Defined Style 1 Chi Option 1 Case**

		COMP1	COMP2	COMP3	COMP4
Chi	Group 1	N/A	9.500000E-01	9.725954E-01	1.000000E+00
	Group 2	N/A	5.000000E-02	2.740455E-02	0.000000E+00

The standard, auxiliary, and COMPXS outputs from this case were compared their equivalents produced by the User-Defined Style 1 case computed with the chi processing option set at 0. The only differences observed, aside from input echoes and case title prints, were limited to the printed values of chi as well as the DIF3D solution iterations and final result. The latter is expected since if the fission spectrum changes, then so too should the solution. All reported values of chi for all four compositions in the outputs evaluated match those provided in Table 46.

### 3.1.1.2.8 A.HMG4C Chi Processing Option 2 Verification

The previous section described the three options for the Type 02 card (Problem Options) in the A.HMG4C block. The options valued 0 and 1 were tested earlier and in the previous section, respectively. This section will verify that option 2,  $v\Sigma_{\text{fission}}$  weighting, performs as expected.

This will be performed by changing the parameter in question of the Type 02 card of the A.HMG4C block to a value of 2 for two cases: the base case and the User-Defined Style 1 case. These two cases are used to handle the cases of when a set-wide chi vector is or is not provided. These are discussed separately below.

#### 3.1.1.2.8.1 A.HMG4C Chi Procession Option 2 Verification: Base Case

To test this option, the fourth line of the base case input file from Figure 9 was modified as shown in the highlighted sections of Figure 18. Here we see that the title was changed (in this line and also for the A.NIP3 and A.DIF3D blocks; these other changes are not shown) as well as the parameter of question.

February 13, 2020

```

1 BLOCK=STP021
2 DATASET=A.HMG4C
3 01 3D XYZ - MCC Micro XS ISOTXS & Chi Opt = 2
4 02 900000 0 3 3 0 2 0 3

```

**Figure 18. Modified A.HMG4C Option for Chi Processing Option 2**

The expected values of chi, computed using the previously provided equations, composition data from Table 22, and the nuclear data provided in Table 13, are provided for each of the four compositions in Table 47.

**Table 47. Hand-Calculated Chi Vectors for Chi Option 2 Case**

		COMP1	COMP2	COMP3	COMP4
Chi	Group 1	N/A	9.500000E-01	9.778163E-01	1.000000E+00
	Group 2	N/A	5.000000E-02	2.751181E-02	0.000000E+00

The standard, auxiliary, and the COMPS outputs from this case were compared their equivalents produced by the base case computed with the chi processing option set at 0. The only differences observed, aside from input echoes and case title prints, were limited to the printed values of chi as well as the DIF3D solution iterations and final result. The latter is expected since if the fission spectrum changes, then so too should the solution. All reported values of chi for all four compositions in the outputs evaluated match those provided in Table 47.

### 3.1.1.2.8.2 A.HMG4C Chi Procession Option 2 Verification: User-Defined Style 1 Case

This option was tested in a completely analogous fashion to the base case described above, including changing the parameter on line 4 of Figure 18 from the User-Defined Style 1 case to a value of 2 in this evaluation.

The expected values of chi, computed using the previously provided equations, composition data from Table 22, and the nuclear data provided in Table 13, are the same as those provided for each of the four compositions in Table 47. Obtaining the same results from a different calculation path is expected in this case since the ISOTXS file was previously verified to not contain a chi vector and to rely on the set-wide chi by the verification in the previous case for Processing Option 1 as well as the original User-Defined Style 1 case.

The standard, auxiliary, and the COMPS outputs from this case were compared their equivalents produced by the User-Defined Style 1 case computed with the chi processing option set at 0. The only differences observed, aside from input echoes and case title prints, were limited to the printed values of chi as well as the DIF3D solution iterations and final result. The latter is expected since if the fission spectrum changes, then so too should the solution. All reported values of chi for all four compositions match those provided in Table 47.

### 3.1.1.2.9 Isotope Classification Verification

The ISOTXS file allows an isotope to be classified as “undefined”, “fissile”, “fertile”, “other actinide”, “fission product”, “structure”, “coolant”, or “control” so this information is available for interfacing with other software systems or pieces of the ARC suite. The verification of this section’s base case has already investigated if the “undefined”, “fissile”, and “coolant” classifications are handled well as shown in Table 12. The verification effort thus far has identified that the “undefined” classification is passed to the NDXSRF file incorrectly as shown in Table 36. These cases will examine if this occurs for other isotopes.

To perform this check, the base case will be perturbed to generate three additional cases. The first two perturbed cases cover the five out of eight remaining isotope classifications without introducing new isotopes to the ISOTXS file, therefore minimizing the amount of reference solutions that must be generated. In addition, perturbation case 2 assigns isotope “ISO3” a classification of “control” thereby uncovering if DIF3D is applying any other special meaning to this classification. The third and final perturbation case is not necessary for the verification of DIF3D but is performed to understand the limits of these classification categories and so will examine what happens if arbitrarily chosen values are chosen. The only differences between all three of these new cases and the base case will be the isotope classifications within the ISOTXS input. The base case’s isotope classifications as well as the three perturbation cases are provided in Table 48. This table shows the classification type (for the first two perturbed cases) and enumerated value shows the numerical value used in the ISOTXS file to represent each classification type.

**Table 48. Isotope Classification Case Summary**

Case	ISO1	ISO2	ISO3	ISO4
<b>Base</b>	Undefined, 0	Coolant, 6	Fissile, 1	Fissile, 1
<b>Perturbed 1</b>	Structure, 5	Fission product, 4	Other Actinide, 3	Fertile, 2
<b>Perturbed 2</b>	Undefined, 0	Coolant, 6	Control, 7	Fissile, 1
<b>Perturbed 3</b>	8	9	10	11

The ISOTXS corresponding to the three perturbed cases are shown in Figure 19 through Figure 21, respectively. The yellow highlighting in each of these figures shows the specific values changed from the base case ISOTXS file, as shown in Figure 4.

These cases were executed in DIF3D and binary outputs converted to ASCII as has been performed previously. Of note, DIF3D completed execution of the third perturbed case without raising an error or warning due to the erroneous isotope classification.

February 13, 2020

```

1 0V ISOTXS *2G * 1
2 1D 2 4 2 2 1 0 5 1
3 2D * Custom *
4 * * ISO1 ISO2 ISO3 ISO4
5 7.73210E+01 4.37393E+05 2.00000E+07 1.00000E+00 0.00000E+00
6 0 7 14 21
7 4D ISO1 BYHAND NONE
8 1.00000E+00 1.10000E-11 2.20000E-12 2.94000E+02 1.10000E+00 1.20000E+00
9 5 0 0 0 0 0 0 2 1 0 100
10 101 200 201 300 1 1 1 1 1 1 2 1
11 2 1 2 1 2 1 2 1 1 1 1 1
12 1 1 1 1 1
13 5D 1.10683E-01 3.63550E-01 1.10683E-01 3.63550E-01 1.10683E-02
14 3.63550E-02 8.48029E-06 1.60000E-04
15 7D 1.09674E-01 3.63390E-01 1.00060E-03
16 7D 0.00000E+00 0.00000E+00 0.00000E+00
17 7D 0.00000E+00 0.00000E+00 0.00000E+00
18 7D 0.00000E+00 0.00000E+00 0.00000E+00
19 7D 0.00000E+00 0.00000E+00 0.00000E+00
20 4D ISO2 BYHAND NONE
21 2.00000E+00 2.20000E-11 4.40000E-12 3.94000E+02 2.10000E+00 2.20000E+00
22 4 0 0 1 1 1 1 2 1 0 100
23 101 200 201 300 1 1 1 1 1 1 2 1
24 2 1 2 1 2 1 2 1 1 1 1 1
25 1 1 1 1 1
26 5D 1.33152E+00 4.37350E+00 1.33152E+00 4.37350E+00 1.33152E-01
27 4.37350E-01 2.48615E-04 9.40000E-03 9.94458E-05 3.76000E-03 7.45844E-05
28 2.82000E-03 2.50000E-02 0.00000E+00 4.97229E-05 1.88000E-03 2.48615E-05
29 9.40000E-04
30 7D 1.15138E+00 4.35470E+00 1.04640E-01
31 7D 0.00000E+00 0.00000E+00 0.00000E+00
32 7D 0.00000E+00 0.00000E+00 0.00000E+00
33 7D 0.00000E+00 0.00000E+00 0.00000E+00
34 7D 5.00000E-02 0.00000E+00 0.00000E+00
35 4D ISO3 BYHAND NONE
36 3.00000E+00 3.30000E-11 6.60000E-12 4.94000E+02 3.10000E+00 3.20000E+00
37 3 1 1 1 1 1 1 2 1 0 100
38 101 200 201 300 1 1 1 1 1 1 2 1
39 2 1 2 1 2 1 2 1 1 1 1 1
40 1 1 1 1 1
41 5D 3.74796E-01 1.68707E+00 6.56960E-01 2.52025E+00 6.56960E-02
42 2.52025E-01 5.02300E-04 1.28940E-02 1.04840E-03 5.06320E-02 2.00000E+00
43 2.50000E+00 9.50000E-01 5.00000E-02 2.00920E-04 5.15760E-03 1.50690E-04
44 3.86820E-03 1.50000E-03 0.00000E+00 1.00460E-04 2.57880E-03 5.02300E-05
45 1.28940E-03
46 7D 6.19680E-01 2.44383E+00 2.92270E-02
47 7D 2.74590E-01 8.33180E-01 7.57370E-03
48 7D 1.50000E-03 0.00000E+00 0.00000E+00
49 7D 0.00000E+00 0.00000E+00 0.00000E+00
50 7D 3.00000E-03 0.00000E+00 0.00000E+00
51 4D ISO4 BYHAND NONE
52 4.00000E+00 4.40000E-11 8.80000E-12 5.94000E+02 4.10000E+00 4.20000E+00
53 2 1 1 0 0 0 2 1 0 100
54 101 200 201 300 1 1 1 1 1 2 2 2
55 2 2 2 2 2 2 2 2 1 2 1 2
56 1 2 1 2 1
57 5D 2.69337E-01 4.91890E-01 3.35880E-01 5.46280E-01 3.35880E-02
58 5.46280E-02 8.70780E-03 2.51800E-02 2.81700E-03 9.70000E-02 2.10000E+00
59 2.40000E+00 1.00000E+00 0.00000E+00
60 7D 1.00000E-04 3.18300E-01 4.24000E-01 4.55500E-03
61 7D 1.00000E-05 6.69400E-02 5.43800E-02 3.97200E-04
62 7D 0.00000E+00 0.00000E+00 0.00000E+00 0.00000E+00
63 7D 0.00000E+00 0.00000E+00 0.00000E+00 0.00000E+00
64 7D 0.00000E+00 3.00000E-03 0.00000E+00 0.00000E+00

```

Figure 19. Perturbed Case 1 ISOTXS

February 13, 2020

```

1 0V ISOTXS *2G * 1
2 1D 2 4 2 2 1 0 5 1
3 2D * Custom *
4 * * ISO1 ISO2 ISO3 ISO4
5 7.73210E+01 4.37393E+05 2.00000E+07 1.00000E+00 0.00000E+00
6 0 7 14 21
7 4D ISO1 BYHAND NONE
8 1.00000E+00 1.10000E-11 2.20000E-12 2.94000E+02 1.10000E+00 1.20000E+00
9 0 0 0 0 0 0 0 2 1 0 100
10 101 200 201 300 1 1 1 1 1 1 2 1
11 2 1 2 1 2 1 2 1 1 1 1 1
12 1 1 1 1 1
13 5D 1.10683E-01 3.63550E-01 1.10683E-01 3.63550E-01 1.10683E-02
14 3.63550E-02 8.48029E-06 1.60000E-04
15 7D 1.09674E-01 3.63390E-01 1.00060E-03
16 7D 0.00000E+00 0.00000E+00 0.00000E+00
17 7D 0.00000E+00 0.00000E+00 0.00000E+00
18 7D 0.00000E+00 0.00000E+00 0.00000E+00
19 7D 0.00000E+00 0.00000E+00 0.00000E+00
20 4D ISO2 BYHAND NONE
21 2.00000E+00 2.20000E-11 4.40000E-12 3.94000E+02 2.10000E+00 2.20000E+00
22 6 0 0 1 1 1 1 2 1 0 100
23 101 200 201 300 1 1 1 1 1 1 2 1
24 2 1 2 1 2 1 2 1 1 1 1 1
25 1 1 1 1 1
26 5D 1.33152E+00 4.37350E+00 1.33152E+00 4.37350E+00 1.33152E-01
27 4.37350E-01 2.48615E-04 9.40000E-03 9.94458E-05 3.76000E-03 7.45844E-05
28 2.82000E-03 2.50000E-02 0.00000E+00 4.97229E-05 1.88000E-03 2.48615E-05
29 9.40000E-04
30 7D 1.15138E+00 4.35470E+00 1.04640E-01
31 7D 0.00000E+00 0.00000E+00 0.00000E+00
32 7D 0.00000E+00 0.00000E+00 0.00000E+00
33 7D 0.00000E+00 0.00000E+00 0.00000E+00
34 7D 5.00000E-02 0.00000E+00 0.00000E+00
35 4D ISO3 BYHAND NONE
36 3.00000E+00 3.30000E-11 6.60000E-12 4.94000E+02 3.10000E+00 3.20000E+00
37 7 1 1 1 1 1 1 2 1 0 100
38 101 200 201 300 1 1 1 1 1 1 2 1
39 2 1 2 1 2 1 2 1 1 1 1 1
40 1 1 1 1 1
41 5D 3.74796E-01 1.68707E+00 6.56960E-01 2.52025E+00 6.56960E-02
42 2.52025E-01 5.02300E-04 1.28940E-02 1.04840E-03 5.06320E-02 2.00000E+00
43 2.50000E+00 9.50000E-01 5.00000E-02 2.00920E-04 5.15760E-03 1.50690E-04
44 3.86820E-03 1.50000E-03 0.00000E+00 1.00460E-04 2.57880E-03 5.02300E-05
45 1.28940E-03
46 7D 6.19680E-01 2.44383E+00 2.92270E-02
47 7D 2.74590E-01 8.33180E-01 7.57370E-03
48 7D 1.50000E-03 0.00000E+00 0.00000E+00
49 7D 0.00000E+00 0.00000E+00 0.00000E+00
50 7D 3.00000E-03 0.00000E+00 0.00000E+00
51 4D ISO4 BYHAND NONE
52 4.00000E+00 4.40000E-11 8.80000E-12 5.94000E+02 4.10000E+00 4.20000E+00
53 1 1 1 0 0 0 0 2 1 0 100
54 101 200 201 300 1 1 1 1 1 2 2 2
55 2 2 2 2 2 2 2 2 1 2 1 2
56 1 2 1 2 1
57 5D 2.69337E-01 4.91890E-01 3.35880E-01 5.46280E-01 3.35880E-02
58 5.46280E-02 8.70780E-03 2.51800E-02 2.81700E-03 9.70000E-02 2.10000E+00
59 2.40000E+00 1.00000E+00 0.00000E+00
60 7D 1.00000E-04 3.18300E-01 4.24000E-01 4.55500E-03
61 7D 1.00000E-05 6.69400E-02 5.43800E-02-3.97200E-04
62 7D 0.00000E+00 0.00000E+00 0.00000E+00 0.00000E+00
63 7D 0.00000E+00 0.00000E+00 0.00000E+00 0.00000E+00
64 7D 0.00000E+00 3.00000E-03 0.00000E+00 0.00000E+00

```

Figure 20. Perturbed Case 2 ISOTXS

February 13, 2020

```

1 0V ISOTXS *2G * 1
2 1D 2 4 2 2 1 0 5 1
3 2D * Custom *
4 * * ISO1 ISO2 ISO3 ISO4
5 7.73210E+01 4.37393E+05 2.00000E+07 1.00000E+00 0.00000E+00
6 0 7 14 21
7 4D ISO1 BYHAND NONE
8 1.00000E+00 1.10000E-11 2.20000E-12 2.94000E+02 1.10000E+00 1.20000E+00
9 8 0 0 0 0 0 0 2 1 0 100
10 101 200 201 300 1 1 1 1 1 1 2 1
11 2 1 2 1 2 1 2 1 1 1 1 1
12 1 1 1 1 1
13 5D 1.10683E-01 3.63550E-01 1.10683E-01 3.63550E-01 1.10683E-02
14 3.63550E-02 8.48029E-06 1.60000E-04
15 7D 1.09674E-01 3.63390E-01 1.00060E-03
16 7D 0.00000E+00 0.00000E+00 0.00000E+00
17 7D 0.00000E+00 0.00000E+00 0.00000E+00
18 7D 0.00000E+00 0.00000E+00 0.00000E+00
19 7D 0.00000E+00 0.00000E+00 0.00000E+00
20 4D ISO2 BYHAND NONE
21 2.00000E+00 2.20000E-11 4.40000E-12 3.94000E+02 2.10000E+00 2.20000E+00
22 9 0 0 1 1 1 1 2 1 0 100
23 101 200 201 300 1 1 1 1 1 1 2 1
24 2 1 2 1 2 1 2 1 1 1 1 1
25 1 1 1 1 1
26 5D 1.33152E+00 4.37350E+00 1.33152E+00 4.37350E+00 1.33152E-01
27 4.37350E-01 2.48615E-04 9.40000E-03 9.94458E-05 3.76000E-03 7.45844E-05
28 2.82000E-03 2.50000E-02 0.00000E+00 4.97229E-05 1.88000E-03 2.48615E-05
29 9.40000E-04
30 7D 1.15138E+00 4.35470E+00 1.04640E-01
31 7D 0.00000E+00 0.00000E+00 0.00000E+00
32 7D 0.00000E+00 0.00000E+00 0.00000E+00
33 7D 0.00000E+00 0.00000E+00 0.00000E+00
34 7D 5.00000E-02 0.00000E+00 0.00000E+00
35 4D ISO3 BYHAND NONE
36 3.00000E+00 3.30000E-11 6.60000E-12 4.94000E+02 3.10000E+00 3.20000E+00
37 10 1 1 1 1 1 1 2 1 0 100
38 101 200 201 300 1 1 1 1 1 1 2 1
39 2 1 2 1 2 1 2 1 1 1 1 1
40 1 1 1 1 1
41 5D 3.74796E-01 1.68707E+00 6.56960E-01 2.52025E+00 6.56960E-02
42 2.52025E-01 5.02300E-04 1.28940E-02 1.04840E-03 5.06320E-02 2.00000E+00
43 2.50000E+00 9.50000E-01 5.00000E-02 2.00920E-04 5.15760E-03 1.50690E-04
44 3.86820E-03 1.50000E-03 0.00000E+00 1.00460E-04 2.57880E-03 5.02300E-05
45 1.28940E-03
46 7D 6.19680E-01 2.44383E+00 2.92270E-02
47 7D 2.74590E-01 8.33180E-01 7.57370E-03
48 7D 1.50000E-03 0.00000E+00 0.00000E+00
49 7D 0.00000E+00 0.00000E+00 0.00000E+00
50 7D 3.00000E-03 0.00000E+00 0.00000E+00
51 4D ISO4 BYHAND NONE
52 4.00000E+00 4.40000E-11 8.80000E-12 5.94000E+02 4.10000E+00 4.20000E+00
53 11 1 1 0 0 0 0 2 1 0 100
54 101 200 201 300 1 1 1 1 1 2 2 2
55 2 2 2 2 2 2 2 2 1 2 1 2
56 1 2 1 2 1
57 5D 2.69337E-01 4.91890E-01 3.35880E-01 5.46280E-01 3.35880E-02
58 5.46280E-02 8.70780E-03 2.51800E-02 2.81700E-03 9.70000E-02 2.10000E+00
59 2.40000E+00 1.00000E+00 0.00000E+00
60 7D 1.00000E-04 3.18300E-01 4.24000E-01 4.55500E-03
61 7D 1.00000E-05 6.69400E-02 5.43800E-02 3.97200E-04
62 7D 0.00000E+00 0.00000E+00 0.00000E+00 0.00000E+00
63 7D 0.00000E+00 0.00000E+00 0.00000E+00 0.00000E+00
64 7D 0.00000E+00 3.00000E-03 0.00000E+00 0.00000E+00

```

Figure 21. Perturbed Case 3 ISOTXS

The standard outputs from the three perturbed cases were each compared to the base case using the same Python diffilib library as has been used extensively in this work. This comparison verified

that the only changes to the standard output were in the case title echoes and the ISOTXS file edits which state the isotope classification for each isotope. These classifications of the first two perturbed cases were verified to match those stated in Table 48; all matched. The same comparison was performed for the auxiliary outputs and no deficiencies were noted with the first two perturbed cases. These findings confirm that DIF3D does not take into account isotope classification for performing the neutronics calculations.

However, since the third perturbed case used classification enumerated values that were not defined by the ISOTXS listing, no reference values exist. The isotope classifications for the four isotopes were reported by DIF3D in the standard and auxiliary output to be: “TOTAL”, “ELASTIC”, “INELASTIC”, and “(N,2N)” for ISO1, ISO2, ISO3, and ISO4, respectively. This implies that DIF3D has hardcode enumerated types; since no error checking is performed on the range of classification values it should be expected that it is possible for the user to provide an isotope classification value that leads to a runtime error within DIF3D.

The next set of files to evaluate are the GEODST, NDXSFR, ZNATDN, COMPXS, and LABELS binary files. The only differences expected between the perturbed cases and the base case in these files are the classifications provided in the NDXSFR file.

This was explicitly confirmed to be the case for all three of the perturbed cases, including case three which used enumerated values not in the ISOTXS specification. Further, the isotope classification integers printed in the NDXSFR files match exactly those provided in the NDXSFR listing except for the previously identified mislabeling of “undefined” as an enumerated value of 0 in the NDXSFR file. This evaluation allows it to be stated that either the NDXSFR file is printing using the ISOTXS classification numbering scheme instead of the NDXSFR scheme, or that the NDXSFR listing is incorrect. Specifically, these two schemes are only inconsistent for the case of the “undefined” classification, which has an enumerated value of 0 in an ISOTXS file but an enumerated value of greater than 7 if in the NDXSFR file. DIF3D is using the ISOTXS classification numbering scheme for both.

#### *3.1.1.2.10 Edit Options Verification*

This section will evaluate the edit control options shown in Table 16. These cards and options that have yet to be evaluated are provided in Table 49. To ensure the scope of this verification effort is appropriately bounded, these options will not be tested for any cross-correlations. Instead each option will be tested one-by-one and it is assumed that the effect of the value of one option has no effect on DIF3D’s ability to execute another option.

Each of the card types and options will be evaluated in the subsections that follow. In all the cases that follows, there will be differences in the output file that are expected, specifically, page numbers and input echoes obviously should change as the number of pages printed changes or the input file changes. These differences will not be discussed explicitly below.

**Table 49. Edit Control Perturbations**

Card Type & Option	Description	Option in Base Case	Perturbations to Base
<b>A.HMG4C 2.3</b>	Print file master control flag	0	1
<b>A.HMG4C 2.4</b>	COMPXS edit flag	3	0, 1, 2
<b>A.HMG4C 2.5</b>	ISOTXS edit flag	3	0, 1, 2, 3
<b>A.HMG4C 2.8</b>	Aux output file master control flag	0	1
<b>A.HMG4C 2.9</b>	Edit for supplied COMPXS	3	0, 1, 2
<b>A.NIP3 2.3</b>	Geometry processing edits	3	0, 1, 2
<b>A.NIP3 2.9</b>	Cross section processing edits	3	0, 1, 2
<b>A.NIP3 2.10</b>	Region/mesh interval plotter edits	3	0, 1, 2
<b>A.NIP3 2.11</b>	Zone/mesh interval plotter edits	3	0, 1, 2
<b>A.DIF3D 4.2</b>	Problem description edit	3	0, 1, 2
<b>A.DIF3D 4.3</b>	Geometry (region to mesh interval) map edit	3	0, 1, 2
<b>A.DIF3D 4.4</b>	Geometry (zone to mesh interval) map edit	3	0, 1, 2
<b>A.DIF3D 4.5</b>	Macroscopic cross section edit	33	00, 01, 02, 03, 10, 11, 12, 13, 20, 21, 22, 23, 30, 31, 32

### 3.1.1.2.10.1 A.HMG4C Type 02 Card Option 3

The third option of the Type 02 card of the A.HMG4C input block takes either a 0 or 1 value, as shown in Table 49. The cases evaluated up to this Edit Options section have left this as a 0 value, indicating that general run information and requested edits will be printed. In this modified case, this value is set to 1, indicating that all printing is suppressed to the standard output except the diagnostics. With this option, standard output, auxiliary output, and the binary interface files are still written, however the content of the standard output is expected to be significantly reduced as all requested edits and run information specifically from the HMG4C module is not printed.

The base case input was modified accordingly and reran in DIF3D. To verify, the auxiliary and standard output files were compared against the base case to ensure that the HMG4C output is limited to the diagnostic information for standard output. It is also expected that there should be no changes to the auxiliary output.

The HMG4C output begins on line 866 of the standard output in the base case with summary information and followed by isotopic and composition details. All of this information was verified to not be present in the modified case as the standard output progressed directly to the DIF3D module outputs. It is also confirmed that there are no differences between the base and modified cases' auxiliary outputs.



#### *3.1.1.2.10.2.A.HMG4C Type 02 Card Option 4*

The fourth option of the Type 02 card of the A.HMG4C input block takes a 0, 1, 2, or 3 value, as shown in Table 49. The cases evaluated up to this Edit Options section have left this as a 3 value, indicating that edits of the COMPXS file will be printed to both standard and auxiliary outputs. In this case, this value will be set to 0, 1, and 2 indicating that the edit will not exist on standard or auxiliary output, only on standard output, or only on auxiliary output, respectively.

The base case input was modified accordingly with three different inputs capturing the 0, 1, and 2 values for this option discussed above. DIF3D was run for all three cases. To verify, the auxiliary and standard output files for each of the three cases were compared against the base case to ensure that the HMG4C COMPXS edit option is respected.

The first modified case shall print no COMPXS edits in either standard or auxiliary output. This was explicitly confirmed by comparing both outputs with the base case equivalent. The base case, beginning on line 1326 of the standard output includes the COMPXS edit printed from the HMG4C module; this is not present in the standard output of the modified case. Similarly, line 1322 of the base case's auxiliary output also includes this information and it is again not present in the modified case's auxiliary output.

The second modified case is expected to print the COMPXS edit to the standard output but not the auxiliary output. Unfortunately, this option was not respected and the COMPXS edit tables were printed to both standard and auxiliary outputs.

The third modified case is expected to print the COMPXS edit to only the auxiliary output. This option was also confirmed to not be respected as the COMPXS edit tables were printed to both standard and auxiliary outputs.

The above verification work found that the fourth option of the Type 02 card in the HMG4C module does not respect options that print COMPXS edit output to one of standard or auxiliary outputs: if the user wants this information printed to one output, it will be in both locations. If the user does not wish for the output to be printed, it will be suppressed in both edits.

#### *3.1.1.2.10.3.A.HMG4C Type 02 Card Option 5*

The fifth option of the Type 02 card of the A.HMG4C input block takes a 0, 1, 2, or 3 value, as shown in Table 49. These options refer to editing only the isotopes in the ISOTXS file that are referenced in the model. The ISOTXS file used for all other cases in this section have used an ISOTXS file that only included the isotopes used in the model, ISO1 through ISO4. This case will therefore have an additional arbitrary isotope added to the ISOTXS file, named ISO5, to ensure it is not included in these edits. The inclusion of this additional isotope also means that all four of this option's values can be tested.

The base case input was modified accordingly with three different inputs capturing the 0, 1, 2, and 3 values for this option discussed above using an ISOTXS library that contains ISO5, that is simply

a copy of ISO1 with a different name. DIF3D was run for all three cases. To verify, the auxiliary and standard output files for each of the three cases were compared against the base case to ensure that the HMG4C ISOTXS edit option is respected and that ISO1, ISO2, ISO3, and ISO4 are the only isotopes that remain in the output for the cases when the ISOTXS edit outputs are printed.

The first modified case shall print no ISOTXS edits in either standard or auxiliary output and all other outputs should be the same as the base case since the additional isotope should have no impact on any edited information. This was explicitly confirmed by comparing both outputs with the base case equivalent. The base case, beginning on line 876 of the standard output includes the ISOTXS edit printed from the HMG4C module; this is not present in the standard output of the modified case. Similarly, line 874 of the base case's auxiliary output also includes this information and it is again not present in the modified case's auxiliary output. It is also confirmed that the standard output does not include the ISO5 data as it is not included in the model.

The second modified case is expected to print the ISOTXS edit to the standard output but not the auxiliary output; again all other output should be the same as the base case despite the presence of ISO5 in the ISOTXS file. Unlike the equivalent COMPXS option, the value of this option was successfully interpreted, as the auxiliary output did not include the ISOTXS edit while the standard output did.

The third modified case is expected to print the ISOTXS edit to only the auxiliary output; and all other output should be the same as the base case despite the presence of ISO5 in the ISOTXS file. Unlike the equivalent COMPXS option, the value of this option was successfully interpreted, as the standard output did not include the ISOTXS edit but the auxiliary output did.

The final modified case shall print the ISOTXS edit to both output streams and should have the same output as the base case despite the presence of the ISO5 isotope in the ISOTXS file. This was verified explicitly to be true, including not printing the edit of ISO5.

#### *3.1.1.2.10.4A.HMG4C Type 02 Card Option 8*

The eighth option of the Type 02 card of the A.HMG4C input block takes either a 0 or 1 value, as shown in Table 49. The cases evaluated up to this Edit Options section have left this as a 0 value, indicating that general run information and requested edits will be printed to the auxiliary output. In this modified case, this value is set to 1, indicating that all printing is suppressed to the auxiliary output except the diagnostics. With this option, standard output, auxiliary output, and the binary interface files are still written, however the content of the auxiliary output is expected to be significantly reduced as all requested edits and run information specifically from the HMG4C module is not printed. The standard output is expected to remain the same.

The base case input was modified accordingly and reran in DIF3D. To verify, the auxiliary and standard output files were compared against the base case to ensure that the HMG4C output is limited to the diagnostic information for auxiliary output. It is also expected that there should be no changes to the standard output.

The HMG4C output begins on line 867 of the auxiliary output in the base case with summary information and followed by isotopic and composition details. All of this information was verified to not be present in the modified case as the auxiliary output progressed directly to the DIF3D module outputs. It is also confirmed that there are no differences between the base and modified cases' standard outputs. Interestingly, the file reference numbers for the NDXSRF, ZNATDN, LABELS, ISOTXS, and COMPXS were printed in the auxiliary output for this modified case even though it is present for the base case.

#### *3.1.1.2.10.5A.HMG4C Type 02 Card Option 9*

The ninth option of the Type 02 card of the A.HMG4C input block takes a 0, 1, 2, or 3 value, as shown in Table 49. The cases evaluated up to this Edit Options section have left this as a 3 value, indicating that edits of the provided COMPXS file will be printed to both standard and auxiliary outputs. However, all previous cases had HMG4C explicitly generate a COMPXS file. This case was re-run all four option values (0, 1, 2, and 3) with a supplied COMPXS file and verify that the supplied COMPXS edit option is respected.

This was done by declaring the existence of the COMPXS dataset with the BLOCK=OLD command. This tells DIF3D to not compute the COMPXS file and simply to use the one that already exists in the present working directory.

The next step was to ensure that the supplied COMPXS file was actually used. This was performed with the A.HMG4C Type 02 card option 9 parameter set to its default value of printing everything (option 3) from the supplied COMPXS file. This case was run and it was noted that the computer file system's modified time and date of the COMPXS was not changed, indicating it was not overwritten. The standard and auxiliary outputs of these options were then compared to the base case, that computes the COMPXS file data during execution, to ensure that the results obtained and intermediate output tables produced are consistent, DIF3D executed to completion with no errors, and the final eigenvalue solution is unchanged. These were found to be true. It should be noted, however, that the GNIP4C module's ISOTXS, ZNATDN, and NDXSRF edits, as well as the HMG4C module's ISOTXS edits were not produced when a COMPXS file is supplied; this makes sense as the computations necessary to produce these files are unnecessary when a COMPXS is already present. Further, the ZNATDN and NDXSRF files were confirmed to have not been created.

The final evaluation for this case is to test the validity of the of the A.HMG4C Type 02 card's ninth option. This was done by modifying this card to have values of 0, 1, 2, and 3. DIF3D was run for all four cases. This case will evaluate the 0, 1, and 2 options which print no supplied COMPXS edits, print no supplied COMPXS edits only to standard output, and no supplied COMPXS edits only to auxiliary output, respectively.

The first modified case shall print no supplied COMPXS edits in either standard or auxiliary output and all other outputs should be the same as the base case. This was explicitly confirmed by comparing both outputs with the base case equivalent

However, the second and third modified cases are expected to print only to either standard or auxiliary output, respectively. However in both cases, the output was written to both standard and auxiliary output. This behavior is akin to if the HMG4C module is either reading a value for the A.HMG4C Type 02 card, option 9, that is either 0, or nonzero. If the value is 0, it successfully does not print to standard or auxiliary output; if it is nonzero, then it is printed to both the standard and auxiliary outputs.

#### *3.1.1.2.10.6 A.NIP3 Type 02 Card Option 3*

The third option of the Type 02 card of the A.NIP3 input block accepts values of 0, 1, 2, or 3 as shown in Table 49. The cases evaluated thus far have kept this option at a value of 3, indicating that geometry edits will be printed to both standard and auxiliary output. This case will evaluate the 0, 1, and 2 options which print no GNIP4C module edits, print GNIP4C edits only to standard output, and print NIP3 edits only to auxiliary output.

The base case input was modified accordingly with three different inputs capturing the 0, 1, 2, and 3 values for this option discussed above. DIF3D was run for all three cases. To verify, the auxiliary and standard output files for each of the three cases were compared against the base case to ensure that the A.NIP3 edit option is respected.

The first modified case shall print no GNIP4C module edits in either standard or auxiliary output and all other outputs should be the same as the base case. This was explicitly confirmed by comparing both outputs with the base case equivalent. The base case, beginning on line 285 of the standard output includes the GNIP4C edits printed from the A.NIP3 module; this is not present in the standard output of the modified case. It is noted that the GNIP4C edits still output the reactor region map, but do not include the GNIP4C edits of the cross section information; this is interesting as the A.NIP3 listing is unclear on what exactly a “geometry processing module edit” entails. The same findings exist for the auxiliary output.

The second modified case is expected to print the GNIP4C edits to the standard output but not the auxiliary output. The value of this option was successfully interpreted, as the auxiliary output did not include the GNIP4C edits but the standard output did. Similar to the above case, the GNIP4C edits in the auxiliary output still output the reactor region map, but do not include the GNIP4C edits of the cross section information.

The third modified case is expected to print the GNIP4C edits to only the auxiliary output; and all other output should be the same as the base. The value of this option was successfully interpreted, as the standard output did not include the GNIP4C edits but the auxiliary output did, with the same caveat as is found for the previous two cases.

#### *3.1.1.2.10.7 A.NIP3 Type 02 Card Option 9*

The ninth option of the Type 02 card of the A.NIP3 input block accepts values of 0, 1, 2, or 3 as shown in Table 49. The cases evaluated thus far have kept this option at a value of 3, indicating that cross section processing edits will be printed to both standard and auxiliary output. This case

will evaluate the 0, 1, and 2 options which print no GNIP4C cross section processing edits, print GNIP4C cross section processing edits only to standard output, and print GNIP4C cross section processing edits only to auxiliary output.

The first modified case shall print no cross section processing edits in either standard or auxiliary output and all other outputs should be the same as the base case. However, this option is not followed by the A.NIP3 module as in the modified casestill contained the same standard and auxiliary outputs as the base case.

The same finding holds for the remaining two case modifications (values of 1 and 2 applied to this option) as there is no difference between the outputs from these modified cases and the base case outputs.

#### *3.1.1.2.10.8 A.NIP3 Type 02 Card Option 10*

The tenth option of the Type 02 card of the A.NIP3 input block accepts values of 0, 1, 2, or 3 as shown in Table 49. The cases evaluated thus far have kept this option at a value of 3, indicating that region/mesh interval printer-plotter maps will be printed to both standard and auxiliary output. This case will evaluate the 0, 1, and 2 options which print no region/mesh interval printer-plotter maps, print region/mesh interval printer-plotter maps only to standard output, and print region/mesh interval printer-plotter maps only to auxiliary output.

The first modified case shall print no reactor region maps in either standard or auxiliary output and all other outputs should be the same as the base case. This was explicitly confirmed by comparing both outputs with the base case equivalent. The base case, beginning on line 392 of the standard output includes the region maps printed from the A.NIP3 module; this is not present in the standard output of the modified case. The same findings exist for the auxiliary output.

The second modified case is expected to print the reactor region maps to the standard output but not the auxiliary output. The value of this option was successfully interpreted, as the auxiliary output did not include the map but the standard output did.

The third modified case is expected to print the reactor region maps to only the auxiliary output; and all other output should be the same as the base. The value of this option was successfully interpreted, as the standard output did not include the reactor region maps but the auxiliary output did.

#### *3.1.1.2.10.9 A.NIP3 Type 02 Card Option 11*

The eleventh option of the Type 02 card of the A.NIP3 input block accepts values of 0, 1, 2, or 3 as shown in Table 49. The cases evaluated thus far have kept this option at a value of 3, indicating that zone (composition) / mesh interval printer-plotter maps will be printed to both standard and auxiliary output. This case will evaluate the 0, 1, and 2 options which print no zone (composition)/mesh interval printer-plotter maps, print zone (composition) / mesh interval printer-

plotter maps only to standard output, and print zone (composition) / mesh interval printer-plotter maps only to auxiliary output.

The first modified case shall print no reactor zone maps in either standard or auxiliary output and all other outputs should be the same as the base case. This was explicitly confirmed by comparing both outputs with the base case equivalent for both standard and auxiliary output files.

The second modified case is expected to print the reactor zone maps to the standard output but not the auxiliary output. The value of this option was successfully interpreted, as the auxiliary output did not include the map but the standard output did.

The third modified case is expected to print the reactor zone maps to only the auxiliary output; and all other output should be the same as the base. The value of this option was successfully interpreted, as the standard output did not include the reactor zone maps but the auxiliary output did.

#### *3.1.1.2.10.10 A.DIF3D Type 04 Card Option 2*

The second option of the Type 04 card of the A.DIF3D input block accepts values of 0, 1, 2, or 3, as shown in Table 49. The cases evaluated thus far have kept this option at a value of 3, indicating that the problem description edits will be printed to both standard and auxiliary output. This case will evaluate the 0, 1, and 2 options which print no problem description edits, print problem description edits only to standard output, and problem description edits only to auxiliary output.

The first modified case shall print no problem description edits in either standard or auxiliary output and all other outputs should be the same as the base case. This was explicitly confirmed by comparing both outputs with the base case equivalent for both standard and auxiliary output files.

The second modified case is expected to print the problem description edits to the standard output but not the auxiliary output. The value of this option was successfully interpreted, as the auxiliary output did not include the problem description edits but the standard output did.

The third modified case is expected to print the problem description edits to only the auxiliary output; and all other output should be the same as the base. The value of this option was successfully interpreted, as the standard output did not include the problem description edits but the auxiliary output did.

#### *3.1.1.2.10.11 A.DIF3D Type 04 Card Option 3*

The third option of the Type 04 card of the A.DIF3D input block accepts values of 0, 1, 2, or 3 as shown in Table 49. The cases evaluated thus far have kept this option at a value of 3, indicating that the DIF3D module will print region/mesh interval printer-plotter maps to both standard and auxiliary output. This case will evaluate the 0, 1, and 2 options which print no region/mesh interval printer-plotter maps, print region/mesh interval printer-plotter maps only to standard output, and print region/mesh interval printer-plotter maps only to auxiliary output.



The first modified case shall print no region maps in either standard or auxiliary output and all other outputs should be the same as the base case. This was explicitly confirmed by comparing both outputs with the base case equivalent

The second modified case is expected to print the region maps to the standard output but not the auxiliary output. The value of this option was successfully interpreted, as the auxiliary output did not include the map but the standard output did.

The third modified case is expected to print the region maps to only the auxiliary output; and all other output should be the same as the base. The value of this option was successfully interpreted, as the standard output did not include the reactor region maps but the auxiliary output did.

#### *3.1.1.2.10.12 A.DIF3D Type 04 Card Option 4*

The fourth option of the Type 04 card of the A.DIF3D input block accepts values of 0, 1, 2, or 3 as shown in Table 49. The cases evaluated thus far have kept this option at a value of 3, indicating that the DIF3D module will print zone/mesh interval printer-plotter maps to both standard and auxiliary output. This case will evaluate the 0, 1, and 2 options which print no zone/mesh interval printer-plotter maps, print zone/mesh interval printer-plotter maps only to standard output, and print zone/mesh interval printer-plotter maps only to auxiliary output.

The first modified case shall print no zone maps in either standard or auxiliary output and all other outputs should be the same as the base case. This was explicitly confirmed by comparing both outputs with the base case equivalent

The second modified case is expected to print the zone maps to the standard output but not the auxiliary output. The value of this option was successfully interpreted, as the auxiliary output did not include the map but the standard output did.

The third modified case is expected to print the zone maps to only the auxiliary output; and all other output should be the same as the base. The value of this option was successfully interpreted, as the standard output did not include the reactor region maps but the auxiliary output did.

#### *3.1.1.2.10.13 A.DIF3D Type 04 Card Option 5*

The fifth option of the Type 04 card of the A.DIF3D input block accepts a two digit number where the first digit controls the scattering and principal cross section composition edits and the second digit controls just the principal cross section edits. The accepted values for each digit are 0, 1, 2, or 3 as shown in Table 49. The cases evaluated thus far have kept both parameters at the value of 3 (thus, the input value is 33), indicating that the DIF3D module will print these quantities to both standard and auxiliary output. This case will evaluate setting each of the values for each digit to the values of 0, 1, and 2 (no edits, to standard out only, and to auxiliary out only, respectively) while keeping the other digit constant. Thus the modified cases to evaluate within this subsection are the values of 00, 01, 02, 03, 10, 11, 12, 13, 20, 21, 22, 23, 30, 31, and 32. This set evaluates every possible combination.

For the 00 case, it is expected that the standard and auxiliary outputs do *not* contain the DIF3D composition cross section edits, whether they be principal or scattering. This was verified explicitly and found to be true.

For the 01 case, it is expected that the auxiliary output does not contain any DIF3D composition cross section edits, while the standard output contains only principal cross sections and no scattering matrices. This was verified explicitly and found to be true.

For the 02 case, it is expected that the standard output does not contain any DIF3D composition cross section edits, while the auxiliary output contains only principal cross sections and no scattering matrices. This was verified explicitly and found to be true.

For the 03 case, it is expected that both the standard and auxiliary outputs contains only principal cross sections and no scattering matrices. This was verified explicitly and found to be true.

For the 10 case, it is expected that the auxiliary output does not contain any DIF3D composition cross section edits, while the standard output contains principal cross sections and scattering matrices. This was verified explicitly and found to be true.

For the 11 case, it is expected that the auxiliary output does not contain any DIF3D composition cross section edits, while the standard output contains principal cross sections and scattering matrices. This was verified explicitly and found to be true.

For the 12 case, it is expected that the auxiliary output contains edits of the principal cross sections, while the standard output contains principal cross sections and scattering matrices. This was verified explicitly and found to be true.

For the 13 case, it is expected that the auxiliary output contains edits of the principal cross sections, while the standard output contains principal cross sections and scattering matrices. This was verified explicitly and found to be true.

For the 20 case, it is expected that the auxiliary output contains principal cross sections and scattering matrices while the standard output contains no cross section edits. This was verified explicitly and found to be true.

For the 21 case, it is expected that the auxiliary output contains principal cross sections and scattering matrices while the standard output contains principal cross section edits only. This was verified explicitly and found to be true.

For the 22 case, it is expected that the auxiliary output contains principal cross sections and scattering matrices while the standard output contains no cross section edits. This was verified explicitly and found to be true.



For the 23 case, it is expected that the auxiliary output contains principal cross sections and scattering matrices while the standard output contains principal cross section edits only. This was verified explicitly and found to be true.

For the 30, 31, and 32 cases, it is expected that the standard and auxiliary output contains principal cross sections and scattering matrix edits. These were verified explicitly and found to be true.

#### *3.1.1.2.11 Rodded Model Verification*

Verification that the A.NIP3 Type 44 card (region assignment to control rod banks) is working as planned, a unique geometric model was developed that was as simple as possible while still allowing for testing of the use cases of the Type 44 card. Specifically, to verify the Type 44 card, this work will exercise the Type 44 card in six ways:

1. Simply define a control rod bank that is composed of a single region
2. Define a control rod bank that is composed of two regions, but each region is assigned to the bank on their own Type 44 card
3. Define a control rod bank composed of two regions assigned on the same Type 44 card
4. Define a control rod bank with an area
5. Define a control rod bank with no name
6. Define a control rod bank with both an area and region being assigned to it.

The above implies that at least six unique control rod banks must be defined with most of these banks containing multiple regions. The minimum number of regions required for the above cases was 10, if we assume the area mentioned in approach 4 has at least 2 regions. A simple 4x3 grid in the X-Y plane was chosen to accommodate this with dimensions of 40 cm by 30 cm with each coarse mesh region being 10 cm by 10 cm.

Further, control rod banks must be defined with at least region below each control rod to allow for rod insertion and replacement of the rod region during a withdrawal. This sets the minimum number of regions in each axial slice to two. However, to enable the application of this test case to downstream verification efforts of the REBUS software, which will use control rod banks during the fuel cycle calculations, this model will be developed so some control rod banks have regions above and below the rods while other control rod banks only have regions below. Therefore the 4x3 X-Y plane will be extruded to 30 cm each with control rod banks starting 10cm above the bottom and a subset of the control rods extending the remaining 20 cm while the remaining control rod banks extending only 10 cm with an additional 10 cm of non-control material above. This was practically implemented by modeling a 3x3x3 grid of regions, 10 cm on each side with a 1x3x2 (X,Y, and Z dimensions, respectively) grid of regions that are 10 cm long in the X and Y dimensions, and the lower Z region is 10 cm tall and the upper Z region is 20 cm tall.

The regions and areas that will compose the control rod banks are shown in Figure 22; these region labels are the labels in the second coarse mesh plane from the bottom in the Z dimension. The six corresponding control rod banks are shown in Figure 23. Note that the numbering of the control

February 13, 2020

rod banks corresponds to the six strategies to apply the Type 44 card. Note that BANK6 is on the right hand side of the 4x3 grid and therefore BANK6 has a region below the control rod regions but not above; all other control rod banks have regions above and below the control rod regions.

REG27	REG28	REG29	REG06
REG24, AREA1	REG25, AREA1	REG26, AREA1	REG05, AREA2
REG21	REG22	REG23	REG04, AREA2

**Figure 22. Control Rod Bank Problem Regions and Areas**

BANK3		(blank)	BANK6
BANK4			
BANK1	BANK2		

**Figure 23. Control Rod Bank Problem Bank Assignments**

The geometric representation of this model will not be explicitly verified and documented here as this capability was already documented by previous sections. Instead this documentation will verify that the A.NIP3 module properly interprets these options via direct inspection of the standard and auxiliary outputs as well as the LABELS binary file, the binary file that contains the control rod bank information.

The final A.NIP3 block of the input file is included in Figure 24, noting that the 33 lines each for composition definitions and assignments have been truncated. The A.DIF3D and A.HMG4C

blocks are the same as the base case discussed throughout the rest of this section. The ISOTXS file is the same as the base case, though only ISO3 as it is the only isotope applied.

The control rod channel specifications begin on line 790 of the standard output as is provided in Figure 25. This table shows each of the six control rod banks and their properties like the regions assigned and the boundaries between the control rods and the regions below and above it. Starting with the bank position, all are at 10 cm above the bottom ( $Z=0$ ) of the model, exactly as incorporated in the model. The rod-tip region labels should match that observed from comparing Figure 22 and Figure 23 when focusing only on the region labels; these labels indeed match. All control rod channels were defined on a  $2 \times 2$  meshed region and therefore 4 mesh cells in the channel is correct. The six columns on the right, the channel descriptions, should tell us there is a region below the rod that starts at 0 cm and extends to 10cm. The 5 banks in the  $3 \times 3 \times 3$  region of the problem (with a region above each the rods) should extend to 20 cm and the bank in the  $1 \times 3 \times 2$  region should have no region above it. These are all confirmed accurate.

Finally, as can be interpreted from the A.NIP3 block in Figure 24, the regions below the rod tips in the  $3 \times 3 \times 3$  region are numbered REG1#, in the rod region they are numbered as REG2#, and above the rod tips are numbered as REG3# with the digit in the ones place (i.e., the “#”), being unique to the X-Y plane location of the region. Therefore the regions below the rod tips for the banks in the  $3 \times 3 \times 3$  region (BANK1 through the fifth bank named with a blank) should have a region number ten less than in the rodded region, and the regions above the tips should have a region number ten greater than in the rodded region. This is clearly seen in Figure 25. The  $1 \times 2 \times 3$  region has a different numbering scheme (since the  $3 \times 3 \times 3$  region used all the digits between 1 and 9) where the region below the tips should have a region number three less than in the rodded region and there should be no regions above the rods. This is also confirmed in Figure 25.

The auxiliary output was confirmed to contain the same control rod region table as is shown in Figure 25 and therefore that output is also verified.

The LABELS file is a binary representation of the model’s region and composition labels, area data, half heights, nuclide set labels, alias zone labels, control rod model data, and burnup-dependent cross section data. Previous LABELS comparisons used the CCCC\_convert program to convert the binary data to ASCII as well as using the CCCC\_PrintTables program. CCCC\_convert, when used to convert this case’s LABELS file reports that “CONTROL ROD stuff not supported by CCCC\_convert.” CCCC\_PrintTables also encounters a segmentation fault during the processing of the LABELS file. This issue does not impact the DIF3D software and only indicates that improvements to the CCCC\_convert.x and CCCC\_PrintTables.x software is necessary.

The custom Python program written to output LABELS information named “read\_LABELS.py” was therefore utilized again and produced a human-readable form of the LABELS file. This output, too long to show here at ~230 lines, was compared with the input and the Figure 25 edits. It was found to correctly represent the control rod banks and the mesh entries containing those rods, including adequately handling the cases with and without movable regions above the rods.

February 13, 2020

```

5  UNIFORM=A.NIP3
6  01  CONTROL ROD BANK
7  02 0 3 40000000 40000000 40000000 40000000 0 3 3 3
8  03 44
9  04      3      3      3      3      3      3
10 c
11 c Define geometry
12 c 3x3x3 grid appended by a 1x3x2 slab on right
13 06 REG11 0.0 10.0 0 2 0.0 10.0
14 06 REG12 10.0 20.0 0 2 0.0 10.0
15 06 REG13 20.0 30.0 0 2 0.0 10.0
16 06 REG14 0.0 10.0 0 2 10.0 20.0
17 06 REG15 10.0 20.0 0 2 10.0 20.0
18 06 REG16 20.0 30.0 0 2 10.0 20.0
19 06 REG17 0.0 10.0 0 2 20.0 30.0
20 06 REG18 10.0 20.0 0 2 20.0 30.0
21 06 REG19 20.0 30.0 0 2 20.0 30.0
22 c
23 06 REG21 0.0 10.0 2 4 0.0 10.0
24 06 REG22 10.0 20.0 2 4 0.0 10.0
25 06 REG23 20.0 30.0 2 4 0.0 10.0
26 06 REG24 0.0 10.0 2 4 10.0 20.0
27 06 REG25 10.0 20.0 2 4 10.0 20.0
28 06 REG26 20.0 30.0 2 4 10.0 20.0
29 06 REG27 0.0 10.0 2 4 20.0 30.0
30 06 REG28 10.0 20.0 2 4 20.0 30.0
31 06 REG29 20.0 30.0 2 4 20.0 30.0
32 c
33 06 REG31 0.0 10.0 4 6 0.0 10.0
34 06 REG32 10.0 20.0 4 6 0.0 10.0
35 06 REG33 20.0 30.0 4 6 0.0 10.0
36 06 REG34 0.0 10.0 4 6 10.0 20.0
37 06 REG35 10.0 20.0 4 6 10.0 20.0
38 06 REG36 20.0 30.0 4 6 10.0 20.0
39 06 REG37 0.0 10.0 4 6 20.0 30.0
40 06 REG38 10.0 20.0 4 6 20.0 30.0
41 06 REG39 20.0 30.0 4 6 20.0 30.0
42 c
43 c Add 1x3x2 slab on right side
44 06 REG01 30.0 40.0 0 2 0.0 10.0
45 06 REG02 30.0 40.0 0 2 10.0 20.0
46 06 REG03 30.0 40.0 0 2 20.0 30.0
47 06 REG04 30.0 40.0 2 6 0.0 10.0
48 06 REG05 30.0 40.0 2 6 10.0 20.0
49 06 REG06 30.0 40.0 2 6 20.0 30.0
50 c Set a middle row area of 2nd plane
51 07 AREA1 REG24 REG25 REG26
52 c Set an area for most of the rightmost slab
53 07 AREA2 REG04 REG05
54 c
55 c Set fine mesh structure, 2x2x2 mesh in each of the coarse mesh blocks
56 09 X 2 10.0 2 20.0 2 30.0
57 09 X 2 40.0
58 09 Y 2 10.0 2 20.0 2 30.0
59 09 Z 2 10.0 2 20.0 2 30.0
60 c
61 c Define Compositions (varying amounts of ISO3)
62 14 CMP01 ISO3 0.1
63-94 ...
95 c
96 c Assign compositions
97 15 CMP01 REG01
98-129 ...
130 c
131 c Assign rod banks:
132 c 1) Single rod defined with one region
133 44 BANK1 REG21
134 c 2) Bank defined with two regions, each on separate lines
135 44 BANK2 REG22
136 44 BANK2 REG23
137 c 3) Bank defined with two regions on same lines
138 44 BANK3 REG27 REG28
139 c 4) Bank defined with an area
140 44 BANK4 AREA1
141 c 5) Bank with no name
142 44 "" REG29
143 c 6) Bank defined with area and region together
144 44 BANK6 AREA2 REG06

```

Figure 24. Control Rod Bank Problem A.NIP3 Input Block

February 13, 2020

```

790                                     *** CONTROL-ROD CHANNEL SPECIFICATIONS ***
791
792
793          CONTROL-ROD BANK
794          NO. LABEL POSITION
795
796          0 1 BANK1 10.00
797          0 2 BANK2 10.00
798
799          0 3 BANK3 10.00
800
801          0 4 BANK4 10.00
802
803
804          0 5 "" 10.00
805          0 6 BANK6 10.00
806
807
          ROD-TIP REGION NO. OF
          LABEL MESH CELLS
          CHANNEL DESCRIPTION (BOUNDARY, REGION, BOUNDARY, ETC.)
          REG21 4 0.00 REG11 10.00 REG21 20.00 REG31
          REG22 4 0.00 REG12 10.00 REG22 20.00 REG32
          REG23 4 0.00 REG13 10.00 REG23 20.00 REG33
          REG27 4 0.00 REG17 10.00 REG27 20.00 REG37
          REG28 4 0.00 REG18 10.00 REG28 20.00 REG38
          REG24 4 0.00 REG14 10.00 REG24 20.00 REG34
          REG25 4 0.00 REG15 10.00 REG25 20.00 REG35
          REG26 4 0.00 REG16 10.00 REG26 20.00 REG36
          REG29 4 0.00 REG19 10.00 REG29 20.00 REG39
          REG04 4 0.00 REG01 10.00 REG04
          REG05 4 0.00 REG02 10.00 REG05
          REG06 4 0.00 REG03 10.00 REG06

```

Figure 25. Snippet of Relevant Standard Output for Control Rod Bank Problem

### 3.1.2 Multigroup Infinite Homogeneous Eigenvalue Verification

The multigroup eigenvalue solution methodology in DIF3D uses a conventional power method with either coarse mesh rebalance or Tchebychev acceleration. The purpose of this test is to demonstrate that that algorithm is working in 3D Cartesian geometry diffusion theory for both DIF3D-FD and DIF3D-VARIANT and transport for DIF3D-VARIANT. To start, the two macroscopic sets that will be used are provided in Table 50. The first data set has no up-scattering and the second one has up-scattering from group 3 to group 2.

Table 50. Macroscopic Multigroup Cross Sections for Infinite Homogeneous Test

Group	Total	Gamma	Fission	v	$\chi$	Scatter From		
						Group 1	Group 2	Group 3
1	0.240	0.006	0.006	3.00	0.96	0.024	0.000	0.000
2	0.975	0.040	0.060	2.50	0.04	0.171	0.600	0.000
3	3.100	0.200	0.900	2.00	0.00	0.033	0.275	2.000
Group	Total	Gamma	Fission	v	$\chi$	Group 1	Group 2	Group 3
1	0.240	0.006	0.006	3.00	0.96	0.024	0.000	0.000
2	0.975	0.040	0.060	2.50	0.04	0.171	0.600	1.000
3	3.100	0.200	0.900	2.00	0.00	0.033	0.275	1.000

Because this problem is an infinite homogeneous single mixture problem, the diffusion and transport equations both produce the simple diffusion theory result. The multigroup flux solution and eigenvalue can both be easily obtained by performing Gaussian elimination or some other simple factorization methodology. The forward eigenvalue problem using the first cross section set can be written in the matrix form with an associated eigenvalue and eigenvector of:

$$\begin{bmatrix} \phi_1 \\ \phi_2 \\ \phi_3 \end{bmatrix} = \frac{1}{k_{eff}} \begin{bmatrix} 0.080 & 0.666 & 8.0 \\ 0.0384 & 0.32 & 3.84 \\ 0.012 & 0.1 & 1.2 \end{bmatrix} \begin{bmatrix} \phi_1 \\ \phi_2 \\ \phi_3 \end{bmatrix} \quad k_{eff} = 1.6 \quad \hat{e} = \begin{bmatrix} 0.893391 \\ 0.428828 \\ 0.134009 \end{bmatrix}. \quad (16)$$

The matrix on the right hand side of this equation is singular because of the fission source matrix and thus the system has only one non-zero eigenvalue and associated eigenvector. The adjoint system can be written as the simple transpose of each operator

$$\bar{A}^T \bar{\phi}^\dagger = \frac{1}{k_{eff}} [\bar{\nu} \bar{\Sigma} \cdot \bar{\chi}^T] \bar{\phi}^\dagger. \quad (17)$$

The matrix form again has a single eigenvalue and eigenvector and can be written as

$$\begin{bmatrix} \phi_1^\dagger \\ \phi_3^\dagger \\ \phi_3^\dagger \end{bmatrix} = \frac{1}{k_{eff}} \begin{bmatrix} 1.536 & 0.064 & 0 \\ 1.536 & 0.064 & 0 \\ 1.57909 & 0.06545 & 0 \end{bmatrix} \begin{bmatrix} \phi_1^\dagger \\ \phi_3^\dagger \\ \phi_3^\dagger \end{bmatrix} \quad k_{eff} = 1.6 \quad \hat{e} = \begin{bmatrix} 0.572977 \\ 0.572977 \\ 0.585999 \end{bmatrix}. \quad (18)$$

Using the second cross section set the following forward and adjoint eigenvalue systems are obtained

$$\begin{bmatrix} \phi_1 \\ \phi_2 \\ \phi_3 \end{bmatrix} = \frac{1}{k_{eff}} \begin{bmatrix} 0.080 & 0.666 & 8.0 \\ 0.0642 & 0.535 & 6.416 \\ 0.00966 & 0.0805 & 0.9659 \end{bmatrix} \begin{bmatrix} \phi_1 \\ \phi_2 \\ \phi_3 \end{bmatrix} \quad k_{eff} = 1.5804878049 \quad \hat{e} = \begin{bmatrix} 0.776688 \\ 0.622866 \\ 0.093771 \end{bmatrix} \\ \begin{bmatrix} \phi_1^\dagger \\ \phi_3^\dagger \\ \phi_3^\dagger \end{bmatrix} = \frac{1}{k_{eff}} \begin{bmatrix} 1.5173 & 0.06322 & 0 \\ 1.5173 & 0.06322 & 0 \\ 1.5454 & 0.06439 & 0 \end{bmatrix} \begin{bmatrix} \phi_1^\dagger \\ \phi_3^\dagger \\ \phi_3^\dagger \end{bmatrix} \quad k_{eff} = 1.5804878049 \quad \hat{e} = \begin{bmatrix} 0.573787 \\ 0.573787 \\ 0.584412 \end{bmatrix}. \quad (19)$$

The two cross section sets have very similar eigenvalues and eigenvectors, but the inclusion of significant up-scattering reduces the eigenvalue as it puts more neutrons into the group with a less favorable capture to fission ratio.

The DIF3D-FD and DIF3D-VARIANT solvers both produce the correct eigenvalue solutions as shown in Table 51. As can be seen, the results are only slightly off when compared to the analytic values above. This is directly attributable to the single precision storage of the cross section data in DIF3D that introduces errors in the tenth significant digit for this problem. The flux solution is also printed in the regular DIF3D output and it is a simple normalization to show that the forward and adjoint solutions are identical to the above listed eigenvectors.

**Table 51. DIF3D eigenvalue results for the Infinite Homogeneous Test Problem**

		DIF3D-FD	DIF3D-VARIANT Diffusion	DIF3D-VARIANT P <sub>5</sub> transport
Problem #1	Forward	1.6000 0001	1.6000 0001	1.6000 0001
	Adjoint	1.6000 0001	1.6000 0001	1.6000 0000
Problem #2	Forward	1.5804 8782	1.5804 8781	1.5804 8781
	Adjoint	1.5804 8782	1.5804 8781	1.5804 8781

The above case was also used to verify the forward and adjoint eigenvalue capabilities of the DIF3D-FD Triangular-Z and DIF3D-VARIANT Hexagonal-Z solvers. This was done trivially with the Triangular-Z solver by making an infinite homogeneous medium problem with the addition of a background region composed of the same composition as above. The eigenvalue for this case matched the reference solutions for both cross section sets to all significant figures.

Mimicking this infinite homogenous medium model is not as trivial in Hexagonal-Z, however it was done with a 2-ring model with an assembly pitch of  $10^6$  cm. This large pitch was necessary to minimize the leakage effects near the irregular edge geometry of the hexagonal geometry. The eigenvalue for this case matched the reference solutions for both cross section sets to all significant figures.

Based upon these results, it is concluded that the DIF3D diffusion and transport solvers are properly solving the steady-state forward and adjoint multigroup calculation for all geometry types.

Finally, this model provides a good opportunity to verify the correctness of the RTFLUX and ATFLUX files, as well as to ensure that the A.DIF3D block's Type 03 card option 3 for calculating the forward flux, adjoint flux, or both, is working properly. This was done for all of the aforementioned geometry and solver types; all created correct and consistent RTFLUX and ATFLUX files as well as heeding the Type 03 card option 3.

### 3.1.3 Multi-group Infinite Homogeneous Fixed Source Verification

The preceding test problem verified the power method in DIF3D and this test problem was constructed to further verify the fixed source algorithm and to display the preceding eigenvector solution. The easy way to do this is to take the fission source from the previous problem and enter it as the fixed source. This should produce the identical eigenvector used to construct the fission source and instead of solving both problems defined by Table 50, we only solve the first one in this case. Note that this requires the fission cross sections to be set to zero in the cross section data in Table 50 and the neutron capture cross section adjusted to produce an equivalent total absorption cross section.

The two fixed sources for the forward and adjoint system are

$$\bar{S} = \frac{1}{k_{eff}} \begin{bmatrix} 0.01728 & 0.144 & 1.728 \\ 0.00072 & 0.006 & 0.072 \\ 0 & 0 & 0 \end{bmatrix} \begin{bmatrix} 0.893391 \\ 0.428828 \\ 0.134009 \end{bmatrix} = \begin{bmatrix} 0.192973 \\ 0.008041 \\ 0.0 \end{bmatrix}. \quad (20)$$

$$\bar{S}^\dagger = \frac{1}{k_{eff}} \begin{bmatrix} 0.01728 & 0.00072 & 0 \\ 0.144 & 0.006 & 0 \\ 1.728 & 0.072 & 0 \end{bmatrix} \begin{bmatrix} 0.572977 \\ 0.572977 \\ 0.585999 \end{bmatrix} = \begin{bmatrix} 0.006446 \\ 0.053717 \\ 0.644599 \end{bmatrix}. \quad (21)$$

February 13, 2020

Figure 26 shows the additional fixed source input (card type 19 for A.NIP3) for the forward and adjoint problems along with the flux solution details.

Forward Input Sample								
19	DOMAIN	1	1	0.192972554773992				
19	DOMAIN	2	2	0.008040523115583				
19	DOMAIN	3	3	0.0				
Forward Output Sample								
REGION	ZONE	ZONE	VOLUME	AVG TOTAL FLUX	GROUP	GROUP	GROUP	
NO.	NAME	NO.	NAME	(CC)	(NEUTRON/CM2-SEC)	1	2	3
1	DOMAIN	1	SRC	1.00000E+06	1.45623E+00	8.93391E-01	4.28828E-01	1.34009E-01
	TOTALS			1.00000E+06	1.45623E+00	8.93391E-01	4.28828E-01	1.34009E-01
Adjoint Input Sample								
19	DOMAIN	3	3	0.006445990112973				
19	DOMAIN	2	2	0.053716584274774				
19	DOMAIN	1	1	0.644599011297287				
Adjoint Output Sample								
REGION	ZONE	ZONE	VOLUME	AVG TOTAL FLUX	GROUP	GROUP	GROUP	
NO.	NAME	NO.	NAME	(CC)	(NEUTRON/CM2-SEC)	1	2	3
1	DOMAIN	1	SRC	1.00000E+06	1.73195E+00	5.72977E-01	5.72977E-01	5.85999E-01
	TOTALS			1.00000E+06	1.73195E+00	5.72977E-01	5.72977E-01	5.85999E-01

**Figure 26. DIF3D Forward and Adjoint Input and Output Samples for the Infinite Homogeneous Fixed Source Test Case**

Note that for the adjoint, the fixed source is re-ordered with respect to energy such that group 3 is entered as group 1 and vice versa. This is required as DIF3D does not internally re-order the fixed source inputs for adjoint problems (neither FIXSRC or VARSRC are re-ordered). In both cases, the DIF3D results identically produce the correct eigenvectors used as input in equation 3.49. This problem demonstrates that both the eigenvalue and fixed source capabilities of DIF3D are working properly for multi-group problems.

### 3.1.4 One-Region Analytic Spatial Eigenvalue Solution

Section 3.1.2 verified multigroup eigenvalues are implemented correctly, but using a single homogenous region, thus it is not sensitive to spatial variations. Such a problem cannot be relied upon to identify errors in the spatial transport of neutrons throughout the system. Therefore this section will evaluate DIF3D's ability to perform the spatial transport of neutrons in DIF3D. Further, the reader will note that since DIF3D-VARIANT can also solve a simplified transport method that is consistent with the diffusion equation, this work will also be used to bolster the verification of the DIF3D-VARIANT spatial transport ability.

The one-group diffusion equation can be written in Cartesian Coordinates as



$$\begin{aligned}
& -D(x, y, z) \nabla^2 \phi(x, y, z) + \Sigma_R(x, y, z) \phi(x, y, z) = S(x, y, z) \\
& \left| \begin{aligned} S(x, y, z) &= \frac{1}{k_{eff}} \nu \Sigma_f(x, y, z) \phi(x, y, z) \\ S(x, y, z) &= q(x, y, z) \\ S(x, y, z) &= \nu \Sigma_f(x, y, z) \phi(x, y, z) + q(x, y, z) \end{aligned} \right. , \quad (22)
\end{aligned}$$

where  $D(x, y, z)$  is the diffusion coefficient,  $\Sigma_R(x, y, z)$  is the removal cross section,  $\phi(x, y, z)$  is the flux solution, and  $S(x, y, z)$  is the source. Three different source representations are provided in this equation, the first of which is meant for a homogeneous k-eigenvalue steady state flux solution with  $\nu \Sigma_f(x, y, z)$  as the combined fission cross section and neutrons produced per fission. The second source example defines a fixed source component  $q(x, y, z)$  that is independent of the flux solution. The third source example contains both a fission source, without  $k_{eff}$ , and a fixed source component. This form is typically referred to as an inhomogeneous fixed source problem as it contains a homogeneous solution component derived from the fission source and a particular solution component derived from the fixed source. In this situation, the system should not be critical or supercritical as it has no steady state solution. This problem can be particularly difficult to solve if the fixed source is orthogonal to the fission source.

As discussed previously, the usage of DIF3D requires that all three source options be verified. The easiest option to obtain an analytic solution for is the steady state eigenvalue solution that has the simple differential form of

$$\begin{aligned}
& \nabla^2 \phi(x, y, z) + B(x, y, z) \phi(x, y, z) = 0, \quad \phi(\vec{r} \in \Gamma) = 0, x \in 0, X, y \in 0, Y, z \in 0, Z \\
& B(x, y, z) = \frac{\frac{1}{k_{eff}} \cdot \nu \Sigma_f(x, y, z) - \Sigma_R(x, y, z)}{D(x, y, z)} . \quad (23)
\end{aligned}$$

To make the problem non-trivial, vacuum boundary conditions are applied on the entire exterior of the domain. The standard way to solve this problem is to assume separation of variables such that

$$\phi(x, y, z) = A(x) \cdot B(y) \cdot C(z) . \quad (24)$$

For simplicity, the cross sections are set as constant throughout the domain to arrive at

$$\begin{aligned}
& \nabla^2 \phi(x, y, z) + B \cdot \phi(x, y, z) = 0, \quad \phi(\vec{r} \in \Gamma) = 0 \\
& B = \frac{\frac{1}{k_{eff}} \nu \Sigma_f - \Sigma_R}{D} = \left( \frac{1}{k_{eff}} \nu \Sigma_f - \Sigma_R \right) \cdot 3 \cdot \Sigma_{tr} . \quad (25)
\end{aligned}$$

In this case, the general solution for a 1-D Cartesian geometry homogeneous system like this has the form:

$$A(x) = \sum_{i=1}^{\infty} a_i \cdot \cos^i(h_i \cdot x) + c_i \cdot \sin^i(h_i \cdot x). \quad (26)$$

This is an infinite series result that will produce a unique solution for the set of coefficients associated with the expansion at each truncation point. Because we desire the fundamental mode solution, this expansion truncates to the minimum first order representation of

$$A(x) = a + b \cdot \cos(h \cdot x) + c \cdot \sin(h \cdot x). \quad (27)$$

By inspection,  $a = 0$  as this is a homogeneous solution (i.e. no fixed source) and that  $h = \sqrt{B}$ . The remaining terms can be found via application of the boundary conditions as:

$$A(x) = b \cdot \cos(\sqrt{B} \cdot x) + c \cdot \sin(\sqrt{B} \cdot x)$$

$$A(0) = 0 = b + c \cdot 0 \rightarrow b \equiv 0$$

$$A(X) = c \cdot \sin(\sqrt{B} \cdot X) \rightarrow \sqrt{B} \cdot X = X \cdot \sqrt{\left(\frac{1}{k_{eff}} \nu \Sigma_f - \Sigma_R\right) \cdot 3 \cdot \Sigma_{tr}} \equiv n \cdot \pi. \quad (28)$$

$$k_{eff} = \frac{\nu \Sigma_f}{\frac{1}{3 \cdot \Sigma_{tr}} \left(\frac{n \cdot \pi}{X}\right)^2 + \Sigma_R}$$

As seen, the application of the boundary conditions restricts the eigenvalue such that the relationship is satisfied thereby inferring multiple solutions (eigenvalues) are possible. Since the fundamental mode represents the largest value of  $k_{eff}$ , the largest value of  $k_{eff}$  that corresponds to the smallest value of  $n$  is desired. Setting  $n = 0$  leads to the trivial solution that  $c = 0$  and thus the flux is zero. Setting the coefficient  $n = 1$ , the coefficient  $c$  is determined by normalizing the flux magnitude to meet the stated power of the system. The typical way of writing the fundamental mode analytic solution is

$$\phi(x) = c \cdot \sin\left(\frac{x}{X} \cdot \pi\right) \quad k_{eff} = \frac{\nu \Sigma_f}{\frac{1}{3 \cdot \Sigma_{tr}} \left(\frac{\pi}{X}\right)^2 + \Sigma_R}. \quad (29)$$

The same technique can be applied to 2D and 3D domains leading to the analytic solutions of

$$\phi(x, y) = c \cdot \sin\left(\frac{x}{X} \cdot \pi\right) \cdot \sin\left(\frac{y}{Y} \cdot \pi\right) \quad k_{eff} = \frac{\nu \Sigma_f}{\frac{1}{3 \cdot \Sigma_{tr}} \left\{ \left(\frac{\pi}{X}\right)^2 + \left(\frac{\pi}{Y}\right)^2 \right\} + \Sigma_R}, \quad (30)$$

$$\phi(x, y, z) = c \cdot \sin\left(\frac{x}{X} \cdot \pi\right) \cdot \sin\left(\frac{y}{Y} \cdot \pi\right) \cdot \sin\left(\frac{z}{Z} \cdot \pi\right) \quad k_{eff} = \frac{\nu \Sigma_f}{\frac{1}{3 \cdot \Sigma_{tr}} \left\{ \left(\frac{\pi}{X}\right)^2 + \left(\frac{\pi}{Y}\right)^2 + \left(\frac{\pi}{Z}\right)^2 \right\} + \Sigma_R}. \quad (31)$$

To verify the DIF3D result, the above analytic solutions were put into MathCAD and the average flux solution was computed for each mesh in the DIF3D approximation. A comparison to both the eigenvalue and flux are pursued since comparing only the eigenvalue could be misleading as the spatial meshing approximation can lead to some cancellation of eigenvalue error. The analytic solution above is sufficient to test out the 3D solver functionality with all vacuum boundary

conditions. To test out the reflected boundary conditions in the 3D solver, we apply them in pairs such that the 2D analytic solution applies in the transverse plane. As an example, to test out the reflected boundary conditions in the x-direction, we apply reflected boundary conditions at  $0$  and  $X$  and thus the y-z plane should identically reproduce the analytic solution with the appropriate variable substitution ( $x \rightarrow y$ ,  $y \rightarrow z$ ). To additionally test reflected boundary conditions, we apply the reflected boundary conditions on two paired surfaces, such as x and y, that should produce the 1D analytic solution above. The final test we apply is to make use of the symmetry of the analytic solution and only model  $1/8^{\text{th}}$  of the domain in DIF3D and apply a single reflected boundary condition on each coordinate direction. Combined, the above stated problem set will fully demonstrate the accuracy of the Cartesian diffusion theory solution scheme and application of the boundary conditions.

A cubic domain of size 100 cm and cross sections of  $\Sigma_{tr} = 0.5$ ,  $\nu = 6$ ,  $\Sigma_c = 0.2$ ,  $\Sigma_f = 0.05$ , and  $\Sigma_s = 0.25$  was used. Table 52 provides the eigenvalue solutions for the DIF3D-FD solver on the analytic test problems defined above. Starting with the 3D results, there is clear asymptotic convergence to the reference solution as the mesh is refined from 10 to 80 in all coordinate directions. The symmetry problem was setup to identically match the 40x40x40 mesh case and one can see that it produces an identical eigenvalue solution. No mesh refinement studies were done in the 2D or 1D cases but all geometries were again setup with the same 40x40x40 mesh. Comparing the accuracy of the eigenvalue in the 3D case with 2D and 1D, one can see that the same meshing appears to produce a more accurate solution in the lower dimensional cases (0.48 versus 0.32 versus 0.16 pcm). This is not uncommon for any solution methodology as the error introduced by the leakage approximation is progressively reduced as the dimensionality of the model is decreased.

**Table 52. DIF3D-FD Eigenvalue for the Cartesian Analytic Diffusion Benchmark**

Description	DIF3D	Reference	Error (pcm)
<b>3D 10x10x10 Meshes</b>	1.19067 59	1.19059 94	7.65
<b>3D 20x20x20 Meshes</b>	1.19061 86	1.19059 94	1.92
<b>3D 40x40x40 Meshes</b>	1.19060 42	1.19059 94	0.48
<b>3D 80x80x80 Meshes</b>	1.19060 06	1.19059 94	0.12
<b>3D 20x20x20 Meshes Symmetry</b>	1.19060 42	1.19059 94	0.48
<b>2D 40x40x40 Meshes y-z</b>	1.19371 98	1.19371 65	0.32
<b>2D 40x40x40 Meshes x-z</b>	1.19371 97	1.19371 65	0.32
<b>2D 40x40x40 Meshes x-y</b>	1.19371 97	1.19371 65	0.32
<b>1D 40x40x40 Meshes z</b>	1.19685 16	1.19685 00	0.16
<b>1D 40x40x40 Meshes x</b>	1.19685 16	1.19685 00	0.16
<b>1D 40x40x40 Meshes y</b>	1.19685 16	1.19685 00	0.16

Overall, the preceding DIF3D-FD solutions demonstrate that the solution algorithm is producing the correct eigenvalue. As mentioned previously, the flux distribution is checked by computing

the average flux solution from the analytic solution for the DIF3D mesh. Comparing the detailed solution is a considerable undertaking and thus the first axial mesh plane in each DIF3D case is chosen for comparison and the RMS error for that plane is reported here as the DIF3D solution should be least accurate near the vacuum boundary condition. Figure 27 shows the spatial flux distribution of the DIF3D-FD methodology on the 3D analytic benchmark. The left hand picture shows the 3D flux distribution while the right hand picture shows the flux solution on the plane we chose for the comparison.

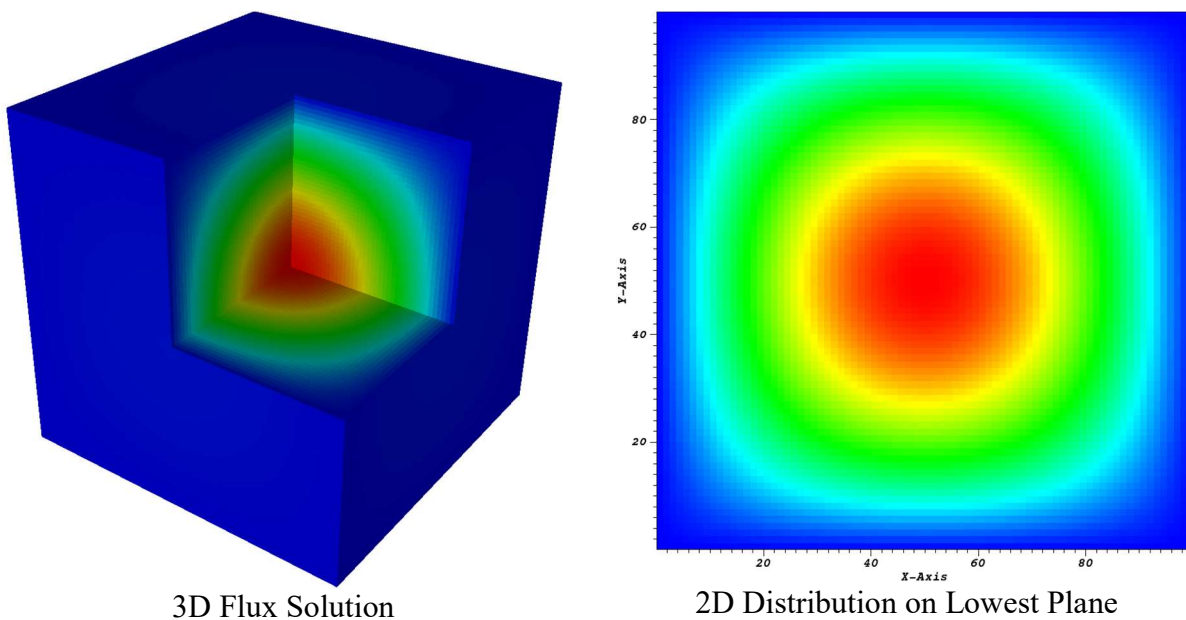


**Figure 27. DIF3D-FD Flux Solution for 3D Domain in Lowest Z Plane**

Table 53 summarizes the computed maximum and Root-mean-squared (RMS) errors of DIF3D for the four mesh refinement problems in Table 52 on the lower plane. As can be seen, both the peak and RMS error initially decrease, but both tend to start increasing as the mesh is refined further. This is not a surprise as the solution we are trying to compute becomes consistently more difficult as we do mesh refinement. We can integrate the flux on the finer meshes to produce the average fluxes on the coarsest 10x10 mesh and provide the peak and RMS flux errors in Table 53. As can be seen, the coarse level flux solution details are also not improved by the progressive mesh refinement indicating that the accuracy of the solution is consistently limited by some other factor.

**Table 53. DIF3D-FD Peak and RMS Errors on the Lowest Plane**

<b>DIF3D Meshing</b>	<b>Peak Flux Error</b>	<b>RMS Flux Error</b>
10x10x10	1.3E-04	8.1E-05
20x20x20	4.3E-06	1.5E-06
40x40x40	5.2E-06	1.5E-06
80x80x80	6.3E-06	1.7E-06
20→10	1.2E-04	7.1E-05
40→10	1.3E-04	7.8E-05
80→10	1.5E-04	8.7E-05

One such aspect is the error due to the iterative algorithm used in DIF3D. DIF3D does not have a residual based error check on the flux solution and thus there is some uncertainty about how much error remains. We decreased the DIF3D input convergence settings for the error reduction factor from the default of 0.04 to 1.0E-8 along with the pointwise fission source tolerance to 1.0E-8 and thereby push the DIF3D flux solution error on the 40→10 result above to 4.0E-5 for the peak flux and 2.5E-5 for the RMS flux. While these are clear improvements, it is not obvious that decreasing the error targets further will resolve the issue. The source of the remaining error can be attributed to the fact that the flux magnitude drops by six orders of magnitude from the center of the domain to the domain edge. This means that a slight amount of error in the flux solution at the center of the domain can propagate to a considerably large error at the periphery which is the observed behavior here as the error in the high flux region was pushed to 8 significant digits of accuracy. Given this situation, the errors seen in Table 53 are more than acceptable for low flux regions in the routine use of DIF3D.

Using the same input problems, the DIF3D-VARIANT solver can be tested for its accuracy on solving diffusion theory problems like this. Table 54 provides the eigenvalue results for DIF3D-VARIANT using a fixed 6<sup>th</sup> order polynomial flux/source approximation and 1<sup>st</sup> order leakage approximation. It is noted that a much coarser mesh is used in DIF3D-VARIANT than was used in DIF3D-FD. While the accuracy of the coarsest mesh is very poor, the remaining meshes produce solutions that are generally more accurate than DIF3D-FD using considerably fewer meshes. This is expected as DIF3D-VARIANT uses a much higher order spatial basis approximation than DIF3D-FD.

In Table 54, asymptotic convergence to the reference solution is observable as the mesh is refined from 2 per coordinate direction to 16. The symmetry conditions applied to a 4x4x4 mesh case, equivalent to the 8x8x8 mesh case, produces a result identical to the non-symmetry model. Following the mesh refinement results, the calculated results are provided using the paired reflected boundary conditions that match the 2D or 1D analytic solution. As was the case with the DIF3D-FD problems, the eigenvalue accuracy is much better on the lower dimensional models such that the error is on the order of the convergence tolerance applied to the solver.

**Table 54. DIF3D-VARIANT Eigenvalue for the Cartesian Analytic Diffusion Benchmark**

<b>Description</b>	<b>DIF3D</b>	<b>Reference</b>	<b>Error (pcm)</b>
<b>3D 2x2x2 Meshes</b>	1.19093 13	1.19059 94	33.19
<b>3D 4x4x4 Meshes</b>	1.19062 51	1.19059 94	2.57
<b>3D 8x8x8 Meshes</b>	1.19060 11	1.19059 94	0.17
<b>3D 16x16x16 Meshes</b>	1.19059 95	1.19059 94	0.01
<b>3D 4x4x4 Meshes Symmetry</b>	1.19060 11	1.19059 94	0.17
<b>2D 8x8x8 Meshes y-z</b>	1.19371 66	1.19371 65	0.002
<b>2D 8x8x8 Meshes x-z</b>	1.19371 66	1.19371 65	0.002
<b>2D 8x8x8 Meshes x-y</b>	1.19371 66	1.19371 65	0.002
<b>1D 8x8x8 Meshes z</b>	1.19685 00	1.19685 00	-0.005
<b>1D 8x8x8 Meshes x</b>	1.19685 00	1.19685 00	-0.005
<b>1D 8x8x8 Meshes y</b>	1.19685 00	1.19685 00	-0.005

Table 55 provides the peak and RMS errors for the four meshes used in the mesh refinement study along with the integrated results of the 8x8x8 and 16x16x16 based meshes collapsed to a 4x4x4 base mesh. The 2x2x2 mesh result has a zero error because there is only 1 mesh by symmetry and the normalization requires the average flux result to be identical. The remaining meshes show a slight increase in the peak and RMS flux error as the mesh is refined. As was the case with DIF3D-FD, collapsing to the 4x4x4 mesh did not significantly improve the error. The remaining error is observed in this table with DIF3D-VARIANT is also traceable to the iterative algorithm. One particular difference to note, however, is that the residual error with the DIF3D-VARIANT results are considerably smaller than those seen in DIF3D-FD (almost 2 orders of magnitude). This is just an artifact of the different iterative solution schemes and coarser meshing in DIF3D-VARIANT.

**Table 55. DIF3D-VARIANT Peak and RMS Errors on the Lowest Planer Flux Distribution**

<b>DIF3D Meshing</b>	<b>Peak Flux Error</b>	<b>RMS Flux Error</b>
<b>2x2x2</b>	0.0	0.0
<b>4x4x4</b>	6.8E-06	3.8E-06
<b>8x8x8</b>	8.4E-06	5.1E-06
<b>16x16x16</b>	1.3E-05	6.6E-06
<b>8→4</b>	6.1E-06	3.7E-06
<b>16→4</b>	6.7E-06	4.3E-06

Because DIF3D-VARIANT can use a higher order spatial basis, refinements in those approximations must also be considered. Using a fixed 3x3x3 spatial mesh, Table 56 shows the impact of changing the spatial order of the polynomial for the flux and leakage noting that the source approximation was set to be the same as the flux. From this Table, one should see quite easily that the flux approximation is of secondary importance to the leakage approximation. From the results in Table 54, one can see that using a quadratic leakage approximation on a 3x3x3 mesh can produce results comparable to the 8x8x8 mesh with a linear leakage approximation. Using a cubic and quartic leakage approximation shows additional improvement to the reference solution

within the iterative error applied to the problem. In both cases, the higher order leakage approximation requires a higher order flux approximation to be used that is generally the main computational penalty that favors doing simple mesh refinement to improve the solution accuracy.

**Table 56. DIF3D-VARIANT P-refinement for the Cartesian Analytic Diffusion Benchmark**

Spatial Flux & Source Order	Spatial Leakage Order	DIF3D	Reference	Error (pcm)
4	1	1.19067 34	1.19059 94	7.40
6	1	1.19067 62	1.19059 94	7.68
8	1	1.19067 64	1.19059 94	7.70
6	2	1.19060 05	1.19059 94	0.11
8	2	1.19060 05	1.19059 94	0.11
8	3	1.19059 94	1.19059 94	-0.003
10	4	1.19059 94	1.19059 94	-0.004

Because a coarse mesh was used in the polynomial order (p-refinement) study, there is no point in comparing the average flux error. The preceding eigenvalue and flux results are sufficient to demonstrate that DIF3D-VARIANT can properly solve this analytic diffusion theory problem.

To complete the study, the domain is modified to be a 100x90x80 cm with the same cross sections. Because the flux comparison has already been completed with this analytic solution, only the eigenvalue accuracy is used to verify that DIF3D properly handles the different spatial dimensions of the domain. Table 57 provides the eigenvalue results obtained with DIF3D-FD and DIF3D-VARIANT showing that both obtain the analytic solution for the non-cube geometry consistent with the error obtained in the cube geometry. It is important to note that the reference solution changes in the various 2D and 1D geometries and only the error for the DIF3D results is provided. These results show that both DIF3D-FD and DIF3D-VARIANT are able to reproduce the analytic solution given sufficient spatial mesh refinement.



Table 57. DIF3D Eigenvalue Results for the Modified Analytic Diffusion Benchmark

Description	DIF3D-FD	Error (pcm)	VARIANT	Error (pcm)
<b>3D 2x2x2 Meshes</b>	1.18822 29	9.64	1.18854 75	42.10
<b>3D 4x4x4 Meshes</b>	1.18815 06	2.42	1.18815 90	3.25
<b>3D 8x8x8 Meshes</b>	1.18813 25	0.60	1.18812 86	0.21
<b>3D 16x16x16 Meshes</b>	1.18812 80	0.15	1.18812 66	0.01
<b>3D 4x4x4 Meshes Symmetry</b>	1.18813 25	0.61	1.18812 86	0.21
<b>2D 8x8x8 Meshes y-z</b>	1.19123 51	0.45	1.19123 07	0.005
<b>2D 8x8x8 Meshes x-z</b>	1.19196 53	0.41	1.19196 12	0.004
<b>2D 8x8x8 Meshes x-y</b>	1.19298 75	0.36	1.19298 39	0.002
<b>1D 8x8x8 Meshes z</b>	1.19508 79	0.25	1.19508 53	-0.007
<b>1D 8x8x8 Meshes x</b>	1.19685 16	0.16	1.19685 00	-0.005
<b>1D 8x8x8 Meshes y</b>	1.19611 55	0.20	1.19611 34	-0.011

The final aspect to consider is the accuracy of the adjoint calculation. Because the diffusion equation is self-adjoint, and this is one group problem, the adjoint flux solution will be identical to the forward solution. This makes the comparison process rather straight-forward although the adjoint has no normalization to power while the forward does. Thus the adjoint flux solution coming out of DIF3D requires an additional normalization step to carry out the comparison.

Because the forward and adjoint flux solution are identical the actual iterative solution from DIF3D-FD and DIF3D-VARIANT yields identical eigenvalues for the forward and adjoint and thus it is not included here. Selecting just a part of the 10x10x10 mesh flux output, it is rather easy to show that the two flux solutions are identical except for the normalization. Table 58 provides the selected flux data from the forward and adjoint DIF3D-FD flux solutions to the 100x100x100 cm problem and the ratio of the two solutions at each mesh point. As can be seen, there is a constant multiplier required to make the flux solution identical at each mesh point.

The same result can be observed with DIF3D-VARIANT in Table 59 where the 8x8x8 mesh was selected for the same 100x100x100 cm problem. What should be clear is that the DIF3D-FD forward flux magnitudes are very similar to the DIF3D-VARIANT forward flux magnitudes. The adjoint flux solution in VARIANT is considerably larger than that observed for DIF3D-FD. This is because the flux solution in DIF3D-FD is initialized to 1.0 while DIF3D-VARIANT is initialized to  $10^{10}$ . This normalization was chosen for DIF3D-NODAL, and thus for DIF3D-VARIANT, to be consistent with the actual flux magnitudes observed in a reactor problem. Because the flux magnitude is only important when the desired power is met, the actual initialization value is not entirely relevant although it does lead to abnormally different flux magnitudes in these cases.

Comparing the ratio of the adjoint and forward flux, one finds the actual normalization constant between DIF3D-FD and DIF3D-VARIANT is similar except for the magnitude. This is not always the case as the iterative solution schemes of the two solvers can cause the flux magnitude to drift



considerably from the initialization condition. Combined, these two tables are sufficient proof to demonstrate that the forward and adjoint spatial flux solution schemes in DIF3D-FD and DIF3D-VARIANT are implemented correctly.

**Table 58. DIF3D-FD Forward and Adjoint Flux Comparison for the Diffusion Benchmark**

Y mesh	Forward		Adjoint		Adjoint/Forward	
	X mesh 1	X mesh 2	X mesh 1	X mesh 2	X mesh 1	X mesh 2
10	5.86E+03	1.70E+04	1.74E-02	5.06E-02	2.9767E-06	2.9767E-06
9	1.70E+04	4.94E+04	5.06E-02	1.47E-01	2.9767E-06	2.9767E-06
8	2.65E+04	7.69E+04	7.89E-02	2.29E-01	2.9767E-06	2.9767E-06
7	3.34E+04	9.69E+04	9.94E-02	2.88E-01	2.9767E-06	2.9767E-06
6	3.70E+04	1.07E+05	1.10E-01	3.20E-01	2.9767E-06	2.9767E-06
5	3.70E+04	1.07E+05	1.10E-01	3.20E-01	2.9767E-06	2.9767E-06
4	3.34E+04	9.69E+04	9.94E-02	2.88E-01	2.9767E-06	2.9767E-06
3	2.65E+04	7.69E+04	7.89E-02	2.29E-01	2.9767E-06	2.9767E-06
2	1.70E+04	4.94E+04	5.06E-02	1.47E-01	2.9767E-06	2.9767E-06
1	5.86E+03	1.70E+04	1.74E-02	5.06E-02	2.9767E-06	2.9767E-06

**Table 59. DIF3D-VARIANT Forward and Adjoint Flux Comparison for the Diffusion Benchmark**

Y mesh	Forward		Adjoint		Adjoint/Forward	
	X mesh 1	X mesh 2	X mesh 1	X mesh 2	X mesh 1	X mesh 2
8	1.13E+04	3.22E+04	3.36E+08	9.57E+08	2.9765E+04	2.9765E+04
7	3.22E+04	9.16E+04	9.57E+08	2.73E+09	2.9765E+04	2.9765E+04
6	4.81E+04	1.37E+05	1.43E+09	4.08E+09	2.9765E+04	2.9765E+04
5	5.68E+04	1.62E+05	1.69E+09	4.81E+09	2.9765E+04	2.9765E+04
4	5.68E+04	1.62E+05	1.69E+09	4.81E+09	2.9765E+04	2.9765E+04
3	4.81E+04	1.37E+05	1.43E+09	4.08E+09	2.9765E+04	2.9765E+04
2	3.22E+04	9.16E+04	9.57E+08	2.73E+09	2.9765E+04	2.9765E+04
1	1.13E+04	3.22E+04	3.36E+08	9.57E+08	2.9765E+04	2.9765E+04

### 3.1.5 One-Region Analytic Spatial Fixed-Source Verification

The purpose of this test problem is to demonstrate that DIF3D produces the correct solution to a given fixed source problem and that the fixed source input into DIF3D works. This again will be performed with DIF3D-FD and DIF3D-VARIANT.

In this case the same diffusion equation as in the previous section is used with the second source option,  $q(x, y, z)$ . The analytic solution depends upon the cross section distribution and the source functionalization itself. Taking the simplest source representation of

$$q(x, y, z) = q, \quad (32)$$

the differential equation can be simplified to

$$-D(x, y, z) \nabla^2 \phi(x, y, z) + \Sigma_R(x, y, z) \phi(x, y, z) = q, \quad (33)$$

Taking the same vacuum boundary conditions, and constant cross sections the diffusion equation can be written as

$$-\nabla^2 \phi(x, y, z) + \frac{\Sigma_R}{D} \phi(x, y, z) = \frac{q}{D}, \quad \phi(\vec{r} \in \Gamma) = 0, x \in 0, X, y \in 0, Y, z \in 0, Z \quad (34)$$

This equation is not solvable because at the domain boundary, the flux must be zero yet the source at that point is non-zero. Thus a compact analytic solution is not achievable. At this point the options are either continue with a two-region problem where the source is discontinuous in space, or a source that actually reaches zero at the boundary must be used. The latter aspect is ideal to test out both the fixed source input of DIF3D and still keep the analytic solution rather simple. To get a compact analytic solution that is consistent with the boundary conditions, a source distribution with the same shape as the preceding homogeneous eigenvalue fission source is assumed:

$$q(x) = q \cdot \sin\left(\frac{x}{X} \cdot \pi\right) \quad (35)$$

and the differential equation to solve:

$$-\frac{d^2}{dx^2} \phi(x) + \frac{\Sigma_R}{D} \phi(x) = \frac{q}{D} \cdot \sin\left(\frac{x}{X} \cdot \pi\right), \quad \phi(x=0) = 0, \phi(x=X) = 0. \quad (36)$$

The analytic solution for the flux takes on the same shape as the source and thus can be written as

$$\phi(x) = a_0 \sin\left(\frac{x}{X} \cdot \pi\right). \quad (37)$$

Plugging this into the differential equation above, the following expressions must hold

$$\begin{aligned} a_0 \left(\frac{\pi}{X}\right)^2 \sin\left(\frac{x}{X} \cdot \pi\right) + \frac{\Sigma_R}{D} a_0 \sin\left(\frac{x}{X} \cdot \pi\right) &= \frac{q}{D} \cdot \sin\left(\frac{x}{X} \cdot \pi\right) \\ a_0 \left(\frac{\pi}{X}\right)^2 + a_0 \frac{\Sigma_R}{D} &= \frac{q}{D} \rightarrow a_0 = \frac{q}{D \frac{\pi^2}{X^2} + \Sigma_R} \end{aligned} \quad (38)$$

This gives the final analytic solution of

$$\phi(x) = \frac{q}{\frac{1}{3 \cdot \Sigma_r} \left(\frac{\pi}{X}\right)^2 + \Sigma_R} \cdot \sin\left(\frac{x}{X} \cdot \pi\right), \quad (39)$$

that is trivially easy to show satisfies the desired boundary conditions. It is important to note that this answer is nearly identical to the preceding homogeneous eigenvalue scheme and thus a source magnitude equivalent to  $\nu \Sigma_f$  can be used.

Because of the near identical setup, the 2D and 3D approaches can be obtained using simple transformations of the previous homogeneous eigenvalue problem as

$$\phi(x, y) = \frac{q}{\frac{1}{3 \cdot \Sigma_{tr}} \left\{ \left( \frac{\pi}{X} \right)^2 + \left( \frac{\pi}{Y} \right)^2 \right\} + \Sigma_R} \cdot \sin\left(\frac{x}{X} \cdot \pi\right) \cdot \sin\left(\frac{y}{Y} \cdot \pi\right), \quad (40)$$

$$\phi(x, y, z) = \frac{q}{\frac{1}{3 \cdot \Sigma_{tr}} \left\{ \left( \frac{\pi}{X} \right)^2 + \left( \frac{\pi}{Y} \right)^2 + \left( \frac{\pi}{Z} \right)^2 \right\} + \Sigma_R} \cdot \sin\left(\frac{x}{X} \cdot \pi\right) \cdot \sin\left(\frac{y}{Y} \cdot \pi\right) \cdot \sin\left(\frac{z}{Z} \cdot \pi\right). \quad (41)$$

In testing of DIF3D-FD, only constant sources in each mesh can be specified. Therefore the accuracy of the test is limited by the spatial mesh refinement itself. For DIF3D-VARIANT, the higher order polynomial treatment allows for a better approximation of the source distribution although it requires the sine based function to be fit with the VARIANT basis set. This can also be tested similarly to the DIF3D-FD approach by using a fine mesh input. Because of the need to verify the inclusion of the VARSRC file for its usage in PERSENT, both paths will be tested for DIF3D-VARIANT.

Starting with DIF3D-FD similar cross sections to the previous benchmark of  $\Sigma_{tr} = 0.5$ ,  $\Sigma_c = 0.25$ , and  $\Sigma_s = 0.25$  were used. The problem dimensions are set to  $X=100$ ,  $Y=90$ , and  $Z=80$  and use 10, 20, 40, 60, and 80 mesh intervals in each coordinate direction to show the impact of mesh refinement. This not only refines the mesh itself, but also requires source input refinement. Because of the overwhelming amount of tabulated data, the results are presented visually and the summary of the average flux error and peak flux error in Table 60.

**Table 60. DIF3D-FD Flux Error Results for the Fixed Source Analytic Diffusion Benchmark**

Mesh	Peak Error	Average Error
10x10x10	8.6E-05	8.1E-05
20x20x20	2.9E-05	2.0E-05
40x40x40	1.1E-04	4.7E-06
60x60x60	2.1E-04	7.1E-06
80x80x80	4.3E-04	1.7E-05

The results in Table 60 indicate that the flux solution is not monotonically improving. Figure 28 shows the spatial error distribution where all error plots use the same scale shown. Starting at the coarsest mesh of 10x10x10, one can see that the entire domain has error on the order of 0.0001. As the mesh is refined, one can see that the 20x20x20 shows improvement with a factor of 10. From there, each progressive mesh refinement shows a reduced error in the internal part of the domain but the solution along the x-axis ( $Y=0$  and  $Z=0$ ) has a growing error contribution. This error is a result of the iterative solution algorithm where the cited set of meshes always have the largest iterative error as it is updated the least frequently. Because DIF3D-FD does not have an error check on the flux, the observed solution is the best that can be achieved without using the restart feature of DIF3D-FD as DIF3D-FD uses the same number of iterations for all of the meshes.

The same problems can be identically executed using DIF3D-VARIANT leading to the peak and average flux error shown in Table 61 and the spatial distribution of that error shown in Figure 28. Starting with the tabulated data, one can clearly see a monotonic decrease in the peak and average flux error as the mesh is refined. Of concern is that the error seen in the DIF3D-VARIANT solution is considerably larger than that seen in DIF3D-FD from Table 60.

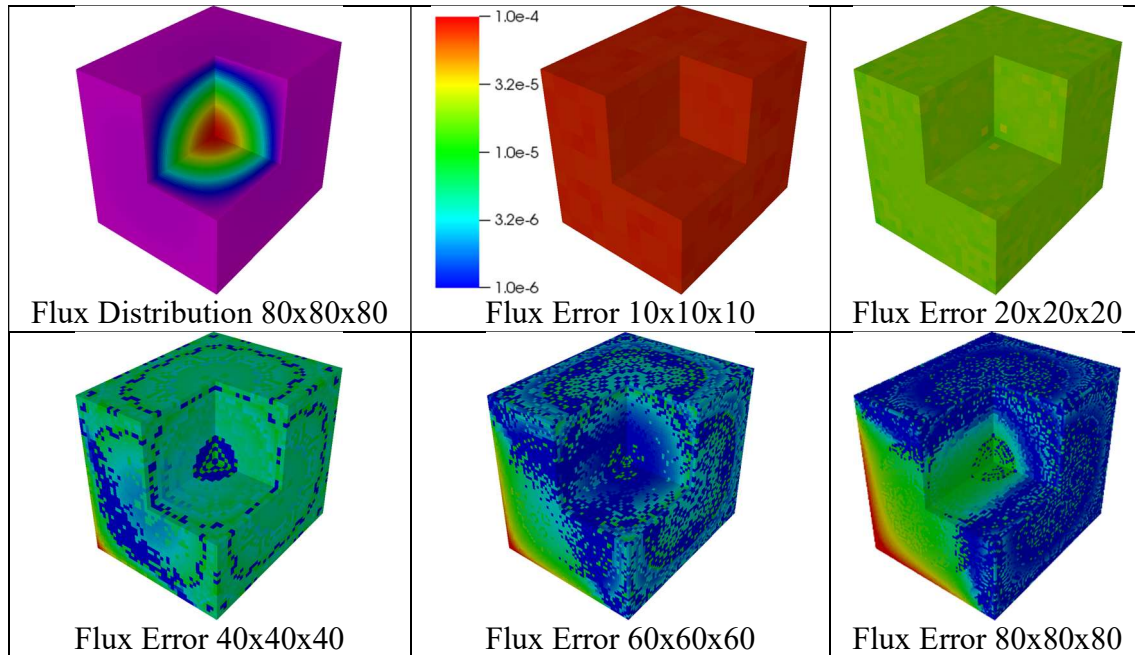


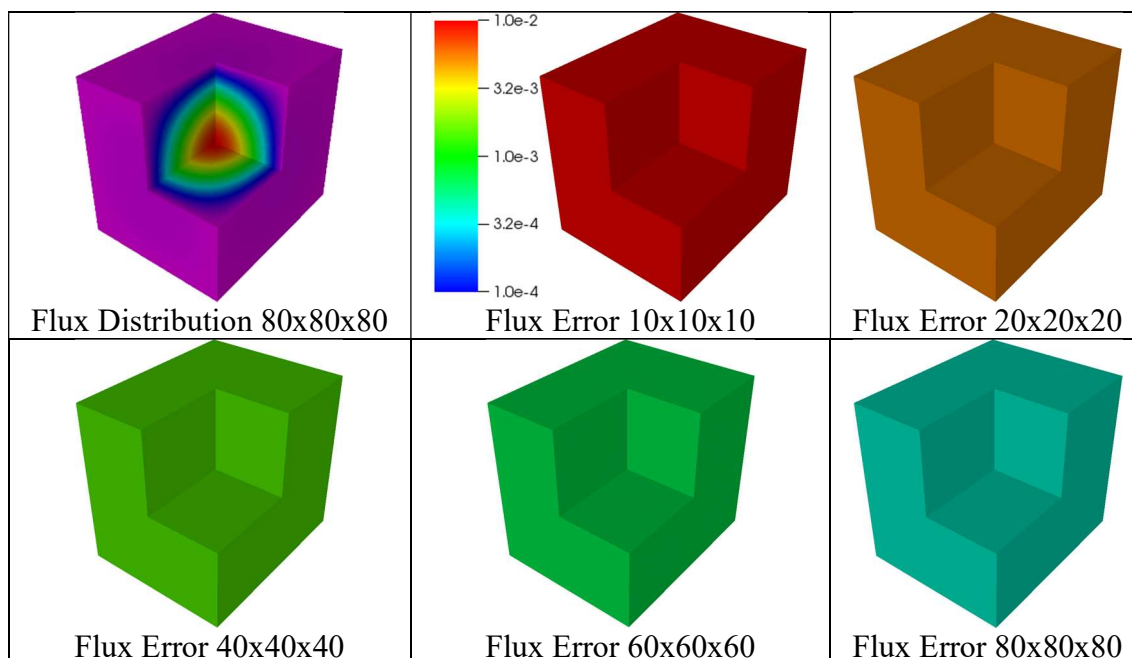
**Figure 28. The DIF3D-FD Flux Error Distribution for the Fixed Source Diffusion Benchmark**

This is the reverse of that observed behavior in the homogeneous eigenvalue solution and is traceable to how the underlying methodology handles the fixed source. Noting that the DIF3D-FD results are not converged, the approximation of the source exactly suits the approximation of the flux that can appear to produce a very accurate solution although the interpolation of the flux between meshes is not likely to be correct. In DIF3D-VARIANT, the approximation of the source is not consistent with the approximation made for the flux and thus the flux error introduced by the poor source approximation can only be resolved if the source representation is improved.

Unlike DIF3D-FD, the flux distribution error in DIF3D-VARIANT in Figure 29 is nearly uniform over the entire domain for each mesh approximation. No convergence problems are observable in DIF3D-VARIANT as it allows the user to directly control the number of iterations used in the solution. This means with proper input, the DIF3D-VARIANT solver is more reliable than DIF3D-FD on fixed source problems although both of them require considerable mesh refinement to obtain the correct solution to this problem.

**Table 61. DIF3D-VARIANT Flux Error Results for the Fixed Source Diffusion Benchmark**

Mesh	Peak Error	Average Error
<b>10x10x10</b>	1.71E-02	1.71E-02
<b>20x20x20</b>	5.49E-03	5.48E-03
<b>40x40x40</b>	1.50E-03	1.49E-03
<b>60x60x60</b>	6.84E-04	6.76E-04
<b>80x80x80</b>	3.91E-04	3.82E-04

**Figure 29. The DIF3D-VARIANT Error Distribution for the Fixed Source Diffusion Benchmark**

The preceding approach tests out the card type 19 input option of A.NIP3. With this input, DIF3D generates the FIXSRC binary file that could alternatively be provided by the user similar to ISOTXS without using card type 19 input. For DIF3D-VARIANT, the preceding work shows that the FIXSRC file leads to some accuracy issues. The VARSRC file is an alternative to FIXSRC that allows the user to define a source with the same spatial expansion used by DIF3D-VARIANT during the solve phase. To create this file, a utility program was created to generate the VARSRC file for a given input mesh size. To demonstrate the p-refinement, a fixed 3x3x3 mesh is used in DIF3D-VARIANT that should maximize the error of the fixed source polynomial approximation. To demonstrate convergence the polynomial order of the flux and the source approximation stored in VARSRC are both increased. It is important to note that the VARSRC polynomial representation will not be able to exactly match the fixed source in this analytic benchmark problem and thus there will always be some level of residual error.

Table 62 provides the summary error details of the 3x3x3 mesh calculation using the VARSRC binary file. As can be seen, the error between the analytic solution and the DIF3D-VARIANT solution drops consistently as the polynomial order is refined.

**Table 62. DIF3D-VARIANT P-Refinement Error for the Fixed Source Diffusion Benchmark**

VARIANT Flux/Source Order	VARIANT Leakage Order	Peak Error	Average Error
4	1	3.83E-05	3.69E-05
6	1	3.83E-05	3.43E-05
6	2	2.46E-06	2.46E-06
10	3	1.64E-07	1.64E-07

The leakage approximation itself is considerably important here because of the small number of meshes and large dimension of the geometry. The remaining error in this case is a mixture of residual iterative convergence error and the base error on the source approximation.

As was the case for the preceding eigenvalue problem, the adjoint flux solution is again identical to the forward flux solution. The only exception here is that a fixed source problem has no power normalization and thus one would expect the two solvers to identically produce the same answer given identical fixed source inputs. Table 63 provides a comparison of a selected part of the DIF3D-FD forward and adjoint flux solution for a 10x10x10 mesh approximation and Table 64 provides the DIF3D-VARIANT comparison. As can be seen, the forward and adjoint flux solutions are identical in both cases and similar to each other with respect to DIF3D-FD and DIF3D-VARIANT.

**Table 63. DIF3D-FD Forward and Adjoint Flux Comparison for the Fixed Source Benchmark**

Y mesh	Forward		Adjoint		Adjoint/Forward	
	X mesh 1	X mesh 2	X mesh 1	X mesh 2	X mesh 1	X mesh 2
10	4.49E-03	1.30E-02	4.49E-03	1.30E-02	1.00000E+00	1.00000E+00
9	1.30E-02	3.78E-02	1.30E-02	3.78E-02	1.00000E+00	1.00000E+00
8	2.03E-02	5.89E-02	2.03E-02	5.89E-02	1.00000E+00	1.00000E+00
7	2.56E-02	7.43E-02	2.56E-02	7.43E-02	1.00000E+00	1.00000E+00
6	2.84E-02	8.23E-02	2.84E-02	8.23E-02	1.00000E+00	1.00000E+00
5	2.84E-02	8.23E-02	2.84E-02	8.23E-02	1.00000E+00	1.00000E+00
4	2.56E-02	7.43E-02	2.56E-02	7.43E-02	1.00000E+00	1.00000E+00
3	2.03E-02	5.89E-02	2.03E-02	5.89E-02	1.00000E+00	1.00000E+00
2	1.30E-02	3.78E-02	1.30E-02	3.78E-02	1.00000E+00	1.00000E+00
1	4.49E-03	1.30E-02	4.49E-03	1.30E-02	1.00000E+00	1.00000E+00

**Table 64. VARIANT Forward and Adjoint Flux Comparison for the Fixed Source Benchmark**

Y mesh	Forward		Adjoint		Adjoint/Forward	
	X mesh 1	X mesh 2	X mesh 1	X mesh 2	X mesh 1	X mesh 2
10	4.42E-03	1.28E-02	4.42E-03	1.28E-02	1.00000E+00	1.00000E+00
9	1.28E-02	3.72E-02	1.28E-02	3.72E-02	1.00000E+00	1.00000E+00
8	2.00E-02	5.79E-02	2.00E-02	5.79E-02	1.00000E+00	1.00000E+00
7	2.52E-02	7.30E-02	2.52E-02	7.30E-02	1.00000E+00	1.00000E+00
6	2.79E-02	8.09E-02	2.79E-02	8.09E-02	1.00000E+00	1.00000E+00
5	2.79E-02	8.09E-02	2.79E-02	8.09E-02	1.00000E+00	1.00000E+00
4	2.52E-02	7.30E-02	2.52E-02	7.30E-02	1.00000E+00	1.00000E+00
3	2.00E-02	5.79E-02	2.00E-02	5.79E-02	1.00000E+00	1.00000E+00
2	1.28E-02	3.72E-02	1.28E-02	3.72E-02	1.00000E+00	1.00000E+00
1	4.42E-03	1.28E-02	4.42E-03	1.28E-02	1.00000E+00	1.00000E+00

The combined results shown in Table 60, Table 61, and Table 62 are sufficient to demonstrate that the fixed source solution algorithm of DIF3D is working as intended and that both DIF3D-FD and DIF3D-VARIANT obtain the analytic solution correctly. This result is consistent with the previous homogeneous eigenvalue solution. Together, these results demonstrate that the spatial flux approximation methodology is working properly in diffusion theory in both DIF3D-FD and DIF3D-VARIANT for both forward and adjoint solver modes.

### 3.1.6 Inhomogeneous Diffusion Equation Verification

The purpose of this test problem is to demonstrate that DIF3D produces the correct solution to a given inhomogeneous fixed source problem that contains both a fixed and fission source. This again will be performed with DIF3D-FD and DIF3D-VARIANT. This capability requires the system to be sub-critical. In this case the diffusion equation defined in Section 3.1.4 with the third source option is used to arrive at

$$-D(x, y, z)\nabla^2\phi(x, y, z) + \Sigma_R(x, y, z)\phi(x, y, z) = \nu\Sigma_f(x, y, z)\phi(x, y, z) + q(x, y, z). \quad (42)$$

Based upon the previous two approaches to generating an analytic solution, it should be obvious that the easiest analytic solution for this problem is to assume the overall source and flux have a spatial distribution of

$$q(x) = (\nu\Sigma_f + q)\sin\left(\frac{x}{X}\cdot\pi\right) = p\cdot\sin\left(\frac{x}{X}\cdot\pi\right) \quad (43)$$

$$\phi(x) = a_0\sin\left(\frac{x}{X}\cdot\pi\right). \quad (44)$$

In this case, the solution is slightly different from the previous fixed source one with a modified magnitude of



$$\phi(x) = \frac{q}{\frac{1}{3\Sigma_{tr}}\left(\frac{\pi}{X}\right)^2 + \Sigma_R - \nu\Sigma_f} \cdot \sin\left(\frac{x}{X} \cdot \pi\right). \quad (45)$$

Focusing on the denominator of the flux one finds the additional requirement that the homogeneous eigenvalue problem

$$-D(x, y, z)\nabla^2\phi(x, y, z) + \Sigma_R(x, y, z)\phi(x, y, z) = \frac{1}{k_{eff}}\nu\Sigma_f(x, y, z)\phi(x, y, z), \quad (46)$$

has a  $k_{eff}$  that is less than 1 or

$$k_{eff} = \frac{\nu\Sigma_f}{\frac{1}{3\Sigma_{tr}}\left\{\left(\frac{\pi}{X}\right)^2 + \left(\frac{\pi}{Y}\right)^2 + \left(\frac{\pi}{Z}\right)^2\right\} + \Sigma_R} < 1.0. \quad (47)$$

If this is not met, the preceding system will either be singular (critical system) or negative definite ( $>1.0$ ) for which DIF3D will not converge. The analytic 3D flux solution is found to be

$$\phi(x, y, z) = \frac{q}{\frac{1}{3\Sigma_{tr}}\left\{\left(\frac{\pi}{X}\right)^2 + \left(\frac{\pi}{Y}\right)^2 + \left(\frac{\pi}{Z}\right)^2\right\} + \Sigma_R - \nu\Sigma_f} \cdot \sin\left(\frac{x}{X} \cdot \pi\right) \cdot \sin\left(\frac{y}{Y} \cdot \pi\right) \cdot \sin\left(\frac{z}{Z} \cdot \pi\right). \quad (48)$$

for the 3D source

$$q(x) = q \sin\left(\frac{x}{X} \cdot \pi\right) \sin\left(\frac{y}{Y} \cdot \pi\right) \sin\left(\frac{z}{Z} \cdot \pi\right). \quad (49)$$

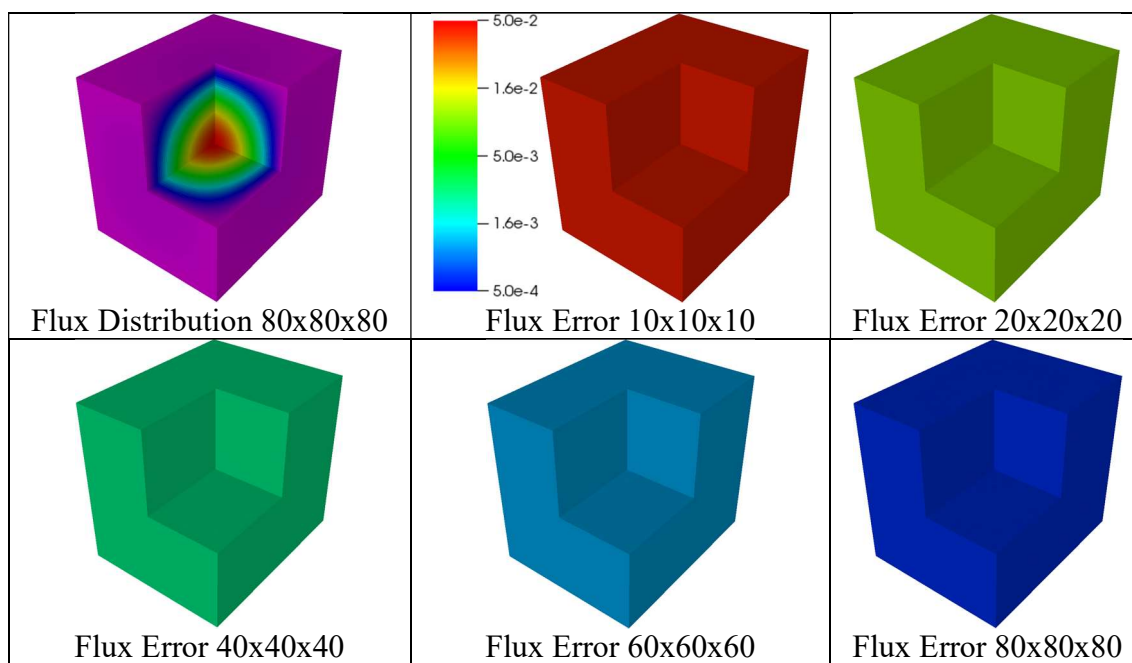
Taking the dimensions  $X=100$ ,  $Y=90$ , and  $Z=80$  and cross sections of  $\Sigma_{tr} = 0.5$ ,  $\nu = 5.04$ ,  $\Sigma_c = 0.2$ ,  $\Sigma_f = 0.05$ , and  $\Sigma_s = 0.25$  the eigenvalue of the homogeneous problem is  $k_{eff} = 0.998026$  that satisfies the limiting relation and should prove a difficult test of the inhomogeneous solver of DIF3D. A fixed source strength of  $5.921272 \times 10^{-4}$  is used such that the flux solution should identically match that of the previous fixed source problem.

The verification will begin with DIF3D-FD and use 10, 20, 40, 60, and 80 mesh intervals in each coordinate direction to show the impact of mesh refinement. Similar to the previous case, the source input is refined as the mesh is refined. Table 65 provides the summary of peak and average error on the spatial distribution while Figure 30 provides a visual assessment of the error in each mesh. From the tabulated data, it should be clear that as the mesh is refined the error drops consistently indicating that the error in the input source distribution is key to the solution. This is counter to the previous fixed source result where DIF3D-FD had relatively good accuracy. In this case, the flux dependent fission source adds error to the overall solution as the flux solution is not accurate. Thus when both a fixed and fission source are present, the DIF3D-FD solver reverts back to the behavior observed in the homogeneous eigenvalue problem with respect to accuracy.



**Table 65. DIF3D-FD Flux Error Results for the Inhomogeneous Diffusion Benchmark**

Mesh	Peak Error	Average Error
10x10x10	4.29E-02	4.28E-02
20x20x20	1.04E-02	1.04E-02
40x40x40	2.58E-03	2.57E-03
60x60x60	1.15E-03	1.14E-03
80x80x80	6.44E-04	6.36E-04

**Figure 30. The DIF3D-FD Flux Error Distribution for the Inhomogeneous Diffusion Benchmark**

As evident from Figure 30, the spatial distribution of the error has considerably improved over that obtained in the fixed source benchmark. This is a consequence of the inhomogeneous solver monitoring the fission source error. Since that is an iterative process, DIF3D-FD performs many more iterations to obtain the flux solution and thus the lack of iterative convergence vanishes. The actual number of iterations DIF3D-FD performed in the previous benchmark was 8 while the current one uses  $\sim 10,000$ . This higher iteration requirement comes from the lack of any acceleration on the fission source and high value of  $k_{\text{eff}}$  chosen. While DIF3D does have a near critical source extrapolation algorithm, it was not enabled on this problem and thus it required over a thousand fission source iterations. Overall, the DIF3D-FD solver is properly solving the inhomogeneous benchmark noting that no flux normalization is needed in this case.

Continuing with DIF3D-VARIANT, the identical calculations to DIF3D-FD were executed with DIF3D-VARIANT and produced the results in Table 66. There is no point in showing the spatial distribution as it is similar to that of DIF3D-FD. As was the case with the homogeneous eigenvalue problem, for the same mesh, the DIF3D-VARIANT solver produces a more accurate solution than

that of DIF3D-FD. As was the case with the previous analytic benchmarks, the DIF3D-VARIANT results decrease consistently with mesh refinement indicating that the error in the fixed source input is the reason for the error in the DIF3D flux solution.

**Table 66. DIF3D-VARIANT Flux Error Results for the Inhomogeneous Diffusion Benchmark**

Mesh	Peak Error	Average Error
10x10x10	2.40E-02	2.40E-02
20x20x20	6.14E-03	6.13E-03
40x40x40	1.55E-03	1.54E-03
60x60x60	7.00E-04	6.91E-04
80x80x80	4.10E-04	4.00E-04

The next task to demonstrate is again the VARSRC file that allows DIF3D-VARIANT to use a polynomial representation of the flux. A 3x3x3 mesh is used again as this will maximize the error in the source representation. Table 67 provides the peak and average flux errors as the polynomial flux and leakage approximations are refined. One can observe clear convergence towards the reference solution as the polynomial approximation is refined. Further, one can see that at low order spatial approximations, the error in the flux dependent fission source dominates the error in the overall solution as it is easy to show the error in the VARSRC source representation is less than  $10^{-7}$  at a 4<sup>th</sup> order polynomial approximation.

**Table 67. DIF3D-VARIANT P-Refinement Error for the Inhomogeneous Diffusion Benchmark**

VARIANT Flux/Source Order	VARIANT Leakage Order	Peak Error	Average Error
4	1	4.14E-02	4.14E-02
6	1	4.31E-02	4.31E-02
6	2	5.92E-04	5.92E-04
10	3	2.10E-06	2.10E-06

The last aspect to verify is that the adjoint solution capability is working. Because the power normalization again does not factor in here, the forward and adjoint flux solution from DIF3D-FD and DIF3D-VARIANT should be identical. Table 68 provides the 10x10x10 mesh result for DIF3D-FD and Table 69 provides it for DIF3D-VARIANT. As can be seen, the forward and adjoint flux solution are identical for both DIF3D-FD and DIF3D-VARIANT that is the expected result. As noted in the preceding work, the flux solution between DIF3D-VARIANT and DIF3D-FD are comparable although there are notable differences.

**Table 68. DIF3D-FD Forward and Adjoint Flux Comparison for the Fixed Source Benchmark**

Y mesh	Forward		Adjoint		Adjoint/Forward	
	X mesh 1	X mesh 2	X mesh 1	X mesh 2	X mesh 1	X mesh 2
10	4.69E-03	1.36E-02	4.69E-03	1.36E-02	1.00000E+00	1.00000E+00
9	1.36E-02	3.95E-02	1.36E-02	3.95E-02	1.00000E+00	1.00000E+00
8	2.12E-02	6.15E-02	2.12E-02	6.15E-02	1.00000E+00	1.00000E+00
7	2.67E-02	7.74E-02	2.67E-02	7.74E-02	1.00000E+00	1.00000E+00
6	2.96E-02	8.58E-02	2.96E-02	8.58E-02	1.00000E+00	1.00000E+00
5	2.96E-02	8.58E-02	2.96E-02	8.58E-02	1.00000E+00	1.00000E+00
4	2.67E-02	7.74E-02	2.67E-02	7.74E-02	1.00000E+00	1.00000E+00
3	2.12E-02	6.15E-02	2.12E-02	6.15E-02	1.00000E+00	1.00000E+00
2	1.36E-02	3.95E-02	1.36E-02	3.95E-02	1.00000E+00	1.00000E+00
1	4.69E-03	1.36E-02	4.69E-03	1.36E-02	1.00000E+00	1.00000E+00

**Table 69. VARIANT Forward and Adjoint Flux Comparison for the Fixed Source Benchmark**

Y mesh	Forward		Adjoint		Adjoint/Forward	
	X mesh 1	X mesh 2	X mesh 1	X mesh 2	X mesh 1	X mesh 2
10	4.38E-03	1.27E-02	4.38E-03	1.27E-02	1.00000E+00	1.00000E+00
9	1.27E-02	3.69E-02	1.27E-02	3.69E-02	1.00000E+00	1.00000E+00
8	1.98E-02	5.75E-02	1.98E-02	5.75E-02	1.00000E+00	1.00000E+00
7	2.50E-02	7.25E-02	2.50E-02	7.25E-02	1.00000E+00	1.00000E+00
6	2.77E-02	8.03E-02	2.77E-02	8.03E-02	1.00000E+00	1.00000E+00
5	2.77E-02	8.03E-02	2.77E-02	8.03E-02	1.00000E+00	1.00000E+00
4	2.50E-02	7.25E-02	2.50E-02	7.25E-02	1.00000E+00	1.00000E+00
3	1.98E-02	5.75E-02	1.98E-02	5.75E-02	1.00000E+00	1.00000E+00
2	1.27E-02	3.69E-02	1.27E-02	3.69E-02	1.00000E+00	1.00000E+00
1	4.38E-03	1.27E-02	4.38E-03	1.27E-02	1.00000E+00	1.00000E+00

Combined, the previous three analytic benchmarks are sufficient proof to demonstrate that the spatial details of the DIF3D-FD and DIF3D-VARIANT diffusion solvers are implemented properly. Both reflected and vacuum boundary conditions were demonstrated on the homogeneous eigenvalue problem and there is no reason to believe they will not work consistently on the fixed source or inhomogeneous fixed source problems as the solution algorithm used is independent upon the problem type. The three different solver options of DIF3D all are proven to work and convergence towards the reference solution is demonstrated although the fixed source option of DIF3D-FD requires additional care to ensure an accurate solution.

### 3.1.7 Power and Flux Peaking Verification

The verification test problems of the previous few sections demonstrate that the method of manufactured solutions (MMS) technique is working in DIF3D-FD and DIF3D-VARIANT. This will be used again later to verify DIF3D's internal peaking calculation.

To test the peaking calculation, a multigroup flux solution must be defined that has significant variance. This work is performed using the inhomogeneous fixed source solver of DIF3D as fission must be present to get the desired peak power output edits from DIF3D. An example of the specific output under review is given in Figure 31 and labeled as “PEAK DENSITY” and “PEAK TO AVG.” Additionally, the peak flux data must be verified. An example of this is shown in Figure 32 where the “PEAK FLUX” and “PEAK FAST FLUX” are the two quantities of importance. This must be verified as correct for both the region and the area edits.

As can be seen in Figure 31 and Figure 32, a test problem must be manufactured that includes multiple regions, has areas, and has identifiable peaks in each spatial region. Because the power calculation involves a sum over energy group, a two-group energy structure is chosen. With this stated, the coupled set of diffusion equations can be written as

$$\begin{aligned} -D_1 \nabla^2 \phi_1 + \Sigma_{R,1} \phi_1 &= \chi_1 \nu_1 \Sigma_{f,1} \phi_1 + \chi_1 \nu_2 \Sigma_{f,2} \phi_2 + q_1 \\ -D_2 \nabla^2 \phi_2 + \Sigma_{R,2} \phi_2 &= \chi_2 \nu_1 \Sigma_{f,1} \phi_1 + \chi_2 \nu_2 \Sigma_{f,2} \phi_2 + \Sigma_{s,1 \rightarrow 2} \phi_1 + q_2 \end{aligned}, \quad (50)$$

where the spatial dependence of all variables is neglected. For simplicity, only a single composition is used in the domain with the cross sections shown in Table 70.

**Table 70. Cross Sections for the Diffusion Theory Peaking Problem**

	Group	Upper Energy	Lower Energy	$\Sigma_t$	$\Sigma_\gamma$	$\chi$	$\nu$	$\Sigma_f$	$\Sigma_s$	
<b>Zone 1</b>	1	10 MeV	0.1 MeV	0.10	0.01	1.00	2.00	0.01	0.03	0.0
	2	0.1 MeV	0.1 meV	1.00	0.10	0.00	2.00	0.10	0.05	0.8

These cross sections are somewhat consistent with thermal spectrum cross sections and more than one composition cannot be used as it typically will cause a discontinuity at the interface between the zones that is difficult to then define a smooth functional relationship for the flux. While a discrete approximation consistent with the DIF3D approximation can be obtained, an analytic solution that can prove the MMS scheme works is pursued.

For the flux solution, the sine functions are combined with “witch” functions to yield:

$$\begin{aligned}
\phi_1 &= \sin\left(\frac{x\pi}{X}\right)\sin\left(\frac{y\pi}{Y}\right)\sin\left(\frac{z\pi}{Z}\right) \cdot \left[4 + f(1.0, 0.3, 0.3, 0.3) + f(0.8, 0.7, 0.7, 0.7)\right] \\
\phi_2 &= \sin\left(\frac{x\pi}{X}\right)\sin\left(\frac{y\pi}{Y}\right)\sin\left(\frac{z\pi}{Z}\right) \cdot \left[1 + f(0.25, 0.7, 0.3, 0.7) + f(0.3, 0.3, 0.7, 0.3)\right] \quad (51) \\
f(a, b, c, d) &= \frac{a}{\left(\frac{x}{X} - b\right)^2 + \left(\frac{y}{Y} - c\right)^2 + \left(\frac{z}{Z} - d\right)^2 + \frac{1}{64}}
\end{aligned}$$

In this form, the source is easy to compute using calculus. A utility program was developed (hosted in the repository with the DIF3D source code) to take a given user domain (user defines X, Y, Z domain sizes) and cross sections to create the fixed source. As was the case with the previous analytic benchmarks, zero flux boundary conditions are applied.

February 13, 2020

REGION NO.	NAME	ZONE NO.	ZONE NAME	VOLUME (CC)	INTEGRATION (1) WEIGHT FACTOR	POWER (WATTS)	POWER DENSITY (WATTS/CC)	PEAK DENSITY (WATTS/CC) (2)	PEAK TO AVG. POWER DENSITY	POWER FRACTION
1	RA1101	1	RA1101	3.57163E+04	1.00000E+00	3.30081E+03	9.24175E-02	5.14415E-01	5.56621E+00	1.10027E-05
2	RA1201	2	RA1201	3.57163E+04	1.00000E+00	6.09302E+03	1.70595E-01	7.77456E-01	4.55732E+00	2.03101E-05
3	RA1301	3	RA1301	3.57163E+04	1.00000E+00	7.74460E+03	2.16837E-01	9.43112E-01	4.34941E+00	2.58153E-05
4	RA1401	4	RA1401	3.57163E+04	1.00000E+00	8.76525E+03	2.45413E-01	1.04243E+00	4.24767E+00	2.92175E-05
5	RA1501	5	RA1501	3.57163E+04	1.00000E+00	9.22439E+03	2.58269E-01	1.07943E+00	4.17947E+00	3.07480E-05
6	RA1601	6	RA1601	3.57163E+04	1.00000E+00	9.13062E+03	2.55643E-01	1.07740E+00	4.21448E+00	3.04354E-05
7	RA1701	7	RA1701	3.57163E+04	1.00000E+00	8.52243E+03	2.38615E-01	1.03485E+00	4.33691E+00	2.84081E-05
8	RA1801	8	RA1801	3.57163E+04	1.00000E+00	7.43684E+03	2.08220E-01	9.34262E-01	4.48690E+00	2.47895E-05
9	RA1901	9	RA1901	3.57163E+04	1.00000E+00	5.80333E+03	1.62484E-01	7.66432E-01	4.71696E+00	1.93444E-05
10	RA1A01	10	RA1A01	3.57163E+04	1.00000E+00	3.12715E+03	8.75554E-02	5.03043E-01	5.74543E+00	1.04238E-05
11	RA1001	11	RA1001	3.57163E+04	1.00000E+00	6.08272E+03	1.70307E-01	7.76025E-01	4.55663E+00	2.02757E-05
12	R90X01	12	R90X01	3.57163E+04	1.00000E+00	1.33405E+04	3.73513E-01	1.24684E+00	3.33815E+00	4.44683E-05
13	R90Y01	13	R90Y01	3.57163E+04	1.00000E+00	1.80176E+04	5.04466E-01	1.54310E+00	3.05888E+00	6.00588E-05
14	R90Z01	14	R90Z01	3.57163E+04	1.00000E+00	2.10319E+04	5.88859E-01	1.73167E+00	2.94071E+00	7.01062E-05
15	R91001	15	R91001	3.57163E+04	1.00000E+00	2.26860E+04	6.35174E-01	1.81219E+00	2.85306E+00	7.56201E-05
16	R91101	16	R91101	3.57163E+04	1.00000E+00	2.30319E+04	6.44858E-01	1.81195E+00	2.80985E+00	7.67731E-05
17	R91201	17	R91201	3.57163E+04	1.00000E+00	2.22764E+04	6.23703E-01	1.81166E+00	2.90468E+00	7.42545E-05
18	R91301	18	R91301	3.57163E+04	1.00000E+00	2.04258E+04	5.71891E-01	1.74760E+00	3.05583E+00	6.80861E-05
19	R91401	19	R91401	3.57163E+04	1.00000E+00	1.73868E+04	4.86804E-01	1.56982E+00	3.22474E+00	5.79561E-05
20	R91501	20	R91501	3.57163E+04	1.00000E+00	1.27868E+04	3.58012E-01	1.25182E+00	3.49658E+00	4.26228E-05
21	RA1B01	21	RA1B01	3.57163E+04	1.00000E+00	5.80590E+03	1.62556E-01	7.66797E-01	4.71712E+00	1.93530E-05
22	RA0Z01	22	RA0Z01	3.57163E+04	1.00000E+00	7.71270E+03	2.15944E-01	9.39226E-01	4.34940E+00	2.57090E-05
23	R90W01	23	R90W01	3.57163E+04	1.00000E+00	1.79768E+04	5.03322E-01	1.53975E+00	3.05918E+00	5.99226E-05
24	R80T01	24	R80T01	3.57163E+04	1.00000E+00	2.49933E+04	6.99773E-01	1.84318E+00	2.63397E+00	8.33109E-05
25	R80U01	25	R80U01	3.57163E+04	1.00000E+00	2.93805E+04	8.22608E-01	1.97943E+00	2.40629E+00	9.79350E-05
26	R80V01	26	R80V01	3.57163E+04	1.00000E+00	3.20874E+04	8.98397E-01	2.08611E+00	2.32204E+00	1.06958E-04
27	R80W01	27	R80W01	3.57163E+04	1.00000E+00	3.27350E+04	9.16528E-01	2.04735E+00	2.23382E+00	1.09117E-04
...										
AREA NO.	AREA NAME			VOLUME (CC)	INTEGRATION (1) WEIGHT FACTOR	POWER (WATTS)	POWER DENSITY (WATTS/CC)	PEAK DENSITY (WATTS/CC) (2)	PEAK TO AVG. POWER DENSITY	POWER FRACTION
1	MAXPO			3.57163E+04	0.00000E+00	6.09581E+06	1.70673E+02	7.21456E+02	4.22712E+00	2.03194E-02
2	ATA_PL			9.97661E+04	0.00000E+00	3.99327E+04	4.00263E-01	2.64681E+00	6.61266E+00	1.33109E-04
3	ATA_EM			4.71694E+05	0.00000E+00	1.26898E+05	2.69026E-01	6.66951E-01	2.47913E+00	4.22993E-04

Figure 31. The DIF3D Example Power Peaking Table of Output

February 13, 2020

REGION NO.	ZONE NAME	ZONE NO.	ZONE NAME	VOLUME (CC)	TOTAL FLUX (NEUTRON-CM/SEC)	PEAK FLUX (1) (NEUTRON/CM2-SEC)	TOTAL FAST FLUX (NEUTRON-CM/SEC)	PEAK FAST FLUX (1) (NEUTRON/CM2-SEC)
1	P50301	1	P50301	1.78581E+04	4.29930E+19	4.61162E+15	2.74643E+19	3.31451E+15
2	P50302	2	P50302	6.23538E+02	9.32171E+17	2.09051E+15	5.71828E+17	1.34838E+15
3	P50303	3	P50303	6.23538E+02	7.46662E+17	1.67877E+15	4.31806E+17	1.01985E+15
4	P50304	4	P50304	1.45160E+03	1.28239E+18	1.42179E+15	6.84138E+17	8.14474E+14
5	P50305	5	P50305	1.04256E+03	6.33317E+17	9.53240E+14	3.06187E+17	4.82203E+14
6	P50306	6	P50306	1.86064E+03	7.30850E+17	7.14228E+14	3.18923E+17	3.30693E+14
7	P50307	7	P50307	6.02089E+03	7.62890E+17	4.15248E+14	2.67280E+17	1.64643E+14
8	P50308	8	P50308	6.23538E+03	1.39883E+17	6.00890E+13	2.23175E+16	1.26707E+13
9	P50309	9	P50309	0.00000E+00	0.00000E+00	0.00000E+00	0.00000E+00	0.00000E+00
10	P50501	10	P50501	6.85892E+03	5.52585E+18	2.12932E+15	2.07905E+18	1.13315E+15
11	P50502	11	P50502	6.23538E+02	1.20323E+18	2.39882E+15	6.53232E+17	1.44342E+15
12	P50503	12	P50503	6.23538E+02	1.35836E+18	2.71309E+15	8.16453E+17	1.78616E+15
13	P50504	13	P50504	1.45160E+03	3.82138E+18	3.46241E+15	2.47979E+18	2.42053E+15
14	P50505	14	P50505	1.04256E+03	3.22973E+18	3.84482E+15	2.15834E+18	2.71868E+15
15	P50506	15	P50506	1.86064E+03	6.31274E+18	4.10375E+15	4.25542E+18	2.91540E+15
16	P50507	16	P50507	6.02089E+03	1.58366E+19	4.10181E+15	1.04655E+19	2.91440E+15
17	P50508	17	P50508	9.75214E+03	3.42378E+18	1.60998E+15	1.63307E+18	9.56662E+14
18	P50509	18	P50509	7.48246E+03	9.34821E+16	7.24054E+13	2.32257E+16	1.98847E+13
19	P50701	19	P50701	1.78581E+04	4.30175E+19	4.61328E+15	2.74804E+19	3.31606E+15
20	P50702	20	P50702	6.23538E+02	9.34370E+17	2.09638E+15	5.73121E+17	1.35202E+15
21	P50703	21	P50703	6.23538E+02	7.48649E+17	1.68413E+15	4.32916E+17	1.02301E+15
22	P50704	22	P50704	1.45160E+03	1.28617E+18	1.42665E+15	6.86121E+17	8.17224E+14
23	P50705	23	P50705	1.04256E+03	6.35273E+17	9.56642E+14	3.07137E+17	4.83959E+14
24	P50706	24	P50706	1.86064E+03	7.33018E+17	7.16615E+14	3.19894E+17	3.31848E+14
25	P50707	25	P50707	6.02089E+03	7.64433E+17	4.16399E+14	2.67913E+17	1.65139E+14
26	P50708	26	P50708	6.23538E+03	1.38549E+17	5.97244E+13	2.22118E+16	1.26523E+13
...								
AREA NO.	AREA NAME			VOLUME (CC)	TOTAL FLUX (NEUTRON-CM/SEC)	PEAK FLUX (1) (NEUTRON/CM2-SEC)	TOTAL FAST FLUX (NEUTRON-CM/SEC)	PEAK FAST FLUX (1) (NEUTRON/CM2-SEC)
1	MAXPO			3.57163E+04	7.18775E+19	6.00879E+15	4.67055E+19	4.41072E+15
2	ATA_PL			9.97661E+04	1.40481E+19	9.85620E+14	3.91227E+18	3.06349E+14
3	ATA_EM			4.71694E+05	7.52107E+20	6.00945E+15	4.63578E+20	4.39674E+15
4	ALPLUG			5.16290E+05	5.41557E+20	3.49251E+15	2.34665E+20	2.24138E+15

Figure 32. The DIF3D Example Flux Peaking Table of Output

February 13, 2020

The flux distribution is plotted in Figure 33 and the power distribution in Figure 34 in such a way to show the peaking within a cubic domain with a dimension of 100 cm on all axes. Figure 33 provides the group 1 results on the left and the group 2 results on the right. As can be seen in Figure 33, the solution is very low in most of the domain (zero at the domain boundaries) and reaches its maximum at the witch peak points of (30,30,30) cm and (70,70,70) cm in group 1 and (30,70,30) cm and (70,30,70) cm in group 2. One can also note that the group 1 flux is a little over 3 times larger than the group 2 flux. When combined, the power distribution shows a dominance by group 2 due to the higher fission and capture cross sections and the relative difference in the flux magnitude. From Figure 32, the fast flux magnitude needs to be verified. To do this, the energy boundary between the two group case is set such that group 1 is entirely a fast spectrum group and group 2 is not. Later perturbations will adjust this energy boundary using the same flux solution to demonstrate that the fast flux computation is correct.

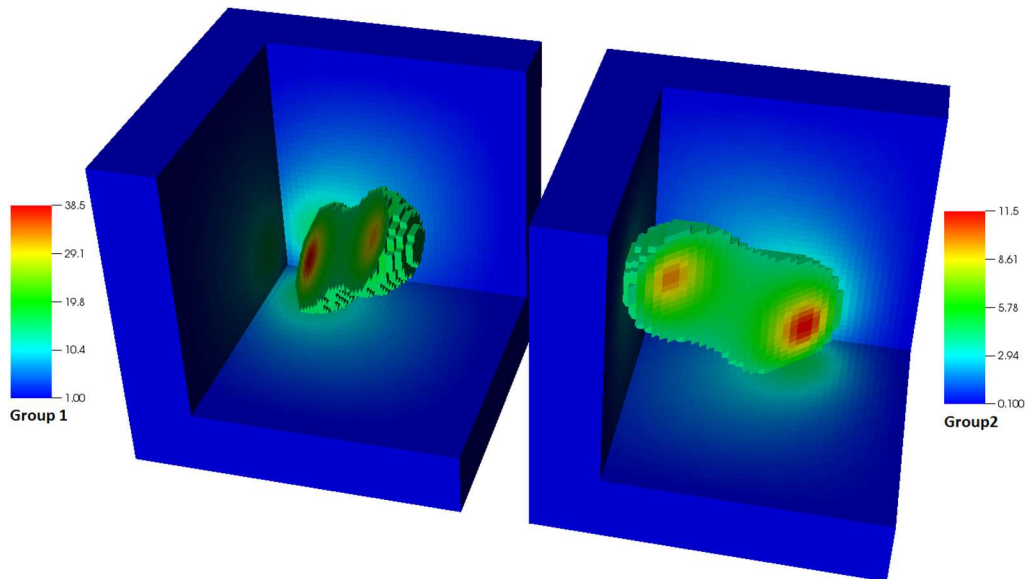


**Figure 33. The Flux Distribution for the Diffusion Theory Peaking Problem**



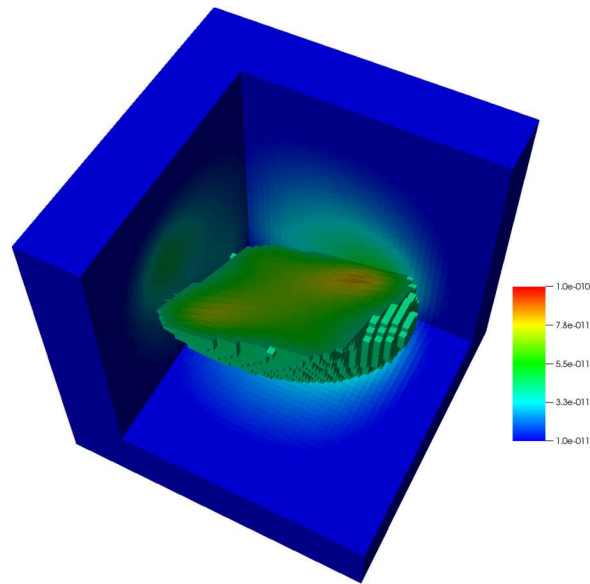


**Figure 34. The Power Distribution for the Diffusion Theory Peaking Problem**

To produce more usable data, the (100,100,100) cm domain is separated into 8 equal sized pieces and define areas that combine the regions and areas shown in Table 71. This type of setup simplifies the area edits and the region edits given that the maximum value in any given region can be analytically determined along with the integral over the sub-domains.

**Table 71. Region and Area Definitions for the Diffusion Theory Peaking Problem**

Region Name	X Range (cm)	Y Range (cm)	Z Range (cm)	Included in Areas
REG1	0-50	0-50	0-50	ALLZ1, BOTHLF, TCORE
REG2	50-100	0-50	0-50	ALLZ2, BOTHLF, TCORE
REG3	0-50	50-100	0-50	ALLZ1, BOTHLF, TCORE
REG4	50-100	50-100	0-50	ALLZ2, BOTHLF, TCORE
REG5	0-50	0-50	50-100	ALLZ2, UPPHLF, TCORE
REG6	50-100	0-50	50-100	ALLZ1, UPPHLF, TCORE
REG7	0-50	50-100	50-100	ALLZ2, UPPHLF, TCORE
REG8	50-100	50-100	50-100	ALLZ2, UPPHLF, TCORE

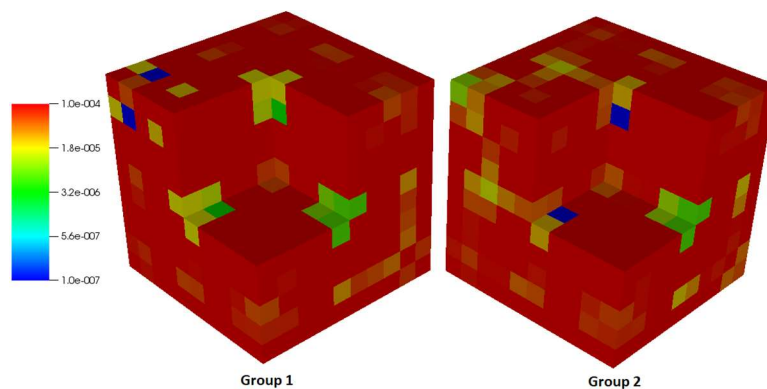
The first task is to verify the region edit output of the flux. For DIF3D-VARIANT, two inputs with 10x10x10 meshes and 20x20x20 meshes were used and each combined with several different polynomial approximations where the utility program creates a VARSRC file for each polynomial approximation. For DIF3D-FD, 10x10x10, 20x20x20, and 50x50x50 meshes were used nothing that the same VARIANT-based utility program will create the flat source FIXSRC file. Because the DIF3D-FD solution is limited to a flat source within each mesh, convergence towards the reference solution with mesh refinement is achievable, but an exact match will not be pursued.

Figure 35 shows the spatial flux errors for the DIF3D-VARIANT solver for two different meshes and two different polynomial approximations. As can be seen, even with a coarse polynomial approximation and coarse mesh, the solution produces errors less than  $10^{-4}$ . As the polynomial approximation or mesh is refined, the spatial flux errors reduce consistently. It is very difficult to push the error to zero on this problem because of the more complex flux solution, the base error in representing the source with polynomials, and the residual error DIF3D has in the fission source.

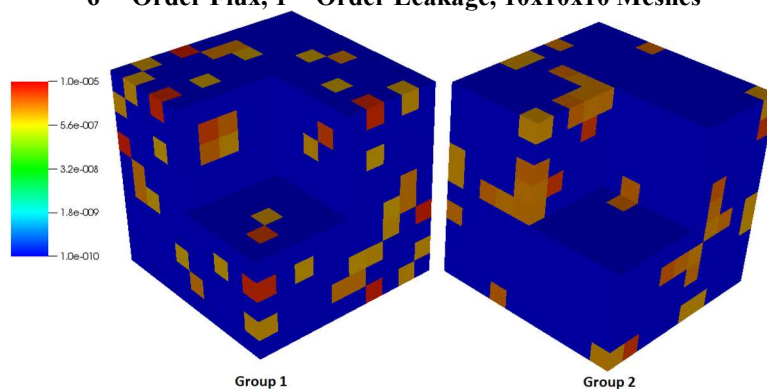
Figure 36 shows the spatial flux errors for the DIF3D-FDD solver for two different meshes. The color scale was set to be the same on both error distributions to demonstrate that with spatial mesh refinement, the DIF3D-FD error is reduced. Compared with the DIF3D-VARIANT results, the DIF3D-FD results contain a considerably larger amount of error. This is due to the witch functions and the difficulty in approximating the source in the flat source based FIXSRC input.

While it is possible to refine the mesh further in both DIF3D-VARIANT and DIF3D-FD, the goal is to compare the region and area integral results shown earlier. Thus, overall, these results are ample evidence that DIF3D-VARIANT and DIF3D-FD produce the correct flux solution given that the source input is properly defined. This evaluation begins with the DIF3D errors on the region flux totals like those provided in Figure 32. Table 72 provides the DIF3D errors for the total flux column of data while Table 73 provides the peak of the total flux column. Similarly, Table 74 provides the total fast flux and Table 75 provides the peak fast flux. The analytic reference solution is provided in each table in the far right column with all other columns providing the DIF3D solver, the spatial mesh, and for DIF3D-VARIANT, the polynomial spatial approximation that was used.

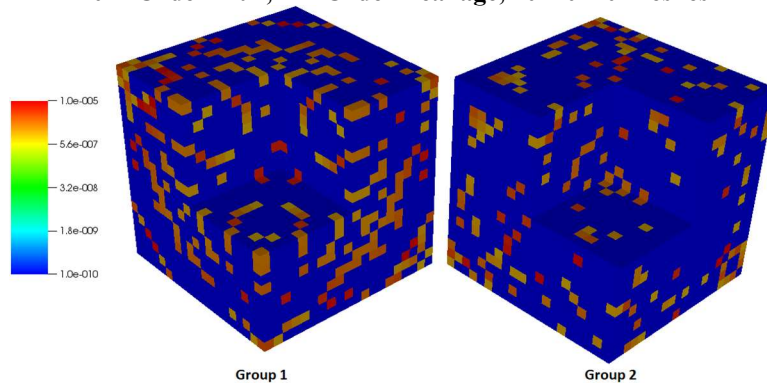
February 13, 2020



**6<sup>TH</sup> Order Flux, 1<sup>ST</sup> Order Leakage, 10x10x10 Meshes**



**10<sup>TH</sup> Order Flux, 4<sup>TH</sup> Order Leakage, 10x10x10 Meshes**



**10<sup>TH</sup> Order Flux, 4<sup>TH</sup> Order Leakage, 20x20x20 Meshes**

**Figure 35. DIF3D-VARIANT Spatial Flux Convergence for the Diffusion Peaking Problem**

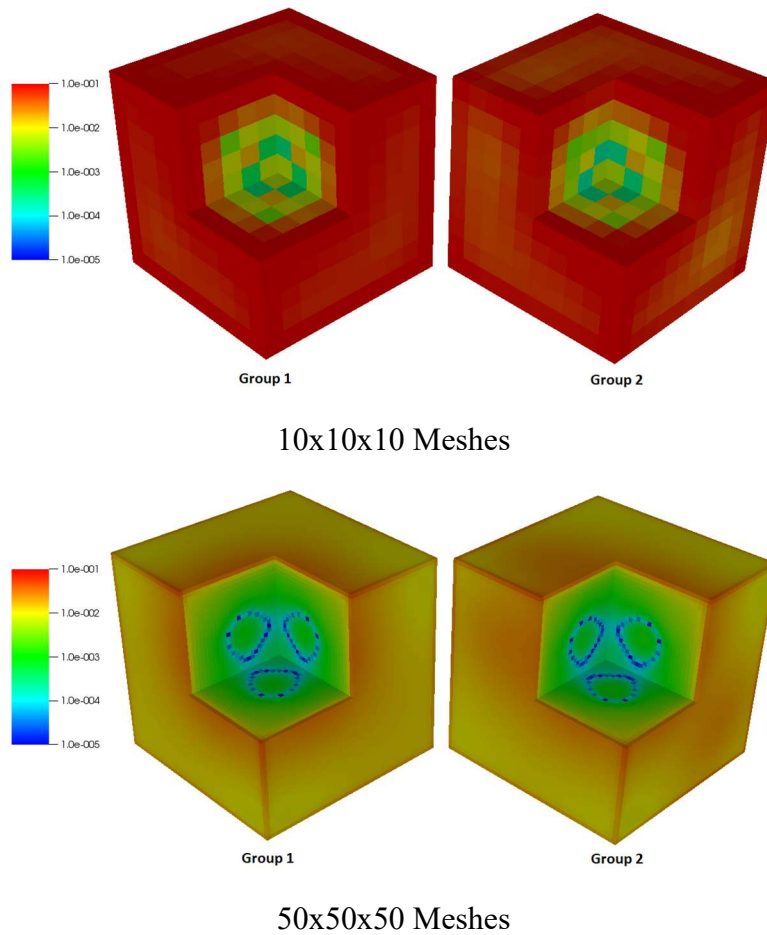


**Figure 36. DIF3D-FD Spatial Flux Convergence for the Diffusion Theory Peaking Problem**

Starting with Table 72, one can see that the DIF3D-VARIANT solutions are very accurate at both coarse meshing and coarse polynomial approximations. It is interesting to note that most of the differing spatial mesh and polynomial approximations all yield the same results that indicates that there is some common issue causing error in each calculation that is likely the base approximation of the source with the polynomial approximation. As expected, the DIF3D-FD results are notably worse than DIF3D-VARIANT but show mesh refinement convergence towards the reference.

Continuing with the peak of the total flux data in Table 73, it is clear that the DIF3D-VARIANT solution is dependent upon the mesh approximation used. This is a consequence of the rather inaccurate algorithm used to estimate the peak flux. To demonstrate that DIF3D-VARIANT can predict the peak flux, a utility program provided with DIF3D, EvaluateFlux, was used to evaluate the flux solution at the peak value coordinate locations in the analytic solution. The tabulated results for the peak of the total flux are provided in Table 75. This demonstrates that the existing peaking algorithm used within DIF3D is the source of the error rather than a deficiency in the DIF3D-VARIANT methodology.

February 13, 2020

**Table 72. Region Errors for the Total Flux in the Diffusion Theory Peaking Problem**

Solver	DIF3D-VARIANT						DIF3D-FD			Analytic
Mesher	10x10x10	10x10x10	10x10x10	10x10x10	10x10x10	20x20x20	10x10x10	20x20x20	50x50x50	-
Flux	6 <sup>th</sup>	6 <sup>th</sup>	8 <sup>th</sup>	10 <sup>th</sup>	12 <sup>th</sup>	10 <sup>th</sup>	-	-	-	-
Leakage	1 <sup>st</sup>	2 <sup>nd</sup>	3 <sup>rd</sup>	4 <sup>th</sup>	5 <sup>th</sup>	4 <sup>th</sup>	-	-	-	-
REG1	1.7E-04	-1.0E-07	-1.0E-07	-1.0E-07	-1.0E-07	-1.0E-07	-8.5E-03	-1.9E-03	-3.1E-04	9.7E+05
REG2	-8.7E-06	-1.1E-06	-1.1E-06	-1.1E-06	-1.1E-06	-1.1E-06	-1.6E-02	-4.0E-03	-6.5E-04	5.3E+05
REG3	-1.5E-07	-1.5E-07	-1.5E-07	-1.5E-07	-1.5E-07	-1.5E-07	-1.3E-02	-3.2E-03	-5.3E-04	6.6E+05
REG4	2.0E-05	-9.7E-07	-9.7E-07	-9.7E-07	-9.7E-07	-9.7E-07	-1.6E-02	-4.0E-03	-6.5E-04	5.2E+05
REG5	-8.7E-06	-1.1E-06	-1.1E-06	-1.1E-06	-1.1E-06	-1.1E-06	-1.6E-02	-4.0E-03	-6.5E-04	5.3E+05
REG6	2.4E-05	-1.6E-07	-1.6E-07	-1.6E-07	-1.6E-07	-1.6E-07	-1.3E-02	-3.4E-03	-5.5E-04	6.2E+05
REG7	2.0E-05	-9.7E-07	-9.7E-07	-9.7E-07	-9.7E-07	-9.7E-07	-1.6E-02	-4.0E-03	-6.5E-04	5.2E+05
REG8	1.6E-04	-5.9E-07	-5.9E-07	-5.9E-07	-5.9E-07	-5.9E-07	-9.1E-03	-2.1E-03	-3.4E-04	8.5E+05

**Table 73. Region Errors for the Peak of the Total Flux in the Diffusion Theory Peaking Problem**

Solver	DIF3D-VARIANT						DIF3D-FD			Analytic
Mesher	10x10x10	10x10x10	10x10x10	10x10x10	10x10x10	20x20x20	10x10x10	20x20x20	50x50x50	-
Flux	6 <sup>th</sup>	6 <sup>th</sup>	8 <sup>th</sup>	10 <sup>th</sup>	12 <sup>th</sup>	10 <sup>th</sup>	-	-	-	-
Leakage	1 <sup>st</sup>	2 <sup>nd</sup>	3 <sup>rd</sup>	4 <sup>th</sup>	5 <sup>th</sup>	4 <sup>th</sup>	-	-	-	-
REG1	-10.62%	-10.76%	-10.76%	-10.75%	-10.75%	-2.35%	-6.81%	0.92%	-1.04%	41.5
REG2	0.61%	0.60%	0.60%	0.60%	0.60%	0.27%	-1.84%	-0.44%	-0.10%	22.8
REG3	-1.83%	-1.87%	-1.87%	-1.87%	-1.87%	-0.18%	2.07%	0.43%	-0.09%	24.2
REG4	0.68%	0.72%	0.72%	0.72%	0.72%	-0.23%	-4.89%	-1.75%	-0.51%	22.4
REG5	0.61%	0.60%	0.60%	0.60%	0.60%	0.27%	-1.84%	-0.44%	-0.10%	22.8
REG6	-1.09%	-1.06%	-1.06%	-1.06%	-1.06%	-0.64%	-2.20%	-1.58%	-0.50%	22.4
REG7	0.68%	0.72%	0.72%	0.72%	0.72%	-0.23%	-4.89%	-1.75%	-0.51%	22.4
REG8	-9.78%	-9.92%	-9.91%	-9.91%	-9.91%	-1.81%	-5.26%	1.36%	-0.34%	34.4

February 13, 2020

**Table 74. Region Errors for the Total Fast Flux in the Diffusion Theory Peaking Problem**

Solver	DIF3D-VARIANT						DIF3D-FD			Analytic
Meshes	10x10x10	10x10x10	10x10x10	10x10x10	10x10x10	20x20x20	10x10x10	20x20x20	50x50x50	-
Flux	6 <sup>th</sup>	6 <sup>th</sup>	8 <sup>th</sup>	10 <sup>th</sup>	12 <sup>th</sup>	10 <sup>th</sup>	-	-	-	-
Leakage	1 <sup>st</sup>	2 <sup>nd</sup>	3 <sup>rd</sup>	4 <sup>th</sup>	5 <sup>th</sup>	4 <sup>th</sup>	-	-	-	-
REG1	1.6E-04	-3.5E-07	-3.5E-07	-3.5E-07	-3.5E-07	-3.5E-07	-7.8E-03	-1.8E-03	-2.9E-04	8.49E+05
REG2	-8.2E-06	-9.6E-07	-9.6E-07	-9.6E-07	-9.6E-07	-9.6E-07	-1.6E-02	-4.1E-03	-6.6E-04	4.16E+05
REG3	-9.6E-07	-9.6E-07	-9.6E-07	-9.6E-07	-9.6E-07	-9.6E-07	-1.6E-02	-4.1E-03	-6.5E-04	4.16E+05
REG4	2.1E-05	7.5E-07	7.5E-07	7.5E-07	7.5E-07	7.5E-07	-1.6E-02	-4.2E-03	-6.7E-04	3.98E+05
REG5	-8.2E-06	-9.6E-07	-9.6E-07	-9.6E-07	-9.6E-07	-9.6E-07	-1.6E-02	-4.1E-03	-6.6E-04	4.16E+05
REG6	3.1E-05	7.5E-07	7.5E-07	7.5E-07	7.5E-07	7.5E-07	-1.6E-02	-4.2E-03	-6.7E-04	3.98E+05
REG7	2.1E-05	7.5E-07	7.5E-07	7.5E-07	7.5E-07	7.5E-07	-1.6E-02	-4.2E-03	-6.7E-04	3.98E+05
REG8	1.5E-04	-4.1E-07	-4.1E-07	-4.1E-07	-4.1E-07	-4.1E-07	-8.5E-03	-2.0E-03	-3.2E-04	7.31E+05

**Table 75. Region Errors for the Peak Fast Flux in the Diffusion Theory Peaking Problem**

Solver	DIF3D-VARIANT						DIF3D-FD			Analytic
Meshes	10x10x10	10x10x10	10x10x10	10x10x10	10x10x10	20x20x20	10x10x10	20x20x20	50x50x50	-
Flux	6 <sup>th</sup>	6 <sup>th</sup>	8 <sup>th</sup>	10 <sup>th</sup>	12 <sup>th</sup>	10 <sup>th</sup>	-	-	-	-
Leakage	1 <sup>st</sup>	2 <sup>nd</sup>	3 <sup>rd</sup>	4 <sup>th</sup>	5 <sup>th</sup>	4 <sup>th</sup>	-	-	-	-
REG1	-11.9%	-12.0%	-12.0%	-12.0%	-12.0%	-2.7%	-10.6%	-0.1%	-1.2%	39.3
REG2	-0.6%	-0.6%	-0.6%	-0.6%	-0.6%	0.1%	2.0%	0.4%	-0.1%	18.7
REG3	-0.6%	-0.6%	-0.6%	-0.6%	-0.6%	0.1%	2.1%	0.4%	-0.1%	18.7
REG4	0.1%	0.1%	0.1%	0.1%	0.1%	-0.5%	-2.9%	-2.0%	-0.7%	17.3
REG5	-0.6%	-0.6%	-0.6%	-0.6%	-0.6%	0.0%	2.0%	0.4%	-0.1%	18.7
REG6	0.1%	0.1%	0.1%	0.1%	0.1%	-0.5%	-2.8%	-2.0%	-0.7%	17.3
REG7	0.1%	0.1%	0.1%	0.1%	0.1%	-0.5%	-2.9%	-2.0%	-0.7%	17.3
REG8	-11.3%	-11.4%	-11.4%	-11.4%	-11.4%	-2.4%	-9.3%	0.1%	-1.3%	32.3

**Table 76. Peak of the Total Flux Positions and DIF3D-VARIANT Error**

	<b>X Position (cm)</b>	<b>Y Position (cm)</b>	<b>Z Position (cm)</b>	<b>DIF3D-VARIANT Error 20x20x20 Mesh 10<sup>th</sup> Order Flux 4<sup>th</sup> Order Leakage</b>
<b>REG1</b>	32.02000	32.16667	32.02000	2.2E-08
<b>REG2</b>	50.00000	42.16667	41.83333	1.7E-07
<b>REG3</b>	38.33333	50.00000	38.33333	2.1E-07
<b>REG4</b>	50.00000	50.00000	47.03833	1.9E-07
<b>REG5</b>	41.83333	42.16667	50.00000	1.7E-07
<b>REG6</b>	50.00000	48.33333	50.00000	1.8E-07
<b>REG7</b>	47.03833	50.00000	50.00000	1.9E-07
<b>REG8</b>	68.33333	68.33333	68.33333	6.1E-08

The DIF3D-FD solution to the peak of the total flux also shows spatial mesh convergence towards the reference solution as expected. It is important to note that several of the coordinates in Table 76 are on the boundaries between regions and thus the mesh approximation is important as the peak occurs at the surface between meshes. This is one of the reasons for the poor DIF3D-VARIANT peaking results as it only considers the net flux on the interface or the average flux within the mesh when determining the peak.

Continuing with the total fast flux in Table 74, similar to the previous total flux result, DIF3D-VARIANT produces a very accurate result for almost all meshes and polynomial approximations. The DIF3D-FD results are again worse than DIF3D-VARIANT, but understandable given the errors introduced by the flat source approximation in FIXSRC. Combined, one can conclude that both of the solvers are demonstrating consistent solutions with the reference solution.

The last output to compare for the flux is the peak of the fast flux in Table 81. As was the case with the peak of the total flux, DIF3D-VARIANT again shows a poor result while DIF3D-FD shows general improvement as the mesh is refined. Again the peak flux estimation algorithm in DIF3D is rather inaccurate. For completeness, the locations of the peak fast flux (group 1) are provided with the DIF3D-VARIANT error in Table 77 where the EvaluateFlux utility was used.

**Table 77. Peak of the Fast Flux Positions and DIF3D-VARIANT Error**

	<b>X Position (cm)</b>	<b>Y Position (cm)</b>	<b>Z Position (cm)</b>	<b>DIF3D-VARIANT Error 20x20x20 Mesh 10<sup>th</sup> Order Flux 4<sup>th</sup> Order Leakage</b>
<b>REG1</b>	31.88333	31.88333	31.88333	-3.7E-08
<b>REG2</b>	50.00000	38.33333	38.33333	-1.7E-07
<b>REG3</b>	38.33333	50.00000	38.33333	-2.1E-07
<b>REG4</b>	50.00000	50.00000	47.00000	-1.9E-07
<b>REG5</b>	38.33333	38.33333	50.00000	-1.8E-07
<b>REG6</b>	50.00000	47.00000	50.00000	-1.8E-07
<b>REG7</b>	47.00000	50.00000	50.00000	-1.9E-07
<b>REG8</b>	68.33333	68.33333	68.33333	-6.9E-08

As was the case before, the DIF3D-VARIANT software is seen to nearly exactly match the analytic solution. Take note that the peak spatial positions change considerably between these two evaluations. This work in effect demonstrates the accuracy of both DIF3D-VARIANT and the EvaluateFlux utility program.

The next output to check is the power density and peak power density computations. Similar to the preceding tables, we tabulate the power density errors in Table 93 and the peak power density errors in Table 94. The power density results mimic the accuracy observed in the total flux and total fast flux estimators shown previously; DIF3D-VARIANT has a consistently good result while DIF3D-FD shows clear improvement as the mesh is refined. Combined, we can conclude that the two solvers can produce excellent estimates of the region flux and power integrals. The peak power density results in Table 79 are generally consistent with the observed behavior in the peak total flux and peak fast flux results.

It is noteworthy that the largest error shifts from REG1 to REG3 in this table. To understand this, the coordinate points for the peak power density from the analytic solution are provided along with the DIF3D-VARIANT results obtained with Evaluate Flux. As was the case with the previous two peaking results, the coordinates again shift (due to the different group fission and capture cross sections) but the DIF3D-VARIANT results are effectively exact.



**Table 78. Peak of the Power Density Positions and the DIF3D-VARIANT Error**

	<b>X Position (cm)</b>	<b>Y Position (cm)</b>	<b>Z Position (cm)</b>	<b>DIF3D-VARIANT Error 20x20x20 Mesh 10<sup>th</sup> Order Flux 4<sup>th</sup> Order Leakage</b>
<b>REG1</b>	38.33333	50.00000	38.33333	-5.2E-07
<b>REG2</b>	50.00000	50.00000	48.33333	-3.8E-07
<b>REG3</b>	32.00000	68.33333	32.00000	-1.5E-07
<b>REG4</b>	50.00000	56.66667	43.33333	-4.0E-07
<b>REG5</b>	48.33333	50.00000	50.00000	-3.8E-07
<b>REG6</b>	68.33333	32.16667	68.33333	-1.7E-07
<b>REG7</b>	43.33333	56.66667	50.00000	-4.0E-07
<b>REG8</b>	50.00000	51.66667	50.00000	-6.9E-08

Overall, one can conclude that the DIF3D-FD and DIF3D-VARIANT solvers are producing the expected results for the cited output tables of peaking data. Because regions cannot overlap in DIF3D, the preceding results are the only actual values that need to be checked with respect to the areas. The peaking data calculated by DIF3D for areas is a simple maximum operation applied to the given regions that are within the area. For integrals, it is simply a volume weighted sum operation of the contained region data. The best way to demonstrate this here is to dissect an input from DIF3D, for which the 20x20x20 DIF3D-VARIANT result is provided in Figure 37.

Starting with area “ALLZ1,” we can see from Table 71 that it consists of REG1, REG3, and REG6. From Figure 37 we can observe that ALLZ1 takes the peak value for the power density from REG3 while it takes the peak total flux and peak fast flux from REG1. Area “ALLZ2” contains REG2, REG4, REG5, REG7, and REG8 and from Table 71 one can see that the peak power density comes from REG4 while the peak total flux and peak fast flux come from REG8. All of these results are of course 100% correct given the maximum in each region with the respective areas.

The area “UPPHLF” consists of REG5 to REG8 while “BOTHLF” consists of REG1 to REG4 and TCORE consists of all regions in the domain. Much like the preceding results, the peak power density for UPPHLF comes from REG6, BOTHLF comes from REG3, and TCORE assumes the peak of the entire domain from REG3. The peak total flux and peak fast flux have similar results for these areas where the peak in UPPHLF comes from REG8, BOTHLF comes from REG1, and TCORE comes from REG1.

Excluding the volume, the remaining columns in each of these tables is derived from the other data. As an example, the “PEAK TO AVG.” column is simply the peak density divided by the adjacent power density result. As an example, for REG1:  $1.467891\text{E-}10/3.26762\text{E-}11=4.49537\text{E+}00$  ignoring the round off error associated with the provided precision. Similarly, the “POWER (WATTS)” column is simply the “POWER DENSITY” column multiplied by the volume. For REG 1:  $3.26762\text{E-}11*1.25\text{E+}05=4.08452\text{E-}06$ . Finally, the “POWER FRACTION”

column is simply the “POWER (WATTS)” column divided by the total power listed at the bottom of the “POWER (WATTS)” column that is the sum over the entire domain. For REG1:  $4.08452\text{E-}06/3.14620\text{E-}05=1.29824\text{E-}01$ . It is a trivial matter to use EXCEL to verify the remaining columns of data are correct given the region-wise values are correct which has already been demonstrated above.

The last aspect to verify is the fast flux computation when there are multiple groups present. DIF3D presently defines the fast flux boundary as 0.1 MeV. To check the multigroup aspect, especially the case where an energy group is cut in parts due to the 0.1 MeV boundary, the energy boundaries of the cross section data in Table 70 were changed from 0.1 MeV to 0.25 MeV. This causes DIF3D to weight the group 2 flux according to the following relation:

$$\phi_{fast} = \phi_1 + \frac{\ln\left(\frac{100000}{250000}\right)}{\ln\left(\frac{0.00001}{250000}\right)} \phi_2 = \phi_1 + 0.03827 \cdot \phi_2. \quad (52)$$

As inferred, this slight change in the energy group representation will only impact the fast flux in a minor way. Because this does not impact the flux distribution or the source representation, the overall flux distribution and the output tables of the total flux and power related data will remain identical. In this regard, the important aspect of making this change is to observe that the total fast flux and peak fast flux change. The location of the peak fast flux will also change.

For brevity, only results for the 20x20x20 DIF3D-VARIANT solution using a 10<sup>th</sup> order flux and 4<sup>th</sup> order leakage approximations are presented. Table 81 provides the region-wise errors for the test case with the 0.1 MeV and 0.25 MeV energy boundary between group 1 and 2. This table provides the total fast flux results and the peak fast flux errors. For the total fast flux, the change in the energy boundary alters the magnitude in each region consistently upwards. With the stated settings, the DIF3D-VARIANT solver matches the reference results very well.

Continuing with the peak fast flux results in Table 81, the result from the DIF3D output table is provided along with the one obtained using the EvaluateFlux utility program using the location of the peak flux from the analytic solution. As was the case for the total fast flux, the peak fast flux goes up in all regions. The DIF3D output tables display a consistent accuracy for the two energy boundaries chosen while the EvaluateFlux result indicates that the DIF3D-VARIANT solution is consistent with the analytic solution.

February 13, 2020

**Table 79. Region Errors for the Power Density in the Diffusion Theory Peaking Problem**

Solver	DIF3D-VARIANT						DIF3D-FD			Analytic
Mesher	10x10x10	10x10x10	10x10x10	10x10x10	10x10x10	20x20x20	10x10x10	20x20x20	50x50x50	-
Flux	6 <sup>th</sup>	6 <sup>th</sup>	8 <sup>th</sup>	10 <sup>th</sup>	12 <sup>th</sup>	10 <sup>th</sup>	-	-	-	-
Leakage	1 <sup>st</sup>	2 <sup>nd</sup>	3 <sup>rd</sup>	4 <sup>th</sup>	5 <sup>th</sup>	4 <sup>th</sup>	-	-	-	-
REG1	2.3E-04	1.6E-06	-1.5E-06	-1.5E-06	-1.5E-06	1.6E-06	-1.1E-02	-2.5E-03	-3.8E-04	3.3E-11
REG2	-9.4E-06	-1.4E-06	-1.4E-06	-1.4E-06	-1.4E-06	-1.4E-06	-1.5E-02	-3.8E-03	-6.2E-04	2.5E-11
REG3	-1.2E-06	-1.2E-06	-1.2E-06	-1.2E-06	-1.2E-06	-1.2E-06	-8.3E-03	-2.2E-03	-3.6E-04	4.6E-11
REG4	1.8E-05	-1.9E-06	-1.9E-06	-1.9E-06	-1.9E-06	-1.9E-06	-1.4E-02	-3.7E-03	-5.9E-04	2.5E-11
REG5	-9.4E-06	-1.4E-06	-1.4E-06	-1.4E-06	-1.4E-06	-1.4E-06	-1.5E-02	-3.8E-03	-6.2E-04	2.5E-11
REG6	1.5E-05	8.9E-07	8.9E-07	8.9E-07	8.9E-07	8.9E-07	-9.0E-03	-2.4E-03	-3.9E-04	4.1E-11
REG7	1.8E-05	-1.9E-06	-1.9E-06	-1.9E-06	-1.9E-06	-1.9E-06	-1.4E-02	-3.7E-03	-5.9E-04	2.5E-11
REG8	2.0E-04	9.0E-07	9.0E-07	9.0E-07	9.0E-07	9.0E-07	-1.1E-02	-2.6E-03	-4.0E-04	3.0E-11

**Table 80. Region Errors for the Peak Power Density in the Diffusion Theory Peaking Problem**

Solver	DIF3D-VARIANT						DIF3D-FD			Analytic
Mesher	10x10x10	10x10x10	10x10x10	10x10x10	10x10x10	20x20x20	10x10x10	20x20x20	50x50x50	-
Flux	6 <sup>th</sup>	6 <sup>th</sup>	8 <sup>th</sup>	10 <sup>th</sup>	12 <sup>th</sup>	10 <sup>th</sup>	-	-	-	-
Leakage	1 <sup>st</sup>	2 <sup>nd</sup>	3 <sup>rd</sup>	4 <sup>th</sup>	5 <sup>th</sup>	4 <sup>th</sup>	-	-	-	-
REG1	-1.9%	-1.9%	-1.9%	-1.9%	-1.9%	-0.2%	2.0%	0.4%	-0.1%	1.5E-10
REG2	1.1%	1.2%	1.2%	1.2%	1.2%	0.0%	-4.3%	-1.5%	-0.4%	1.4E-10
REG3	-10.6%	-10.6%	-10.6%	-10.6%	-10.6%	-2.2%	-14.3%	-2.7%	-1.5%	2.5E-10
REG4	0.8%	0.8%	0.8%	0.8%	0.8%	0.3%	-2.4%	-0.4%	-0.1%	1.4E-10
REG5	1.1%	1.2%	1.2%	1.2%	1.2%	0.0%	-4.3%	-1.5%	-0.4%	1.4E-10
REG6	-10.2%	-10.1%	-10.1%	-10.1%	-10.1%	-2.0%	-13.1%	-2.4%	-1.1%	2.1E-10
REG7	0.8%	0.8%	0.8%	0.8%	0.8%	0.3%	-2.4%	-0.4%	-0.1%	1.4E-10
REG8	-0.9%	-0.9%	-0.9%	-0.9%	-0.9%	-0.5%	-1.3%	-1.0%	-0.4%	1.4E-10

February 13, 2020

REGION NO.	NAME	ZONE NO.	ZONE NAME	VOLUME (CC)	INTEGRATION (1) WEIGHT FACTOR	POWER (WATTS)	POWER DENSITY (WATTS/CC)	PEAK DENSITY (WATTS/CC) (2)	PEAK TO AVG. POWER DENSITY	POWER FRACTION
1	REG1	1	COMP1	1.25000E+05	1.00000E+00	4.08452E-06	3.26762E-11	1.46891E-10	4.49537E+00	1.29824E-01
2	REG2	2	COMP2	1.25000E+05	1.00000E+00	3.12847E-06	2.50277E-11	1.36032E-10	5.43526E+00	9.94362E-02
3	REG3	3	COMP3	1.25000E+05	1.00000E+00	5.80915E-06	4.64732E-11	2.43032E-10	5.22950E+00	1.84640E-01
4	REG4	4	COMP4	1.25000E+05	1.00000E+00	3.18259E-06	2.54607E-11	1.38140E-10	5.42560E+00	1.01157E-01
5	REG5	5	COMP5	1.25000E+05	1.00000E+00	3.12847E-06	2.50277E-11	1.36032E-10	5.43526E+00	9.94362E-02
6	REG6	6	COMP6	1.25000E+05	1.00000E+00	5.18654E-06	4.14924E-11	2.09091E-10	5.03927E+00	1.64851E-01
7	REG7	7	COMP7	1.25000E+05	1.00000E+00	3.18259E-06	2.54607E-11	1.38140E-10	5.42560E+00	1.01157E-01
8	REG8	8	COMP8	1.25000E+05	1.00000E+00	3.75970E-06	3.00776E-11	1.35023E-10	4.48916E+00	1.19499E-01
TOTALS				1.00000E+06	0.00000E+00	3.14620E-05	3.14620E-11	2.43032E-10	7.72460E+00	1.00000E+00

AREA NO.	NAME	VOLUME (CC)	INTEGRATION (1) WEIGHT FACTOR	POWER (WATTS)	POWER DENSITY (WATTS/CC)	PEAK DENSITY (WATTS/CC) (2)	PEAK TO AVG. POWER DENSITY	POWER FRACTION
1	ALLZ1	3.75000E+05	0.00000E+00	1.50802E-05	4.02139E-11	2.43032E-10	6.04347E+00	4.79315E-01
2	ALLZ2	6.25000E+05	0.00000E+00	1.63818E-05	2.62109E-11	1.38140E-10	5.27032E+00	5.20685E-01
3	UPPHLF	5.00000E+05	0.00000E+00	1.52573E-05	3.05146E-11	2.09091E-10	6.85217E+00	4.84943E-01
4	BOTHLF	5.00000E+05	0.00000E+00	1.62047E-05	3.24095E-11	2.43032E-10	7.49879E+00	5.15057E-01
5	TCORE	1.00000E+06	0.00000E+00	3.14620E-05	3.14620E-11	2.43032E-10	7.72460E+00	1.00000E+00

...

REGION NO.	NAME	ZONE NO.	ZONE NAME	VOLUME (CC)	TOTAL FLUX (NEUTRON-CM/SEC)	PEAK FLUX (1) (NEUTRON/CM2-SEC)	TOTAL FAST FLUX (NEUTRON-CM/SEC)	PEAK FAST FLUX (1) (NEUTRON/CM2-SEC)
1	REG1	1	COMP1	1.25000E+05	9.68012E+05	4.04989E+01	8.48651E+05	3.82045E+01
2	REG2	2	COMP2	1.25000E+05	5.30581E+05	2.28750E+01	4.15731E+05	1.87612E+01
3	REG3	3	COMP3	1.25000E+05	6.64616E+05	2.41869E+01	4.15731E+05	1.87612E+01
4	REG4	4	COMP4	1.25000E+05	5.17049E+05	2.23574E+01	3.97689E+05	1.72479E+01
5	REG5	5	COMP5	1.25000E+05	5.30581E+05	2.28750E+01	4.15731E+05	1.87544E+01
6	REG6	6	COMP6	1.25000E+05	6.17247E+05	2.22151E+01	3.97689E+05	1.72479E+01
7	REG7	7	COMP7	1.25000E+05	5.17049E+05	2.23574E+01	3.97689E+05	1.72479E+01
8	REG8	8	COMP8	1.25000E+05	8.46196E+05	3.37676E+01	7.31346E+05	3.15542E+01
TOTALS				1.00000E+06	5.19133E+06	4.04989E+01	4.02026E+06	3.82045E+01

AREA NO.	NAME	VOLUME (CC)	TOTAL FLUX (NEUTRON-CM/SEC)	PEAK FLUX (1) (NEUTRON/CM2-SEC)	TOTAL FAST FLUX (NEUTRON-CM/SEC)	PEAK FAST FLUX (1) (NEUTRON/CM2-SEC)
1	ALLZ1	3.75000E+05	2.24987E+06	4.04989E+01	1.66207E+06	3.82045E+01
2	ALLZ2	6.25000E+05	2.94146E+06	3.37676E+01	2.35819E+06	3.15542E+01
3	UPPHLF	5.00000E+05	2.51107E+06	3.37676E+01	1.94245E+06	3.15542E+01
4	BOTHLF	5.00000E+05	2.68026E+06	4.04989E+01	2.07780E+06	3.82045E+01
5	TCORE	1.00000E+06	5.19133E+06	4.04989E+01	4.02026E+06	3.82045E+01

Figure 37. The DIF3D-VARIANT 20x20x20 Mesh Result for the Peaking Output Tables

February 13, 2020

**Table 81. Region Errors for the Total Fast Flux and Peak Fast Flux in the Diffusion Theory Peaking Problem**

Region	Results for 0.1 MeV Energy Boundary					Results for 0.25 MeV Energy Boundary				
	Total Fast Flux		Peak Fast Flux			Total Fast Flux		Peak Fast Flux		
	Error	Reference	DIF3D Output Table Error	Evaluate Flux Output Error	Reference	Error	Reference	DIF3D Output Table Error	Evaluate Flux Output Error	Reference
<b>REG1</b>	-3.5E-07	8.49E+05	-2.70%	-3.7E-08	39.26	-4.2E-07	8.53E+05	-2.68%	-3.1E-08	39.35
<b>REG2</b>	-9.6E-07	4.16E+05	0.08%	-1.7E-07	18.75	3.9E-07	4.20E+05	0.09%	-2.0E-07	18.89
<b>REG3</b>	-9.6E-07	4.16E+05	0.08%	-2.1E-07	18.75	-1.1E-06	4.25E+05	0.06%	-2.4E-07	18.96
<b>REG4</b>	7.5E-07	3.98E+05	-0.53%	-1.9E-07	17.34	5.9E-07	4.02E+05	-0.51%	-2.0E-07	17.53
<b>REG5</b>	-9.6E-07	4.16E+05	0.04%	-1.8E-07	18.75	3.9E-07	4.20E+05	0.06%	-2.0E-07	18.89
<b>REG6</b>	7.5E-07	3.98E+05	-0.53%	-1.8E-07	17.34	-1.1E-06	4.06E+05	-0.53%	-1.9E-07	17.53
<b>REG7</b>	7.5E-07	3.98E+05	-0.53%	-1.9E-07	17.34	5.9E-07	4.02E+05	-0.51%	-2.0E-07	17.53
<b>REG8</b>	-4.1E-07	7.31E+05	-2.39%	-6.9E-08	32.33	3.6E-07	7.36E+05	-2.36%	-6.4E-08	32.40

February 13, 2020

Given the preceding results, one can conclude that the DIF3D-FD and DIF3D-VARIANT solvers are able to correctly solve this test problem. Further, the DIF3D summary tables for region edits of the total flux, the peak of the total flux, the total fast flux, the peak of the fast flux, the power density and peak power density were all shown to identically produce the analytic solution. All of the other quantities in these tables were derivative quantities given these base pieces of information and the geometry volume. While DIF3D-FD requires substantial mesh refinement to reduce the errors to zero, there is clear convergence towards the solution. DIF3D-VARIANT requires a considerable polynomial order to match the reference solution to less than  $10^{-4}$  error. Of some concern is that the algorithm used to evaluate the peak fast flux in DIF3D-VARIANT can be quite unreliable due to the peaking of the flux within the mesh. While it is not clear whether this issue impacts current design projects, it is a trivial matter to use the EvaluateFlux routine to check the DIF3D output tables as demonstrated on this problem.

### 3.1.8 Radial Periodic Boundary Conditions Verification

To verify DIF3D's ability to apply periodic boundary conditions in the radial plane, a simple 3D Cartesian model was created comprising of two regions. This model was represented in a full-core DIF3D model as well as an equivalent periodic model and the results compared. Figure 38 provides the A.NIP3 blocks (top) and resultant DIF3D core map (bottom) for these models; the full-core model is on the left and the periodic is on the right. This particular layout was chosen for its simplicity and because it could not be represented with a reflective boundary condition.

<pre> UNFORM=A.NIP3 01 FULL_CORE 02 0 3 40000000 40000000 40000000 40000000 0 3 3 3 03 44 04 2 2 2 2 10 10 06 REG1 0. 40. 0 2 0. 40. 06 REG3 30. 40. 0 2 20. 30. 06 REG3 10. 20. 0 2 30. 40. 06 REG3 0. 10. 0 2 10. 20. 06 REG3 20. 30. 0 2 0. 10. 09 X 4 40. 09 Y 4 40. 09 Z 2 50. 14 COMP1 ISO1 1.0 15 COMP1 REG1 14 COMP3 ISO3 1.0 15 COMP3 REG3 </pre>	<pre> UNFORM=A.NIP3 01 PERIODIC 02 0 3 40000000 40000000 40000000 40000000 0 3 3 3 03 44 04 7 2 2 2 10 10 06 REG1 0. 20. 0 2 0. 20. 06 REG3 10. 20. 0 2 0. 10. 09 X 2 20. 09 Y 2 20. 09 Z 2 50. 14 COMP1 ISO1 1.0 15 COMP1 REG1 14 COMP3 ISO3 1.0 15 COMP3 REG3 </pre>
<pre> 0 1 2 3 4 ***** 4 * 1 2 1 1 4 + * * * * + ***** 3 * 1 1 1 2 3 + * * * * + ***** 2 * 2 1 1 1 2 + * * * * + ***** 1 * 1 1 2 1 1 + * * * * + ***** 1 2 3 4 </pre>	<pre> 0 1 2 ***** 2 * 1 1 * 2 * * * * 1 * 1 * 2 * 1 ***** 1 2 </pre>

Figure 38. 3D Cartesian Periodic Input and Core Map

Proper DIF3D handling of these boundaries should result in similar eigenvalues and flux distributions between the two models, with allowances granted for the differing error residuals during convergence for these cases. After execution, it was found that the eigenvalue error between the full-core and periodic cases is 0.004269 pcm. Similarly, the flux values differed by a factor of approximately 4.007. This factor of four is expected due to the full-core model having four times the volume, and thus having a normalization factor that differs by a factor of four. Therefore the periodic and full-core case fluxes match and this capability is verified.

### 3.1.9 Extrapolated and Reflected Boundary Conditions Verification

The previous problems analyzed either escape, reflective, or periodic boundary conditions on all six faces of the 3D Cartesian problem domain. This problem will verify the extrapolated flux boundary condition. This will be done with the infinite-medium, multigroup, analytical eigenvalue case from Section 3.1.2 using the first cross section dataset provided in Table 50.

Specifically, this will be performed for each of the six faces by replacing the initial reflective boundary condition with an escape boundary condition ( $\phi = 0$ ). Then, this escape boundary condition will be replaced with an extrapolated boundary condition option with an extrapolation constant mathematically consistent with an escape boundary condition. The escape boundary and extrapolated-escape boundary shall yield the same eigenvalue. Next, the extrapolation constant will be reduced to a value of 0 (with a few steps along the way) to mimic a reflective boundary condition. Along the way, the default value of 0.4692 will be manually entered as well as left blank to verify the correctness of the manual that this is the default value.

Before progressing, the extrapolated boundary condition used by DIF3D is provided below. In this equation, the constant  $A$  is the user input and  $D$  is the typical diffusion coefficient. To mimic an escape flux boundary condition,  $\phi = 0$ , using this equation, it is clear that  $A$  must be significantly larger than  $D$ . Therefore, this work a value of  $10^{10}$  will be used for  $A$ . Next, since reflective boundary conditions are defined as  $\phi' = 0$ , this can be mimicked by setting  $A$  to a value of 0.

$$D\phi' + A\phi = 0 \quad (53)$$

The values of  $A$  used for this case and the resultant eigenvalues are provided in Table 82 for each of the six surfaces. For each of the presented cases, the five faces that are not provided in the surface column a reflective boundary condition applied. For convenience, the values in Table 82 that are expected to match have matching text colors for the eigenvalue. As can be seen, all values match to the 9<sup>th</sup> significant digit. Further, it is confirmed that as  $A$  approaches 0, the eigenvalue increases. This agrees with physical intuition as this applies a reflective boundary condition is approached and less neutron leakage is present. These results therefore show that the radial and axial reflective, vacuum, and extrapolated boundary conditions are verified for the DIF3D-FD Cartesian solver.

Table 82. Cartesian DIF3D-FD Extrapolated Boundary Condition Results

Surf.	Boundary Condition	A	Eigenvalue	Surf.	Boundary Condition	A	Eigenvalue
All	Reflected	N/A	1.60000001001	-			
Lower X	Escape	N/A	1.36533288176	Upper Y	Escape	N/A	1.36533288155
	Extrapolated	$10^{10}$	1.36533288176		Extrapolated	$10^{10}$	1.36533288155
		10	1.37029149130			10	1.37029149109
		0.46920 (manually entered)	1.43882439700			0.46920 (manually entered)	1.43882439683
		0.46920 (DIF3D default)	1.43882439700			0.46920 (DIF3D default)	1.43882439683
		0	1.60000001001			0	1.60000001001
Upper X	Escape	N/A	1.36533288176	Lower Z	Escape	N/A	1.36533288147
	Extrapolated	$10^{10}$	1.36533288176		Extrapolated	$10^{10}$	1.36533288147
		10	1.37029149130			10	1.37029149120
		0.46920 (manually entered)	1.43882439700			0.46920 (manually entered)	1.43882439675
		0.46920 (DIF3D default)	1.43882439700			0.46920 (DIF3D default)	1.43882439675
		0	1.60000001001			0	1.60000001001
Lower Y	Escape	N/A	1.36533288147	Upper Z	Escape	N/A	1.36533288155
	Extrapolated	$10^{10}$	1.36533288147		Extrapolated	$10^{10}$	1.36533288155
		10	1.37029149120			10	1.37029149109
		0.46920 (manually entered)	1.43882439675			0.46920 (manually entered)	1.43882439683
		0.46920 (DIF3D default)	1.43882439675			0.46920 (DIF3D default)	1.43882439683
		0	1.60000001001			0	1.60000001001

### 3.1.10 Iteration and Convergence Control Verification

Table 9 of the reference [6] plan identified that the iteration and convergence control options (A.DIF3D Type 3.4, 3.6, 3.9, 3.10, 3.11, 3.12, 5.2, 5.3, and 5.4) would be verified by way of the Integral Verification case. These options will be verified in this section, however, a DIF3D-FD version of the multigroup eigenvalue problem discussed for transport verification in Section 3.3.3 will be used instead. This was done for no other reason than that problem is smaller than the integral benchmark problem and thus runs faster, but also converges slowly enough that the effect of these options will be readily apparent. Note that this is only performed for a forward eigenvalue case and not repeated for a fixed source or adjoint case as the same convergence control code is exercised for any of these solves.



This will be performed by first running a base case that leaves all relevant parameters to their internal defaults. Then, a case will be performed where the defaults are explicitly specified in their respective cards. Next, using the explicitly listed defaults as the starting point, the options verified by this section will be modified from their default to the possible values. The possible values will either be every value in the discrete set, or if the variable can be continuous (like the number of iterations) then a sufficient number will be evaluated. The specific parameters, their defaults, and their perturbations are provided in Table 83. After executing all these cases, the output will be analyzed to ensure that DIF3D respected the option according to the description provided in the A.DIF3D listing. The restart capability will then be checked with two additional cases discussed in the final subsection.

**Table 83. Iteration Control Options for the Diffusion Solver**

Card Type	Summary	Default Value	Perturbed Values
3.4	Tchebyshev Acceleration	0	1
3.6	Outer Iteration Control	30	-4, -3, -2, -1, 10
3.9	Upscatter Iterations per Outer Iteration	5	20
3.10	Concurrent Iteration Efficiency	0	1
3.11	Accel. Of Opt. Overrelaxation	0	1
3.12	Opt. Overrelaxation Factor Calculation Control	50	2
5.2	Eigenvalue Criterion	$10^{-7}$	$10^{-3}$
5.3	Pointwise Fiss. Source Criterion	$10^{-5}$	$10^{-4}$
5.4	Avg. Fiss. Source Criterion	$10^{-5}$	$10^{-4}$

#### 3.1.10.1 Base and Default Cases

As noted, the first step performed was to first execute a case where all of the above values were simply not included in the input, and thereby DIF3D applied the default value. Then, a case was executed with these values explicitly stated. The outputs were compared using a python Diff tool, and it was found that the outputs indeed matched, except for the input edits and some slight changes to a few of the iteration times, that are subject to external factors and cannot be controlled. Therefore the default case will be used as the starting point going forward.

While not a part of this verification effort, it was noted that the A.DIF3D listing states that the Type 03 card's 5<sup>th</sup> parameter (minimum plane-block size for input/output transfer) has a default of 4500, however this was found to actually be 10,000.

All cases that remain will compare to this default case, but modified to utilize 2,000 iterations to convergence so that the total number of iterations to convergence can be observed as these options change.

#### 3.1.10.2 Card 3 Option 4 Perturbations

Card 3 Option 4 sets whether or not Tchebyshev acceleration of the outer iterations is performed. The default value, 0, indicates it shall be performed, while a value of 1 turns off this acceleration. Therefore, when the value of 1 is used, one should expect that either more iterations will be required to converge. Additionally, DIF3D's echo repeat should acknowledge the setting of this option.

The correct echo repeat was confirmed. Additionally, the case with the acceleration was found to converge in 46 iterations while the case without the acceleration required 169 iterations. The eigenvalue and flux values matched the default cases to within 0.3 pcm and 0.3%, respectively.

#### 3.1.10.3 Card 3 Option 6 Perturbations

Card 3 Option 6 controls the number of outer iterations in a case. The possible values are -1 (data management parameters, overrelaxation factors, and neutronics edits are performed), -2 (same as -1 without overrelaxation factors), -3 (DIF3D module is bypassed), -4 (same as -2, but with leakage results derived from the balance equation with zero residual), or some number greater than 0 that simply sets the maximum number of DIF3D outer iterations. The default value is 30 total iterations. This case will evaluate the 4 negative options as well as ensuring 10 total iterations are obeyed.

Option -4 was verified to skip the DIF3D iteration and skip the inner iteration optimization strategy edits as well as the outer iteration summary (i.e., DIF3D did not solve the diffusion equation). Further, the balance edits were compared between this and the base case. Here, the leakage terms were clearly derived from the balance residual, as the leakages were the equivalent to the default case's balance + leakage.

Option -3 was verified to not execute the DIF3D module, instead only processing the geometry and zone information from the A.NIP3 and A.HMG4C blocks.

Option -2 produced the same output as option -4 except for the balance edits, that were the same in Option -2 as the base case.

Option -1 computed the over relaxation factors, but did not perform the diffusion system solve.

Finally, a value of +10 performed exactly as expected, yielding 10 total iterations before quitting.

#### 3.1.10.4 Card 3 Option 9 Perturbations

Card 3 Option 9 sets the number of upscatter iterations per outer iteration. The default is 5. This parameter's impact is only indirectly observed in a diffusion solve. Specifically, it was found that the per-iteration convergence metrics and final results did vary in the final significant digit. The

eigenvalue matched the default and the flux had an RMSE error on the order of  $10^{-10}$ . This does indicate additional iterations were performed.

#### 3.1.10.5 Card 3 Option 10 Perturbations

Card 3 Option 10 sets a flag that instructs DIF3D to either perform the estimated number of inner iterations for each group (option 0), or to avoid the last pass of the inner iterations in groups whose number of iterations are less than some non-user-facing threshold. The default value is not specified by the A.DIF3D listing.

For the given problem this option seems to have no effect. This could very well be because the iterations are always greater than the threshold. The eigenvalue and flux matched the default to all reported digits.

#### 3.1.10.6 Card 3 Option 11 Perturbations

Card 3 Option 11 sets a flag that instructs DIF3D to either not perform acceleration of the optimum overrelaxation factor calculation (option 0, default), or apply asymptotic source extrapolation of the power iterations during the spectral radius calculation (option 1).

This was observed by a message indicating the truncation of the convergence on the optimum overrelaxation factor calculation iteration, as well as different omega values and a different iteration history though the same total number of iterations. The eigenvalues matched exactly and the flux had a RMS error on the order of  $10^{-11}$ .

#### 3.1.10.7 Card 3 Option 12 Perturbations

Card 3 Option 12 sets the number of iterations when determining the optimum overrelaxation factors. A positive integer is supplied and a value of 50 is strongly recommended. In this case a value of 2 was applied instead.

This problem yielded omegas with values of 1.0 for all three groups. This implies the factors did not modify (significantly) from their initial guess of 1.0 after the 2<sup>nd</sup> iteration. This affected the convergence history and required 2 more total power history iterations. The eigenvalues matched exactly and the flux had a RMS error on the order of  $10^{-9}$ .

#### 3.1.10.8 Card 5 Option 2 Perturbations

Card 5 Option 2 provides the floating point eigenvalue convergence criterion. The default is a value of  $10^{-7}$ . This case will apply a value of  $10^{-4}$ . To ensure the eigenvalue convergence is limiting, the pointwise and average fission source convergence tolerances were set to 0.01. Therefore one can expect that increasing the eigenvalue convergence (compared to the base case) should reduce the total number of iterations such that the fission source convergence is limiting.

This was indeed observed, as the case with a  $10^{-4}$  eigenvalue convergence criterion converged in 15 iterations instead of the base case's 46 iterations. Further, this was achieved when the eigenvalue dropped below  $10^{-4}$ ; the fission source measures had already passed 0.01.

#### 3.1.10.9 Card 5 Option 3 Perturbations

Card 5 Option 3 provides the floating point pointwise fission source convergence criterion. The default is a value of  $10^{-5}$ . This perturbation case will apply a value of  $10^{-4}$ . Like the previous case, the other convergence parameters were set so the pointwise fission source convergence criterion was limiting. Specifically, this means that the eigenvalue and average fission source criterion were 0.01 while the pointwise fission source criterion was  $10^{-4}$ . In this case, one can expect to see the problem execution to end when the fission source criterion is met.

This was observed, as the case with a  $10^{-4}$  pointwise fission source convergence criterion converged in 31 iterations instead of the base case's 46 iterations. Further, this convergence was achieved when the pointwise fission source was converged to less than  $10^{-4}$ , the provided value.

#### 3.1.10.10 Card 5 Option 4 Perturbations

Card 5 Option 4 provides the floating point average fission source convergence criterion. The default is a value of  $10^{-5}$ . This perturbation case will apply a value of  $10^{-4}$ . Since the default case reaches the eigenvalue convergence after the fission source is converged to the stated value, then the parameters were also set that the average fission source convergence criterion was limiting. Specifically, this means that the eigenvalue and pointwise fission source criterion were 0.01 while the average fission source criterion was  $10^{-4}$ . In this case, one can expect the problem execution to end when the fission source criterion is met.

This was the observed behavior, as the case with a  $10^{-4}$  average fission source convergence criterion converged in 28 iterations instead of the base case's 46 iterations. Further, this convergence was achieved when the rel. sum error of the fission source was converged to less than  $10^{-4}$ , the provided value.

#### 3.1.10.11 Restart Calculation

A restart computation can be performed with three approaches in DIF3D: (1) the binary DIF3D and RTFLUX files from the previous computation are provided via the "BLOCK=OLD" input block; (2) a restart is performed with the RTFLUX (or NHFLUX if DIF3D-VARIANT) file and a combination of A.DIF3D Type 06 and possibly 07 cards; or (3) DIF3D is executed and then restarted with tighter convergence criterion (or number of iterations) from within the same input. This sub-section will test these approaches using a restart from the default case that terminated itself after 30 iterations.

The first approach was performed with the BLOCK=OLD RTFLUX and DIF3D files, and a single card in the A.DIF3D block that set the maximum number of iterations to 2,000 instead of the 30 from the previous computation (and thus in the DIF3D binary file). After running this in DIF3D,

it is expected that (1) DIF3D's user input specifications echo would the changes to the number of iterations, state that this is a restart, and include the  $k_{\text{eff}}$  from the restart RTFLUX file (2) the initial  $k_{\text{eff}}$  from the 1<sup>st</sup> iteration of the new calculation should differ from the original calculation's first guess, (3) the outer iterations should continue until the new calculation's convergence criteria are met, and (4) the final eigenvalue and reported fluxes should match to on the order of the convergence criterion. All of these were observed, indicating the binary file-based restart was successful.

The second approach (previous RTFLUX and Type 06/Type 07 cards) was also performed with only the BLOCK=OLD RTFLUX file and Type 06 and Type 07 cards. The A.DIF3D module was modified to include the  $k_{\text{eff}}$  and dominance ratio from the 30 iteration calculation, and the restart flag set to 1 (indicating a restart should be performed). The restart case also had the number of iterations set to 2,000. After running this in DIF3D, it is expected that 1) DIF3D's user input specifications echo would the changes to the number of iterations, state that this is a restart, and include the initial  $k_{\text{eff}}$  2) the initial  $k_{\text{eff}}$  from the 1<sup>st</sup> iteration of the new calculation should differ from the original calculation's first guess, 3) the outer iterations should continue until the new calculation's convergence criteria are met, and (4) the final eigenvalue and reported fluxes should match to on the order of the convergence criterion. All of these were observed, indicating the restart was successful.

The third approach (restarting within same input file) was performed by executing the original DIF3D case to 30 iterations, using the DIF3D and RTFLUX files which were just generated with modifications for an increase number of iterations, and re-executing DIF3D. Similar behavior should be observed with this case compared to the original. This was confirmed, indicating this restart methodology was successful. Further, these methods output files and convergence histories matched to within the convergence criterion, indicating they effectively perform the same function within DIF3D.

#### 3.1.11 *Solution Edit Verification*

DIF3D prints a balance of the solution results in the form of neutron balance edits, power edits, flux edits, zone-averaged flux edits, and region-averaged flux edits. In addition to these are the writing of the SFEDIT, RZFLUX, and PWDINT interface files. All of these are controlled by options 6 through 11 of the A.DIF3D module's Type 04 card. This section will verify that these options are correctly obeyed. This section will also verify the correctness of the neutron balance tables, as these are the only tables that are not verified elsewhere.

The verification that the edit toggles can be performed with any model. The verification of the correctness of the neutron balances requires a model that utilizes multiple regions, one or more areas, and has cross sections with more than one group. Further, as the individual parameters will be calculated independent from DIF3D, a small model is desirable.

To that end, the four composition cross sections used in Section 3.1.1 (defined in Table 23 and Table 26) will be applied in a 10cm cube model. The region between 0 and 5 cm in X, 0 to 10 cm in Y, and 0 to 5 cm in Z are assigned REG1 filled with COMP1. The region between 5 cm in X

(and the same Y and Z as REG1) is assigned REG2 that is filled with COMP2. The top 5 cm in the Z plane are filled with REG3 (COMP3) on the left, and REG4 (COMP4) on the right. Reflective boundary conditions are applied on all sides. Finally, AREA1 is defined as all four regions while AREA2 is only REG1. The A.NIP3 input (aside from the composition definitions) is provided in Figure 39.

```

UNFORM=A.NIP3
01 3D XYZ - EDITS
02 0 3 40000000 40000000 40000000 40000000 0 3 3 3
03 44
04 3 3 3 3 3 3
06 REG1 0.0 5.0 0 1 0.0 10.0
06 REG2 5.0 10.0 0 1 0.0 10.0
06 REG3 0.0 5.0 1 2 0.0 10.0
06 REG4 5.0 10.0 1 2 0.0 10.0
09 X 1 5.0 1 10.
09 Y 2 10.
09 Z 1 5.0 1 10.
07 AREA1 REG1 REG2 REG3 REG4
07 AREA2 REG1

```

**Figure 39. XYZ Diffusion Edit Table Model**

To verify that the edit toggles were correctly verified the A.DIF3D Type 04 cards provided in Table 84 were applied. The first four do not print the binary interface files while the last two do. The first is the base case that prints none of the edits of interest. The second prints all edits to standard and auxiliary output. The third prints only to auxiliary output. The fourth to only standard output. The final two cases print the surface fast flux and power density to the SFEDIT file in mesh cell order and then in region order.

**Table 84. XYZ Diffusion Edit Table Perturbations**

Case	A.DIF3D Type 04 Card
1	04 3 3 3 33 000 00 000 0 0 0000 -1
2	04 3 3 3 33 333 33 333 3 3 0000 -1
3	04 3 3 3 33 222 22 222 2 2 0000 -1
4	04 3 3 3 33 111 11 111 1 1 0000 -1
5	04 3 3 3 33 000 00 000 0 0 1111 -1
6	04 3 3 3 33 000 00 000 0 0 2211 -1

Each of these six tasks was verified to ensure the output was produced where intended; no deficiencies were noted.

The next task is to verify the correctness of the PWDINT file. This was performed by comparing these files, after conversion to ASCII with the afore-mentioned CCCC\_convert utility, to the power density values provided in the already-verified DIF3D ASCII edits.

Similarly, the RZFLUX files were verified to be consistent with the already verified flux edit tables as well as by comparing the neutron loss terms to those provided in the standard output (and

February 13, 2020

verified later in this section). This was performed by evaluating the binary files using a custom Python program quite similar to the RTFLUX reading interface. Interestingly, it was identified that the total neutron losses and absorption values in this file were zero, despite the problem containing losses and absorption. All other terms, including the zone-averaged fluxes were as expected.

It was then verified that the SFEDIT files were printed, and that the case 5 SFEDIT file is different from the case 6 SFEDIT file by comparing the MD5 hashes of each file. The accuracy of the contents of these files, however, was not verified as part of this work.

The final task to be performed in this section is the verification of the correctness of the neutron balance tables. DIF3D outputs these quantities in one table per group, and a final table containing the information integrated over all energy groups. Each of these tables contains three sets of balance information. The data within each of these balance sets are provided in Table 85, Table 86, and Table 87, respectively. In addition to this region data, similar data was output for areas. The areas were chosen such that this comparison was trivial, AREA1 was all four regions, and thus should be equivalent to the Total row; AREA2 was defined as REG1 and therefore should be equivalent to the corresponding REG1 row. This was verified to be true.

Table 85. DIF3D Neutron Balance Table Set 1

Region	Net Leakage	Absorption Rate	Out-Scatter	In-Scatter	Fission Production	External Source	Balance
<b>Group 1</b>							
<b>REG1</b>	-4.3555E+08	3.6603E+06	4.3189E+08	0.0000E+00	0.0000E+00	0.0000E+00	-9.1195E-06
<b>REG2</b>	-2.2267E+08	8.1188E+08	1.1004E+10	0.0000E+00	1.1593E+10	0.0000E+00	3.5960E+01
<b>REG3</b>	-7.6464E+08	1.1670E+09	1.2870E+10	4.2179E+06	1.3268E+10	0.0000E+00	-3.4205E+01
<b>REG4</b>	1.4229E+09	5.2742E+09	1.8546E+09	4.9110E+06	8.5468E+09	0.0000E+00	2.0874E+00
<b>Total</b>	0.0000E+00	7.2567E+09	2.6160E+10	9.1289E+06	3.3408E+10	0.0000E+00	3.8425E+00
<b>Group 2</b>							
<b>REG1</b>	3.9527E+08	3.6617E+07	0.0000E+00	4.3189E+08	0.0000E+00	0.0000E+00	1.7881E-07
<b>REG2</b>	5.1743E+08	1.1690E+10	-2.3581E-06	1.1597E+10	6.1016E+08	0.0000E+00	1.8927E+00
<b>REG3</b>	2.5597E+09	1.3606E+10	4.2179E+06	1.5796E+10	3.7385E+08	0.0000E+00	-9.6379E-01
<b>REG4</b>	-3.4724E+09	6.0081E+09	4.9110E+06	2.5406E+09	0.0000E+00	0.0000E+00	-9.5367E-07
<b>Total</b>	4.7684E-07	3.1340E+10	9.1289E+06	3.0365E+10	9.8401E+08	0.0000E+00	9.2886E-01
<b>Group-Integrated</b>							
<b>REG1</b>	-4.0277E+07	4.0277E+07	4.3189E+08	4.3189E+08	0.0000E+00	0.0000E+00	-8.9407E-06
<b>REG2</b>	2.9476E+08	1.2501E+10	1.1004E+10	1.1597E+10	1.2203E+10	0.0000E+00	3.7853E+01
<b>REG3</b>	1.7951E+09	1.4773E+10	1.2874E+10	1.5800E+10	1.3642E+10	0.0000E+00	-3.5169E+01
<b>REG4</b>	-2.0496E+09	1.1282E+10	1.8595E+09	2.5455E+09	8.5468E+09	0.0000E+00	2.0874E+00
<b>Total</b>	4.7684E-07	3.8597E+10	2.6169E+10	3.0374E+10	3.4392E+10	0.0000E+00	4.7714E+00



February 13, 2020

Table 86. DIF3D Neutron Balance Table Set 2

Region	X Leakage	Y Leakage	Z Leakage	Tot. Buckling	X Buckling	Y Buckling	Z Buckling
<b>Group 1</b>							
<b>REG1</b>	-4.3994E+08	0.0000E+00	4.3891E+06	-3.3506E-04	-3.3844E-04	0.0000E+00	3.3765E-06
<b>REG2</b>	4.3994E+08	0.0000E+00	-6.6261E+08	-5.2989E-04	1.0469E-03	0.0000E+00	-1.5768E-03
<b>REG3</b>	-7.6025E+08	0.0000E+00	-4.3891E+06	-2.7863E-03	-2.7703E-03	0.0000E+00	-1.5994E-05
<b>REG4</b>	7.6025E+08	0.0000E+00	6.6261E+08	3.5472E-03	1.8953E-03	0.0000E+00	1.6519E-03
<b>Total</b>	0.0000E+00	0.0000E+00	-1.1921E-07	0.0000E+00	0.0000E+00	0.0000E+00	-4.9761E-20
<b>Group 2</b>							
<b>REG1</b>	8.1926E+08	0.0000E+00	-4.2399E+08	1.8837E-03	3.9044E-03	0.0000E+00	-2.0206E-03
<b>REG2</b>	-8.1926E+08	0.0000E+00	1.3367E+09	1.4203E-02	-2.2488E-02	0.0000E+00	3.6691E-02
<b>REG3</b>	2.1357E+09	0.0000E+00	4.2399E+08	5.3102E-02	4.4306E-02	0.0000E+00	8.7958E-03
<b>REG4</b>	-2.1357E+09	0.0000E+00	-1.3367E+09	-1.8146E-01	-1.1161E-01	0.0000E+00	-6.9851E-02
<b>Total</b>	0.0000E+00	0.0000E+00	0.0000E+00	1.5205E-18	0.0000E+00	0.0000E+00	0.0000E+00
<b>Group-Integrated</b>							
<b>REG1</b>	3.7933E+08	0.0000E+00	-4.1960E+08	-2.6678E-05	2.5126E-04	0.0000E+00	-2.7793E-04
<b>REG2</b>	-3.7933E+08	0.0000E+00	6.7408E+08	6.4546E-04	-8.3066E-04	0.0000E+00	1.4761E-03
<b>REG3</b>	1.3755E+09	0.0000E+00	4.1960E+08	5.5638E-03	4.2633E-03	0.0000E+00	1.3006E-03
<b>REG4</b>	-1.3755E+09	0.0000E+00	-6.7408E+08	-4.8769E-03	-3.2729E-03	0.0000E+00	-1.6040E-03
<b>Total</b>	0.0000E+00	0.0000E+00	-1.1921E-07	1.7600E-19	0.0000E+00	0.0000E+00	-4.4001E-20

Table 87. DIF3D Neutron Balance Table Set 3

Region	Capture Rate	Fission Rate	(n,2n) Source	Net Prod'n	Median E. Fiss Src	Median E. Abs. Rate	Med E. Flux
<b>Group 1</b>							
<b>REG1</b>	3.6603E+06	0.0000E+00	-	-	-	-	-
<b>REG2</b>	3.9747E+08	4.1441E+08	-	-	-	-	-
<b>REG3</b>	8.0966E+08	3.5736E+08	-	-	-	-	-
<b>REG4</b>	3.9860E+09	1.2882E+09	-	-	-	-	-
<b>Total</b>	5.1967E+09	2.0600E+09	-	-	-	-	-
<b>Group 2</b>							
<b>REG1</b>	3.6617E+07	0.0000E+00	-	-	-	-	-
<b>REG2</b>	3.9465E+09	7.7431E+09	-	-	-	-	-
<b>REG3</b>	4.7090E+09	8.8965E+09	-	-	-	-	-
<b>REG4</b>	1.2444E+09	4.7636E+09	-	-	-	-	-
<b>Total</b>	9.9365E+09	2.1403E+10	-	-	-	-	-
<b>Group-Integrated</b>							
<b>REG1</b>	4.0277E+07	0.0000E+00	0.0000E+00	0.0000E+00	0.0000E+00	6.5052E-03	5.1875E+01
<b>REG2</b>	4.3439E+09	8.1575E+09	5.9292E+08	1.2796E+10	2.8733E+03	5.4845E-03	1.7305E+02
<b>REG3</b>	5.5187E+09	9.2539E+09	2.9257E+09	1.6568E+10	3.5290E+03	6.0089E-03	2.6327E+01
<b>REG4</b>	5.2304E+09	6.0519E+09	6.8595E+08	9.2327E+09	4.4721E+03	5.0491E-01	1.8134E+03
<b>Total</b>	1.5133E+10	2.3463E+10	4.2046E+09	3.8597E+10	3.4913E+03	1.3582E-02	1.4943E+02



To verify these, an independent computation of these values is necessary. These quantities are trivial nuclear-engineering quantities that can generally be obtained through standard reaction-rate quantities. Further, the DIF3D output provides notes on what specific quantities compose each of these balance columns. The only quantities that were not trivially computed are the median energies (last three columns of Table 87) and the leakage terms. The median energies are thoroughly defined in Chapter 3 of the DIF3D-FD manual [1]. The leakage terms are the same as one would expect with diffusion theory; these are defined in Chapter 2 of the DIF3D-FD manual and specifically in Eq. 2.15 and Table 2.2 of [1]. The Table 85 through Table 87 quantities were computed in such a way using a Python script that used information accessible in Python via the same scripts used to convert the DIF3D inputs to an equivalent MCNP information. Namely, the RTFLUX, GEODST, and COMPXS information.

These computed reference balance values are provided in Table 88 through Table 90 in the same format as the DIF3D output values above. As can be seen, the differences are exceedingly small, and usually less than the printed tolerance. The largest errors are seen with the total balance, however, these values are significantly less than the terms in the rows, which are summed to produce the balance. Thus this also is simply numerical truncation error. Finally, a sanity check was performed by ensuring that the leakage, absorption, fission, and (n,2n) production rates, when combined as shown in the equation below yields the same eigenvalue as reported by DIF3D. This was observed to be true. Therefore this table is considered verified.

$$k_{eff} = \frac{\text{Fiss Source Rate}}{\text{Leakage Rate} + \text{Abso Rate} - (\text{n,2n}) \text{ Rate}} \quad (54)$$

The median energy values in this table required some iteration. Since the ISOTXS file provided defined the lower energy group boundary as 0.0 eV, the conversion to lethargy would naturally produce an invalid number. DIF3D internally replaces 0 eV group boundaries with a value, avoiding this problem. To identify which value DIF3D uses, a search was performed, and the 0 eV seems to be replaced with  $1.382882 \times 10^{-5}$  eV. This energy was therefore used internally by DIF3D in generating the results of Table 90. It was separately verified that when a non-zero lower group boundary is used (i.e.,  $10^{-5}$  eV), DIF3D and the hand-computations match.

February 13, 2020

Table 88. Reference Neutron Balance Table Set 1

Region	Net Leakage	Absorption Rate	Out-Scatter	In-Scatter	Fission Production	External Source	Balance
<b>Group 1</b>							
REG1	-4.3555E+08	3.6603E+06	4.3189E+08	0.0000E+00	0.0000E+00	0.0000E+00	-8.9407E-06
REG2	-2.2267E+08	8.1188E+08	1.1004E+10	0.0000E+00	1.1593E+10	0.0000E+00	-1.9221E+02
REG3	-7.6464E+08	1.1670E+09	1.2870E+10	4.2179E+06	1.3268E+10	0.0000E+00	-2.9534E+02
REG4	1.4229E+09	5.2742E+09	1.8546E+09	4.9110E+06	8.5468E+09	0.0000E+00	-1.6613E+02
Total	0.0000E+00	7.2567E+09	2.6160E+10	9.1289E+06	3.3408E+10	0.0000E+00	-6.5368E+02
<b>Group 2</b>							
REG1	3.9527E+08	3.6617E+07	0.0000E+00	4.3189E+08	0.0000E+00	0.0000E+00	4.1723E-07
REG2	5.1743E+08	1.1690E+10	-2.3581E-06	1.1597E+10	6.1016E+08	0.0000E+00	-1.0116E+01
REG3	2.5597E+09	1.3606E+10	4.2179E+06	1.5796E+10	3.7385E+08	0.0000E+00	-8.3218E+00
REG4	-3.4724E+09	6.0081E+09	4.9110E+06	2.5406E+09	0.0000E+00	0.0000E+00	0.0000E+00
Total	4.7684E-07	3.1340E+10	9.1289E+06	3.0365E+10	9.8401E+08	0.0000E+00	-1.8438E+01
<b>Group-Integrated</b>							
REG1	-4.0277E+07	4.0277E+07	4.3189E+08	4.3189E+08	0.0000E+00	0.0000E+00	-8.5235E-06
REG2	2.9476E+08	1.2501E+10	1.1004E+10	1.1597E+10	1.2203E+10	0.0000E+00	-2.0233E+02
REG3	1.7951E+09	1.4773E+10	1.2874E+10	1.5800E+10	1.3642E+10	0.0000E+00	-3.0367E+02
REG4	-2.0496E+09	1.1282E+10	1.8595E+09	2.5455E+09	8.5468E+09	0.0000E+00	-1.6613E+02
Total	2.3842E-07	3.8597E+10	2.6169E+10	3.0374E+10	3.4392E+10	0.0000E+00	-6.7212E+02

Table 89. Reference Neutron Balance Table Set 2

Region	X Leakage	Y Leakage	Z Leakage	Tot. Buckling	X Buckling	Y Buckling	Z Buckling
<b>Group 1</b>							
REG1	-4.3994E+08	0.0000E+00	4.3891E+06	-3.3506E-04	-3.3844E-04	0.0000E+00	3.3765E-06
REG2	4.3994E+08	0.0000E+00	-6.6261E+08	-5.2989E-04	1.0469E-03	0.0000E+00	-1.5768E-03
REG3	-7.6025E+08	0.0000E+00	-4.3891E+06	-2.7863E-03	-2.7703E-03	0.0000E+00	-1.5994E-05
REG4	7.6025E+08	0.0000E+00	6.6261E+08	3.5472E-03	1.8953E-03	0.0000E+00	1.6519E-03
Total	0.0000E+00	0.0000E+00	0.0000E+00	0.0000E+00	0.0000E+00	0.0000E+00	0.0000E+00
<b>Group 2</b>							
REG1	8.1926E+08	0.0000E+00	-4.2399E+08	1.8837E-03	3.9044E-03	0.0000E+00	-2.0206E-03
REG2	-8.1926E+08	0.0000E+00	1.3367E+09	1.4203E-02	-2.2488E-02	0.0000E+00	3.6691E-02
REG3	2.1357E+09	0.0000E+00	4.2399E+08	5.3102E-02	4.4306E-02	0.0000E+00	8.7958E-03
REG4	-2.1357E+09	0.0000E+00	-1.3367E+09	-1.8146E-01	-1.1161E-01	0.0000E+00	-6.9851E-02
Total	0.0000E+00	0.0000E+00	0.0000E+00	0.0000E+00	0.0000E+00	0.0000E+00	0.0000E+00
<b>Group-Integrated</b>							
REG1	3.7933E+08	0.0000E+00	-4.1960E+08	-2.6678E-05	2.5126E-04	0.0000E+00	-2.7793E-04
REG2	-3.7933E+08	0.0000E+00	6.7408E+08	6.4547E-04	-8.3066E-04	0.0000E+00	1.4761E-03
REG3	1.3755E+09	0.0000E+00	4.1960E+08	5.5639E-03	4.2633E-03	0.0000E+00	1.3006E-03
REG4	-1.3755E+09	0.0000E+00	-6.7408E+08	-4.8769E-03	-3.2729E-03	0.0000E+00	-1.6040E-03
Total	0.0000E+00	0.0000E+00	0.0000E+00	0.0000E+00	0.0000E+00	0.0000E+00	0.0000E+00

Table 90. Reference Neutron Balance Table Set 3

Region	Capture Rate	Fission Rate	(n,2n) Source	Net Prod'n	Median E. Fiss Src	Median E. Abs. Rate	Med E. Flux
<b>Group 1</b>							
<b>REG1</b>	3.6603E+06	0.0000E+00	-	-	-	-	-
<b>REG2</b>	3.9747E+08	4.1441E+08	-	-	-	-	-
<b>REG3</b>	8.0966E+08	3.5736E+08	-	-	-	-	-
<b>REG4</b>	3.9860E+09	1.2882E+09	-	-	-	-	-
<b>Total</b>	5.1967E+09	2.0600E+09	-	-	-	-	-
<b>Group 2</b>							
<b>REG1</b>	3.6617E+07	0.0000E+00	-	-	-	-	-
<b>REG2</b>	3.9465E+09	7.7431E+09	-	-	-	-	-
<b>REG3</b>	4.7090E+09	8.8965E+09	-	-	-	-	-
<b>REG4</b>	1.2444E+09	4.7636E+09	-	-	-	-	-
<b>Total</b>	9.9365E+09	2.1403E+10	-	-	-	-	-
<b>Group-Integrated</b>							
<b>REG1</b>	4.0277E+07	0.0000E+00	0.0000E+00	0.0000E+00	0.0000E+00	6.5052E-03	5.1875E+01
<b>REG2</b>	4.3439E+09	8.1575E+09	5.9292E+08	1.2796E+10	2.8733E+03	5.4845E-03	1.7305E+02
<b>REG3</b>	5.5187E+09	9.2539E+09	2.9257E+09	1.6568E+10	3.5290E+03	6.0089E-03	2.6327E+01
<b>REG4</b>	5.2304E+09	6.0519E+09	6.8595E+08	9.2327E+09	4.4721E+03	5.0491E-01	1.8134E+03
<b>Total</b>	1.5133E+10	2.3463E+10	4.2046E+09	3.8597E+10	3.4913E+03	1.3582E-02	1.4943E+02

### 3.1.12 A.SUMMAR Output

The SUMMAR module aggregates binary output produced by DIF3D and creates summary tables (and formerly, plots) which provide engineering information to the user. This module can be called within DIF3D by specifying an A.SUMMAR input block. This section will verify the specific capabilities within the SUMMAR module that are applicable to stand-alone DIF3D usage. The remaining capabilities, if necessary, will be verified by future work or otherwise disabled. As a final note before getting in to the details, SUMMAR only takes output from DIF3D and does not interact directly with the solver. Therefore this verification need not be repeated for DIF3D-FD and DIF3D-VARIANT, nor for the different geometry types.

To perform this verification, a DIF3D-FD 3D Cartesian model was created which used the same four isotopic cross sections defined in Table 12 through Table 14. These four isotopes were combined into three unique regions, and each assigned to a 10x10x10 cm block arranged next to each other. The corresponding A.NIP3 model definition is provided in Figure 40. Note that this model also utilizes three areas to allow for an evaluation of areas which are combinations of fissile and non-fissile regions.

February 13, 2020

```

UNFORM=A.NIP3
01  SUMMAR TEST
02 0 3 40000000 40000000 40000000 40000000 0 3 3 3
03 44
04 3 3 3 3 3
06 REG1 0. 10. 0 2 0. 10.
06 REG2 10. 20. 0 2 0. 10.
06 REG3 20. 30. 0 2 0. 10.
09 X 3 30.
09 Y 2 10.
09 Z 2 10.
07 AREA1 REG2
07 AREA2 REG1 REG3
07 AREA3 REG1 REG2 REG3
c Define Compositions
c Composition 1
14 COMP1 ISO1 1.0
15 COMP1 REG1
c Composition 2
14 COMP2 ISO2 0.5 ISO3 0.5
15 COMP2 REG2
c Composition 3
14 COMP3 ISO3 0.05 ISO4 0.95
15 COMP3 REG3

```

**Figure 40. SUMMAR Verification Model A.NIP3 Block**

Figure 41 provides the A.SUMMAR block included in this DIF3D input. In this block, the Type 01 card is used to request the standard output edits and include the effective one-group microscopic cross section edits. The Type 04 cards allow the user to specify the isotope type of the four isotopes (coolant, coolant, fertile, and fissile, respectively). The Type 06 cards provide SUMMAR with the relationship between the isotopes and those in the built-in ENDF/B dataset. The atomic masses of the four isotopes were chosen arbitrarily (1, 16, 50, and 100).

```

UNFORM=A.SUMMAR
01 0 0 30000000 0 0 0 1
04 6 ISO1
04 6 ISO2
04 2 ISO3
04 1 ISO4
06 H1__7 SPEC 1.0 ISO1
06 O16__7 SPEC 16.0 ISO2
06 U238__7 FERT 50.0 ISO3
06 PU2397 FISS 100.0 ISO4

```

**Figure 41. SUMMAR Verification Model A.SUMMAR Block**

The specific tables which will be verified herein are the reaction integral tables for regions and areas. These are shown in Figure 42 with the region integral table on the left and the area table on the right. Each of these quantities presented will be verified. Note that in this output, the blank lines have been removed and the output for all but the first of each isotope are excluded.

February 13, 2020

REACTION INTEGRALS				REACTION INTEGRALS			
IN DIRECTION OF CALCULATION				IN DIRECTION OF CALCULATION			
REGION	1 REG1	2 REG2	3 REG3	AREA	1 AREA1	2 AREA2	3 AREA3
0H1___7 ENDF/B MAT. H1___7		SPEC(6)	ATOMIC MASS =	0H1___7 ENDF/B MAT. H1___7		SPEC(6)	ATOMIC MASS =
1.000000				1.000000			
MASS(KG)	1.66043E+00	0.00000E+00	0.00000E+00	MASS(KG)	0.00000E+00	1.66043E+00	1.66043E+00
GM-ATOM	1.66043E+03	0.00000E+00	0.00000E+00	GM-ATOM	0.00000E+00	1.66043E+03	1.66043E+03
CAPTURES	1.54531E+08	0.00000E+00	0.00000E+00	CAPTURES	0.00000E+00	1.54531E+08	1.54531E+08
N2N PROD	0.00000E+00	0.00000E+00	0.00000E+00	N2N PROD	0.00000E+00	0.00000E+00	0.00000E+00
FISSIONS	0.00000E+00	0.00000E+00	0.00000E+00	FISSIONS	0.00000E+00	0.00000E+00	0.00000E+00
NUSIGF	0.00000E+00	0.00000E+00	0.00000E+00	NUSIGF	0.00000E+00	0.00000E+00	0.00000E+00
ALPHA	0.00000E+00	0.00000E+00	0.00000E+00	ALPHA	0.00000E+00	0.00000E+00	0.00000E+00
MACRO CAP	1.09217E-04	0.00000E+00	0.00000E+00	MACRO CAP	0.00000E+00	8.03131E-05	4.76470E-05
MACRO FIS	0.00000E+00	0.00000E+00	0.00000E+00	MACRO FIS	0.00000E+00	0.00000E+00	0.00000E+00
MACRO N2N	0.00000E+00	0.00000E+00	0.00000E+00	MACRO N2N	0.00000E+00	0.00000E+00	0.00000E+00
NU BAR	NaN	0.00000E+00	0.00000E+00	NU BAR	0.00000E+00	NaN	NaN
ETA	0.00000E+00	0.00000E+00	0.00000E+00	ETA	0.00000E+00	0.00000E+00	0.00000E+00
MICRO CAP	1.09217E-04	0.00000E+00	0.00000E+00	MICRO CAP	0.00000E+00	1.60626E-04	1.42941E-04
MICRO FIS	0.00000E+00	0.00000E+00	0.00000E+00	MICRO FIS	0.00000E+00	0.00000E+00	0.00000E+00
MICRO N2N	0.00000E+00	0.00000E+00	0.00000E+00	MICRO N2N	0.00000E+00	0.00000E+00	0.00000E+00
0016___7 ENDF/B MAT. 016___7		SPEC(6)	ATOMIC MASS =	0016___7 ENDF/B MAT. 016___7		SPEC(6)	ATOMIC MASS =
16.000000				16.000000			
...				...			
0U238___7 ENDF/B MAT. U238___7		FERT(2)	ATOMIC MASS =	0U238___7 ENDF/B MAT. U238___7		FERT(2)	ATOMIC MASS =
50.000000				50.000000			
...				...			
0PU2397 ENDF/B MAT. PU2397		FISS(1)	ATOMIC MASS =	0PU2397 ENDF/B MAT. PU2397		FISS(1)	ATOMIC MASS =
100.000000				100.000000			
...				...			

Figure 42. SUMMAR Module Output

These values were verified with a Python program to compute each of these quantities using data obtained from the ZNATDN (number densities), RZFLUX (region fluxes), ISOTXS (isotopic cross sections), and the GEODST file (region volumes). As these quantities are relatively trivial, the findings from this investigation are as follows:

- In SUMMAR, the capture reaction channel is defined as the (n, $\gamma$ ), (n,  $\alpha$ ), (n,d), (n,t), and (n,p) reactions.
- The term “ALPHA” refers not to the (n, $\alpha$ ) reaction channel, but instead to the typical capture-to-fission ratio.
- A NaN (“not a number”) appears in the SUMMAR output when non-fissile isotopes are defined and the data is uninitialized. These should be understood as 0 when present.

With this script, the data tables of Figure 42 were verified and all found correct, with only one digit off due to rounding error (the macroscopic capture cross sections of ISO2/<sup>16</sup>O was reported by SUMMAR as  $5.63031 \times 10^{-3}$  1/cm in REG2, whereas the Python script reported it as  $5.63030 \times 10^{-3}$  1/cm. Since this is the last significant digit, no further investigation is warranted. These edit tables of the SUMMAR module are therefore considered verified.

### 3.1.13 Integral Verification

Before 1975, the finite difference methodology was the primary approach to solving the 2D R-Z diffusion theory problems of that era. As the computing technology improved, the ability to solve 3D diffusion equations became a reality. The first extensions of the finite difference methodology to full 3D proved problematic due to the large number of meshes required to get spatial

convergence. In the early 1980s, the transverse integrated nodal diffusion theory methods arrived that applied higher order spatial approximations in each mesh. The nodal methodologies received substantial research and development over that decade and the following 30 years received almost no research focus other than on alternative acceleration methodologies. All of the early history is well discussed and covered by Lawrence in [10]. As a consequence of the near dearth in research for 30 years, most of the published test problems and collaborative efforts to solve them exist in the literature in the late 1980s. The most widely used one during that time period is referred to as the IAEA benchmark [12].

Reference [10] provides the calculated results from eight participants while reference [11] provides the solutions from seven participants where there is some overlap in the used software and solutions between these two references. The reference solution is extrapolated from finite difference calculations as discussed in reference [12]. Figure 43 provides the geometric layout of the problem along with the axially integrated assembly power map. Each assembly is 20 cm in the x and y directions and 340 cm tall. The model places a radial reflector of thickness 20 cm around the active core and an axial reflector that is 20 cm thick above and below the active core. A rodged composition for the reflector and fuel type 2 is used to create an axial offset in the power distribution. Other than  $k_{\text{eff}}$ , the reference solution provides axially integrated assembly powers for each assembly and mesh-wise fluxes and powers. The mesh-wise data provides one value per assembly for 19 axial planes (20 cm axial sections) for the 45 degree symmetry portion of the domain.

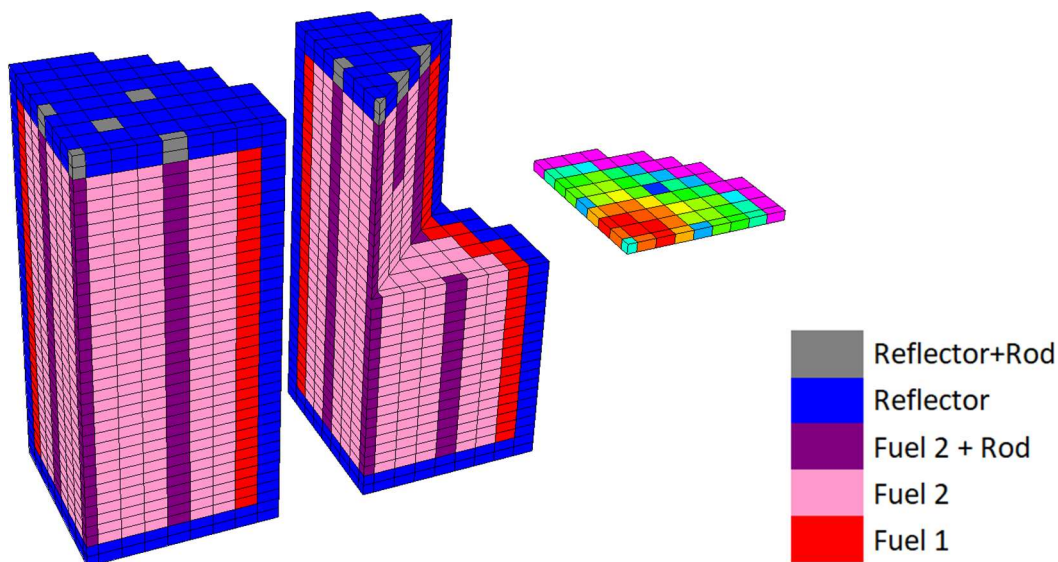


**Figure 43. IAEA Benchmark Model and Average Assembly Power Map**

Most of the reported results only focus on the  $k_{\text{eff}}$  accuracy and axially integrated assembly power detail. This is because of the effort involved in comparing the detailed flux and power distribution

to that from any given code was cumbersome at the time. Today, performing the mesh-wise flux and power comparison is onerous due to the poor quality of the text conversion of the historical report. Consequently, the axially integrated power distribution is assumed to be a sufficient measure of the spatial flux accuracy given that the DIF3D code is restricted to using equal mesh refinements in all directions. This conclusion is also supported by the use of a partially inserted control rod and thus lack of radial or axial symmetry. For finite difference codes, the 3D meshing requirements are significant and the literature reports considerable errors when using 1.6 cm radial and 3.3 cm axial meshing.

The DIF3D compiled results for the IAEA benchmark are tabulated in Table 91 while the closest external solutions taken from reference [10] and [11] are provided in Table 92. The reference solution was only documented in 3 and 4 significant digits that restricts the accuracy comparison to at most 3 significant digits hence the error measures in both tables being truncated at a tenth of a percent. Starting with the DIF3D-FD results, it should be clear that convergence of the power distribution to the reference solution is observable with spatial mesh refinement. The  $k_{\text{eff}}$  convergence is not as good because the coarsest mesh result is uncharacteristically accurate. This is attributable to cancellation of error and the  $k_{\text{eff}}$  convergence behavior is consistent with the literature reported finite difference solutions. It is interesting to note that the 2 cm mesh results of DIF3D-FD are very comparable to the ~2 cm meshing used in the VENTURE code, also a finite difference based methodology, from almost 40 years previous. The fact that the 1 cm meshed DIF3D-FD result is higher than the provided reference solution (extrapolated), is a good indication that that reference solution is not the true one as DIF3D-FD should display an asymptotic convergence to the true solution.

**Table 91. DIF3D  $k_{\text{eff}}$  and Power Distribution Errors for the IAEA Benchmark**

	DIF3D-FD				DIF3D-VARIANT		
					6 <sup>th</sup> 4 <sup>th</sup> 1 <sup>st</sup>	8 <sup>th</sup> 8 <sup>th</sup> 3 <sup>rd</sup>	8 <sup>th</sup> 8 <sup>th</sup> 3 <sup>rd</sup>
<b>Mesh Size (cm)</b>	10	5	2	1	20	20	10
<b><math>K_{\text{eff}}</math></b>	1.02906	1.02866	1.02895	1.02904	1.02906 8	1.02907 3	1.02907 4
<b><math>K_{\text{eff}}</math> Error (pcm)</b>	3	-37	-8	1	4	4	4
<b>RMS Error</b>	10.5%	6.2%	1.4%	0.2%	0.2%	0.2%	0.3%
<b>Average Error</b>	8.2%	4.8%	1.1%	0.2%	0.2%	0.2%	0.2%
<b>Peak Powered Assembly Error</b>	7.7%	4.6%	1.0%	0.1%	0.0%	-0.2%	-0.2%
<b>Maximum Assembly Error</b>	23.8%	14.1%	3.3%	0.6%	0.8%	0.5%	0.5%



**Table 92. External keff and Power Distribution Errors for the IAEA Benchmark**

	NEM	NODLEG	QUANDRY	NGFM	VENTURE	IQSBOX	TRIDENT
<b>Mesh Size (cm)</b>	20	20	20	20	1.67/3.33	-	-
<b>K<sub>eff</sub></b>	1.02911	1.02895	1.02902	1.02909	1.02896	1.02911	1.02914
<b>K<sub>eff</sub> Error (pcm)</b>	8	-8	-1	6	-7	8	11
<b>Average Error</b>	--	0.7%	0.2%	--	--	0.3%	1.5%
<b>Maximum Assembly Error</b>	0.9%	1.3%	0.7%	0.4%	2.1%	0.9%	--

Moving to the DIF3D-VARIANT solutions, mesh sizes of 10 and 20 cm were chosen the latter of which is consistent with the approach taken with other nodal methodologies of that era as seen in Table 92 (NEM, NODLEG, QUANDRY, NGFM). Take note that at the coarsest polynomial approximation attempted, the DIF3D-VARIANT error profile is very similar to the NEM and QUANDRY results indicating some level of equivalence. As the DIF3D-VARIANT polynomial approximation is refined, the average error drops to 0.2% with a peak error of 0.5%. Refinement of the mesh or polynomial order further makes negligible differences in the distribution or  $k_{eff}$  errors. This would again indicate that the DIF3D-VARIANT code has likely converged to the true reference solution.

In conclusion, the preceding DIF3D results for Cartesian geometries indicate that the DIF3D software is producing consistent results to diffusion codes developed by external parties, increasing confidence in the DIF3D verification. As stated, in all likelihood, the highest order DIF3D-VARIANT solutions presented are actually the true reference solution given the near negligible differences that occur with spatial mesh refinement. In that regard, all of the other code packages likely need additional spatial mesh refinement or increases in polynomial expansion to match the DIF3D-VARIANT result or even the provided reference solutions.

### **3.2 Triangular-Z Diffusion Verification**

#### **3.2.1 Model Building Verification**

As is discussed in Section 3.2.1 of [6], a Model Building case will be used to verify the ability of NIP3 and HMG4C to create the user-specified Triangular-Z diffusion model by creating a simple two-group, multi-isotope, multi-composition, multi-region triangular-Z model. This case will specifically be used to verify the following card types and options consistent with Tables 7 through 9 of [6]: card Types 1, 2 (options 3, 9, 10, and 11), 7, 9, 13, 14, 15, 29, 30, 31, and 44 of the NIP3 module; card Types 1, 2 (options 3, 4, 5, 7, 8, and 9) of the HMG4C module; and card Types 1, 4 (Options 2, 3, 4, and 5) of the DIF3D module.

The verification of these options will be similar to, and if applicable, rely on, the equivalent verification performed for the 3D Cartesian diffusion in Section 3.1.1. This case will be designed to use the same microscopic cross sections and material/compositions data. Therefore, this work



will verify the macroscopic cross section data computed by the DIF3D software is the same as that produced in the 3D Cartesian diffusion model building case. Since the geometry will be Triangular-Z rather than 3D Cartesian, the geometry edits will naturally be different. This verification effort will therefore rely heavily on the 3D Cartesian diffusion verification, and will not repeat perturbation cases that relate to the composition cross sections since that functionality is not affected by the geometric solution scheme.

### 3.2.1.1 *Model Definition*

#### 3.2.1.1.1 *Geometry*

DIF3D allows the user to input a triangular-Z reactor with the A.NIP3 Type 29 card to specify the overall hexagonal dimensions, A.NIP3 Type 30 card to establish the laydown of regions within each hexagonal ring, the A.NIP3 Type 31 card to specify the background region (i.e., the material that exists within the triangular-Z grid outside of the hexagonal lattice, and the A.NIP3 Type 09 card to specify the Z-dimensions. The model used for this verification should sufficiently test the options available via these cards, either by directly including the use of these cards options in the base input model (the “base case”) or by later performing perturbations to the base case to fully test remaining options.

Before defining attributes of the base case that result from the A.NIP3 Type 29-31 and 9 cards, the following starting point will be established:

1. The base case model will utilize a full core Triangular-Z geometry
  - a. Perturbation cases will verify that other triangular-Z geometries are consistent with this full core;
2. The axial and outward radial boundary conditions will be set as reflecting;
3. The same compositions used in the 3D Cartesian diffusion model will be applied here
  - a. To this point the HMG4C module’s ability to handle the multiple ISOTXS formats has been adequately verified and thus only the Microscopic XS ISOTXS format will be utilized (i.e., the same as shown in Figure 4);
4. This model will utilize four regions, one per composition.
5. This model will use only one area since the 3D Cartesian model thoroughly examined the concept of areas already.
6. The base model will utilize a “null” background, perturbations will add a user-specified composition to the background regions;
7. The rodged case will be treated separately.

The following A.NIP3 cards to be specifically tested here impose the following additional constraints:

1. The Type 29 card provides the following option or input format flexibility:
  - a. This card allows the user to specify the number of equal parts into which the hexagons will be subdivided and provides a default value of 6 triangles per hexagon
    - i. The base model will utilize the default number of triangles per hexagonal region, where perturbations will vary this value;
2. The Type 30 card provides the following option or input format flexibility:
  - a. Regions can be assigned to an entire ring
  - b. Regions can be assigned to individual locations within a ring
  - c. Regions can be assigned to ranges of locations within a ring
  - d. Any of the above can be overlaid wherein the latest Type 30 card data supersedes earlier data
  - e. Options are provided for lower and upper Z boundaries of a region
  - f. All of the above can be incorporated the following three rings:
    - i. Ring 1, which has one position, will be defined to be filled by a region and then overlaid with another composition, making that overlay the final region
    - ii. Ring 1 will be defined to have two axial extents, a lower portion and an upper portion, each with unique compositions
    - iii. Ring 2, which has 2 unique positions in sixth-core symmetry, will be defined with a region assigned to the entire ring, but using a range definition
    - iv. Ring 3, which has three unique positions in sixth-core symmetry, will be defined with a region assigned to the entire ring and then overlaid so that the regions between the regions along lines of sixth-core symmetry are of a single different composition than the region applied along the symmetric axes;
3. The Type 31 card provides the following option or input format flexibility:
  - a. The background region can either be defined or not (by not providing the Type 31 card or by assigning a blank for the background region name value)
    - i. The base model will utilize the default value of providing no Type 31 card; perturbations will vary this value;
4. The Type 09 card provides the following option or input format flexibility:
  - a. This card must be defined for the Z-dimension for triangular-z geometries and this should be provided to support the Type 30 card axial extent definitions.

The geometric constraints yield a core laydown for the two planes as shown in Figure 44. Each color corresponds to a unique composition. Specifically, red, blue, green, and yellow correspond to COMP1, COMP2, COMP3, and COMP4, respectively, where the compositions are the same as utilized in Section 3.1.1. Since COMP1 through COMP4 are also assigned to regions REG1 through REG4, respectively, the red, blue, green, and yellow also correspond to REG1 through REG4. Further, to maintain an area-to-region assignment in this model, REG1 and REG4 are both assigned to the area labelled AREA1. The A.NIP3 module input that corresponds to this geometry is provided in Figure 45.

February 13, 2020

---

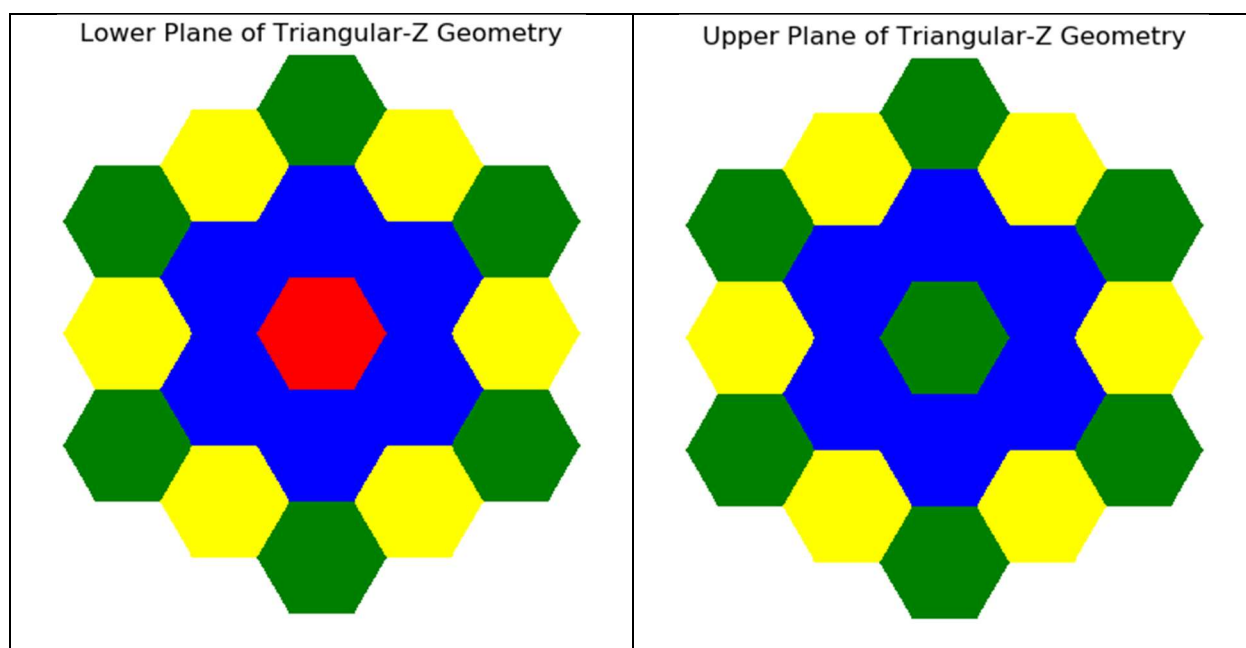


Figure 44. Triangular-Z Reference Geometry axially between 0 - 10cm (left) and 10 - 30 cm (right)

February 13, 2020

```

5  UNIFORM=A.NIP3
6  01      TRIZ - MCC Micro XS ISOTXS
7  02 0 3 40000000 40000000 40000000 40000000 0 3 3 3
8  03 100
9  04      2      2      2      2      2      2
10 c Define hexagon dimensions
11 29 10.0 3
12 c Add Z-dimension mesh structure
13 09 Z 2 10. 3 30.
14 c Define ring 1 which will have lower and upper regions
15 c Start with an overlay test region
16 c (this should be replaced by next two Type 30 Cards)
17 30 REG4 1
18 30 REG1 1 1 1 0. 10.
19 30 REG3 1 1 1 10. 30.
20 c Define ring 2 with the same region in each position
21 c Will be defined using the range definition
22 30 REG2 2 1 6 0. 30.
23 c Define ring 3, with alternating regions in each position
24 c define the ring by using a blanket ring fill and then
25 c overlaying every other position with the alternating
26 c region
27 30 REG3 3 0 0 0. 30.
28 30 REG4 3 2 2 0. 30.
29 30 REG4 3 4 4 0. 30.
30 30 REG4 3 6 6 0. 30.
31 30 REG4 3 8 8 0. 30.
32 30 REG4 3 10 10 0. 30.
33 30 REG4 3 12 12 0. 30.
34 c Define an area to test that capability
35 07 AREA1 REG1
36 07 AREA1 REG4
37 c Define Compositions
38 c Composition 1
39 14 COMP1 IS01 1.0
40 15 COMP1 REG1
41 c Composition 2
42 13 MIS03 IS03 2.0
43 14 COMP2 MIS03 0.25 IS01 0.1
44 14 COMP2 MIS03 0.2
45 15 COMP2 REG2
46 c Composition 3
47 13 MAT31 IS04 0.4 IS01 0.6
48 14 COMP32 IS03 0.6 IS02 0.4
49 14 COMP3 MAT31 0.4 COMP32 0.4
50 14 COMP3 COMP32 0.2
51 15 COMP3 REG3
52 c Composition 4
53 14 COMP41 IS04 2.0
54 14 COMP42 IS01 2.0
55 14 COMP4 COMP41 0.5 COMP42 0.5
56 15 COMP4 REG4

```

**Figure 45 A.NIP3 Triangular-Z Model Geometry Definition**

Line 11 of Figure 45 shows that an assembly pitch of 10cm is applied. Line 13 of Figure 45, two fine mesh elements are used for the first axial plane (between 0 and 10 cm) and three are applied for the second plane. This geometry definition yields the total volumes for each of the four regions and AREA1 that are listed in Table 93.

**Table 93. Triangular-Z Geometry Hand-Calculated Volumes**

Region Name	Tot. Volume [cc]
REG1	8.660E+02
REG2	1.559E+04
REG3	1.732E+04
REG4	1.559E+04
AREA1	1.645E+04

The discussion above highlighted various perturbations that should be performed for verifying the geometry creation. These perturbations, as well as those related to the geometry-processing related edit controls, must be performed as indicated in Table 94. No cross section processing edits will be exercised for this case due to the degree to which these options have been exercised thus far and the fact that the geometry type and cross section processing edits are independent.

**Table 94. Diffusion Theory Triangular-Z Perturbation Cases**

<b>A.NIP3</b>				
<b>Card Type &amp; Option</b>	<b>Description</b>	<b>Option in Base Case</b>	<b>Perturbations to Base</b>	<b>Evaluated in Sections</b>
2.3	Geometry processing edits	3	0, 1, 2	3.2.1.2.3.1
2.10	Region/mesh interval plotter edits	3	0, 1, 2	3.2.1.2.3.2
2.11	Zone/mesh interval plotter edits	3	0, 1, 2	3.2.1.2.3.3
3.2	Geometry Type	100	90, 94	3.2.1.2.2.1
29.4	Triangle Subdivisions	Default (1)	2	3.2.1.2.2.2
30.2	Background Region	Default (0)	REG1	3.2.1.2.2.3
<b>A.DIF3D</b>				
<b>Card Type &amp; Option</b>	<b>Description</b>	<b>Option in Base Case</b>	<b>Perturbations to Base</b>	<b>Evaluated in Sections</b>
4.2	Problem description edit	3	0, 1, 2	3.2.1.2.3.4
4.3	Geometry (region to mesh interval) map edit	3	0, 1, 2	3.2.1.2.3.5
4.4	Geometry (zone to mesh interval) map edit	3	0, 1, 2	3.2.1.2.3.6

### 3.2.1.2 *Verification*

The previous section defined the base case of the model to examine. This section will compare the DIF3D processing of this base case and show that DIF3D correctly handles the inputs provided to it. As stated above, this verification will utilize the base case discussed above with the Microscopic XS ISOTXS format of Figure 4. After verification of this base case, the perturbations to this base case provided in Table 94 will be performed and verified to be implemented correctly in DIF3D.

#### 3.2.1.2.1 *Base Case*

The DIF3D input for the base case is the same as defined in Figure 45, Figure 4, and Figure 9. The output to screen (i.e., standard output) was redirected to a text file; this and all other output files from this run are stored in an isolated directory.

The remainder of this section will progress by first traversing the standard output and the edited information compared to the independently computed values. Next, the auxiliary output file (fort.10) will be evaluated to ensure that all of the expected output edits are present and correct. The evaluation will then progress to the binary output files relating to the model definition (i.e., GEODST, NDXSRF, ZNATDN, COMPSX, and LABELS) are correct. Intermediate files (e.g., ADIF3D, ISOTXS, and ARC) and those related to the solution of the given model (e.g., RTFLUX) will not be evaluated as they are either not directly used by designers or will be verified in later sections of this work.

##### 3.2.1.2.1.1 *Standard Output Edit Verification*

This section will progress through the DIF3D standard output file and evaluate the correctness of the outputted data, based upon the model description provided previously. These outputs are 2,000 lines long and therefore, the information replicated within the main body of this document will be minimized. Due to the use of the same cross sections and compositions as previous problems, all ISOTXS and composition-related edits will be compared directly to the standard output from the diffusion theory 3D Cartesian model building base case. Geometry-related information, however, will be directly compared to the expected configurations presented in Figure 44, Table 93 or others as needed.

Aside from an echo of the input file and the separation of inputs into the individual module's components, the first edit encountered that requires verification is the general GNIP3C module parameter echo and outputs related to defining the problem geometry. This is shown from the

February 13, 2020

output in Figure 46. This output table provides an echo of the input information, including the geometry type, the number of regions, compositions, coarse and fine mesh intervals.

305			*** MODEL DESCRIPTION ***
306			
307	17	IGOM	GEOMETRY TYPE, TRIANGULAR-Z
308	4	NZONE	NO. OF ZONES (COMPOSITIONS)
309	4	NREG	NO. OF REGIONS
310	1	NZCL	NO. OF ZONE CLASSIFICATIONS
311	17	NCINTI	NO. OF 1ST DIMENSION COARSE MESH INTERVALS
312	10	NCINTJ	NO. OF 2ND DIMENSION COARSE MESH INTERVALS
313	2	NCINTK	NO. OF 3RD DIMENSION COARSE MESH INTERVALS
314	17	NINTI	NO. OF 1ST DIMENSION FINE MESH INTERVALS
315	10	NINTJ	NO. OF 2ND DIMENSION FINE MESH INTERVALS
316	5	NINTK	NO. OF 3RD DIMENSION FINE MESH INTERVALS
317	0	IMB1	FIRST BOUNDARY CONDITION, FIRST DIMENSION, ZERO FLUX
318	0	IMB2	LAST BOUNDARY CONDITION, FIRST DIMENSION, ZERO FLUX
319	0	JMB1	FIRST BOUNDARY CONDITION, SECOND DIMENSION, ZERO FLUX
320	0	JMB2	LAST BOUNDARY CONDITION, SECOND DIMENSION, ZERO FLUX
321	0	KMB1	FIRST BOUNDARY CONDITION, THIRD DIMENSION, ZERO FLUX
322	0	KMB2	LAST BOUNDARY CONDITION, THIRD DIMENSION, ZERO FLUX
323	1	NBS	NO. OF BUCKLING SPECIFICATIONS
324	1	NBCS	NO. OF CONSTANTS FOR EXTERNAL BOUNDARIES
325	1	NIBCS	NO. OF CONSTANTS FOR INTERNAL BOUNDARIES
326	0	NZWBB	NO. OF BLACKNESS THEORY ZONES
327	0	NRASS	0/1, REGION ASSIGNMENTS TO COARSE/FINE MESH
328	2	NTRIAG	OUTER BOUNDARY SHAPE, RECTANGLE
329	1	NTHPT	ORIENTATION OF (1,1) MESH TRIANGLE - POINTS AWAY FROM 1ST DIMENSION AXIS
330	1.0000E+01	FLAT	HEXAGON FLAT-TO-FLAT DISTANCE
331	5.7735E+00	SIDE	LENGTH OF MESH-TRIANGLE SIDE

**Figure 46. GNIP4C Model Description Edit**

To compare the number of mesh intervals, the rectangular boundary domain for the triangular-Z geometry was visualized by appending grid lines consistent with those provided in the DIF3D user's manual (Figure 2.6 of [1]). Figure 47 provides this structure sketched on the core layout previously shown in Figure 44. Counting across the lower-left row of triangles it is clear that there are seventeen partial triangles in the model. This is consistent with the NCINTI parameter on line 311 of the Figure 46 output. Similarly, counting up from the lower left reveals ten triangles, again consistent with the NCINTJ parameter. The NCINTK parameter is simply the number of coarse mesh intervals in the Z direction, which is two per the Type 09 card for the A.NIP3 block in Figure 45. The fine-mesh intervals are provided in NINTI, NINTJ, and the NINTK parameters. NINTI and NINTJ are the same as NCINTI and NCINTJ, respectively, since the number of triangle subdivisions provided in the A.NIP3 Type 29 card was left as the default. The fine-mesh intervals in the z direction, NINTK, are 5, again consistent with the number of fine-mesh intervals provided

February 13, 2020

in total on the Type 09 card. The remaining parameters are self-explanatory and verified consistent with the user input.

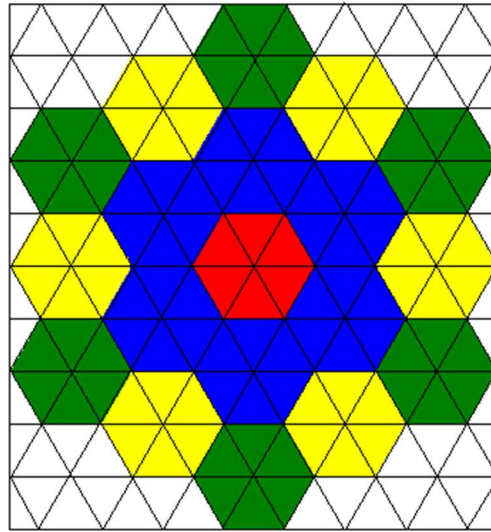


**Figure 47. Rectangular Boundary Domain Triangular-Z Grid Sketch**

The next output table on line 334 is the Z-direction fine mesh interval boundaries; the values reported by DIF3D are 0, 5, 10, 16.67, 23.3 and 30 cm. These values match expectations as there are two equal divisions for the first 10 cm, and three equal subdivisions of the upper 20 cm for the Type 09 card.

Next, the region volumes and composition assignments are provided as shown in Figure 48 from line 340 of the standard output. These values are verified to be correct as they match the volume values calculated and provided in Table 93 as well as the region assignments defined in the model input in Figure 45.

REGION/ZONE SPECIFICATIONS							
REGION NO.	REGION NAME	REGION VOLUME	ZONE NO.	ZONE NAME	ZONE CLASS.	BUCKLING BY GROUP (...)	
1	REG4	1.559E+04	4	COMP4	0	0.000E+00	
2	REG1	8.660E+02	1	COMP1	0	0.000E+00	
3	REG3	1.732E+04	3	COMP3	0	0.000E+00	
4	REG2	1.559E+04	2	COMP2	0	0.000E+00	

**Figure 48. Region and Zone Specifications Output**

Line 351 provides the internal boundary condition constants where a single value of 0 is reported; no internal boundaries were specified, thus this is as expected.

Line 357 is the table describing the regions comprising each area. Per the model input in Figure 45, one area was used and it was composed of REG1 and REG4. This matches the output.



February 13, 2020

Line 365 begins the region/composition map for the hexagonal geometry. There are two of these maps, one for the lower plane (between 0 and 10 cm axially) and another for the upper plane (between 10 and 30 cm). These maps are shown in Figure 49 below with the lower plane on the left and the upper plane on the right.

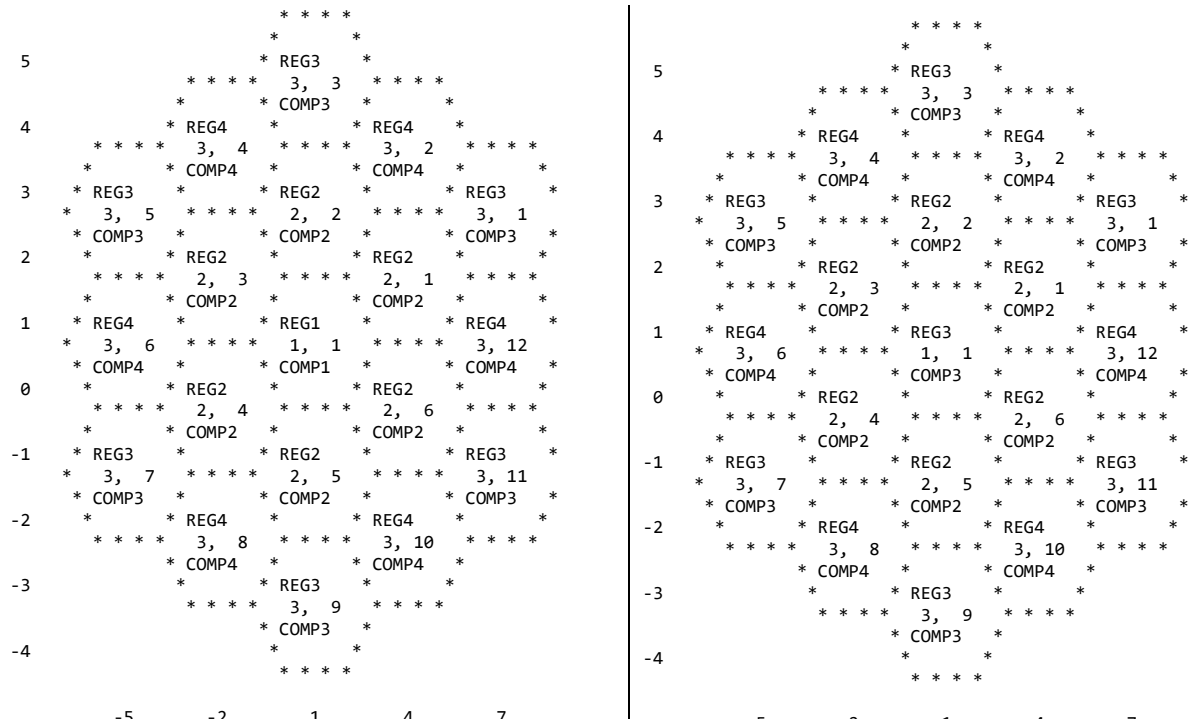


**Figure 49. DIF3D Region/Composition Map for Triangular-Z Geometry Model; the lower plane is on the left, and the upper plane is on the right**

Lines 443 to 535 contain the GNIP4C module edit of the ISOTXS and ZNATDN file information. Immediately after this begins the HMG4C module edits of the ISOTXS and COMPXS information printed on Lines 536 through 1135 where the DIF3D module edits begin. The ISOTXS, ZNATDN, and COMPXS edits should be the same as produced in the equivalent blocks for the 3D Cartesian diffusion base case described in Section 3.1.1 as they are only dependent upon the isotopic and composition makeup of the model that was, by design, the same in the 3D Cartesian and Triangular-Z problems. Therefore these cases will be evaluated by utilizing the same Python diffliB package as was used extensively in Section 3.1.1 to evaluate the perturbations to that 3D Cartesian base case. This difference comparison should find no unexpected differences within the ISOTXS and COMPXS edit blocks. This was confirmed true as the only differences were limited to the problem title repeated at the start of each page within these edit blocks. Therefore the ISOTXS, ZNATDN and COMPXS edit blocks in the standard output are verified.

The DIF3D edits begin on line 1136 with file identifiers, storage allocation and scratch file information that is not verified as part of this work. Line 1184 begins an edit of the user input specifications for the problem; all are confirmed to match expectations based upon the A.DIF3D module input specified by Figure 9.

Line 1237 begins the problem description table including the number of mesh intervals in each dimension, number of zones, regions, energy groups, z-direction mesh interval boundaries and midpoints, boundary conditions, internal black boundary condition constants, and the region and zone assignments. These are mostly repeated from earlier tables and are confirmed to match expectations. The z-direction mesh interval midpoints were not printed but were verified earlier; however, by inspection it is clear that the mesh midpoints match expectations.

The reactor region by mesh point map is provided for the two planes on line 1292 and 1319, respectively. The lower plane edit produced by DIF3D is provided on the top of Figure 50 and the sketch of the triangular mesh shown earlier as Figure 47 is reproduced on the bottom for easy comparison. The DIF3D output provides numbers corresponding to the order of appearance in the model as is shown in Figure 51. The grid sketch uses the same coloring scheme as before where regions REG1, REG2, REG3, and REG4 are colored as red, blue, green, and yellow, respectively. This same color scheme has been applied by the authors to the numbers in the top portion of Figure 50 to provide for an easier comparison. This comparison clearly shows that there are six mesh points per hexagon as expected, the regions in this plane are laid down correctly, and the background triangle mesh points are assigned a value of 0, as expected.

A similar figure is repeated for the top plane; for brevity, this will not be repeated here. However, it was manually verified that the only differences are the replacement of the central hexagon with reactor region 3, which is REG3 per Figure 51. This is again as expected based upon the model definition input.

Line 1343 begins the two maps of reactor zones by mesh point; with one map for each of the two planes. These are the same type of figure as provided in the top portion of Figure 50 except here the integer identifier corresponds to the composition number with 1 referring to COMP1, 2 is COMP2, etc. Again for brevity, these are not repeated here, but they were manually verified to match the expectations, including the identifier of 0 for the background region.

Lines 1398 through 1474 are a repeat of the COMPXS edits, except this time by the DIF3D module. Like the previous COMPXS edits by the HMG4C module, these were compared to the 3D Cartesian diffusion theory equivalent output edit using the Python diffliB package. No differences occurred.

The remainder of the standard output is related to the solution itself; this output will be verified by other verification problems and thus will not be examined in this case.

No adverse findings are noted with regard to this section's verification of the standard output file.

February 13, 2020

1289	0	REACTOR REGION BY MESH POINT															Z	-DIM	MAP FOR PLANES		1	-	2							
1290	0	Y-DIM																												
1291		X-DIM TRIANGULAR																												
1292	0		1	2	3	4	5	6	7	8	9	10	11	12	13	14	15	16	17											
1293		*****																												
1294	10	*	0	0	0	0	0	0	0	*	3	3	4	*	0	0	0	0	0	0	0	*	10							
1295		*	*****																											
1296	9	*	0	0	0	0	0	*	1	1	1	*	3	3	4	*	1	1	1	*	0	0	0	0	*	9				
1297		*	*****																											
1298	8	*	0	*	3	3	3	*	1	1	1	*	4	4	4	*	1	1	1	*	3	3	3	*	0	*	8			
1299		*	*****																											
1300	7	*	0	*	3	3	3	*	4	4	4	4	4	4	4	4	4	4	4	*	3	3	3	*	0	*	7			
1301		*	*****																											
1302	6	*	0	*	1	1	1	*	4	4	4	4	*	2	2	2	*	4	4	4	4	*	1	1	1	*	0	*	6	
1303		*	*****																											
1304	5	*	0	*	1	1	1	*	4	4	4	4	*	2	2	2	*	4	4	4	4	*	1	1	1	*	0	*	5	
1305		*	*****																											
1306	4	*	0	*	3	3	3	*	4	4	4	4	4	4	4	4	4	4	4	*	3	3	3	*	0	*	4			
1307		*	*****																											
1308	3	*	0	*	3	3	3	*	1	1	1	1	*	4	4	4	4	*	1	1	1	1	*	3	3	3	*	0	*	3
1309		*	*****																											
1310	2	*	0	0	0	0	0	*	1	1	1	1	*	3	3	3	4	*	1	1	1	1	*	0	0	0	0	*	2	
1311		*	*****																											
1312	1	*	0	0	0	0	0	0	0	0	0	*	3	3	3	4	*	0	0	0	0	0	0	0	0	0	*	1		
1313		*****																												
1314			1	2	3	4	5	6	7	8	9	10	11	12	13	14	15	16	17											

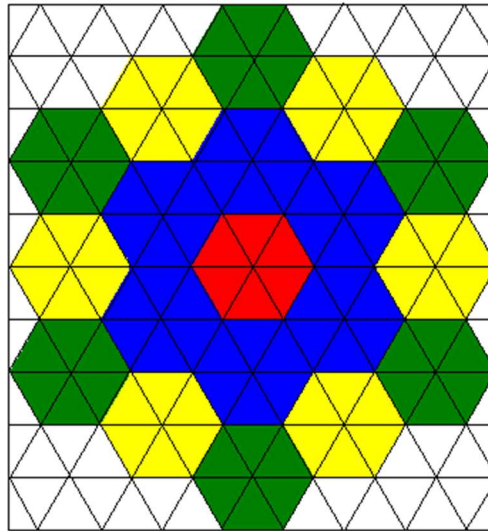


Figure 50. DIF3D Reactor Region by Mesh Point Comparison to Triangular-Z Geometry Reference

1283		REGION NUMBER AND ASSIGNMENT TO ZONE											
1284	0	REGION	ZONE	ZONE	REGION	ZONE	ZONE	REGION	ZONE	ZONE	REGION	ZONE	ZONE
1285		NO.	NAME	NO.	NAME	NO.	NAME	NO.	NAME	NO.	NAME	NO.	NAME
1286		1	REG4	4	COMP4	2	REG1	1	COMP1	3	REG3	3	COMP3
1287												4	REG2
												2	COMP2

Figure 51. Region Number to Name Assignments

### 3.2.1.2.1.2 Auxiliary Output Edit Verification

This base case requested every output table be printed to both the standard and auxiliary outputs. This section will examine the auxiliary output (i.e., the “fort.10” file) to ensure the content there

is correct and consistent with the expectations. This evaluation will utilize the previous standard output verification heavily, and primarily focus on comparing to the already-verified standard outputs as opposed to comparing back to reference hand-calculations.

This comparison (again with the `diff` Python package) revealed that the only differences between the standard and auxiliary outputs are:

1. The page breaks are inconsistent between the two outputs and so page numbers may be different.
2. The standard output includes additional information that was not verified by the standard output work (output file number assignments, memory storage sizes, and runtime warnings about over-relaxation factors reaching the iteration threshold).
3. The auxiliary output is apparently using non-ASCII characters to print composition names whereas the standard output was using ASCII (note it may be possible that the GNU/Linux shell used, `bash`, was converting these behind the scenes). Specifically, the standard output says: “EDIT OF (NONFISSIONABLE COMPOSITION COMP1” while the auxiliary output says “EDIT OF (NONFISSIONABLE COMPOSITION ”. This is only seen in the composition edits. Note that both are missing closing parentheses.

These differences are not important to this verification work, and since the content of the files match, the auxiliary output file is considered verified.

#### *3.2.1.2.1.3 Binary Output Verification*

The final set of outputs to verify are the CCCC-formatted [8] and ANL-specific binary output files relating to the model definition (i.e., GEODST, NDXSRF, ZNATDN, COMPXS, and LABELS). As stated earlier, intermediate files such (e.g., ADIF3D, ISOTXS, and ARC) and those related to the solution of the given model (e.g., RTFLUX) will not be evaluated as they are either not directly used by designers or will be verified in later sections of this work. The binary files that will be evaluated will be first converted to an ASCII format with the `"/software/ARC/CCCC_convert_v11.0_r3012_d2019_03_14.x"` executable that is distributed with the ARC suite.

Of these five binary files, only the NDXSRF, GEODST, and LABELS files should depend on the geometric definition of the model. Therefore the ZNATDN, and COMPXS files were compared by converting to ASCII and then confirming that there are no differences between these files and those produced during the execution of the 3D Cartesian diffusion base case verification. The comparison was performed for ZNATDN and COMPXS using the Python `diff` package and it was confirmed that there are no differences.

The only geometry-specific data within the NDXSRF file is the volumes of zones and subzones. It was confirmed that these volumes are the only information that is different between this case and the 3D Cartesian diffusion base case; the volume fractions of zones within a primary zone, and subzone to primary zone compositions are consistent, as expected. The volumes reported in

the NDXSRF file for this case are reported as shown in Table 95. The NDXSRF values are in the central column and the rightmost column are the hand-calculated reference volumes previously shown in Table 93, but with precision matching that in the NDXSRF file, for the zones and subzones. Differences are highlighted in red. The subzone volumes within the NDXSRF file are computed based upon the ratio of that subzone within the zone. Based on lines 15 and 16 of Figure 3, the ratio of the subzone volume to the zone volume should be  $(0.4 + 0.2)$ , or 0.6. Thus, given the volume of COMP3 is  $1.732050\text{E}+04$ , the COMP32 subzone will have 60% of that volume, or  $1.0392\text{E}+04 \text{ cm}^3$ . Similarly, COMP41 and COMP42 are both half of COMP4 and thus they should half the volume of COMP4, or  $7.794\text{E}+03 \text{ cm}^3$ . The reference and NDXSRF volumes match to six significant digits, indicating that a likely insignificant round-off error is occurring somewhere along the way during the DIF3D computation.

**Table 95. Triangular-Z NDXSRF Volumes**

Zone Type and ID	NDXSRF Volume [ $\text{cm}^3$ ]	Reference Volume [ $\text{cm}^3$ ]
Zone 1 [COMP1]	8.660255E+02	8.660254E+02
Zone 2 [COMP2]	1.558845E+04	1.558846E+04
Zone 3 [COMP3]	1.732050E+04	1.732051E+04
Zone 4 [COMP4]	1.558845E+04	1.558846E+04
Subzone 1 [COMP32]	1.039230E+04	1.039230E+04
Subzone 2 [COMP41]	7.794225E+03	7.794229E+03
Subzone 3 [COMP42]	7.794225E+03	8.227241E+03

The LABELS file also contains some geometric information such as the composition identifiers and names, region identifiers and names, and area identifiers, names, and region assignments. These were all evaluated explicitly and found to match expectations.

Finally, the GEODST file contains the mesh structure of the solution scheme (i.e., the information necessary to reproduce the triangles of Figure 47). Since this Triangular-Z GEODST file is completely different than the version produced by the 3D Cartesian case, it will be verified explicitly instead of relying on a comparison to the underlying data after comparison to ASCII directly with the CCCC\_convert\_v11.0\_r3012\_d2019\_03\_14.x program.

The output from CCCC\_convert\_v11.0\_r3012\_d2019\_03\_14.x for the GEODST file is provided in Figure 52, after the removal of some invalid characters in the HOLLERITH USER IDENTIFICATION parameter of the file identification record which did not allow the file to be displayed in all text editors. This file, and the GEODST format specification [CCCC reference] were used to populate Table 96, which contains both the expected values and actual values from within the GEODST file.

The expected values provided in Table 96 were obtained from the model definition information provided in Figure 44, Figure 45, Figure 51, and Table 93. In addition to Table 96, Figure 53 is provided to more clearly illustrate the GEODST file's interpretation of the region to coarse-mesh interval assignments. The contents of Figure 53 are simply the two 6D records seen on lines 17 through 46 of Figure 52, one for each plane of the model, reformatted to be a 17 x 10 array and

colored to match the region/composition coloring utilized in Figure 44. Comparing Figure 52 to Figure 44 reveals no disagreement and verifies that the GEODST file is capturing the correct region to coarse-mesh interval assignments.

The values in Table 96 highlighted in red indicate that there is a difference between the expected values and DIF3D values in a few cases. These, and their dispositions, are discussed separately below:

1. NZCL (number of zone classifications): this quantity is not well defined in the DIF3D manuals, GEODST format, or the CCCC format specification document. For that reason a reference value was not readily determined and since the variable is not used in the ARC system, the reported values can be ignored.
2. NBS (number of buckling specifications), NBCS (number of constants for external boundaries), and NIBCS (number of constants for internal boundaries): These parameters are either related to the application of internal or external boundary conditions. Since no buckling, only reflective boundaries, and no internal boundaries were modeled in the problem, the expected value for each of these is 0. However, the GEODST file contains values of 1 here, indicating there is a single value for each that applies everywhere. Since a value of 0 was only allowed in the CCCC format in version 4 [8], and there is no functional difference between no value and a single value everywhere if that value is a zero or ignored; the maintainers of the ARC suite chose to continue applying a single value everywhere instead of using the new 0 value feature of the standard. No further work is necessary.
3. BSQ(N) (buckling values): The expected outcome is that this data is not present because it is expected that NBS would be 0. However, the GEODST file does contain a value of 1 for NBS and thus a value for BSQ(N) of 0.0. This is equivalent to no buckling, and therefore not an error.
4. BNDC(N) (boundary constants): This value is the boundary constant derived from  $D\phi' + A\phi = 0$  per the A.NIP3 input format specification (and equivalently  $D\phi' + C\phi = 0$  in the GEODST format guide). The expectation is that since a reflective boundary condition is used,  $A$  (or  $C$ ) are either not supplied or are zero. However, the value in the GEODST file is 0.4692. This is listed as the default value in the A.NIP3 manual, if extrapolated boundary conditions are specified but no A.NIP3 Type 05 card (external boundary condition constants) is provided. Therefore, it is obvious that DIF3D populates this value as the default even though it is never needed. Later problems verifying the treatment of boundary conditions will verify if this value truly is ignored by the solver with boundary conditions where it is not relevant.
5. BNCI(N) (internal black boundary constants): The expected output is that this data is not present because it is expected that NIBCS would be 0. However, the GEODST file does contain a value of 1 for NIBCS and thus a value for BNCI(N) of 0.0. This is equivalent to no internal black boundary constant, and therefore is not in error.

February 13, 2020

6. NZC(N) (zone classification assignments): Similar to NZCL, it is unclear what a zone classification is and thus expected values are difficult to identify. Since the values are not used by the ARC software, the GEODST file's four values of 0 (one 0 for each of the four zones) is not an error.

Based on the above, the GEODST file contents are considered verified for this problem; later cases with reference flux and eigenvalue solutions will examine the impact of the boundary condition constant value of 0.4692 that is in the GEODST file.

```

1 0V GEODST*      1
2 1D      17      4      4      1      17      10      2      17      10      5      0
3      0      0      0      0      0      1      1      1      0      2      0      1
4      100      0      0      0
5 4D 0.00000E+00 2.88675E+00 0.00000E+00 0.00000E+00 0.00000E+00
6 0.00000E+00 0.00000E+00 0.00000E+00 0.00000E+00 0.00000E+00 0.00000E+00
7 0.00000E+00 0.00000E+00 0.00000E+00 0.00000E+00 0.00000E+00 0.00000E+00
8 0.00000E+00 0.00000E+00 0.00000E+00 0.00000E+00 0.00000E+00 0.00000E+00
9 0.00000E+00 0.00000E+00 0.00000E+00 0.00000E+00 0.00000E+00 0.00000E+00
10 0.00000E+00 1.00000E+01 3.00000E+01
11      1      1      1      1      1      1      1      1      1      1      1      1
12      1      1      1      1      1      1      1      1      1      1      1      1
13      1      1      1      2      3
14 5D 1.55885E+04 8.66025E+02 1.73205E+04 1.55885E+04 0.00000E+00
15 4.69200E-01 0.00000E+00
16      0      0      0      0      4      1      3      2
17 6D      0      0      0      0      0      0      0      0      3      3      3      0
18      0      0      0      0      0      0      0      0      0      0      1      1
19      1      3      3      3      1      1      1      1      0      0      0      0
20      3      3      3      1      1      1      4      4      4      1      1      1
21      3      3      3      0      0      3      3      3      4      4      4      4
22      4      4      4      4      4      3      3      3      0      0      1      1
23      1      4      4      4      2      2      2      4      4      4      1      1
24      1      0      0      1      1      1      4      4      4      2      2      2
25      4      4      4      1      1      1      0      0      3      3      3      4
26      4      4      4      4      4      4      4      4      3      3      3      0
27      0      3      3      3      1      1      1      4      4      4      1      1
28      1      3      3      3      0      0      0      0      0      1      1      1
29      3      3      3      1      1      1      0      0      0      0      0      0
30      0      0      0      0      0      3      3      3      0      0      0      0
31      0      0      0      0
32 6D      0      0      0      0      0      0      0      0      3      3      3      0
33      0      0      0      0      0      0      0      0      0      0      1      1
34      1      3      3      3      1      1      1      0      0      0      0      0
35      3      3      3      1      1      1      4      4      4      1      1      1
36      3      3      3      0      0      3      3      3      4      4      4      4
37      4      4      4      4      4      3      3      3      0      0      1      1
38      1      4      4      4      3      3      3      4      4      4      1      1
39      1      0      0      1      1      1      4      4      4      3      3      3
40      4      4      4      1      1      1      0      0      3      3      3      4
41      4      4      4      4      4      4      4      4      3      3      3      0
42      0      3      3      3      1      1      1      4      4      4      1      1
43      1      3      3      3      0      0      0      0      0      1      1      1
44      3      3      3      1      1      1      0      0      0      0      0      0
45      0      0      0      0      0      3      3      3      0      0      0      0
46      0      0      0

```

Figure 52. Triangular-Z Base Case GEODST File

February 13, 2020

```
1 6D Record: Region Numbers to
Coarse-Mesh Intervals for Plane 1
2 0 0 0 0 0 0 0 3 3 0 0 0 0 0 0 0
3 0 0 0 0 1 1 1 3 3 1 1 1 0 0 0 0
4 0 3 3 1 1 1 4 4 4 1 1 1 3 3 3 0
5 0 3 3 4 4 4 4 4 4 4 4 4 3 3 3 0
6 0 1 1 1 4 4 4 2 2 2 4 4 4 1 1 1 0
7 0 1 1 1 4 4 4 2 2 2 4 4 4 1 1 1 0
8 0 3 3 3 4 4 4 4 4 4 4 4 4 3 3 3 0
9 0 3 3 3 1 1 1 4 4 4 1 1 1 3 3 3 0
10 0 0 0 0 1 1 1 3 3 3 1 1 1 0 0 0 0
11 0 0 0 0 0 0 0 3 3 0 0 0 0 0 0 0
12
13 6D Record: Region Numbers to
Coarse-Mesh Intervals for Plane 2
14 0 0 0 0 0 0 0 3 3 3 0 0 0 0 0 0 0
15 0 0 0 0 1 1 1 3 3 3 1 1 1 0 0 0 0
16 0 3 3 3 1 1 1 4 4 4 1 1 1 3 3 3 0
17 0 3 3 3 4 4 4 4 4 4 4 4 4 3 3 3 0
18 0 1 1 1 4 4 4 3 3 3 4 4 4 1 1 1 0
19 0 1 1 1 4 4 4 3 3 3 4 4 4 1 1 1 0
20 0 3 3 3 4 4 4 4 4 4 4 4 4 3 3 3 0
21 0 3 3 3 1 1 1 4 4 4 1 1 1 3 3 3 0
22 0 0 0 0 1 1 1 3 3 3 1 1 1 0 0 0 0
23 0 0 0 0 0 0 0 3 3 3 0 0 0 0 0 0 0
```

Figure 53. GEODST File Coarse-Mesh Interval Region Assignments



February 13, 2020

Table 96. Comparison of GEODST Values for Triangular-Z Problem

Variable	Expected Value	DIF3D Value	Variable	Expected Value	DIF3D Value	Variable	Expected Value	DIF3D Value
<b>Specifications (1D Record)</b>			<b>1D Mesh Boundaries (2D Record)</b>			<b>Geometry Data (5D Record)</b>		
<i>IGOM</i>	17 (tri-Z)	17	<i>Not present since 3D</i>			<i>VOLR(N)</i>	NREG Values: 1.55885E+04, 8.66025E+02, 1.73205E+04, 1.55885E+04	1.55885E+04, 8.66025E+02, 1.73205E+04, 1.55885E+04
<i>NZONE</i>	4	4	<b>2D Mesh Boundaries (3D Record)</b>			<i>BSQ(N)</i>	NBS Values: Not Present	0
<i>NREG</i>	4	4	<i>Not present since 3D</i>			<i>BND(C,N)</i>	NBCS Values: Not Present	0.4692
<i>NZCL</i>	1	1	<b>3D Mesh Boundaries (4D Record)</b>			<i>BNCI(N)</i>	NIBCS Values: Not Present	0
<i>NCINTI</i>	17	17	<i>XMESH(I)</i>	NCINTI+1 Values: 0., 2.88675, 0*16	0., 2.88675, 0*16	<i>NZHBB(N)</i>	NZWBB Values: Not Present	Not Present
<i>NCINTJ</i>	10	10	<i>YMESH(J)</i>	NCINTJ+1 Values: 0*11	0*11	<i>NZC(N)</i>	NZONE Values: Unclear	0,0,0,0
<i>NCINTK</i>	2	2	<i>ZMESH(K)</i>	NCINTK+1 Values: 0, 10, 30	0, 10, 30	<i>NZNR</i>	NREG Values: 1,2,3,4,4,3,2,1	1,2,3,4,4,3,2,1
<i>NINTI</i>	17	17	<i>IFINTS(I)</i>	NCINTI Values 1*17	1*17	<b>Region Assignments to Coarse Mesh (6D Record)</b>		
<i>NINTJ</i>	10	10	<i>JFINTS(J)</i>	NCINTJ Values 1*10	1*10	<i>MR(I,J,K=1)</i>	NCINTI $\times$ NCINTJ Values: See Figure	See Figure
<i>NINTK</i>	5	5	<i>KFINTS(K)</i>	NCINTK Values 2, 3	2, 3	<i>MR(I,J,K=2)</i>	NCINTI $\times$ NCINTJ Values: See Figure	See Figure
<i>IMB1</i>	0	0				<b>Region Assignments to Fine Mesh (7D Record)</b>		
<i>IMB2</i>	0	0				<i>Not present since NRASS=0</i>		
<i>JMB1</i>	0	0						
<i>JMB2</i>	0	0						
<i>KMB1</i>	0	0						
<i>KMB2</i>	0	0						
<i>NBS</i>	0	1						
<i>NBCS</i>	0	1						
<i>NIBCS</i>	0	1						
<i>NZWBB</i>	0	0						
<i>NTRIAG</i>	2	2						
<i>NRASS</i>	0	0						
<i>NTHPT</i>	1	1						
<i>NGOP</i>	Reserved	100, 0, 0, 0						

### 3.2.1.2.2 Verification of Triangular-Z Geometric Perturbations

Table 94 provided the perturbation cases that need to be evaluated for the Triangular-Z diffusion solver verification. Included in these were the perturbations to the A.NIP3 options relating to geometry type, the number of triangle subdivisions, and the setting of the region filling the model background. These geometric perturbations to the triangular-Z base case will be evaluated in this section. Each of these perturbation options will be discussed separately in the subsections that follow.

#### 3.2.1.2.2.1 Geometry Type Perturbations

Thus far this work has evaluated the “Triangular-Z, rectangular boundary in plane, full core in plane” geometry type. However, consistent with [6], the Triangular-Z, rhombic boundary in the plane with sixth-core symmetry and Triangular-Z, rhombic boundary in the plane with third-core symmetry should also be verified. This section will mimic the same core as shown in Figure 44 except utilizing these geometry options.

##### 3.2.1.2.2.1.1 Sixth-Core Symmetric Representation

The first perturbation made was to model the core as a sixth-core with rhombic boundaries. The perturbations made are shown in Figure 54 with changes highlighted in yellow. Figure 54 shows that the boundary conditions on the A.NIP3 Type 04 card were also modified; this was done to add reflective boundary conditions on the lower X and left Y faces of the model simply so that the base and modified solutions were consistent within the specified tolerances. The actual verification of these boundary conditions will be addressed by later problems specifically focused on the boundary conditions.

```

5  UNFORM=A.NIP3
6  01  TRIZ - MCC Micro XS ISOTXS
7  02 0 3 400000000 400000000 400000000 400000000 0 3 3 3
8  03 90
9  04      3      2      3      2      2      2

```

Figure 54. A.NIP3 Changes for Sixth-Core Geometry

With this change, it is expected that the standard and auxiliary output edited region maps will only show 1/6 the core instead of the whole core, the same region maps will also be adjusted to reflect the rhombic vice rectangular boundary, the number of mesh intervals in the X and Y directions will change, the echos of the modified input options, the volumes will be 1/6 as large, and the solution convergence approach will change. These expectations were confirmed true by using the Python diffliib package that highlighted the differences in the outputs. It was found that these areas were the only areas of deviation, as expected. Further, the only binary files with deviations were the GEODST file and only the volumes within the NDXSRF file.

Next, the areas that did change need to be verified. Beginning on line 305, the first relevant difference in the standard output is the number of coarse and fine mesh intervals in the X and Y directions. Figure 55 provides a sketch of the triangular mesh, with rhombic boundary conditions, overlaid on top of the relevant portion of the Figure 44 geometry. From this figure it is expected

that there should be eight coarse mesh and fine mesh intervals in the X dimension and four in the Y dimension. However, DIF3D reports that the number of 1<sup>st</sup> dimension (i.e., the X dimension) coarse and fine-mesh intervals are 7. The number in the 2<sup>nd</sup> dimension (Y) are consistent. This same information, and the same values, are repeated by the DIF3D module's Problem Description Table on lines 1200 through 1250. This was verified as being an internal mesh reduction by DIF3D that is correct and will have no effect. This was checked with by adding a background region, thus making the white triangles of Figure 55 being filled with a color, and thus non-negligible by DIF3D. In this case, the NCINTI and NINTI values were correctly increased from 7 (without the background region) to 8.

The same table also contains the integer identifiers for the boundary conditions and outer boundary shape; these were changed exactly as expected.

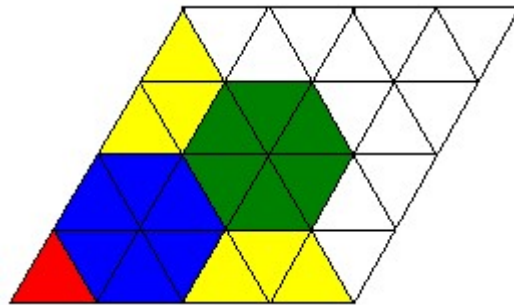


**Figure 55. Sixth-Core Geometry Mesh Sketch**

Line 342 provides the region and zone specifications, including the volumes of each region. These values were verified to be exactly 1/6 that of the base case values, provided in Figure 48; this is the expected result.

Line 364 begins the region/composition map for the hexagonal geometry. There are two of these maps, one for the lower plane (between 0 and 10 cm axially) and another for the upper plane (between 10 and 30 cm). These maps are shown in Figure 56 below with the lower plane on the left and the upper plane on the right. By inspection, these are equivalent to the top-right sixth of the core provided in Figure 49 and the sixth-core provided in Figure 55 (for the lower plane) with red, blue, green, and yellow corresponding to REG1 through REG4 as they have in all previous figures of this model. Interestingly, the DIF3D output does not print the composition label for the bottom row of assemblies; this is not considered to impact the correctness of DIF3D, but is noted here for completeness.

February 13, 2020

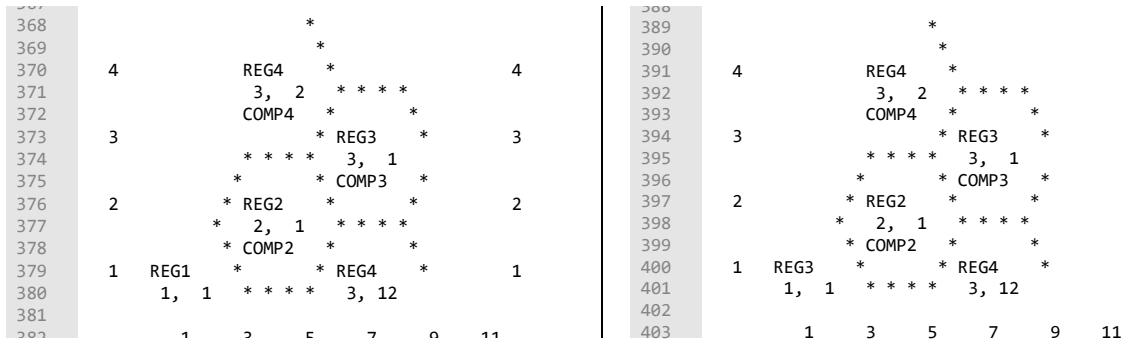


Figure 56. DIF3D Region/Composition Map for the Sixth-Core Triangular-Z Geometry Model; the lower plane is on the left, and the upper plane is on the right

The final differences to discuss are the DIF3D module's output of the reactor region and zone mesh-point assignment maps. The region by mesh-point map for the lower plane of the core is provided in Figure 57, with the region identifiers colored consistent with that used in Figure 55. The DIF3D output provides numbers corresponding to the order of appearance in the model; these are consistent with that shown in Figure 51. REG1, REG2, REG3, and REG4 are colored as red, blue, green, and yellow, respectively in Figure 57. This same color scheme has been applied by the authors to the numbers in the top portion of Figure 50 to provide for an easier comparison. This comparison clearly shows that there are six mesh points per hexagon as expected, the regions in this plane are laid down correctly, and the background triangle mesh points are assigned a value of 0, as expected. This map fails to display the last upper triangle in each row that are present as seen in Figure 55.

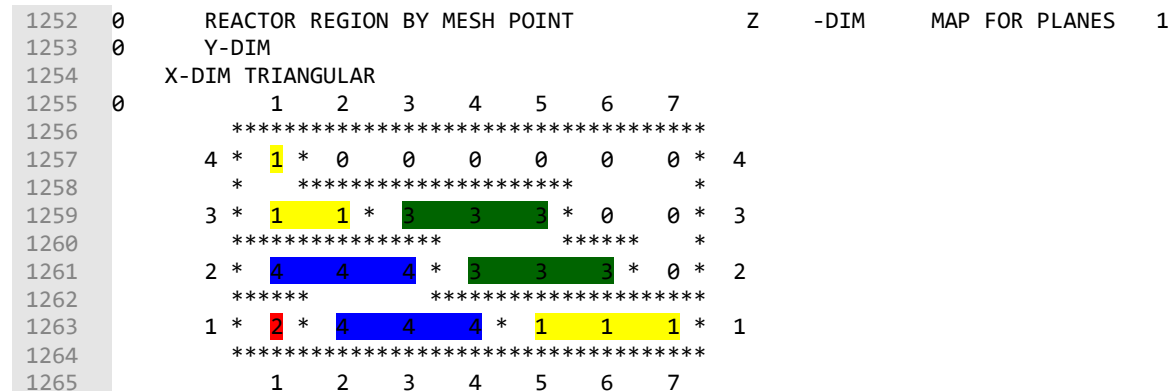


Figure 57. Sixth-Core Reactor Region Map for the Lower Plane

The lines that follow line 1265 provide the same plot for the upper plans (lines 1270-1280), and the reactor zone by mesh-point plots for each plane (lines 1285 to 1310). These were manually verified and the region and zone laydowns were as expected.

Finally, as an indication that the DIF3D manipulation of this geometry is likely correct, both the base case and this sixth-core model yield the same final, converged, eigenvalue to all reported significant digits.

To verify the auxiliary output, the auxiliary output was compared to the standard output; the only differences were related to the different content in the auxiliary and standard outputs, none of that was impacted by this change of geometry.

Next, the NDXSRF file was converted to ASCII and compared to the same file for the base case. Unsurprisingly, the only differences are that the volumes have been modified by a factor of one sixth, as expected.

The GEODST file contains extensive differences as one would expect, due to the introduction of the sixth-core geometry. In the 1D record, these differences are limited to the number of coarse and fine mesh intervals in the X and Y dimensions; the sixth-core model has values of 7 (X) and 4 (Y) for these as already discussed. The boundary conditions are also modified as expected, as is the geometry option signifying that this is a rhombic boundary. In the 3D record, the coarse mesh and fine mesh interval boundaries have been updated to consistently reflect the updated number of coarse and fine mesh intervals. The volumes again have been reduced by a factor of one-sixth, as expected. Finally, the GEODST file includes the region assignments to the coarse mesh intervals in the 6D record. Like in Figure 53 for the base case, these arrays will be converted to a regular grid and colored to more clearly provide the verification basis. This is provided in Figure 58. Based on comparison with the GEODST listing and the numbering of elements in a triangular-Z grid with a rhombic boundary, these region to mesh assignments should be inverted so that the first row printed is actually the first row of the mesh at the bottom of the core. When factoring this in, the GEODST file mesh assignments in Figure 58 match the expected layout shown in Figure 55.

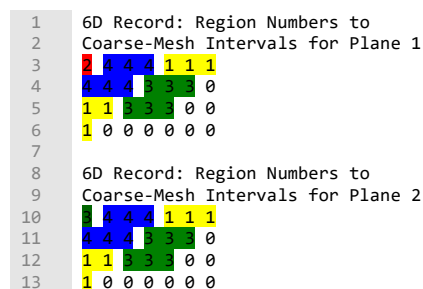


**Figure 58. Sixth-Core Geometry GEODST File Region to Mesh Assignments**

#### 3.2.1.2.2.1.2 Third-Core Symmetric Representation

The second perturbation made was to model the core as a third-core with rhombic boundaries. The perturbations made are shown in Figure 59 with changes highlighted in yellow. Figure 59 shows that the boundary conditions on the A.NIP3 Type 04 card were also modified; this was done to add reflective boundary conditions on the lower X and left Y faces of the model simply so that the base and modified solutions were consistent within the specified tolerances. The actual verification

February 13, 2020

of these boundary conditions will be addressed by later problems specifically focused on the boundary conditions.

```

5  UNFORM=A.NIP3
6  01      TRIZ - MCC Micro XS ISOTXS
7  02 0 3  40000000 40000000 40000000 40000000 0 3 3 3
8  03 94
9  04      3      2      3      2      2      2

```

**Figure 59. A.NIP3 Changes for Third-Core Geometry**

With this change, it is expected that the standard and auxiliary output edited region maps will only show 1/3 of the full core, the same region maps will also be adjusted to reflect the rhombic boundary, the number of mesh intervals in the X and Y directions will change, the echos of the modified input options, the volumes will be 1/3 as large, and the solution convergence approach will change. These expectations were confirmed true by using the Python diffliib package to which highlighted the differences in the outputs. It was found that these areas were the only areas of deviation, as expected. Further, the only binary files with deviations were most of the GEODST file and the volumes within the NDXSRF file.

Next, the areas that did change need to be verified. Beginning on line 305, the first relevant difference in the standard output is the number of coarse and fine mesh intervals in the X and Y directions. Figure 60 provides a sketch of the triangular mesh, with rhombic boundary conditions, overlaid on top of the relevant portion of the Figure 44 geometry. From this figure it is expected that there should be ten coarse mesh and fine mesh intervals in the X dimension and five in the Y dimension. This is consistent with the reported values from DIF3D. This same information, and the same values, are repeated by the DIF3D module's Problem Description Table on lines 1206 through 1248.

The same table also contains the integer identifiers for the boundary conditions and outer boundary shape; these were changed exactly as expected.

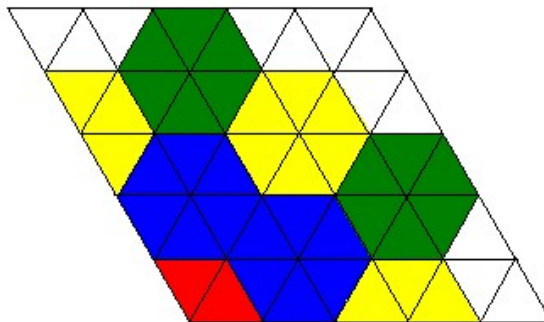


**Figure 60. Third-Core Geometry Mesh Sketch**

February 13, 2020

Line 340 provides the region and zone specifications, including the volumes of each region. These values were verified to be exactly 1/3 that of the base case values, provided in Figure 48; this is the expected result.

Line 364 begins the region/composition map for the hexagonal geometry. There are two of these maps, one for the lower plane (between 0 and 10 cm axially) and another for the upper plane (between 10 and 30 cm). These maps are shown in Figure 61 below with the lower plane on the left and the upper plane on the right. By inspection, these are equivalent to the top-right third of the core provided in Figure 49 and the third-core provided in Figure 60 (for the lower plane) with red, blue, green, and yellow corresponding to REG1 through REG4 as they have in all previous figures of this model. Interestingly, the DIF3D output does not print the composition label for the bottom row of assemblies; this is not considered to impact the correctness of DIF3D, but is noted here for completeness. Additionally, the final assembly in Ring 3 is not printed; later examinations show that DIF3D is aware of this assembly (see Figure 62) and so this is just a convenience taken for the plotting.

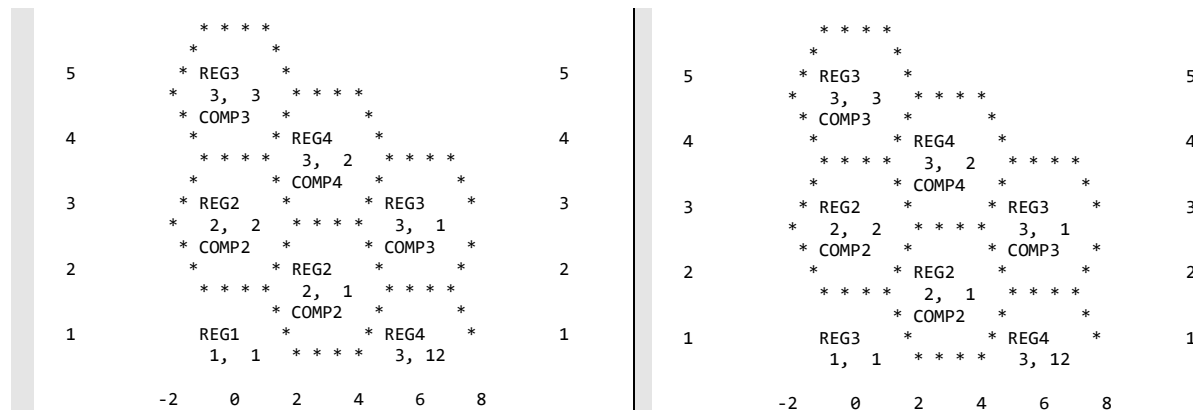


**Figure 61. DIF3D Region/Composition Map for the Third-Core Triangular-Z Geometry Model; the lower plane is on the left, and the upper plane is on the right**

The final differences to discuss are the DIF3D module's output of the reactor region and zone mesh-point assignment maps. The region by mesh-point map for the lower plane of the core is provided in Figure 62, with the region identifiers colored consistent with that used in Figure 60. The DIF3D output provides numbers corresponding to the order of appearance in the model; these are consistent with that shown in Figure 51. REG1, REG2, REG3, and REG4 are colored as red, blue, green, and yellow, respectively in Figure 62. This same color scheme has been applied via post-processing to the numbers in the top portion of Figure 50 to provide for an easier comparison. This comparison clearly shows that there are six mesh points per hexagon as expected, the regions in this plane are laid down correctly, and the background triangle mesh points are assigned a value of 0, as expected.

February 13, 2020

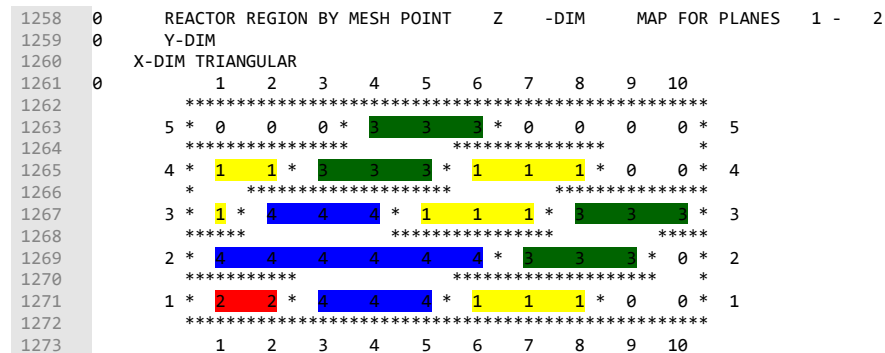


**Figure 62. Third-Core Reactor Region Map for the Lower Plane**

The lines that follow line 1273 provide the same plot for the upper plans (lines 1275-1290), and the reactor zone by mesh-point plots for each plane (lines 1295 to 1324). These were manually verified and the region and zone laydowns were as expected.

Finally, as an indication that the DIF3D manipulation of this geometry is likely correct, both the base case and the 1/3 core model yield the same final, converged, eigenvalue to all reported significant digits.

To verify the auxiliary output, the auxiliary output was compared to the standard output; the only differences were related to the different content in the auxiliary and standard outputs, none of which was impacted by this change of geometry.

Next, the NDXSRF file was converted to ASCII and compared to the same file for the base case. Unsurprisingly, the only differences are the volumes that have been modified exactly by a factor of one third, as expected.

The GEODST file contains extensive differences as expected, due to the introduction of the sixth-core geometry. In the 1D record, these differences are limited to the number of coarse and fine mesh intervals in the X and Y dimensions; the third-core model has values of 10 (X) and 5 (Y) for these as already discussed. The boundary conditions are also modified as expected, as is the geometry option signifying that this is a rhombic boundary. In the 3D record, the coarse mesh and fine mesh interval boundaries have been updated to consistently reflect the updated number of coarse and fine mesh intervals. The volumes again have been reduced by a factor of one third, as expected. Finally, the GEODST file includes the region assignments to the coarse mesh intervals in the 6D record. Like in Figure 53 for the base case, these arrays will be converted to a regular grid and colored to more clearly provide the verification basis. This is provided in Figure 63. Based on comparison with the GEODST listing and the numbering of elements in a triangular-Z grid with a rhombic boundary, these region to mesh assignments should be inverted such that the first row printed is actually the first row of the mesh at the bottom of the core. When factoring this in, the GEODST file mesh assignments in Figure 63 match the expected layout shown in Figure 60.



1	6D Record: Region Numbers to
2	Coarse-Mesh Intervals for Plane 1
3	2 2 4 4 4 1 1 1 0 0
4	4 4 4 4 4 4 3 3 0
5	1 4 4 4 1 1 1 3 3
6	1 1 3 3 1 1 1 0 0
7	0 0 0 3 3 0 0 0 0
8	
9	6D Record: Region Numbers to
10	Coarse-Mesh Intervals for Plane 2
11	3 3 4 4 4 1 1 1 0 0
12	4 4 4 4 4 4 3 3 0
13	1 4 4 4 1 1 1 3 3
14	1 1 3 3 1 1 1 0 0
15	0 0 0 3 3 0 0 0 0

**Figure 63. Third-Core Geometry GEODST File Region to Mesh Assignments**

Based on the above evaluation, this case should be considered verified.

#### 3.2.1.2.2.2 Triangle Subdivisions Perturbation

The A.NIP3 block contains an option on the Type 29 card that controls the triangular subdivision of the mesh. This value tells DIF3D to subdivide the hexagon's six equilateral triangles into a number of equal parts. More specifically, doubling this number from the default of 1 to a value of 2 will cut the spacing between the endpoints of the mesh lines traversing the reactor model in half.

To verify the A.NIP3 block's Type 29 card option to subdivide the mesh grid's equilateral triangles, the base case (full-core), sixth-core, and third-core geometries will each have the A.NIP3 Type 29 card, Option 4, default value of 1 increased to a value of 2. This will yield three additional perturbations to test in this subsection. Each of these will be discussed separately below.

##### 3.2.1.2.2.2.1 Full-Core Representation with Two Triangle Subdivisions

This case is the same as the base case discussed previously except the A.NIP3 Type 29 card, Option 4, has an assigned value of 2. A sketch of the expected triangular mesh is presented in Figure 64 below, which is a modified version of Figure 47 with the mesh spacing reduced to half as much in the X and Y dimensions, thus creating a total of 24 triangles per hexagon in each 2D plane. Across the X dimension there are 33 triangles while the Y dimension has 20 triangles. The side of each triangle is reduced from 5.7735cm per side to half that, 2.8868cm per side. Finally, the first triangle in the first row is pointing towards the X axis.

The above changes, the region and zone maps, the edits of computer memory required, page headers, and the solution are all that are expected to change. Therefore this section will verify this is true by comparing the standard output, auxiliary output, and binary files to the equivalent configuration that left the A.NIP3 Type 29 card at its' default value of 1 (referred to as the reference configuration). Then, the differences will be confirmed consistent with the mesh of Figure 64.

When comparing the standard, and auxiliary output, the GEODST file, and the NDXSRF file to the reference case, it was found that the high-precision volumes printed in the GEODST and NDXSRF differ in the last two of seven significant digits. This is not an issue, but an indication that some precision is lost when creating the mesh and storing the triangular dimensions. The

standard and auxiliary outputs report the same volumes since less significant digits are reported in that output.

The file comparison confirms that, aside from the above volume discrepancy, the differences are limited to the differences expected as previously discussed. These specific values will be verified now.

Line 305 of the standard output begins the GNIP4C module's model description, containing the number of mesh intervals in the X and Y dimensions, the orientation of the lower-left triangle, and the length of the side of each triangle. All of these values are exactly as expected. Further, these same outputs are repeated (and confirmed correct) in the DIF3D module's problem description table (line 1237), the equivalent tables in auxiliary output, and in the GEODST file.

The reactor region core map on line 365 contains the same core map as before, except the coarse mesh indexing not reflects the updated number of mesh intervals; this is confirmed accurate.

Lines 1289 to 1663 contain the reactor region to mesh interval map for the lower and upper planes, followed by the reactor zone to mesh interval map for the lower and upper planes, in that order. The region by mesh-point map for the lower plane of the core is provided in Figure 65. This figure includes post-processing such as combining the mesh to exist on one line, and coloring the region identifiers consistent with that used in Figure 64, and removing all asterisks used by DIF3D to represent boundaries to reduce the space required by the figure. The DIF3D output provides numbers corresponding to the order of appearance in the model; these are consistent with that shown in Figure 51. REG1, REG2, REG3, and REG4 are colored as red, blue, green, and yellow, respectively in Figure 65. This comparison clearly shows that there are 24 mesh points per hexagon as expected, the regions in this plane are laid down correctly, and the background triangle mesh points are assigned a value of 0, as expected.

The remaining planes were manually verified to be correct; no discrepancies were identified.

The above comparisons were performed for the auxiliary output and verified to be the same as in the standard output.

The LABELS file contains one value that changed: the number of triangles per hexagon. This was verified to have increased from 6 to 24 triangles per hexagon.

The remaining output to check is the region number assignments for the two planes in the GEODST file. Like previous comparisons, this was done by taking the binary GEODST file, converting to ASCII, and then reformatting the two 6D records so that the region number arrays are a 33 by 10 array, mimicking the core laydown. This laydown was then compared with the expectations based upon the equivalent data shown in Figure 66 and Figure 67 and has been confirmed to match for both planes of the reactor.

February 13, 2020

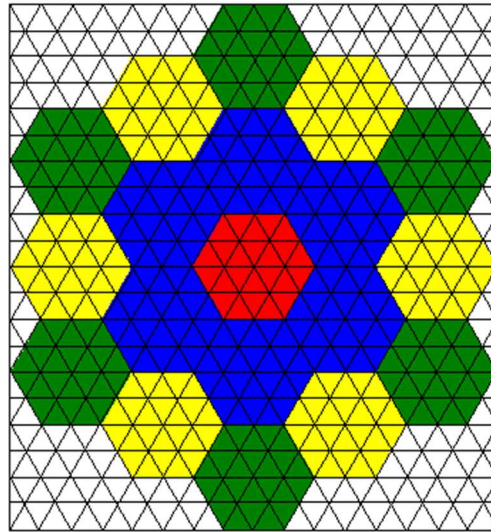


Figure 64. Sketch of the Full-Core Mesh with Type 29 Card 4 Set to 2

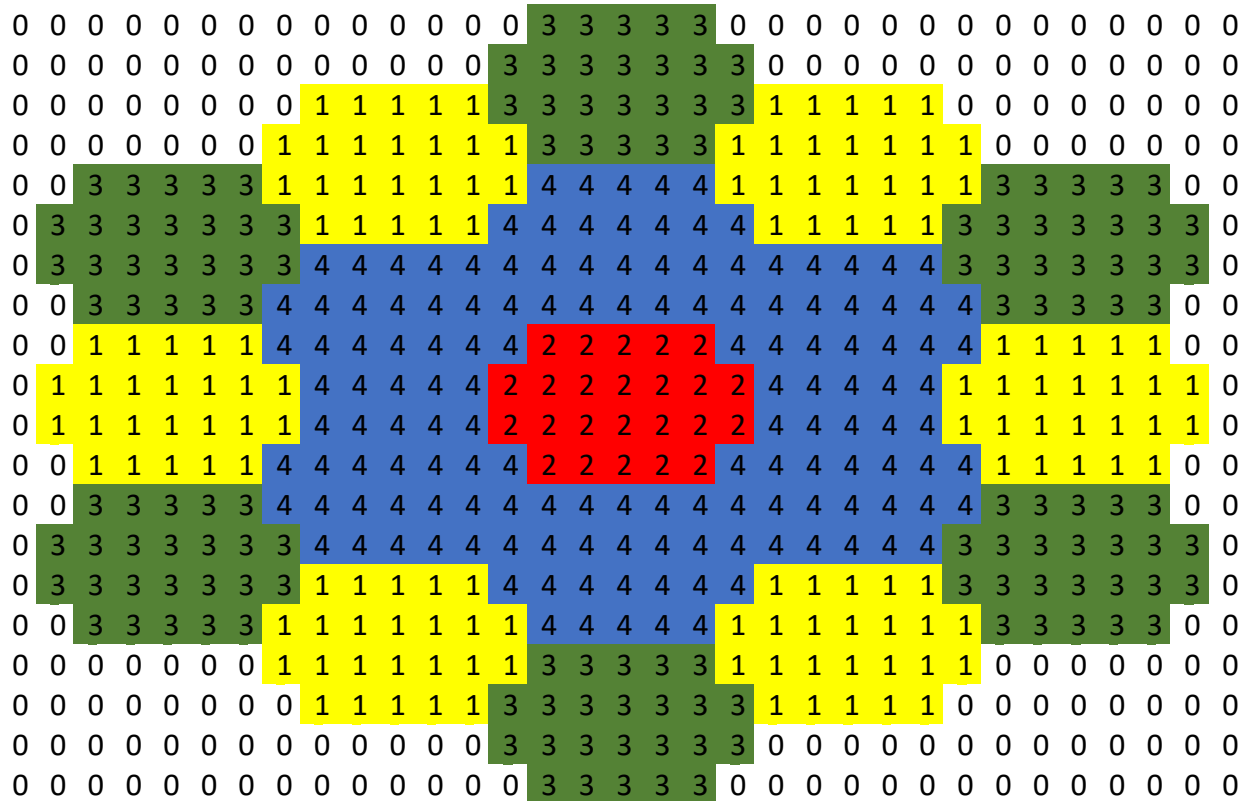


Figure 65. DIF3D Region to Mesh Interval Map for Plane 1 of Full-Core Model



February 13, 2020

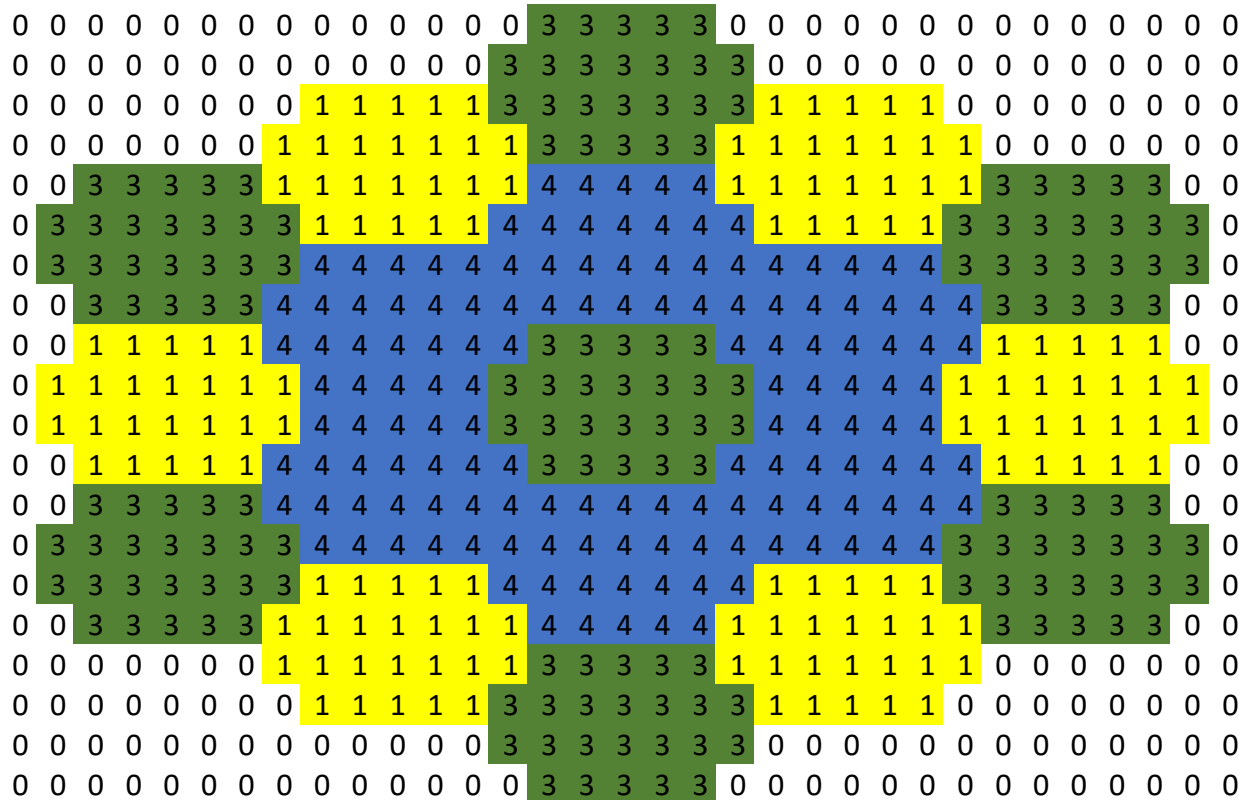


Figure 67. DIF3D GEODST File 6D Record for Plane 2 of Full-Core Model

### 3.2.1.2.2.2 Sixth-Core Representation with Two Triangle Subdivisions

This case is the same as the sixth-core case discussed previously except the A.NIP3 Type 29 card, Option 4, has an assigned value of 2. A sketch of the expected triangular mesh is presented in Figure 68 below, which is a modified version of Figure 55 with the mesh spacing reduced to half as much in the X and Y dimensions, thus creating a total of 24 triangles per hexagon in each 2D plane. Across the X dimension there are 16 triangles; across the Y dimension there are 8. The side of each triangle is reduced from 5.7735cm per side to half that, 2.8868cm per side. Finally, the lower left mesh triangle is pointing away from the X axis.

The above changes, the region and zone maps, the edits of computer memory required, page headers, and the solution are all that are expected to change. Therefore this section will verify this is true by comparing the standard output, auxiliary output, and binary files to the equivalent configuration that left the A.NIP3 Type 29 card at its' default value of 1 (referred to as the reference configuration). Then, the differences will be confirmed consistent with the mesh in Figure 68.

In contrast with the full-core case, all volumes reported in the standard and auxiliary outputs, GEODST, and NDXSRF files match the reference case to the reported number of digits.

The file comparison confirms that the differences are limited to the differences expected as previously discussed. These specific values will be verified in the sections that follow.

Line 305 of the standard output begins the GNIP4C module's model description, containing the number of mesh intervals in the X and Y dimensions, the orientation of the lower-left triangle, and the length of the side of each triangle. The only discrepancy noted herein is that DIF3D reports that there are 15 triangles across the X dimension instead of the expected 16. This is the same issue identified when discussing the sixth-core model in the previous section; there it was found to have no effect. The remaining values match. All of these values are exactly as expected. Further, these same outputs are repeated (and confirmed correct) in the DIF3D module's problem description table (line 1204), the equivalent tables in auxiliary output, and in the GEODST file.

The reactor region core map on line 365 contains the same core map as before, except the coarse mesh indexing does not reflect the updated number of mesh intervals; this is confirmed accurate.

Lines 1255 to 1342 contain the reactor region to mesh interval map for the lower and upper planes, followed by the reactor zone to mesh interval map for the lower and upper planes, in that order. The region by mesh-point map for the lower plane of the core is provided in Figure 69. This figure includes post-processing such as combining the mesh to exist on one line, and coloring the region identifiers consistent with that used in Figure 68, and removing all asterisks used by DIF3D to represent boundaries to reduce the space required by the figure. The DIF3D output provides numbers corresponding to the order of appearance in the model; these are consistent with that shown in Figure 51. REG1, REG2, REG3, and REG4 are colored as red, blue, green, and yellow, respectively in Figure 69. This comparison clearly shows that there are 24 mesh points per hexagon as expected, the regions in this plane are laid down correctly, and the background triangle mesh points are assigned a value of 0, as expected. The 15 triangles per row discrepancy is also present here as we see there is no background triangle to the right of the last of the REG4 entries (yellow) on the first row as there is in Figure 68.

The remaining planes were manually verified to be correct; no discrepancies were identified.

The above comparisons were performed for the auxiliary output and verified to be the same as in the standard output.

The LABELS file contains one value that changed: the number of triangles per hexagon. This was verified to have increased from 6 to 24 triangles per hexagon.

The remaining output to check is the region number assignments for the two planes in the GEODST file. Like previous comparisons, this was done by taking the binary GEODST file, converting to ASCII, and then reformatting the two 6D records so that the region number arrays are a 15 by 8 array, mimicking the core laydown interpreted by DIF3D. This laydown was then compared with the expectations based upon the equivalent data shown in Figure 70 and has been confirmed to match for both planes of the reactor when factoring the reversed ordering of these arrays as discussed earlier.

February 13, 2020

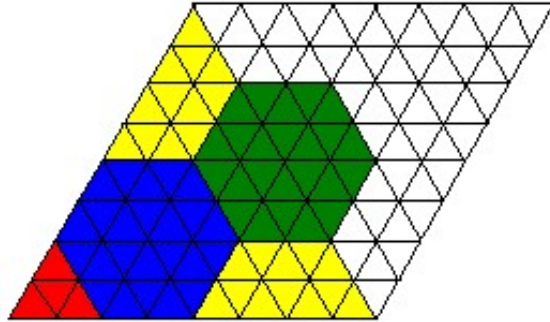


Figure 68. Sketch of the Sixth-Core Mesh with Type 29 Card 4 Set to 2

1255	0	1	2	3	4	5	6	7	8	9	10	11	12	13	14	15
1256		*****														
1257	8	*	1	*	0	0	0	0	0	0	0	0	0	0	0	*
1258		*	*****													
1259	7	*	1	1	1	*	0	0	0	0	0	0	0	0	0	*
1260		*	*****													
1261	6	*	1	1	1	1	*	3	3	3	3	*	0	0	0	*
1262		*	*****													
1263	5	*	1	1	1	1	*	3	3	3	3	3	*	0	0	*
1264		*	*****													
1265	4	*	4	4	4	4	4	*	3	3	3	3	3	3	*	*
1266		*	*****													
1267	3	*	4	4	4	4	4	4	*	3	3	3	3	*	0	*
1268		*	*****													
1269	2	*	2	*	4	4	4	4	4	4	*	1	1	1	1	*
1270		*	*****													
1271	1	*	2	2	2	*	4	4	4	4	4	*	1	1	1	*
1272		*	*****													
1273		1	2	3	4	5	6	7	8	9	10	11	12	13	14	15

Figure 69. Region Map for Sixth-Core Model

1	6D Record: Region Numbers to
2	Coarse-Mesh Intervals for Plane 1
3	2 2 2 4 4 4 4 4 1 1 1 1 1 1 1
4	2 4 4 4 4 4 4 4 1 1 1 1 1 0 0
5	4 4 4 4 4 4 4 4 3 3 3 3 3 0 0
6	4 4 4 4 4 4 3 3 3 3 3 3 3 0 0
7	1 1 1 1 1 3 3 3 3 3 3 3 3 0 0
8	1 1 1 1 1 3 3 3 3 3 3 3 3 0 0
9	1 1 1 1 0 0 0 0 0 0 0 0 0 0 0
10	1 0 0 0 0 0 0 0 0 0 0 0 0 0 0
11	
12	6D Record: Region Numbers to
13	Coarse-Mesh Intervals for Plane 2
14	3 3 3 4 4 4 4 4 1 1 1 1 1 1 1
15	4 4 4 4 4 4 4 4 1 1 1 1 1 0 0
16	4 4 4 4 4 4 4 4 3 3 3 3 3 0 0
17	4 4 4 4 4 4 3 3 3 3 3 3 3 0 0
18	1 1 1 1 1 3 3 3 3 3 3 3 3 0 0
19	1 1 1 1 1 3 3 3 3 3 3 3 3 0 0
20	1 1 1 1 0 0 0 0 0 0 0 0 0 0 0
21	1 0 0 0 0 0 0 0 0 0 0 0 0 0 0

Figure 70. DIF3D GEODST File 6D Record for both Planes of the Sixth-Core Model

### 3.2.1.2.2.2.3 Third-Core Representation with Two Triangle Subdivisions

This case is the same as the third-core case discussed previously except the A.NIP3 Type 29 card, Option 4, has an assigned value of 2. A sketch of the expected triangular mesh is presented in Figure 71 below, which is a modified version of Figure 60 with the mesh spacing reduced to half as much in the X and Y dimensions, thus creating a total of 24 triangles per hexagon in each 2D plane. Across the X dimension there are 20 triangles while the Y dimension has 10 triangles. The side of each triangle is reduced from 5.7735cm per side to half that, 2.8868cm per side. Finally, the first triangle on the first row is pointing to the X axis.

The above changes, the region and zone maps, the edits of computer memory required, page headers, and the solution are all that are expected to change. Therefore this section will verify this is true by comparing the standard output, auxiliary output, and binary files to the equivalent configuration that left the A.NIP3 Type 29 card at its' default value of 1 (referred to as the reference configuration). Then, the differences will be confirmed consistent with the mesh in Figure 71.

When comparing the standard, and auxiliary output, the GEODST file, and the NDXSRF file to the reference case, it was found that the high-precision volumes printed in the GEODST and NDXSRF differ in the last two of seven significant digits. This is not an issue, but an indication that some precision is lost when creating the mesh and storing the triangular dimensions. The standard and auxiliary outputs report the same volumes since less significant digits are reported in that output.

The file comparison confirms that, aside from the above volume discrepancy, the differences are limited to the differences expected as previously discussed. These specific values will be verified now.

Line 305 of the standard output begins the GNIP4C module's model description, containing the number of mesh intervals in the X and Y dimensions, the orientation of the lower-left triangle, and the length of the side of each triangle. All of these values are exactly as expected. Further, these same outputs are repeated (and confirmed correct) in the DIF3D module's problem description table (line 1206), the equivalent tables in auxiliary output, and in the GEODST file.

The reactor region core map on line 365 contains the same core map as before, except the coarse mesh indexing not reflects the updated number of mesh intervals; this is confirmed accurate.

Lines 1260 to 1364 contain the reactor region to mesh interval map for the lower and upper planes, followed by the reactor zone to mesh interval map for the lower and upper planes, in that order. The region by mesh-point map for the lower plane of the core is provided in Figure 72. This figure includes post-processing such as combining the mesh to exist on one line, and coloring the region identifiers consistent with that used in Figure 71, and removing all asterisks used by DIF3D to represent boundaries to reduce the space required by the figure. The DIF3D output provides numbers corresponding to the order of appearance in the model; these are consistent with that shown in Figure 51. REG1, REG2, REG3, and REG4 are colored as red, blue, green, and yellow, respectively in Figure 72. This comparison clearly shows that there are 24 mesh points per hexagon as expected, the regions in this plane are laid down correctly, and the background triangle mesh



February 13, 2020

points are assigned a value of 0, as expected. The remaining planes were manually verified to be correct; no discrepancies were identified.

The above were repeated for the auxiliary output and were the same as standard output.

The LABELS file contains one value that changed: the number of triangles per hexagon. This was verified to have increased from 6 to 24 triangles per hexagon.

The remaining output to check is the region number assignments for the two planes in the GEODST file. Like previous comparisons, this was done by taking the binary GEODST file, converting to ASCII, and then reformatting the two 6D records so that the region number arrays are a 20 by 10 array, mimicking the core laydown interpreted by DIF3D. This laydown was then compared with the expectations based upon the equivalent data shown in Figure 73 and has been confirmed to match for both planes of the reactor when factoring the reversed ordering of these arrays as discussed earlier.

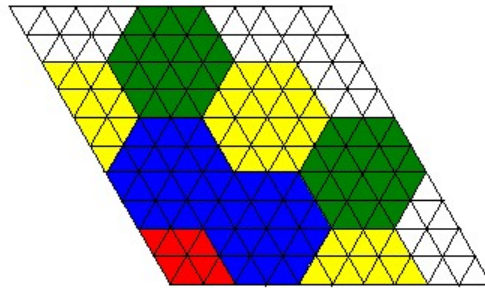


Figure 71. Sketch of the Third-Core Mesh with Type 29 Card 4 Set to 2

1261	0	1	2	3	4	5	6	7	8	9	10	11	12	13	14	15	16	17	18	19	20
1262		*****	*****	*****	*****	*****	*****	*****	*****	*****	*****	*****	*****	*****	*****	*****	*****	*****	*****	*****	*****
1263	10	*	0	0	0	0	0	0	*	3	3	3	3	*	0	0	0	0	0	0	0
1264		*								*****				*							*
1265	9	*	0	0	0	0	0	0	*	3	3	3	3	3	*	0	0	0	0	0	0
1266		*								*****					*****						*
1267	8	*	1	1	1	1	*	3	3	3	3	3	3	*	1	1	1	1	1	*	0
1268		*								*****					*						*
1269	7	*	1	1	1	1	*	3	3	3	3	3	3	*	1	1	1	1	1	1	0
1270		*								*****					*						*
1271	6	*	1	1	1	1	*	4	4	4	4	4	4	*	1	1	1	1	1	1	3
1272		*								*****					*						*
1273	5	*	1	*	4	4	4	4	4	4	4	4	4	*	1	1	1	1	1	1	3
1274		*								*****					*						*
1275	4	*	4	4	4	4	4	4	4	4	4	4	4	*	3	3	3	3	3	3	0
1276		*												*							*
1277	3	*	4	4	4	4	4	4	4	4	4	4	4	*	3	3	3	3	3	3	0
1278		*												*							*
1279	2	*	2	2	2	2	*	4	4	4	4	4	4	*	1	1	1	1	1	1	0
1280		*												*							*
1281	1	*	2	2	2	2	*	4	4	4	4	4	4	*	1	1	1	1	1	1	0
1282		*												*							*
1283			1	2	3	4	5	6	7	8	9	10	11	12	13	14	15	16	17	18	19

Figure 72. Region Map for Third-Core Model

February 13, 2020

1	6D Record: Region Numbers to																							
2	Coarse-Mesh Intervals for Plane 1																							
3	2	2	2	2	4	4	4	4	4	1	1	1	1	1	1	1	0	0	0	0	0	0	0	0
4	2	2	2	2	4	4	4	4	4	4	1	1	1	1	1	1	0	0	0	0	0	0	0	0
5	4	4	4	4	4	4	4	4	4	4	4	4	4	4	4	3	3	3	3	3	0	0	0	0
6	4	4	4	4	4	4	4	4	4	4	4	4	4	4	4	3	3	3	3	3	3	0	0	0
7	1	4	4	4	4	4	4	4	4	1	1	1	1	1	1	3	3	3	3	3	3	3	3	3
8	1	1	1	1	4	4	4	4	4	1	1	1	1	1	1	3	3	3	3	3	3	3	3	3
9	1	1	1	1	3	3	3	3	3	1	1	1	1	1	1	0	0	0	0	0	0	0	0	0
10	1	1	1	1	3	3	3	3	3	3	1	1	1	1	1	0	0	0	0	0	0	0	0	0
11	0	0	0	0	0	3	3	3	3	3	3	0	0	0	0	0	0	0	0	0	0	0	0	0
12	0	0	0	0	0	0	3	3	3	3	3	0	0	0	0	0	0	0	0	0	0	0	0	0
13																								
14	6D Record: Region Numbers to																							
15	Coarse-Mesh Intervals for Plane 2																							
16	3	3	3	3	4	4	4	4	4	1	1	1	1	1	1	0	0	0	0	0	0	0	0	0
17	3	3	3	3	4	4	4	4	4	4	1	1	1	1	1	0	0	0	0	0	0	0	0	0
18	4	4	4	4	4	4	4	4	4	4	4	4	4	4	4	3	3	3	3	3	0	0	0	0
19	4	4	4	4	4	4	4	4	4	4	4	4	4	4	4	3	3	3	3	3	3	0	0	0
20	1	4	4	4	4	4	4	4	4	1	1	1	1	1	1	3	3	3	3	3	3	3	3	3
21	1	1	1	1	4	4	4	4	4	1	1	1	1	1	1	3	3	3	3	3	3	3	3	3
22	1	1	1	1	3	3	3	3	3	1	1	1	1	1	1	0	0	0	0	0	0	0	0	0
23	1	1	1	1	3	3	3	3	3	3	1	1	1	1	1	0	0	0	0	0	0	0	0	0
24	0	0	0	0	0	3	3	3	3	3	3	0	0	0	0	0	0	0	0	0	0	0	0	0
25	0	0	0	0	0	0	3	3	3	3	3	0	0	0	0	0	0	0	0	0	0	0	0	0

Figure 73. DIF3D GEODST File 6D Record for both Planes of the Third-Core Model

### 3.2.1.2.2.3 Background Region Perturbation

The A.NIP3 block contains an option on the Type 31 card that controls the setting of the background region in the model. This is the region assigned to the region of the reactor outside of the hexagonal map defined by the Type 30 cards. DIF3D defaults to applying a “0” region, i.e., no region or material, to these regions; this was used in all triangular-Z models thus far.

To verify the A.NIP3 block’s Type 31 card, REG1 will be applied to the background for the full-core, sixth-core, and third-core cases. For these cases, the only differences expected are that the volume of REG1 will increase, and the region and zone to mesh interval maps should have the “0”s on the core periphery replaced with “2” (for region maps) or “1” (for zone maps). Table 97 provides the computed volumes based upon computing the areas of the white regions of Figure 47, Figure 55, and Figure 60 for the full-core, sixth-core, and third-core cases, respectively.

**Table 97. Volumes for REG1 in Background**

Case	REG1 Volumes [cm <sup>3</sup> ]
Base	8.660254E+02
Full-Core	2.078461E+04
Sixth-Core	5.773503E+03
Third-Core	5.484828E+03

To perform this verification, the standard, auxiliary, and binary outputs from cases with REG1 assigned to the background will be compared to their equivalents with no background region assigned.

This comparison was performed, and no discrepancies were found. However it is noted that the volumes computed above match for the sixth-core case despite the Figure 55 mesh sketch and DIF3D not agreeing on the number of mesh cells along the X dimension. This is because when a background is applied, DIF3D adds the additional triangle back in as the Sixth-Core case had 8 triangles along the X-Dimension as expected per Figure 55. This capability is therefore verified for Triangular-Z geometries.

#### *3.2.1.2.3 Verification of Triangular-Z Edit Control Perturbations*

Table 94 provided the perturbation cases that need to be evaluated for the Triangular-Z diffusion solver verification. Of these, only the edit control options remain to be verified. This section will perform that verification.

The six edit control options from Table 94 that must be verified are summarized in Table 98. Each of these will be verified separately in the subsections that follow. These specific edit control options are those relating to the geometry; those relating to composition or isotopic data have been thoroughly vetted by other problems.

Table 98. Diffusion Theory Triangular-Z Perturbation Cases

A.NIP3 Module Options			
Card Type & Option	Description	Option in Base Case	Perturbations to Base
2.3	Geometry processing edits	3	0, 1, 2
2.10	Region/mesh interval plotter edits	3	0, 1, 2
2.11	Zone/mesh interval plotter edits	3	0, 1, 2
A.DIF3D Module Options			
Card Type & Option	Description	Option in Base Case	Perturbations to Base
4.2	Problem description edit	3	0, 1, 2
4.3	Geometry (region to mesh interval) map edit	3	0, 1, 2
4.4	Geometry (zone to mesh interval) map edit	3	0, 1, 2

### 3.2.1.2.3.1 A.NIP3 Type 02 Card Option 3

The third option of the Type 02 card of the A.NIP3 input block accepts values of 0, 1, 2, or 3 as shown in Table 98. The cases evaluated thus far have kept this option at a value of 3, indicating that geometry edits will be printed to both standard and auxiliary output. This case will evaluate the 0, 1, and 2 options that print no GNIP4C module edits, print GNIP4C edits only to standard output, and print GNIP4C edits only to auxiliary output.

The base case input was modified accordingly with three different inputs capturing the 0, 1, 2, and 3 values for this option discussed above. DIF3D was run for all three cases. To verify, the auxiliary and standard output files for each of the three cases were compared against the base case to ensure that the A.NIP3 edit option is respected.

The first modified case shall print no GNIP4C module edits in either standard or auxiliary output and all other outputs should be the same as the base case. This was explicitly confirmed by comparing both outputs with the base case equivalent. The base case, beginning on line 293 of the standard output includes the GNIP4C edits printed from the A.NIP3 module; this is not present in the standard output of the modified case. It is noted that the GNIP4C edits still output the reactor region map, but do not include the GNIP4C edits of the cross section information; this is interesting as the A.NIP3 listing is unclear on what exactly a “geometry processing module edit” entails. The same findings exist for the auxiliary output.

The second modified case is expected to print the GNIP4C edits to the standard output but not the auxiliary output. The value of this option was successfully interpreted, as the auxiliary output did not include the GNIP4C edits but the standard output did. Similar to the above case, the GNIP4C edits in the auxiliary output still output the reactor region map, but do not include the GNIP4C edits of the cross section information.

The third modified case is expected to print the GNIP4C edits to only the auxiliary output; and all other output should be the same as the base. The value of this option was successfully interpreted, as the standard output did not include the GNIP4C edits but the auxiliary output did, with the same caveat as is found for the previous two cases. Interestingly, this specific option did not translate the isotope names to ASCII correctly in the auxiliary output as lines 475 through 521 of the auxiliary output includes a “<0x00>” code for each character in the isotope name. The other cases in this A.NIP3 Type 02 card Option 3 cases had no issue with this.

#### *3.2.1.2.3.2 A.NIP3 Type 02 Card Option 10*

The tenth option of the Type 02 card of the A.NIP3 input block accepts values of 0, 1, 2, or 3 as shown in Table 98. The cases evaluated thus far have kept this option at a value of 3, indicating that region/mesh interval printer-plotter maps will be printed to both standard and auxiliary output. This case will evaluate the 0, 1, and 2 options that print no region/mesh interval printer-plotter maps, print region/mesh interval printer-plotter maps only to standard output, and print region/mesh interval printer-plotter maps only to auxiliary output.

This verification found that the A.NIP3 Type 02 card’s 10<sup>th</sup> option is not regarded and the region/mesh interval map is always plotted to both the standard and auxiliary outputs.

#### *3.2.1.2.3.3 A.NIP3 Type 02 Card Option 11*

The eleventh option of the Type 02 card of the A.NIP3 input block accepts values of 0, 1, 2, or 3 as shown in Table 98. The cases evaluated thus far have kept this option at a value of 3, indicating that zone (composition) / mesh interval printer-plotter maps will be printed to both standard and auxiliary output. This case will evaluate the 0, 1, and 2 options that print no zone (composition) / mesh interval printer-plotter maps, print zone (composition) / mesh interval printer-plotter maps only to standard output, and print zone (composition) / mesh interval printer-plotter maps only to auxiliary output.

This verification found that the A.NIP3 Type 02 card’s 11<sup>th</sup> option is not regarded and the zone/mesh interval map is always plotted to both the standard and auxiliary outputs.

#### *3.2.1.2.3.4 A.DIF3D Type 04 Card Option 2*

The second option of the Type 04 card of the A.DIF3D input block accepts values of 0, 1, 2, or 3, as shown in Table 98. The cases evaluated thus far have kept this option at a value of 3, indicating that the problem description edits will be printed to both standard and auxiliary output. This case will evaluate the 0, 1, and 2 options that print no problem description edits, print problem description edits only to standard output, and problem description edits only to auxiliary output.

The first modified case shall print no problem description edits in either standard or auxiliary output and all other outputs should be the same as the base case. This was explicitly confirmed by comparing both outputs with the base case equivalent for both standard and auxiliary output files.

The second modified case is expected to print the problem description edits to the standard output but not the auxiliary output. The value of this option was successfully interpreted, as the auxiliary output did not include the problem description edits but the standard output did.

The third modified case is expected to print the problem description edits to only the auxiliary output; and all other output should be the same as the base. The value of this option was successfully interpreted, as the standard output did not include the problem description edits but the auxiliary output did.

#### *3.2.1.2.3.5 A.DIF3D Type 04 Card Option 3*

The third option of the Type 04 card of the A.DIF3D input block accepts values of 0, 1, 2, or 3 as shown in Table 98. The cases evaluated thus far have kept this option at a value of 3, indicating that the DIF3D module will print region/mesh interval printer-plotter maps to both standard and auxiliary output. This case will evaluate the 0, 1, and 2 options that print no region/mesh interval printer-plotter maps, print region/mesh interval printer-plotter maps only to standard output, and print region/mesh interval printer-plotter maps only to auxiliary output.

The first modified case shall print no region maps in either standard or auxiliary output and all other outputs should be the same as the base case. This was explicitly confirmed by comparing both outputs with the base case equivalent.

The second modified case is expected to print the region maps to the standard output but not the auxiliary output. The value of this option was successfully interpreted, as the auxiliary output did not include the map but the standard output did.

The third modified case is expected to print the region maps to only the auxiliary output; and all other output should be the same as the base. The value of this option was successfully interpreted, as the standard output did not include the reactor region maps but the auxiliary output did.

#### *3.2.1.2.3.6 A.DIF3D Type 04 Card Option 4*

The fourth option of the Type 04 card of the A.DIF3D input block accepts values of 0, 1, 2, or 3 as shown in Table 98. The cases evaluated thus far have kept this option at a value of 3, indicating that the DIF3D module will print zone/mesh interval printer-plotter maps to both standard and auxiliary output. This case will evaluate the 0, 1, and 2 options that print no zone/mesh interval printer-plotter maps, print zone/mesh interval printer-plotter maps only to standard output, and print zone/mesh interval printer-plotter maps only to auxiliary output.

The first modified case shall print no zone maps in either standard or auxiliary output and all other outputs should be the same as the base case. This was explicitly confirmed by comparing both outputs with the base case equivalent

The second modified case is expected to print the zone maps to the standard output but not the auxiliary output. The value of this option was successfully interpreted, as the auxiliary output did not include the map but the standard output did.

The third modified case is expected to print the zone maps to only the auxiliary output; and all other output should be the same as the base. The value of this option was successfully interpreted, as the standard output did not include the reactor region maps but the auxiliary output did.

#### *3.2.1.2.4 Rodded Model Verification*

Verification that the A.NIP3 Type 44 card (region assignment to control rod banks) is working as planned, a unique Triangular-Z model was developed that was as simple as possible while still allowing for testing of the use cases of the Type 44 card. To adequately verify the Type 44 card, this work will exercise the Type 44 card in the same six ways previously discussed in the 3D Cartesian diffusion model building section:

1. Simply define a control rod bank that is composed of a single region
2. Define a control rod bank that is composed of two regions, but each region is assigned to the bank on their own Type 44 card
3. Define a control rod bank composed of two regions assigned on the same Type 44 card
4. Define a control rod bank with an area
5. Define a control rod bank with a “blank” name
6. Define a control rod bank with both an area and region being assigned to it.

The above implies that at least six unique control rod banks must be defined with most of these banks containing multiple regions. The minimum number of regions required for the above cases was 10, if we assume the area mentioned in approach 4 has at least 2 regions. Therefore, the three-ring model shown in Figure 44 will be the baseline for this model. It should be noted that the verification of the blank bank name performed in Section 3.1.1.2.11 will not be repeated herein as that work showed that quotation marks, indicating a blank, merely are treated as valid ASCII characters and thus need not be repeated again. Instead this section will still use six banks, but the fifth will be named “BANK5” instead of “ “.

Further, control rod banks must be defined with at least region below each control rod to allow for rod insertion and replacement of the rod region during a withdrawal. This sets the minimum number of regions in each axial slice to two. However, to enable the application of this test case to downstream verification efforts of the REBUS software, which will use these control rod banks for criticality searches, this model will be developed so some control rod banks have regions above and below the rods while other control rod banks only have regions below. Therefore the Figure 44 model will be extruded to consist of three planes, each 10 cm tall, for a total height of 30 cm.



February 13, 2020

All control rod banks will start 10cm above the bottom and a subset of the control rods extending the remaining 20 cm while the remaining control rod banks (specifically, those in the third ring) extending only 10 cm with an additional 10 cm of non-control material above.

The hexagonal regions are labeled with a numbering scheme as “RXYZZ” where X is the plane number (1, 2, or 3), Y is the ring number (1, 2, or 3), and Z is a two digit position within the ring (where the 1 position follows the thirty degree diagonal from the X-axis. The areas that will be used to compose the control rod banks are shown on the left side of Figure 74; these areas are assigned to the second coarse mesh plane from the bottom in the Z dimension. Each hexagon is its own unique region with its own unique composition. The six corresponding control rod banks are shown on the right side of Figure 74. Note that the numbering of the control rod banks corresponds to the six strategies one can apply with the Type 44 card. All banks in the third ring have regions above and below the control rods while all other regions have regions only below the control rods.

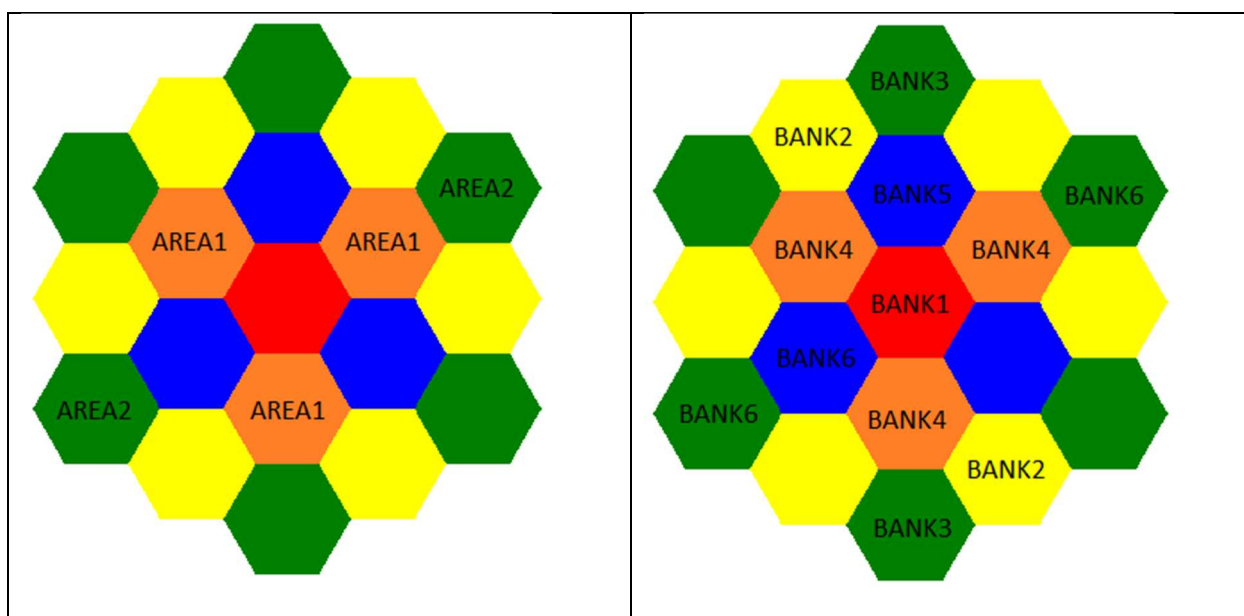


**Figure 74. Control Rod Bank Problem Areas (Left) and Bank Assignments (Right)**

The geometric representation of this model will not be explicitly verified and documented here as this capability was already documented by previous sections. Instead this documentation will verify that the A.NIP3 module properly interprets these options via direct inspection of the standard and auxiliary outputs as well as the LABELS binary file, the only binary file containing control rod information.

The control rod channel specifications begin on line 922 of the standard output as is provided in Figure 75. This table shows each of the six control rod banks and their properties like the regions assigned and the boundaries between the control rods and the regions below and above it. Starting with the bank position, all are at 10 cm above the bottom ( $Z=0$ ) of the model, exactly as



February 13, 2020

incorporated in the model. Additionally, only banks within ring 3 have a region above the rod region. The rod-tip region labels should match that observed based upon the bank locations in Figure 75. These region locations (again, using the RXYZ numbering scheme) indeed match.

The auxiliary output was confirmed to contain the same control rod region table as is shown in Figure 75 and therefore the auxiliary output is also verified.

The LABELS file is a binary representation of the model's region and composition labels, area data, half heights, nuclide set labels, alias zone labels, control rod model data, and burnup-dependent cross section data. Previous LABELS comparisons used the CCCC\_convert program to convert the binary data to ASCII as well as using the CCCC\_PrintTables program. CCCC\_convert, when used to convert this case's LABELS file reports that "CONTROL ROD stuff not supported by CCCC\_convert." CCCC\_PrintTables also encounters a segmentation fault during the processing of the LABELS file.

The custom Python program written to output LABELS information (named "read\_LABELS.py") was therefore utilized again. This output, too long to show here at ~230 lines, was compared with the input, the Figure 75 edits, the triangular meshing scheme sketched in Figure 47, and the rod bank locations in Figure 75. It was found to represent the control rod banks, their rods, and the mesh entries containing those rods faithfully, including adequately handling the cases with and without movable regions above the rods.

922	*** CONTROL-ROD CHANNEL SPECIFICATIONS ***									
923										
924					ROD-TIP	NO. OF				
925	CONTROL-ROD BANK				REGION	MESH CELLS				
926	NO. LABEL		POSITION	LABEL	IN CHANNEL	CHANNEL DESCRIPTION (BOUNDARY, REGION, BOUNDARY, ETC.)				
927										
928	0	1	BANK1	10.00	R2101	6	0.00 R1101	10.00 R2101		
929	0	2	BANK2	10.00	R2310	6	0.00 R1310	10.00 R2310	20.00 R3310	
930					R2304	6	0.00 R1304	10.00 R2304	20.00 R3304	
931	0	3	BANK3	10.00	R2309	6	0.00 R1309	10.00 R2309	20.00 R3309	
932					R2303	6	0.00 R1303	10.00 R2303	20.00 R3303	
933	0	4	BANK4	10.00	R2205	6	0.00 R1205	10.00 R2205		
934					R2203	6	0.00 R1203	10.00 R2203		
935					R2201	6	0.00 R1201	10.00 R2201		
936	0	5	BANK5	10.00	R2202	6	0.00 R1202	10.00 R2202		
937	0	6	BANK6	10.00	R2307	6	0.00 R1307	10.00 R2307	20.00 R3307	
938					R2204	6	0.00 R1204	10.00 R2204		
939					R2301	6	0.00 R1301	10.00 R2301	20.00 R3301	

**Figure 75. Snippet of Relevant Standard Output for Control Rod Bank Problem**

### 3.2.2 One-Region Spatial Eigenvalue Verification

Both hexagonal and triangular-Z geometries in DIF3D have an irregular outer boundaries. Consequently, it is very difficult to construct a simple analytic solution let alone a manufactured solution. The preceding Cartesian benchmarks demonstrate that the fixed source functionality of DIF3D-FD and DIF3D-VARIANT work properly and that an analytic flux solution can be used to assess the accuracy of both solution schemes. The DIF3D-VARIANT functionality is again

verified with DIF3D-FD as DIF3D-VARIANT can also solve the diffusion equation with usage of appropriate angular orders.

Given this approach, in the following set of problems, an analytic solution is desired that can again be used to test the accuracy of the hexagonal geometry. For DIF3D-VARIANT, spatial mesh refinement is not possible as a hexagonal grid is not self-divisible into another hexagonal grid and one must instead rely upon p-refinement. Based upon the preceding Cartesian geometry examples, this approach should be more than sufficient to demonstrate the accuracy of DIF3D-VARIANT in diffusion theory. For DIF3D-FD, the number of triangles used per hexagonal mesh can be refined without changing the number of, an example of which is displayed in Figure 76.

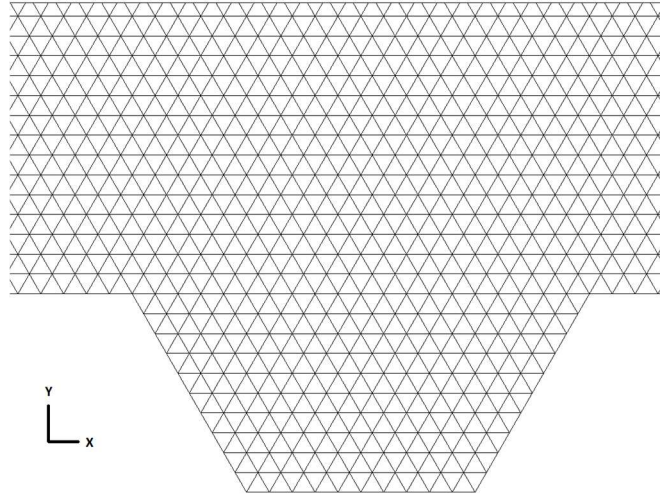


**Figure 76. Triangular-Z Example Sub-meshing of Hex Geometry Input**

This work use the one-group diffusion equation defined earlier as

$$\begin{aligned}
 & -D(x, y, z) \nabla^2 \phi(x, y, z) + \Sigma_R(x, y, z) \phi(x, y, z) = S(x, y, z) \\
 & \left| \begin{aligned}
 S(x, y, z) &= \frac{1}{k_{eff}} \nu \Sigma_f(x, y, z) \phi(x, y, z) \\
 S(x, y, z) &= q(x, y, z) \\
 S(x, y, z) &= \nu \Sigma_f(x, y, z) \phi(x, y, z) + q(x, y, z)
 \end{aligned} \right. \quad . \quad (55)
 \end{aligned}$$

For this work, three example hexagonal geometries shown in Figure 77 are considered. There are two straightforward ways to create an analytic solution. First, a solution can be created in cylindrical coordinates and then conformally map it to the specific hexagonal geometry shown. Alternatively, a solution can be constructed that has an arbitrary solution within the domain but is truncated by the boundary conditions as

$$\phi(x, y, z) = f(x, y, z) \cdot BC(x, y, z) . \quad (56)$$

The easiest example of the second case is to look at the single hex case that has the following six zero flux boundary conditions at the domain x-y interfaces:

$$\left. \begin{aligned} x - \frac{P}{2} &= 0 \\ x + \frac{P}{2} &= 0 \\ \sqrt{3} \cdot y - x - P &= 0 \\ \sqrt{3} \cdot y + x - P &= 0 \\ \sqrt{3} \cdot y - x + P &= 0 \\ \sqrt{3} \cdot y + x + P &= 0 \end{aligned} \right\} \phi = 0. \quad (57)$$

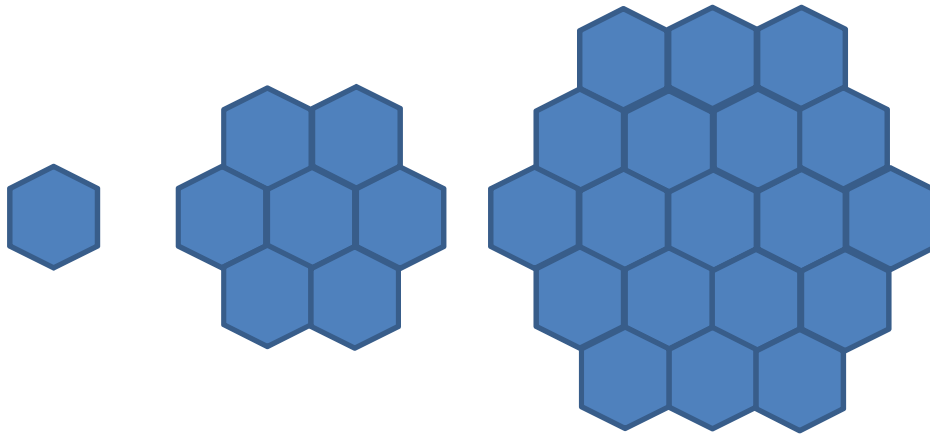


**Figure 77. One, Two, and Three Ring Hexagonal Geometries**

For equation (58), this would translate to the following basic boundary condition definition:

$$BC(x, y) = \left( x - \frac{P}{2} \right) \cdot \left( x + \frac{P}{2} \right) \cdot \left( \sqrt{3} \cdot y - x - P \right) \cdot \left( \sqrt{3} \cdot y + x - P \right) \cdot \left( \sqrt{3} \cdot y - x + P \right) \cdot \left( \sqrt{3} \cdot y + x + P \right) \quad (59)$$

This of course imposes a 6<sup>th</sup> order polynomial function that is zero at the boundary and negative at the center of the domain with a minimum of  $-\frac{1}{4}P^6$ . To make this function more practical for a general application, it can be normalized to

$$BC(x, y) = -\frac{4}{P^6} \left( x - \frac{P}{2} \right) \cdot \left( x + \frac{P}{2} \right) \cdot \left( \sqrt{3} \cdot y - x - P \right) \cdot \left( \sqrt{3} \cdot y + x - P \right) \cdot \left( \sqrt{3} \cdot y - x + P \right) \cdot \left( \sqrt{3} \cdot y + x + P \right) \quad (60)$$

Whatever function is chosen for  $f(x, y, z)$  will still allow the exploration of peaking or spatial asymmetries in the flux solution.

While this approach would seem to be viable, care is necessary to not overrun the possible polynomial basis in DIF3D-VARIANT. To understand, if the same methodology is extended to the two and three ring examples in Figure 77, there would be 12 unique and 18 unique boundary conditions for the two and three ring geometries, respectively. As one should infer, this implies a  $P^{18}$  normalization factor and  $x^{18}$  order polynomial basis. Using a lower order basis expansion in DIF3D-VARIANT will invariably introduce a source approximation inconsistent with the boundary conditions and thus prevent DIF3D-VARIANT from getting an accurate solution. Similarly, the DIF3D-FD spatial mesh approximation would need to be considerably fine to properly capture the complicated source representation defined by such a function.

While this does effectively eliminate this specific scheme, a better behaved scheme can be imposed by using simple sine and cosine functions. Focusing again on the single hex case of Figure 77, a boundary condition function is used as follows:

$$BC(x, y) = \cos\left(\pi \cdot \frac{x}{P}\right) \cdot \cos\left(\pi \cdot \frac{\frac{1}{2}x + \frac{\sqrt{3}}{2}y}{P}\right) \cdot \cos\left(\pi \cdot \frac{-\frac{1}{2}x + \frac{\sqrt{3}}{2}y}{P}\right). \quad (61)$$

This function meets the zero boundary condition at all interfaces and is positive throughout the domain. Extending it to a two or three ring hex case is more problematic as it requires us to take advantage of the periodicity of the cosine function to force the flux to zero at intervals of  $\frac{P}{2}$ . It has the additional problem that for at least half of the domain, it will have a negative flux solution. While the negative flux aspect can be remedied by squaring each cosine function, this will invariably lead to a negative source evaluation at the zero points of the flux. Nevertheless, this can be defined generally as

$$BC(x, y, z) = \sin^2\left(2\pi \frac{x}{P}\right) \cdot \sin^2\left(2\pi \cdot \frac{\frac{1}{2}x + \frac{\sqrt{3}}{2}y}{P}\right) \cdot \sin^2\left(2\pi \cdot \frac{-\frac{1}{2}x + \frac{\sqrt{3}}{2}y}{P}\right) \sin\left(\pi \frac{z}{Z}\right), \quad (62)$$

that is usable on any size hexagonal geometry grid noting that it will display zero flux solutions within the domain and cause a negative source at those points. To introduce peaks in the domain, witch functions are again used to define  $f(x, y, z)$  of the form:

$$f(x, y, z) = \frac{a}{\left(\frac{x}{X} - b\right)^2 + \left(\frac{y}{Y} - c\right)^2 + \left(\frac{z}{Z} - d\right)^2 + \frac{1}{64}}. \quad (63)$$

In this equation, the X and Y values are the maximum and minimum x and y values that occur for a given hexagonal grid that for N rings is determined as  $X = N \cdot P - \frac{P}{2}$  and  $Y = \frac{\sqrt{3}}{2} X$ .

The source representation for this expression is considerably complex and cannot be compactly written in this document. However, it is implemented in a utility program for use with the DIF3D solver. To understand how that was done, the basic logic here is presented herein. The flux solution is first represented as the product of multiple functions

$$\phi(x, y, z) = \prod_{i=1}^I g_i(x, y, z) + \prod_{i=1}^I h_i(x, y, z) + \dots, \quad (64)$$

where the  $g_i(x, y, z)$  functions consist of the separated components of equation (65). The  $h_i(x, y, z)$  represents the inclusion of some other witch function as done previously. In this approach, there would be a maximum of five  $g_i(x, y, z)$  functions and five  $h_i(x, y, z)$ . The source that must be approximated is given as

$$q(x, y, z) = -D\nabla^2\phi(x, y, z) + \Sigma_R\phi(x, y, z) - \chi V\Sigma_f\phi(x, y, z). \quad (66)$$

Focusing on the evaluation of the double derivative the following outcome is obtained

$$\begin{aligned} \nabla^2\phi(x, y, z) &= \frac{\partial}{\partial x} \frac{\partial}{\partial x} \phi(x, y, z) + \frac{\partial}{\partial y} \frac{\partial}{\partial y} \phi(x, y, z) + \frac{\partial}{\partial z} \frac{\partial}{\partial z} \phi(x, y, z) \\ \frac{\partial}{\partial x} \frac{\partial}{\partial x} \phi(x, y, z) &= \frac{\partial}{\partial x} \frac{\partial}{\partial x} \prod_{i=1}^I g_i(x, y, z) + \dots \\ &= \frac{\partial}{\partial x} \sum_{i=1}^I g x_i(x, y, z) \cdot \prod_{\substack{j=1 \\ j \neq i}}^I g_j(x, y, z) \\ &= \sum_{i=1}^I g x x_i(x, y, z) \cdot \prod_{\substack{j=1 \\ j \neq i}}^I g_j(x, y, z) + \sum_{i=1}^I g x_i(x, y, z) \cdot \sum_{\substack{j=1 \\ j \neq i}}^I g x_j(x, y, z) \cdot \prod_{\substack{k=1 \\ k \neq i \\ k \neq j}}^I g_k(x, y, z) \end{aligned} \quad (67)$$

As can be seen, the second derivative with respect to x requires evaluation of the base functions,  $g_i(x, y, z)$ , their single derivatives with respect to x,  $g x_i(x, y, z)$ , and their double derivatives with respect to x,  $g x x_i(x, y, z)$ . The double derivatives with respect to y and z have an identical outcome although the derivatives are obviously with respect to the other dimensions. Given this form, one can envision a simple combination of the  $g_i(x, y, z)$  functions and their derivatives to obtain the flux solution. Given this function is projected onto the basis of the DIF3D-VARIANT polynomial set, the above can trivially be evaluated using Gaussian numerical integration that is the essence of the utility program.

For triangular-Z grids, the above is only slightly more complicated as the domain is a triangle and its orientation changes as shown in Figure 76 (upward and downward facing triangles). Gauss integration points for a triangle for the two triangle systems are thus used. The next step is to determine a separate coordinate transformation for an upward and downward triangle. One primary issue with using the triangle sub-division is that the DIF3D system does not maintain any guidance on where the coordinate center (i.e. central hex position) is located that makes the generic boundary conditions above difficult to use. To identify the originating grid, the first triangle that appears on the first row should always be downward facing if it is the corner of an originating hex. Because

the originating input pitch is not known, the utility program must have the input pitch hardwired into the source code. Given the originating pitch, the boundary conditions can be set based entirely on this one triangle as the boundary conditions are periodic.

To understand what the boundary conditions in equation 3.39 look like, the resulting flux shape without witch functions is shown in Figure 78. As can be seen, the flux profile is very regular and is identical in every hexagon. This picture was made using a 2,640 triangles per hex which is the 20 triangle per side setting of DIF3D-FD. While it may resemble a detailed representation of the flux profile in Figure 78, looking at the legend, one can see that even at this setting, the DIF3D-FD representation of the flux is quite poor. One should also note that the DIF3D-VARIANT polynomial representation of the flux will be less accurate than before because of the more complex flux profile. Consequently, the analysis of this work is limited to a 3 ring hex system with a 40 cm height and 10 cm hexagonal pitch to reduce the computational burden on both DIF3D-FD and DIF3D-VARIANT. From the displayed flux profile, it should be obvious that considerable mesh refinement will be needed in DIF3D-FD.

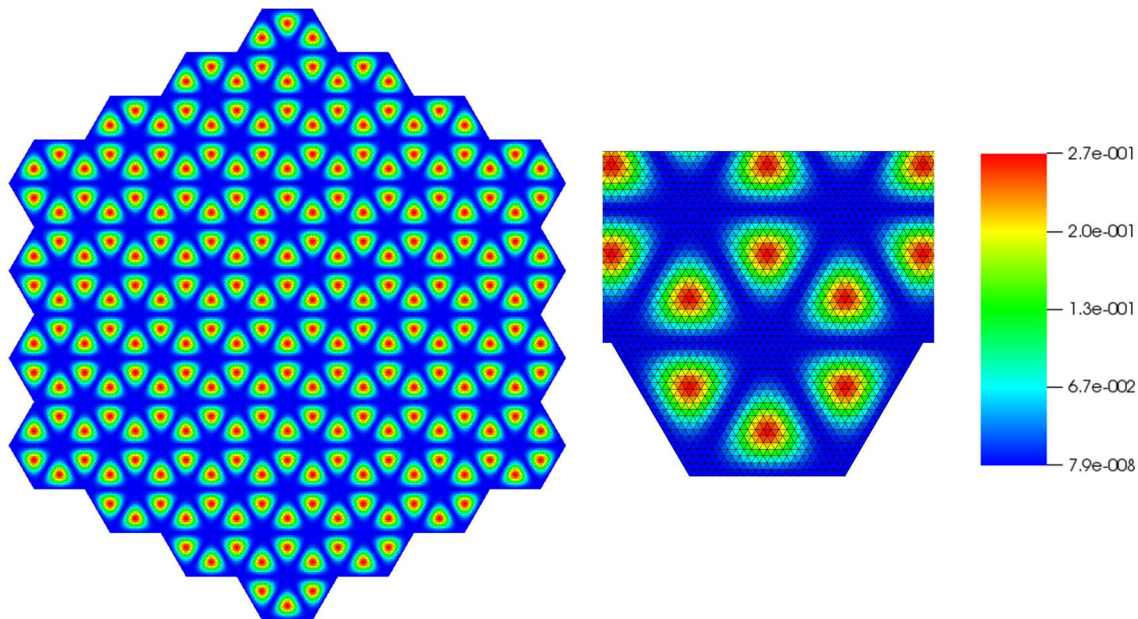


**Figure 78. Four Ring Hexagonal Geometry Boundary Condition Based Flux Profile**

To understand how the witch functions impact the solution, the flux profile of the targeted problem is provided in Figure 79. The witch functions were set to have maximum values at axial positions 4 cm and 28 cm and on opposite sides of the domain. The planer slice shown at the bottom of Figure 79 shows how the two witch functions combine to cause a complex axial flux shape. The x-y position of the peaks will always fall entirely within a given hex because of the boundary condition functions and thus the DIF3D input defines every hex as its own region such that the peaking estimator can be checked. The DIF3D-VARIANT prediction of the peak flux will be considerably off.



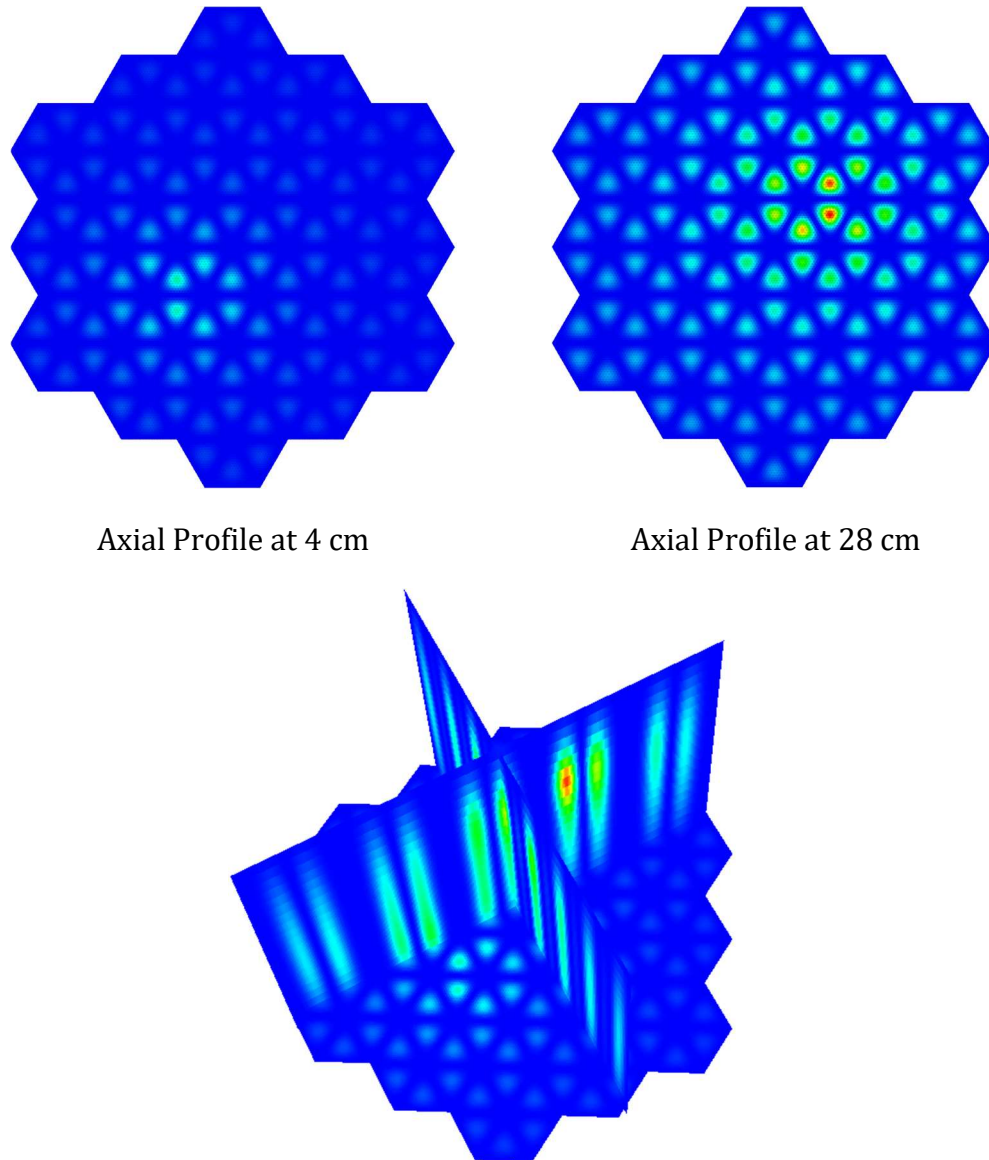


**Figure 79. Flux Profile for the Three Ring Test Problem**

DIF3D-FD was used to solve the described problem using several different mesh settings and the results are shown for the first two meshes in Figure 80. Clearly using 5 axial meshes and 5 meshes per hexagonal edge will yield a rather poor solution as is evident from the 80% errors in Figure 80. What is not expected is that refinement of the mesh to 10 axial meshes and 10 meshes per hexagon edge leads to a much larger error in DIF3D-FD. However, close inspect shows that these errors are associated with the spatial points where the flux reaches its minimum values (i.e. internal zeros). Given the difficult flux profile that is being imposed, it should come as no surprise that

DIF3D-FD struggles to accurately assess these near zero fluxes. If the absolute error is inspected instead of the relative error as defined by equation (68) below, then convergence towards the analytical solution can be observed in Figure 81 with mesh refinement.

$$e = |\phi_{reference} - \phi_{DIF3DFD}| \quad (69)$$

In this case, one can see that the maximum error in any given flux magnitude is consistently dropping as the mesh is refined. Setting a 4 significant digit threshold (i.e. any flux value <0.001 is set to zero) to eliminate the small trivial fluxes, one can observe the average error for each progressive mesh refinement in Figure 81 to be 38%, 34%, 4.8%, and 3.7%. This is further indication that if the zero fluxes are ignored, the error is reduced consistently with mesh refinement.

Because of the computational effort involved with further mesh refinements, the results presented here are sufficient evidence that DIF3D-FD is correctly solving the stated problem given the constraints of accuracy that can be applied with the fixed source input. The assessment of the peaking calculation is deferred to later in this report.

Because radial mesh refinement is not possible in DIF3D-VARIANT, the polynomial order approximation (p-refinement) is the focus of the refinement analysis. In addition, using a 3 ring system provides little information on the spatial distribution and thus a 5 ring system with 4 axial meshes is used. While one would ideally like to contrast DIF3D-FD to DIF3D-VARIANT on the same problem, because the spatial domain is rotated 30 degrees relative to DIF3D-FD, the witch functions appear at different locations of the domain without introducing further geometric rotations. Also, the DIF3D-VARIANT results can at best only compare the average flux solution in each hex that is equivalent to determining whether it computes the average value per hex correctly in DIF3D-FD as opposed to the demonstrated fine mesh details.



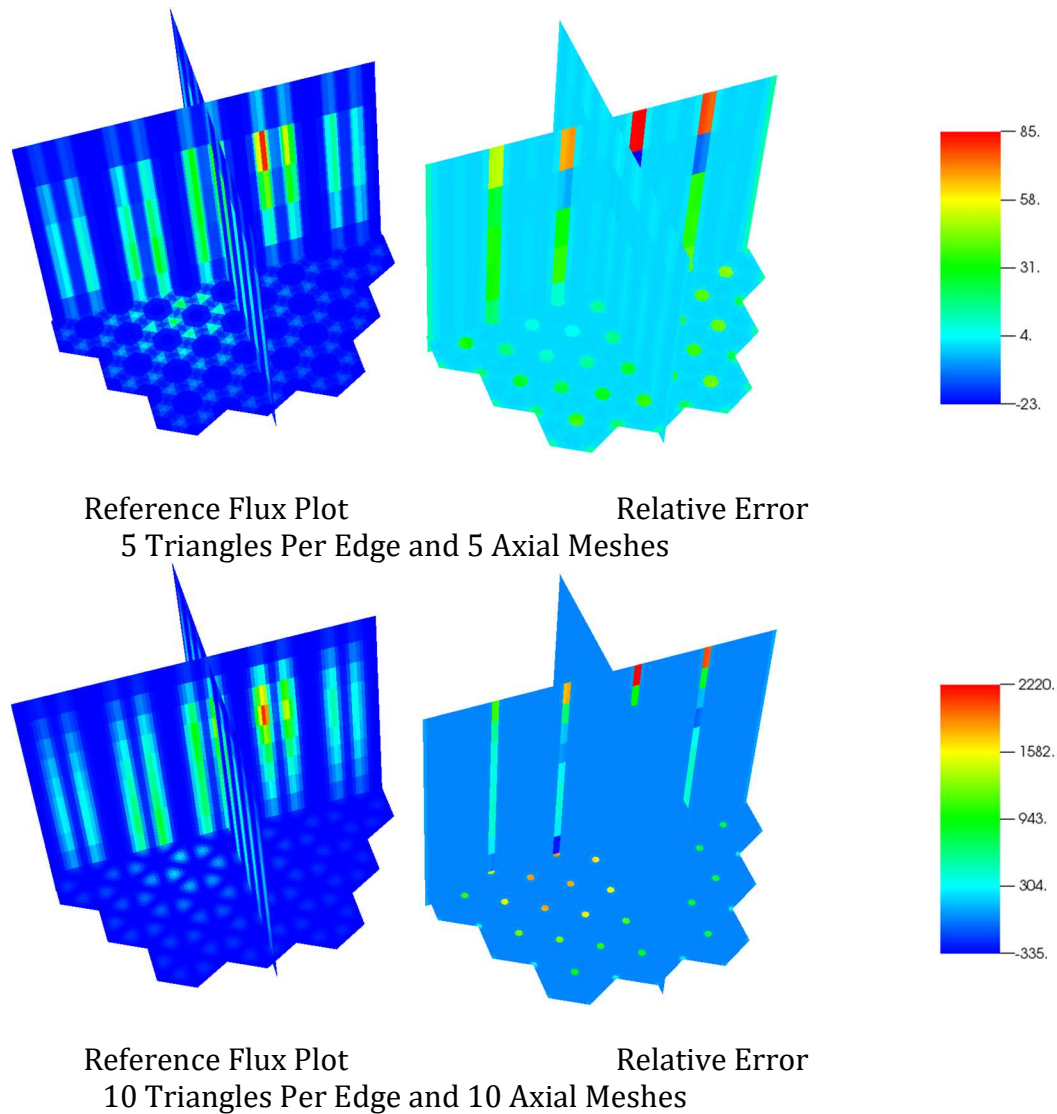


**Figure 80. DIF3D-FD Flux and Error Profile for Two Meshes of the Three Ring Test Problem**

The flux and relative error profiles, averaged over each hex, are given for four different polynomial approximations in Figure 82 and Figure 83. For each calculation, the flux profile is displayed at each of the four axial meshes noting that internal to each hex the flux and source are just as complicated as those presented in Figure 78 and Figure 79. Above each flux distribution is the relative error that is the error between the analytic solution to the average flux per hex and that obtained with DIF3D-VARIANT. At the lowest order approximation, the peak error is 0.67% error and one can see that for the follow on two approximations that it drops consistently to 0.14% and 0.072% error. At the highest polynomial approximation attempted, it increases to 0.37%. Comparing the four error plots one finds that the highest order polynomial approximation has a much higher error on the domain boundary. It is not clear what is causing this particular issue, but the most likely problem is that the representation of the complex flux shape with the polynomial

February 13, 2020

basis is failing. Thus cancellation of error in the low order approximations disappears as the flux order becomes high enough to actually model the real source and flux shape. Because the Gaussian integration scheme is limited by the programmed triangle cubature (18<sup>th</sup> order) in DIF3D-VARIANT, higher polynomial treatments are not presently possible.

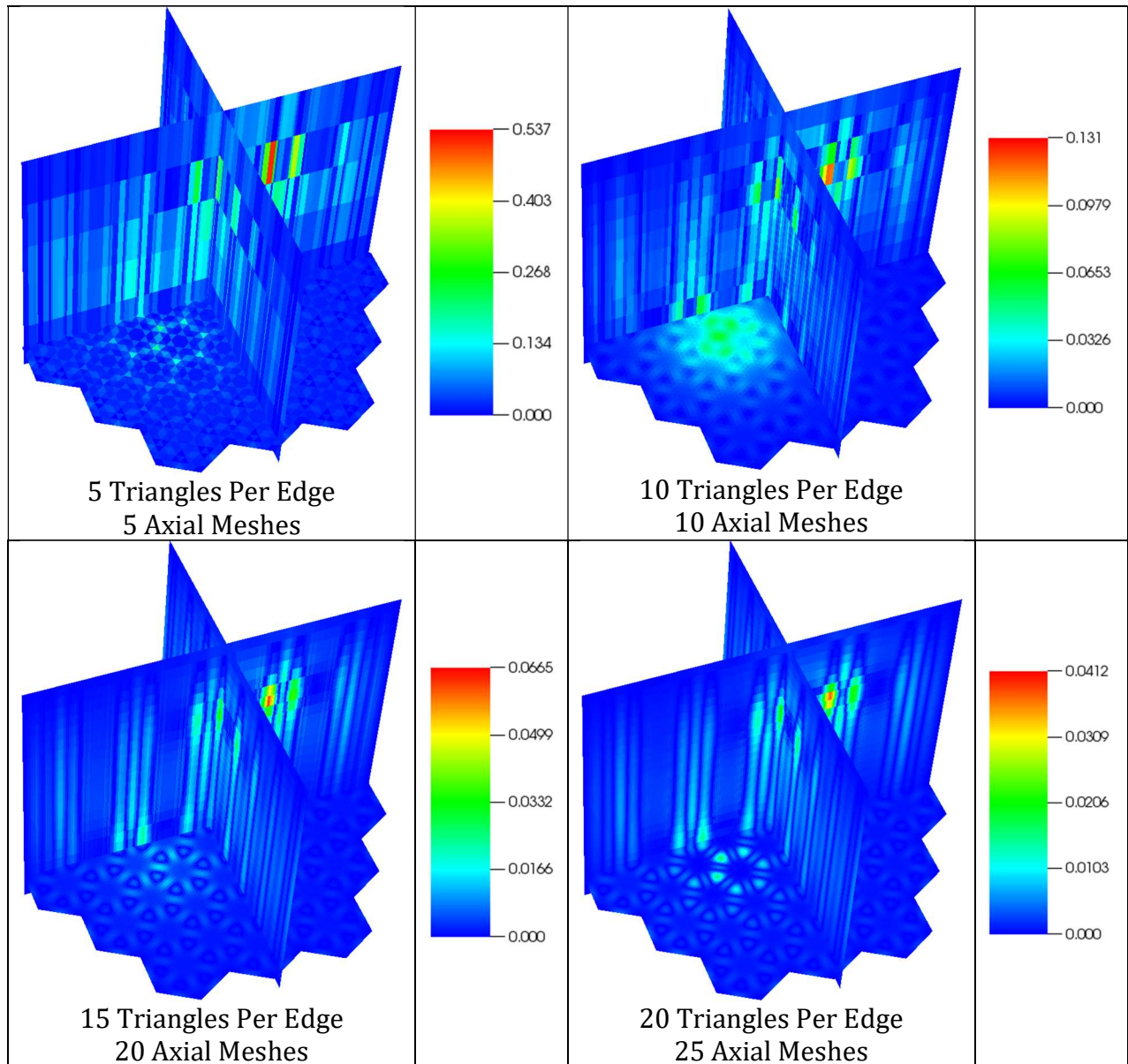
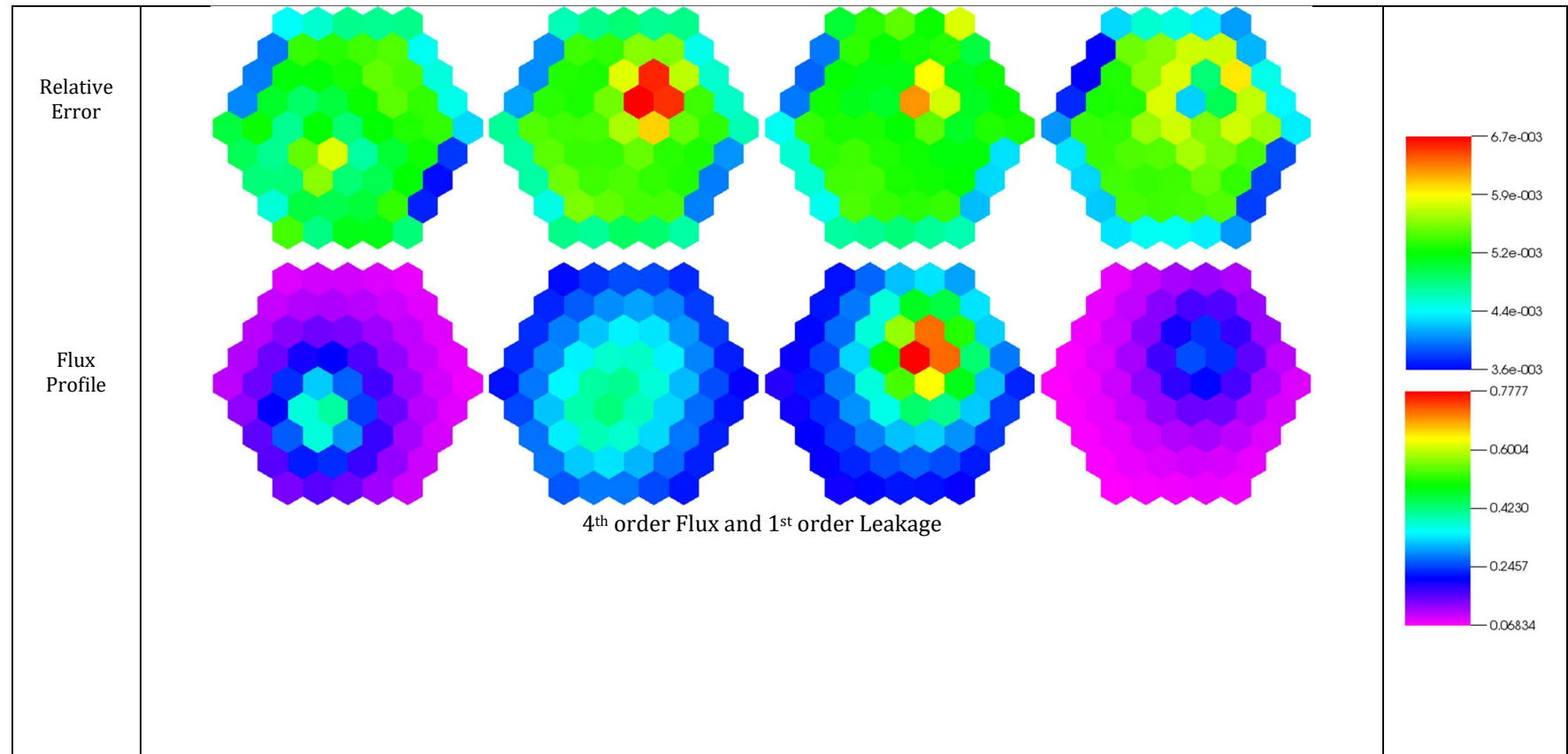
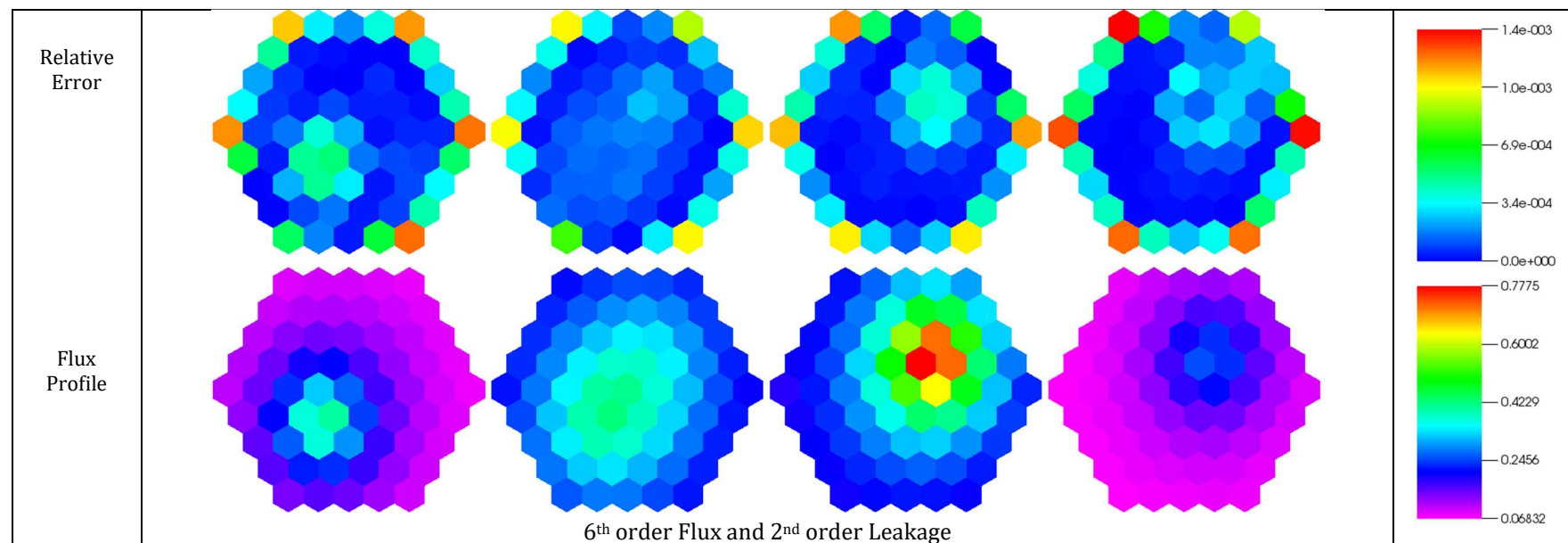


Figure 81. DIF3D-FD Absolute Error Profiles for the Three Ring Test Problem

February 13, 2020

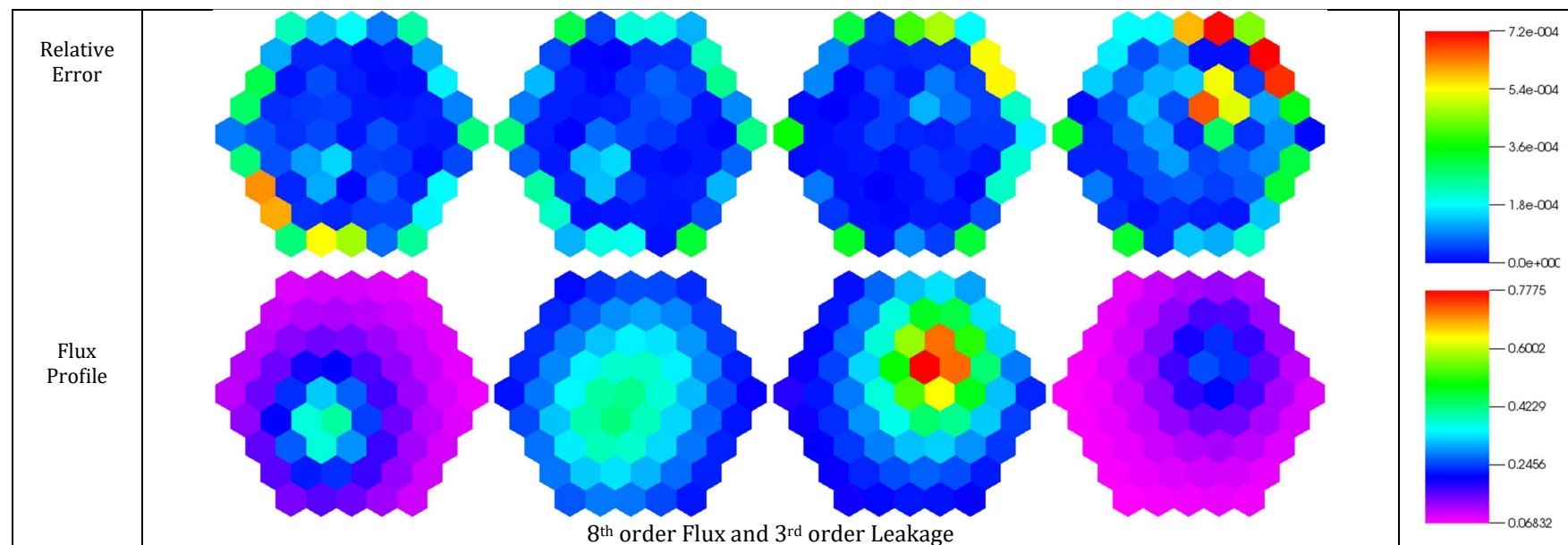


February 13, 2020



**Figure 82. DIF3D-VARIANT Low Order Polynomial Flux and Relative Error Profiles for Five Ring Test Problem**

February 13, 2020



February 13, 2020

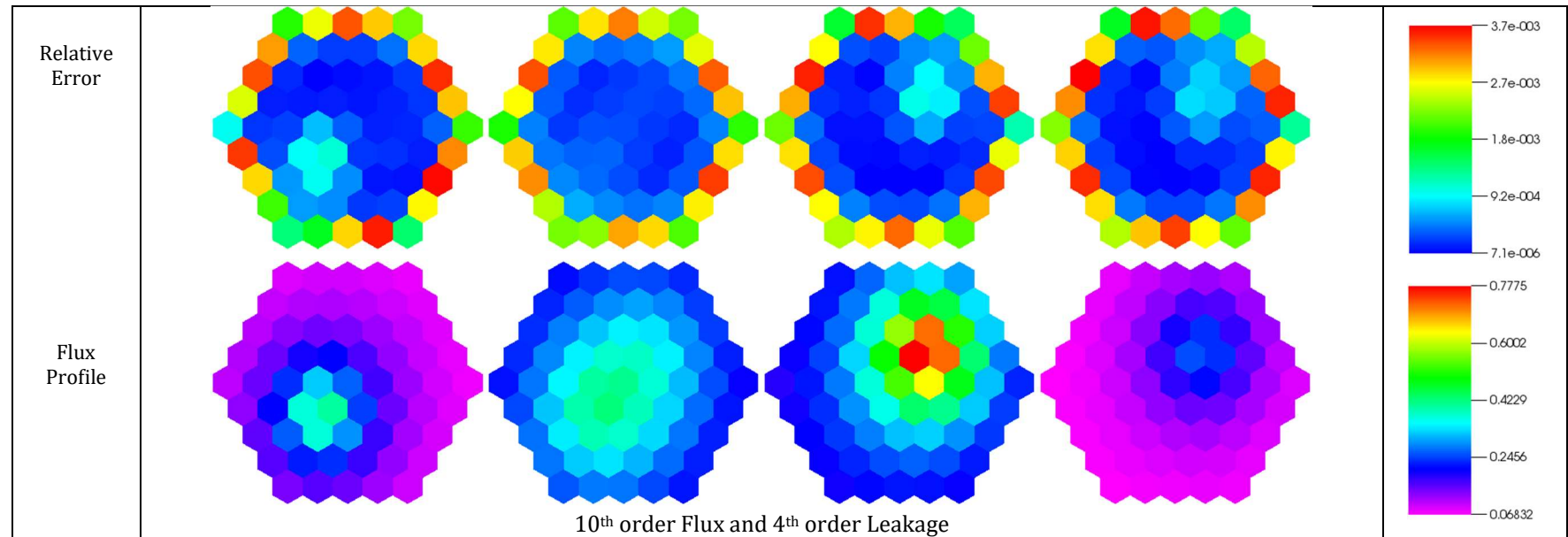


**Figure 83. DIF3D-VARIANT High Order Polynomial Flux and Relative Error Profiles for a Five Ring Test Problem**



February 13, 2020

The last part to verify with this hexagonal geometry problem is the peaking calculation. For both DIF3D-FD and DIF3D-VARIANT, the peak of the flux in each hex can be identified and compared against the actual peak flux output produced by DIF3D. For DIF3D-VARIANT, the EvaluateFlux utility will need to be used to actually obtain comparable peak flux values as the reported numbers are simply the maximum mesh flux values.

Starting with DIF3D-FD, Table 99 provides the peak flux calculations printed out by DIF3D for the four meshes shown previously. Focusing on the finest mesh result, one can observe a very good agreement with the DIF3D-FD result with almost every value 2 significant digits accurate except for HEX201 and HEX204. These two hexes are of course where the witch functions peak and additional mesh refinement is necessary to better represent the steeply peaked flux shape. It is important to note that while the finest mesh attempted is rather accurate, some of the coarse meshes are also sufficiently accurate with the coarsest mesh having mostly unacceptable accuracy. Overall, these results are more than acceptable and convergence towards the analytic solution is observable in almost all of the peak flux results.

Table 99. Peak Flux Predictions of DIF3D-FD

Triangles per Edge	5	10	15	20	Analytic
Axial Meshes	5	10	20	25	
HEX101	3.43	3.69	3.76	3.80	3.84
HEX201	4.14	4.44	4.58	4.63	4.72
HEX202	3.23	3.42	3.47	3.50	3.55
HEX203	1.73	1.80	1.79	1.83	1.84
HEX204	2.11	2.69	2.72	2.79	2.82
HEX205	1.91	2.08	2.17	2.21	2.25
HEX206	2.20	2.37	2.33	2.39	2.39
HEX301	1.63	1.78	1.77	1.81	1.81
HEX302	2.03	2.17	2.12	2.17	2.24
HEX303	1.31	1.37	1.35	1.39	1.42
HEX304	1.34	1.39	1.36	1.40	1.41
HEX305	1.15	1.17	1.14	1.18	1.18
HEX306	1.38	1.40	1.39	1.43	1.43
HEX307	1.34	1.35	1.34	1.38	1.39
HEX308	1.51	1.55	1.52	1.56	1.57
HEX309	1.13	1.18	1.16	1.20	1.21
HEX310	1.24	1.25	1.23	1.26	1.27
HEX311	1.21	1.23	1.20	1.24	1.25
HEX312	1.69	1.84	1.83	1.87	1.88

For DIF3D-VARIANT, the enlargement of the domain and rotation relative to DIF3D-FD leads to a slight alteration and magnitude in the location of the peak values of the flux. There are five rings of data that can be compared and, for brevity, only a subset of the data is compared as seen in Table 100. The DIF3D-VARIANT values in this table are the direct output from DIF3D and generally represent the maximum of the average flux in each hex position. As a consequence, it is no surprise that the DIF3D-VARIANT results do not compare well against the Analytic solution.

**Table 100. Peak Flux Predictions of DIF3D-VARIANT reported by DIF3D**

Flux Order	4	6	8	10	Analytic
Leakage Order	1	2	3	4	
HEX101	0.58	0.57	0.57	0.57	3.17
HEX201	0.69	0.69	0.69	0.69	3.92
HEX202	0.87	0.87	0.87	0.87	4.92
HEX203	0.53	0.53	0.53	0.53	2.91
HEX204	0.46	0.46	0.46	0.46	2.43
HEX205	0.56	0.55	0.55	0.55	2.87
HEX206	0.46	0.46	0.46	0.46	2.40
HEX301	0.52	0.51	0.51	0.51	2.79
HEX302	0.80	0.80	0.80	0.80	4.62
HEX303	0.80	0.80	0.80	0.80	4.59
HEX304	0.63	0.62	0.62	0.62	3.53
HEX305	0.40	0.40	0.40	0.40	2.01
HEX306	0.36	0.36	0.36	0.36	1.76
HEX307	0.37	0.37	0.37	0.37	1.88
HEX308	0.51	0.51	0.51	0.51	2.81
HEX309	0.51	0.51	0.51	0.51	2.76
HEX310	0.42	0.42	0.42	0.42	2.22
HEX311	0.35	0.35	0.35	0.35	1.70
HEX312	0.44	0.44	0.44	0.44	2.30
HEX401	0.34	0.34	0.34	0.34	1.69
HEX501	0.25	0.25	0.25	0.25	1.20

Using the EvaluateFlux utility program, the peak flux values (left table) in Table 101 are obtained from DIF3D-VARIANT at each peak location determined using the analytic solution. Also included (right table) are the flux evaluations at the center of each hex. Looking at the peak flux values, one can see that with low order polynomial approximations, the solutions from DIF3D-VARIANT are very poor with errors  $\gg 100\%$ . As the polynomial order is refined, the peaking results improve, but even at the highest order approximation attempted, it still has significant errors of 20-30%. To better understand why this is occurring, the EvaluateFlux utility was used to check the flux value at the very center of each hex that should be identically equal to zero from the



February 13, 2020

---

imposed flux shape. As was the case with the peaking values, there are substantial errors in the flux magnitude and all of them show that the flux is negative at the chosen point. While the errors are consistently reduced as the polynomial order is increased, it should be clear that even if the 20<sup>th</sup> order polynomial limit is attempted, there will still be errors in the complicated flux shape. Knowing that the integration cubature is not be able to properly evaluate the fixed source in such a high order implementation, no additional effort was spent to evaluate higher order polynomial approximations.

The preceding results demonstrate that the DIF3D-FD and DIF3D-VARIANT solvers are both solving the hexagonal geometry based diffusion equation correctly. No additional checks on the DIF3D output were made beyond verifying the average hexagonal flux and peak flux in each hex. This test problem was very difficult to create and, based upon the results above, there is no point in constructing additional test problems as they would invariably be more difficult to solve and at best be duplicative of the presented case. Because the flux solution for both solvers is quite good and consistent with the analytic solution, the presented results for DIF3D-FD and DIF3D-VARIANT are considered to be sufficient evidence for verification. This conclusion is further supported by the previous usage of the same technique to study the Cartesian geometry implementation where DIF3D-VARIANT performed excellently.

February 13, 2020

**Table 101. Peak Flux (left) and Zero Flux (right) Predictions of DIF3D-VARIANT reported by the EvaluateFlux Utility**

Flux	4	6	8	10	13	Analytic
Leakage	1	2	3	4	5	
HEX101	0.94	1.32	1.51	2.22	3.00	3.17
HEX201	1.16	1.62	1.85	2.66	3.66	3.92
HEX202	1.43	1.99	2.28	3.27	4.59	4.92
HEX203	0.88	1.20	1.41	2.16	2.86	2.91
HEX204	0.71	0.96	1.14	1.57	2.30	2.43
HEX205	0.85	1.16	1.34	1.78	2.58	2.87
HEX206	0.72	1.01	1.15	1.69	2.28	2.40
HEX301	0.84	1.17	1.33	1.93	2.62	2.79
HEX302	1.38	1.91	2.17	2.98	4.17	4.62
HEX303	1.35	1.88	2.15	3.03	4.24	4.59
HEX304	1.05	1.45	1.67	2.42	3.32	3.53
HEX305	0.61	0.84	0.98	1.52	1.99	2.01
HEX306	0.53	0.74	0.84	1.25	1.69	1.76
HEX307	0.57	0.73	0.90	1.22	1.85	1.88
HEX308	0.81	1.10	1.30	1.82	2.63	2.81
HEX309	0.80	1.09	1.28	1.79	2.58	2.76
HEX310	0.67	0.88	1.05	1.44	2.13	2.22
HEX311	0.52	0.73	0.82	1.19	1.63	1.70
HEX312	0.70	0.98	1.10	1.61	2.17	2.30
HEX401	0.52	0.74	0.82	1.14	1.56	1.69
HEX501	0.37	0.52	0.58	0.80	1.11	1.20

Flux	4	6	8	10	13
Leakage	1	2	3	4	5
HEX101	0.33	-0.39	-0.48	-0.25	-0.08
HEX201	0.36	-0.32	-0.47	-0.27	-0.07
HEX202	0.39	-0.32	-0.49	-0.28	-0.08
HEX203	0.33	-0.35	-0.46	-0.25	-0.07
HEX204	0.27	-0.40	-0.45	-0.21	-0.07
HEX205	0.26	-0.43	-0.46	-0.21	-0.07
HEX206	0.30	-0.37	-0.45	-0.23	-0.07
HEX301	0.32	-0.26	-0.40	-0.24	-0.06
HEX302	0.37	-0.28	-0.45	-0.27	-0.07
HEX303	0.37	-0.27	-0.45	-0.27	-0.07
HEX304	0.35	-0.29	-0.44	-0.26	-0.07
HEX305	0.29	-0.29	-0.39	-0.21	-0.06
HEX306	0.26	-0.33	-0.40	-0.20	-0.06
HEX307	0.23	-0.35	-0.38	-0.18	-0.06
HEX308	0.22	-0.41	-0.42	-0.18	-0.06
HEX309	0.22	-0.41	-0.41	-0.18	-0.06
HEX310	0.25	-0.38	-0.42	-0.19	-0.06
HEX311	0.26	-0.31	-0.39	-0.20	-0.06
HEX312	0.30	-0.29	-0.41	-0.22	-0.06
HEX401	0.26	-0.22	-0.33	-0.19	-0.05
HEX501	0.20	-0.18	-0.26	-0.15	-0.04

### 3.2.3 *Extrapolated and Reflected Boundary Conditions Verification*

This problem will verify the extrapolated flux boundary condition on these faces. This will be done with the infinite-medium, multigroup, analytical eigenvalue case from Section 3.1.2 using the first cross section dataset provided in Table 50.

This will be performed using the same methodology discussed for the 3D Cartesian equivalent in Section 3.1.9. As a reminder, this will be done for each of the faces by replacing the initial reflective boundary condition with an escape boundary condition. Then, this escape boundary condition will be replaced with an extrapolated boundary condition option with an extrapolation constant mathematically consistent with an escape boundary condition. At this stage it is expected that the escape boundary and extrapolated-escape boundary shall yield the same eigenvalue. Next, the extrapolation constant will be reduced to a value of 0 (with a few steps along the way) to mimic a reflective boundary condition. Along the way, the default value of 0.4692 will be manually entered as well as left blank to verify the correctness of the manual that this is the default value.

As discussed previously, an escape flux boundary condition can be mimicked by setting the extrapolated boundary condition constant,  $A$ , to an infinitely large value. In this case  $10^{10}$  will be used. A reflective boundary condition can similarly be mimicked by setting  $A$  to 0. For each of the evaluated cases, the five faces that are not provided in the surface column have a reflective boundary condition applied. To ensure a true infinite homogeneous medium problem, the 3-Group material used in the Cartesian problem above also had to be used as a background material. This was repeated for full-core (A.NIP3 geometry type 100), sixth-core (geometry type 90), and third-core (geometry type 94) Triangular-Z geometries. Performing each of these geometry types is necessary as the mesh and orientation of the triangles is different for each of these cases. The resultant eigenvalue results are provided in Table 102 and its follow-on tables.

The coloring scheme used in Table 82 is applied here as well wherein each consistent colors imply the values are expected to be similar. From these tables it is clear that the infinite homogeneous results (the red eigenvalues) are all consistent. However, it is evident in these tables that the eigenvalues within each color set have surface-specific eigenvalues. For example, in the full-core results of Table 102, we see that the escape eigenvalue (blue) is 1.56764 on the X surfaces, 1.56999 on the Y surfaces, and 1.36533 on the Z surfaces. The X surface and Y surfaces yield different results due to differences in the triangular orientations on the edges leading to a different mesh along each of these axes. Theoretically these would converge as the number of triangles is increased, however that was not performed. Finally, the Z surface results match those obtained in Table 82 (to the 10<sup>th</sup> digit) as the Z axis is the same in 3D Cartesian and Triangular-Z geometries.

Since these differences are understood, and the general trends of eigenvalue increasing as reflective BCs are approached, this capability is considered verified for the Triangular-Z diffusion solver.

February 13, 2020

Table 102. Full-Core Triangular-Z DIF3D-FD Extrapolated Boundary Condition Results

Surf.	Boundary Condition	A	Eigenvalue	Surf.	Boundary Condition	A	Eigenvalue
All	Reflected	N/A	1.60000000916	-			
Lower X	Escape	N/A	1.56764344167	Upper Y	Escape	N/A	1.56999394075
	Extrapolated	$10^{10}$	1.56764344167		Extrapolated	$10^{10}$	1.56999394075
		10	1.56791208689			10	1.57024020048
		0.46920 (manually entered)	1.57203914701			0.46920 (manually entered)	1.57436316737
		0.46920 (DIF3D default)	1.57203914701			0.46920 (DIF3D default)	1.57436316737
		0	1.60000000916			0	1.60000000916
Upper X	Escape	N/A	1.56764344167	Lower Z	Escape	N/A	1.36533288123
	Extrapolated	$10^{10}$	1.56764344167		Extrapolated	$10^{10}$	1.36533288124
		10	1.56791208689			10	1.37029149079
		0.46920 (manually entered)	1.57203914701			0.46920 (manually entered)	1.43882439651
		0.46920 (DIF3D default)	1.57203914701			0.46920 (DIF3D default)	1.43882439651
		0	1.60000000916			0	1.60000000916
Lower Y	Escape	N/A	1.56999394048	Upper Z	Escape	N/A	1.36533288123
	Extrapolated	$10^{10}$	1.56999394048		Extrapolated	$10^{10}$	1.36533288124
		10	1.57024020021			10	1.37029149079
		0.46920 (manually entered)	1.57436316711			0.46920 (manually entered)	1.43882439651
		0.46920 (DIF3D default)	1.57436316711			0.46920 (DIF3D default)	1.43882439651
		0	1.60000000916			0	1.60000000916

February 13, 2020

**Table 103. Sixth-Core Triangular-Z DIF3D-FD Extrapolated Boundary Condition Results**

Surf.	Boundary Condition	A	Eigenvalue	Surf.	Boundary Condition	A	Eigenvalue
All	Reflected	N/A	1.60000000911	-			
Lower X	Escape	N/A	1.40863927233	Upper Y	Escape	N/A	1.40863927240
	Extrapolated	$10^{10}$	1.40863927233		Extrapolated	$10^{10}$	1.40863927241
		10	1.41219612087			10	1.41219612094
		0.46920 (manually entered)	1.46229037735			0.46920 (manually entered)	1.46229037745
		0.46920 (DIF3D default)	1.46229037735			0.46920 (DIF3D default)	1.46229037745
		0	1.60000000911			0	1.60000000911
Upper X	Escape	N/A	1.40863927245	Lower Z	Escape	N/A	1.36533288120
	Extrapolated	$10^{10}$	1.40863927246		Extrapolated	$10^{10}$	1.36533288121
		10	1.41219612099			10	1.37029149076
		0.46920 (manually entered)	1.46229037749			0.46920 (manually entered)	1.43882439647
		0.46920 (DIF3D default)	1.46229037749			0.46920 (DIF3D default)	1.43882439647
		0	1.60000000911			0	1.60000000911
Lower Y	Escape	N/A	1.40863927238	Upper Z	Escape	N/A	1.36533288120
	Extrapolated	$10^{10}$	1.40863927238		Extrapolated	$10^{10}$	1.36533288121
		10	1.41219612091			10	1.37029149076
		0.46920 (manually entered)	1.46229037739			0.46920 (manually entered)	1.43882439647
		0.46920 (DIF3D default)	1.46229037739			0.46920 (DIF3D default)	1.43882439647
		0	1.60000000911			0	1.60000000911

**Table 104. Third-Core Triangular-Z DIF3D-FD Extrapolated Boundary Condition Results**

Surf.	Boundary Condition	A	Eigenvalue	Surf.	Boundary Condition	A	Eigenvalue
All	Reflected	N/A	1.60000000912	-			
Lower X	Escape	N/A	1.50676960755	Upper Y	Escape	N/A	1.56999394075
	Extrapolated	$10^{10}$	1.50676960755		Extrapolated	$10^{10}$	1.56999394075
		10	1.50807467663			10	1.57024020048
		0.46920 (manually entered)	1.52758821556			0.46920 (manually entered)	1.57436316737
		0.46920 (DIF3D default)	1.52758821556			0.46920 (DIF3D default)	1.57436316737
		0	1.60000000912			0	1.60000000916
	Escape	N/A	1.50676960736		Escape	N/A	1.36533288123
Upper X	Extrapolated	$10^{10}$	1.50676960736	Lower Z	Extrapolated	$10^{10}$	1.36533288124
		10	1.50807467643			10	1.37029149079
		0.46920 (manually entered)	1.52758821538			0.46920 (manually entered)	1.43882439651
		0.46920 (DIF3D default)	1.52758821538			0.46920 (DIF3D default)	1.43882439651
		0	1.60000000912			0	1.60000000916
	Escape	N/A	1.50676960745		Escape	N/A	1.36533288123
	Escape	N/A	1.50676960745		Escape	N/A	1.36533288124
Lower Y	Extrapolated	$10^{10}$	1.50807467652	Upper Z	Extrapolated	$10^{10}$	1.37029149079
		0.46920 (manually entered)	1.52758821546			0.46920 (manually entered)	1.43882439651
		0.46920 (DIF3D default)	1.52758821546			0.46920 (DIF3D default)	1.43882439651
		0	1.60000000912			0	1.60000000916
	Escape	N/A	1.50676960745		Escape	N/A	1.36533288123
	Escape	N/A	1.50676960745		Escape	N/A	1.36533288124
	Escape	N/A	1.50676960745		Escape	N/A	1.36533288124

### 3.2.4 Radial Periodic Boundary Conditions Verification

To verify DIF3D's ability to apply periodic boundary conditions in the radial plane, a simple Hexagonal-Z model was created comprising of two unique regions. This model was represented in a full-core DIF3D model as well as an equivalent periodic model and the results compared. This was repeated for both sixth-core and third-core symmetric models.

Figure 84 provides the A.NIP3 blocks for the sixth-core symmetric models; the full-core model is on the left and the periodic model is on the right. Unlike the similar cases presented for 3D Cartesian and Hexagonal-Z elsewhere in this document, the resultant reactor region mesh is not provided as with Triangular-Z geometry this is a quite large plot. The same comparison is essentially provided in Figure 138, which is the same model, but for the Hexagonal-Z geometry. However, these were inspected and verified consistent. This particular core laydown was chosen

February 13, 2020

amongst others for its simplicity but also because it could not be represented with a reflective boundary condition. The error between the full-core and periodic models was 0.67 pcm. The flux values matched, when accounting for the factor of six increase in the area-normalized flux and the tenuous rearrangement due to the different triangular meshing strategies applied, to the 3<sup>rd</sup> or 4<sup>th</sup> significant digit.

UNIFORM=A.NIP3 01 FULL_CORE 02 0 3 40000000 40000000 40000000 40000000 0 3 3 3 03 100 04 9 9 9 9 10 10 09 Z 2 50. 29 10. 4 30 REG1 1 1 1 0. 50. 30 REG1 2 1 6 0. 50. 30 REG1 3 1 12 0. 50. 30 REG1 4 1 18 0. 50. 30 REG3 4 2 2 0. 50. 30 REG3 4 5 5 0. 50. 30 REG3 4 8 8 0. 50. 30 REG3 4 11 11 0. 50. 30 REG3 4 14 14 0. 50. 30 REG3 4 17 17 0. 50. 14 COMP1 ISO1 1.0 15 COMP1 REG1 14 COMP3 ISO3 1.0 15 COMP3 REG3	UNIFORM=A.NIP3 01 PERIODIC 02 0 3 40000000 40000000 40000000 40000000 0 3 3 3 03 90 04 7 9 9 9 10 10 09 Z 2 50. 29 10. 4 30 REG1 1 1 1 0. 50. 30 REG1 2 1 6 0. 50. 30 REG1 3 1 12 0. 50. 30 REG1 4 1 18 0. 50. 30 REG3 4 2 2 0. 50. 30 REG3 4 5 5 0. 50. 30 REG3 4 8 8 0. 50. 30 REG3 4 11 11 0. 50. 30 REG3 4 14 14 0. 50. 30 REG3 4 17 17 0. 50. 14 COMP1 ISO1 1.0 15 COMP1 REG1 14 COMP3 ISO3 1.0 15 COMP3 REG3
--	--

Figure 84. Sixth-Core Periodic Triangular-Z Input and Core Map

Similarly, Figure 85 provides the A.NIP3 blocks for the third-core symmetric models. Again, this particular core laydown was chosen amongst others for its simplicity but also because it could not be represented with a reflective boundary condition. The error in the full-core and periodic models was 1 pcm. The flux values matched, when accounting for the factor of six increase in the area-normalized flux and the tenuous rearrangement due to the different triangular meshing strategies applied, to the 3<sup>rd</sup> or 4<sup>th</sup> significant digit.

UNIFORM=A.NIP3 01 FULL_CORE 02 0 3 40000000 40000000 40000000 40000000 0 3 3 3 03 100 04 9 9 9 9 10 10 09 Z 2 50. 29 10. 4 30 REG1 1 1 1 0. 50. 30 REG1 2 1 6 0. 50. 30 REG1 3 1 12 0. 50. 30 REG1 4 1 18 0. 50. 30 REG3 4 5 5 0. 50. 30 REG3 4 11 11 0. 50. 30 REG3 4 17 17 0. 50. 14 COMP1 ISO1 1.0 15 COMP1 REG1 14 COMP3 ISO3 1.0 15 COMP3 REG3	UNIFORM=A.NIP3 01 PERIODIC 02 0 3 40000000 40000000 40000000 40000000 0 3 3 3 03 94 04 7 9 9 9 10 10 09 Z 2 50. 29 10. 4 30 REG1 1 1 1 0. 50. 30 REG1 2 1 6 0. 50. 30 REG1 3 1 12 0. 50. 30 REG1 4 1 18 0. 50. 30 REG3 4 5 5 0. 50. 30 REG3 4 11 11 0. 50. 30 REG3 4 17 17 0. 50. 14 COMP1 ISO1 1.0 15 COMP1 REG1 14 COMP3 ISO3 1.0 15 COMP3 REG3
--	--

Figure 85. Third-Core Periodic Triangular-Z Input and Core Map

### 3.2.5 Iteration and Convergence Control Verification

Table 9 of the [6] plan identified that the iteration and convergence control options (A.DIF3D Type 3.4, 3.6, 3.9, 3.10, 3.11, 3.12, 5.2, 5.3, 5.4, 12.5, 12.6, and 12.11) would be verified by way of the Integral Verification case. These options will be verified in this section, however, a

February 13, 2020

DIF3D-FD version of the multigroup eigenvalue problem discussed for transport verification in Section 3.4.3 will be used instead. This was done for no other reason than that problem is smaller than the integral benchmark problem and thus runs faster, but also converges slowly enough that the effect of these options will be readily apparent. Note that this is only performed for a forward eigenvalue case and not repeated for a fixed source or adjoint case as the same convergence control code is exercised for any of these solves.

This test will be performed by first running a base case that leaves all relevant parameters to their internal defaults. Then, a case will be performed where the defaults are explicitly specified in their respective cards. Next, using the explicitly listed defaults as the starting point, the options verified by this section will be modified from their default to the possible values. The possible values will either be every value in the discrete set, or if the variable can be continuous (like the number of iterations) then a sufficient number will be evaluated. The specific parameters, their defaults, and their perturbations are provided in Table 105. After executing all these cases, the output will be analyzed to ensure that DIF3D respected the option according to the description provided in the A.DIF3D listing. The restart capability will then be checked with two additional cases discussed in the final subsection.

**Table 105. Iteration Control Options for the Diffusion Solver**

Card Type	Summary	Default Value	Perturbed Values
3.4	Tchebyshev Acceleration	0	1
3.6	Outer Iteration Control	30	-4, -3, -2, -1, 10
3.9	Upscatter Iterations per Outer Iteration	5	20
3.10	Concurrent Iteration Efficiency	0	1
3.11	Accel. Of Opt. Overrelaxation	0	1
3.12	Opt. Overrelaxation Factor Calculation Control	50	2
5.2	Eigenvalue Criterion	$10^{-7}$	$10^{-3}$
5.3	Pointwise Fiss. Source Criterion	$10^{-5}$	$10^{-4}$
5.4	Avg. Fiss. Source Criterion	$10^{-5}$	$10^{-4}$

### 3.2.5.1 Base and Default Cases

As noted, the first step performed was to first execute a case where all of the above values were simply not included in the input, and thereby DIF3D applied the default value. Then, a case was executed with these values explicitly stated. The outputs were compared using a python Diff tool, and it was found that the outputs indeed matched, except for the input edits and some slight changes to a few of the iteration times, which are subject to external factors and cannot be controlled. Therefore the default case will be used as the starting point going forward.



While not a part of this verification effort, it was noted that the A.DIF3D listing states that the Type 03 card's 5<sup>th</sup> parameter (minimum plane-block size for input/output transfer) has a default of 4500, however this was found to actually be 10000.

All cases that remain will compare to this default case, but modified to utilize 2,000 iterations to convergence so that the total number of iterations to convergence can be observed as these options change.

### 3.2.5.2 Card 3 Option 4 Perturbations

Card 3 Option 4 sets whether or not Tchebyshev acceleration of the outer iterations is performed. The default value, 0, indicates it shall be performed, while a value of 1 turns off this acceleration. Therefore, when the value of 1 is used, one should expect that either more iterations will be required to converge. Additionally, DIF3D's echo repeat should acknowledge the setting of this option.

The correct echo repeat was confirmed. Additionally, the case with acceleration was found to converge in 55 iterations while the case without acceleration required 256 iterations. The eigenvalue matched exactly and the flux values matched the default case to within 3-4 significant figures.

### 3.2.5.3 Card 3 Option 6 Perturbations

Card 3 Option 6 controls the number of outer iterations in a case. The possible values are -1 (data management parameters, overrelaxation factors, and neutronics edits are performed), -2 (same as -1 without overrelaxation factors), -3 (DIF3D module is bypassed), -4 (same as -2, but with leakage results derived from the balance equation with zero residual), or some number greater than 0 that simply sets the maximum number of DIF3D outer iterations. The default value is 30 total iterations. This case will evaluate the 4 negative options as well as ensuring 10 total iterations are obeyed.

Option -4 was verified to skip the DIF3D iteration and skip the inner iteration optimization strategy edits as well as the outer iteration summary (i.e., DIF3D did not solve the diffusion equation). Further, the balance edits were compared between this and the base case. Here, the leakage terms were clearly derived from the balance residual, as the leakages were the equivalent to the default case's balance + leakage.

Option -3 was verified to not execute the DIF3D module, instead only processing the geometry and zone information from the A.NIP3 and A.HMG4C blocks.

Option -2 produced the same output as option -4 except for the balance edits, which were the same in Option -2 as the base case.

Option -1 computed the over relaxation factors, but did not perform the diffusion system solve.

Finally, a value of +10 performed exactly as expected, yielding 10 total iterations before quitting.

### 3.2.5.4 Card 3 Option 9 Perturbations

Card 3 Option 9 sets the number of upscatter iterations per outer iteration. The default is 5, and this case applied 20. Since DIF3D-FD does not print the number of upscatters for each outer iteration, this can only be indirectly inferred. Specifically, it was found that the per-iteration convergence metrics and final results did vary in the final significant digit, further an additional 3 iterations were required to converge, indicating that the additional upscatter iterations were necessary. The eigenvalue matched the default and the flux matched to the third or fourth significant digit. This does indicate a different inner iteration strategy was performed.

### 3.2.5.5 Card 3 Option 10 Perturbations

Card 3 Option 10 sets a flag that instructs DIF3D to either perform the estimated number of inner iterations for each group (option 0), or to avoid the last pass of the inner iterations in groups whose number of iterations are less than some non-user-facing threshold. The default value is not specified by the A.DIF3D listing.

For the given problem this option seems to have no effect. This could very well be because the iterations are always greater than the threshold. The eigenvalue and flux matched the default to all reported digits.

### 3.2.5.6 Card 3 Option 11 Perturbations

Card 3 Option 11 sets a flag that instructs DIF3D to either not perform acceleration of the optimum overrelaxation factor calculation (option 0, default), or apply asymptotic source extrapolation of the power iterations during the spectral radius calculation (option 1).

This was observed by a message indicating the truncation of the convergence on the optimum overrelaxation factor calculation iteration, as well as different omega values and a different iteration history though the same total number of iterations. The eigenvalues matched exactly and only the last significant digit of one region (and one group) flux was different.

### 3.2.5.7 Card 3 Option 12 Perturbations

Card 3 Option 12 sets the number of iterations when determining the optimum overrelaxation factors. A positive integer is supplied and a value of 50 is strongly recommended. In this case a value of 2 was applied instead.

This problem yielded omegas with values of 1.0 for all three groups. This implies the factors did not modify (significantly) from their initial guess of 1.0 after the 2<sup>nd</sup> iteration. This affected the convergence history though the same number of outer iterations were required. The eigenvalue matched the default and the flux matched to the third or fourth significant digit.

### 3.2.5.8 Card 5 Option 2 Perturbations

Card 5 Option 2 provides the floating point eigenvalue convergence criterion. The default is a value of  $10^{-7}$ . This case will apply a value of  $10^{-4}$ . To ensure the eigenvalue convergence is limiting, the pointwise and average fission source convergence tolerances were set to 0.01. Therefore, increasing the eigenvalue convergence (compared to the base case) should reduce the total number of iterations such that the fission source convergence is limiting.

This was indeed observed, as the case with a  $10^{-4}$  eigenvalue convergence criterion converged in 15 iterations instead of the base case's 55 iterations. Further, this was achieved when the eigenvalue dropped below  $10^{-4}$ ; the fission source measures had already passed 0.01.

### 3.2.5.9 Card 5 Option 3 Perturbations

Card 5 Option 3 provides the floating point pointwise fission source convergence criterion. The default is a value of  $10^{-5}$ . This perturbation case will apply a value of  $10^{-4}$ . Like the previous case, the other convergence parameters were set so the pointwise fission source convergence criterion was limiting. Specifically, this means that the eigenvalue and average fission source criterion were 0.01 while the pointwise fission source criterion was  $10^{-4}$ . In this case, we should see the iterations end when the fission source criterion is met.

This was indeed observed, as the case with a  $10^{-4}$  pointwise fission source convergence criterion converged in 40 iterations instead of the base case's 55 iterations. Further, this convergence was achieved when the pointwise fission source was converged to less than  $10^{-4}$ , the provided value.

### 3.2.5.10 Card 5 Option 4 Perturbations

Card 5 Option 4 provides the floating point average fission source convergence criterion. The default is a value of  $10^{-5}$ . This perturbation case will apply a value of  $10^{-4}$ . Since the default case reaches the eigenvalue convergence after the fission source is converged to the stated value, then the parameters were also set that the average fission source convergence criterion was limiting. Specifically, this means that the eigenvalue and pointwise fission source criterion were 0.01 while the average fission source criterion was  $10^{-4}$ . In this case, the iterations should complete when the fission source criterion is met.

This was indeed observed, as the case with a  $10^{-4}$  average fission source convergence criterion converged in 37 iterations instead of the base case's 55 iterations. Further, this convergence was achieved when the rel. sum error of the fission source was converged to less than  $10^{-4}$ , the provided value.

### 3.2.5.11 Restart Calculation

A restart computation can be performed with three approaches in DIF3D: (1) the binary DIF3D and RTFLUX files from the previous computation are provided via the "BLOCK=OLD" input block; (2) a restart is performed with the RTFLUX (or NHFLUX if DIF3D-VARIANT) file and a combination of A.DIF3D Type 06 and possibly 07 cards; or (3) DIF3D is executed and then

restarted with tighter convergence criterion (or number of iterations) from within the same input. This sub-section will test these approaches using a restart from the default case that terminated itself after 30 iterations.

The first approach was performed with the BLOCK=OLD RTFLUX and DIF3D files, and a single card in the A.DIF3D block that set the maximum number of iterations to 2,000 instead of the 30 of the previous computation (and thus in the DIF3D binary file). After running this in DIF3D, it is expected that (1) DIF3D's user input specifications would echo the changes to the number of iterations, state that this is a restart, and include the  $k_{\text{eff}}$  from the restart RTFLUX file (2) the initial  $k_{\text{eff}}$  from the 1<sup>st</sup> iteration of the new calculation should differ from the original calculation's first guess, (3) the outer iterations should continue until the new calculation's convergence criteria are met, and (4) the final eigenvalue and reported fluxes should match to the precision of the convergence criterion. All of these were observed, indicating the binary file-based restart was successful.

The second approach (previous RTFLUX and Type 06/Type 07 cards) was also performed with only the BLOCK=OLD RTFLUX file and Type 06 and Type 07 cards. The A.DIF3D module was modified to include the  $k_{\text{eff}}$  and dominance ratio from the 30 iteration calculation, and the restart flag set to 1 (indicating a restart should be performed). The restart case also had the number of iterations set to 2,000. After running this in DIF3D, it is expected that 1) DIF3D's user input specifications echo would the changes to the number of iterations, state that this is a restart, and include the initial  $k_{\text{eff}}$  2) the initial  $k_{\text{eff}}$  from the 1<sup>st</sup> iteration of the new calculation should differ from the original calculation's first guess, 3) the outer iterations should continue until the new calculation's convergence criteria are met, and (4) the final eigenvalue and reported fluxes should match to on the order of the convergence criterion. All of these were observed, indicating the restart was successful.

The third approach (restarting within same input file) was performed by executing the original DIF3D case to 30 iterations, using the DIF3D and RTFLUX files which were just generated with modifications for an increase number of iterations, and re-executing DIF3D. Similar behavior should be observed with this case compared to the original. This was confirmed, indicating this restart methodology was successful.

Further, these methods output files and convergence histories matched to within the convergence criterion, indicating both effectively perform the same function within DIF3D.

### 3.2.6 Solution Edit Verification

DIF3D prints a balance of the solution results in the form of neutron balance edits, power edits, flux edits, zone-averaged flux edits, and region-averaged flux edits. In addition to these changes are the writing of the SFEDIT, RZFLUX, and PWDINT interface files. All of these are controlled by options 6 through 11 of the A.DIF3D module's Type 04 card. This section will verify that these options are correctly obeyed. This section will also verify the correctness of the neutron balance tables, as these are the only tables that are not verified elsewhere.

The verification that the edit toggles can be performed with any model. The verification of the correctness of the neutron balances requires a model that utilizes multiple regions, one or more areas, and has cross sections with more than one group. Further, as the individual parameters will be calculated independent from DIF3D, a small model is desirable.

To that end, the four composition cross sections used in Section 3.1.1 and defined in Table 23 and Table 26 will be applied with a 2-ring, 10cm pitch, and 10 cm tall triangular-Z model. The lower 5 cm of the core has REG1 in the central position and REG2 in the 2<sup>nd</sup> ring. The upper 5 cm has REG3 in the central position and REG4 in the outer ring. The model is modelled in sixth-core symmetry and with reflective boundary conditions applied on all sides. Finally, AREA1 is defined as all four regions while AREA2 is only REG1. The A.NIP3 input (aside from the composition definitions) is provided in Figure 86.

```

UNFORM=A.NIP3
01  TRIZ - EDITS
02 0 3 40000000 40000000 40000000 40000000 0 3 3 3
03 96
04 3 3 3 3 3 3
09 Z 1 5.0 1 10.
29 10. 2
30 REG1 1 1 1 0. 5.
30 REG2 2 1 6 0. 5.
30 REG3 2 1 6 5. 10.
30 REG4 1 1 1 5. 10.
07 AREA1 REG1 REG2 REG3 REG4
07 AREA2 REG1

```

**Figure 86. Triangular-Z Diffusion Edit Table Model**

To verify that the edit toggles were correctly verified, the same A.DIF3D Type 04 cards used in Section 3.1.11 and provided in Table 84 were applied. Again, the first four do not print the binary interface files while the last two do. The first should print none of the edits of interest. The second prints all edits to standard and auxiliary output. The third prints only to auxiliary output. The fourth to only standard output. The final two cases print the surface fast flux and power density to the SFEDIT file in mesh cell order and then in region order. Each of these six tasks was verified to ensure the output was produced as intended; no deficiencies were noted.

The next task is to verify the correctness of the PWDINT file. This was performed by comparing these files, after conversion to ASCII with the afore-mentioned CCCC\_convert utility, to the power density values provided in the already-verified DIF3D ASCII edits.

Similarly, the RZFLUX files were verified consistent with the already verified flux edit tables as well as by comparing the neutron loss terms to those provided in the standard output (and verified later in this section). This was performed by evaluating the binary files using a custom Python program quite similar to the RTFLUX reading interface. Similar to the 3D Cartesian DIF3D-FD case, it was identified that the total neutron losses and absorption values in this file were zero, despite the problem containing losses and absorption. All other terms, including the zone-averaged fluxes were as expected.

February 13, 2020

It was then verified that the SFEDIT files were printed, and that the case 5 SFEDIT file is different from the case 6 SFEDIT file by comparing the MD5 hashes of each file. The accuracy of the contents of these files, however, was not verified as part of this work.

The final task to be performed in this section is the verification of the correctness of the neutron balance tables. DIF3D outputs these quantities in one table per group, and a final table containing the information integrated over all energy groups. Each of these tables contains three sets of balance information. The data within each of these balance sets are provided in Table 106, Table 107, and Table 108, respectively. In addition to this region data, similar output was provided for areas. The areas were chosen such that this comparison was trivial, AREA1 was all four regions, and thus should be equivalent to the Total row; AREA2 was defined as REG1 and therefore should be equivalent to the corresponding REG1 row. This was verified to be true.

**Table 106. DIF3D Neutron Balance Table Set 1**

Region	Net Leakage	Absorption Rate	Out-Scatter	In-Scatter	Fission Production	External Source	Balance
<b>Group 1</b>							
<b>REG1</b>	-9.1833E+07	7.7176E+05	9.1061E+07	0.0000E+00	0.0000E+00	0.0000E+00	3.8743E-06
<b>REG2</b>	8.8495E+07	9.9860E+08	1.3535E+10	0.0000E+00	1.4622E+10	0.0000E+00	1.4890E+02
<b>REG3</b>	-8.6239E+08	1.4381E+09	1.5859E+10	5.5663E+06	1.6429E+10	0.0000E+00	-1.3969E+02
<b>REG4</b>	8.6572E+08	1.1052E+09	3.8864E+08	1.5384E+06	2.3581E+09	0.0000E+00	5.8417E+00
<b>Total</b>	1.1921E-07	3.5426E+09	2.9873E+10	7.1047E+06	3.3409E+10	0.0000E+00	1.5048E+01
<b>Group 2</b>							
<b>REG1</b>	8.6218E+07	4.8427E+06	0.0000E+00	9.1061E+07	0.0000E+00	0.0000E+00	4.7684E-07
<b>REG2</b>	-7.0147E+08	1.5735E+10	-3.1742E-06	1.4264E+10	7.6956E+08	0.0000E+00	7.8366E+00
<b>REG3</b>	1.9665E+09	1.7955E+10	5.5663E+06	1.9464E+10	4.6291E+08	0.0000E+00	-3.9360E+00
<b>REG4</b>	-1.3512E+09	1.8821E+09	1.5384E+06	5.3239E+08	0.0000E+00	0.0000E+00	-5.9605E-07
<b>Total</b>	2.3842E-07	3.5577E+10	7.1047E+06	3.4351E+10	1.2325E+09	0.0000E+00	3.9006E+00
<b>Group-Integrated</b>							
<b>REG1</b>	-5.6145E+06	5.6145E+06	9.1061E+07	9.1061E+07	0.0000E+00	0.0000E+00	4.3511E-06
<b>REG2</b>	-6.1298E+08	1.6734E+10	1.3535E+10	1.4264E+10	1.5391E+10	0.0000E+00	1.5673E+02
<b>REG3</b>	1.1041E+09	1.9393E+10	1.5864E+10	1.9470E+10	1.6892E+10	0.0000E+00	-1.4363E+02
<b>REG4</b>	-4.8550E+08	2.9873E+09	3.9018E+08	5.3393E+08	2.3581E+09	0.0000E+00	5.8417E+00
<b>Total</b>	3.5763E-07	3.9119E+10	2.9880E+10	3.4358E+10	3.4641E+10	0.0000E+00	1.8949E+01

February 13, 2020

Table 107. DIF3D Neutron Balance Table Set 2

Region	Planar Leakage	Y Leakage	Z Leakage	Tot. Buckling	X Buckling	Y Buckling	Z Buckling
<b>Group 1</b>							
<b>REG1</b>	1.7024E+08	0.0000E+00	-2.6207E+08	-3.3506E-04	6.2113E-04	0.0000E+00	-9.5620E-04
<b>REG2</b>	-1.7024E+08	0.0000E+00	2.5873E+08	1.7121E-04	-3.2936E-04	0.0000E+00	5.0058E-04
<b>REG3</b>	-6.0365E+08	3.7253E-09	-2.5873E+08	-2.5502E-03	-1.7851E-03	1.1016E-20	-7.6511E-04
<b>REG4</b>	6.0365E+08	0.0000E+00	2.6207E+08	1.0299E-02	7.1816E-03	0.0000E+00	3.1178E-03
<b>Total</b>	0.0000E+00	3.7253E-09	0.0000E+00	9.8263E-20	0.0000E+00	3.0707E-21	0.0000E+00
<b>Group 2</b>							
<b>REG1</b>	-2.3936E+08	0.0000E+00	3.2558E+08	3.1068E-03	-8.6253E-03	0.0000E+00	1.1732E-02
<b>REG2</b>	2.3936E+08	3.7253E-09	-9.4084E+08	-1.4305E-02	4.8811E-03	7.5966E-20	-1.9186E-02
<b>REG3</b>	1.0256E+09	-5.5879E-9	9.4084E+08	3.0913E-02	1.6123E-02	-8.784E-20	1.4790E-02
<b>REG4</b>	-1.0256E+09	0.0000E+00	-3.2558E+08	-2.2541E-01	-1.7110E-01	0.0000E+00	-5.4313E-02
<b>Total</b>	1.1921E-07	-1.8627E-9	5.9605E-08	1.6286E-18	8.1428E-19	-1.272E-20	4.0714E-19
<b>Group-Integrated</b>							
<b>REG1</b>	-6.9127E+07	0.0000E+00	6.3512E+07	-1.8602E-05	-2.2903E-04	0.0000E+00	2.1043E-04
<b>REG2</b>	6.9127E+07	3.7253E-09	-6.8210E+08	-1.0832E-03	1.2215E-04	6.5829E-21	-1.2053E-03
<b>REG3</b>	4.2199E+08	-1.8627E-9	6.8210E+08	2.7480E-03	1.0503E-03	-4.636E-21	1.6977E-03
<b>REG4</b>	-4.2199E+08	0.0000E+00	-6.3512E+07	-5.3914E-03	-4.6861E-03	0.0000E+00	-7.0530E-04
<b>Total</b>	1.1921E-07	1.8627E-09	5.9605E-08	2.6305E-19	8.7682E-20	1.3700E-21	4.3841E-20



Table 108. DIF3D Neutron Balance Table Set 3

Region	Capture Rate	Fission Rate	(n,2n) Source	Net Prod'n	Median E. Fiss Src	Median E. Abs. Rate	Med E. Flux
<b>Group 1</b>							
<b>REG1</b>	7.7176E+05	0.0000E+00	-	-	-	-	-
<b>REG2</b>	4.8888E+08	5.0972E+08	-	-	-	-	-
<b>REG3</b>	9.9769E+08	4.4036E+08	-	-	-	-	-
<b>REG4</b>	8.3527E+08	2.6995E+08	-	-	-	-	-
<b>Total</b>	2.3226E+09	1.2200E+09	-	-	-	-	-
<b>Group 2</b>							
<b>REG1</b>	4.8427E+06	0.0000E+00	-	-	-	-	-
<b>REG2</b>	5.3122E+09	1.0423E+10	-	-	-	-	-
<b>REG3</b>	6.2144E+09	1.1741E+10	-	-	-	-	-
<b>REG4</b>	3.8983E+08	1.4922E+09	-	-	-	-	-
<b>Total</b>	1.1921E+10	2.3655E+10	-	-	-	-	-
<b>Group-Integrated</b>							
<b>REG1</b>	5.6145E+06	0.0000E+00	0.0000E+00	0.0000E+00	0.0000E+00	9.0696E-03	2.7317E+02
<b>REG2</b>	5.8011E+09	1.0932E+10	7.2928E+08	1.6121E+10	2.8733E+03	5.3038E-03	1.2732E+02
<b>REG3</b>	7.2121E+09	1.2181E+10	3.6052E+09	2.0497E+10	3.5290E+03	5.8208E-03	1.8288E+01
<b>REG4</b>	1.2251E+09	1.7622E+09	1.4374E+08	2.5018E+09	4.4721E+03	9.9345E-02	1.1601E+03
<b>Total</b>	1.4244E+10	2.4876E+10	4.4782E+09	3.9119E+10	3.2798E+03	6.4912E-03	7.0132E+01

To verify these, an independent computation of these values is necessary. These quantities were obtained from standard reaction-rate calculations given the edited DIF3D flux solution. The DIF3D output provides notes on what specific quantities compose each of these balance columns. The only quantities that were not trivially computed are the median energies (last three columns of Table 87) and the leakage terms. The median energies are thoroughly defined in Chapter 3 of the DIF3D-FD manual [1]. The leakage terms are the same as one would expect with diffusion theory; these are defined in Chapter 2 of the DIF3D-FD manual and specifically in Eq. 2.15 and Table 2.2 of [1]. The quantities that are provided in the three tables that follow were computed in such a way using a Python script that used information accessible in Python via the same scripts used to convert the DIF3D inputs to an equivalent MCNP information. Namely, the RTFLUX, GEODST, and COMPS information.

These computed reference balance values are provided in the following tables are in the same format as the DIF3D output values above. As can be seen, the reference and DIF3D values match very well, with differences being less than the significant digits shown here. The largest errors are seen with the total balance, however, these values are significantly less than the terms in the rows, that are summed to produce the balance. Thus this also is simply numerical truncation error. A sanity check was performed by ensuring that the leakage, absorption, fission, and (n,2n) production



February 13, 2020

rates yields the same eigenvalue as reported by DIF3D. This was observed to be true. Like the DIF3D-FD 3D Cartesian case, the median energy computations in DIF3D replace a 0 eV group boundary with  $1.382882 \times 10^{-5}$  eV. This energy was therefore used internally by DIF3D in generating the reference results.

Therefore this DIF3D edit table is considered verified. It should be noted that for completeness, the above was also repeated for third- and full-core symmetry options, these also matched.

**Table 109. Reference Neutron Balance Table Set 1**

Region	Net Leakage	Absorption Rate	Out-Scatter	In-Scatter	Fission Production	External Source	Balance
<b>Group 1</b>							
<b>REG1</b>	-9.1833E+07	7.7176E+05	9.1061E+07	0.0000E+00	0.0000E+00	0.0000E+00	3.9488E-06
<b>REG2</b>	8.8495E+07	9.9860E+08	1.3535E+10	0.0000E+00	1.4622E+10	0.0000E+00	4.2065E+02
<b>REG3</b>	-8.6239E+08	1.4381E+09	1.5859E+10	5.5663E+06	1.6429E+10	0.0000E+00	1.6566E+02
<b>REG4</b>	8.6572E+08	1.1052E+09	3.8864E+08	1.5384E+06	2.3581E+09	0.0000E+00	4.9668E+01
<b>Total</b>	-1.1921E-07	3.5426E+09	2.9873E+10	7.1047E+06	3.3409E+10	0.0000E+00	6.3598E+02
<b>Group 2</b>							
<b>REG1</b>	8.6218E+07	4.8427E+06	0.0000E+00	9.1061E+07	0.0000E+00	0.0000E+00	4.6194E-07
<b>REG2</b>	-7.0147E+08	1.5735E+10	-3.1742E-06	1.4264E+10	7.6956E+08	0.0000E+00	2.2140E+01
<b>REG3</b>	1.9665E+09	1.7955E+10	5.5663E+06	1.9464E+10	4.6291E+08	0.0000E+00	4.6677E+00
<b>REG4</b>	-1.3512E+09	1.8821E+09	1.5384E+06	5.3239E+08	0.0000E+00	0.0000E+00	-4.7684E-07
<b>Total</b>	2.3842E-07	3.5577E+10	7.1047E+06	3.4351E+10	1.2325E+09	0.0000E+00	2.6807E+01
<b>Group-Integrated</b>							
<b>REG1</b>	-5.6145E+06	5.6145E+06	9.1061E+07	9.1061E+07	0.0000E+00	0.0000E+00	4.4107E-06
<b>REG2</b>	-6.1298E+08	1.6734E+10	1.3535E+10	1.4264E+10	1.5391E+10	0.0000E+00	4.4279E+02
<b>REG3</b>	1.1041E+09	1.9393E+10	1.5864E+10	1.9470E+10	1.6892E+10	0.0000E+00	1.7033E+02
<b>REG4</b>	-4.8550E+08	2.9873E+09	3.9018E+08	5.3393E+08	2.3581E+09	0.0000E+00	4.9668E+01
<b>Total</b>	1.3411E-07	3.9119E+10	2.9880E+10	3.4358E+10	3.4641E+10	0.0000E+00	6.6279E+02

February 13, 2020

Table 110. Reference Neutron Balance Table Set 2

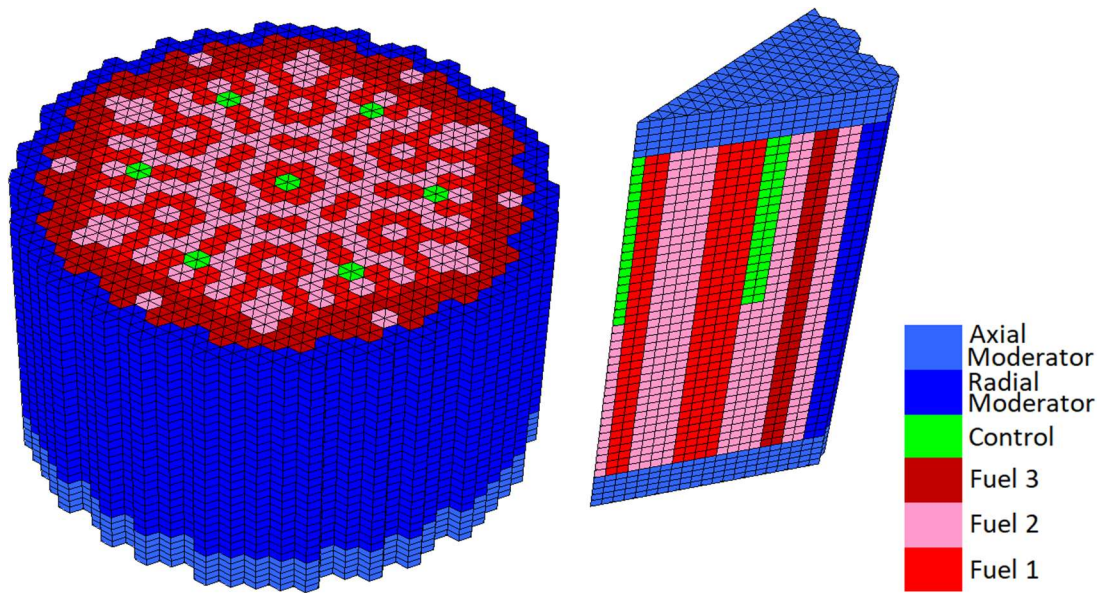
Region	Planar Leakage	Y Leakage	Z Leakage	Tot. Buckling	X Buckling	Y Buckling	Z Buckling
<b>Group 1</b>							
<b>REG1</b>	1.7024E+08	0.0000E+00	-2.6207E+08	-3.3506E-04	6.2113E-04	0.0000E+00	-9.5620E-04
<b>REG2</b>	-1.7024E+08	0.0000E+00	2.5873E+08	1.7121E-04	-3.2936E-04	0.0000E+00	5.0058E-04
<b>REG3</b>	-6.0365E+08	-1.8627E-9	-2.5873E+08	-2.5502E-03	-1.7851E-03	0.0000E+00	-7.6511E-04
<b>REG4</b>	6.0365E+08	0.0000E+00	2.6207E+08	1.0299E-02	7.1816E-03	0.0000E+00	3.1178E-03
<b>Total</b>	0.0000E+00	-1.8627E-9	0.0000E+00	0.0000E+00	0.0000E+00	0.0000E+00	0.0000E+00
<b>Group 2</b>							
<b>REG1</b>	-2.3936E+08	0.0000E+00	3.2558E+08	3.1068E-03	-8.6253E-03	0.0000E+00	1.1732E-02
<b>REG2</b>	2.3936E+08	-2.7940E-9	-9.4084E+08	-1.4305E-02	4.8811E-03	0.0000E+00	-1.9186E-02
<b>REG3</b>	1.0256E+09	-5.5879E-9	9.4084E+08	3.0913E-02	1.6123E-02	0.0000E+00	1.4790E-02
<b>REG4</b>	-1.0256E+09	0.0000E+00	-3.2558E+08	-2.2541E-01	-1.7110E-01	0.0000E+00	-5.4313E-02
<b>Total</b>	0.0000E+00	-8.3819E-9	0.0000E+00	0.0000E+00	0.0000E+00	0.0000E+00	0.0000E+00
<b>Group-Integrated</b>							
<b>REG1</b>	-6.9127E+07	0.0000E+00	6.3512E+07	-1.8602E-05	-2.2903E-04	0.0000E+00	2.1043E-04
<b>REG2</b>	6.9127E+07	-2.7940E-9	-6.8210E+08	-1.0832E-03	1.2215E-04	0.0000E+00	-1.2053E-03
<b>REG3</b>	4.2199E+08	-7.4506E-9	6.8210E+08	2.7480E-03	1.0503E-03	0.0000E+00	1.6977E-03
<b>REG4</b>	-4.2199E+08	0.0000E+00	-6.3512E+07	-5.3914E-03	-4.6861E-03	0.0000E+00	-7.0530E-04
<b>Total</b>	0.0000E+00	-1.0245E-8	0.0000E+00	0.0000E+00	0.0000E+00	0.0000E+00	0.0000E+00

Table 111. Reference Neutron Balance Table Set 3

Region	Capture Rate	Fission Rate	(n,2n) Source	Net Prod'n	Median E. Fiss Src	Median E. Abs. Rate	Med E. Flux
<b>Group 1</b>							
<b>REG1</b>	7.7176E+05	0.0000E+00	-	-	-	-	-
<b>REG2</b>	4.8888E+08	5.0972E+08	-	-	-	-	-
<b>REG3</b>	9.9769E+08	4.4036E+08	-	-	-	-	-
<b>REG4</b>	8.3527E+08	2.6995E+08	-	-	-	-	-
<b>Total</b>	2.3226E+09	1.2200E+09	-	-	-	-	-
<b>Group 2</b>							
<b>REG1</b>	4.8427E+06	0.0000E+00	-	-	-	-	-
<b>REG2</b>	5.3122E+09	1.0423E+10	-	-	-	-	-
<b>REG3</b>	6.2144E+09	1.1741E+10	-	-	-	-	-
<b>REG4</b>	3.8983E+08	1.4922E+09	-	-	-	-	-
<b>Total</b>	1.1921E+10	2.3655E+10	-	-	-	-	-
<b>Group-Integrated</b>							
<b>REG1</b>	5.6145E+06	0.0000E+00	0.0000E+00	0.0000E+00	0.0000E+00	9.0696E-03	2.7317E+02
<b>REG2</b>	5.8011E+09	1.0932E+10	7.2928E+08	1.6121E+10	2.8733E+03	5.3038E-03	1.2732E+02
<b>REG3</b>	7.2121E+09	1.2181E+10	3.6052E+09	2.0497E+10	3.5290E+03	5.8208E-03	1.8288E+01
<b>REG4</b>	1.2251E+09	1.7622E+09	1.4374E+08	2.5018E+09	4.4721E+03	9.9345E-02	1.1601E+03
<b>Total</b>	1.4244E+10	2.4876E+10	4.4782E+09	3.9119E+10	3.2798E+03	6.4912E-03	7.0132E+01

### 3.2.7 Integral Verification

The purpose of the integral verification test is to compare both the eigenvalue and flux distribution against externally obtained solutions. The VVER-440 model [13] was chosen as the comparison case given the available external solutions in the literature. The full-core geometry for this case is shown in Figure 87. This core has 30 degree symmetry and thus the 30 degree sector of interest is shown. Two group cross sections were provided in [13]. The hexagonal pitch is 14.7 cm. The total geometry height is 300 cm; the active core region is 250 cm and there are 25 cm of moderator regions above and below the active core. A portion of control rods are inserted 150 cm from the bottom.



**Figure 87. VVER-440 Benchmark Model**

The original reference solution was obtained in [13] by extrapolating the DIF3D-FD  $k_{\text{eff}}$  to the  $k_{\text{eff}}$  that would be obtained when using an infinitesimally small mesh element size. The result was a  $k_{\text{eff}}$  of 1.01132. A whole core power distribution assuming ten axial regions for each assembly was also provided. Table 112 provides the triangular mesh size (side length of the triangle), the axial mesh size, and the resulting DIF3D-FD  $k_{\text{eff}}$  result converged to an iterative error of  $10^{-8}$ . Because convergence with respect to axial mesh refinement is observed at an axial mesh size of 1.25 cm, extrapolation to the infinitesimally small mesh element size was performed based only on the radial mesh refinement. Using the 2.12 cm and 1.70 cm triangle meshing results with 1.0 cm axial meshing leads to an eigenvalue of 1.01155. Using the 1.70 cm and 1.41 cm triangle meshing results with 1.0 cm axial meshing leads to 1.01150. In addition to these linear extrapolations, two least squared approaches were also used. The first used a basis of  $(1, x, y)$ , yielding an eigenvalue of 1.01135. The second used a basis of  $(1, x, y, x \cdot y)$  and yielded an eigenvalue of 1.01168. These are all included in Table 112. In the literature, the well-established methodology for extrapolating finite difference diffusion theory calculations was used to obtain the reference solution 1.01132 where an eigenvalue error of  $\pm 20$  pcm around the reference solution is assumed to be considered accurate given the variance in the above extrapolation schemes.

**Table 112. DIF3D-FD VVER-440 Eigenvalue Results**

<b>Triangular Mesh Size (cm)</b>	<b>Axial Mesh Size (cm)</b>	<b><math>k_{\text{eff}}</math></b>
8.49	6.25	1.01007
4.24	3.125	1.01049
2.83	1.5625	1.01085
2.12	1.25	1.01104
2.12	1.0	1.01104
1.70	1.0	1.01114
1.41	1.0	1.01120
0.0	0.0	1.01155*
		1.01150*
		1.01135*
		1.01168*

\* Extrapolated Results

The power distribution from DIF3D-FD was compared to the reference via a mesh-wise comparison for all axial meshes of all 37 assemblies. In Table 113 we provide four measures to describe the accuracy of the power distribution. The RMS error is the standard root-mean-square of the mesh-wise error in power density (all meshes have the same volume). The average error is the average of the absolute value of the mesh-wise error in power density. The peak powered mesh error is the error in the mesh with the maximum power density that occurs in axial mesh 4 of assembly 25 or ring 10 position 3. Finally, the maximum mesh error is the maximum error in any mesh from any assembly.

Table 113 includes results from multiple sources and cases: DIF3D-FD with the 1.70 cm triangle and 1.0 axial mesh case from Table 112; DIF3D-VARIANT with the  $P_1$  angular approximation (i.e., diffusion); a new DIF3D-FD solution with meshing that matches the meshing scheme used for the stated reference solution [13]; and results from references [13] and [14] that do *not* rely on DIF3D. From these results, it is clear that the updated DIF3D-FD results contain a non-trivial amount of error in it compared with the published reference solution. The DIF3D-VARIANT solution is slightly closer to the reference solution also having a maximum error well under 1%. The DIF3D-FD solution with a mesh that matches the reference interestingly contains non-zero errors in all mesh locations. This implies that either different convergence settings were used in the DIF3D-FD calculations (i.e. iterative error) or the stated reference is also an extrapolated result that was not stated in the literature. Regardless, the error measures are similar to DIF3D-VARIANT and accurate with respect to the reference solution.

**Table 113. DIF3D-FD VVER 440 Power Distribution Errors**

	<b>DIF3D-FD</b>	<b>DIF3D-VARIANT</b>	<b>Match Reference</b>	<b>ANC-H</b>	<b>PARCS</b>	<b>COREDAX</b>
<b><math>k_{\text{eff}}</math> Error (pcm)</b>	12	3	7	25	45	102
<b>RMS Error</b>	0.255%	0.175%	0.168%	-	-	-
<b>Average Error</b>	0.203%	0.132%	0.133%	1.28%	-	-
<b>Peak Powered Mesh Error</b>	0.218%	-0.024%	0.141%	-	-	-
<b>Maximum Mesh Error</b>	0.766%	0.612%	0.478%	-	21.7%	1.28%

In reference [13], only a 1.28% average error is reported for ANC-H along with a  $k_{\text{eff}}$  error of 25 pcm. In reference [14], only the maximum mesh error is given for the coarsest mesh approximations although  $k_{\text{eff}}$  solutions for multiple meshes are provided. For the coarsest PARCS solution, the  $k_{\text{eff}}$  error is 45 pcm and the maximum mesh error was reported as 21.7%. The coarsest COREDAX solution had a  $k_{\text{eff}}$  error of 102 pcm and a maximum reported mesh error of 1.28%. For the finest mesh  $k_{\text{eff}}$  results reported, PARCS had a 45 pcm error and COREDAX had a 6 pcm error and thus one can assume that the power distribution errors were significantly reduced as well even though they were not provided. Excluding the PARCS result, these solutions are reasonably consistent with the DIF3D-FD and DIF3D-VARIANT solutions.

### 3.3 3D Cartesian Transport Verification

#### 3.3.1 Model Building Verification

As is discussed in Section 3.1.1 of [6], a Model Building case will be used to verify the ability of NIP3 and HMG4C to create the user-specified 3D Cartesian transport model by creating a simple two-group, multi-isotope, multi-composition, multi-region 3D Cartesian model. This case will specifically be used to verify the following card types and options consistent with Tables 7 through 9 of [6]: card Types 1, 2 (options 3, 9, 10, and 11), 6, 7, 9, 13, 14, 15, and 44 of the NIP3 module; card Types 1, 2 (options 3, 4, 5, 7, and 8) of the HMG4C module; and card Types 1, 4 (Options 2, 3, 4, and 5) of the DIF3D module.

The verification of these options will be similar to, and, when applicable, rely on, the equivalent verification performed for the 3D Cartesian diffusion Model Building case in Section 3.1.1. Specifically, the change to a transport solver will only impact the edits of the specific composition cross sections and the output related to the actual solution (verified elsewhere). Isotopic cross sections are not expected to change since the edits of the ISOTXS file include all data within the ISOTXS file and do not include diffusion-specific information like the diffusion coefficient. Therefore output options relating to the ISOTXS file will not be exercised. Otherwise, this verification effort will repeat the base and perturbation cases from Section 3.1.1, modified to use the transport solver, and comparing the ASCII and binary outputs to the equivalent files from the 3D Cartesian diffusion cases. Any differences will be either explained or their impact on DIF3D verification understood and stated.

### 3.3.1.1 Model Definition

The geometry and material composition data used for verification of DIF3D's 3D Cartesian transport model building capability will be the same as for the 3D Cartesian diffusion model building capability as shown in Figure 1 and described in the related tables. Like the diffusion case, the cross section data will also be tested in the various forms shown in Table 15 and explicitly provided in Figure 4 through Figure 8. The base case referred to throughout this section will again use the microscopic XS ISOTXS format shown in Figure 4.

To enable the transport solver, the A.DIF3D block shown in the 3D Cartesian diffusion model building verification case (Figure 9) was modified with the addition of a single card as highlighted in Figure 88. In this card, the default spatial and angular approximations are applied, exercising a quadratic source approximation, 4<sup>th</sup> order flux approximation, and linear leakage approximation in space, and a third-order spherical harmonic flux and leakage expansion for the angular variable.

```

1  BLOCK=STP021
2  DATASET=A.HMG4C
3  01      3D XYZ - MCC Micro XS ISOTXS
4  02      9000000      0      3      3      0      0      0      3
5  UNFORM=A.NIP3
6  01      3D XYZ - MCC Micro XS ISOTXS
7  02 0 3 40000000 40000000 40000000 40000000 0 3 3 3
8  ...
9  ... See A.NIP3 Model Geometry Definition Listing
10 ...
11 ... See A.NIP3 Model Composition Definition Listing
12 ...
13 C
14 UNFORM=A.DIF3D
15 01      3D XYZ - MCC Micro XS ISOTXS
16 02      30000000 15000000 0
17 03      0 2 0 4500 200
18 04      3 3 3 33 000 00 000 0 0 0000 -1
19 05 1.0E-06 1.0E-07 1.0E-08
20 12 20401 10303
21 NOSORT=A.ISO
22 ...
23 ... See Micro XS ISOTXS Listing
24 ...

```

**Figure 88. Remaining DIF3D Input Options**

### 3.3.1.2 Verification

In this section the DIF3D processing of the previously-defined base case will be evaluated to show how DIF3D handles the inputs provided to it when the transport solver is used on 3D Cartesian geometry. This verification will begin by examining the above base case with the microscopic XS ISOTXS format of Figure 4. Finally, the perturbations to this base case discussed in the next paragraph will be performed and verified to be implemented correctly in DIF3D. The ISOTXS formats described in Table 15 will not be verified for the transport solver case as the source code for DIF3D is written so the neutronics solvers obtain data from the COMPXS files; since the 3D Cartesian diffusion model building verification work already verified these COMPXS files are correct, this does not need to be repeated.



These perturbations were provided earlier in Table 16 for the 3D Cartesian diffusion model building verification work. Table 114 is a modified version of Table 16 except here only the A.DIF3D block perturbations are included since re-verifying the A.NIP3 and A.HMG4C block options they would be duplicitous with the diffusion equivalent cases.

**Table 114. DIF3D Transport Control Options and Their Perturbations**

A.DIF3D				
Card Type & Option	Description	Option in Base Case	Perturbations to Base	Evaluated in Sections
4.2	Problem description edit	3	0, 1, 2	3.3.1.2.2.1
4.3	Geometry (region to mesh interval) map edit	3	0, 1, 2	3.3.1.2.2.2
4.4	Geometry (zone to mesh interval) map edit	3	0, 1, 2	3.3.1.2.2.3
4.5	Macroscopic cross section edit	33	00, 01, 02, 03, 10, 11, 12, 13, 20, 21, 22, 23, 30, 31, 32	3.3.1.2.2.4
12.9	Aniso. Scattering Approx NPNO	0	1, 2	3.3.1.2.2.5
12.10	Extended Transport Approximation	0	-1, <= NPNO, > NPNO	3.3.1.2.2.6

### 3.3.1.2.1 Microscopic XS ISOTXS Base Case

The DIF3D input for the microscopic XS ISOTXS base case is the same as defined in Figure 2, Figure 3, Figure 4, and Figure 88. Like all other cases in this work, this input was executed on the KOOKIE cluster with the DIF3D executable located at /software/ARC/dif3d\_v11.0\_r3012\_d2019\_03\_14\_512GB.x. The output to screen (i.e., standard output) was redirected to a text file; this and all other output files from this run are stored in an isolated directory.

The remainder of this section will compare the standard and auxiliary outputs to the base case from the 3D Cartesian diffusion model building base case. The majority of these files are expected to be the same, with the only differences being related to the composition cross section edits and the solver iterations and results edits. These expectations will be verified, and then the composition cross sections will be compared to the expected values to verify that DIF3D is correctly computing the macroscopic cross sections needed for the transport solver.

After verifying these ASCII output files, the binary output files related to the model definition (i.e., GEODST, NDXXSRF, ZNATDN, COMPTS, and LABELS) will be compared to their already verified diffusion equivalents. Like in the diffusion case, intermediate files (e.g., ADIF3D, ISOTXS, and ARC) and those related to the solution of the given model (e.g., RTFLUX) will not



be evaluated as they are either not directly used by designers or will be verified in later sections of this work.

#### *3.3.1.2.1.1 Standard Output Edit Verification*

This section will progress through the differences in the DIF3D standard output file from this case compared to the diffusion base case. The differences will be discussed with the goal of showing that the change in solver type does not introduce any additional issues in the execution of DIF3D.

The majority of differences in the input are limited to the differences in the repeat of the input file and prints of the total storage/words used for processing and storing data. These are all to be expected and the specific values are not the focus of this verification work.

The geometry region and zone maps and the mesh structure as edited by both the GNIP4C and DIF3D modules were verified to be the exact same between diffusion and transport cases, as expected. The ISOTXS edits also were verified to be the exact same.

The HMG4C module's composition cross section edits were also the same between both cases; this is acceptable since at this point the HMG4C module is just printing what is in the COMPXS file. The COMPXS file format and data within it is independent of the downstream data; it contains both diffusion coefficients and higher-order total, transport, and scattering moments.

Line 1814 of the transport solver's standard output file begins the variational nodal option edits. Unsurprisingly, this is not included in the diffusion solver case's file since the card containing these options were not present. This is repeated in Figure 89. The nodal parameters that were specifically input as shown in the A.DIF3D Type 12 card in Figure 88 (i.e., 20401 and 10303) were verified accurate. The remaining options were left as their default values and should agree with the default values specified in the DIF3D manual. These nodal parameter values are as expected, except the DIF3D output states that the number of axial partial current sweeps per group per outer iteration defaults to a value of 2, however the reported value is 0, despite the default being used. This is only an editorial issue that could utilize additional clarity.

Similarly, the Problem Description section of Figure 89 is reporting how DIF3D's transport solver is interpreting the solution mesh. The number of nodes (and active nodes) in a plane is simply the number of x mesh elements multiplied by the number of y elements. From Table 10, these values are 6 and 22, respectively. Multiplying these yields 132, verifying this value in Figure 89. The number of axial planes is also obtained from Table 10 and it is confirmed to be 17 planes. The number of nodes is reported as 2,244; since multiplying 132 and 17 produces 2,244 this number is also as expected. It is unclear what the number of unique node types refers to. Finally, the 45 degree symmetry edit (a value of -1) is inconsistent with the edit stating the values can either be 0 or +1 and inconsistent with the manual that is consistent with this output. Therefore this should be clarified.

February 13, 2020

```

1815                                     *** VARIATIONAL NODAL OPTION ***
1816
1817
1818
1819                                     *** NODAL PARAMETERS ***
1820
1821          20401      IAPRX      ORDER OF SPATIAL APPROXIMATION
1822          10303      IAPRXZ     ORDER OF ANGULAR APPROXIMATION
1823          -1        NFMCMX     NUMBER OF FINE MESH PER REBALANCE MESH IN X- AND Y-DIRECTIONS (-1 = NO COARSE-
MESH REBALANCE)
1824          0        NXYSWP     NUMBER OF XY-PLANE PARTIAL CURRENT SWEEPS PER GROUP PER AXIAL SWEEP (0 = LET
CODE DECIDE)
1825          0        NZSWP      NUMBER OF AXIAL PARTIAL CURRENT SWEEPS PER GROUP PER OUTER ITERATION (DEFAULT =
2)
1826          1        ISXTRP     ASYMPTOTIC EXTRAPOLATION OF OUTERS (0 = EXTRAPOLATE, 1 = DON'T
EXTRAPOLATE)
1827          0        NPNO       SCATTERING ANISOTROPY ORDER
1828          0        NXTR       EXTENDED TRANSPORT APPROXIMATION ON TOTAL CROSS SECTION
1829          0        IOMAC      OMEGA TRANSFORMATION ACCELERATION (0/1 = YES/NO)
1830          0        IFUL       INNER ITERATION ALGORITHM (0/1 = PARTITIONED/FULL MATRIX
1831          0        IWNHFL      NHFLUX CONTENT (0/1/2 = BOTH/FLUX/PARTIAL CURRENTS)
1832          0        IPERT      PERTURBATION OPTION (0/1 = NO EFFECT/USE SAME APPROXIMATION FOR SOURCE AS FLUX)
1833          0        IHARM       HARMONIC TO BE CALCULATED (NOT YET OPERATIONAL)
1834          0
1835
1836                                     *** PROBLEM DESCRIPTION ***
1837
1838
1839          NO. OF NODES IN PLANE                = 132
1840          NO. OF ACTIVE NODES IN PLANE         = 132
1841          NO. OF AXIAL PLANES                  = 17
1842          NO. OF NODES                         = 2244
1843          NO. OF UNIQUE NODE TYPES             = 24
1844          45 DEGREE SYMMETRY USED (0/1 = NO/YES) = -1

```

**Figure 89. Variational Nodal Option Output**

Immediately after the above output is the COMPXS edit after processing by the DIF3D module. This section is expected to have differences from the diffusion case because no diffusion coefficients would be present in a transport solve.

A value-by-value comparison revealed that the absorption cross sections, removal cross sections, fission cross sections, fission spectra, and neutrons per fission, and power conversion factors are exactly equivalent, as expected, between the diffusion and transport cases for all four compositions in the problem.

The transport solver's principal cross section edit also includes what is reported as the total cross sections for the four compositions. However, based upon the "NXTR" option in Figure 89, DIF3D is going to use the transport cross section from the COMPXS file for the transport cross section and so it is expected that the composition total cross section reported by DIF3D will actually be the transport cross section. The expected values for both the total and transport cross sections were previously reported in Table 23. These are repeated in Table 115 along with what DIF3D is reporting as the total cross section. This table shows that DIF3D is reporting the transport cross section, as expected, and that it is faithfully computing this value.

**Table 115. Transport Case Total and Transport Cross Sections**

Comp #	Grp	Reference Total [1/cm]	Reference Transport [1/cm]	DIF3D Total [1/cm]
1	1	1.106830E-01	1.106830E-01	1.106830E-01
	2	3.635500E-01	3.635500E-01	3.635500E-01
2	1	6.023323E-01	3.483847E-01	3.483847E-01
	2	2.304580E+00	1.554718E+00	1.554718E+00
3	1	6.363751E-01	5.241492E-01	5.241492E-01
	2	2.131587E+00	1.822940E+00	1.822940E+00
4	1	4.465630E-01	3.800200E-01	3.800200E-01
	2	9.098300E-01	8.554400E-01	8.554400E-01

Also included in DIF3D's composition cross section edit are the  $P_0$  total scattering matrices for each of the four compositions. The expected values for these were previously reported in Table 26 and are repeated in Table 116, which also includes the values reported by DIF3D. These values show that DIF3D is accurately reporting the  $P_0$  total scattering matrices for the case of the transport solver. Note this is different from the diffusion solver as deficiencies in the scattering matrix edit output were noted there.

**Table 116. Transport Case  $P_0$  Total Scattering Matrices**

Comp #	To Grp	Expected $P_0$ , From Group		DIF3D $P_0$ , From Group	
		1	2	1	2
1	1	1.096740E-01	0.000000E+00	1.096740E-01	0.000000E+00
	2	1.000600E-03	3.633900E-01	1.000600E-03	3.633900E-01
2	1	5.727294E-01	0.000000E+00	5.727294E-01	0.000000E+00
	2	2.640436E-02	2.235786E+00	2.640436E-02	2.235786E+00
3	1	5.907658E-01	1.600000E-05	5.907658E-01	1.600000E-05
	2	3.660426E-02	2.079960E+00	3.660427E-02	2.079961E+00
4	1	4.309740E-01	1.000000E-04	4.309740E-01	1.000000E-04
	2	5.555600E-03	7.873900E-01	5.555600E-03	7.873900E-01

All remaining information in the standard output is related specifically to the solution obtained by DIF3D and so is out of scope for this model building verification work.

#### *3.3.1.2.1.2 Auxiliary Output Edit Verification*

Similar to the standard output verification, the auxiliary output was compared to the diffusion theory auxiliary output. All differences were found to be completely consistent with the differences identified above for the standard output.

#### *3.3.1.2.1.3 Binary Output Verification*

The binary output files (GEODST, NDXSRF, ZNATDN, COMPXS, and LABELS) were first converted to ASCII as discussed in the diffusion theory model building verification section, and then compared to the diffusion ASCII counterparts. No differences were noted. This is expected because the information in these binary files is solver agnostic by design of the binary file formats. Therefore the binary file outputs is equivalently verified for transport as it is for diffusion theory. It should be noted that the GEODST file produced by the transport solver still contains the boundary constant value of 0.4692 as was present in the equivalent diffusion case. Again, later cases will verify if this impacts the solution.

#### *3.3.1.2.2 Edit Options Verification*

This section will evaluate the edit control options shown in Table 114. These cards and options that have yet to be evaluated are provided in Table 117. To ensure the scope of this verification effort is appropriately bounded, these options will not be tested for any cross-correlations. Instead each option will be tested one-by-one and it is assumed that the effect of the value of one option has no effect on DIF3D's ability to execute another option.

Each of the card types and options will be evaluated in the subsections that follow. In all the cases that follows, there will be expected differences in the output file. Specifically, page numbers and input echoes obviously should change as the number of pages printed changes or the input file changes. These differences will not be discussed explicitly below.

Table 117. Edit Control Perturbations

Card Type & Option	Description	Option in Base Case	Perturbations to Base
4.2	Problem description edit	3	0, 1, 2
4.3	Geometry (region to mesh interval) map edit	3	0, 1, 2
4.4	Geometry (zone to mesh interval) map edit	3	0, 1, 2
4.5	Macroscopic cross section edit	33	00, 01, 02, 03, 10, 11, 12, 13, 20, 21, 22, 23, 30, 31, 32
12.9	Aniso. Scattering Approx NPNO	0	1, 2
12.10	Extended Transport Approximation	0	-1, <= NPNO, > NPNO

#### 3.3.1.2.2.1 A.DIF3D Type 04 Card Option 2

The second option of the Type 04 card of the A.DIF3D input block accepts values of 0, 1, 2, or 3, as shown in Table 117. The cases evaluated thus far have kept this option at a value of 3, indicating that the problem description edits will be printed to both standard and auxiliary output. This case will evaluate the 0, 1, and 2 options that print no problem description edits, print problem description edits only to standard output, and problem description edits only to auxiliary output.

The first modified case shall print no problem description edits in either standard or auxiliary output and all other outputs should be the same as the base case. This was explicitly confirmed by comparing both outputs with the base case equivalent for both standard and auxiliary output files.

The second modified case is expected to print the problem description edits to the standard output but not the auxiliary output. The value of this option was successfully interpreted, as the auxiliary output did not include the problem description edits but the standard output did.

The third modified case is expected to print the problem description edits to only the auxiliary output; and all other output should be the same as the base. The value of this option was successfully interpreted, as the standard output did not include the problem description edits but the auxiliary output did.

#### 3.3.1.2.2.2 A.DIF3D Type 04 Card Option 3

The third option of the Type 04 card of the A.DIF3D input block accepts values of 0, 1, 2, or 3 as shown in Table 117. The cases evaluated thus far have kept this option at a value of 3, indicating

that the DIF3D module will print region/mesh interval printer-plotter maps to both standard and auxiliary output. This case will evaluate the 0, 1, and 2 options that print no region/mesh interval printer-plotter maps, print region/mesh interval printer-plotter maps only to standard output, and print region/mesh interval printer-plotter maps only to auxiliary output.

The first modified case shall print no region maps in either standard or auxiliary output and all other outputs should be the same as the base case. This was explicitly confirmed by comparing both outputs with the base case equivalent

The second modified case is expected to print the region maps to the standard output but not the auxiliary output. The value of this option was successfully interpreted, as the auxiliary output did not include the map but the standard output did.

The third modified case is expected to print the region maps to only the auxiliary output; and all other output should be the same as the base. The value of this option was successfully interpreted, as the standard output did not include the reactor region maps but the auxiliary output did.

#### *3.3.1.2.2.3 A.DIF3D Type 04 Card Option 4*

The fourth option of the Type 04 card of the A.DIF3D input block accepts values of 0, 1, 2, or 3 as shown in Table 117. The cases evaluated thus far have kept this option at a value of 3, indicating that the DIF3D module will print zone/mesh interval printer-plotter maps to both standard and auxiliary output. This case will evaluate the 0, 1, and 2 options that print no zone/mesh interval printer-plotter maps, print zone/mesh interval printer-plotter maps only to standard output, and print zone/mesh interval printer-plotter maps only to auxiliary output.

The first modified case shall print no zone maps in either standard or auxiliary output and all other outputs should be the same as the base case. This was explicitly confirmed by comparing both outputs with the base case equivalent

The second modified case is expected to print the zone maps to the standard output but not the auxiliary output. The value of this option was successfully interpreted, as the auxiliary output did not include the map but the standard output did.

The third modified case is expected to print the zone maps to only the auxiliary output; and all other output should be the same as the base. The value of this option was successfully interpreted, as the standard output did not include the reactor region maps but the auxiliary output did.

#### *3.3.1.2.2.4 A.DIF3D Type 04 Card Option 5*

The fifth option of the Type 04 card of the A.DIF3D input block accepts a two digit number where the first digit controls the scattering and principal cross section composition edits and the second digit controls just the principal cross section edits. The accepted values for each digit are 0, 1, 2, or 3 as shown in Table 117. The cases evaluated thus far have kept both parameters at the value of 3 (thus, the input value is 33), indicating that the DIF3D module will print these quantities to both

standard and auxiliary output. This case will evaluate setting each of the values for each digit to the values of 0, 1, and 2 (no edits, to standard out only, and to auxiliary out only, respectively) while keeping the other digit constant. Thus the modified cases to evaluate within this subsection are the values of 00, 01, 02, 03, 10, 11, 12, 13, 20, 21, 22, 23, 30, 31, and 32. This set evaluates every possible combination.

For the 00 case, it is expected that the standard and auxiliary outputs do *not* contain the DIF3D composition cross section edits, whether they be principal or scattering. This was verified explicitly and found to be true.

For the 01 case, it is expected that the auxiliary output does not contain any DIF3D composition cross section edits, while the standard output contains only principal cross sections and no scattering matrices. This was verified explicitly and found to be true.

For the 02 case, it is expected that the standard output does not contain any DIF3D composition cross section edits, while the auxiliary output contains only principal cross sections and no scattering matrices. This was verified explicitly and found to be true.

For the 03 case, it is expected that both the standard and auxiliary outputs contains only principal cross sections and no scattering matrices. This was verified explicitly and found to be true.

For the 10 case, it is expected that the auxiliary output does not contain any DIF3D composition cross section edits, while the standard output contains principal cross sections and scattering matrices. This was verified explicitly and found to be true.

For the 11 case, it is expected that the auxiliary output does not contain any DIF3D composition cross section edits, while the standard output contains principal cross sections and scattering matrices. This was verified explicitly and found to be true.

For the 12 case, it is expected that the auxiliary output contains edits of the principal cross sections, while the standard output contains principal cross sections and scattering matrices. This was verified explicitly and found to be true.

For the 13 case, it is expected that the auxiliary output contains edits of the principal cross sections, while the standard output contains principal cross sections and scattering matrices. This was verified explicitly and found to be true.

For the 20 case, it is expected that the auxiliary output contains principal cross sections and scattering matrices while the standard output contains no cross section edits. This was verified explicitly and found to be true.

For the 21 case, it is expected that the auxiliary output contains principal cross sections and scattering matrices while the standard output contains principal cross section edits only. This was verified explicitly and found to be true.

For the 22 case, it is expected that the auxiliary output contains principal cross sections and scattering matrices while the standard output contains no cross section edits. This was verified explicitly and found to be true.

For the 23 case, it is expected that the auxiliary output contains principal cross sections and scattering matrices while the standard output contains principal cross section edits only. This was verified explicitly and found to be true.

For the 30, 31, and 32 cases, it is expected that the standard and auxiliary output contains principal cross sections and scattering matrix edits. These were verified explicitly and found to be true.

#### *3.3.1.2.2.5 A.DIF3D Type 12 Card Option 9*

The ninth option of the Type 12 card of the A.DIF3D input block accepts values of 0, or the scattering order N that in this case the ISOTXS data only supplies up to order 1, as shown in Table 117. The cases evaluated thus far have kept this option at a value of 0, indicating isotropic scattering will be applied. This case will evaluate the 1, and 2 options that use  $P_1$  scattering and  $P_2$  scattering, respectively. The  $P_2$  case is expected to fail as the data does not supply  $P_2$  scattering cross section data, but this is included to ensure this happens.

For the case of  $P_1$  scattering, the extended transport approximation option states that if the scattering order is greater than 0 and equal to the maximum number of orders in the COMPXS file, then the total cross section will be applied instead of the transport cross section. Therefore it is expected that  $P_1$  data will be present in the DIF3D COMPXS edits in standard and auxiliary outputs and that the data reported as the “total cross section” will actually be the total cross section. The total cross section data in each of these outputs was compared to the reference total cross section provided in Table 115 and found to match exactly to all reported digits. Similarly, the  $P_1$  scattering matrices were compared with the values calculated by hand and provided previously in Table 26 and found to match exactly to all reported digits. The  $P_0$  data was not modified from the base case, as expected.

The  $P_2$  scattering case failed, as expected, with the following error message: “0 ANISOTROPIC MAX ORDER 1 ON COMPXS FILE IS LESS THAN NPNO 2 REQUIRED IN NODAL CALCULATION.”

#### *3.3.1.2.2.6 A.DIF3D Type 12 Card Option 10*

The tenth option of the Type 12 card of the A.DIF3D input block accepts values of -1, 0, or some positive integer N as shown in Table 117. The effect on DIF3D of this option depends on the value of the NPNO value supplied in the ninth option of the Type 12 card. Specifically, the following options are possible where NPNO refers to the value of the ninth option of the Type 12 card, and NXTR is the value of the tenth option, and MAXORD is the maximum number of orders in the ISOTXS file (this is 1 for the Microscopic XS ISOTXS dataset):



- If NXTR is -1, then:
  - If NPNO is 0, then the total cross section will be used
  - If NPNO is not 0, then the transport cross section will be used.
- If NXTR is 0 (the default), then:
  - If NPNO is 0, then the transport cross section will be used
  - If NPNO is greater than 0 and NPNO is equal to MAXORD, then the total cross section will be used;
  - If NPNO is greater than 0 and NPNO is less than MAXORD, then the extended transport approximation will be applied using the  $P_{NPNO+1}$  scattering cross section.
- If NXTR is greater than 0 and less than or equal to NPNO, then:
  - The total cross section will be used;
- If NXTR is greater than 0 but greater than NPNO, then;
  - The extended transport approximation will be applied on the total cross section from the total cross section orders from  $NPNO + 1$  to NXTR.

These paths require an ISOTXS file that contains a MAXORD greater than 1. To accommodate this with a minimum number of ISOTXS modifications, the User-Defined XS Style 2 will be used as the starting point, as the ISOTXS modifications necessary are minimum for this starting point. Specifically, the ISO4 isotope will have  $P_2$  data added that is the same as its  $P_1$  data, but a factor of 10 smaller. This ISOTXS file is provided for reference in Figure 90. Additions to the data from Figure 8 are highlighted in green and modifications are in yellow.

The total composition macroscopic cross sections of interest that will change due to the addition of this  $P_2$  data are included in Table 118.

February 13, 2020

```

64 0V ISOTXS *2G          *      1
65 1D      2      4      2      2      2      1      1      1
66 2D * Custom *
67 *      * IS01 IS02 IS03 IS04
68 9.50000E-01 5.00000E-02
69 7.73210E+01 4.37393E+05 2.00000E+07 1.00000E+00 0.00000E+00
70      0      3      6      9
71 4D IS01 BYHAND NONE
72 1.00000E+00 1.10000E-11 2.20000E-12 2.94000E+02 1.10000E+00 1.20000E+00
73      0      0      0      0      0      0      0      1      1      0      0
74      1      1      2      1      1
75 5D 1.10683E-01 3.63550E-01 1.10683E-01 3.63550E-01 8.48029E-06
76 1.60000E-04
77 7D 1.09674E-01 3.63390E-01 1.00060E-03
78 4D IS02 BYHAND NONE
79 2.00000E+00 2.20000E-11 4.40000E-12 3.94000E+02 2.10000E+00 2.20000E+00
80      6      0      0      1      1      1      1      1      1      1      0      0
81      1      1      2      1      1
82 5D 1.33152E+00 4.37350E+00 1.33152E+00 4.37350E+00 2.48615E-04
83 9.40000E-03 9.94458E-05 3.76000E-03 7.45844E-05 2.82000E-03 2.50000E-02
84 0.00000E+00 4.97229E-05 1.88000E-03 2.48615E-05 9.40000E-04
85 7D 1.17638E+00 4.35470E+00 1.04640E-01
86 4D IS03 BYHAND NONE
87 3.00000E+00 3.30000E-11 6.60000E-12 4.94000E+02 3.10000E+00 3.20000E+00
88      1      0      1      1      1      1      1      1      1      1      0      0
89      2      1      2      1      1
90 5D 3.74796E-01 1.68707E+00 6.56960E-01 2.52025E+00 5.02300E-04
91 1.28940E-02 1.04840E-03 5.06320E-02 2.00000E+00 2.50000E+00 2.00920E-04
92 5.15760E-03 1.50690E-04 3.86820E-03 1.50000E-03 0.00000E+00 1.00460E-04
93 2.57880E-03 5.02300E-05 1.28940E-03
94 7D 6.21180E-01 2.44383E+00 2.92270E-02 2.74590E-01 8.33180E-01
95 7.57370E-03
96 4D IS04 BYHAND NONE
97 4.00000E+00 4.40000E-11 8.80000E-12 5.94000E+02 4.10000E+00 4.20000E+00
98      1      1      1      0      0      0      0      1      1      0      0
99      3      2      2      2      1
100 5D 2.69337E-01 4.91890E-01 3.35880E-01 5.46280E-01 8.70780E-03
101 2.51800E-02 2.81700E-03 9.70000E-02 2.10000E+00 2.40000E+00 1.00000E+00
102 0.00000E+00
103 7D 1.00000E-04 3.19800E-01 4.24000E-01 4.55500E-03 1.00000E-05
104 6.69400E-02 5.43800E-02 3.97200E-04 1.00000E-06 6.69400E-03 5.43800E-03
105 -3.97200E-05

```

Figure 90. P<sub>2</sub> Modified User-Defined Style 2 ISOTXS File

With this new ISOTXS file, the combined values for NPNO and NXTR that will access all branches are as follows; these cases are ordered consistently with the cases listed above:

- NXTR = -1, NPNO = 0
- NXTR = -1, NPNO = 1
- NXTR = 0, NPNO = 0
- NXTR = 0, NPNO = 2
- NXTR = 0 NPNO = 1
- NXTR = 1, NPNO = 1
- NXTR = 2, NPNO = 1

The verification of each of these will be discussed separately below.

**Table 118. Composition Cross Sections for P<sub>2</sub> ISOTXS File Data**

	COMP1	COMP2	COMP3	COMP4
<b>Transport<sub>1</sub></b>	1.106830E-01	3.483847E-01	5.241492E-01	3.800200E-01
<b>Transport<sub>2</sub></b>	3.635500E-01	1.554718E+00	1.822940E+00	8.554400E-01
<b>Total<sub>1</sub></b>	1.106830E-01	6.023323E-01	6.363751E-01	4.465630E-01
<b>Total<sub>2</sub></b>	3.635500E-01	2.304580E+00	2.131587E+00	9.098300E-01
<b>Scatter<sub>0,1-&gt;1</sub></b>	1.096740E-01	5.700294E-01	5.834458E-01	4.294740E-01
<b>Scatter<sub>0,1-&gt;2</sub></b>	1.000600E-03	2.640436E-02	3.660426E-02	5.555600E-03
<b>Scatter<sub>0,2-&gt;1</sub></b>	0.000000E+00	0.000000E+00	1.600000E-05	1.000000E-04
<b>Scatter<sub>0,2-&gt;2</sub></b>	3.633900E-01	2.235786E+00	2.079960E+00	7.873900E-01
<b>Scatter<sub>1,1-&gt;1</sub></b>	0.000000E+00	2.471310E-01	1.095628E-01	6.694000E-02
<b>Scatter<sub>1,1-&gt;2</sub></b>	0.000000E+00	6.816330E-03	2.662980E-03	-3.972000E-04
<b>Scatter<sub>1,2-&gt;1</sub></b>	0.000000E+00	0.000000E+00	1.600000E-06	1.000000E-05
<b>Scatter<sub>1,2-&gt;2</sub></b>	0.000000E+00	7.498620E-01	3.086456E-01	5.438000E-02
<b>Scatter<sub>2,1-&gt;1</sub></b>	0.000000E+00	0.000000E+00	1.071040E-03	6.694000E-03
<b>Scatter<sub>2,1-&gt;2</sub></b>	0.000000E+00	0.000000E+00	-6.355200E-06	-3.972000E-05
<b>Scatter<sub>2,2-&gt;1</sub></b>	0.000000E+00	0.000000E+00	1.600000E-07	1.000000E-06
<b>Scatter<sub>2,2-&gt;2</sub></b>	0.000000E+00	0.000000E+00	8.700800E-04	5.438000E-03

#### 3.3.1.2.2.6.1 Card 12 Option 10, Case 1

For this case, NXTR is -1 and NPNO is 0. Therefore it is expected that the DIF3D module's COMPXS edits will utilize the total cross sections from Table 118. Further, since NPNO is 0, only P<sub>0</sub> scattering matrices will be printed. These values and the scattering matrices were manually compared digit-by-digit to the data in Table 118 in both the standard and auxiliary outputs. All match to all but the last reported significant digit due to round-off error, while most match to all digits.

#### 3.3.1.2.2.6.2 Card 12 Option 10, Case 2

For this case, NXTR is -1 and NPNO is 1. Therefore it is expected that the DIF3D module's COMPXS edits will utilize the transport cross sections from Table 118. Further, since NPNO is 1, P<sub>0</sub> and P<sub>1</sub> scattering matrices will be printed. These values and the scattering matrices were manually compared digit-by-digit to the data in Table 118 in both the standard and auxiliary outputs. All match to all but the last reported significant digit due to round-off error, while most match to all digits.

### 3.3.1.2.2.6.3 Card 12 Option 10, Case 3

For this case, NXTR is 0 and NPNO is 0. Therefore it is expected that the DIF3D module's COMPXS edits will utilize the total cross sections from Table 118. Further, since NPNO is 0, only  $P_0$  scattering matrices will be printed. These values and the scattering matrices were manually compared digit-by-digit to the data in Table 118 in both the standard and auxiliary outputs. All match to all but the last reported significant digit due to round-off error, while most match to all digits.

### 3.3.1.2.2.6.4 Card 12 Option 10, Case 4

For this case, NXTR is 0 and NPNO is 2. Therefore it is expected that the DIF3D module's COMPXS edits will utilize the transport cross sections from Table 118. Further, since NPNO is 2,  $P_0$ ,  $P_1$ , and  $P_2$  scattering matrices will be printed. These values and the scattering matrices were manually compared digit-by-digit to the data in Table 118 in both the standard and auxiliary outputs. All match to all but the last reported significant digit due to round-off error, while most match to all digits.

### 3.3.1.2.2.6.5 Card 12 Option 10, Case 5

For this case, NXTR is 0 and NPNO is 1. Therefore it is expected that the DIF3D module's COMPXS edits will calculate the transport cross sections using the extended transport approximation with the  $P_2$  data. Further, since NPNO is 1,  $P_0$  and  $P_1$  scattering matrices will be printed.

The Bell-Hansen-Sandmeier extended transport approximation that applies in this case is per the following operations:

$$\tilde{\Sigma}_{total,g} = \Sigma_{total,g} - \sum_{g_{outgoing}} \Sigma_{scatter, NPNO+ , g \rightarrow g_{outgoing}}$$

$$\tilde{\Sigma}_{scatter,n,g \rightarrow g} = \Sigma_{scatter,n,g \rightarrow g} - \sum_{g_{outgoing}} \Sigma_{scatter, NPNO+ , g \rightarrow g_{outgoing}} ; \text{ for } n \leq NPNO$$

The reference values, after applying this with NPNO equal to 1, are provided in Table 119.

**Table 119. Card 12 Option 10, Case 5 Reference Solution**

	COMP1	COMP2	COMP3	COMP4
<b>Total<sub>1</sub></b>	1.106830E-01	6.023323E-01	6.353104E-01	4.399087E-01
<b>Total<sub>2</sub></b>	3.635500E-01	2.304580E+00	2.130717E+00	9.043910E-01
<b>Scatter<sub>0,1-&gt;1</sub></b>	1.096740E-01	5.700294E-01	5.823811E-01	4.228197E-01
<b>Scatter<sub>0,1-&gt;2</sub></b>	1.000600E-03	2.640436E-02	3.660426E-02	5.555600E-03
<b>Scatter<sub>0,2-&gt;1</sub></b>	0.000000E+00	0.000000E+00	1.600000E-05	1.000000E-04
<b>Scatter<sub>0,2-&gt;2</sub></b>	3.633900E-01	2.235786E+00	2.079090E+00	7.819510E-01
<b>Scatter<sub>1,1-&gt;1</sub></b>	0.000000E+00	2.471310E-01	1.084981E-01	6.028572E-02
<b>Scatter<sub>1,1-&gt;2</sub></b>	0.000000E+00	6.816330E-03	2.662980E-03	-3.972000E-04
<b>Scatter<sub>1,2-&gt;1</sub></b>	0.000000E+00	0.000000E+00	1.600000E-06	1.000000E-05
<b>Scatter<sub>1,2-&gt;2</sub></b>	0.000000E+00	7.498620E-01	3.077754E-01	4.894100E-02

These values and the scattering matrices were manually compared digit-by-digit to the data in Table 119 in both the standard and auxiliary outputs. All match to all but the last reported significant digit due to round-off error, while most match to all digits.

#### *3.3.1.2.2.6.6 Card 12 Option 10, Case 6*

For this case, NXTR is 1 and NPNO is 1. Therefore it is expected that the DIF3D module's COMPXS edits will utilize the transport cross sections from Table 118. Further, since NPNO is 1,  $P_0$  and  $P_1$  scattering matrices will be printed. These values and the scattering matrices were manually compared digit-by-digit to the data in Table 118 in both the standard and auxiliary outputs. All match to all but the last reported significant digit due to round-off error, while most match to all digits.

#### *3.3.1.2.2.6.7 Card 12 Option 10, Case 7*

For this case, NXTR is 2 and NPNO is 1. Therefore it is expected that the DIF3D module's COMPXS edits will calculate the transport cross sections using the extended transport approximation with the  $P_2$  data. Further, since NPNO is 1,  $P_0$  and  $P_1$  scattering matrices will be printed. In this case the transport approximation reduces to the same as that used in the Case 5 for this card and option. Therefore the standard and auxiliary outputs were compared directly with the outputs obtained in that case and all were found to match exactly.

### 3.3.2 Multigroup Fixed Source Verification

As discussed in Section 3.3.3 of [6], a two-group, up-scattering, anisotropic, 3D Cartesian, fixed source verification case must be generated that utilizes a multigroup source in at least one of the regions and applies reflective boundary conditions on all six surfaces of the XYZ domain. This case will be such a problem.

The reference solution was stated in [6] to be determined from a multigroup Monte Carlo code. In this case, MCNP 6.2 [15] will be used to solve the exact same source, geometry, material, and cross sections used in the DIF3D model. Further, the MCNP 6.2 tally regions will be defined exactly consistent with the fine-mesh regions in the DIF3D model to avoid any coarsening of results when performing the code-to-code comparison. Since a code-to-code comparison will be used for verification of DIF3D, the features of the MCNP 6.2 code used to generate this reference solution must also be verified. The verification of relevant MCNP 6.2 features are documented in Section 4.

The following approach will be taken when comparing the DIF3D and MCNP fixed source results. First, the calculated flux distribution will be compared through three metrics: the maximal (normalized) region-averaged flux value and location, the root-mean-squared-error of the DIF3D flux compared to the MCNP flux distributions for each group, and finally a graphical comparison of the differences in flux distributions will be displayed. It is unlikely that the DIF3D and MCNP results will match exactly, because of each method's distinct error sources that cannot be practically removed from the analysis. Therefore, instead of striving for an exact match, this work will instead show that refining DIF3D's spatial and angular order is approaching the MCNP reference result.

Before progressing that it should be noted this problem was also used to verify the correct definition of a multigroup DIF3D-FD source. This was indeed observed in the FIXSRC file and the solution's flux ratios implying the spectra was correctly applied.

#### 3.3.2.1 Model Definition

Based on the above considerations, a cuboid 30 cm to a side was chosen for the modeled extent. The resultant cuboid is broken into two cuboids. The innermost cuboid is 20 cm on a side and is composed of a material named REG2. This inner cuboid's lower-left corner is the lower-left of the entire model at the origin. The remainder of this original 30 cm cuboid is filled with another region, REG1. All boundaries are reflective.

The two group macroscopic cross sections for each of these two regions are provided in Table 120. The REG1 cross sections were defined as follows: group 1 had a mean-free-path (mfp) of 30 cm and group 2 had a mfp of 10 cm; there was no up-scatter; the scatter-to-total ratio for both groups was 20%; and the  $P_1/P_0$  moment ratio was 10%. Similarly, the REG2 cross sections were defined as follows: group 1 had a mean-free-path (mfp) of 30 cm and group 2 had a mfp of 20 cm; there was 10% up-scattering from group 2 to group 1; the scatter-to-total ratio for both groups was 30%; and the  $P_1/P_0$  moment ratio was 5%. These  $P_1/P_0$  moment ratios were chosen such that they had a

value less than 1/3; if they were greater then a negative angular distribution would be encountered during the MCNP computations potentially leading to significant discrepancies between a deterministic and Monte Carlo solver.

**Table 120. 3D Cartesian Transport Multigroup Fixed Source Macroscopic Cross Sections; units of cross sections are 1/cm**

	REG1		REG2	
	Group 1	Group 2	Group 1	Group 2
$\Sigma_{\text{total}}$	3.33333E-02	1.00000E-01	3.33333E-02	5.00000E-02
$\Sigma_{\text{abs}}$	2.66667E-02	8.00000E-02	2.33333E-02	3.50000E-02
$\nu\Sigma_{\text{fission}}$	-	-	-	-
$\chi$	-	-	-	-
$\Sigma_{\text{scatter},0,1\rightarrow g}$	1.33333E-03	5.33333E-03	2.00000E-03	8.00000E-03
$\Sigma_{\text{scatter},0,2\rightarrow g}$	0.00000E+0 0	2.00000E-02	1.50000E-03	1.35000E-02
$\Sigma_{\text{scatter},1,1\rightarrow g}$	1.33333E-04	5.33333E-04	1.00000E-04	4.00000E-04
$\Sigma_{\text{scatter},1,2\rightarrow g}$	0.00000E+0 0	2.00000E-03	7.50000E-05	6.75000E-04

Finally, the volumetric fixed source is uniformly distributed in the lower-left of the model (and in the REG2 cuboid), between 0 and 10 cm in the X-, Y-, and Z- dimensions. 75% of the unit source is deposited in group 1 and 25% in group 2.

### 3.3.2.2 Reference MCNP Results

The previously described model was converted to an MCNP model via the `create_mcnpy.py` script. This script reads a DIF3D model's geometry from the GEODST file and the composition cross sections from the COMPXS file and creates an exact duplicate of the model in MCNP. The MCNP file created from this script only utilizes planar surfaces and cells assigned to the root universe, minimizing the amount of MCNP features that must be verified to support this work. The MCNP input file included tally regions for each of the DIF3D fine-mesh blocks and for each energy group of the problem. Finally, this script creates the multigroup nuclear data library for MCNP by way of the `'simple_ace_mg.pl'` script that is distributed by Los Alamos National Laboratory with MCNP [16]. After the script created the MCNP input file, it was manually modified to establish the fixed source region as the script only creates eigenvalue inputs.

The MCNP reference case was run with 1.6 billion histories. Due to the large number of histories, the L'Ecuyer 63-bit generator (number 1) was used with its' period of  $9.2 \times 10^{18}$  numbers. The relative errors for all tally bins were less than 0.03% and are significantly smaller than any expected code-to-code differences and therefore no further visualization or description of their behavior follows.

February 13, 2020

This case yielded a flux distribution one would expect with neutrons streaming away from the volumetric source in a slightly larger than exponential fashion due to the combination of the absorption losses and slightly forward peaked scattering. This flux distribution is provided in Figure 91 and Figure 92. These figures show a slice of the flux distribution computed by MCNP in both the X-Y (left) and Y-Z (right) planes for the two groups, respectively. In these figures, the color-scale is chosen so that low flux values are blue, the median is white, and the highest flux regions are shown in red. The specific flux values are the MCNP-reported flux, that is the region and energy integrated flux, normalized to the number of source particles. The minimum and maximum values to generate these color schemes are based on the flux extremes over all energy groups, hence the same color scale is applied to Figure 91 and Figure 92.

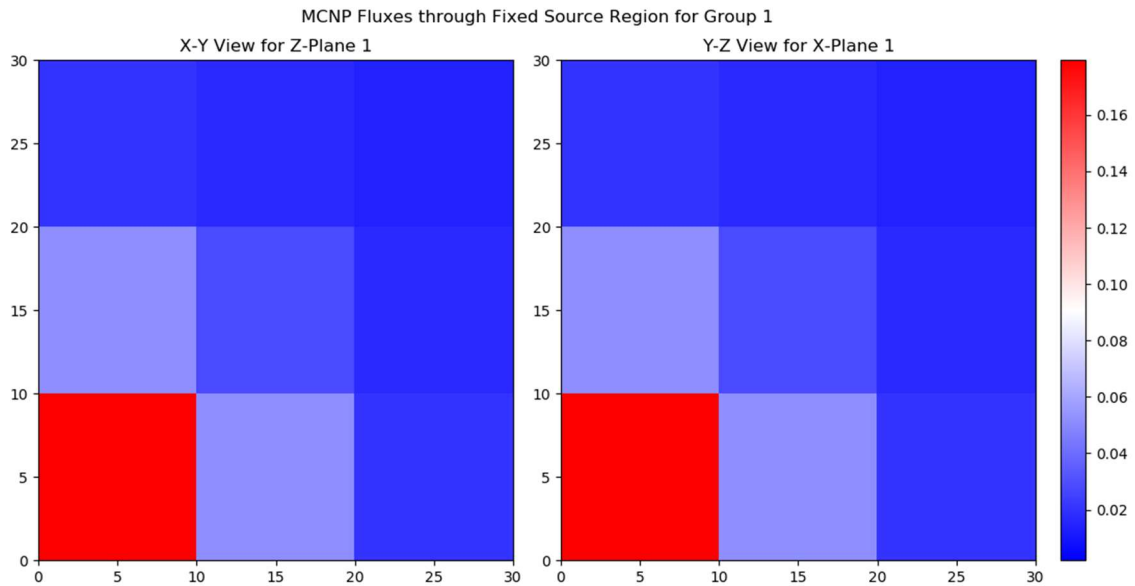


**Figure 91. XYZ MG Fixed Source MCNP Reference Flux in Group 1**



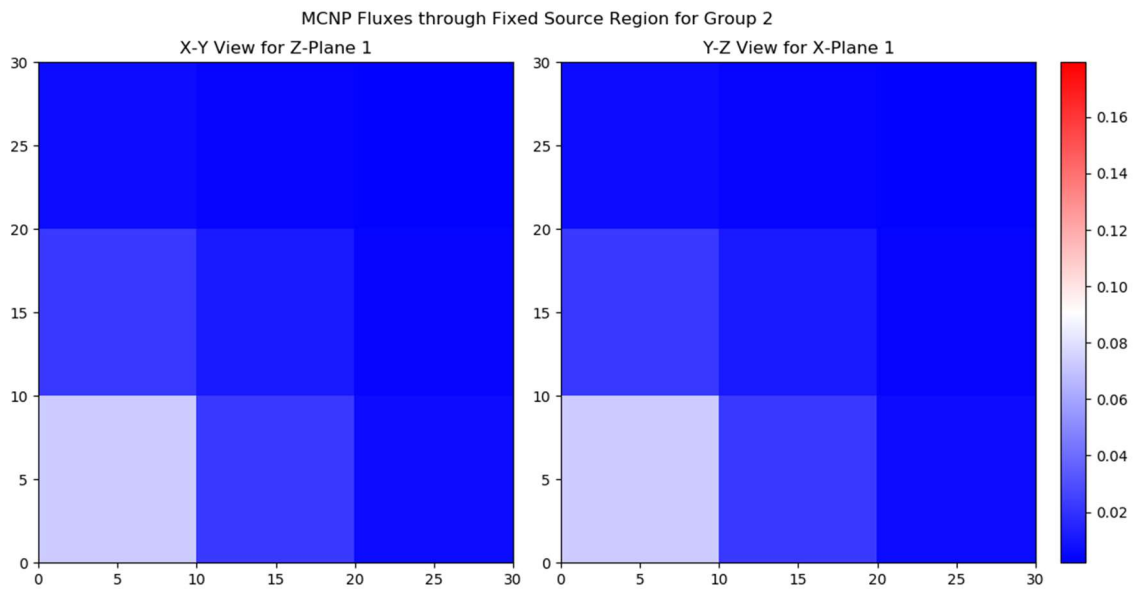


Figure 92. XYZ MG Fixed Source MCNP Reference Flux in Group 2

### 3.3.2.3 DIF3D Results

The transport solver within DIF3D, DIF3D-VARIANT, was used to solve the same configuration that was analyzed by MCNP. Since, as previously stated, an exact analytical match cannot be expected, this verification will focus on ensuring that the DIF3D solution is converging to the MCNP reference solution as the spatial and angular orders are increased. This analysis will not consider additional mesh refinement in DIF3D is not as impactful as increasing the polynomial order first. The metrics used to evaluate the accuracy of the DIF3D solution include the value and location of the maximum region-averaged fluxes for each group, and the root-mean-squared-error of the group- and region-wise fluxes.

All of the cases used an eigenvalue convergence criterion of  $10^{-8}$ , a pointwise fission source convergence of  $10^{-7}$ , average fission source convergence of  $10^{-8}$ , 200 XY-plane partial current sweeps per group per outer iteration, and 200 axial partial current sweeps per outer iteration. All other iteration parameters were left at the DIF3D defaults.

Table 121 provides the difference in the maximum region-averaged group-wise flux between the DIF3D solutions and the MCNP reference. These locations are in the bottom-left region for the MCNP reference and all DIF3D cases; this is expected as this is where the source is located. In these tables, ‘-’ denotes that the case was not possible due to limitations in the amount of memory that the tested version of DIF3D can allocate to solve a model. The ‘\*’ denotes cases that encountered numerical issues and did not converge.

Similarly, Table 122 provides the root-mean-squared-error of the flux across the entire spatial and energy domain of the problem.

**Table 121. XYZ MG DIF3D Peak Flux Errors in units of percent**

Flux	6 <sup>th</sup>	7 <sup>th</sup>	8 <sup>th</sup>	8 <sup>th</sup>	10 <sup>th</sup>	12 <sup>th</sup>	10 <sup>th</sup>	10 <sup>th</sup>
Leakage	1 <sup>st</sup>	2 <sup>nd</sup>	3 <sup>rd</sup>	3 <sup>rd</sup>	3 <sup>rd</sup>	3 <sup>rd</sup>	4 <sup>th</sup>	5 <sup>th</sup>
Source	4 <sup>th</sup>	7 <sup>th</sup>	8 <sup>th</sup>	5 <sup>th</sup>	5 <sup>th</sup>	5 <sup>th</sup>	5 <sup>th</sup>	5 <sup>th</sup>
<b>Group 1</b>								
P <sub>1</sub>	49.43	49.55	49.56	49.56	49.56	49.56	49.56	49.56
P <sub>3</sub>	27.26	28.27	28.31	28.31	28.31	28.31	28.32	28.32
P <sub>5</sub>	10.71	16.29	16.51	16.51	16.5	16.49	*	*
P <sub>7</sub>	-4.24	9.29	10.15	10.15	10.1	10.07	10.24	*
P <sub>9</sub>	-14.38	4.58	6.55	6.55	6.4	-	6.7	-
P <sub>11</sub>	-19.6	1.58	4.31	4.3	-	-	-	-
P <sub>13</sub>	-22.82	-0.43	-	-	-	-	-	-
P <sub>15</sub>	-24.49	-	-	-	-	-	-	-
<b>Group 2</b>								
P <sub>1</sub>	42.24	42.39	42.4	42.4	42.4	42.4	42.4	42.4
P <sub>3</sub>	16.04	17.28	17.34	17.34	17.34	17.34	17.34	17.35
P <sub>5</sub>	2.22	7.38	7.64	7.64	7.62	7.62	*	*
P <sub>7</sub>	-6.59	3.26	4.03	4.03	3.98	3.95	4.09	*
P <sub>9</sub>	-11.64	1.05	2.39	2.39	2.29	-	2.53	-
P <sub>11</sub>	-14.26	-0.3	1.42	1.43	-	-	-	-
P <sub>13</sub>	-15.69	-1.17	-	-	-	-	-	-
P <sub>15</sub>	-16.49	-	-	-	-	-	-	-

In these tables, the spatial source approximation is truncated to reduce memory; this is acceptable as in the fixed source region, the source is effectively flat and thus a 0<sup>th</sup> order approximation would suffice. Outside of the fixed source region, the source is only due to the scattering present in the problem. Since the scattering source depends on the flux, and the total mean-free-paths are on the order of 10s of cm, the scattering source will be slowly varying within a region and therefore low orders will suffice. This can be observed when comparing the 8-3-8 (Flux-Leakage-Source) column's errors to the 8-3-5 column's errors. This comparison shows that reducing the source's

February 13, 2020

---

polynomial order by three orders had no effect on the errors but the 8-3-5 case was able to run a higher angular approximation due to the reduced memory requirements of the 5<sup>th</sup> order spatial source approximation.

The spatial flux convergence is achieved at the eighth order; this can be observed by comparing the 8-3-5, 10-3-5, and 12-3-5 results in Table 121 and Table 122. Here, the only change is the order of the spatial flux polynomials used, yet there is at most a third significant digit change in the peak and root-mean-squared errors.

Similarly, spatial leakage convergence is achieved by the third leakage order as seen by comparing the 10-3-5, 10-4-5, and 10-5-5 results in Table 121 and Table 122. Only the leakage is changed in these three calculations and only the last significant digit of each metric is changed.

This case is easily converged in space as the spatial flux distribution is generally smooth. Specifically, the flux will exhibit the standard exponential decay through a material whose cross sections are such that neutrons have a mean-free-path of at least 10 cm. If a strong absorber like a thermal reactor control rod was included, then more spatial orders would naturally be necessary.

The angular refinement is the last component to consider and one can observe that convergence is not yet observed as the highest two possible angular orders for each Flux-Leakage-Source combination are still changing. This is expected behavior in a problem with a discrete volumetric fixed source. Within the fixed source region, the angular flux order may not need to be much larger than the defined fixed source, which in this case is isotropic. However, the angular leakage order representing the angular dependence of the leakage from the source region to its neighboring regions will need to be large as the leakage is skewed strongly away from the source region. In the non-source regions, the angular flux order will need to be high due to the leakage from the source region; further, without strong scattering the angular leakage order in non-source regions will also need to be high. In general, the Table 121 and Table 122 error metrics show that the error is strongly driven by the angular order and any case that is sufficiently converged spatially (i.e., not 6-1-4) will benefit from increasing the angular order.

Table 122. XYZ MG DIF3D Flux Root-Mean-Squared-Errors

Flux	6 <sup>th</sup>	7 <sup>th</sup>	8 <sup>th</sup>	8 <sup>th</sup>	10 <sup>th</sup>	12 <sup>th</sup>	10 <sup>th</sup>	10 <sup>th</sup>
Leakage	1 <sup>st</sup>	2 <sup>nd</sup>	3 <sup>rd</sup>	3 <sup>rd</sup>	3 <sup>rd</sup>	3 <sup>rd</sup>	4 <sup>th</sup>	5 <sup>th</sup>
Source	4 <sup>th</sup>	7 <sup>th</sup>	8 <sup>th</sup>	5 <sup>th</sup>	5 <sup>th</sup>	5 <sup>th</sup>	5 <sup>th</sup>	5 <sup>th</sup>
<b>Group 1</b>								
P <sub>1</sub>	1.78E-02	1.79E-02	1.79E-02	1.79E-02	1.79E-02	1.79E-02	1.79E-02	1.79E-02
P <sub>3</sub>	9.68E-03	1.00E-02	1.01E-02	1.01E-02	1.01E-02	1.01E-02	1.01E-02	1.01E-02
P <sub>5</sub>	4.05E-03	5.98E-03	6.06E-03	6.06E-03	6.06E-03	6.06E-03	*	*
P <sub>7</sub>	2.95E-03	3.55E-03	3.89E-03	3.89E-03	3.87E-03	3.86E-03	3.94E-03	*
P <sub>9</sub>	6.41E-03	1.81E-03	2.59E-03	2.59E-03	2.52E-03	-	2.66E-03	-
P <sub>11</sub>	8.34E-03	8.12E-04	1.72E-03	1.72E-03	-	-	-	-
P <sub>13</sub>	9.57E-03	8.44E-04	-	-	-	-	-	-
P <sub>15</sub>	1.02E-02	-	-	-	-	-	-	-
<b>Group 2</b>								
P <sub>1</sub>	6.04E-03	6.06E-03	6.06E-03	6.06E-03	6.06E-03	6.06E-03	6.06E-03	6.06E-03
P <sub>3</sub>	2.38E-03	2.56E-03	2.57E-03	2.57E-03	2.57E-03	2.57E-03	2.57E-03	2.57E-03
P <sub>5</sub>	5.15E-04	1.15E-03	1.20E-03	1.20E-03	1.19E-03	1.19E-03	*	*
P <sub>7</sub>	1.13E-03	5.08E-04	6.38E-04	6.38E-04	6.29E-04	6.23E-04	6.51E-04	*
P <sub>9</sub>	1.96E-03	1.69E-04	3.76E-04	3.76E-04	3.57E-04	-	4.03E-04	-
P <sub>11</sub>	2.39E-03	1.63E-04	2.20E-04	2.22E-04	-	-	-	-
P <sub>13</sub>	2.63E-03	2.91E-04	-	-	-	-	-	-
P <sub>15</sub>	2.76E-03	-	-	-	-	-	-	-

With these findings, the 7-2-7 P<sub>11</sub> case will be considered the converged DIF3D result for the qualitative region-wise flux comparisons. These are shown in Figure 93 and Figure 94 for groups 1 and 2, respectively. Each of these figures provides two plots; the left is the bottom-most plane of model (i.e., that with the fixed source) and the right is the top-most plane (i.e., the furthest from the source). Within each of these figures is the DIF3D-to-MCNP flux ratios in each of the 9 regions of the plane. The ratio is provided numerically as well as by color where blue indicates the DIF3D result is less than the MCNP, white implying they are close, and red implying the DIF3D result is larger than in MCNP. These results show overall very close agreement for the majority of the central regions.

February 13, 2020

In these figures, the largest errors are present in the central region on the bottom plane (5.6% error in group 1) and at the top-right of the top plane (3.7% error in group 1). The central region on the bottom plane is located on the diagonal from the fixed source region in the lower-left. This case is likely because for particles to enter the central region on the bottom plane, in reality (and the reference), they are most likely simply streaming from the source to this region directly. DIF3D-VARIANT cannot directly stream to a diagonal region in a Cartesian geometry like this and instead neutrons must first be passed to the right (or up) via inter-node leakage, and then passed up (or right, respectively) to the diagonal node. Each of these moves accrues additional error due to the spatial and angular approximations in place.

The upper-right region is the furthest from the source and naturally sees the errors build-up as the particles are transported from the source. Further, this region is located on the periphery of the model and also has error from the vacuum boundary condition that is difficult to capture with the spherical harmonics angular expansion as previously discussed.

Given that the vast majority of the model is within 2% of the analog MCNP solution, and the solution is shown to be convergent to the correct solution, the DIF3D capability for the XYZ geometry is considered verified. Further, since the RTFLUX files were utilized to prepare these comparisons (and similar comparisons across the other geometry types of this work) to the MCNP results, and the RTFLUX files were compared to the edits of the real flux information in DIF3D's standard output, the content of the RTFLUX files are also considered verified.

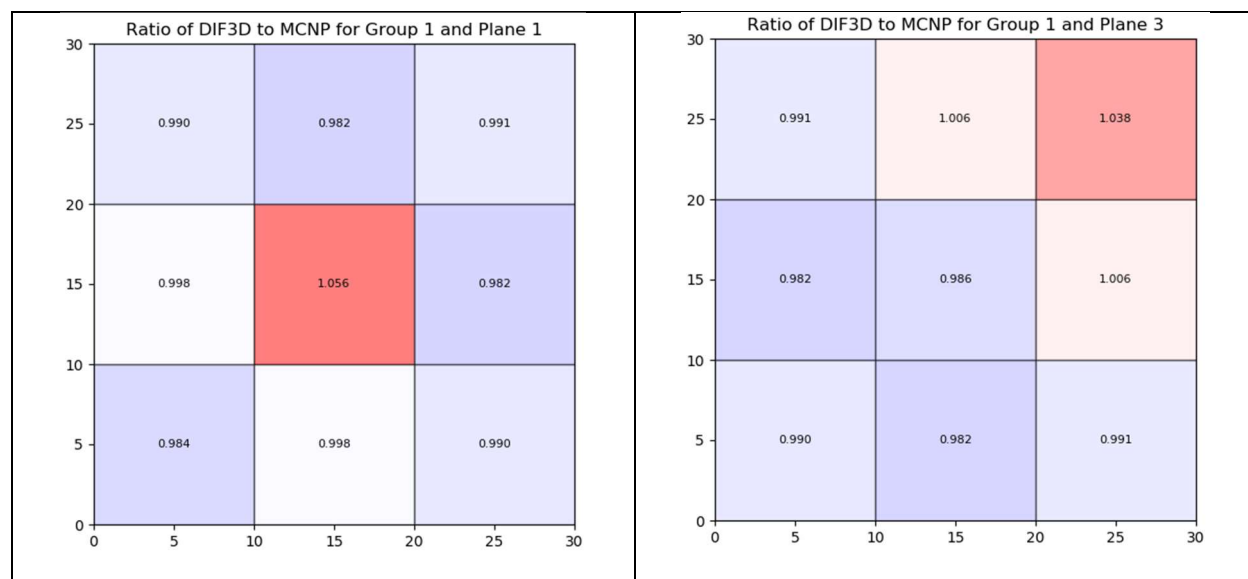


Figure 93. XYZ MG DIF3D to MCNP Flux Ratios in Group 1

February 13, 2020

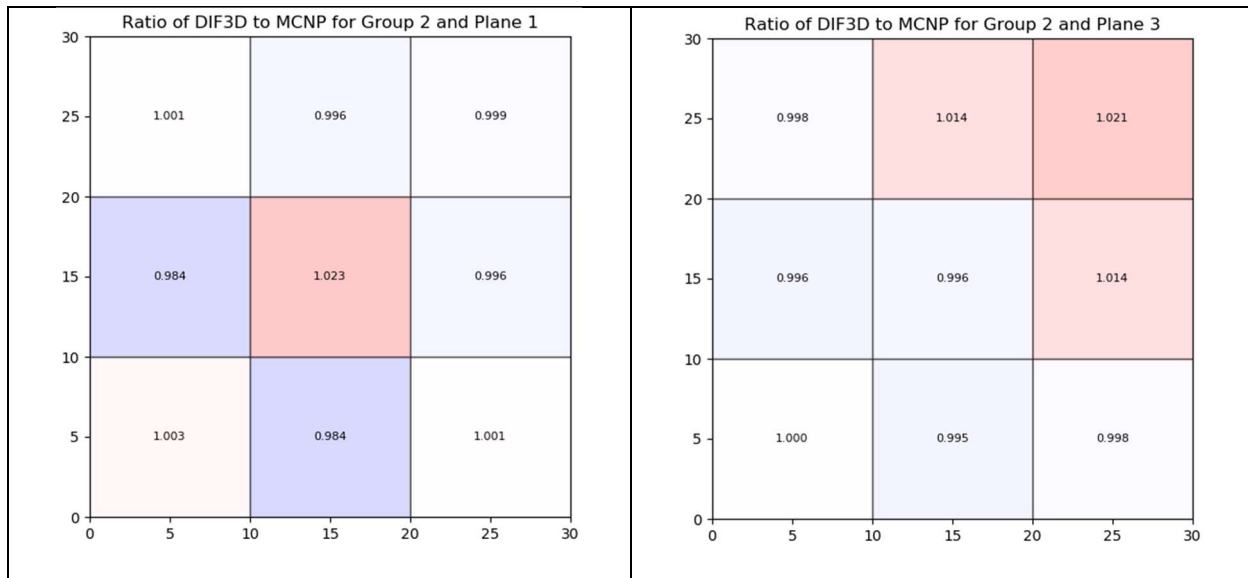


Figure 94. XYZ MG DIF3D to MCNP Flux Ratios in Group 2

### 3.3.2.4 Verification of Important Anisotropic Scattering

As discussed in [6], to utilize this anisotropic scattering case as verification that anisotropic scattering is working, it must be verified that a different and sensible result is obtained when isotropic scattering (with the same data) compared to the anisotropic result. In this case, the same 7-2-7  $P_{11}$  case was re-ran with isotropic scattering via option 9 of the Type 12 card in the A.DIF3D input block. Similarly, DIF3D was told to utilize the total cross section instead of the transport cross section. Thus the problem is truly isotropic in nature.

Since this model is forward-scattering (i.e.,  $P_1/P_0$  is positive), the isotropic case should have less neutrons at locations further from the source. Further, since the  $P_1/P_0$  is larger in the 2<sup>nd</sup> group, this effect should be exacerbated in group 2. Figure 95 and Figure 96 provide plots similar to Figure 93 through Figure 94 except the ratio in this case is the isotropic flux compared to the anisotropic flux in each of the two groups. A ratio less than one should be observable further out from the source in the lower left, and even more so in the second group. This is exactly what is observed in Figure 95 and Figure 96.

February 13, 2020

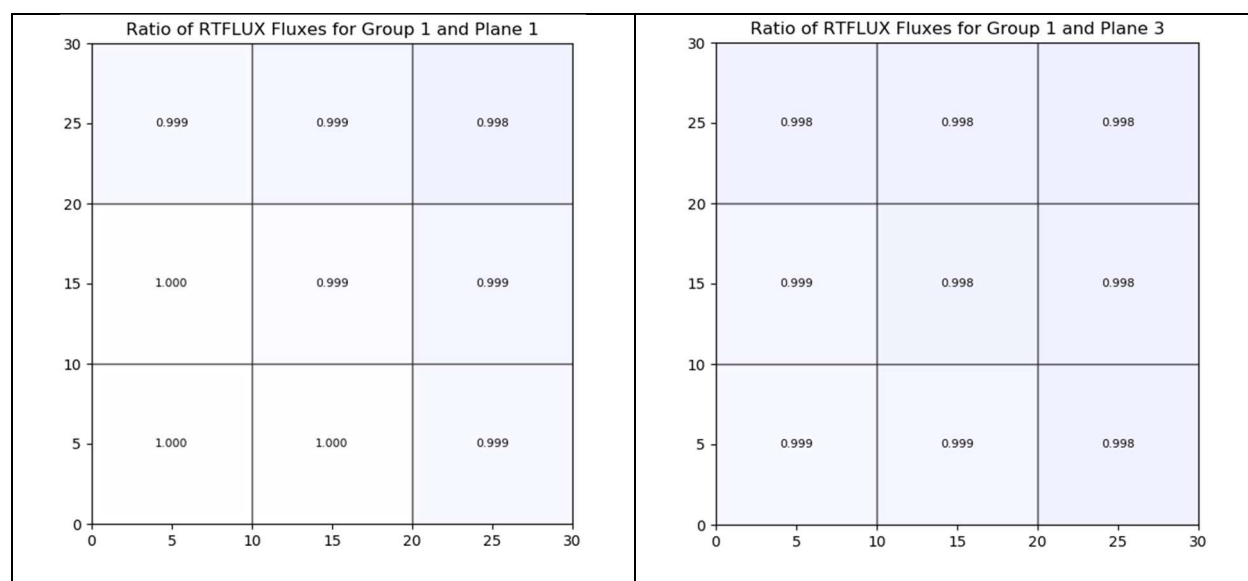


Figure 95. XYZ MG Isotropic to Anisotropic DIF3D Flux Ratios in Group 1

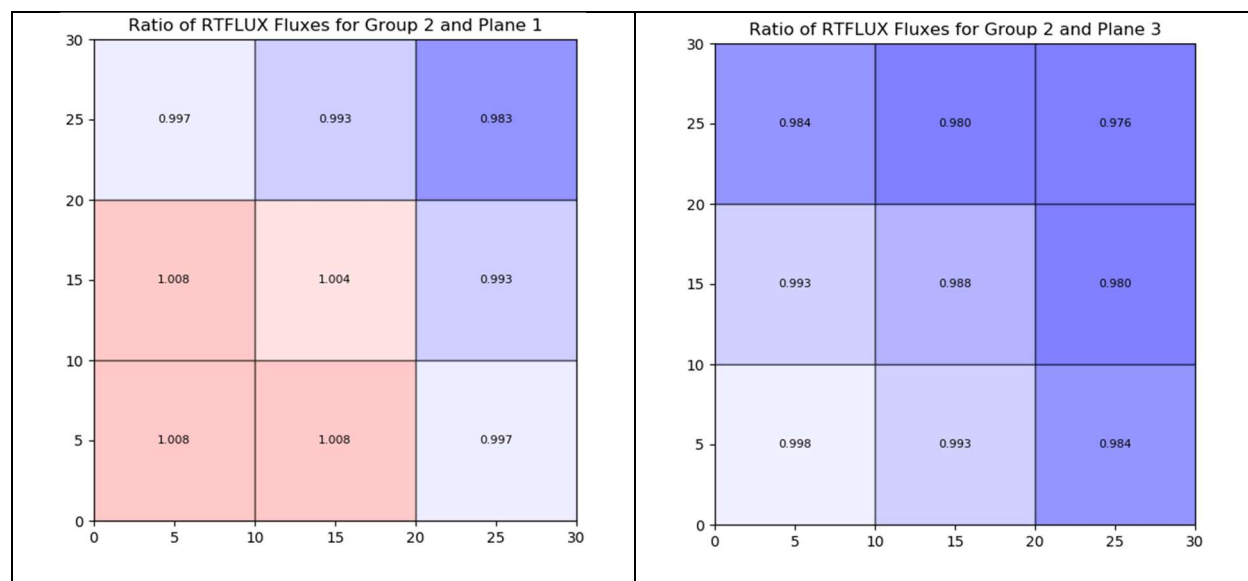


Figure 96. XYZ MG Isotropic to Anisotropic DIF3D Flux Ratios in Group 2

### 3.3.2.5 Inhomogeneous Fixed Source Verification

In addition to the traditional fixed source capability, DIF3D also provides the capability to compute an inhomogeneous fixed source calculation. That is, a fixed source problem with fissile media. While this capability was previously included in the manufactured solution verification discussed earlier in Section 3.1.6, that case only considered a single region and one energy group. To ensure the capability works as expected in a multi-region, multigroup case the fixed source model discussed above was modified to include fission.

Specifically, the fixed source, scattering source, and fission source are combined in DIF3D to create the total within group source for the solution of each inner iteration. With this equation, it is clear that the total within group source will stay the same if some amount of up- or down-scattering is removed from the  $P_0$  scattering term and replaced with an equivalent fission cross section, fission multiplicity, and fission spectrum. For this case the  $P_0$  up-scatter from group 2 to group 1 of the REG2 material defined in Table 120 was replaced with the cross sections defined in the “Modified REG2” set in Table 123.

**Table 123. Modified Multigroup Macroscopic Cross Sections for Inhomogeneous Case; units of cross sections are 1/cm**

	REG2		Modified REG2	
	Group 1	Group 2	Group 1	Group 2
$\Sigma_{\text{total}}$	3.33333E-02	5.00000E-02	3.33333E-02	5.00000E-02
$\Sigma_{\text{abs}}$	2.33333E-02	3.50000E-02	2.33333E-02	3.50000E-02
$\nu$	-	-	5.00000E-01	5.00000E-01
$\Sigma_{\text{fission}}$	-	-	0.00000E+00	1.50000E-03
$\nu\Sigma_{\text{fission}}$	-	-	0.00000E+00	7.50000E-04
$\chi$	-	-	1.00000E+00	0.00000E+00
$\Sigma_{\text{scatter},0,1 \rightarrow g}$	2.00000E-03	8.00000E-03	2.00000E-03	8.00000E-03
$\Sigma_{\text{scatter},0,2 \rightarrow g}$	1.50000E-03	1.35000E-02	0.00000E+00	1.35000E-02
$\Sigma_{\text{scatter},1,1 \rightarrow g}$	1.00000E-04	4.00000E-04	1.00000E-04	4.00000E-04
$\Sigma_{\text{scatter},1,2 \rightarrow g}$	7.50000E-05	6.75000E-04	7.50000E-05	6.75000E-04

These cross sections, when combined with an input  $k_{\text{eff}}$  value of 0.5, result in a total source (Q) that is equivalent between REG2 and the Modified REG2. Therefore DIF3D should yield the same flux distribution in space and energy regardless of if REG2 or the Modified REG2 are applied. This modified case was run and it was explicitly verified that the resultant DIF3D fluxes were the exact same between the two cases to all reported significant figures, though it is noted that DIF3D required 5 iterations to converge in this case instead of just two iterations as is for the case that included no fission.

### 3.3.3 Multigroup Eigenvalue Verification

As discussed in Section 3.3.4 of [6], a three-group (with up-scattering), anisotropic, 3D Cartesian, eigenvalue verification case must be generated to test the ability of DIF3D-VARIANT to compute multigroup, multi-region eigenvalue solutions. This case will utilize multiple regions with different cross sections, and have vacuum boundary conditions on all six surfaces of the XYZ domain.

Since a multigroup, 3D, multi-region analytical solution to the neutron transport equation is infeasible, the reference solution was stated in [6] to be determined from a multigroup Monte Carlo code. In this case, MCNP 6.2 [15] will be used to solve the exact same geometric, material, and



cross sections used in the DIF3D model. Further, the MCNP 6.2 tally regions will be defined exactly consistent with the fine-mesh regions in the DIF3D model to avoid any coarsening of results when performing the code-to-code comparison. Since a code-to-code comparison will be used for verification of DIF3D, the features of the MCNP 6.2 code used to generate this reference solution must also be verified. The verification of relevant MCNP 6.2 features are documented in Section 4.

The specific model definition chosen must be one that both solvers should be expected to practically solve while still challenging DIF3D in its' ability to solve a model with characteristics relevant to hexagonal-Z fast reactor analyses. DIF3D's variational transport method makes the following approximations, among others: 1) uses polynomial basis functions to represent the spatial distribution of the neutron flux, 2) expands the angular flux within the node and on the nodal surface with spherical harmonics, and 3) each of these expansions must be truncated to fit within the memory constraints of the solver and/or computer. These approximations limit the type of model that can be used for this verification. Specifically, these approximations mean one should expect that DIF3D's accuracy will be limited in problems with strong spatial and angular flux gradients as anticipated primarily near vacuum boundary conditions. These can also occur near strong absorbers, however, since the targeted application is a fast reactor these internal strongly absorbing regions will not be considered as they are not present. Therefore, a challenging yet solvable verification problem for DIF3D should have enough neutron leakage that this effect is visible, however, this neutron leakage and associated anisotropy should not dominate the solution. Practically this means the reactor size should be not too small and not too large.

The following approach will be taken when comparing the DIF3D and MCNP results. First, the calculated eigenvalues will be compared. Then, the calculated flux distribution will be compared through three metrics: the maximal (normalized) region-averaged flux value and location, the root-mean-squared-error of the DIF3D flux compared to the MCNP flux distributions for each group, and finally a graphical comparison of the differences in flux distributions will be displayed. It is unlikely that the DIF3D and MCNP results will match exactly, because of each method's distinct iterative error sources that cannot be practically removed from the analysis. Therefore, instead of striving for an exact match, this work will instead show that refining DIF3D's spatial and angular order does converge towards the MCNP reference result.

### 3.3.3.1 *Model Definition*

Based on the above considerations, a cuboid 100 cm to a side was chosen for the total problem extent; including 20 cm of reflection in the XY plane and 10 cm in the Z dimension. The reflector was found to be necessary to reduce the neutron flux anisotropy near the fissionable region's periphery while also mimicking the geometry of the typical fast reactors.

The resultant 100 cm x 100 cm x 100 cm is composed of three unique concentric parallelepipeds. The innermost region, REG1, is a square (in the XY plane) 20 cm on a side extending from 10cm to 90cm above the bottom of the model (in the Z-direction). This innermost region is surrounded by another region, REG2, which is a square (in the XY plane) 60 cm on a side and also extending

from 10cm to 90cm above the bottom of the model. The remainder of the 100 cm cuboid is composed of REG3. REG1 and REG2 are fissionable while REG3 is not. Both the DIF3D and MCNP representations of this model are discretized with an equal-width mesh spacing of 10 cm in each of the X, Y, and Z dimensions.

The three group macroscopic cross sections for each of these regions are provided in Table 120; all significant digits are shown. This shows that all three regions scatter from group 1 into all other groups, group 2 only down-scatters, and group 3 has a large amount of up-scatter. Each region includes linearly anisotropic scattering. The  $P_1/P_0$  moment ratio for REG1 is 0.25, for REG2 it is 0.23, and REG3 is 0.05. Importantly, all of these ratios are less than 1/3; if they were greater than 1/3 a negative angular distribution would be encountered during the MCNP computations potentially leading to significant (100s to 1,000s of pcm) discrepancies between a deterministic and Monte Carlo solver.

**Table 124. 3D Cartesian Transport Multigroup Eigenvalue Cross Sections; units of cross sections are 1/cm**

	REG1			REG2			REG3		
	Group 1	Group 2	Group 3	Group 1	Group 2	Group 3	Group 1	Group 2	Group 3
$\Sigma_{\text{total}}$	2.400E-01	9.750E-01	3.100E+00	2.628E-01	1.065E+00	3.370E+00	2.454E-01	9.750E-01	3.100E+00
$\Sigma_{\text{abs}}$	1.200E-02	1.000E-01	1.100E+00	1.200E-02	1.020E-01	1.170E+00	6.000E-03	4.000E-02	2.000E-01
$\nu\Sigma_{\text{fission}}$	1.800E-02	1.500E-01	1.800E+00	1.980E-02	1.650E-01	1.980E+00	0.000E+00	0.000E+00	0.000E+00
$\chi$	9.600E-01	4.000E-02	0.000E+00	9.000E-01	5.000E-02	5.000E-02	0.000E+00	0.000E+00	0.000E+00
$\Sigma_{\text{scatter},0,1\rightarrow g}$	2.400E-02	1.710E-01	3.300E-02	2.640E-02	1.881E-01	3.630E-02	2.520E-02	1.796E-01	3.465E-02
$\Sigma_{\text{scatter},0,2\rightarrow g}$	0.000E+00	6.000E-01	2.750E-01	0.000E+00	6.600E-01	3.025E-01	0.000E+00	6.411E-01	2.939E-01
$\Sigma_{\text{scatter},0,3\rightarrow g}$	0.000E+00	1.000E+00	1.000E+00	0.000E+00	1.100E+00	1.100E+00	0.000E+00	1.450E+00	1.450E+00
$\Sigma_{\text{scatter},1,1\rightarrow g}$	6.000E-03	4.275E-02	8.250E-03	6.000E-03	4.275E-02	8.250E-03	1.260E-03	8.978E-03	1.733E-03
$\Sigma_{\text{scatter},1,2\rightarrow g}$	0.000E+00	1.500E-01	6.875E-02	0.000E+00	1.500E-01	6.875E-02	0.000E+00	3.206E-02	1.469E-02
$\Sigma_{\text{scatter},1,3\rightarrow g}$	0.000E+00	2.500E-01	2.500E-01	0.000E+00	2.500E-01	2.500E-01	0.000E+00	7.250E-02	7.250E-02

### 3.3.3.2 Reference MCNP Results

The previously described model was converted to an MCNP model via the `create_mcnpy` script. This script reads a DIF3D model's geometry from the GEODST file and the composition cross sections from the COMPTS file and creates an exact duplicate of the model in MCNP. The MCNP file created from this script only utilizes planar surfaces and cells assigned to the root universe, minimizing the amount of MCNP features that must be verified to support this work. The MCNP

February 13, 2020

input file included tally regions for each of the DIF3D fine-mesh blocks and for each energy group of the problem. Finally, this script creates the multigroup nuclear data library for MCNP by way of the `simple\_ace\_mg.pl` script that is distributed by Los Alamos National Laboratory with MCNP [16].

The MCNP reference case was run with 400,000 histories per batch, 100 inactive batches, and 16,000 active batches for a total of 6.4 billion active histories. The resultant value of  $k_{\text{eff}}$  predicted by MCNP was 1.58684 with an estimated standard deviation of 0.00001. The L'Ecuyer 63-bit generator (number 1) was used due to its period of  $9.2 \times 10^{18}$  numbers, six orders of magnitude larger than the default Lehmer 48-bit congruential generator, and for consistency with other MCNP models included in this work. The relative errors for all tally bins were distributed as is shown in Figure 97. The majority of these relative errors are significantly smaller than any expected code-to-code differences and therefore no further visualization or description of their behavior follows.

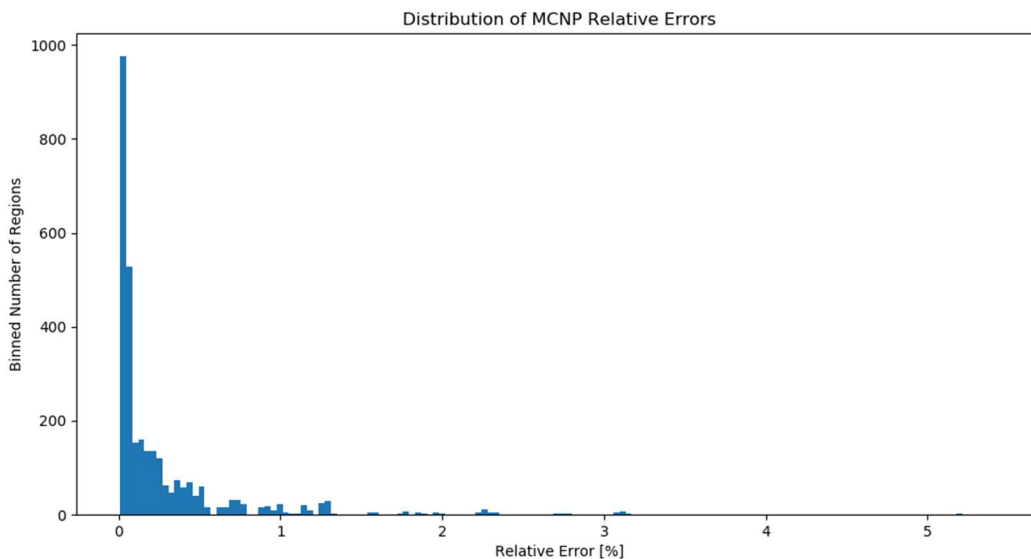


**Figure 97. XYZ MG Eigenvalue MCNP Flux Rel. Err. Distribution**

This case yielded a flux distribution that is generally sinusoidal in shape in the radial (XY) and axial dimensions. This flux distribution is provided in Figure 98 through Figure 100. These figures show a slice of the flux distribution computed by MCNP through a central slice of both the X-Y (left) and Y-Z (right) planes for the fast, epithermal, and thermal groups, respectively. In these figures, and other flux distribution figures throughout this Section, the color-scale is chosen so that low flux values are blue, the median is white, and the highest flux regions are shown in red. The minimum and maximum values to generate these color schemes are based on the flux extremes over all energy groups, hence the same color scale is applied to Figure 98 through Figure 100. Given this coloring scheme, it is clearly evident that the fissile region is between 30 and 50 cm in the X and Y dimensions and 10 to 90 cm in the Z dimension.

February 13, 2020

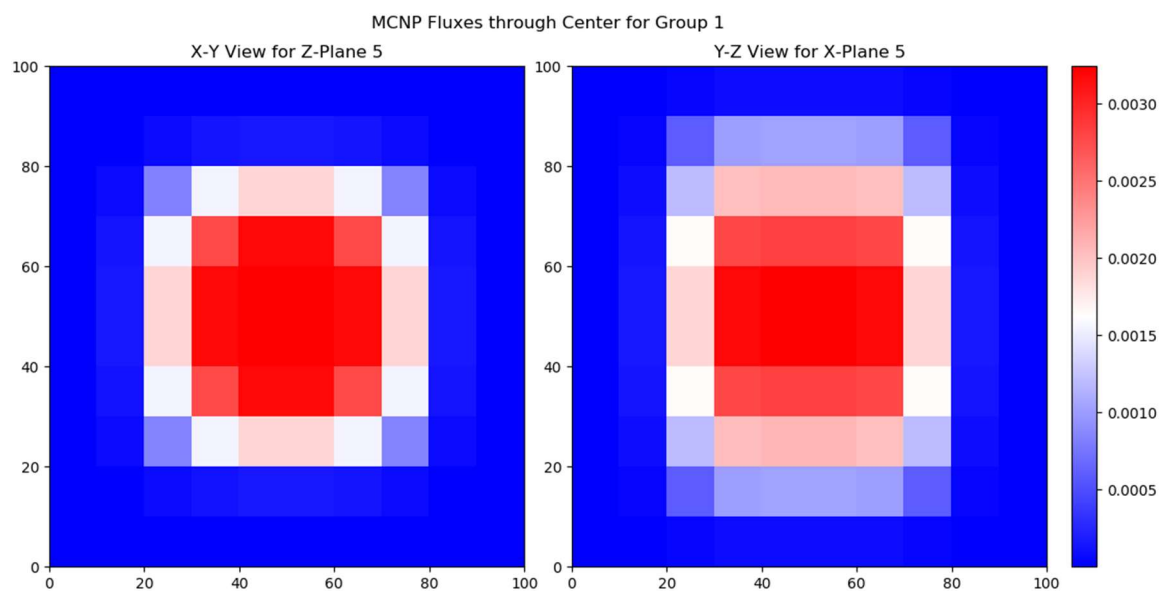


**Figure 98. XYZ MG Eigenvalue MCNP Reference Flux in Group 1**

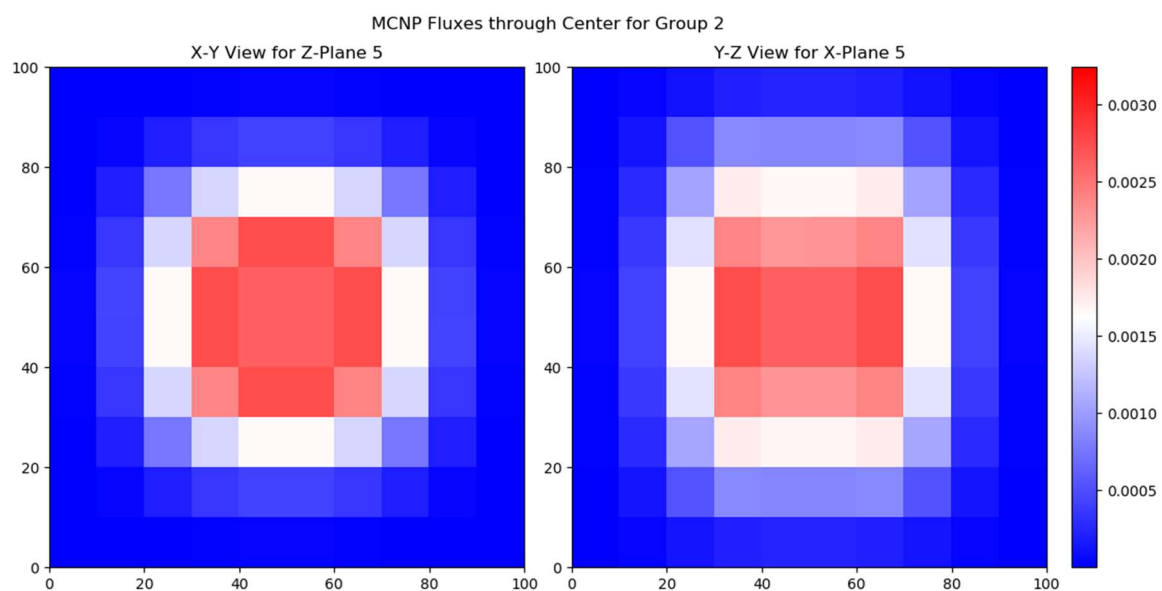


**Figure 99. XYZ MG Eigenvalue MCNP Reference Flux in Group 2**

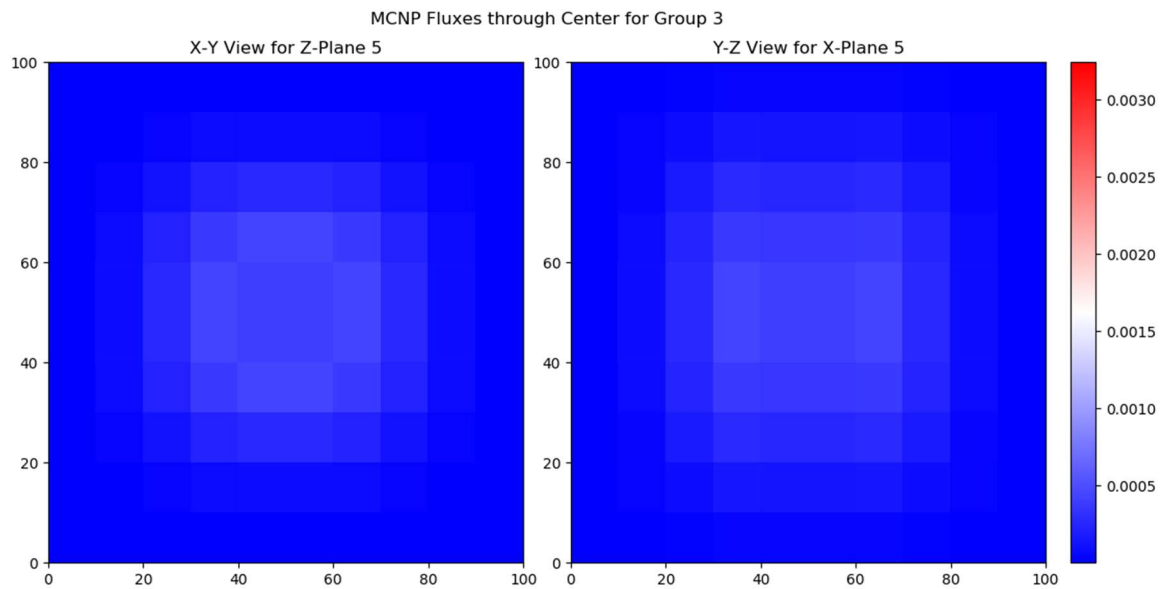


Figure 100. XYZ MG Eigenvalue MCNP Reference Flux in Group 3

### 3.3.3.3 DIF3D Results

The transport solver within DIF3D, DIF3D-VARIANT, was used to solve the same reactor and multigroup cross sections that was analyzed by MCNP. Since, as previously stated, an exact analytical match cannot be expected, this verification will focus on ensuring that the DIF3D solution is converging to the MCNP reference solution as the spatial and angular orders are increased. This analysis will not consider additional mesh refinement in DIF3D as it is not as impactful as increasing the polynomial order first. The metrics used to evaluate the accuracy of the DIF3D solution include the eigenvalue accuracy, value and location of the maximum region-averaged fluxes for each group, and the root-mean-squared-error of the group- and region-wise fluxes.

All of the cases used an eigenvalue convergence criterion of  $10^{-8}$ , a pointwise fission source convergence of  $10^{-7}$ , average fission source convergence of  $10^{-8}$ , 80 XY-plane partial current sweeps per group per outer iteration, and 80 axial partial current sweeps per outer iteration. All other iteration parameters were left at the DIF3D defaults.

Table 125 provides the DIF3D-VARIANT computed eigenvalue errors for this model as a function of both the spatial (columns) and angular approximations (rows). In these tables, '-' denotes that the case was not possible due to limitations in the amount of memory that the tested version of DIF3D can allocate to solve a model.

Table 125. XYZ MG DIF3D Eigenvalue Errors in units of pcm

Flux	6 <sup>th</sup>	7 <sup>th</sup>	8 <sup>th</sup>	8 <sup>th</sup>	10 <sup>th</sup>	12 <sup>th</sup>	10 <sup>th</sup>	10 <sup>th</sup>
Leakage	1 <sup>st</sup>	2 <sup>nd</sup>	3 <sup>rd</sup>	3 <sup>rd</sup>	3 <sup>rd</sup>	3 <sup>rd</sup>	4 <sup>th</sup>	5 <sup>th</sup>
Source	4 <sup>th</sup>	7 <sup>th</sup>	8 <sup>th</sup>	5 <sup>th</sup>	5 <sup>th</sup>	5 <sup>th</sup>	5 <sup>th</sup>	5 <sup>th</sup>
P <sub>1</sub>	-257	-263	-263	-262	-263	-263	-263	-263
P <sub>3</sub>	11	-15	-15	-14	-14	-14	-14	-14
P <sub>5</sub>	30	-4	-5	-4	-4	-4	-4	-4
P <sub>7</sub>	36	-1	-3	-1	-2	-2	-2	-2
P <sub>9</sub>	37	0	-2	-1	-1	-	-1	-
P <sub>11</sub>	38	0	-2	0	-	-	-	-
P <sub>13</sub>	38	0	-	-	-	-	-	-
P <sub>15</sub>	38	-	-	-	-	-	-	-

In the table, the spatial source approximation is truncated for two reasons: 1) it is generally not as important as the flux or leakage approximations and 2) it is done to reduce the memory requirements of high order space-angle approximations. This can be observed when comparing the 8-3-8 (Flux-Leakage-Source) column's errors to the 8-3-5 column's errors where the reduction in the source's polynomial order by three orders impacted the eigenvalue by one pcm.

The spatial flux convergence is achieved at the eighth order; this can be observed by comparing the 8-3-5, 10-3-5, and 12-3-5 results in Table 121. Here, the only change is the order of the spatial flux polynomials used, yet there is at most a 1 pcm change in the eigenvalue. Spatial leakage convergence is achieved by the third leakage order. This is seen by comparing the 10-3-5, 10-4-5, and 10-5-5 results in Table 121. Only the leakage is changed in these three calculations and no error change is observed. The angular refinement is the last component to consider and one can observe that at the highest orders that have been computed, there is 0-1 pcm of change in the eigenvalue.

Table 126 provides the difference in the maximum region-averaged group-wise flux between the DIF3D solutions and the MCNP reference. The locations of the peak were verified to be either in the same location as the MCNP reference, or in a symmetric location to the MCNP reference. The same general trends as discussed in the eigenvalue with the spatial orders are seen here, however the peak flux errors increase as the angular order increases at orders greater than P<sub>3</sub>. These orders generally saturate at around P<sub>7</sub> or P<sub>9</sub>.

Table 126. XYZ MG DIF3D Peak Flux Errors in units of percent

Flux	6 <sup>th</sup>	7 <sup>th</sup>	8 <sup>th</sup>	8 <sup>th</sup>	10 <sup>th</sup>	12 <sup>th</sup>	10 <sup>th</sup>	10 <sup>th</sup>
Leakage	1 <sup>st</sup>	2 <sup>nd</sup>	3 <sup>rd</sup>	3 <sup>rd</sup>	3 <sup>rd</sup>	3 <sup>rd</sup>	4 <sup>th</sup>	5 <sup>th</sup>
Source	4 <sup>th</sup>	7 <sup>th</sup>	8 <sup>th</sup>	5 <sup>th</sup>	5 <sup>th</sup>	5 <sup>th</sup>	5 <sup>th</sup>	5 <sup>th</sup>
Group 1								
P <sub>1</sub>	-3.02	-3.11	-3.12	-3.12	-3.12	-3.12	-3.12	-3.12
P <sub>3</sub>	0.24	-0.15	-0.16	-0.15	-0.16	-0.16	-0.15	-0.15
P <sub>5</sub>	0.57	0.06	0.04	0.05	0.04	0.03	0.05	0.05
P <sub>7</sub>	0.66	0.11	0.09	0.09	0.08	0.07	0.09	0.09
P <sub>9</sub>	0.68	0.13	0.10	0.11	0.09	-	0.10	-
P <sub>11</sub>	0.69	0.13	0.11	0.11	-	-	-	-
P <sub>13</sub>	0.69	0.14	-	-	-	-	-	-
P <sub>15</sub>	0.69	-	-	-	-	-	-	-
Group 2								
P <sub>1</sub>	-0.50	-0.48	-0.48	-0.49	-0.49	-0.49	-0.49	-0.49
P <sub>3</sub>	0.09	-0.03	-0.02	-0.02	-0.03	-0.03	-0.03	-0.03
P <sub>5</sub>	0.24	0.09	0.10	0.09	0.08	0.08	0.09	0.09
P <sub>7</sub>	0.28	0.13	0.13	0.13	0.11	0.11	0.12	0.12
P <sub>9</sub>	0.30	0.14	0.14	0.14	0.12	-	0.13	-
P <sub>11</sub>	0.30	0.14	0.14	0.14	-	-	-	-
P <sub>13</sub>	0.30	0.15	-	-	-	-	-	-
P <sub>15</sub>	0.30	-	-	-	-	-	-	-
Group 3								
P <sub>1</sub>	-0.51	-0.48	-0.49	-0.51	-0.52	-0.52	-0.52	-0.51
P <sub>3</sub>	0.09	-0.02	-0.03	-0.03	-0.05	-0.05	-0.04	-0.04
P <sub>5</sub>	0.24	0.10	0.09	0.08	0.07	0.06	0.08	0.08
P <sub>7</sub>	0.28	0.13	0.12	0.11	0.10	0.09	0.10	0.10
P <sub>9</sub>	0.30	0.15	0.13	0.13	0.11	-	0.11	-
P <sub>11</sub>	0.30	0.15	0.14	0.13	-	-	-	-
P <sub>13</sub>	0.30	0.15	-	-	-	-	-	-
P <sub>15</sub>	0.30	-	-	-	-	-	-	-

Table 127 provides the root-mean-squared-error (RMSE) of the DIF3D and MCNP region-averaged group-wise fluxes. The same general trends are observed; increasing the spatial order generally improves the RMSE. Increasing angular order does increase the RMSE for the 6-1-4 case after P<sub>3</sub>, approaching an asymptote after P<sub>9</sub>; for the others the error effectively maintains constant except for the last reported significant digit at angular orders greater than P<sub>3</sub>. These differences are inconsequentially small and since the error growth is on the order of the fission

February 13, 2020

source and eigenvalue convergence criteria ( $10^{-7}$  and  $10^{-8}$ , respectively), no further investigation will be performed.

Table 127. XYZ MG DIF3D Flux Root-Mean-Squared-Errors

Flux	6 <sup>th</sup>	7 <sup>th</sup>	8 <sup>th</sup>	8 <sup>th</sup>	10 <sup>th</sup>	12 <sup>th</sup>	10 <sup>th</sup>	10 <sup>th</sup>
Leakage	1 <sup>st</sup>	2 <sup>nd</sup>	3 <sup>rd</sup>	3 <sup>rd</sup>	3 <sup>rd</sup>	3 <sup>rd</sup>	4 <sup>th</sup>	5 <sup>th</sup>
Source	4 <sup>th</sup>	7 <sup>th</sup>	8 <sup>th</sup>	5 <sup>th</sup>	5 <sup>th</sup>	5 <sup>th</sup>	5 <sup>th</sup>	5 <sup>th</sup>
<b>Group 1</b>								
P <sub>1</sub>	1.82E-05	1.85E-05	1.86E-05	1.86E-05	1.86E-05	1.86E-05	1.86E-05	1.86E-05
P <sub>3</sub>	1.46E-06	2.50E-06	2.68E-06	2.66E-06	2.70E-06	2.71E-06	2.68E-06	2.68E-06
P <sub>5</sub>	2.91E-06	9.14E-07	1.19E-06	1.18E-06	1.19E-06	1.20E-06	1.20E-06	1.22E-06
P <sub>7</sub>	3.61E-06	8.06E-07	8.86E-07	8.85E-07	8.83E-07	8.84E-07	9.10E-07	9.30E-07
P <sub>9</sub>	3.87E-06	8.66E-07	8.15E-07	8.19E-07	8.08E-07	-	8.30E-07	-
P <sub>11</sub>	3.97E-06	9.12E-07	7.99E-07	8.05E-07	-	-	-	-
P <sub>13</sub>	4.01E-06	9.40E-07	-	-	-	-	-	-
P <sub>15</sub>	4.02E-06	-	-	-	-	-	-	-
<b>Group 2</b>								
P <sub>1</sub>	1.48E-05	1.50E-05	1.50E-05	1.50E-05	1.50E-05	1.50E-05	1.50E-05	1.50E-05
P <sub>3</sub>	1.21E-06	1.65E-06	1.59E-06	1.57E-06	1.61E-06	1.63E-06	1.58E-06	1.58E-06
P <sub>5</sub>	2.24E-06	7.70E-07	7.66E-07	7.62E-07	7.90E-07	8.02E-07	7.67E-07	7.65E-07
P <sub>7</sub>	2.63E-06	7.13E-07	7.01E-07	7.04E-07	7.13E-07	7.19E-07	7.06E-07	7.05E-07
P <sub>9</sub>	2.76E-06	7.20E-07	6.99E-07	7.05E-07	7.05E-07	-	7.02E-07	-
P <sub>11</sub>	2.80E-06	7.27E-07	7.03E-07	7.08E-07	-	-	-	-
P <sub>13</sub>	2.81E-06	7.31E-07	-	-	-	-	-	-
P <sub>15</sub>	2.82E-06	-	-	-	-	-	-	-
<b>Group 3</b>								
P <sub>1</sub>	2.42E-06	2.46E-06	2.47E-06	2.47E-06	2.48E-06	2.48E-06	2.48E-06	2.48E-06
P <sub>3</sub>	1.85E-07	2.50E-07	2.54E-07	2.51E-07	2.63E-07	2.67E-07	2.58E-07	2.58E-07
P <sub>5</sub>	3.61E-07	1.16E-07	1.21E-07	1.21E-07	1.28E-07	1.31E-07	1.24E-07	1.24E-07
P <sub>7</sub>	4.25E-07	1.13E-07	1.11E-07	1.12E-07	1.14E-07	1.16E-07	1.13E-07	1.13E-07
P <sub>9</sub>	4.46E-07	1.17E-07	1.11E-07	1.12E-07	1.13E-07	-	1.12E-07	-
P <sub>11</sub>	4.53E-07	1.19E-07	1.12E-07	1.13E-07	-	-	-	-
P <sub>13</sub>	4.55E-07	1.20E-07	-	-	-	-	-	-
P <sub>15</sub>	4.56E-07	-	-	-	-	-	-	-

With these findings, the 8-3-5 P<sub>9</sub> case will be used as the reference DIF3D result for the following region-wise flux comparisons. These are shown in Figure 101 through Figure 103 for groups 1-3, respectively. Each of these figures provides two plots; the left is the bottom-most plane of the



February 13, 2020

fictitious reactor and the right is the plane with MCNP's peak flux in that group. Within each of these figures is the DIF3D-to-MCNP flux ratios in each region of the plane. The ratio is provided numerically as well as by color where blue indicates the DIF3D result is less than the MCNP, white implying they are close, and red implying the DIF3D result is larger than in MCNP. These results show overall very close agreement for the majority of the central regions. The largest errors are present on the periphery of the model; the magnitude of the error depends on the number of a region's surfaces adjacent to the vacuum boundary. For example, the largest errors are found in the corner regions of the lowest plane, where three out of six faces have a vacuum boundary condition applied. Known inaccuracies exist for the variational nodal transport method used within DIF3D, as previously discussed, so these findings are not unexpected. Further, these weakness areas are also located in the same regions where the analog Monte Carlo method has the largest uncertainty: areas with relatively low fluxes. For example, the regions located in the eight corners of the cuboidal reactor had stochastic uncertainties as large as 5%. Given that the all non-reflector regions of the reactor are within 1% of the analog MCNP solution, and the areas actually near the peak flux are significantly closer, the DIF3D capability for the XYZ geometry is considered verified.

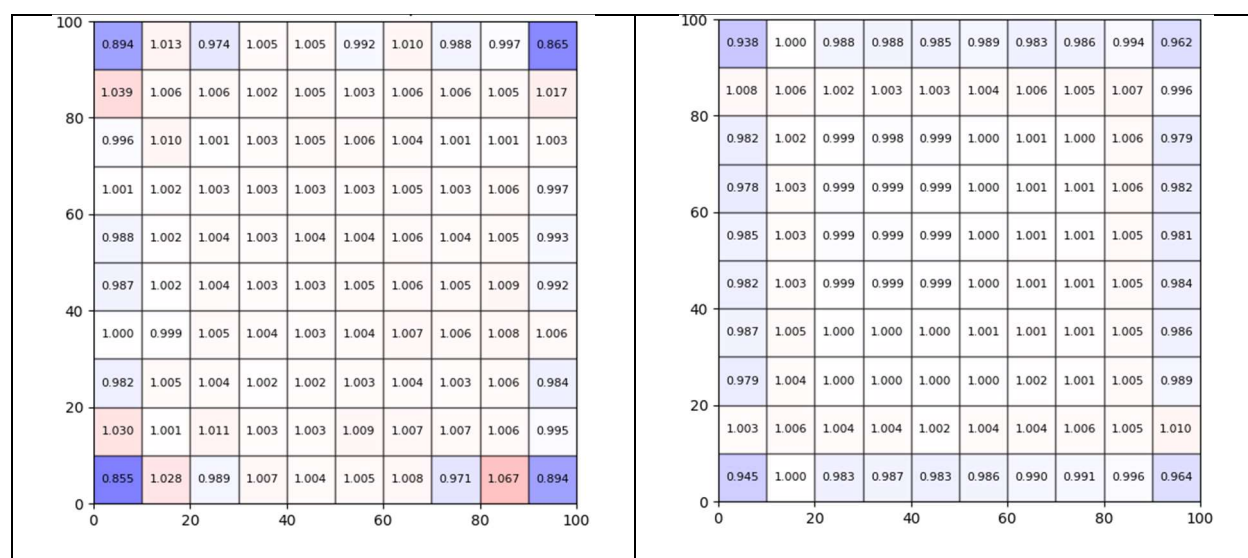


Figure 101. XYZ MG DIF3D to MCNP Flux Ratios in Group 1

February 13, 2020

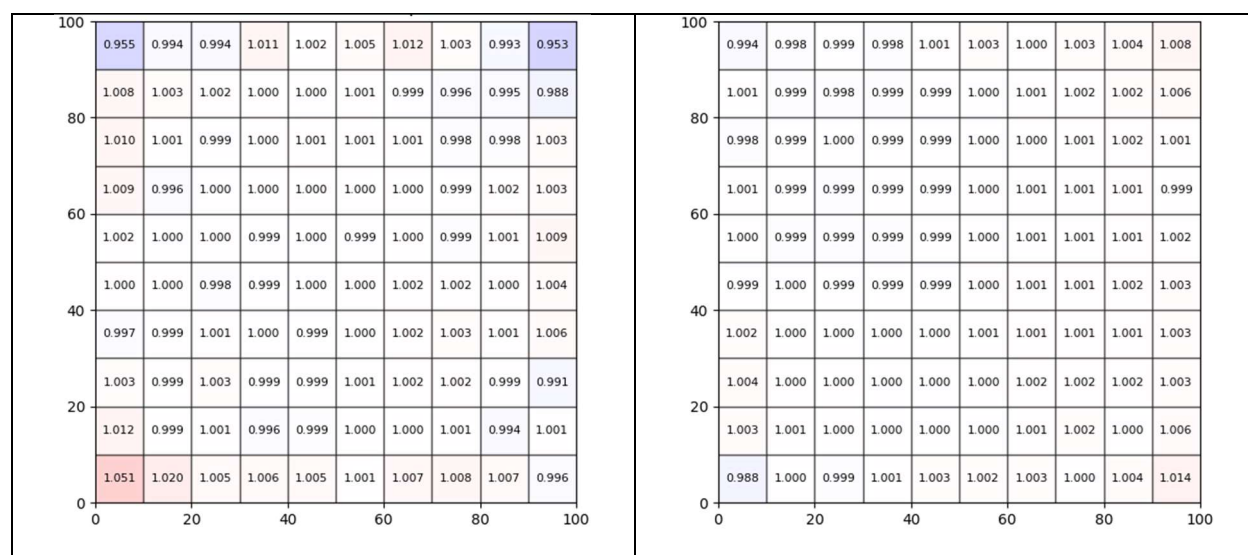


Figure 102. XYZ MG DIF3D to MCNP Flux Ratios in Group 2

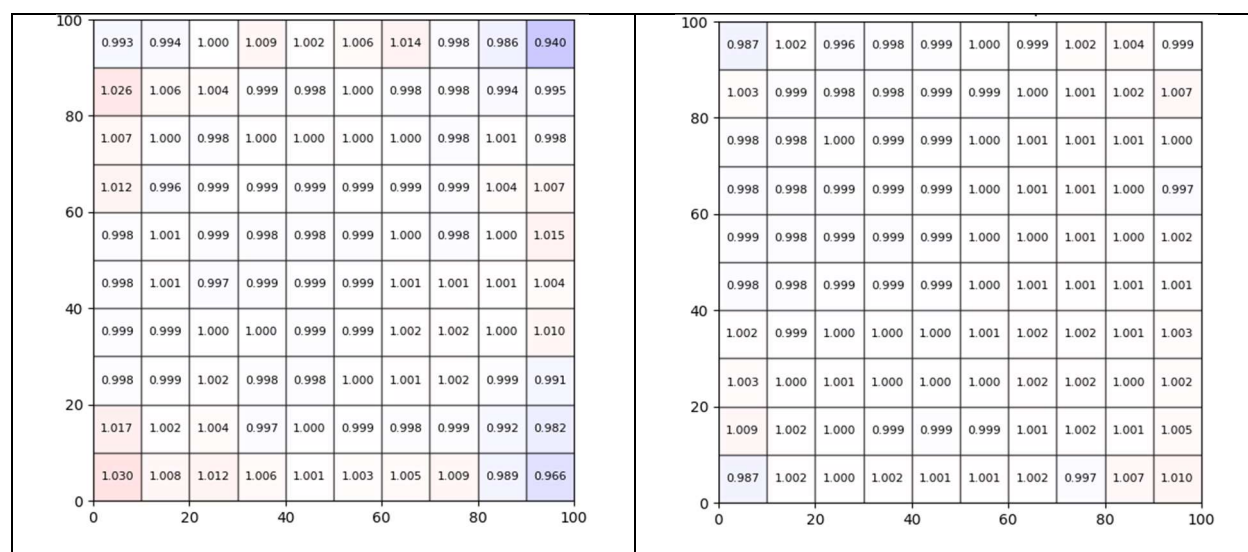


Figure 103. XYZ MG DIF3D to MCNP Flux Ratios in Group 3

### 3.3.3.4 Verification of Anisotropic Scattering Importance

As discussed in [6], to utilize this anisotropic scattering case as verification that anisotropic scattering is working, it must be verified that a different and sensible result is obtained when isotropic scattering (with the same data) compared to the anisotropic result. In this case, the same 8-3-5 P<sub>9</sub> case was re-ran with isotropic scattering via option 9 of the Type 12 card in the A.DIF3D input block. Similarly, DIF3D was told to utilize the total cross section instead of the transport cross section. Thus the problem is truly isotropic in nature.

February 13, 2020

As a reminder, the cross sections from this case were such that the  $P_1/P_0$  moment ratio for REG1 is 0.25, for REG2 it is 0.23, and REG3 is 0.05. Each of these are forward-scattering since the  $P_1/P_0$  moment ratios are positive; further REG3 is significantly closer to isotropic than REG1 and REG2. Since REG1 and REG2 are located in the inner portions of the core, it is expected that applying isotropic scattering will result in fewer neutrons reaching the REG3 “reflector” and more staying in the REG1 and REG2 “active core”. This should also result in a higher eigenvalue as the leakage would be reduced.

The 8-3-5  $P_9$  anisotropic eigenvalue was 1.58684 while the isotropic eigenvalue was 1.591313, indicating that the isotropic case had a 447 pcm eigenvalue bias compared to anisotropic. This confirms the initial reasoned change discussed above.

Figure 104 through Figure 106 provide plots similar to Figure 93 through Figure 103 except the ratio in this case is the isotropic flux compared to the anisotropic flux in each of the three groups. As discussed above, the “reflector” region should have a lower flux than the flux in the core. Since the reflector region is the outer regions, the ratios in Figure 104 through Figure 106 confirm the initial suspicions, indicating that the DIF3D solver is in fact applying anisotropic scattering when it should be.

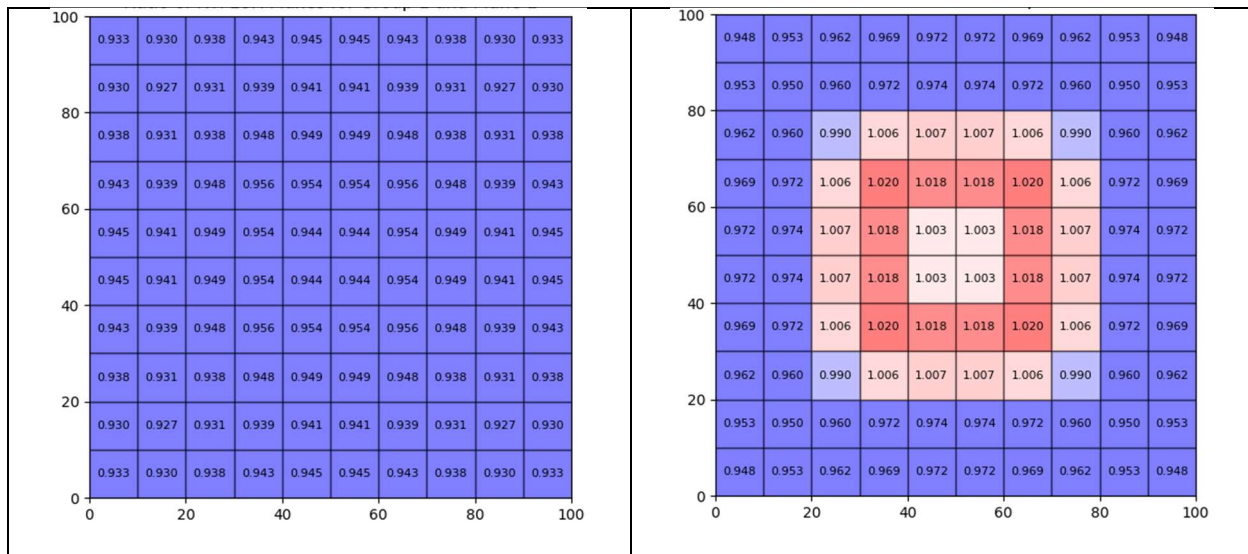


Figure 104. XYZ MG Isotropic to Anisotropic DIF3D Flux Ratios in Group 1

February 13, 2020

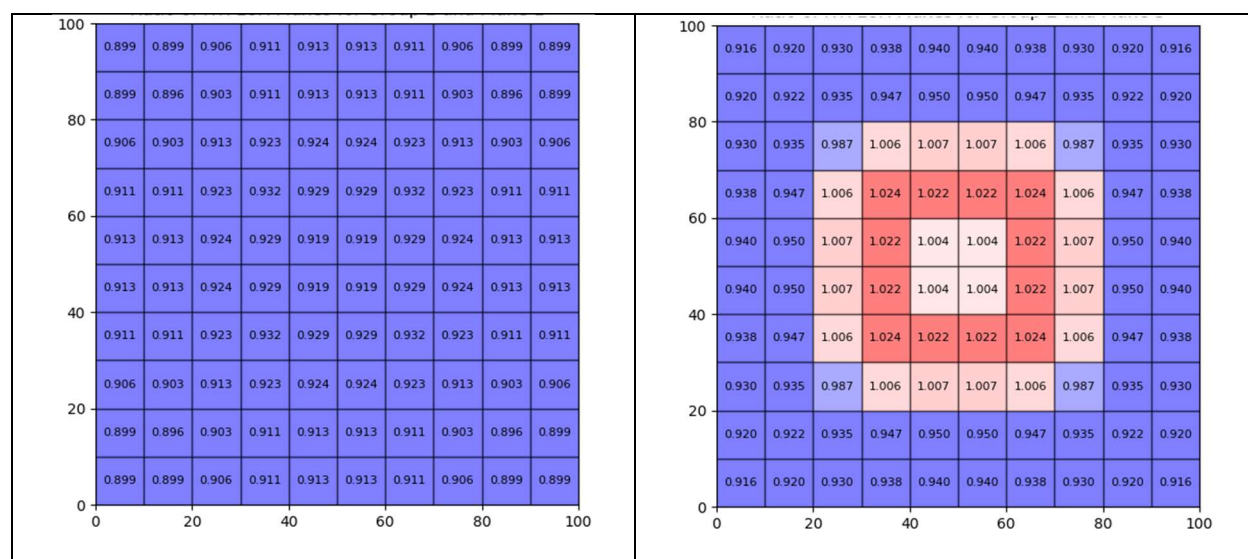


Figure 105. XYZ MG Isotropic to Anisotropic DIF3D Flux Ratios in Group 2

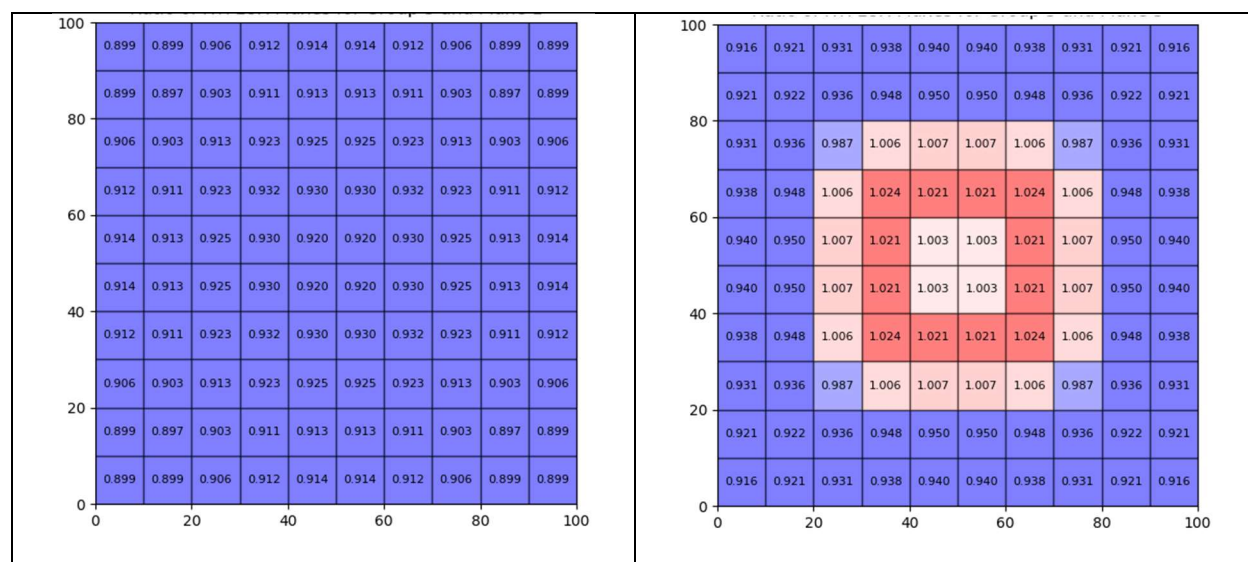


Figure 106. XYZ MG Isotropic to Anisotropic DIF3D Flux Ratios in Group 3

### 3.3.4 Reflective Boundary Conditions Verification

The previous problems analyzed vacuum or reflective boundary conditions on a subset of the six faces of the 3D Cartesian problem domain. However, the problem discussed in Section 3.1.2 showed that reflective boundary conditions were correctly implemented by their ability to recreate an infinite homogenous medium. Since A.DIF3D allows either the vacuum boundary conditions to be defined with either a value of 2 ( $\phi = 0$ , for diffusion) or 9 (incoming angular flux is zero), and that the reflective boundary conditions can be established with either 3 ( $\phi' = 0$ , for diffusion)

or option 10 (reflective), this problem will show that these are in fact interchangeable with the transport solver. This was performed using the same infinite problem as discussed in Section 3.1.2 and Section 3.1.9, again using the first cross section dataset provided in Table 50.

This was performed for each of the six faces by replacing the initial reflective boundary condition (option 10) with each of the above types and comparing the result to expectations. The results of these cases are provided in Table 142. Here all eigenvalues that are in red are expected to have the same value as they should all be infinite homogeneous. All eigenvalues that are black should have one leakage surface of the same area, and similarly should also have a consistent eigenvalue. Both are validated to be true. This indicates that these diffusion coefficient boundary condition options are swapped for their equivalent transport versions internally to DIF3D.

**Table 128. Cartesian DIF3D-VARIANT Extrapolated Boundary Condition Results**

Surf.	Boundary Condition	Eigenvalue	Surf.	Boundary Condition	Eigenvalue
All	10, Reflected	1.60000001			
Lower X	2, Escape	1.44179550	Upper Y	2, Escape	1.44179550
	9, Vacuum	1.44179550		9, Vacuum	1.44179550
	3, Diff. Refl.	1.60000001		3, Diff. Refl.	1.60000001
Upper X	2, Escape	1.44179550	Lower Z	2, Escape	1.44179550
	9, Vacuum	1.44179550		9, Vacuum	1.44179550
	3, Diff. Refl.	1.60000001		3, Diff. Refl.	1.60000001
Lower Y	2, Escape	1.44179550	Upper Z	2, Escape	1.44179550
	9, Vacuum	1.44179550		9, Vacuum	1.44179550
	3, Diff. Refl.	1.60000001		3, Diff. Refl.	1.60000001

### 3.3.5 Iteration and Convergence Control Verification

Table 9 of the [6] plan identified that the iteration and convergence control options (A.DIF3D Type 3.4, 3.6, 3.9, 3.10, 3.11, 3.12, 5.2, 5.3, 5.4, 12.5, 12.6, and 12.11) would be verified by way of the Integral Verification case. These options will be verified in this section, however, the multigroup eigenvalue problem discussed in Section 3.3.3 will be used instead. This was done for no other reason than that problem is smaller than the integral benchmark problem and thus runs faster, but also converges slowly enough (more than 100 iterations are required) that the effect of these options will be readily apparent. Note that this is only performed for a forward eigenvalue case and not repeated for a fixed source or adjoint case as the same convergence control code is exercised for any of these solves. Specifically, this case will utilize the 040601 spatial and 10303 ( $P_3$ ) angular approximation options with  $P_1$  scattering and the total cross section used.

This test will be performed by first running a base case that leaves all relevant parameters to their internal defaults. Then, a case will be performed where the defaults are explicitly specified in their respective cards. Next, using the explicitly listed defaults as the starting point, the options verified by this section will be modified from their default to the possible values. The possible values will either be every value in the discrete set, or if the variable can be continuous (like the number of iterations) then a sufficient number will be evaluated. The specific parameters, their defaults, and their perturbations are provided in Table 129. After executing all these cases, the output will be



analyzed to ensure that DIF3D respected the option according to the description provided in the A.DIF3D listing. The restart capability will then be checked with two additional cases discussed in the final subsection.

**Table 129. Iteration Control Options for Cartesian Transport**

Card Type	Summary	Default Value	Perturbed Values
3.4	Tchebyshev Acceleration	0	1
3.6	Outer Iteration Control	30	-4, -3, -2, -1, 10
3.9	Upscatter Iterations per Outer Iteration	5	20
3.10	Concurrent Iteration Efficiency	0	1
3.11	Accel. Of Opt. Overrelaxation	0	1
3.12	Opt. Overrelaxation Factor Calculation Control	50	2
5.2	Eigenvalue Criterion	$10^{-7}$	$10^{-3}$
5.3	Pointwise Fiss. Source Criterion	$10^{-5}$	$10^{-4}$
5.4	Avg. Fiss. Source Criterion	$10^{-5}$	$10^{-4}$
12.5	Num. of X-Y Plane Partial Current Sweeps	0	200
12.6	Num. of Axial Partial Current Sweeps	0	20
12.11	Omega Transformation Acceleration	0	1

### 3.3.5.1 Base and Default Cases

As noted, the first step performed was to execute a case where all of the above values were simply not included in the input, and thereby DIF3D applied the default value. Then, a case was executed with these values explicitly stated. The outputs were compared using a python Diff tool, and it was found that the outputs indeed matched, except for the input edits and some slight changes to a few of the iteration times, which are subject to external factors and cannot be controlled. Therefore the default case will be used as the starting point going forward.

While not a part of this verification effort, it was noted that the A.DIF3D listing states that the Type 03 card's 5<sup>th</sup> parameter (minimum plane-block size for input/output transfer) has a default of 4500, however this was found to actually be 10000.

All cases that remain will compare to this default case, but modified to utilize 2,000 iterations to convergence so that the total number of iterations to convergence can be observed as these options change.

### 3.3.5.2 Card 3 Option 4 Perturbations

Card 3 Option 4 sets whether or not Tchebyshev acceleration of the outer iterations is performed. The default value, 0, indicates it shall be performed, while a value of 1 turns off this acceleration. Therefore, when the value of 1 is used, one should expect that more iterations will be required to converge. Additionally, DIF3D's echo repeat should acknowledge the setting of this option.

The correct echo repeat was confirmed. Additionally, the case with the acceleration was found to converge in 76 iterations while the case without the acceleration required 137 iterations. The eigenvalue and flux values matched the default cases to within 0.1 pcm and 0.01%, respectively.

### 3.3.5.3 Card 3 Option 6 Perturbations

Card 3 Option 6 controls the number of outer iterations in a case. The possible values are -1 (data management parameters, overrelaxation factors, and neutronics edits are performed), -2 (same as -1 without overrelaxation factors), -3 (DIF3D module is bypassed), -4 (same as -2, but with leakage results derived from the balance equation with zero residual), or some number greater than 0 that simply sets the maximum number of DIF3D outer iterations. The default value is 30 total iterations. This case will evaluate the 4 negative options as well as ensuring 10 total iterations are obeyed.

Option -4 was verified to skip the DIF3D iteration and skip the inner iteration optimization strategy edits as well as the outer iteration summary (i.e., DIF3D did not solve the diffusion equation). However, this option did not use the residual neutron balance to derive the leakage results; instead these leakage terms were the same as in the base case, including the non-zero residual.

Option -3 was verified to not execute the DIF3D module, instead only processing the geometry and zone information from the A.NIP3 and A.HMG4C blocks.

Option -2 produced the same output as option -4 except for the balance edits, which were the same in Option -2 as the base case.

Option -1 interestingly performed only one iteration, and seems to be equivalent to providing a single iteration.

Finally, a value of +10 performed exactly as expected, yielding 10 total iterations before quitting.

### 3.3.5.4 Card 3 Option 9 Perturbations

Card 3 Option 9 sets the number of upscatter iterations per outer iteration. The default is 5. This case will verify that 20 is also obeyed. This can be verified in the input echo, by observing the "Ups" column of the DIF3D iteration history, and in the total time for each outer iteration where the iteration time should increase by a factor of 4. It should be noted that the 20 requested iterations

was changed by DIF3D to an odd number, with a corresponding warning to alert the user. Note that this behavior was not stated in the A.DIF3D listing. Factoring in the 21 iterations, the correct number of upscatter iterations was observed. Further, the time per iteration increased with increasing upscatter iterations by a factor between 3.3 and 4.3. Given that only one significant digit is reported for the time, this is considered reasonable agreement. The eigenvalue for this case matched to all reported digits and fluxes matched with an RMS error on the order of  $10^{-9}$ , indicating that the default number of upscatter iterations was sufficient.

#### 3.3.5.5 Card 3 Option 10 Perturbations

Card 3 Option 10 sets a flag that instructs DIF3D to either perform the estimated number of inner iterations for each group (option 0), or to avoid the last pass of the inner iterations in groups whose number of iterations are less than some non-user-facing threshold. This parameter has no effect on DIF3D-VARIANT. This was verified to be true.

#### 3.3.5.6 Card 3 Option 11 Perturbations

Card 3 Option 11 sets a flag that instructs DIF3D to either not perform acceleration of the optimum over-relaxation factor calculation (option 0, default), or apply asymptotic source extrapolation of the power iterations during the spectral radius calculation (option 1). This parameter has no effect on DIF3D-VARIANT. This was verified to be true. Card 3 Option 12 Perturbations

Card 3 Option 12 sets the number of iterations when determining the optimum overrelaxation factors. This parameter has no effect on DIF3D-VARIANT. This was verified to be true.

#### 3.3.5.7 Card 5 Option 2 Perturbations

Card 5 Option 2 provides the floating point eigenvalue convergence criterion. The default is a value of  $10^{-7}$ . This case will apply a value of  $10^{-4}$ . To ensure the eigenvalue convergence is limiting, the pointwise and average fission source convergence tolerances were set to 0.01. Therefore we should expect that increasing the eigenvalue convergence (compared to the base case) should reduce the total number of iterations such that the fission source convergence is limiting.

This was indeed observed, as the case with a  $10^{-4}$  eigenvalue convergence criterion converged in 27 iterations instead of the base case's 76 iterations. Further, this was achieved when the eigenvalue dropped below  $10^{-4}$ ; the fission source measures had already passed 0.01.

#### 3.3.5.8 Card 5 Option 3 Perturbations

Card 5 Option 3 provides the floating point pointwise fission source convergence criterion. The default is a value of  $10^{-5}$ . This perturbation case will apply a value of  $10^{-4}$ . Like the previous case, the other convergence parameters were set so the pointwise fission source convergence criterion was limiting. Specifically, this means that the eigenvalue and average fission source criterion were 0.01 while the pointwise fission source criterion was  $10^{-4}$ . In this case, we should see the iterations end when the fission source criterion is met.



This was indeed observed, as the case with a  $10^{-4}$  pointwise fission source convergence criterion converged in 46 iterations instead of the base case's 76 iterations. Further, this convergence was achieved when the pointwise fission source was converged to less than  $10^{-4}$ , the provided value.

#### 3.3.5.9 Card 5 Option 4 Perturbations

Card 5 Option 4 provides the floating point average fission source convergence criterion. The default is a value of  $10^{-5}$ . This perturbation case will apply a value of  $10^{-4}$ . Since the default case reaches the eigenvalue convergence after the fission source is converged to the stated value, then the parameters were also set that the average fission source convergence criterion was limiting. Specifically, this means that the eigenvalue and pointwise fission source criterion were 0.01 while the average fission source criterion was  $10^{-4}$ . In this case, we should see the iterations end when the fission source criterion is met.

This was indeed observed, as the case with a  $10^{-4}$  average fission source convergence criterion converged in 42 iterations instead of the base case's 76 iterations. Further, this convergence was achieved when the rel. sum error of the fission source was converged to less than  $10^{-4}$ , the provided value.

#### 3.3.5.10 Card 12 Option 5 Perturbations

Card 12 Option 5 sets the number of XY-Plane partial current sweeps per group, per outer iteration. Positive integers are accepted; the default is 0, meaning the code will decide. In the base case, the code decided to use 2 radial inner iterations for each group. Therefore the perturbed case will increase this by a factor of 1000, to 2000 radial inner iterations per group. This should be observable by the edit stating this value, as well as seeing the increase in time per outer iteration. The value of 2000 was chosen so that the runtime impact was noticeable. This runtime impact was indeed observed as the time per iteration increased from 0.3 seconds to 1.4 seconds. The eigenvalues matched to all reported values and the fluxes differed with an RMS on the order of  $10^{-13}$ .

#### 3.3.5.11 Card 12 Option 6 Perturbations

Card 12 Option 6 sets the number of axial partial current sweeps per group, per outer iteration. Positive integers are accepted; the default is 0, meaning the code will decide. In the base case, the code decided to use 2 axial inner iterations for each group. Therefore the perturbed case will increase this by a factor of 10, to 20 axial inner iterations per group. This should be observable by the edit stating this value, as well as seeing the increase in time per outer iteration. This runtime impact was indeed observed as the time per iteration increased from 0.3 seconds to 0.8 seconds. The eigenvalues matched to all reported values and the fluxes differed with an RMS on the order of  $10^{-10}$ .

#### 3.3.5.12 Card 12 Option 11 Perturbations

Card 12 Option 1 sets a flag denoting if the omega transformation acceleration option is applied (option 0, default) or not (option 1). If used, then the number of inner iterations per group, as

decided by the code, should be “significantly reduced”. Since the number of inner groups is already 2 for each group, it is unlikely that this option will have any effect. It was applied and it was found to not change the number of axial inner sweeps, however the omega and gamma parameters printed before the iteration histories were modified with omega having values of 0 for each group and gamma having values of 1 for each group. Some of the last significant digits in the fission and eigenvalue errors were changed, indicating that the convergence is affected by this parameter. The eigenvalues matched to all reported values and the fluxes differed with an RMS on the order of  $10^{-10}$ . This omega acceleration is known to yield inconsistent results compared to the solution without omega acceleration as documented in Section 7.5 of [4]. Therefore no further work is necessary.

### 3.3.5.13 Restart Calculation

A restart computation can be performed with three approaches in DIF3D: (1) the binary DIF3D and NHFLUX files from the previous computation are provided via the “BLOCK=OLD” input block; (2) a restart is performed with the NHFLUX (or NHFLUX if DIF3D-VARIANT) file and a combination of A.DIF3D Type 06 and possibly 07 cards; or (3) DIF3D is executed and then restarted with tighter convergence criterion (or number of iterations) from within the same input. This sub-section will test these approaches using a restart from the default case that terminated itself after 30 iterations.

The first approach was performed with the BLOCK=OLD NHFLUX and DIF3D files, and a single card in the A.DIF3D input that set the maximum number of iterations to 2,000 instead of the 30 of the previous computation (and thus in the DIF3D binary file). After running this in DIF3D, it is expected that (1) DIF3D’s user input specifications echo would the changes to the number of iterations, state that this is a restart, and include the  $k_{\text{eff}}$  from the restart NHFLUX file (2) the initial  $k_{\text{eff}}$  from the 1<sup>st</sup> iteration of the new calculation should differ from the original calculation’s first guess, (3) the outer iterations should continue until the new calculation’s convergence criteria are met, and (4) the final eigenvalue and reported fluxes should match to on the order of the convergence criterion. All of these were observed, indicating the binary file-based restart was successful.

The second approach was also performed with only the BLOCK=OLD NHFLUX file and the Type 06 card. The A.DIF3D input was modified to include the  $k_{\text{eff}}$  and dominance ratio from the 30 iteration calculation, and the restart flag set to 1 (indicating a restart should be performed). The restart case also had the number of iterations set to 2,000. After running this in DIF3D, it is expected that 1) DIF3D’s user input specifications echo would the changes to the number of iterations, state that this is a restart, and include the initial  $k_{\text{eff}}$  2) the initial  $k_{\text{eff}}$  from the 1<sup>st</sup> iteration of the new calculation should differ from the original calculation’s first guess, 3) the outer iterations should continue until the new calculation’s convergence criteria are met, and (4) the final eigenvalue and reported fluxes should match to on the order of the convergence criterion. All of these were observed, indicating the restart was successful.

February 13, 2020

The third approach (restarting within same input file) was performed by executing the original DIF3D case to 30 iterations, using the DIF3D and NHFLUX files which were just generated with modifications for an increase number of iterations, and re-executing DIF3D. Similar behavior should be observed with this case compared to the original. This was confirmed, indicating this restart methodology was successful.

Further, these methods output files and convergence histories matched, indicating both effectively perform the same function within DIF3D.

### 3.3.6 Solution Edit Verification

DIF3D prints a balance of the solution results in the form of neutron balance edits, power edits, flux edits, zone-averaged flux edits, and region-averaged flux edits. In addition to these are the writing of the SFEDIT, RZFLUX, and PWDINT interface files. All of these are controlled by options 6 through 11 of the A.DIF3D module's Type 04 card. This section will verify that these options are correctly obeyed. This section will also verify the correctness of the neutron balance tables, as these are the only tables that are not verified elsewhere.

The verification that the edit toggles can be performed with any model. The verification of the correctness of the neutron balances requires a model that utilizes multiple regions, one or more areas, and has cross sections with more than one group. Further, as the individual parameters will be calculated independent from DIF3D, a small model is desirable.

To that end, the four composition cross sections used in the Model Building section of this verification effort (defined in Table 23 and Table 26) will be applied in a 10cm cube model. The region between 0 and 5 cm in X, 0 to 10 cm in Y, and 0 to 5 cm in Z are assigned REG1 filled with COMP1. The region between 5 cm in X (and the same Y and Z as REG1) is assigned REG2 that is filled with COMP2. The top 5 cm in the Z plane are filled with REG3 (COMP3) on the left, and REG4 (COMP4) on the right. Reflective boundary conditions are applied on all sides. Finally, AREA1 is defined as all four regions while AREA2 is only REG1. The A.NIP3 input (aside from the composition definitions) is provided in Figure 107.

```

UNFORM=A.NIP3
01 3D XYZ - EDITS
02 0 3 40000000 40000000 40000000 40000000 0 3 3 3
03 44
04 3 3 3 3 3 3
06 REG1 0.0 5.0 0 1 0.0 10.0
06 REG2 5.0 10.0 0 1 0.0 10.0
06 REG3 0.0 5.0 1 2 0.0 10.0
06 REG4 5.0 10.0 1 2 0.0 10.0
09 X 1 5.0 1 10.
09 Y 2 10.
09 Z 1 5.0 1 10.
07 AREA1 REG1 REG2 REG3 REG4
07 AREA2 REG1

```

**Figure 107. XYZ Transport Edit Table Model**

To verify that the edit toggles were correctly verified the same A.DIF3D Type 04 cards used in Section 3.1.11 and provided in Table 84 were applied. Again, the first four do not print the binary interface files while the last two do. The first should print none of the edits of interest. The second prints all edits to standard and auxiliary output. The third prints only to auxiliary output. The fourth to only standard output. The final two cases print the surface fast flux and power density to the SFEDIT file in mesh cell order and then in region order. Each of these six tasks was verified to ensure the output was produced as intended; no deficiencies were noted.

The next task is to verify the correctness of the PWDINT file. This was performed by comparing these files, after conversion to ASCII with the afore-mentioned CCCC\_convert utility, to the power density values provided in the already-verified DIF3D ASCII edits.

Similarly, the RZFLUX files were verified consistent with the already verified flux edit tables as well as by comparing the neutron loss terms to those provided in the standard output (and verified later in this section). This was performed by evaluating the binary files using a custom Python program quite similar to the RTFLUX reading interface. Similar to the 3D Cartesian DIF3D-FD case, it was identified that the total neutron losses and absorption values in this file were zero, despite the problem containing losses and absorption. All other terms, including the zone-averaged fluxes were as expected.

It was then verified that the SFEDIT files were printed, and that the case 5 SFEDIT file is different from the case 6 SFEDIT file by comparing the MD5 hashes of each file. The accuracy of the contents of these files, however, was not verified as part of this work.

The final task to be performed in this section is the verification of the correctness of the neutron balance tables. DIF3D outputs these quantities in one table per group, and a final table containing the information integrated over all energy groups. All of these terms that are not leakage or buckling were confirmed to match independent calculations and are thus verified. Further, the area edits were confirmed to match expectations for all reaction and leakage types (AREA1 matches the region TOTALS row, and AREA2 matches the REG1 row).

The group-wise net leakage, group-wise total buckling, group-integrated net leakage, and group-wise total buckling were then verified to in fact be simple sums of their constituent parts. This was found to be true. Since the buckling in each of the cardinal directions is related to the leakage, ( $L_i = B_i D_i^2$ ) with knowledge of the diffusion coefficient, the reported leakage was verified to produce the reported buckling. This was done for each group and direction and it was found that DIF3D is properly representing this function.

The diffusion equivalent of this verification computed the leakage terms directly from one region to another. However, with the transport solver this process is more involved and introduces risk of mistakes in the verification process. Instead, this transport solver verification case will simplify the process and identify the group-integrated net leakage that produces the DIF3D-reported eigenvalue, using independently generated (though previously verified) absorption rates and fission source rates. This required net leakage will then be compared to what DIF3D reports. Since it is also required that the group-wise, direction-dependent leakages match, this method has to be implemented on a model wherein the group-wise, direction-dependent leakages were the sole

contributor to the net leakage. This method thereby verifies both (as well as ensuring the remaining leakages are zero as they should be).

The reference model for this work is based on the model described earlier and shown in Figure 107 except the model was instead a homogeneous model filled with only COMP3. A single leakage boundary was applied to one of the surfaces. Further, a group-wise albedo was supplied with the A.NIP3 Type 05 card such that only one of the two groups on this surface was a leakage boundary, and the other was treated as purely reflecting. An example of this for the right X-boundary is provided in Figure 108. In this way, the net neutron leakage was isolated to a single group and single surface at a time. DIF3D was then run for this model, the fluxes and eigenvalue collected and used to back-calculate the leakage that produces that eigenvalue. This was the reference solution for comparison to DIF3D's leakage edits. This process was repeated for each of the surfaces and each of the groups. Each and every case showed that the DIF3D and reference group-wise, direction-wise leakages matched. Therefore these balance tables are verified.

```

UNFORM=A.NIP3
01 3D XYZ - EDITS
02 0 3 40000000 40000000 40000000 40000000 0 3 3 3
03 44
04 3 4 3 3 3 3
05 XU 1.E10 1
05 XU 0. 2
06 REG3 0.0 5.0 0 1 0.0 10.0
06 REG3 5.0 10.0 0 1 0.0 10.0
06 REG3 0.0 5.0 1 2 0.0 10.0
06 REG3 5.0 10.0 1 2 0.0 10.0
09 X 1 5.0 1 10.
09 Y 2 10.
09 Z 1 5.0 1 10.

```

**Figure 108. XYZ Transport Neutron Leakage Edit Table Model**

### 3.3.7 Integral Verification

The preceding test problems are all manufactured test cases not based upon any real reactors. The series of benchmarks problems discussed in this section were proposed and accepted by NEACRP from Toshikazu Takeda and Hideaki Ikeda in 1988 with the final report issued in 1991 [18]. The intention of these test problems was to have users contribute their solution (diffusion or transport) for four different reactor models. In the final report, the compiled results from all participants are provided and discussed where the reference eigenvalue solution is taken from a compiled average between multiple Monte Carlo solutions. Because of the computational power limitations at the time, most of the Monte Carlo solutions had 50 to 60 pcm of statistical uncertainty reported for the eigenvalue. With the today's substantially improved computational power, the MCNP6.2 Monte Carlo [15] solution error can be less than 1 pcm, thus in this work the reference solutions are redone.

The original focus of the benchmark was to compute the control worth that only involves focused computation of the eigenvalue for two geometrical configurations. With new reference solutions, the amount of information verified against the MCNP reference solution was increased. In

particular, the capture and fission distribution in the domain is compared by isotope to check the accuracy of the DIF3D capabilities.

The third benchmark model is of interest to the verification of the 3D Cartesian DIF3D-VARIANT solver. This model is a 1/8 symmetry model of a Cartesian reactor shown in Figure 109. This reactor model is derived from a Zero Power Reactor and is notably similar to the ZPPR-17 series of experiments carried out at ANL. Because of the computational expense at the time, Figure 109 uses reflected boundary conditions on three surfaces that is not realistic for a real reactor. The three configurations are relatively interesting as the “Core” loading fills the control rod positions with the equivalent adjacent material such that the Cartesian geometry has a more perfect R-Z configuration. The “Rods Out” case identifies a simple layout of primary and secondary control rods where the “Rods In” case only loads control rod materials into symmetric positions. This allowed codes that could only handle 45 degree symmetry to solve the problem by reducing the modeled domain to 1/16<sup>th</sup> of a full core case.

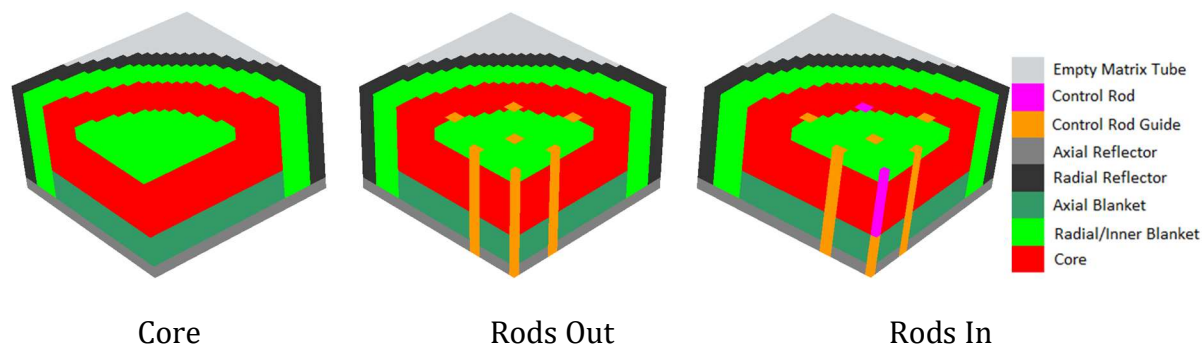


**Figure 109. Takeda 3 Benchmark Model Configurations**

This benchmark poses a rather rigorous test of the multi-group transport methodology. In particular, these problems test the spatial meshing accuracy and the angular refinement. The control rod materials are relatively strong absorbing regions and insufficient spatial meshing will cause significant errors due to the over prediction of absorption in the control rod regions. Similarly, both systems are relatively leaky such that a higher than normal angular approximation is required to model the leakage from the core. By today’s standards, these problems are relatively trivial to execute for DIF3D-VARIANT although the high order space-angle approximations are a bit impractical for most actual reactor analysis and validation efforts.

The three Takeda 3 cases exhibit convergence issues when using higher space-angle approximations. This problem is well known to users of DIF3D-VARIANT and is associated with low density medium or small mesh sizes. In this and other Takeda 3 models, the empty matrix tube region is a low density medium with little to no absorptive properties (the macroscopic absorption cross section is  $\sim 10^{-3} \text{ cm}^{-1}$ ). In the methodology of DIF3D-VARIANT, the iterative convergence algorithm can lose diagonal dominance when the absorptive properties of a given energy group drop below  $\sim 10^{-2} \text{ cm}^{-1}$  and thus it fails to produce a solution. The fix that is typically applied to existing reactor analysis, such as the ZPR and ZPPR validation cases, is to alter the absorption in



the empty matrix tube regions. This technique was applied to all of the Takeda 3 models incorporated in this work, including the reference MCNP reports.

The next section will describe the convergence of the most challenging of these problems, the Rods-In case. The data for the other cases is provided and not discussed in Section 3.3.7.2 and 3.3.7.3 for the Rods-Out and Core cases, respectively.

### 3.3.7.1 Rods-In Case

#### 3.3.7.1.1 Reference MCNP Results

The Monte Carlo solutions published with the benchmark contained 50 to 60 pcm of statistical uncertainty for the reported eigenvalue; these were computed with less than three million histories due to computational limitations of the time. This uncertainty was considered too large for this work and therefore MCNP6.2 was used to recreate the reference solutions. In this case, the goal is to show that the DIF3D results are converging to the MCNP6.2-based reference solution.

The MCNP reference solution was generated here with one million histories per batch, 100 inactive batches, and 16,000 active batches for a total of 16 billion active histories. The resultant value of  $k_{\text{eff}}$  predicted by MCNP was  $0.97176 \pm 0.00004$ . The relative errors for all tally bins are generally quite low, though in the extreme locations and lowest energy group of the model they can be as high as 12.8%. The relative error distribution is shown in Figure 110.

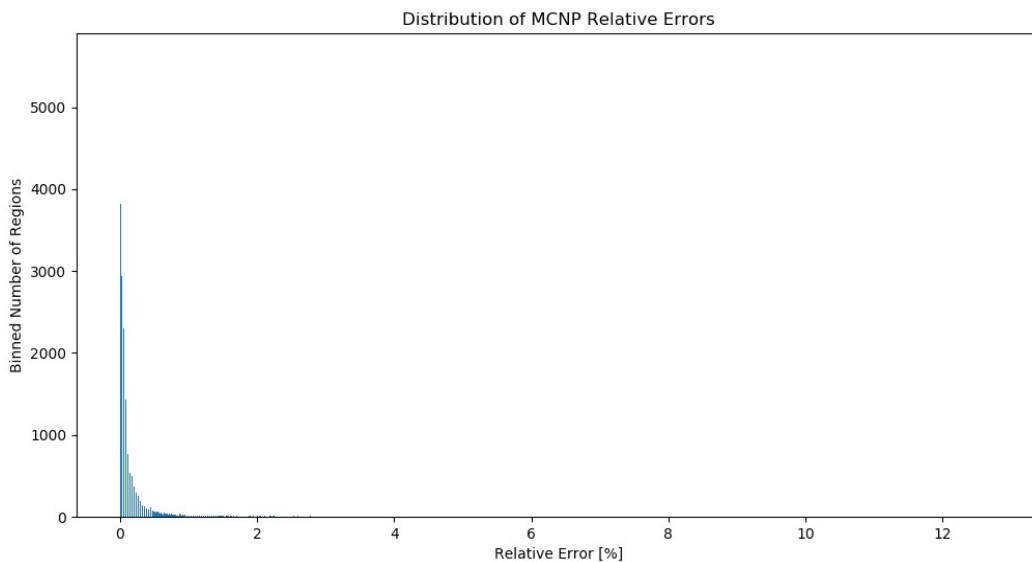


**Figure 110. MCNP Relative Error Distribution for Rods-In Case**

#### 3.3.7.1.2 DIF3D Results

The DIF3D-VARIANT solver was used to solve the same reactor using the same multigroup cross sections as analyzed by MCNP. Since an exact analytical match is not expected, this verification

focuses on ensuring that the DIF3D solution converges to the MCNP solution as the spatial and angular orders are increased.

The DIF3D “Rods In” eigenvalue errors are provided in Table 130. This table is organized similar to the previous case with the flux, leakage, and source spatial approximations in the columns and the angular (flux and leakage) represented with the rows. The dash values (‘-’) in the table are a result of the DIF3D-VARIANT code requiring more memory than DIF3D can allocate and thus the code did not execute. The asterisks (‘\*’) denote cases where DIF3D successfully executed, but was unable to converge to a solution, despite the addition of the previously discussed additional absorption. These cases were run using the standard functions (with a leading 1 on the A.DIF3D Type 12 Card, Option 3).

Table 131, however, was run using the Yang functions (replacing the leading 1 with a leading 3). These results clearly show that the Yang functions converge in cases where the standard functions do not, however, the results are similar for the cases that did converge. More absorption in the Empty matrix Tube regions could have been added, however, it was considered unnecessary as enough convergence information was present from the cases that did converge with the Yang functions. The remainder of the Takeda 3 cases in this Section and Sections 3.3.7.2 and 3.3.7.3 will therefore utilize the Yang functions.

**Table 130. Takeda 3, Rods-In, Eigenvalue Errors with Standard Functions [pcm]**

<b>Flux</b>	<b>6<sup>th</sup></b>	<b>7<sup>th</sup></b>	<b>8<sup>th</sup></b>	<b>8<sup>th</sup></b>	<b>10<sup>th</sup></b>	<b>12<sup>th</sup></b>	<b>10<sup>th</sup></b>	<b>10<sup>th</sup></b>
<b>Leakage</b>	<b>1<sup>st</sup></b>	<b>2<sup>nd</sup></b>	<b>3<sup>rd</sup></b>	<b>3<sup>rd</sup></b>	<b>3<sup>rd</sup></b>	<b>3<sup>rd</sup></b>	<b>4<sup>th</sup></b>	<b>5<sup>th</sup></b>
<b>Source</b>	<b>4<sup>th</sup></b>	<b>7<sup>th</sup></b>	<b>8<sup>th</sup></b>	<b>5<sup>th</sup></b>	<b>5<sup>th</sup></b>	<b>5<sup>th</sup></b>	<b>5<sup>th</sup></b>	<b>5<sup>th</sup></b>
<b>P<sub>1</sub></b>	-706	-708	-709	-709	-709	-709	-709	-709
<b>P<sub>3</sub></b>	-59	-82	*	*	*	*	*	*
<b>P<sub>5</sub></b>	-1	-24	-25	-25	-26	-26	*	*
<b>P<sub>7</sub></b>	20	-11	-14	-14	-14	-14	*	*
<b>P<sub>9</sub></b>	29	-5	-9	-9	-9	-	-	-
<b>P<sub>11</sub></b>	33	-3	-6	-6	-	-	-	-
<b>P<sub>13</sub></b>	36	-1	-	-	-	-	-	-
<b>P<sub>15</sub></b>	37	-	-	-	-	-	-	-

Referring to Table 131, the spatial flux order (8-3-5, 10-3-5, and 12-3-5) changes the eigenvalue error by at most one pcm. The spatial leakage approximation (10-3-5, 10-4-5, and 10-5-5) shows no change in eigenvalue errors and therefore a 3<sup>rd</sup> spatial leakage approximation is more than sufficient. Finally, the spatial source approximation is observed to not be a strong contributor to converge in this model.



The last aspect of refinement to consider is angular refinement. The two 13<sup>th</sup> angular order cases that completed show a few pcm change compared to the equivalent  $P_{11}$  cases. Therefore it may be possible that the angular order is still converging when DIF3D is no longer able to complete the computations, however these results are sufficiently accurate given the inability to further refine the space-angle approximations.

**Table 131. Takeda 3, Rods-In, Eigenvalue Errors with Yang Functions [pcm]**

Flux	6 <sup>th</sup>	7 <sup>th</sup>	8 <sup>th</sup>	8 <sup>th</sup>	10 <sup>th</sup>	12 <sup>th</sup>	10 <sup>th</sup>	10 <sup>th</sup>
Leakage	1 <sup>st</sup>	2 <sup>nd</sup>	3 <sup>rd</sup>	3 <sup>rd</sup>	3 <sup>rd</sup>	3 <sup>rd</sup>	4 <sup>th</sup>	5 <sup>th</sup>
Source	4 <sup>th</sup>	7 <sup>th</sup>	8 <sup>th</sup>	5 <sup>th</sup>	5 <sup>th</sup>	5 <sup>th</sup>	5 <sup>th</sup>	5 <sup>th</sup>
$P_1$	-706	-708	-709	-709	-709	-709	-709	-709
$P_3$	-59	-69	-70	-70	-70	-70	-70	-70
$P_5$	-1	-24	-26	-26	-26	-26	-26	*
$P_7$	20	-11	-14	-14	-14	-14	*	*
$P_9$	29	-6	-9	-9	-9	-	-10	-
$P_{11}$	33	-3	-6	-7	-	-	-	-
$P_{13}$	36	-1	-	-	-	-	-	-
$P_{15}$	37	-	-	-	-	-	-	-

The peak flux and flux root-mean-squared-errors followed similar trends to the eigenvalue errors shown in Table 131 and are repeated in Table 132 and Table 133 below.

Table 132. Takeda 3, Rods-In, Peak Flux Errors [%]

Flux	6 <sup>th</sup>	7 <sup>th</sup>	8 <sup>th</sup>	8 <sup>th</sup>	10 <sup>th</sup>	12 <sup>th</sup>	10 <sup>th</sup>	10 <sup>th</sup>
Leakage	1 <sup>st</sup>	2 <sup>nd</sup>	3 <sup>rd</sup>	3 <sup>rd</sup>	3 <sup>rd</sup>	3 <sup>rd</sup>	4 <sup>th</sup>	5 <sup>th</sup>
Source	4 <sup>th</sup>	7 <sup>th</sup>	8 <sup>th</sup>	5 <sup>th</sup>	5 <sup>th</sup>	5 <sup>th</sup>	5 <sup>th</sup>	5 <sup>th</sup>
<b>Group 1</b>								
P <sub>1</sub>	1.73	1.72	1.72	1.72	1.72	1.72	1.72	1.72
P <sub>3</sub>	-0.2	-0.15	-0.15	-0.15	-0.15	-0.15	-0.15	-0.15
P <sub>5</sub>	-0.21	-0.03	-0.05	-0.05	-0.05	-0.05	-0.05	*
P <sub>7</sub>	-0.16	0.02	-0.01	-0.01	-0.01	-0.01	*	*
P <sub>9</sub>	-0.16	0.03	0	-0.01	0	-	0	-
P <sub>11</sub>	-0.15	0.03	0	0	-	-	-	-
P <sub>13</sub>	-0.15	0.03	-	-	-	-	-	-
P <sub>15</sub>	-0.15	-	-	-	-	-	-	-
<b>Group 2</b>								
P <sub>1</sub>	1.3	1.3	1.3	1.3	1.3	1.3	1.3	1.3
P <sub>3</sub>	0.03	0.01	0	0	0	0	0	0
P <sub>5</sub>	0.03	0	0	0	0	0	0	*
P <sub>7</sub>	0.04	0.01	0	0	0	0	*	*
P <sub>9</sub>	0.04	0.01	0.01	0.01	0.01	-	0.01	-
P <sub>11</sub>	0.05	0.01	0.01	0.01	-	-	-	-
P <sub>13</sub>	0.05	0.01	-	-	-	-	-	-
P <sub>15</sub>	0.05	-	-	-	-	-	-	-
<b>Group 3</b>								
P <sub>1</sub>	-1.35	-1.36	-1.36	-1.36	-1.36	-1.36	-1.36	-1.36
P <sub>3</sub>	-0.09	-0.1	-0.1	-0.1	-0.1	-0.1	-0.1	-0.1
P <sub>5</sub>	0.02	0	0	0	0	0	0	*
P <sub>7</sub>	0.05	0.02	0.02	0.02	0.02	0.02	*	*
P <sub>9</sub>	0.07	0.03	0.02	0.02	0.02	-	0.02	-
P <sub>11</sub>	0.07	0.03	0.02	0.02	-	-	-	-
P <sub>13</sub>	0.07	0.03	-	-	-	-	-	-
P <sub>15</sub>	0.07	-	-	-	-	-	-	-
<b>Group 4</b>								
P <sub>1</sub>	1.84	1.84	1.84	1.84	1.84	1.84	1.84	1.84
P <sub>3</sub>	0.19	0.24	0.25	0.25	0.25	0.25	0.25	0.25
P <sub>5</sub>	-0.05	0.09	0.09	0.09	0.09	0.09	0.09	*
P <sub>7</sub>	-0.15	0.04	0.05	0.05	0.05	0.05	*	*
P <sub>9</sub>	-0.19	0.02	0.03	0.03	0.03	-	0.04	-
P <sub>11</sub>	-0.21	0	0.02	0.02	-	-	-	-
P <sub>13</sub>	-0.22	0	-	-	-	-	-	-
P <sub>15</sub>	-0.23	-	-	-	-	-	-	-

Table 133. Takeda 3, Rods-In, Root-Mean-Squared Flux Errors

Flux	6 <sup>th</sup>	7 <sup>th</sup>	8 <sup>th</sup>	8 <sup>th</sup>	10 <sup>th</sup>	12 <sup>th</sup>	10 <sup>th</sup>	10 <sup>th</sup>
Leakage	1 <sup>st</sup>	2 <sup>nd</sup>	3 <sup>rd</sup>	3 <sup>rd</sup>	3 <sup>rd</sup>	3 <sup>rd</sup>	4 <sup>th</sup>	5 <sup>th</sup>
Source	4 <sup>th</sup>	7 <sup>th</sup>	8 <sup>th</sup>	5 <sup>th</sup>	5 <sup>th</sup>	5 <sup>th</sup>	5 <sup>th</sup>	5 <sup>th</sup>
<b>Group 1</b>								
P <sub>1</sub>	4.65E-07	4.66E-07	4.66E-07	4.66E-07	4.66E-07	4.66E-07	4.66E-07	4.66E-07
P <sub>3</sub>	1.10E-07	1.20E-07	1.20E-07	1.20E-07	1.20E-07	1.20E-07	1.20E-07	1.20E-07
P <sub>5</sub>	3.96E-08	5.26E-08	5.57E-08	5.57E-08	5.56E-08	5.55E-08	5.59E-08	*
P <sub>7</sub>	5.51E-08	2.38E-08	3.00E-08	3.00E-08	2.96E-08	2.94E-08	*	*
P <sub>9</sub>	7.79E-08	1.11E-08	1.75E-08	1.75E-08	1.69E-08	-	1.87E-08	-
P <sub>11</sub>	9.04E-08	1.05E-08	1.09E-08	1.12E-08	-	-	-	-
P <sub>13</sub>	9.75E-08	1.34E-08	-	-	-	-	-	-
P <sub>15</sub>	1.01E-07	-	-	-	-	-	-	-
<b>Group 2</b>								
P <sub>1</sub>	1.23E-06	1.23E-06	1.23E-06	1.23E-06	1.23E-06	1.23E-06	1.23E-06	1.23E-06
P <sub>3</sub>	1.12E-07	1.29E-07	1.31E-07	1.31E-07	1.31E-07	1.31E-07	1.31E-07	1.31E-07
P <sub>5</sub>	4.89E-08	4.15E-08	4.56E-08	4.56E-08	4.53E-08	4.51E-08	4.62E-08	*
P <sub>7</sub>	7.82E-08	1.88E-08	2.33E-08	2.33E-08	2.28E-08	2.25E-08	*	*
P <sub>9</sub>	9.49E-08	1.52E-08	1.58E-08	1.58E-08	1.54E-08	-	1.67E-08	-
P <sub>11</sub>	1.04E-07	1.64E-08	1.33E-08	1.33E-08	-	-	-	-
P <sub>13</sub>	1.08E-07	1.79E-08	-	-	-	-	-	-
P <sub>15</sub>	1.10E-07	-	-	-	-	-	-	-
<b>Group 3</b>								
P <sub>1</sub>	5.87E-07	5.90E-07	5.90E-07	5.90E-07	5.90E-07	5.90E-07	5.90E-07	5.90E-07
P <sub>3</sub>	5.55E-08	6.21E-08	6.35E-08	6.35E-08	6.34E-08	6.33E-08	6.37E-08	6.38E-08
P <sub>5</sub>	4.15E-08	2.23E-08	2.44E-08	2.44E-08	2.42E-08	2.41E-08	2.47E-08	*
P <sub>7</sub>	5.22E-08	1.36E-08	1.51E-08	1.51E-08	1.49E-08	1.47E-08	*	*
P <sub>9</sub>	5.75E-08	1.17E-08	1.21E-08	1.20E-08	1.18E-08	-	1.25E-08	-
P <sub>11</sub>	6.00E-08	1.15E-08	1.09E-08	1.09E-08	-	-	-	-
P <sub>13</sub>	6.12E-08	1.18E-08	-	-	-	-	-	-
P <sub>15</sub>	6.19E-08	-	-	-	-	-	-	-
<b>Group 4</b>								
P <sub>1</sub>	4.21E-08	4.25E-08	4.27E-08	4.27E-08	4.27E-08	4.27E-08	4.27E-08	4.27E-08
P <sub>3</sub>	6.86E-09	8.27E-09	8.60E-09	8.60E-09	8.55E-09	8.54E-09	8.65E-09	8.69E-09
P <sub>5</sub>	5.80E-09	4.20E-09	4.53E-09	4.53E-09	4.48E-09	4.45E-09	4.60E-09	*
P <sub>7</sub>	7.18E-09	3.01E-09	3.31E-09	3.31E-09	3.24E-09	3.20E-09	*	*
P <sub>9</sub>	7.94E-09	2.48E-09	2.73E-09	2.72E-09	2.66E-09	-	2.79E-09	-
P <sub>11</sub>	8.34E-09	2.31E-09	2.42E-09	2.42E-09	-	-	-	-
P <sub>13</sub>	8.55E-09	2.27E-09	-	-	-	-	-	-
P <sub>15</sub>	8.67E-09	-	-	-	-	-	-	-

February 13, 2020

The region-wise flux comparisons for DIF3D and MCNP for the 7-2-7  $P_{11}$  case are provided in Figure 111. This case was chosen as it represents a good balance of low errors in of the above metrics. This figure provides two plots, each showing the ratio of the DIF3D-to-MCNP group 1 fluxes. The left figure shows this ratio in the bottom axial plane while the right figure provides it for the central plane. The color scheme is such that white is exceedingly close to 1.0, red is above 1, and blue is below 1. The maximal and minimal errors are denoted with the textual value of the ratio in the location where the value is obtained.

Overall very close agreement is observed for the majority of the regions, with the maximal errors being observed in the upper right area in the empty matrix tube regions and next to the vacuum boundary. This is an area that most transport solvers would have difficulty with due to the high streaming and lower flux values (as this is an ex-core location). Further, these locations near vacuum boundaries are where DIF3D typically performs the weakest due to the difficulty in representing vacuum boundary conditions with spherical harmonics.

Similar figures for groups 2, 3, and 4 are not provided for brevity; these lower energy groups generally match the MCNP reference quite well with maximal errors on the order of 1%.

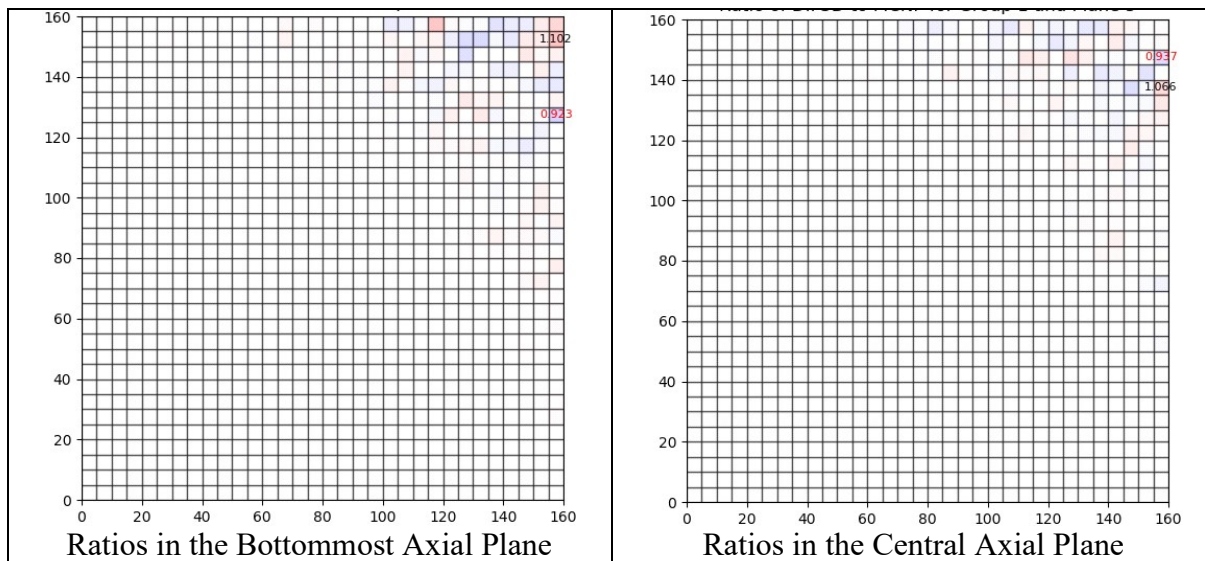


**Figure 111. Ratio of DIF3D to MCNP Fluxes in Group 1**

These results, and those provided in Sections 3.3.7.2 and 3.3.7.3, indicate that the DIF3D can closely match the MCNP reference, converging with increasing spatial and angular orders, and therefore can be used to provide confidence in the verification of DIF3D.

### 3.3.7.2 Rods-Out Case

#### 3.3.7.2.1 Reference MCNP Results

The MCNP reference solution was generated here with one million histories per batch, 100 inactive batches, and 16,000 active batches for a total of 16 billion active histories. The resultant value of  $k_{\text{eff}}$  predicted by MCNP was  $1.00137 \pm 0.000005$ . The relative errors for all tally bins are generally quite low, though in the extreme locations of the model they can be as high as 11% in the lowest energy groups. The relative error distribution is shown in Figure 112.

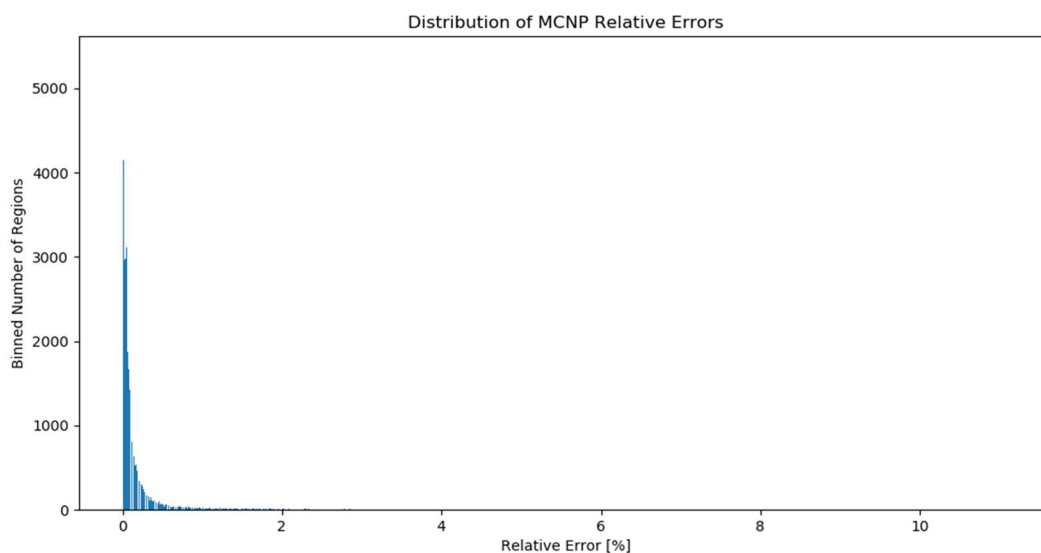


Figure 112. MCNP Relative Error Distribution for Rods-Half Case

#### 3.3.7.2.2 DIF3D Results

The following tables provide the eigenvalue errors, peak flux errors, and the root-mean-squared errors of the mesh-wise fluxes. Similar trends are observed to those discussed in Section 3.3.7.1.

Table 134. Takeda 3, Rods-Out, Eigenvalue Errors [pcm]

Flux	6 <sup>th</sup>	7 <sup>th</sup>	8 <sup>th</sup>	8 <sup>th</sup>	10 <sup>th</sup>	12 <sup>th</sup>	10 <sup>th</sup>	10 <sup>th</sup>
Leakage	1 <sup>st</sup>	2 <sup>nd</sup>	3 <sup>rd</sup>	3 <sup>rd</sup>	3 <sup>rd</sup>	3 <sup>rd</sup>	4 <sup>th</sup>	5 <sup>th</sup>
Source	4 <sup>th</sup>	7 <sup>th</sup>	8 <sup>th</sup>	5 <sup>th</sup>	5 <sup>th</sup>	5 <sup>th</sup>	5 <sup>th</sup>	5 <sup>th</sup>
P <sub>1</sub>	-567	-568	-568	-568	-568	-568	-568	-568
P <sub>3</sub>	-53	-56	-56	-56	-56	-56	-56	-56
P <sub>5</sub>	-12	-22	-22	-22	-22	-22	-23	*
P <sub>7</sub>	4	-12	-13	-13	-13	-13	*	*
P <sub>9</sub>	11	-7	-9	-9	-9	-	*	-
P <sub>11</sub>	15	-5	-7	-7	-	-	-	-
P <sub>13</sub>	17	-3	-	-	-	-	-	-
P <sub>15</sub>	18	-	-	-	-	-	-	-

Table 135. Takeda 3, Rods-Out, Peak Flux Errors [%]

Flux	6 <sup>th</sup>	7 <sup>th</sup>	8 <sup>th</sup>	8 <sup>th</sup>	10 <sup>th</sup>	12 <sup>th</sup>	10 <sup>th</sup>	10 <sup>th</sup>
Leakage	1 <sup>st</sup>	2 <sup>nd</sup>	3 <sup>rd</sup>	3 <sup>rd</sup>	3 <sup>rd</sup>	3 <sup>rd</sup>	4 <sup>th</sup>	5 <sup>th</sup>
Source	4 <sup>th</sup>	7 <sup>th</sup>	8 <sup>th</sup>	5 <sup>th</sup>	5 <sup>th</sup>	5 <sup>th</sup>	5 <sup>th</sup>	5 <sup>th</sup>
<b>Group 1</b>								
P <sub>1</sub>	2.63	2.63	2.63	2.63	2.63	2.63	2.63	2.63
P <sub>3</sub>	-0.04	0.04	0.03	0.03	0.03	0.03	0.03	0.03
P <sub>5</sub>	-0.21	0.04	0.03	0.03	0.03	0.03	0.03	*
P <sub>7</sub>	-0.23	0.07	0.05	0.05	0.04	0.04	*	*
P <sub>9</sub>	-0.24	0.07	0.04	0.04	0.04	-	*	-
P <sub>11</sub>	-0.23	0.07	0.04	0.04	-	-	-	-
P <sub>13</sub>	-0.23	0.06	-	-	-	-	-	-
P <sub>15</sub>	-0.23	-	-	-	-	-	-	-
<b>Group 2</b>								
P <sub>1</sub>	2.06	2.05	2.05	2.05	2.05	2.05	2.05	2.05
P <sub>3</sub>	0.16	0.15	0.15	0.15	0.15	0.15	0.15	0.15
P <sub>5</sub>	0.06	0.04	0.04	0.04	0.04	0.04	0.04	*
P <sub>7</sub>	0.02	0.02	0.02	0.02	0.02	0.02	*	*
P <sub>9</sub>	0.01	0.01	0.01	0.01	0.01	-	*	-
P <sub>11</sub>	0	0	0.01	0	-	-	-	-
P <sub>13</sub>	0	0	-	-	-	-	-	-
P <sub>15</sub>	0	-	-	-	-	-	-	-
<b>Group 3</b>								
P <sub>1</sub>	-0.45	-0.45	-0.45	-0.45	-0.45	-0.45	-0.45	-0.45
P <sub>3</sub>	0.07	0.08	0.08	0.08	0.08	0.08	0.08	0.11
P <sub>5</sub>	0.02	0.03	0.03	0.03	0.03	0.03	0.03	*
P <sub>7</sub>	-0.01	0.02	0.02	0.02	0.02	0.02	*	*
P <sub>9</sub>	-0.02	0.01	0.01	0.01	0.01	-	*	-
P <sub>11</sub>	-0.03	0.01	0.01	0.01	-	-	-	-
P <sub>13</sub>	-0.03	0.01	-	-	-	-	-	-
P <sub>15</sub>	-0.03	-	-	-	-	-	-	-
<b>Group 4</b>								
P <sub>1</sub>	2.00	2.00	2.00	2.00	2.00	2.00	2.00	2.00
P <sub>3</sub>	0.15	0.21	0.21	0.21	0.21	0.21	0.21	0.22
P <sub>5</sub>	-0.12	0.02	0.02	0.02	0.02	0.02	0.02	*
P <sub>7</sub>	-0.23	-0.04	-0.03	-0.03	-0.03	-0.03	*	*
P <sub>9</sub>	-0.28	-0.07	-0.05	-0.05	-0.05	-	*	-
P <sub>11</sub>	-0.30	-0.08	-0.06	-0.06	-	-	-	-
P <sub>13</sub>	-0.31	-0.09	-	-	-	-	-	-
P <sub>15</sub>	-0.32	-	-	-	-	-	-	-

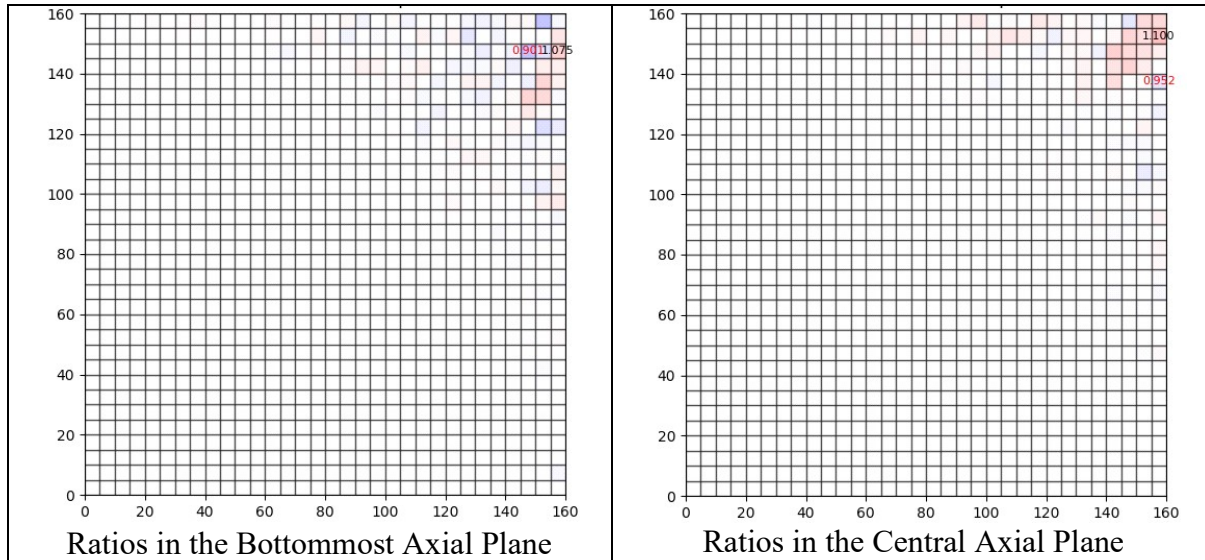
February 13, 2020

Table 136. Takeda 3, Rods-Out, Root-Mean-Squared Flux Errors

Flux	6 <sup>th</sup>	7 <sup>th</sup>	8 <sup>th</sup>	8 <sup>th</sup>	10 <sup>th</sup>	12 <sup>th</sup>	10 <sup>th</sup>	10 <sup>th</sup>
Leakage	1 <sup>st</sup>	2 <sup>nd</sup>	3 <sup>rd</sup>	3 <sup>rd</sup>	3 <sup>rd</sup>	3 <sup>rd</sup>	4 <sup>th</sup>	5 <sup>th</sup>
Source	4 <sup>th</sup>	7 <sup>th</sup>	8 <sup>th</sup>	5 <sup>th</sup>	5 <sup>th</sup>	5 <sup>th</sup>	5 <sup>th</sup>	5 <sup>th</sup>
<b>Group 1</b>								
P <sub>1</sub>	4.46E-07	4.46E-07	4.46E-07	4.46E-07	4.46E-07	4.46E-07	4.46E-07	4.46E-07
P <sub>3</sub>	1.08E-07	1.16E-07	1.17E-07	1.17E-07	1.17E-07	1.17E-07	1.17E-07	1.17E-07
P <sub>5</sub>	3.91E-08	5.17E-08	5.46E-08	5.46E-08	5.45E-08	5.45E-08	5.48E-08	*
P <sub>7</sub>	5.37E-08	2.36E-08	2.96E-08	2.96E-08	2.93E-08	2.91E-08	*	*
P <sub>9</sub>	7.67E-08	1.09E-08	1.74E-08	1.74E-08	1.68E-08	-	*	-
P <sub>11</sub>	8.94E-08	1.04E-08	1.09E-08	1.09E-08	-	-	-	-
P <sub>13</sub>	9.66E-08	1.35E-08	-	-	-	-	-	-
P <sub>15</sub>	1.01E-07	-	-	-	-	-	-	-
<b>Group 2</b>								
P <sub>1</sub>	1.15E-06	1.15E-06	1.15E-06	1.15E-06	1.15E-06	1.15E-06	1.15E-06	1.15E-06
P <sub>3</sub>	1.01E-07	1.06E-07	1.06E-07	1.06E-07	1.06E-07	1.06E-07	1.06E-07	1.06E-07
P <sub>5</sub>	3.88E-08	3.66E-08	3.85E-08	3.85E-08	3.84E-08	3.83E-08	3.87E-08	*
P <sub>7</sub>	5.01E-08	1.89E-08	2.13E-08	2.13E-08	2.11E-08	2.10E-08	*	*
P <sub>9</sub>	6.19E-08	1.49E-08	1.57E-08	1.57E-08	1.56E-08	-	*	-
P <sub>11</sub>	6.87E-08	1.48E-08	1.38E-08	1.38E-08	-	-	-	-
P <sub>13</sub>	7.24E-08	1.54E-08	-	-	-	-	-	-
P <sub>15</sub>	7.44E-08	-	-	-	-	-	-	-
<b>Group 3</b>								
P <sub>1</sub>	5.31E-07	5.32E-07	5.32E-07	5.32E-07	5.32E-07	5.32E-07	5.32E-07	5.32E-07
P <sub>3</sub>	5.54E-08	5.16E-08	5.19E-08	5.19E-08	5.19E-08	5.19E-08	5.20E-08	5.21E-08
P <sub>5</sub>	3.23E-08	2.20E-08	2.28E-08	2.28E-08	2.27E-08	2.26E-08	2.29E-08	*
P <sub>7</sub>	3.12E-08	1.43E-08	1.53E-08	1.53E-08	1.52E-08	1.51E-08	*	*
P <sub>9</sub>	3.28E-08	1.15E-08	1.25E-08	1.25E-08	1.24E-08	-	*	-
P <sub>11</sub>	3.34E-08	1.05E-08	1.12E-08	1.12E-08	-	-	-	-
P <sub>13</sub>	3.40E-08	1.02E-08	-	-	-	-	-	-
P <sub>15</sub>	3.43E-08	-	-	-	-	-	-	-
<b>Group 4</b>								
P <sub>1</sub>	4.16E-08	4.19E-08	4.20E-08	4.20E-08	4.20E-08	4.20E-08	4.20E-08	4.20E-08
P <sub>3</sub>	6.99E-09	8.21E-09	8.48E-09	8.48E-09	8.44E-09	8.42E-09	8.52E-09	8.56E-09
P <sub>5</sub>	5.29E-09	4.21E-09	4.53E-09	4.53E-09	4.47E-09	4.45E-09	4.59E-09	*
P <sub>7</sub>	6.55E-09	2.96E-09	3.30E-09	3.30E-09	3.23E-09	3.20E-09	*	*
P <sub>9</sub>	7.31E-09	2.37E-09	2.70E-09	2.70E-09	2.63E-09	-	*	-
P <sub>11</sub>	7.71E-09	2.16E-09	2.37E-09	2.37E-09	-	-	-	-
P <sub>13</sub>	7.93E-09	2.11E-09	-	-	-	-	-	-
P <sub>15</sub>	8.05E-09	-	-	-	-	-	-	-

February 13, 2020

The region-wise group 1 flux comparisons for DIF3D and MCNP for the 7-2-7 P<sub>11</sub> case are provided in the following figures. This case was chosen as it represents a good balance of low errors in of the above metrics. The left side of this figure shows this ratio in the bottom axial plane while the right side of the figure provides it for the central plane. Similar figures for groups 2 through 4 are omitted as the errors are located in similar regions with a maximum value of around 1.8%.



**Figure 113. Ratio of DIF3D to MCNP Fluxes in Group 1**

### 3.3.7.3 Core Case

#### 3.3.7.3.1 Reference MCNP Results

The MCNP reference solution was generated here with one million histories per batch, 100 inactive batches, and 16,000 active batches for a total of 16 billion active histories. The resultant value of  $k_{\text{eff}}$  predicted by MCNP was  $1.02199 \pm 0.000004$ . The relative errors for all tally bins are generally quite low, though in the extreme locations of the model they can be as high as 12% in the lowest energy groups. The relative error distribution is shown in Figure 114.



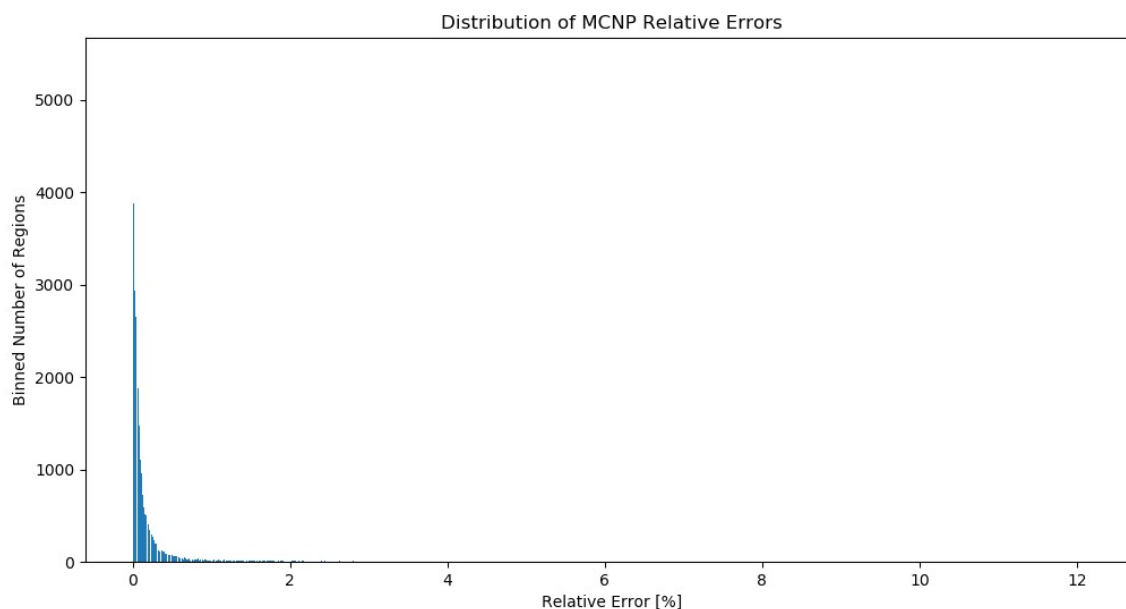


Figure 114. MCNP Relative Error Distribution for Core Case

### 3.3.7.3.2 DIF3D Results

The following tables provide the eigenvalue errors, the errors in the peak fluxes, and the root-mean-squared errors of the fluxes on a per-mesh basis. Similar trends are observed to those discussed in 3.3.7.1.

Table 137. Takeda 3, Core, Eigenvalue Errors [pcm]

Flux	6 <sup>th</sup>	7 <sup>th</sup>	8 <sup>th</sup>	8 <sup>th</sup>	10 <sup>th</sup>	12 <sup>th</sup>	10 <sup>th</sup>	10 <sup>th</sup>
Leakage	1 <sup>st</sup>	2 <sup>nd</sup>	3 <sup>rd</sup>	3 <sup>rd</sup>	3 <sup>rd</sup>	3 <sup>rd</sup>	4 <sup>th</sup>	5 <sup>th</sup>
Source	4 <sup>th</sup>	7 <sup>th</sup>	8 <sup>th</sup>	5 <sup>th</sup>	5 <sup>th</sup>	5 <sup>th</sup>	5 <sup>th</sup>	5 <sup>th</sup>
P <sub>1</sub>	-427	-427	-427	-427	-427	-418	-427	-427
P <sub>3</sub>	-18	-19	-19	-19	-19	-19	-19	-19
P <sub>5</sub>	-2	-7	-7	-7	-7	-7	-7	*
P <sub>7</sub>	3	-4	-5	-5	-5	-5	-5	*
P <sub>9</sub>	5	-3	-4	-4	-4	-	*	-
P <sub>11</sub>	6	-2	-3	-3	-	-	-	-
P <sub>13</sub>	6	-2	-	-	-	-	-	-
P <sub>15</sub>	7	-	-	-	-	-	-	-

Table 138. Takeda 3, Core, Peak Flux Errors [%]

Flux	6 <sup>th</sup>	7 <sup>th</sup>	8 <sup>th</sup>	8 <sup>th</sup>	10 <sup>th</sup>	12 <sup>th</sup>	10 <sup>th</sup>	10 <sup>th</sup>
Leakage	1 <sup>st</sup>	2 <sup>nd</sup>	3 <sup>rd</sup>	3 <sup>rd</sup>	3 <sup>rd</sup>	3 <sup>rd</sup>	4 <sup>th</sup>	5 <sup>th</sup>
Source	4 <sup>th</sup>	7 <sup>th</sup>	8 <sup>th</sup>	5 <sup>th</sup>	5 <sup>th</sup>	5 <sup>th</sup>	5 <sup>th</sup>	5 <sup>th</sup>
<b>Group 1</b>								
P <sub>1</sub>	1.77	1.77	1.77	1.77	1.77	1.77	1.77	1.77
P <sub>3</sub>	-0.13	-0.08	-0.08	-0.08	-0.08	-0.08	-0.08	-0.08
P <sub>5</sub>	-0.18	0.01	-0.01	-0.01	-0.01	-0.01	-0.01	*
P <sub>7</sub>	-0.15	0.04	0.02	0.02	0.02	0.02	0.02	*
P <sub>9</sub>	-0.13	0.05	0.02	0.02	0.02	-	*	-
P <sub>11</sub>	-0.13	0.05	0.02	0.02	-	-	-	-
P <sub>13</sub>	-0.12	0.05	-	-	-	-	-	-
P <sub>15</sub>	-0.12	-	-	-	-	-	-	-
<b>Group 2</b>								
P <sub>1</sub>	1.37	1.37	1.37	1.37	1.37	1.37	1.37	1.37
P <sub>3</sub>	0.02	0	0	0	0	0	0	0
P <sub>5</sub>	0.04	0	0	0	0	0	0	*
P <sub>7</sub>	0.05	0.01	0	0	0	0	0	*
P <sub>9</sub>	0.06	0.01	0.01	0.01	0.01	-	*	-
P <sub>11</sub>	0.07	0.01	0.01	0.01	-	-	-	-
P <sub>13</sub>	0.07	0.01	-	-	-	-	-	-
P <sub>15</sub>	0.07	-	-	-	-	-	-	-
<b>Group 3</b>								
P <sub>1</sub>	-1.15	-1.15	-1.15	-1.15	-1.15	-1.15	-1.15	-1.15
P <sub>3</sub>	0.01	0.01	0.01	0.01	0.01	0.01	0.01	0.01
P <sub>5</sub>	0.03	0.04	0.04	0.04	0.04	0.04	0.04	*
P <sub>7</sub>	0.03	0.04	0.04	0.04	0.04	0.04	0.04	*
P <sub>9</sub>	0.04	0.05	0.04	0.04	0.04	-	*	-
P <sub>11</sub>	0.04	0.05	0.04	0.04	-	-	-	-
P <sub>13</sub>	0.04	0.05	-	-	-	-	-	-
P <sub>15</sub>	0.05	-	-	-	-	-	-	-
<b>Group 4</b>								
P <sub>1</sub>	-0.45	-0.46	-0.46	-0.46	-0.46	-0.46	-0.46	-0.46
P <sub>3</sub>	-0.04	0	0	0	0	0	0	0
P <sub>5</sub>	-0.04	0.02	0.02	0.02	0.02	0.02	0.02	*
P <sub>7</sub>	-0.03	0.03	0.02	0.02	0.02	0.02	0.02	*
P <sub>9</sub>	-0.03	0.03	0.03	0.03	0.03	-	*	-
P <sub>11</sub>	-0.03	0.03	0.03	0.03	-	-	-	-
P <sub>13</sub>	-0.03	0.03	-	-	-	-	-	-
P <sub>15</sub>	-0.02	-	-	-	-	-	-	-

Table 139. Takeda 3, Core, Root-Mean-Squared Flux Errors

Flux	6 <sup>th</sup>	7 <sup>th</sup>	8 <sup>th</sup>	8 <sup>th</sup>	10 <sup>th</sup>	12 <sup>th</sup>	10 <sup>th</sup>	10 <sup>th</sup>
Leakage	1 <sup>st</sup>	2 <sup>nd</sup>	3 <sup>rd</sup>	3 <sup>rd</sup>	3 <sup>rd</sup>	3 <sup>rd</sup>	4 <sup>th</sup>	5 <sup>th</sup>
Source	4 <sup>th</sup>	7 <sup>th</sup>	8 <sup>th</sup>	5 <sup>th</sup>	5 <sup>th</sup>	5 <sup>th</sup>	5 <sup>th</sup>	5 <sup>th</sup>
<b>Group 1</b>								
P <sub>1</sub>	3.91E-07	3.91E-07	3.91E-07	3.91E-07	3.91E-07	3.91E-07	3.91E-07	3.91E-07
P <sub>3</sub>	8.07E-08	8.86E-08	8.91E-08	8.91E-08	8.91E-08	8.91E-08	8.91E-08	8.91E-08
P <sub>5</sub>	3.28E-08	3.81E-08	4.12E-08	4.12E-08	4.11E-08	4.11E-08	4.13E-08	*
P <sub>7</sub>	4.77E-08	1.64E-08	2.21E-08	2.21E-08	2.19E-08	2.17E-08	*	*
P <sub>9</sub>	6.31E-08	7.14E-09	1.30E-08	1.31E-08	1.25E-08	-	-	-
P <sub>11</sub>	7.12E-08	7.46E-09	8.33E-09	8.51E-09	-	-	-	-
P <sub>13</sub>	7.55E-08	9.97E-09	-	-	-	-	-	-
P <sub>15</sub>	7.78E-08	-	-	-	-	-	-	-
<b>Group 2</b>								
P <sub>1</sub>	1.00E-06	1.01E-06	1.01E-06	1.01E-06	1.01E-06	1.01E-06	1.01E-06	1.01E-06
P <sub>3</sub>	5.81E-08	6.28E-08	6.31E-08	6.31E-08	6.31E-08	6.31E-08	6.31E-08	6.32E-08
P <sub>5</sub>	2.80E-08	2.29E-08	2.45E-08	2.45E-08	2.44E-08	2.44E-08	2.46E-08	*
P <sub>7</sub>	4.09E-08	1.57E-08	1.70E-08	1.70E-08	1.69E-08	1.69E-08	*	*
P <sub>9</sub>	4.94E-08	1.51E-08	1.53E-08	1.53E-08	1.53E-08	-	-	-
P <sub>11</sub>	5.41E-08	1.55E-08	1.49E-08	1.49E-08	-	-	-	-
P <sub>13</sub>	5.64E-08	1.59E-08	-	-	-	-	-	-
P <sub>15</sub>	5.77E-08	-	-	-	-	-	-	-
<b>Group 3</b>								
P <sub>1</sub>	4.60E-07	4.61E-07	4.61E-07	4.61E-07	4.61E-07	4.61E-07	4.61E-07	4.61E-07
P <sub>3</sub>	3.12E-08	3.31E-08	3.37E-08	3.37E-08	3.36E-08	3.36E-08	3.38E-08	3.39E-08
P <sub>5</sub>	2.78E-08	1.91E-08	2.00E-08	2.00E-08	1.99E-08	1.99E-08	2.02E-08	*
P <sub>7</sub>	3.29E-08	1.49E-08	1.59E-08	1.59E-08	1.57E-08	1.57E-08	*	*
P <sub>9</sub>	3.65E-08	1.31E-08	1.40E-08	1.40E-08	1.39E-08	-	-	-
P <sub>11</sub>	3.79E-08	1.23E-08	1.30E-08	1.31E-08	-	-	-	-
P <sub>13</sub>	3.89E-08	1.21E-08	-	-	-	-	-	-
P <sub>15</sub>	3.95E-08	-	-	-	-	-	-	-
<b>Group 4</b>								
P <sub>1</sub>	2.80E-08	2.84E-08	2.85E-08	2.85E-08	2.85E-08	2.85E-08	2.86E-08	2.86E-08
P <sub>3</sub>	6.37E-09	7.34E-09	7.58E-09	7.58E-09	7.54E-09	7.53E-09	7.62E-09	7.66E-09
P <sub>5</sub>	4.52E-09	4.11E-09	4.37E-09	4.37E-09	4.32E-09	4.30E-09	4.41E-09	*
P <sub>7</sub>	5.00E-09	2.96E-09	3.26E-09	3.26E-09	3.20E-09	3.17E-09	*	*
P <sub>9</sub>	5.50E-09	2.37E-09	2.69E-09	2.70E-09	2.63E-09	-	-	-
P <sub>11</sub>	5.77E-09	2.14E-09	2.38E-09	2.39E-09	-	-	-	-
P <sub>13</sub>	5.94E-09	2.07E-09	-	-	-	-	-	-
P <sub>15</sub>	6.04E-09	-	-	-	-	-	-	-

The region-wise flux comparisons for DIF3D and MCNP for the 7-2-7 P<sub>11</sub> case are provided in the following figures. This case was chosen as it represents a good balance of low errors in of the above metrics. The left side of this figure shows this ratio in the bottom axial plane while the right side of the figure provides it for the central plane. Similar figures for groups 2 through 4 are omitted as the errors are located in similar regions with a maximum value of around 2.6%.

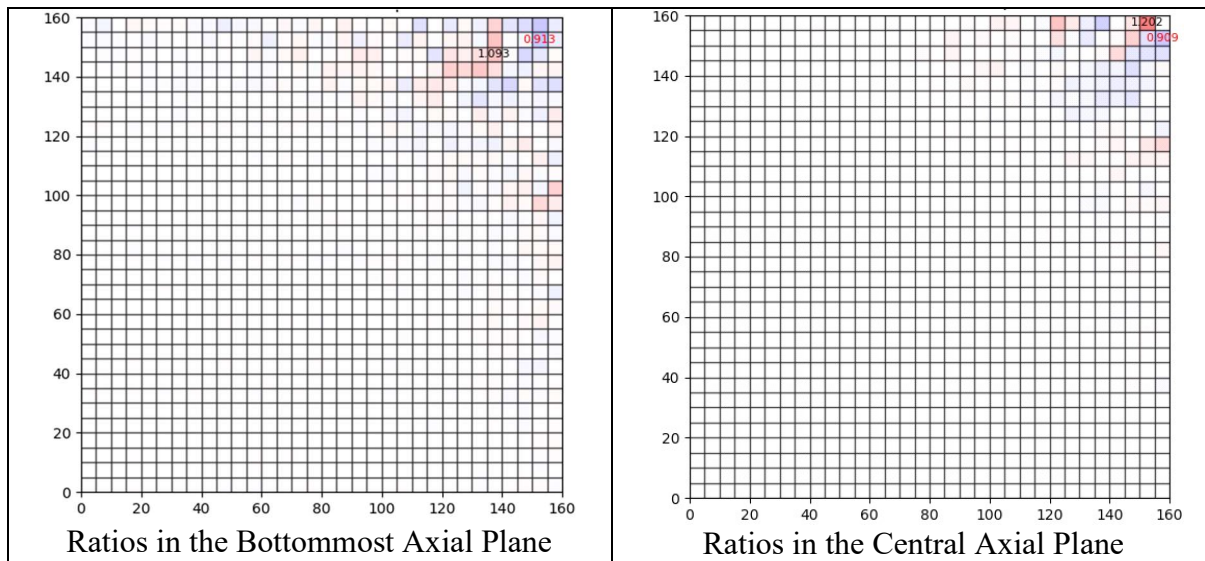


Figure 115. Ratio of DIF3D to MCNP Fluxes in Group 1

### 3.4 Hexagonal-Z Transport Verification

#### 3.4.1 Model Building Verification

As is discussed in Section 3.4.1 of [6], a Model Building case will be used to verify the ability of NIP3 and HMG4C to create the user-specified Hexagonal-Z transport model by creating a simple two-group, multi-isotope, multi-composition, multi-region triangular-Z model. This case will specifically be used to verify the following card types and options consistent with Tables 7 through 9 of [6]: card Types 1, 2 (options 3, 9, 10, and 11), 7, 9, 13, 14, 15, 29, 30, 31, and 44 of the NIP3 module; card Types 1, 2 (options 3, 4, 5, 7, and 8) of the HMG4C module; and card Types 1, 4 (Options 2, 3, 4, and 5) of the DIF3D module.

The verification of these options will be similar to, and rely heavily on, the equivalent verification performed for the 3D Cartesian transport Model Building work in Section 3.1.1 and the same for the Triangular-Z diffusion case in Section 3.2.1. This case will be designed to use the same microscopic cross sections and material/compositions data. Therefore, this work will verify the macroscopic cross section data computed by the DIF3D software is the same as that produced in the 3D Cartesian transport model building case. This case will also use the same geometry used for the Triangular-Z diffusion model building verification case. This verification effort will

therefore rely heavily on comparing this Hexagonal-Z transport outputs with those from 3D Cartesian transport (for the cross section data), and the Triangular-Z diffusion case (for the geometric data, except for the triangular-mesh specific information).

### 3.4.1.1 Model Definition

The models used for this case will be based upon the same model used with the Triangular-Z diffusion theory model building case. The only difference between this model and that will be the inclusion of the A.DIF3D module's Type 12 card as highlighted in yellow in Figure 88 that was provided for the 3D Cartesian transport case as well as changing the geometry type from full-core Triangular-Z to full-core Hexagonal-Z via the A.NIP3 Type 03 card.

This case will utilize the same perturbations performed for both the Triangular-Z diffusion case with differences as noted below. These perturbations, as well as those related to the geometry-processing related edit controls that must be performed are highlighted in Table 140. This table shows that no cross section processing edits will be exercised for this case due to the degree to that these options have been exercised thus far and the fact that the geometry type has no bearing on the cross section processing edits. Note that the A.NIP3 Module's Type 29 card, option 4, should have no bearing on the Hexagonal-Z structure; the applicable perturbation will simply make sure that is true.

**Table 140. Transport Theory Hexagonal-Z Perturbation Cases**

<b>A.NIP3</b>				
<b>Card Type &amp; Option</b>	<b>Description</b>	<b>Option in Base Case</b>	<b>Perturbations to Base</b>	<b>Evaluated in Sections</b>
2.3	Geometry processing edits	3	0, 1, 2	3.4.1.2.3.1
2.10	Region/mesh interval plotter edits	3	0, 1, 2	3.4.1.2.3.2
2.11	Zone/mesh interval plotter edits	3	0, 1, 2	3.4.1.2.3.3
3.2	Geometry Type	100	90, 94	3.4.1.2.2.1
29.4	Triangle Subdivisions	Default (1)	2	3.4.1.2.2.2
30.2	Background Region	Default (0)	REG1	3.4.1.2.2.3
<b>A.DIF3D</b>				
<b>Card Type &amp; Option</b>	<b>Description</b>	<b>Option in Base Case</b>	<b>Perturbations to Base</b>	<b>Evaluated in Sections</b>
4.2	Problem description edit	3	0, 1, 2	3.4.1.2.3.4
4.3	Geometry (region to mesh interval) map edit	3	0, 1, 2	3.4.1.2.3.5
4.4	Geometry (zone to mesh interval) map edit	3	0, 1, 2	3.4.1.2.3.6

### 3.4.1.2 *Verification*

The previous section defined the base case of the model to examine. This section will compare the DIF3D processing of this base case and show that DIF3D correctly handles the inputs provided to it. As stated above, this verification will utilize the base case discussed above with the Microscopic XS ISOTXS format of Figure 4. After verification of this base case, the perturbations to this base case provided in Table 140 will be performed and verified to be implemented correctly in DIF3D.

#### 3.4.1.2.1 *Base Case*

The DIF3D input for the base case is the same as defined in Figure 116 with the addition of the ISOTXS file from Figure 4. This file is the same as that used for the Triangular-Z diffusion theory verification except for the few parameters highlighted in yellow. The output to screen (i.e., standard output) was redirected to a text file; this and all other output files from this run are stored in an isolated directory.

The remainder of this section will progress by first traversing the standard output and the edited information compared to the independently computed values. Next, the auxiliary output file (fort.10) will be evaluated to ensure that all of the expected output edits are present and correct. The evaluation will then progress to the binary output files relating to the model definition (i.e., GEODST, NDXSFR, ZNATDN, COMPTS, and LABELS) are correct. Intermediate files (e.g., ADIF3D, ISOTXS, and ARC) and those related to the solution of the given model (e.g., RTFLUX) will not be evaluated as they are either not directly used by designers or will be verified in later sections of this work.

February 13, 2020

```

1 BLOCK=STP021
2 DATASET=A.HMG4C
3 01 HEXZ - MCC Micro XS ISOTXS
4 02 900000 0 3 3 0 0 0 3
5 UNFORM=A.NIP3
6 01 HEXZ - MCC Micro XS ISOTXS
7 02 0 3 40000000 40000000 40000000 40000000 0 3 3 3
8 03 120
9 04 2 2 2 2 2 2
10 c Define hexagon dimensions
11 29 10.0 3
12 c Add Z-dimension mesh structure
13 09 Z 2 10. 3 30.
14 c Define ring 1 which will have lower and upper regions
15 c Start with an overlay test region
16 c (this should be replaced by next two Type 30 Cards)
17 30 REG4 1
18 30 REG1 1 1 1 0. 10.
19 30 REG3 1 1 1 10. 30.
20 c Define ring 2 with the same region in each position
21 c Will be defined using the range definition
22 30 REG2 2 1 6 0. 30.
23 c Define ring 3, with alternating regions in each position
24 c define the ring by using a blanket ring fill and then
25 c overlaying every other position with the alternating
26 c region
27 30 REG3 3 0 0 0. 30.
28 30 REG4 3 2 2 0. 30.
29 30 REG4 3 4 4 0. 30.
30 30 REG4 3 6 6 0. 30.
31 30 REG4 3 8 8 0. 30.
32 30 REG4 3 10 10 0. 30.
33 30 REG4 3 12 12 0. 30.
34 c Define an area to test that capability
35 07 AREA1 REG1
36 07 AREA1 REG4
37 c Define Compositions
38 c Composition 1
39 14 COMP1 ISO1 1.0
40 15 COMP1 REG1
41 c Composition 2
42 13 MIS03 ISO3 2.0
43 14 COMP2 MIS03 0.25 ISO1 0.1
44 14 COMP2 MIS03 0.2
45 15 COMP2 REG2
46 c Composition 3
47 13 MAT31 ISO4 0.4 ISO1 0.6
48 14 COMP32 ISO3 0.6 ISO2 0.4
49 14 COMP3 MAT31 0.4 COMP32 0.4
50 14 COMP3 COMP32 0.2
51 15 COMP3 REG3
52 c Composition 4
53 14 COMP41 ISO4 2.0
54 14 COMP42 ISO1 2.0
55 14 COMP4 COMP41 0.5 COMP42 0.5
56 15 COMP4 REG4
57 C
58 UNFORM=A.DIF3D
59 01 HEXZ - MCC Micro XS ISOTXS
60 02 30000000 150000000 0
61 03 0 2 0 4500 200
62 04 3 3 3 33 000 00 000 0 0 0000 -1
63 05 1.0E-06 1.0E-07 1.0E-08
64 12 20401 10303

```

Figure 116. Hexagonal-Z Base Case Input

#### *3.4.1.2.1.1 Standard Output Edit Verification*

This section will progress through the DIF3D standard output file and evaluate the correctness of the outputted data, based upon the model description provided previously. These outputs are 2,000 lines long and therefore, the information replicated within the main body of this document will be minimized. Due to the use of the same cross sections and compositions as previous problems, all ISOTXS and composition-related edits will be compared directly to the standard output from the transport theory 3D Cartesian model building base case. Geometry-related information, however, will be directly compared to the expected configurations presented in Figure 44 and Table 93, or others as needed. Comparisons of files will be performed with the Python difflib package.

The first output of interest to this verification effort is the GNIP4C control parameters and model description table that begins on line 297. These values are consistent with those in the equivalent Triangular-Z geometry case except for those that should be expected for a hexagonal, vice triangular, mesh. Specifically, there are five X and Y-dimension mesh intervals since there are two rings and one central ring in the model, further the outer boundary shape is listed as a 120 degree rhombus as one would expect for a hexagonal grid.

The region and zone specifications, area definitions, region map, ISOTXS edits, ZNATDN, produced by the GNIP4C module are all consistent with the Triangular-Z case, as expected.

Line 536 is the beginning of the HMG4C module's edits. This section begins with another ISOTXS edit followed by the COMPXS edit, which, again is correctly consistent with the Triangular-Z case.

The DIF3D module's edits begin on line 1146, starting with edits of the user input specifications, memory storage requirements, the user edit options, and convergence criteria. These were all found to be consistent with the user input.

Line 1197 starts the DIF3D module's edit of the problem description and its' reinterpretation of the geometry in the GEODST file. These, too were found to be consistent.

The reaction region and zone by mesh point maps for each of the lower and upper planes are found on lines 1251 through 1316. These maps are significantly simpler than those for the 3D Cartesian or Triangular-Z cases as there is only a 5x5 grid for each; therefore they are not repeated here. Each was verified by hand to compare with the expected user input and all were found to match the expectations based upon the core laydown shown in Figure 44.

Line 1329 begins the output of the variational nodal parameters. These parameters include the transport option as well as another description of the geometry. The variational nodal parameters were confirmed consistent with the 3D Cartesian transport solver model building case. The geometric information was also compared to expectations and they were confirmed to be correct.



Finally, the DIF3D module's edit of the COMPXS file was confirmed to match exactly with the 3D Cartesian transport solver model's version of this table. This is expected as that problem used the same ISOTXS file, composition definitions, and transport approximation options.

The remainder of the information within this file is the solution itself for which this section will not verify the accuracy of, as this is separately covered by Sections 3.4.2 through 3.4.7.

#### *3.4.1.2.1.2 Auxiliary Output Edit Verification*

This base case requested every output table be printed to both the standard and auxiliary outputs. This section will examine the auxiliary output (i.e., the "fort.10" file) to ensure the content there is correct and consistent with the expectations. This evaluation will utilize the previous standard output verification heavily, and primarily focus on comparing to the already-verified standard outputs as opposed to comparing back to reference hand-calculations.

This comparison (again with the diffli Python package) revealed that the only differences between the standard and auxiliary outputs are:

1. The page breaks are inconsistent between the two outputs and so page numbers may be different.
2. The standard output includes additional information that was not verified by the standard output work (output file number assignments, memory storage sizes, and runtime warnings about over-relaxation factors reaching the iteration threshold).
3. The auxiliary output is apparently using non-ASCII characters to print composition names whereas the standard output was using ASCII (note it may be possible that the GNU/Linux bash shell converted these behind the scenes). Specifically, the standard output says: "EDIT OF (NONFISSIONABLE COMPOSITION COMP1" while the auxiliary output says "EDIT OF (NONFISSIONABLE COMPOSITION". This is only seen in the composition edits. Note that both are missing closing parentheses. This is consistent with the earlier auxiliary output edit verifications discussed earlier.

These differences are not important to this verification work, and since the content of the files match, the auxiliary output file is considered verified.

#### *3.4.1.2.1.3 Binary Output Verification*

The final set of outputs to verify are the CCCC-formatted [8] and ANL-specific binary output files relating to the model definition (i.e., GEODST, NDXSRF, ZNATDN, COMPXS, and LABELS). As stated earlier, intermediate files such (e.g., ADIF3D, ISOTXS, and ARC) and those related to the solution of the given model (e.g., RTFLUX) will not be evaluated as they are either not directly used by designers or will be verified in later sections of this work. The binary files that will be evaluated will be first converted to an ASCII format with the "/software/ARC/CCCC\_convert\_v11.0\_r3012\_d2019\_03\_14.x" executable that is distributed with the ARC suite.

Of these five binary files, the COMPTS, LABELS, NDXSRF, and ZNATDN files are expected to be consistent with the same files generated in the Triangular-Z case. This was confirmed true, save for differences in the last significant digit of the volumes reported in the NDXSRF files. Since it is not unreasonable to expect the volumes to be computed independently, this is an unimportant difference. No further work is necessary.

The GEODST file contains the mesh structure of the solution scheme (i.e., the information necessary to reproduce the hexagonal structure of Figure 44. Since this Hexagonal-Z GEODST file is completely different than the version produced by the 3D Cartesian and Triangular-Z cases, it will be verified explicitly instead of relying on a comparison to the underlying data after comparison to ASCII directly with the CCCC\_convert\_v11.0\_r3012\_d2019\_03\_14.x program.

The output from CCCC\_convert\_v11.0\_r3012\_d2019\_03\_14.x for the GEODST file is provided in Figure 117, after the removal of some invalid characters in the HOLLERITH USER IDENTIFICATION parameter of the file identification record that did not allow the file to be displayed in all text editors. This file, and the GEODST format specification [8] were used to populate Table 141, which contains both the expected values and actual values from within the GEODST file.

In addition to Table 141, Figure 118 is provided to more clearly illustrate the GEODST file's interpretation of the region to coarse-mesh interval assignments. The contents of Figure 118 are simply the two 6D records seen on lines 12 through 17 of Figure 117, one for each plane of the model, reformatted to be a 5 x 5 array and colored to match the region/composition coloring utilized in Figure 44. Comparing Figure 118 to Figure 44 reveals no disagreement and verifies that the GEODST file is capturing the correct region to coarse-mesh interval assignments.

The values in Table 141 highlighted in red indicate that there is a difference between the expected values and DIF3D values in a few cases. These, and their dispositions, are discussed separately below:

1. NZCL (number of zone classifications): this quantity is not well defined in the DIF3D manuals, GEODST format, or the CCCC format specification document. For that reason a reference value was not readily determined. However, the GEODST file has a value of one here, and by context, this value likely refers to the number of zone types in the problem, whether it be standard, internal black boundary, or a rodged region. As this model has no internal black boundaries or rodged regions, a value of 1 for NZCL is reasonable, given this interpretation. No further work is necessary.
2. NBS (number of buckling specifications), NBCS (number of constants for external boundaries), and NIBCS (number of constants for internal boundaries): These parameters are either related to the application of internal or external boundary conditions. Since no buckling, only reflective boundaries, and no internal boundaries were modeled in the problem, the expected value for each of these is 0. However, the GEODST file contains values of 1 here, indicating there is a single value for each that applies everywhere. Since

a value of 0 was only allowed in the CCCC format in version 4 [8], and there is no functional difference between no value and a single value everywhere if that value is a zero or ignored; the maintainers of the ARC suite chose to continue applying a single value everywhere instead of using the new 0 value feature of the standard. No further work is necessary.

3. BSQ(N) (buckling values): The expected value is that this value is not present because it is expected that NBS would be 0. However, the GEODST file does contain a value of 1 for NBS and thus a value for BSQ(N) of 0.0. This is equivalent to no buckling, and therefore is correct.
4. BNDC(N) (boundary constants): This value is the boundary constant derived from  $D\phi' + A\phi = 0$  per the A.NIP3 input format specification (and equivalently  $D\phi' + C\phi = 0$  in the GEODST format guide). The expectation is that since a reflective boundary condition is used,  $A$  (or  $C$ ) are either not supplied or are zero. However, the value in the GEODST file is 0.4692. This is listed as the default value in the A.NIP3 manual, if extrapolated boundary conditions are specified but no A.NIP3 Type 05 card (external boundary condition constants) is provided. Therefore DIF3D must populate this value as the default even if it is never needed. Problems verifying the treatment of boundary conditions will verify that this value truly is ignored by the solver with boundary conditions where it is not relevant.
5. BNCI(N) (internal black boundary constants): The expected value is that this value is not present because it is expected that NIBCS would be 0. However, the GEODST file does contain a value of 1 for NIBCS and thus a value for BNCI(N) of 0.0. This is equivalent to no internal black boundary constant, and therefore is correct.
6. NZC(N) (zone classification assignments): Similar to NZCL, since it is unclear what a zone classification is, expected values are difficult to identify. Given the contextual understanding discussed above with NZCL, the GEODST file's four values of 0 (for each of the four zones) are reasonable and no further work is needed.

Based on the above, the GEODST file contents are considered verified for this problem; later cases with reference flux and eigenvalue solutions will examine the impact of the boundary condition constant value of 0.4692 that is in the GEODST file.

February 13, 2020

```

1 0V GEODST*      *      1
2 1D      18      4      4      1      5      5      2      5      5      5      0
3      0      0      0      0      0      1      1      1      0      0      0      0
4      120      0      0      0
5 4D 0.00000E+00 1.00000E+01 0.00000E+00 0.00000E+00 0.00000E+00 0.00000E+00
6 0.00000E+00 0.00000E+00 0.00000E+00 0.00000E+00 0.00000E+00 0.00000E+00
7 0.00000E+00 0.00000E+00 1.00000E+01 3.00000E+01
8      1      1      1      1      1      1      1      1      1      2      3
9 5D 1.55885E+04 8.66025E+02 1.73205E+04 1.55885E+04 0.00000E+00
10 4.69200E-01 0.00000E+00
11      0      0      0      0      4      1      3      2
12 6D      3      1      3      0      0      1      4      4      1      0      3
13      4      2      4      3      0      1      4      4      1      0      3
14      1      3
15 6D      3      1      3      0      0      1      4      4      1      0      3
16      4      3      4      3      0      1      4      4      1      0      3
17      1      3

```

Figure 117. Hexagonal-Z Base Case GEODST File

```

1 6D Record: Region Numbers to
2 Coarse-Mesh Intervals for Plane 1
3  1 0 0
4  1 2 1 0
5  1 2 1 0
6  0 1 4 1
7  0 0 1
8
9 6D Record: Region Numbers to
10 Coarse-Mesh Intervals for Plane 1
11  1 0 0
12  1 2 1 0
13  1 2 1 0
14  0 1 4 1
15  0 0 1

```

Figure 118. GEODST File Coarse-Mesh Interval Region Assignments

February 13, 2020

Table 141. Comparison of GEODST Values for Hexagonal-Z Problem

Variable	Expected Value	DIF3D Value	Variable	Expected Value	DIF3D Value	Variable	Expected Value	DIF3D Value
<b>Specifications (1D Record)</b>			<b>1D Mesh Boundaries (2D Record)</b>			<b>Geometry Data (5D Record)</b>		
<i>IGOM</i>	18 (hex-Z)	18	<i>Not present since 3D</i>			<i>VOLR(N)</i>	NREG Values: 1.55885E+04, 8.66025E+02, 1.73205E+04, 1.55885E+04	1.55885E+04, 8.66025E+02, 1.73205E+04, 1.55885E+04
<i>NZONE</i>	4	4	<b>2D Mesh Boundaries (3D Record)</b>			<i>BSQ(N)</i>	NBS Values: Not Present	0
<i>NREG</i>	4	4	<i>Not present since 3D</i>			<i>BNDC(N)</i>	NBCS Values: Not Present	0.4692
<i>NZCL</i>	1	1	<b>3D Mesh Boundaries (4D Record)</b>			<i>BNCI(N)</i>	NIBCS Values: Not Present	0
<i>NCINTI</i>	5	5	<i>XMESH(I)</i>	NCINTI+1 Values: 0., 10.0, 0*4	0., 10.0, 0*4	<i>NZHBB(N)</i>	NZWBB Values: Not Present	Not Present
<i>NCINTJ</i>	5	5	<i>YMESH(J)</i>	NCINTJ+1 Values: 0*6	0*6	<i>NZC(N)</i>	NZONE Values: ?	0,0,0,0
<i>NCINTK</i>	2	2	<i>ZMESH(K)</i>	NCINTK+1 Values: 0, 10, 30	0, 10, 30	<i>NZNR</i>	NREG Values: 1,2,3,4,4,3,2,1	1,2,3,4,4,3,2,1
<i>NINTI</i>	5	5	<i>IFINTS(I)</i>	NCINTI Values 1*5	1*5	<b>Region Assignments to Coarse Mesh (6D Record)</b>		
<i>NINTJ</i>	5	5	<i>JFINTS(J)</i>	NCINTJ Values 1*5	1*5	<i>MR(I,J,K=1)</i>	NCINTIxNCINTJ Values: See Figure	See Figure
<i>NINTK</i>	5	5	<i>KFINTS(K)</i>	NCINTK Values 2, 3	2, 3	<i>MR(I,J,K=2)</i>	NCINTIxNCINTJ Values: See Figure	See Figure
<i>IMB1</i>	0	0				<b>Region Assignments to Fine Mesh (7D Record)</b>		
<i>IMB2</i>	0	0				<i>Not present since NRASS=0</i>		
<i>JMB1</i>	0	0						
<i>JMB2</i>	0	0						
<i>KMB1</i>	0	0						
<i>KMB2</i>	0	0						
<i>NBS</i>	0	1						
<i>NBCS</i>	0	1						
<i>NIBCS</i>	0	1						
<i>NZWBB</i>	0	0						
<i>NTRIAG</i>	0	0						
<i>NRASS</i>	0	0						
<i>NTHPT</i>	0	0						
<i>NGOP</i>	Reserved	120, 0, 0, 0						

#### *3.4.1.2.2 Verification of Hexagonal-Z Geometric Perturbations*

Table 140 provided the perturbation cases that need to be evaluated for the Hexagonal-Z transport solver verification. Included in these were the perturbations to the A.NIP3 options relating to geometry type, number of triangle subdivisions, and setting the region filling the model background. These geometric perturbations to the triangular-Z base case will be evaluated in this section. Each of these perturbation options will be discussed separately in the subsections that follow.

##### *3.4.1.2.2.1 Geometry Type Perturbations*

Thus far the full-core Hexagonal-Z case has been tested. The following subsections will verify the sixth- and third-core symmetric representations.

###### *3.4.1.2.2.1.1 Sixth-Core Symmetric Representation*

The sixth-core symmetry can be enabled by settings the geometry type parameter in the A.NIP3 Type 03 card to 124. Further, to obtain an eigenvalue close to the original within tolerance, periodic adjacent boundary conditions are added to the lower X and leftmost Y boundaries.

With this change, it is expected that the standard and auxiliary output edited region maps will only show 1/6 the core instead of the whole core, the number of mesh intervals in the X and Y directions will change, the echoes of the modified input options, the volumes will be 1/6 as large, and the solution convergence approach will change. These expectations were confirmed true by using the Python diffliB package that highlighted the differences in the outputs. It was found that these areas were the only areas of deviation, as expected. Further, the only binary files with deviations were the GEODST file and specifically the volumes within the NDXSFR file.

Next, the areas that did change need to be verified. Beginning on line 307, the first relevant difference in the standard output is the number of coarse and fine mesh intervals in the X and Y directions. Since the reactor model only contains three rings, a third-core model should also contain three intervals in the X and Y dimensions; this was found to match the DIF3D output. This same information, and the same values, are repeated by the DIF3D module's Problem Description Table on lines 1160 through 1211. The same table also contains the integer identifiers for the boundary conditions and outer boundary shape; these were changed exactly as expected.

Line 342 provides the region and zone specifications, including the volumes of each region. These values were verified to be exactly 1/6 that of the base case values; this is the expected result.

Line 364 begins the region/composition map for the hexagonal geometry. There are two of these maps, one for the lower plane (between 0 and 10 cm axially) and another for the upper plane (between 10 and 30 cm). The maps provided are the same as those produced by the equivalent Triangular-Z case, as expected, and therefore are similarly verified. Similar to the Triangular-Z case, the DIF3D output does not print the composition label for the bottom row of assemblies; this is not considered to impact the correctness of DIF3D, but is noted here for completeness.

February 13, 2020

The final differences to discuss are the DIF3D module's output of the reactor region and zone mesh-point assignment maps for the lower and upper planes. These maps were verified manually through comparisons to expectations in Figure 55, neglecting the triangular mesh, and expected to match expectations.

Finally, as an indication that the DIF3D manipulation of this geometry is likely correct, both the base case and this sixth-core model yield the same final, converged, eigenvalue to all reported significant digits.

The auxiliary output was verified through comparison to the standard output; the only differences were related to the expected different types of content in the auxiliary and standard outputs, none of which was impacted by this change of geometry.

Next, the NDXSRF file was converted to ASCII and compared to the same file for the base case. Unsurprisingly, the only differences here are that the volumes have been modified exactly by a factor of one-sixth, as expected.

The GEODST file contains extensive differences as one would expect, due to the introduction of the sixth-core geometry. In the 1D record, these differences are limited to the number of coarse and fine mesh intervals in the X and Y dimensions; the sixth-core model has values of 3 (X) and 3 (Y) for these as already discussed. The boundary conditions are also modified as expected, as is the geometry option signifying that this is a 60 degree rhombic boundary. In the 3D record, the coarse mesh and fine mesh interval boundaries have been updated to consistently reflect the updated number of coarse and fine mesh intervals. The volumes again have been reduced by a factor of one-sixth, as expected. Finally, the GEODST file includes the region assignments to the coarse mesh intervals in the 6D record. Like in Figure 53 for the base case, these arrays will be converted to a regular grid and colored to more clearly provide the verification basis. This is provided in Figure 119. These region to mesh assignments should be inverted so that the first row printed is actually the first row of the mesh at the center of the core as printed in the DIF3D standard output maps. When factoring this in, the GEODST file mesh assignments in Figure 119 matches the expected layout.

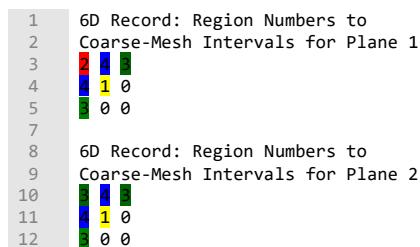


**Figure 119. Sixth-Core Geometry GEODST File Region to Mesh Assignments**

#### 3.4.1.2.2.1.2 Third-Core Symmetric Representation

The third-core symmetry can be enabled by settings the geometry type parameter in the A.NIP3 Type 03 card to 126. Further, to obtain an eigenvalue close to the original within tolerance, periodic adjacent boundary conditions are added to the lower X and leftmost Y boundaries.

February 13, 2020

---

With this change, it is expected that the standard and auxiliary output edited region maps will show 1/3 of the core instead of the whole core, the number of mesh intervals in the X and Y directions will change, the echoes of the modified input options, the volumes will be 1/3 as large, and the solution convergence approach will change. These expectations were confirmed true by using the Python diffliib package that highlighted the differences in the outputs. It was found that these areas were the only areas of deviation, as expected. Further, the only binary files with deviations were the GEODST file and specifically the volumes within the NDXSRF file.

Next, the areas that did change need to be verified. Beginning on line 307, the first relevant difference in the standard output is the number of coarse and fine mesh intervals in the X and Y directions. Since the reactor model only contains three rings, a third-core model should also contain three intervals in the X and Y dimensions; this was found to match the DIF3D output. This same information, and the same values, are repeated by the DIF3D module's Problem Description Table on lines 1166 through 1217. The same table also contains the integer identifiers for the boundary conditions and outer boundary shape; these were changed exactly as expected.

Line 340 provides the region and zone specifications, including the volumes of each region. These values were verified to be exactly 1/3 that of the base case values; this is the expected result.

Line 364 begins the region/composition map for the hexagonal geometry. There are two of these maps, one for the lower plane (between 0 and 10 cm axially) and another for the upper plane (between 10 and 30 cm). The maps provided are the same as those produced by the equivalent third-core Triangular-Z case, as expected, and therefore are similarly verified. Similar to the Triangular-Z case, the DIF3D output does not print the composition label for the bottom row of assemblies; this is not considered to impact the correctness of DIF3D, but is noted here for completeness.

The final differences to discuss are the DIF3D module's output of the reactor region and zone mesh-point assignment maps for the lower and upper planes. These maps were verified manually through comparisons to expectations in Figure 60, neglecting the triangular mesh, and expected to match expectations.

Finally, as an indication that the DIF3D manipulation of this geometry is likely correct, both the base case and this third-core model yield the same final, converged, eigenvalue to all reported significant digits.

The auxiliary output was verified through comparison to the standard output; the only differences were related to the expected different types of content in the auxiliary and standard outputs, none of which was impacted by this change of geometry.

Next, the NDXSRF file was converted to ASCII and compared to the same file for the base case. Unsurprisingly, the only differences here are that the volumes have been modified exactly by a factor of one-third, as expected.



February 13, 2020

The GEODST file contains extensive differences as one would expect, due to the introduction of the third-core geometry. In the 1D record, these differences are limited to the number of coarse and fine mesh intervals in the X and Y dimensions; the third-core model has values of 3 (X) and 3 (Y) for these as already discussed. The boundary conditions are also modified as expected, as is the geometry option signifying that this is a 60 degree rhombic boundary. In the 3D record, the coarse mesh and fine mesh interval boundaries have been updated to consistently reflect the updated number of coarse and fine mesh intervals. The volumes again have been reduced by a factor of one-third, as expected. Finally, the GEODST file includes the region assignments to the coarse mesh intervals in the 6D record. Like in Figure 53 for the base case, these arrays will be converted to a regular grid and colored to more clearly provide the verification basis. This is provided in Figure 120. These region to mesh assignments should be inverted so that the first row printed is actually the first row of the mesh at the center of the core as printed in the DIF3D standard output maps. When factoring this in, the GEODST file mesh assignments in Figure 120 matches the expected layout.

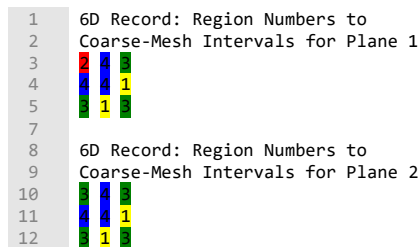


**Figure 120. Third-Core Geometry GEODST File Region to Mesh Assignments**

#### 3.4.1.2.2.2 Triangle Subdivisions Perturbation

Including additional triangles in a hexagonal mesh is expected to have no effect on the solution. This was verified by adding a value of 2 to the fourth parameter of the A.NIP3 Type 29 card (as opposed to the default value) as was done in the equivalent perturbation study for the diffusion solver's Triangular-Z model building verification cases. This was verified to have no effect on the solution of DIF3D and only two minor impacts to the output: (1) the GNIP4C module's reactor map plot saw an increase in the index numbering along the left, right, top and bottom of the map implying that it is still working with a triangular meshing structure, and (2) the LABELS file has a parameter for number of triangles per hex, and this was updated consistent with as if the triangles were actually used (a value of 24 was reported in all the subdivided perturbed cases). This discrepancy was the only noted when comparing all relevant output files. This study was also repeated for the sixth-core, and third-core geometries; the same result was found.

#### 3.4.1.2.2.3 Background Region Perturbation

The A.NIP3 block contains an option on the Type 31 card that controls the setting of the background region in the model. This is the region assigned to the region of the reactor outside of the hexagonal map defined by the Type 30 cards. DIF3D defaults to applying a "0" region, i.e., no region or material, to these regions; this was used in all Hexagonal-Z models thus far.

To verify the A.NIP3 block's Type 31 card, REG1 will be applied to the background for the full-core, sixth-core, and third-core cases. For these cases, the only differences expected are

February 13, 2020

that the volume of REG1 will increase, and the region and zone to mesh interval maps should have the “0”s on the core periphery replaced with “2” (for region maps) or “1” (for zone maps).

Table 142 provides the computed volumes. These volumes were computed by determining how many additional hexagonal regions, filled with REG1, are required to fill a 120 degree rhombus, a 60 degree rhombus, or a 120 degree rhombus for the full-, sixth-, and third-core geometries respectively based upon the core laydowns sketched in Figure 47, Figure 55, and Figure 60. This analysis identified that six additional 30 cm tall hexagons of 10 cm pitch were required for the full-core case, 3 for sixth-core, and none for the third-core case.

**Table 142. Volumes for REG1 in Background**

Case	REG1 Volumes [cm <sup>3</sup> ]
Base	8.660254E+02
Full-Core	1.645448E+04
Sixth-Core	7.938566E+03
Third-Core	2.886751E+02

To perform this verification, the standard, auxiliary, and binary outputs from cases with REG1 assigned to the background will be compared to their equivalents with no background region assigned. The volumes should be as expected and the core maps should identify the number of additional REG1 hexagons. All were found to match expectations with one notable discrepancy: the core maps plotted by the GNIP4C module (for example, that starting on line 369 of the standard output for the full-core model) do not plot the background regions in the core map plot and thus no differences were observed there. This is expected behavior, though slightly misleading.

#### *3.4.1.2.3 Verification of Hexagonal-Z Edit Control Perturbations*

Table 140 provided the perturbation cases that need to be evaluated for the Hexagonal-Z transport solver verification. Of these only the edit control options remain to be verified. This section will perform that verification.

The six edit control options from Table 140 that must be verified are summarized in Table 143. Each of these will be verified separately in the subsections that follow. These specific edit control options are those relating to the geometry; those relating to composition or isotopic data have been thoroughly vetted by other problems.

Table 143. Transport Theory Hexagonal-Z Perturbation Cases

<b>A.NIP3 Module Options</b>			
<b>Card Type &amp; Option</b>	<b>Description</b>	<b>Option in Base Case</b>	<b>Perturbations to Base</b>
2.3	Geometry processing edits	3	0, 1, 2
2.10	Region/mesh interval plotter edits	3	0, 1, 2
2.11	Zone/mesh interval plotter edits	3	0, 1, 2
<b>A.DIF3D Module Options</b>			
<b>Card Type &amp; Option</b>	<b>Description</b>	<b>Option in Base Case</b>	<b>Perturbations to Base</b>
4.2	Problem description edit	3	0, 1, 2
4.3	Geometry (region to mesh interval) map edit	3	0, 1, 2
4.4	Geometry (zone to mesh interval) map edit	3	0, 1, 2

#### 3.4.1.2.3.1 A.NIP3 Type 02 Card Option 3

The third option of the Type 02 card of the A.NIP3 input block accepts values of 0, 1, 2, or 3 as shown in Table 98. The cases evaluated thus far have kept this option at a value of 3, indicating that geometry edits will be printed to both standard and auxiliary output. This case will evaluate the 0, 1, and 2 options that print no GNIP4C module edits, print GNIP4C edits only to standard output, and print GNIP4C edits only to auxiliary output.

The base case input was modified accordingly with three different inputs capturing the 0, 1, 2, and 3 values for this option discussed above. DIF3D was run for all three cases. To verify, the auxiliary and standard output files for each of the three cases were compared against the base case to ensure that the A.NIP3 edit option is respected.

The first modified case shall print no GNIP4C module edits in either standard or auxiliary output and all other outputs should be the same as the base case. This was explicitly confirmed by comparing both outputs with the base case equivalent. The base case, beginning on line 292 of the standard output includes the GNIP4C edits printed from the A.NIP3 module; this is not present in the standard output of the modified case. It is noted that the GNIP4C edits still output the reactor region map, but do not include the GNIP4C edits of the cross section information; this is interesting as the A.NIP3 listing is unclear on what exactly a “geometry processing module edit” entails. The same findings exist for the auxiliary output.

The second modified case is expected to print the GNIP4C edits to the standard output but not the auxiliary output. The value of this option was successfully interpreted, as the auxiliary output did not include the GNIP4C edits but the standard output did. Similar to the above case, the GNIP4C edits in the auxiliary output still output the reactor region map, but do not include the GNIP4C edits of the cross section information.

The third modified case is expected to print the GNIP4C edits to only the auxiliary output; and all other output should be the same as the base. The value of this option was successfully interpreted, as the standard output did not include the GNIP4C edits but the auxiliary output did, with the same caveat as is found for the previous two cases. Interestingly, this specific option did not translate the isotope names to ASCII correctly in the auxiliary output as lines 475 through 521 of the auxiliary output includes a “<0x00>” code for each character in the isotope name. The other cases in this A.NIP3 Type 02 card Option 3 cases had no issue here.

#### *3.4.1.2.3.2 A.NIP3 Type 02 Card Option 10*

The tenth option of the Type 02 card of the A.NIP3 input block accepts values of 0, 1, 2, or 3 as shown in Table 98. The cases evaluated thus far have kept this option at a value of 3, indicating that region/mesh interval printer-plotter maps will be printed to both standard and auxiliary output. This case will evaluate the 0, 1, and 2 options that print no region/mesh interval printer-plotter maps, print region/mesh interval printer-plotter maps only to standard output, and print region/mesh interval printer-plotter maps only to auxiliary output.

This verification found that the A.NIP3 Type 02 card’s 10<sup>th</sup> option is not regarded and the region/mesh interval map is always plotted to both the standard and auxiliary outputs.

#### *3.4.1.2.3.3 A.NIP3 Type 02 Card Option 11*

The eleventh option of the Type 02 card of the A.NIP3 input block accepts values of 0, 1, 2, or 3 as shown in Table 98. The cases evaluated thus far have kept this option at a value of 3, indicating that zone (composition) / mesh interval printer-plotter maps will be printed to both standard and auxiliary output. This case will evaluate the 0, 1, and 2 options that print no zone (composition) / mesh interval printer-plotter maps, print zone (composition) / mesh interval printer-plotter maps only to standard output, and print zone (composition) / mesh interval printer-plotter maps only to auxiliary output.

This verification found that the A.NIP3 Type 02 card’s 11<sup>th</sup> option is not regarded and the zone/mesh interval map is always plotted to both the standard and auxiliary outputs.

#### *3.4.1.2.3.4 A.DIF3D Type 04 Card Option 2*

The second option of the Type 04 card of the A.DIF3D input block accepts values of 0, 1, 2, or 3, as shown in Table 98. The cases evaluated thus far have kept this option at a value of 3, indicating that the problem description edits will be printed to both standard and auxiliary output. This case will evaluate the 0, 1, and 2 options that print no problem description edits, print problem description edits only to standard output, and problem description edits only to auxiliary output.

The first modified case shall print no problem description edits in either standard or auxiliary output and all other outputs should be the same as the base case. This was explicitly confirmed by comparing both outputs with the base case equivalent for both standard and auxiliary output files.

The second modified case is expected to print the problem description edits to the standard output but not the auxiliary output. The value of this option was successfully interpreted, as the auxiliary output did not include the problem description edits but the standard output did.

The third modified case is expected to print the problem description edits to only the auxiliary output; and all other output should be the same as the base. The value of this option was successfully interpreted, as the standard output did not include the problem description edits but the auxiliary output did.

#### *3.4.1.2.3.5 A.DIF3D Type 04 Card Option 3*

The third option of the Type 04 card of the A.DIF3D input block accepts values of 0, 1, 2, or 3 as shown in Table 98. The cases evaluated thus far have kept this option at a value of 3, indicating that the DIF3D module will print region/mesh interval printer-plotter maps to both standard and auxiliary output. This case will evaluate the 0, 1, and 2 options that print no region/mesh interval printer-plotter maps, print region/mesh interval printer-plotter maps only to standard output, and print region/mesh interval printer-plotter maps only to auxiliary output.

The first modified case shall print no region maps in either standard or auxiliary output and all other outputs should be the same as the base case. This was explicitly confirmed by comparing both outputs with the base case equivalent

The second modified case is expected to print the region maps to the standard output but not the auxiliary output. The value of this option was successfully interpreted, as the auxiliary output did not include the map but the standard output did.

The third modified case is expected to print the region maps to only the auxiliary output; and all other output should be the same as the base. The value of this option was successfully interpreted, as the standard output did not include the reactor region maps but the auxiliary output did.

#### *3.4.1.2.3.6 A.DIF3D Type 04 Card Option 4*

The fourth option of the Type 04 card of the A.DIF3D input block accepts values of 0, 1, 2, or 3 as shown in Table 98. The cases evaluated thus far have kept this option at a value of 3, indicating that the DIF3D module will print zone/mesh interval printer-plotter maps to both standard and auxiliary output. This case will evaluate the 0, 1, and 2 options that print no zone/mesh interval printer-plotter maps, print zone/mesh interval printer-plotter maps only to standard output, and print zone/mesh interval printer-plotter maps only to auxiliary output.

The first modified case shall print no zone maps in either standard or auxiliary output and all other outputs should be the same as the base case. This was explicitly confirmed by comparing both outputs with the base case equivalent

The second modified case is expected to print the zone maps to the standard output but not the auxiliary output. The value of this option was successfully interpreted, as the auxiliary output did not include the map but the standard output did.

The third modified case is expected to print the zone maps to only the auxiliary output; and all other output should be the same as the base. The value of this option was successfully interpreted, as the standard output did not include the reactor region maps but the auxiliary output did.

#### *3.4.1.2.4 Rodded Model Verification*

Verification that the A.NIP3 Type 44 card (region assignment to control rod banks) is working as planned, a Hexagonal-Z version of the earlier presented Triangular-Z rodded model was developed (see Figure 74). This model is completely consistent with that model except the Hexagonal-Z geometry and transport solver options were exercised.

The geometric representation of this model will not be explicitly verified and documented here as this capability was already documented by previous sections. Instead this documentation will verify that the A.NIP3 module properly interprets these options via direct inspection of the standard and auxiliary outputs as well as the LABELS binary file, the only binary file containing control rod information.

Before progressing further, it must be noted that despite the note in the A.NIP3 listing that says “NOTE THAT A BLANK CONTROL ROD BANK LABEL IS ACCEPTABLE”, a blank control rod label is not actually acceptable. Specifically the DIF3D code fails with an error during GNIP4C processing of the A.NIP3 block if a blank label is actually used for a control rod bank. This includes the label being in columns 7-12 as specified by the listing and elsewhere. Therefore the following cases will actually apply a label (“BANK5”) to the fifth control rod bank option.

The control rod channel specifications begin on line 922 of the standard output as is provided in Figure 121. This table shows each of the six control rod banks and their properties like the regions assigned and the boundaries between the control rods and the regions below and above it. Starting with the bank position, all are at 10 cm above the bottom ( $Z=0$ ) of the model, exactly as incorporated in the model. Additionally, only banks within ring 3 have a region above the rodded region. The rod-tip region labels should match that observed based upon the bank locations in Figure 74. These region locations (again, using the RXYZZ numbering scheme) indeed match. Further, this table is exactly the same as that created for the Triangular-Z geometry, with the exception that the number of mesh cells in channel is 1 for the hexagonal case and that the order of rods within BANK3 are not the same, though both are correct.

The auxiliary output was confirmed to contain the same control rod region table as is shown in Figure 121 and therefore the auxiliary output is also verified.

The LABELS file is a binary representation of the model’s region and composition labels, area data, half heights, nuclide set labels, alias zone labels, control rod model data, and burnup-dependent cross section data. Previous LABELS comparisons used the CCCC\_convert program to convert the binary data to ASCII as well as using the CCCC\_PrintTables program.



February 13, 2020

CCCC\_convert, when used to convert this case's LABELS file reports that "CONTROL ROD stuff not supported by CCCC\_convert." CCCC\_PrintTables also encounters a segmentation fault during the processing of the LABELS file.

The custom Python program written to output LABELS information (named "read\_LABELS.py") was therefore utilized again. This output, too long to show here at ~230 lines, was compared with the input, the Figure 121 edits, and the bank locations in Figure 74. First, it was expected that this file should only have different mesh indices when compared to the equivalent output from the Triangular-Z Rodded Model Verification case; this was found true. This output was found to represent the control rod banks, their rods, and the mesh entries containing those rods faithfully, including adequately handling the cases with and without movable regions above the rods when factoring in that the (1,1) mesh position begins at the bottom Bank 3 hexagon in Figure 74 and the (5,5) mesh is the topmost Bank 4 hexagon.

*** CONTROL-ROD CHANNEL SPECIFICATIONS ***									
CONTROL-ROD BANK				ROD-TIP	NO. OF				
NO.	LABEL	POSITION		REGION	MESH CELLS				
				LABEL	IN CHANNEL	CHANNEL DESCRIPTION (BOUNDARY, REGION, BOUNDARY, ETC.)			
928	0	1	BANK1	10.00	R2101	1	0.00	R1101	10.00 R2101
929	0	2	BANK2	10.00	R2310	1	0.00	R1310	10.00 R2310 20.00 R3310
930					R2304	1	0.00	R1304	10.00 R2304 20.00 R3304
931	0	3	BANK3	10.00	R2309	1	0.00	R1309	10.00 R2309 20.00 R3309
932					R2303	1	0.00	R1303	10.00 R2303 20.00 R3303
933	0	4	BANK4	10.00	R2205	1	0.00	R1205	10.00 R2205
934					R2201	1	0.00	R1201	10.00 R2201
935					R2203	1	0.00	R1203	10.00 R2203
936	0	5	BANK5	10.00	R2202	1	0.00	R1202	10.00 R2202
937	0	6	BANK6	10.00	R2307	1	0.00	R1307	10.00 R2307 20.00 R3307
938					R2204	1	0.00	R1204	10.00 R2204
939					R2301	1	0.00	R1301	10.00 R2301 20.00 R3301

**Figure 121. Snippet of Relevant Standard Output for Control Rod Bank Problem**

### 3.4.2 Multigroup Fixed Source Verification

As discussed in Section 3.4.2 of [6], a two-group, up-scattering, anisotropic, Hexagonal-Z, fixed source verification case must be generated that utilizes a multigroup source in at least one of the regions, utilizes sixth-core symmetry, and applies vacuum boundary conditions on both Z-axis boundaries as well as in the radial direction. This section describes this verification case.

The reference solution was stated in [6] to be determined from a multigroup Monte Carlo code. In this case, MCNP 6.2 [15] will be used to solve the exact same source, geometry, material, and cross sections used in the DIF3D model. Further, the MCNP 6.2 tally regions will be defined exactly consistent with the fine-mesh regions in the DIF3D model to avoid any coarsening of results when performing the code-to-code comparison. Since a code-to-code comparison will be used for verification of DIF3D, the features of the MCNP 6.2 code used to generate this reference solution must also be verified. The verification of relevant MCNP 6.2 features are documented in Section 4.

The following approach will be taken when comparing the DIF3D and MCNP fixed source results. First, the calculated flux distribution will be compared through three metrics: the maximal (normalized) region-averaged flux value and location, the root-mean-squared-error of the DIF3D flux compared to the MCNP flux distributions for each group, and finally a graphical

February 13, 2020

comparison of the differences in flux distributions will be displayed. It is unlikely that the DIF3D and MCNP results will match exactly, because of each method's distinct iterative error sources that cannot be practically removed from the analysis. Therefore, instead of striving for an exact match, this work will instead show that refining DIF3D's spatial and angular order is approaching the MCNP reference result.

Before progressing that it should be noted this problem was also used to verify the correct definition of a multigroup DIF3D-FD source. This was indeed observed in the FIXSRC file and the solution's flux ratios implying the spectra was correctly applied.

#### 3.4.2.1 Model Definition

Based on the above considerations, a three-ring hexagonal-Z system will be modeled with a hexagon flat-to-flat distance of 25 cm, a total height of 60 cm, and an axial mesh spacing of 10 cm. The bottom and top 10 cm of the model are composed of REG1. The 40 cm between these regions contains REG2 in the first and second rings, and REG1 in the third ring. The REG1 and REG2 cross sections are as defined in Table 144 and previously used for the 3D Cartesian Transport Multigroup Fixed Source case.

**Table 144. 3D Cartesian Transport Multigroup Fixed Source Macroscopic Cross Sections; units of cross sections are 1/cm**

	REG1		REG2	
	Group 1	Group 2	Group 1	Group 2
$\Sigma_{\text{total}}$	3.33333E-02	1.00000E-01	3.33333E-02	5.00000E-02
$\Sigma_{\text{abs}}$	2.66667E-02	8.00000E-02	2.33333E-02	3.50000E-02
$\nu\Sigma_{\text{fission}}$	-	-	-	-
$\chi$	-	-	-	-
$\Sigma_{\text{scatter},0,1 \rightarrow g}$	1.33333E-03	5.33333E-03	2.00000E-03	8.00000E-03
$\Sigma_{\text{scatter},0,2 \rightarrow g}$	0.00000E+0 0	2.00000E-02	1.50000E-03	1.35000E-02
$\Sigma_{\text{scatter},1,1 \rightarrow g}$	1.33333E-04	5.33333E-04	1.00000E-04	4.00000E-04
$\Sigma_{\text{scatter},1,2 \rightarrow g}$	0.00000E+0 0	2.00000E-03	7.50000E-05	6.75000E-04

The volumetric fixed source is uniformly in ring 1 position and axially between 20 and 40 cm. 75% of the unit source is deposited in group 1 and 25% in group 2. Finally, the above description was modeled as a sixth-core and thus with periodic boundary conditions azimuthally.

#### 3.4.2.2 Reference MCNP Results

The previously described model was converted to an MCNP model via the create\_mcnpy script discussed elsewhere. Of note for this application, the periodic boundary conditions (required by DIF3D for sixth-core geometries) were replaced with reflective boundaries in MCNP to simplify the conversion script. As this model exhibits periodic and reflective



February 13, 2020

symmetries, these are equivalent. After the script created the MCNP input file, it was manually modified to establish the fixed source region as the script only creates eigenvalue inputs.

The MCNP reference case was run with 1.6 billion histories. Due to the large number of histories, the L'Ecuyer 63-bit generator (number 1) was used with its' period of  $9.2 \times 10^{18}$  numbers. The relative errors for all tally bins were less than 0.06% and are significantly smaller than any expected code-to-code differences and therefore no further visualization or description of their behavior follows.

This case yielded a flux distribution one would expect with neutrons streaming away from the volumetric source in a slightly larger than exponential fashion due to the combination of the absorption losses and slightly forward peaked scattering. This flux distribution is provided in Figure 91 and Figure 92 showing a slice of the flux distribution computed by MCNP in both the X-Y (left) and Y-Z (right) planes for the two groups, respectively. The color-scale is chosen so that low flux values are blue, the median is white, and the highest flux regions are shown in red. The minimum and maximum values to generate these color schemes are based on the flux extremes over all energy groups, hence the same color scale is applied to Figure 122 and Figure 123.

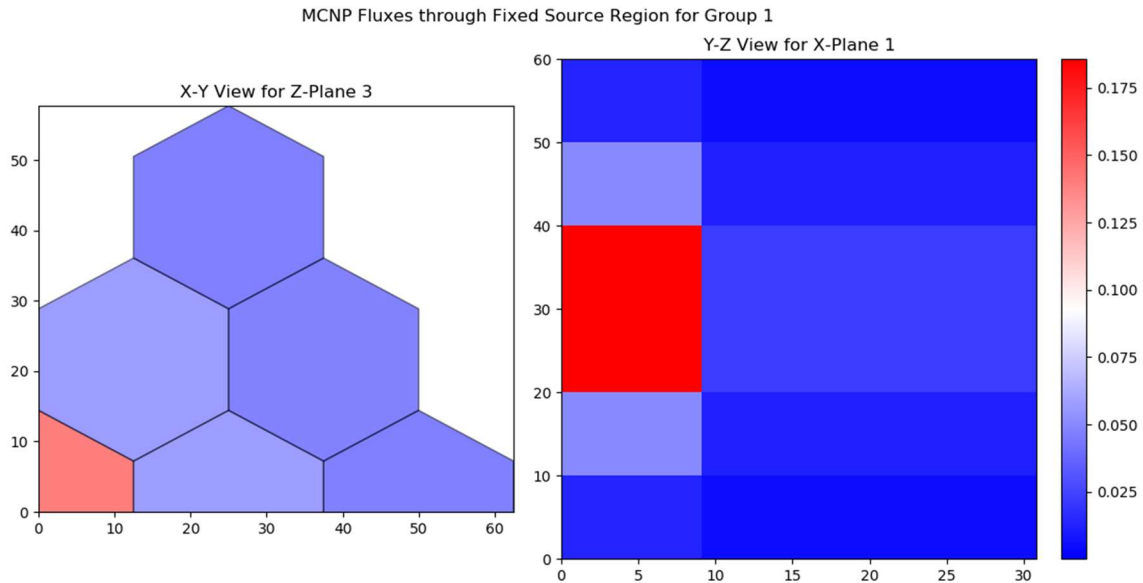


**Figure 122. Hexagonal-Z MG Fixed Source MCNP Reference Flux in Group 1**

February 13, 2020

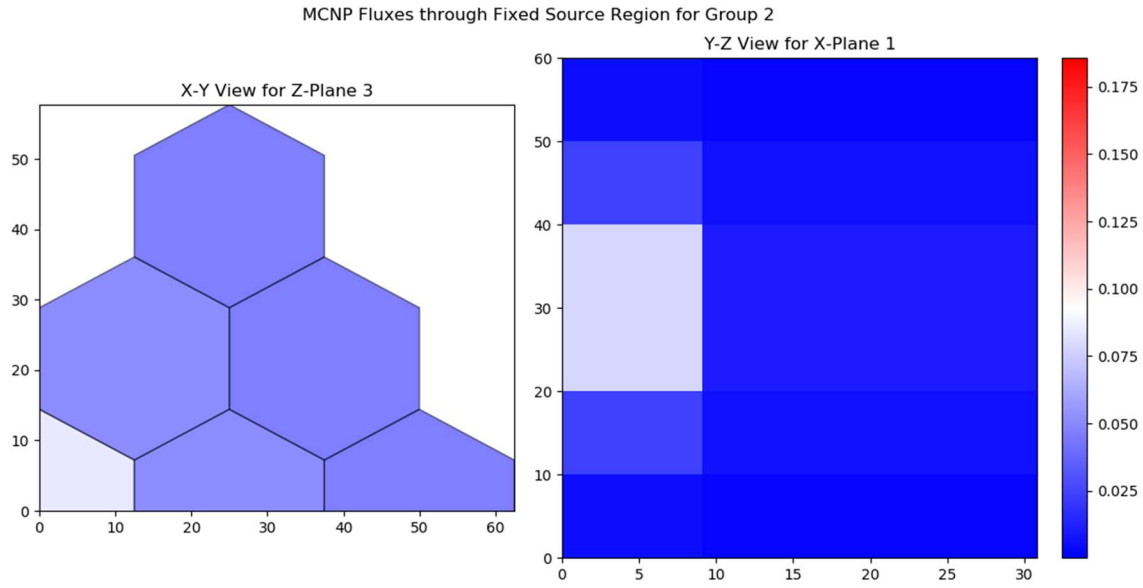


**Figure 123. Hexagonal-Z MG Fixed Source MCNP Reference Flux in Group 2**

### 3.4.2.3 DIF3D Results

The transport solver within DIF3D, DIF3D-VARIANT, was used to solve the same configuration that was analyzed by MCNP. Since, as previously stated, an exact analytical match cannot be expected, this verification will focus on ensuring that the DIF3D solution is generally converging to the MCNP reference solution as the spatial and angular orders are increased. This analysis will not consider additional mesh refinement in DIF3D is not as impactful as increasing the polynomial order first. The metrics used to evaluate the accuracy of the DIF3D solution include the value and location of the maximum region-averaged fluxes for each group, and the root-mean-squared-error of the group- and region-wise fluxes.

All of the cases used a pointwise fission source convergence of  $10^{-7}$ , average fission source convergence of  $10^{-8}$ , 200 XY-plane partial current sweeps per group per outer iteration, and 200 axial partial current sweeps per outer iteration. All other iteration parameters were left at the DIF3D defaults.

Table 145 provides the difference in the maximum region-averaged group-wise flux between the DIF3D solutions and the MCNP reference. These peak locations are unsurprisingly located in the source region. In these tables, '-' denotes that the case was not possible due to limitations in the amount of memory that the tested version of DIF3D can allocate to solve a model.

Similarly, Table 146 provides the root-mean-squared-error of the flux across the entire spatial and energy domain of the problem.

Table 145. Hexagonal-Z MG DIF3D Peak Flux Errors in units of percent

Flux	6 <sup>th</sup>	7 <sup>th</sup>	8 <sup>th</sup>	8 <sup>th</sup>	10 <sup>th</sup>	12 <sup>th</sup>	10 <sup>th</sup>	10 <sup>th</sup>
Leakage	1 <sup>st</sup>	2 <sup>nd</sup>	3 <sup>rd</sup>	3 <sup>rd</sup>	3 <sup>rd</sup>	3 <sup>rd</sup>	4 <sup>th</sup>	5 <sup>th</sup>
Source	4 <sup>th</sup>	7 <sup>th</sup>	8 <sup>th</sup>	5 <sup>th</sup>	5 <sup>th</sup>	5 <sup>th</sup>	5 <sup>th</sup>	5 <sup>th</sup>
<b>Group 1</b>								
P <sub>1</sub>	37.5	38.0	38.0	38.0	38.0	38.0	38.0	38.0
P <sub>3</sub>	18.8	20.8	21.0	21.0	21.0	20.9	21.0	21.0
P <sub>5</sub>	3.0	10.3	11.1	11.1	11.0	11.0	11.2	11.2
P <sub>7</sub>	-7.5	4.2	5.9	5.9	5.7	5.6	6.1	6.3
P <sub>9</sub>	-12.7	0.6	3.1	3.1	2.6	-	-	-
P <sub>11</sub>	-14.9	-1.1	-	-	-	-	-	-
P <sub>13</sub>	-16.1	-1.9	-	-	-	-	-	-
P <sub>15</sub>	-16.8	-	-	-	-	-	-	-
<b>Group 2</b>								
P <sub>1</sub>	27.3	27.8	27.8	27.8	27.8	27.8	27.8	27.8
P <sub>3</sub>	9.2	11.1	11.4	11.4	11.3	11.3	11.4	11.4
P <sub>5</sub>	-0.8	4.2	4.7	4.7	4.6	4.6	4.8	4.8
P <sub>7</sub>	-5.9	1.4	2.2	2.2	2.0	2.0	2.3	2.4
P <sub>9</sub>	-8.2	-0.1	1.0	1.0	0.8	-	-	-
P <sub>11</sub>	-9.1	-0.7	-	-	-	-	-	-
P <sub>13</sub>	-9.7	-1.0	-	-	-	-	-	-
P <sub>15</sub>	-10.03	-	-	-	-	-	-	-

In these tables, the spatial source approximation is truncated to reduce memory; this is acceptable as in the fixed source region, the source is effectively flat and thus a 0<sup>th</sup> order approximation would suffice. Outside of the fixed source region, the source term is only due to the scattering present in the problem. Since the scattering source depends on the flux, and the total mean-free-paths are on the order of 10s of cm, the scattering source will be slowly varying within a region and therefore low orders will suffice. This can be observed when comparing the 8-3-8 (Flux-Leakage-Source) column's errors to the 8-3-5 column's errors. This comparison shows that reducing the source's polynomial order by three orders had no significant effect on the errors but the 8-3-5 case was able to run a higher angular approximation due to the reduced memory requirements of the 5<sup>th</sup> order spatial source approximation.

The spatial flux convergence is achieved at the tenth order; this can be observed by comparing the 8-3-5, 10-3-5, and 12-3-5 results in Table 145 and Table 146. Here, the only change is the

February 13, 2020

---

order of the spatial flux polynomials used, yet there is only a minor change in the peak and root-mean-squared errors.

Similarly, spatial leakage convergence is achieved by the third leakage order as seen by comparing the 10-3-5, 10-4-5, and 10-5-5 results in Table 145 and Table 146. Only the leakage is changed in these three calculations and only the last significant digit of each metric is variant.

This case is easily converged in space as the spatial flux distribution is generally smooth. Specifically, the flux will exhibit the standard exponential decay through a material whose cross sections are such that neutrons have a mean-free-path of at least 10 cm. If a strong absorber like a thermal reactor control rod was included then more spatial orders would be necessary.

The angular refinement is the last component to consider and one can observe that convergence is not yet observed as the highest two possible angular orders for each Flux-Leakage-Source combination are still changing. This is expected behavior in a problem with a discrete volumetric fixed source. Within the fixed source region, the angular flux order does not need to be much larger than the defined fixed source, which in this case is isotropic. However, the angular leakage order representing the angular dependence of the leakage from the source region to its neighboring regions will need to be large as the leakage is skewed strongly away from the source region. In the non-source regions, the angular flux order will need to be high due to the leakage from the source region; further, without strong scattering the angular leakage order in non-source regions will also need to be high. The Table 121 and Table 122 error metrics show that the error is strongly driven by the angular order and any case that is sufficiently converged spatially (i.e., not 6-1-4) will benefit from increasing the angular order to the maximum extent practical.

**Table 146. Hexagonal-Z MG DIF3D Flux Root-Mean-Squared-Errors**

Flux	6 <sup>th</sup>	7 <sup>th</sup>	8 <sup>th</sup>	8 <sup>th</sup>	10 <sup>th</sup>	12 <sup>th</sup>	10 <sup>th</sup>	10 <sup>th</sup>
Leakage	1 <sup>st</sup>	2 <sup>nd</sup>	3 <sup>rd</sup>	3 <sup>rd</sup>	3 <sup>rd</sup>	3 <sup>rd</sup>	4 <sup>th</sup>	5 <sup>th</sup>
Source	4 <sup>th</sup>	7 <sup>th</sup>	8 <sup>th</sup>	5 <sup>th</sup>	5 <sup>th</sup>	5 <sup>th</sup>	5 <sup>th</sup>	5 <sup>th</sup>
<b>Group 1</b>								
P <sub>1</sub>	1.39E-02	1.41E-02	1.41E-02	1.41E-02	1.41E-02	1.41E-02	1.41E-02	1.41E-02
P <sub>3</sub>	7.28E-03	7.96E-03	8.04E-03	8.04E-03	8.03E-03	8.03E-03	8.05E-03	8.05E-03
P <sub>5</sub>	1.94E-03	4.26E-03	4.50E-03	4.50E-03	4.47E-03	4.46E-03	4.52E-03	4.54E-03
P <sub>7</sub>	3.02E-03	2.14E-03	2.56E-03	2.56E-03	2.49E-03	2.45E-03	2.64E-03	2.68E-03
P <sub>9</sub>	4.98E-03	9.71E-04	1.46E-03	1.46E-03	1.32E-03	-	-	-
P <sub>11</sub>	5.85E-03	7.84E-04	-	-	-	-	-	-
P <sub>13</sub>	6.33E-03	8.82E-04	-	-	-	-	-	-
P <sub>15</sub>	6.63E-03	-	-	-	-	-	-	-
<b>Group 2</b>								
P <sub>1</sub>	4.33E-03	4.42E-03	4.42E-03	4.42E-03	4.42E-03	4.42E-03	4.42E-03	4.42E-03
P <sub>3</sub>	1.66E-03	1.94E-03	1.97E-03	1.97E-03	1.97E-03	1.97E-03	1.98E-03	1.98E-03
P <sub>5</sub>	3.90E-04	8.48E-04	9.09E-04	9.10E-04	8.99E-04	8.95E-04	9.20E-04	9.26E-04
P <sub>7</sub>	1.01E-03	3.68E-04	4.45E-04	4.47E-04	4.25E-04	4.16E-04	4.70E-04	4.83E-04
P <sub>9</sub>	1.41E-03	1.66E-04	2.28E-04	2.31E-04	2.00E-04	-	-	-
P <sub>11</sub>	1.59E-03	1.69E-04	-	-	-	-	-	-
P <sub>13</sub>	1.69E-03	1.96E-04	-	-	-	-	-	-
P <sub>15</sub>	1.76E-03	-	-	-	-	-	-	-

Interestingly, the 7-2-7 series of cases performed slightly better than did 8-3-8 with its higher flux, leakage, and source orders. In the review of results it was identified that this is driven by cancellation of errors wherein the 7-2-7 cases had larger flux values in the outer ring that resulted in a decrease in the flux in the remainder of the core, bringing the solution close to the MCNP reference. With these findings, the 7-2-7 P<sub>11</sub> case will be considered the converged DIF3D result for the qualitative region-wise flux comparisons as it has the highest order and has sufficiently high spatial orders. These flux comparisons are shown in Figure 124 and Figure 125 for groups 1 and 2, respectively. Each of these figures provides two plots; the left is the bottom-most plane of model and the right is the third axial plane that is one of the two that contains the fixed source. Within each of these figures is the DIF3D-to-MCNP flux ratios in each of the hexagonal regions of the plane. The ratio is provided numerically as well as by color where blue indicates the DIF3D result is less than the MCNP, white implying they are

February 13, 2020

close, and red implying the DIF3D result is larger than in MCNP. These results show overall very close agreement for the majority of the central regions.

In these figures, the largest errors are present below the source in the central region of the bottom plane (12% error in group 1) and in the source plane but furthest away (6% error for group 1). The errors in both of these regions are due to an accrual of errors in representing the angular flux as they stream from the source region through intermediary regions and into the high-error regions.

Given that the solution is shown to be convergent to the correct solution, this DIF3D capability for the Hexagonal-Z geometry is considered verified.

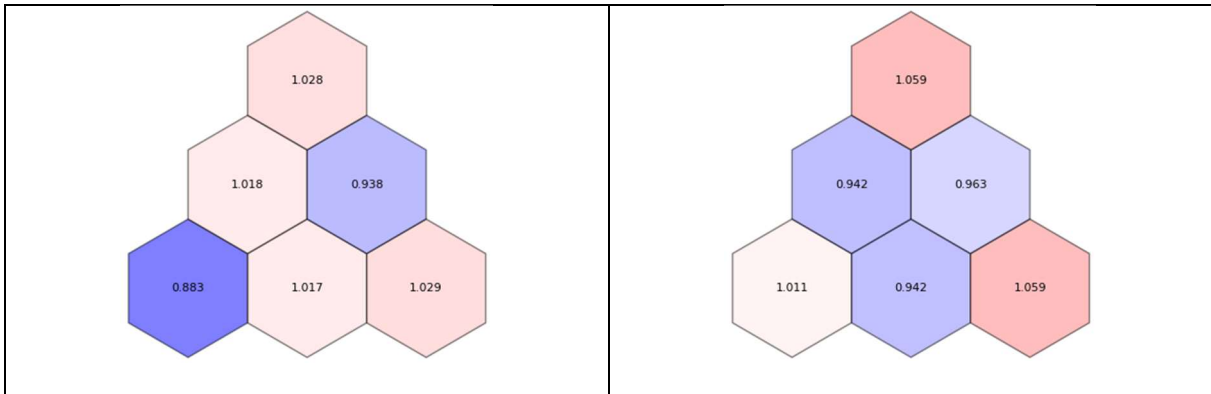


Figure 124. Hexagonal-Z MG DIF3D to MCNP Flux Ratios in Group 1

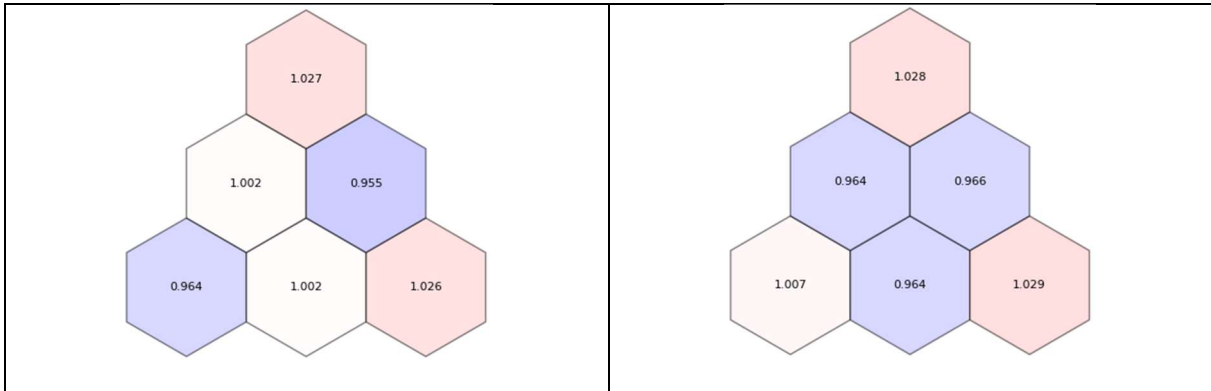


Figure 125. Hexagonal-Z MG DIF3D to MCNP Flux Ratios in Group 2

#### 3.4.2.4 Verification of Important Anisotropic Scattering

As discussed in [6], to utilize this anisotropic scattering case as verification that anisotropic scattering is working, it must be verified that a different and sensible result is obtained when isotropic scattering (with the same data) compared to the anisotropic result. In this case, the same 7-2-7  $P_{11}$  case was re-ran with isotropic scattering via option 9 of the Type 12 card in the A.DIF3D input block. Similarly, DIF3D was told to utilize the total cross section instead of the transport cross section. Thus the problem is truly isotropic in nature.

Since this model is forward-scattering (i.e.,  $P_1/P_0$  is positive), the isotropic case should have less neutrons at locations further from the source. Further, since the  $P_1/P_0$  is larger in the 2<sup>nd</sup>

February 13, 2020

group, this effect should be exacerbated in group 2. Figure 126 and Figure 127 provide plots similar to Figure 124 and Figure 125 except the ratio in this case is the isotropic flux compared to the anisotropic flux in each of the two groups. We should therefore see a ratio less than one the further out from the source in the lower left, and even more so in the second group. This is exactly what is observed in Figure 126 and Figure 127.

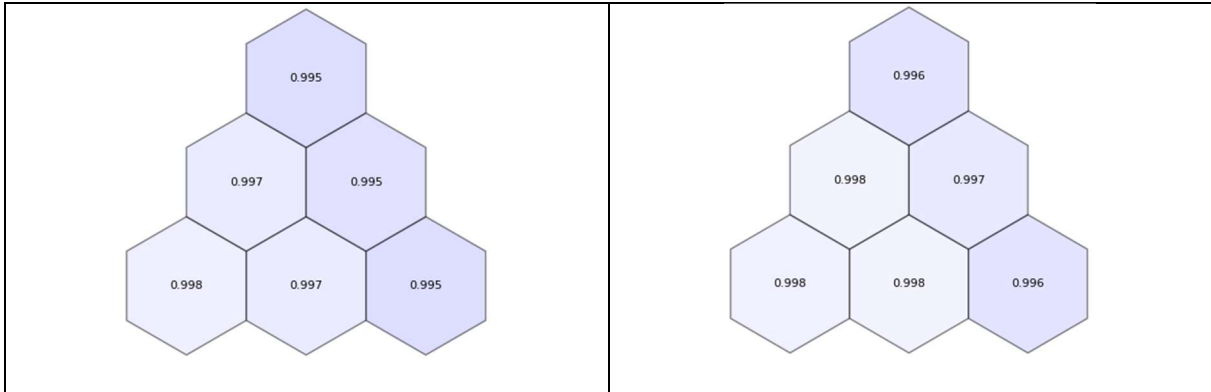


**Figure 126. Hexagonal-Z MG Isotropic to Anisotropic DIF3D Flux Ratios in Group 1**

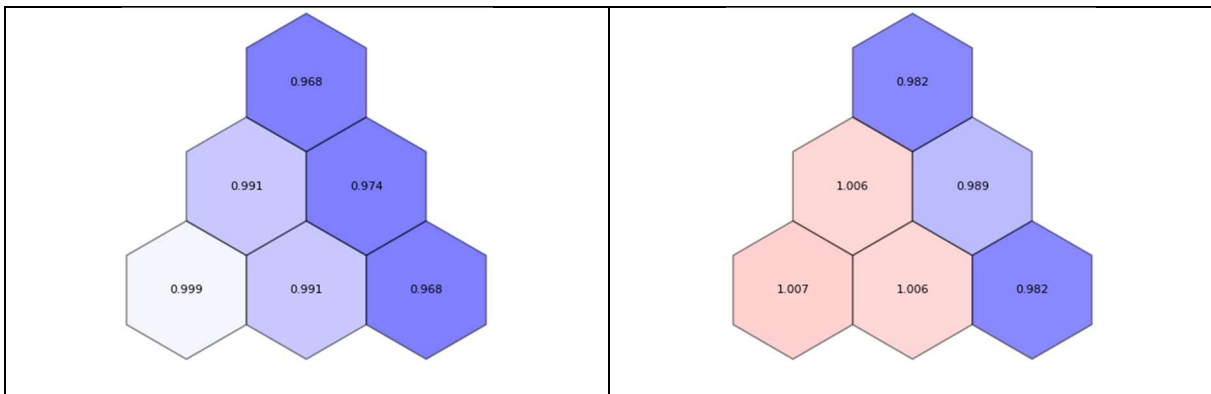


**Figure 127. Hexagonal-Z MG Isotropic to Anisotropic DIF3D Flux Ratios in Group 2**

### 3.4.2.5 Inhomogeneous Fixed Source Verification

In addition to the traditional fixed source capability, DIF3D also provides the capability to compute an inhomogeneous fixed source calculation. That is, a fixed source problem with fissile media. While this capability was previously included in the manufactured solution verification discussed earlier in 3.2.2, that case only considered a single region and one energy group. To ensure the capability works as expected in a multi-region, multigroup case the fixed source model discussed above was modified to include fission.

Specifically, the fixed source, scattering source, and fission source are combined in DIF3D to create the total within group source for the solution of each inner iteration. With this equation, it is clear that the total within group source will stay the same if some amount of up- or down-scatter cross section is removed from the  $P_0$  scattering term and replaced with an equivalent fission cross section, fission multiplicity, and fission spectrum. For this case we chose to replace the  $P_0$  up-scatter from group 2 to group 1 of the REG2 material defined in Table 144 and replace with the cross sections defined in the “Modified REG2” set in Table 147.

**Table 147. Modified Multigroup Macroscopic Cross Sections for Inhomogeneous Case; units of cross sections are 1/cm**

	REG2		Modified REG2	
	Group 1	Group 2	Group 1	Group 2
$\Sigma_{total}$	3.33333E-02	5.00000E-02	3.33333E-02	5.00000E-02
$\Sigma_{abs}$	2.33333E-02	3.50000E-02	2.33333E-02	3.50000E-02
$\nu$	-	-	5.00000E-01	5.00000E-01
$\Sigma_{fission}$	-	-	0.00000E+0 0	1.50000E-03
$\nu\Sigma_{fission}$	-	-	0.00000E+0 0	7.50000E-04
$\chi$	-	-	1.00000E+0 0	0.00000E+00
$\Sigma_{scatter,0,1->g}$	2.00000E-03	8.00000E-03	2.00000E-03	8.00000E-03
$\Sigma_{scatter,0,2->g}$	1.50000E-03	1.35000E-02	0.00000E+0 0	1.35000E-02
$\Sigma_{scatter,1,1->g}$	1.00000E-04	4.00000E-04	1.00000E-04	4.00000E-04
$\Sigma_{scatter,1,2->g}$	7.50000E-05	6.75000E-04	7.50000E-05	6.75000E-04

These cross sections, when combined with an input  $k_{eff}$  value of 0.5, result in a total source (Q) that is equivalent between REG2 and the Modified REG2. Therefore DIF3D should yield the same flux distribution in space and energy regardless of if REG2 or the Modified REG2 are applied. This modified case was run and it was explicitly verified that the resultant DIF3D fluxes were the exact same between the two cases to all reported significant figures, though it is noted that DIF3D required 5 iterations to converge the fission source in this case instead of just two iterations as is for the case that included no fission.

### 3.4.3 Multigroup Eigenvalue Verification

As discussed in Section 3.4.3 of [6], a three-group (with up-scattering), anisotropic, Hexagonal-Z, eigenvalue verification case must be generated. This case will utilize multiple regions with different cross sections, have sixth-core symmetry, and utilize vacuum boundary conditions on the Z-axis boundaries as well as in the radial direction (i.e., perpendicular to the outer ring of assemblies).

This case is similar to the Multigroup Eigenvalue verification performed for the 3D Cartesian Transport Verification work discussed in Section 3.3.3, except in this case Hexagonal-Z is used. Like the Section 3.3.3 case, this case will use MCNP 6.2 [15] as the reference solution to be used as the verification basis for DIF3D. This verification will also progress through the verification by comparing the following quantities between DIF3D and MCNP: (1) the calculated eigenvalues; (2) the maximal (normalized) region-averaged flux values and location; (3) the root-mean-squared-error of the DIF3D flux compared to the MCNP fluxes; and (5) a graphical comparison of the region-wise differences in flux distributions. Like the 3D Cartesian case, this evaluation will also ensure that the DIF3D solution is converging to the MCNP reference result.



#### 3.4.3.1 *Model Definition*

The model considered for the Hexagonal-Z multigroup eigenvalue verification is a 100 cm tall reactor of 25 cm assemblies arranged in four rings. The compositions used in this reactor are the same as were defined for the 3D Cartesian Multigroup Eigenvalue verification case discussed in Section 3.3.3 and thus the multigroup cross sections are the same as those provided in Table 124. In summary, REG1 and REG2 were fissile regions while REG3 was similar in composition to a reflector. The bottom and top 10 cm of the entire core is composed of REG3. Between 10 cm and 90 cm, rings 1, 2, 3, and 4 are composed of REG2, REG1, REG2, and REG3, respectively. The presence of the reflector (COMP3) was found to be necessary to make the flux anisotropy manageable near the edge of the fissile region of the core as was previously discussed.

This reactor is discretized in both DIF3D and MCNP so that the axial mesh is 10 cm tall. The radial mesh is one mesh element per assembly.

#### 3.4.3.2 *Reference MCNP Results*

The previously described model was converted to an MCNP model via the `create_mcnpy` script. This script reads a DIF3D model's geometry from the GEODST file and the composition cross sections from the COMPTS file and creates an exact duplicate of the model in MCNP. The MCNP file created from this script only utilizes planar surfaces, including for the hexagonal assembly surfaces, and cells assigned to the root universe, minimizing the amount of MCNP features that must be verified to support this work. The MCNP input file included tally regions for each of the DIF3D mesh elements and for each energy group of the problem. Finally, this script creates the multigroup nuclear data library for MCNP by way of the `'simple_ace_mg.pl'` script that is distributed by Los Alamos National Laboratory with MCNP [16].

The MCNP reference case was run with 1,000,000 histories per batch, 100 inactive batches, and 16,000 active batches for a total of 16 billion active histories. The resultant value of  $k_{\text{eff}}$  predicted by MCNP was 1.59232 with an estimated standard deviation of 0.00001. Like the equivalent 3D Cartesian MCNP model, the L'Ecuyer 63-bit generator (number 1) was used. The relative errors for all tally bins were distributed as is shown in Figure 128. The majority of these relative errors are significantly smaller than any expected code-to-code differences and therefore no further visualization or description of their behavior follows.

February 13, 2020

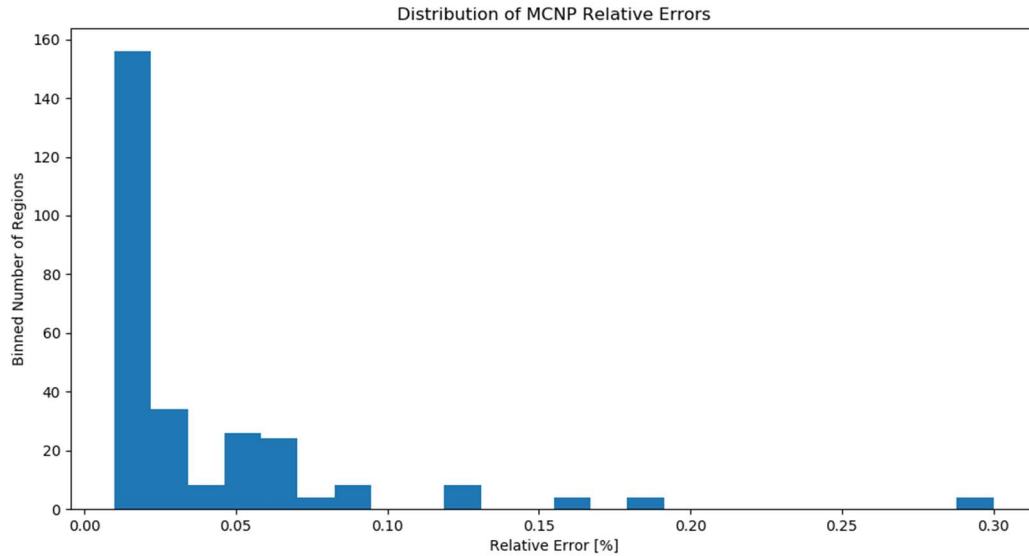


**Figure 128. Hexagonal-Z MG Eigenvalue MCNP Flux Rel. Err. Distribution**

This case yielded a flux distribution that is generally sinusoidal in the Z-direction, and peaked in the central assembly of the 3<sup>rd</sup> ring. This flux distribution is provided in Figure 129 through Figure 131. These figures show a slice of the flux distribution computed by MCNP through a central slice of both the X-Y (left) and Y-Z (right) planes for the fast, epithermal, and thermal groups, respectively. In these figures, and other flux distribution figures throughout this Section, the color-scale is chosen so that low flux values are blue, the median is white, and the highest flux regions are shown in red. The minimum and maximum values to generate these color schemes are based on the flux extremes over all energy groups, hence the same color scale is applied in Figure 129 through Figure 131. Given this coloring scheme, it is clearly evident that the fissile region is between 30 and 50 cm in the X and Y dimensions and 10 to 90 cm in the Z dimension and that a general sinusoidal shape is achieved along each axes.

February 13, 2020

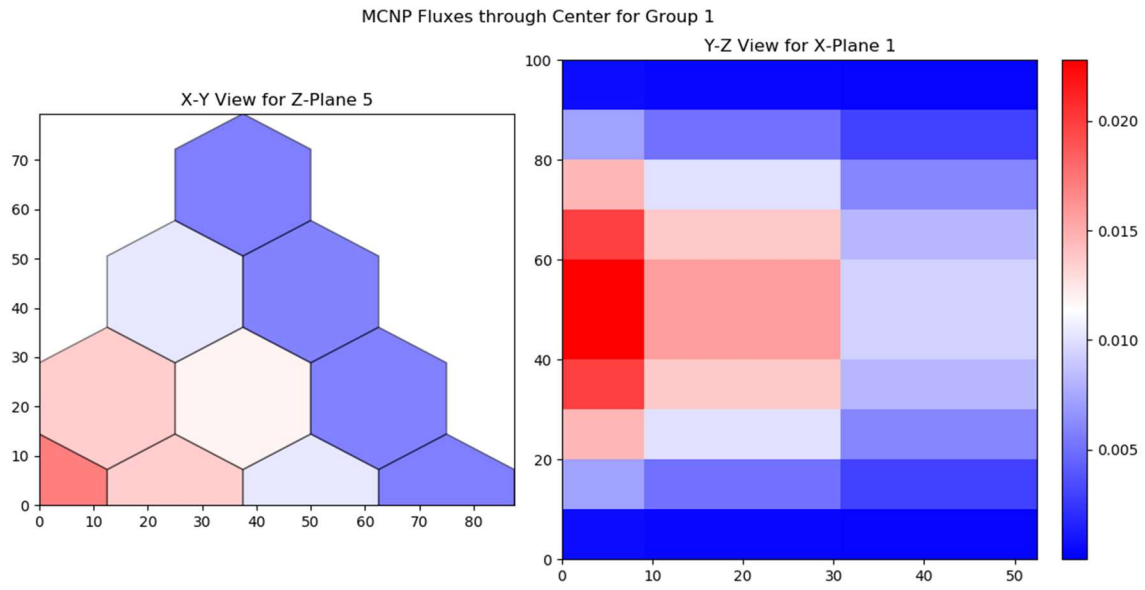


**Figure 129. Hexagonal-Z MG Eigenvalue MCNP Reference Flux in Group 1**

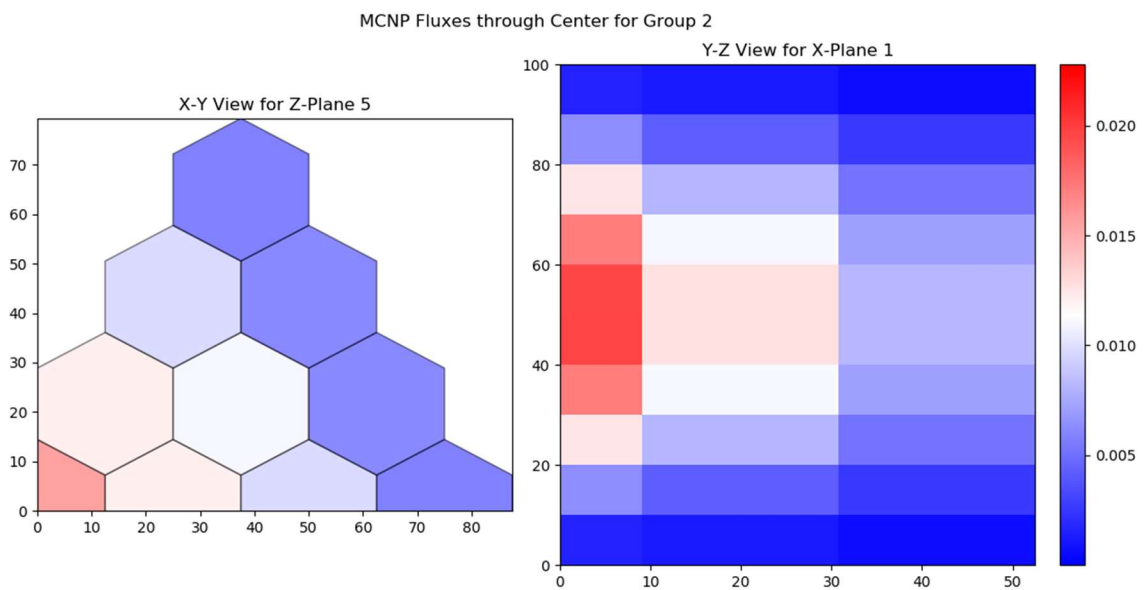


**Figure 130. Hexagonal-Z MG Eigenvalue MCNP Reference Flux in Group 2**

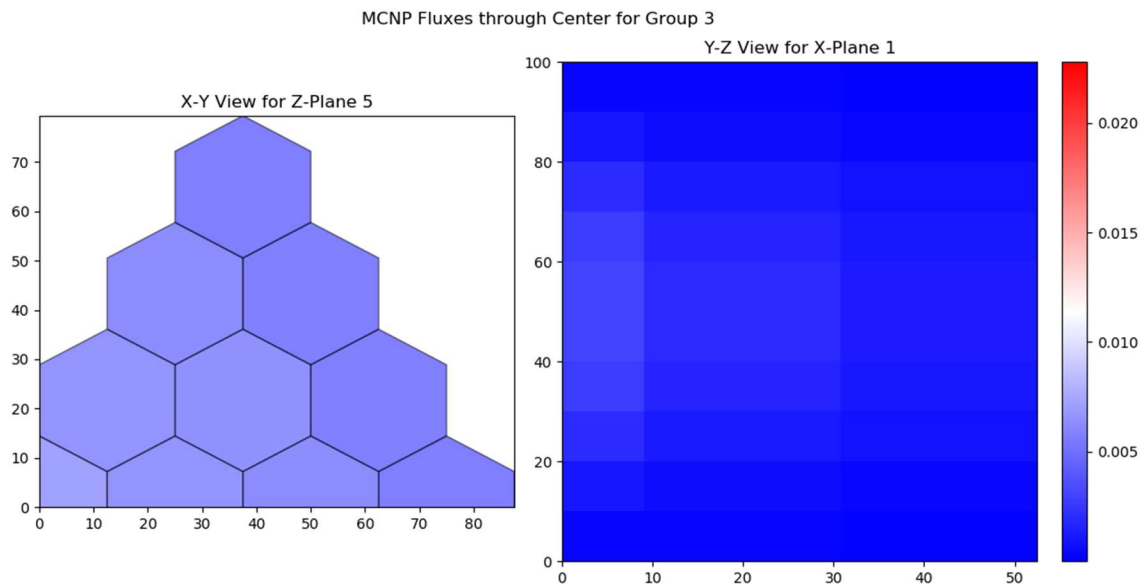


**Figure 131. Hexagonal-Z MG Eigenvalue MCNP Reference Flux in Group 3**

### 3.4.3.3 DIF3D Results

The transport solver within DIF3D, DIF3D-VARIANT, was used to solve the same reactor and multigroup cross sections that was analyzed by MCNP. Since, as previously stated, an exact analytical match cannot be expected, this verification will focus on ensuring that the DIF3D solution is converging to the MCNP reference solution as the spatial and angular orders are increased. This analysis will not consider additional mesh refinement in DIF3D is not as impactful as increasing the polynomial order first. The metrics used to evaluate the accuracy of the DIF3D solution include the eigenvalue accuracy, value and location of the maximum region-averaged fluxes for each group, and the root-mean-squared-error of the group- and region-wise fluxes.

All of the cases used an eigenvalue convergence criterion of  $10^{-8}$ , a pointwise fission source convergence of  $10^{-7}$ , average fission source convergence of  $10^{-8}$ , 80 XY-plane partial current sweeps per group per outer iteration, and 80 axial partial current sweeps per outer iteration. All other iteration parameters were left at the DIF3D defaults.

Table 148 provides the DIF3D-VARIANT computed eigenvalue errors for this model as a function of both the spatial (columns) and angular approximations (rows). In these tables, '-' denotes that the case was not possible due to limitations in the amount of memory that the tested version of DIF3D can allocate to solve a model.

**Table 148. Hexagonal-Z MG DIF3D Eigenvalue Errors in units of pcm**

<b>Flux</b>	<b>6<sup>th</sup></b>	<b>7<sup>th</sup></b>	<b>8<sup>th</sup></b>	<b>8<sup>th</sup></b>	<b>10<sup>th</sup></b>	<b>12<sup>th</sup></b>	<b>10<sup>th</sup></b>	<b>10<sup>th</sup></b>
<b>Leakage</b>	<b>1<sup>st</sup></b>	<b>2<sup>nd</sup></b>	<b>3<sup>rd</sup></b>	<b>3<sup>rd</sup></b>	<b>3<sup>rd</sup></b>	<b>3<sup>rd</sup></b>	<b>4<sup>th</sup></b>	<b>5<sup>th</sup></b>
<b>Source</b>	<b>4<sup>th</sup></b>	<b>7<sup>th</sup></b>	<b>8<sup>th</sup></b>	<b>5<sup>th</sup></b>	<b>5<sup>th</sup></b>	<b>5<sup>th</sup></b>	<b>5<sup>th</sup></b>	<b>5<sup>th</sup></b>
<b>P<sub>1</sub></b>	-143	-163	-165	-160	-161	-162	-161	-161
<b>P<sub>3</sub></b>	57	3	-7	-4	-5	-6	-7	-7
<b>P<sub>5</sub></b>	74	12	-1	2	2	1	0	-1
<b>P<sub>7</sub></b>	78	13	1	3	3	3	1	1
<b>P<sub>9</sub></b>	79	14	1	3	4	-	-	-
<b>P<sub>11</sub></b>	80	14	-	-	-	-	-	-
<b>P<sub>13</sub></b>	80	14	-	-	-	-	-	-
<b>P<sub>15</sub></b>	80	-	-	-	-	-	-	-

In the table, the spatial source approximation is truncated for two reasons: 1) it is generally not as important as the flux or leakage approximations and 2) it is done to reduce the memory requirements of high order space-angle approximations. This can be observed when comparing the 8-3-8 (Flux-Leakage-Source) column's errors to the 8-3-5 column's errors where the reduction in the source's polynomial order by three orders impacted the eigenvalue by only a few pcm.

The spatial flux convergence can be observed by comparing the 8-3-5 (flux-leakage-source), 10-3-5, and 12-3-5 results in Table 148. Here, the only change is the order of the spatial flux polynomials used and there is only a net 1 pcm change between each spatial flux order. Similarly, the spatial leakage convergence is only changing the eigenvalue by 2 pcm between 10-3-5 and 10-4-5. The angular refinement is the last component to consider and one can observe that the eigenvalue errors have converged around 7<sup>th</sup> order.

February 13, 2020

---

Table 149 provides the difference in the maximum region-averaged group-wise flux between the DIF3D solutions and the MCNP reference for group 1. The group 2 and 3 data were also inspected, however they are not shown as one would draw the same conclusions from the data for those groups. The locations of the peak were verified to be in the same position as the MCNP reference for each case. The same general trends as discussed in the eigenvalue with the spatial orders are observed, however the peak flux errors increase slightly as the angular order increases slightly as the angular order increases past 3.

February 13, 2020

Table 149. Hexagonal-Z MG DIF3D Peak Flux Errors in units of percent

Flux	6 <sup>th</sup>	7 <sup>th</sup>	8 <sup>th</sup>	8 <sup>th</sup>	10 <sup>th</sup>	12 <sup>th</sup>	10 <sup>th</sup>	10 <sup>th</sup>
Leakage	1 <sup>st</sup>	2 <sup>nd</sup>	3 <sup>rd</sup>	3 <sup>rd</sup>	3 <sup>rd</sup>	3 <sup>rd</sup>	4 <sup>th</sup>	5 <sup>th</sup>
Source	4 <sup>th</sup>	7 <sup>th</sup>	8 <sup>th</sup>	5 <sup>th</sup>	5 <sup>th</sup>	5 <sup>th</sup>	5 <sup>th</sup>	5 <sup>th</sup>
<b>Group 1</b>								
P <sub>1</sub>	-0.84	-1.34	-1.39	-1.18	-1.28	-1.32	-1.27	-1.27
P <sub>3</sub>	1.21	0.30	0.08	0.28	0.18	0.13	0.13	0.13
P <sub>5</sub>	1.52	0.49	0.25	0.44	0.36	0.31	0.29	0.29
P <sub>7</sub>	1.58	0.53	0.28	0.47	0.41	0.36	0.33	0.33
P <sub>9</sub>	1.60	0.54	0.29	0.48	0.43	-	-	-
P <sub>11</sub>	1.60	0.55	-	-	-	-	-	-
P <sub>13</sub>	1.60	0.55	-	-	-	-	-	-
P <sub>15</sub>	1.60	-	-	-	-	-	-	-
<b>Group 2</b>								
P <sub>1</sub>	-0.85	-1.32	-1.39	-1.19	-1.30	-1.34	-1.29	-1.29
P <sub>3</sub>	1.21	0.33	0.09	0.28	0.17	0.11	0.12	0.13
P <sub>5</sub>	1.53	0.52	0.27	0.44	0.35	0.29	0.29	0.29
P <sub>7</sub>	1.59	0.56	0.30	0.47	0.40	0.34	0.32	0.32
P <sub>9</sub>	1.61	0.58	0.31	0.48	0.41	-	-	-
P <sub>11</sub>	1.61	0.58	-	-	-	-	-	-
P <sub>13</sub>	1.61	0.58	-	-	-	-	-	-
P <sub>15</sub>	1.61	-	-	-	-	-	-	-
<b>Group 3</b>								
P <sub>1</sub>	-0.71	-1.21	-1.33	-1.12	-1.26	-1.32	-1.26	-1.25
P <sub>3</sub>	1.34	0.44	0.15	0.36	0.21	0.14	0.16	0.17
P <sub>5</sub>	1.66	0.64	0.32	0.52	0.39	0.32	0.33	0.33
P <sub>7</sub>	1.72	0.68	0.36	0.55	0.44	0.37	0.37	0.36
P <sub>9</sub>	1.74	0.69	0.37	0.56	0.46	-	-	-
P <sub>11</sub>	1.74	0.70	-	-	-	-	-	-
P <sub>13</sub>	1.75	0.70	-	-	-	-	-	-
P <sub>15</sub>	1.75	-	-	-	-	-	-	-

Table 150 provides the root-mean-squared error (RMS) of the DIF3D and MCNP region-averaged group-wise fluxes for the first group; groups 2 and 3 are also not included as the conclusions are the same. The same general trends as seen thus far are again present; increasing the spatial order generally improves the RMS. Increasing angular order does increase the RMS at orders greater than P<sub>5</sub>, however the error grows slowly as the angular order is increased further. These differences are inconsequentially small and, since the error growth is on the order of the fission source and eigenvalue convergence criteria ( $10^{-7}$  and  $10^{-8}$ , respectively), no further investigation was performed.

Table 150. Hexagonal-Z MG DIF3D Flux Root-Mean-Squared-Errors

Flux	6 <sup>th</sup>	7 <sup>th</sup>	8 <sup>th</sup>	8 <sup>th</sup>	10 <sup>th</sup>	12 <sup>th</sup>	10 <sup>th</sup>	10 <sup>th</sup>
Leakage	1 <sup>st</sup>	2 <sup>nd</sup>	3 <sup>rd</sup>	3 <sup>rd</sup>	3 <sup>rd</sup>	3 <sup>rd</sup>	4 <sup>th</sup>	5 <sup>th</sup>
Source	4 <sup>th</sup>	7 <sup>th</sup>	8 <sup>th</sup>	5 <sup>th</sup>	5 <sup>th</sup>	5 <sup>th</sup>	5 <sup>th</sup>	5 <sup>th</sup>
<b>Group 1</b>								
P <sub>1</sub>	1.13E-04	1.37E-04	1.39E-04	1.32E-04	1.35E-04	1.37E-04	1.35E-04	1.35E-04
P <sub>3</sub>	7.55E-05	1.55E-05	8.64E-06	1.28E-05	1.01E-05	9.25E-06	9.55E-06	9.75E-06
P <sub>5</sub>	9.57E-05	2.44E-05	9.41E-06	1.74E-05	1.42E-05	1.20E-05	1.10E-05	1.08E-05
P <sub>7</sub>	1.00E-04	2.66E-05	1.07E-05	1.86E-05	1.63E-05	1.43E-05	1.23E-05	1.19E-05
P <sub>9</sub>	1.01E-04	2.73E-05	1.10E-05	1.89E-05	1.71E-05	-	-	-
P <sub>11</sub>	1.02E-04	2.75E-05	-	-	-	-	-	-
P <sub>13</sub>	1.02E-04	2.76E-05	-	-	-	-	-	-
P <sub>15</sub>	1.02E-04	-	-	-	-	-	-	-
<b>Group 2</b>								
P <sub>1</sub>	9.00E-05	1.10E-04	1.13E-04	1.06E-04	1.08E-04	1.10E-04	1.08E-04	1.08E-04
P <sub>3</sub>	6.44E-05	1.40E-05	5.19E-06	1.01E-05	6.65E-06	5.43E-06	5.70E-06	5.84E-06
P <sub>5</sub>	8.07E-05	2.20E-05	8.29E-06	1.50E-05	1.18E-05	9.60E-06	9.10E-06	9.06E-06
P <sub>7</sub>	8.43E-05	2.38E-05	9.53E-06	1.61E-05	1.35E-05	1.16E-05	1.04E-05	1.02E-05
P <sub>9</sub>	8.53E-05	2.44E-05	9.87E-06	1.64E-05	1.41E-05	-	-	-
P <sub>11</sub>	8.56E-05	2.46E-05	-	-	-	-	-	-
P <sub>13</sub>	8.58E-05	2.46E-05	-	-	-	-	-	-
P <sub>15</sub>	8.58E-05	-	-	-	-	-	-	-
<b>Group 3</b>								
P <sub>1</sub>	1.42E-05	1.73E-05	1.77E-05	1.65E-05	1.70E-05	1.72E-05	1.70E-05	1.70E-05
P <sub>3</sub>	1.05E-05	2.70E-06	1.08E-06	2.05E-06	1.29E-06	9.81E-07	1.12E-06	1.14E-06
P <sub>5</sub>	1.30E-05	3.91E-06	1.59E-06	2.79E-06	2.08E-06	1.65E-06	1.67E-06	1.66E-06
P <sub>7</sub>	1.36E-05	4.19E-06	1.77E-06	2.95E-06	2.35E-06	1.95E-06	1.86E-06	1.84E-06
P <sub>9</sub>	1.37E-05	4.27E-06	1.82E-06	2.99E-06	2.45E-06	-	-	-
P <sub>11</sub>	1.38E-05	4.30E-06	-	-	-	-	-	-
P <sub>13</sub>	1.38E-05	4.31E-06	-	-	-	-	-	-
P <sub>15</sub>	1.38E-05	-	-	-	-	-	-	-

With these findings, the 8-3-8 P<sub>9</sub> case is chosen as the reference DIF3D result for the region-wise flux comparisons. These are shown in Figure 132 through Figure 134 for groups 1-3, respectively. Each of these figures provides two plots; the left is the bottom-most plane of the fictitious reactor and the right is the central plane that contains the peak flux for all groups. Within each of these figures is the DIF3D-to-MCNP flux ratios in each region of the plane. The ratio is provided numerically as well as by color where blue indicates the DIF3D result is less than the MCNP, white implying they are close, and red implying the DIF3D result is larger than in MCNP. These results show overall very close agreement for the majority of the central regions. These results show overall very close agreement for the majority of the active core regions. The largest errors are present on the outer ring assemblies in the central plane where they approach 2% error. This location for the peak errors are not unsurprising as the spatial and angular flux gradients will be quite large for these assemblies adjacent to the fissile regions and vacuum boundary.



February 13, 2020

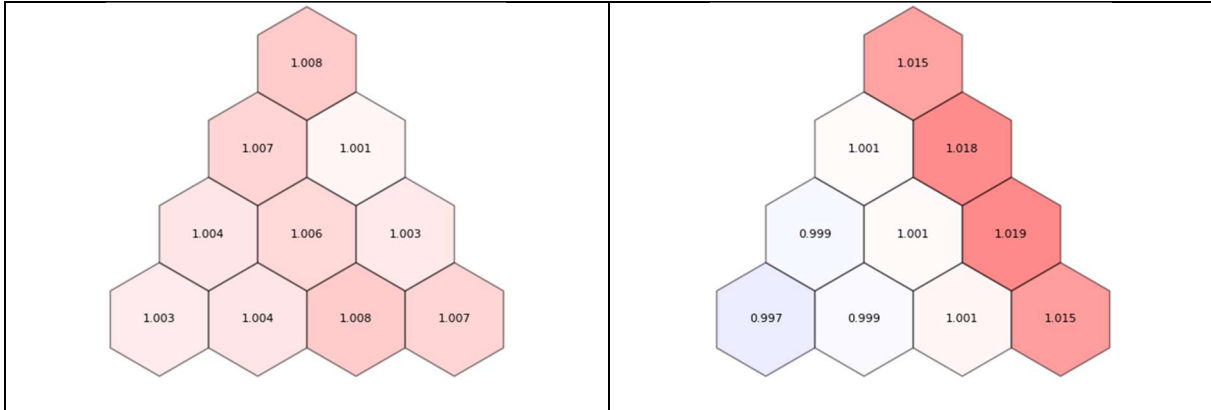


Figure 132. Hexagonal-Z MG DIF3D to MCNP Flux Ratios in Group 1

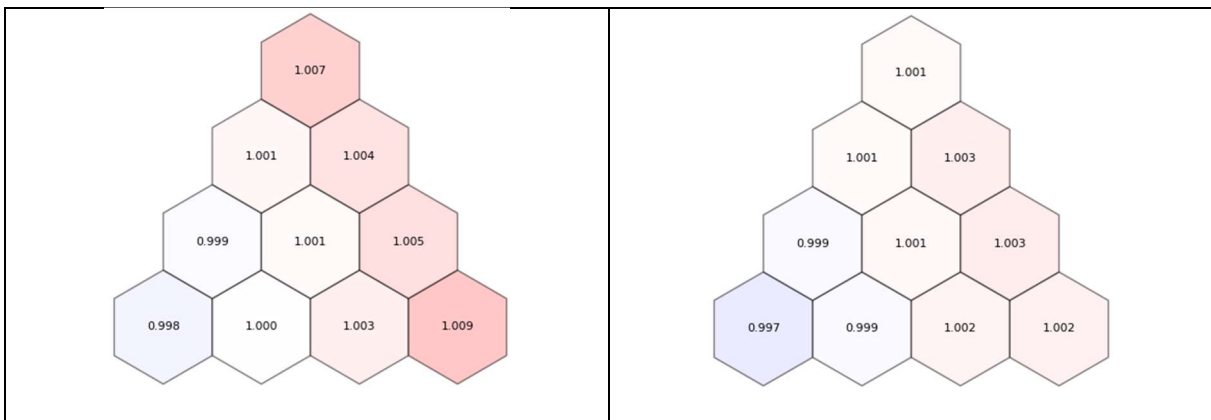


Figure 133. Hexagonal-Z MG DIF3D to MCNP Flux Ratios in Group 2

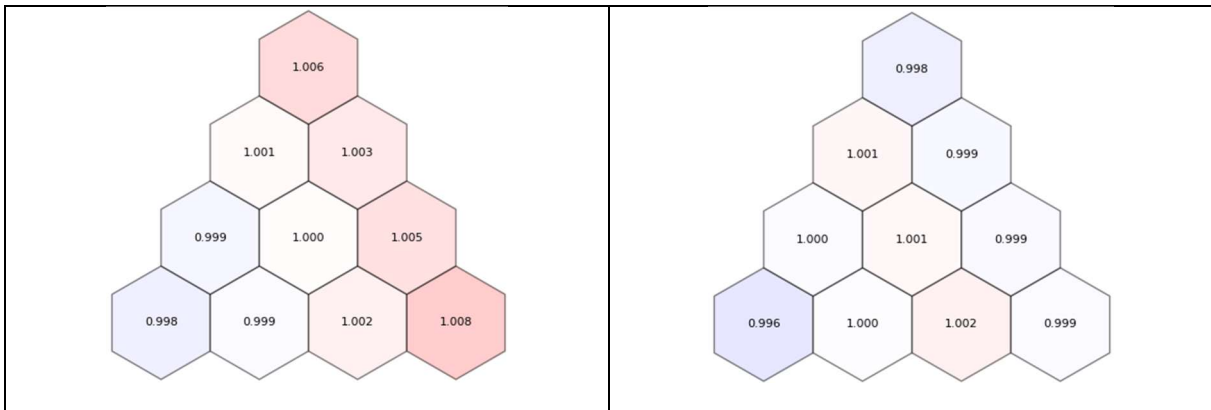


Figure 134. Hexagonal-Z MG DIF3D to MCNP Flux Ratios in Group 3

#### 3.4.3.4 Verification of Important Anisotropic Scattering

As discussed in [6], to utilize this anisotropic scattering case as verification that anisotropic scattering is working, it must be verified that a different and sensible result is obtained when isotropic scattering (with the same data) compared to the anisotropic result. In this case, the 7-2-7 P<sub>7</sub> case was re-ran with isotropic scattering via option 9 of the Type 12 card in the A.DIF3D input block. This case was chosen as it is reasonably converged but significantly

February 13, 2020

faster running than the 8-3-8  $P_9$  case used above. Similarly, DIF3D was set to utilize the total cross section instead of the transport cross section. Thus the problem is truly isotropic in nature.

As a reminder, the cross sections from this case were such that the  $P_1/P_0$  moment ratio for REG1 is 0.25, for REG2 it is 0.23, and REG3 is 0.05. Each of these are forward-scattering since the  $P_1/P_0$  moment ratios are positive; further REG3 is significantly closer to isotropic than REG1 and REG2. Since REG1 and REG2 are located within the first three rings, it is expected that applying isotropic scattering will result in less neutrons reaching the REG3 “reflector” and more staying in the REG1 and REG2 “active core”. This should also result in a higher eigenvalue as the leakage would be reduced.

The 7-2-7  $P_7$  linearly anisotropic eigenvalue was 1.59245 while the isotropic eigenvalue was 1.59555, indicating that the isotropic case had a 310 pcm eigenvalue bias compared to anisotropic. This confirms the initial reasoned change discussed above.

Figure 135 through Figure 137 provide plots similar to Figure 132 through Figure 134 except the ratio in this case is the isotropic flux compared to the anisotropic flux in each of the three groups. As discussed above, the “reflector” region should have lower flux than in-core. Since the reflector region is the outer ring and the bottom plane these Figure 135 through Figure 137 ratios confirm the initial suspicions, indicating that the DIF3D solver is in fact applying anisotropic scattering when it should be.

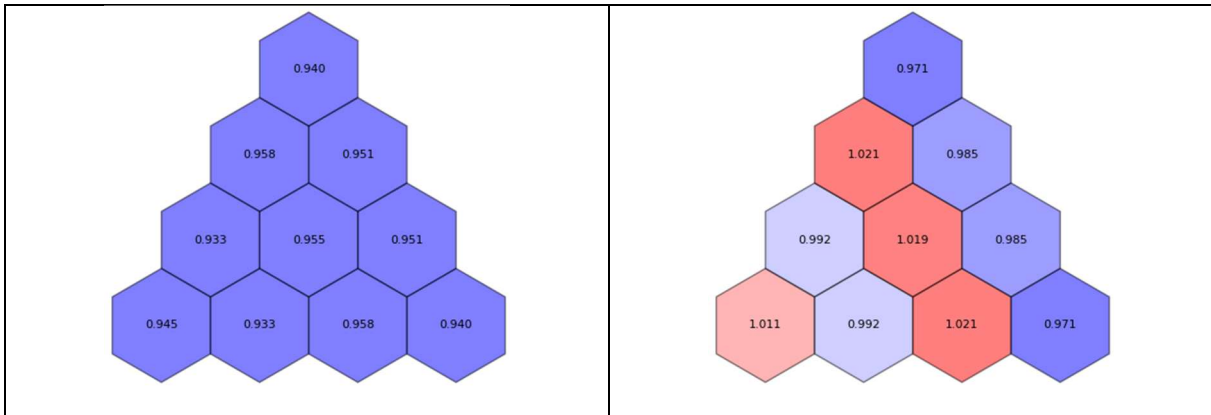


Figure 135. Hexagonal-Z MG Isotropic to Anisotropic DIF3D Flux Ratios in Group 1

February 13, 2020

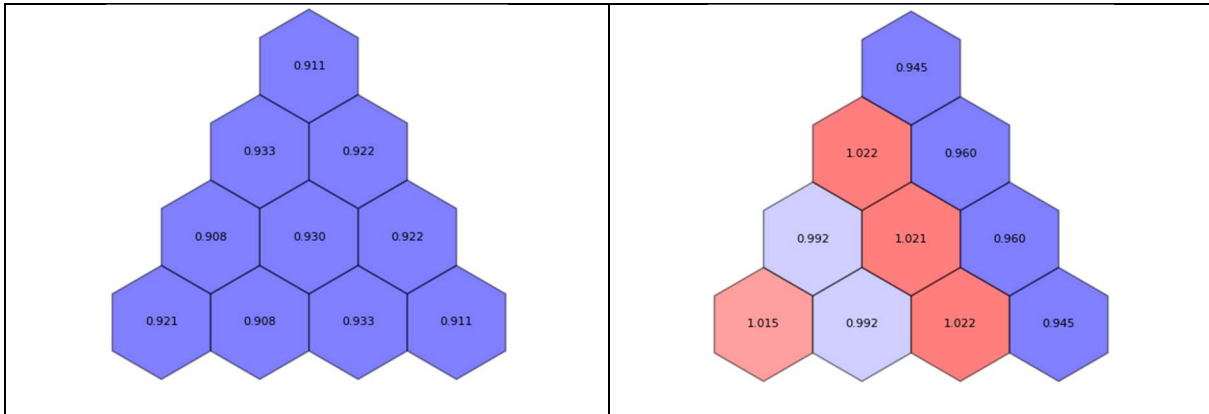


Figure 136. Hexagonal-Z MG Isotropic to Anisotropic DIF3D Flux Ratios in Group 2

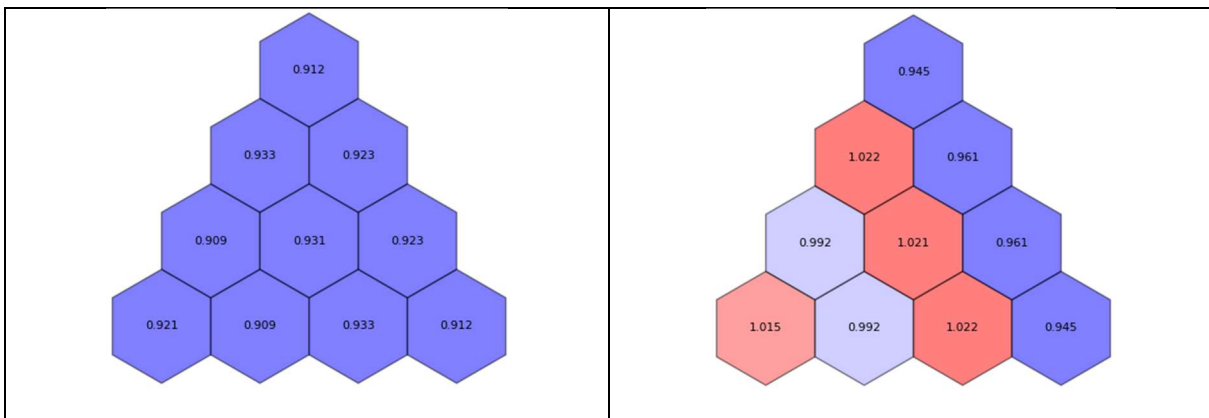


Figure 137. Hexagonal-Z MG Isotropic to Anisotropic DIF3D Flux Ratios in Group 3

### 3.4.3.5 Verification of Angular Approximation with the Yang Trial Functions

The Integral Verification problem for Cartesian neutron transport verified the correctness of the Yang trial functions by comparing the eigenvalue errors (compared to MCNP) using both the standard and Yang trial functions. In that section, the Yang trial functions were used for the final results used for a more thorough comparison to the MCNP reference due to their better convergence properties for that particular model, with the presence of low density material regions. The evaluation of the hexagonal transport model in this section used the standard trial functions were used as no abnormal convergence behavior was present. This subsection will compare the eigenvalue errors computed with the Yang trial functions to those computed with the standard trial functions above to show that these Yang functions are implemented consistently with the standard functions and are thus similarly verified. This will be done for this model vice the integral hexagonal model of Section 3.4.7 as this model is significantly smaller and less computationally expensive.

This was specifically performed by simply re-running all the cases presented in Table 148 but this time with the Yang trial functions. The resultant eigenvalue errors (again, compared to the MCNP reference) were the exact same as in Table 148 and therefore both trial function classes provide the same accuracy for this model.

**Table 151. Hexagonal-Z MG DIF3D Eigenvalue Errors in units of pcm**

<b>Flux</b>	<b>6<sup>th</sup></b>	<b>7<sup>th</sup></b>	<b>8<sup>th</sup></b>	<b>8<sup>th</sup></b>	<b>10<sup>th</sup></b>	<b>12<sup>th</sup></b>	<b>10<sup>th</sup></b>	<b>10<sup>th</sup></b>
<b>Leakage</b>	<b>1<sup>st</sup></b>	<b>2<sup>nd</sup></b>	<b>3<sup>rd</sup></b>	<b>3<sup>rd</sup></b>	<b>3<sup>rd</sup></b>	<b>3<sup>rd</sup></b>	<b>4<sup>th</sup></b>	<b>5<sup>th</sup></b>
<b>Source</b>	<b>4<sup>th</sup></b>	<b>7<sup>th</sup></b>	<b>8<sup>th</sup></b>	<b>5<sup>th</sup></b>	<b>5<sup>th</sup></b>	<b>5<sup>th</sup></b>	<b>5<sup>th</sup></b>	<b>5<sup>th</sup></b>
<b>P<sub>1</sub></b>	-143	-163	-165	-160	-161	-162	-161	-161
<b>P<sub>3</sub></b>	57	3	-7	-4	-5	-6	-7	-7
<b>P<sub>5</sub></b>	74	12	-1	2	2	1	0	-1
<b>P<sub>7</sub></b>	78	13	1	3	3	3	1	1
<b>P<sub>9</sub></b>	79	14	1	3	4	-	-	-
<b>P<sub>11</sub></b>	80	14	-	-	-	-	-	-
<b>P<sub>13</sub></b>	80	14	-	-	-	-	-	-
<b>P<sub>15</sub></b>	80	-	-	-	-	-	-	-

#### 3.4.4 Radial Periodic Boundary Conditions Verification

To verify DIF3D's ability to apply periodic boundary conditions in the radial plane, a simple Hexagonal-Z model was created comprising of two unique regions. This model was represented in a full-core DIF3D model as well as an equivalent periodic model and the results compared. This was repeated for both sixth-core and third-core symmetric models.

Figure 138 provides the A.NIP3 blocks (top) and resultant DIF3D core map (bottom) for the sixth-core symmetric models; the full-core model is on the left and the periodic model is on the right. This particular core laydown was chosen amongst others for its simplicity but also because it could not be represented with a reflective boundary condition. The bias in the full-core and periodic models was 0.4 pcm. The fluxes matched, when accounting for the factor of six increase in the area-normalized flux, to the 4<sup>th</sup> significant digit.

Similarly, Figure 139 provides the A.NIP3 blocks (top) and resultant DIF3D core map (bottom) for the third-core symmetric models. Again, this particular core laydown was chosen amongst others for its simplicity but also because it could not be represented with a reflective boundary condition. The bias in the full-core and periodic models was 3 pcm. The fluxes matched, when accounting for the factor of three increase in the area-normalized flux, to the 4<sup>th</sup> significant digit.

February 13, 2020

<p>UNFORM=A.NIP3  01 FULL_CORE  02 0 3 40000000 40000000 40000000 40000000 0 3 3 3  03 120  04 9 9 9 9 10 10  09 Z 2 50.  29 10. 4  30 REG1 1 1 1 0. 50.  30 REG1 2 1 6 0. 50.  30 REG1 3 1 12 0. 50.  30 REG1 4 1 18 0. 50.  30 REG3 4 2 2 0. 50.  30 REG3 4 5 5 0. 50.  30 REG3 4 8 8 0. 50.  30 REG3 4 11 11 0. 50.  30 REG3 4 14 14 0. 50.  30 REG3 4 17 17 0. 50.  14 COMP1 ISO1 1.0  15 COMP1 REG1  14 COMP3 ISO3 1.0  15 COMP3 REG3</p>	<p>UNFORM=A.NIP3  01 PERIODIC  02 0 3 40000000 40000000 40000000 40000000 0 3 3 3  03 124  04 7 9 9 9 10 10  09 Z 2 50.  29 10. 4  30 REG1 1 1 1 0. 50.  30 REG1 2 1 6 0. 50.  30 REG1 3 1 12 0. 50.  30 REG1 4 1 18 0. 50.  30 REG3 4 2 2 0. 50.  30 REG3 4 5 5 0. 50.  30 REG3 4 8 8 0. 50.  30 REG3 4 11 11 0. 50.  30 REG3 4 14 14 0. 50.  30 REG3 4 17 17 0. 50.  14 COMP1 ISO1 1.0  15 COMP1 REG1  14 COMP3 ISO3 1.0  15 COMP3 REG3</p>
<pre> 0      1      2      3      4      5      6      7 ***** 7 * 0      0      0 * 1      1 * 2 * 1 * 7 *      ***** 6 * 0      0 * 2 * 1      1      1      1 * 6 *      ***** 5 * 0 * 1      1      1      1      1 * 2 * 5 ***** 4 * 1      1      1      1      1      1 * 1 * 4 ***** 3 * 2 * 1      1      1      1      1 * 0 * 3 ***** 2 * 1      1      1      1 * 2 * 0      0 * 2 *      ***** 1 * 1 * 2 * 1      1 * 0      0      0 * 1 ***** 1      2      3      4      5      6      7 </pre>	<pre> 0      1      2      3      4 ***** 4 * 1 * 0      0      0 * 4 *      ***** 3 * 1      1 * 0      0 * 3 *      ***** 2 * 1      1 * 2 * 0 * 2 *      ***** 1 * 1      1      1      1 * 1 ***** 1      2      3      4 </pre>

Figure 138. Sixth-Core Periodic Hexagonal-Z Input and Core Map

<p>UNFORM=A.NIP3  01 FULL_CORE  02 0 3 40000000 40000000 40000000 40000000 0 3 3 3  03 120  04 9 9 9 9 10 10  09 Z 2 50.  29 10. 4  30 REG1 1 1 1 0. 50.  30 REG1 2 1 6 0. 50.  30 REG1 3 1 12 0. 50.  30 REG1 4 1 18 0. 50.  30 REG3 4 5 5 0. 50.  30 REG3 4 11 11 0. 50.  30 REG3 4 17 17 0. 50.  14 COMP1 ISO1 1.0  15 COMP1 REG1  14 COMP3 ISO3 1.0  15 COMP3 REG3</p>	<p>UNFORM=A.NIP3  01 PERIODIC  02 0 3 40000000 40000000 40000000 40000000 0 3 3 3  03 126  04 7 9 9 9 10 10  09 Z 2 50.  29 10. 4  30 REG1 1 1 1 0. 50.  30 REG1 2 1 6 0. 50.  30 REG1 3 1 12 0. 50.  30 REG1 4 1 18 0. 50.  30 REG3 4 5 5 0. 50.  30 REG3 4 11 11 0. 50.  30 REG3 4 17 17 0. 50.  14 COMP1 ISO1 1.0  15 COMP1 REG1  14 COMP3 ISO3 1.0  15 COMP3 REG3</p>
<pre> 0      1      2      3      4      5      6      7 ***** 7 * 0      0      0 * 1      1 * 2 * 1 * 7 *      ***** 6 * 0      0 * 1      1      1      1      1 * 6 *      ***** 5 * 0 * 1      1      1      1      1      1 * 5 ***** 4 * 1      1      1      1      1      1 * 1 * 4 ***** 3 * 2 * 1      1      1      1      1 * 0 * 3 ***** 2 * 1      1      1      1 * 2 * 0      0 * 2 *      ***** 1 * 1      1      1      1 * 0      0      0 * 1 ***** 1      2      3      4      5      6      7 </pre>	<pre> 0      1      2      3      4 ***** 4 * 1      1 * 2 * 1 * 4 *      ***** 3 * 1      1      1      1 * 3 *      ***** 2 * 1      1      1      1 * 2 *      ***** 1 * 1      1      1      1 * 1 ***** 1      2      3      4 </pre>

Figure 139. Third-Core Periodic Hexagonal-Z Input and Core Map

### 3.4.5 Iteration and Convergence Control Verification

Table 9 of the reference [6] plan identified that the iteration and convergence control options (A.DIF3D Type 3.4, 3.6, 3.9, 3.10, 3.11, 3.12, 5.2, 5.3, 5.4, 12.5, 12.6, and 12.11) would be verified by way of the Integral Verification case. These options will be verified in this section, however, the multigroup eigenvalue problem discussed in Section 3.4.3 will be used instead. This was done for no other reason than that problem is smaller than the integral benchmark problem and thus runs faster, but also converges slowly enough (more than 100 iterations are required) that the effect of these options will be readily apparent. Note that this is only performed for a forward eigenvalue case and not repeated for a fixed source or adjoint case as the same convergence control code is exercised for any of these solves. Specifically, this case will utilize the 040601 spatial and 10303 ( $P_3$ ) angular approximation options with  $P_1$  scattering and the total cross section used.

Specifically, this will be performed by first running a base case that leaves all relevant parameters to their internal defaults. Then, a case will be performed where the defaults are explicitly specified in their respective cards. Next, using the explicitly listed defaults as the starting point, the options verified by this section will be modified from their default to the possible values. The possible values will either be every value in the discrete set, or if the variable can be continuous (like the number of iterations) then a sufficient number will be evaluated. The specific parameters, their defaults, and their perturbations are provided in Table 152. After executing all these cases, the output will be analyzed to ensure that DIF3D respected the option according to the description provided in the A.DIF3D listing. The restart capability will then be checked with two additional cases discussed in the final subsection.

**Table 152. Iteration Control Options for Hexagonal Transport**

Card Type	Summary	Default Value	Perturbed Values
3.4	Tchebyshev Acceleration	0	1
3.6	Outer Iteration Control	30	-4, -3, -2, -1, 10
3.9	Upscatter Iterations per Outer Iteration	5	20
3.10	Concurrent Iteration Efficiency	0	1
3.11	Accel. Of Opt. Overrelaxation	0	1
3.12	Opt. Overrelaxation Factor Calculation Control	50	2
5.2	Eigenvalue Criterion	$10^{-7}$	$10^{-3}$
5.3	Pointwise Fiss. Source Criterion	$10^{-5}$	$10^{-4}$
5.4	Avg. Fiss. Source Criterion	$10^{-5}$	$10^{-4}$
12.5	Num. of X-Y Plane Partial Current Sweeps	0	200
12.6	Num. of Axial Partial Current Sweeps	0	20
12.11	Omega Transformation Acceleration	0	1

#### 3.4.5.1 Base and Default Cases

As noted, the first step performed was to first execute a case where all of the above values were simply not included in the input, and thereby DIF3D applied the default value. Then, a case was executed with these values explicitly stated. The outputs were compared using a python Diff tool, and it was found that the outputs indeed matched, except for the input edits and some slight

February 13, 2020

---

changes to a few of the iteration times, which are subject to external factors and cannot be controlled. Therefore the default case will be used as the starting point going forward.

While not a part of this verification effort, it was noted that the A.DIF3D listing states that the Type 03 card's 5<sup>th</sup> parameter (minimum plane-block size for input/output transfer) has a default of 4500, however this was found to actually be 10,000.

All cases that remain will compare to this default case, but modified to utilize 2,000 iterations to convergence so that the total number of iterations to convergence can be observed as these options change.

#### 3.4.5.2 Card 3 Option 4 Perturbations

Card 3 Option 4 sets whether or not Tchebyshev acceleration of the outer iterations is performed. The default value, 0, indicates it shall be performed, while a value of 1 turns off this acceleration. Therefore, when the value of 1 is used, one should expect that either more iterations will be required to converge. Additionally, DIF3D's echo repeat should acknowledge the setting of this option.

The correct echo repeat was confirmed. Additionally, the case with the acceleration was found to converge in 131 iterations while the case without the acceleration required 227 iterations. The eigenvalue and flux values matched the default cases to within 0.3 pcm and 0.03%, respectively.

#### 3.4.5.3 Card 3 Option 6 Perturbations

Card 3 Option 6 controls the number of outer iterations in a case. The possible values are -1 (data management parameters, overrelaxation factors, and neutronics edits are performed), -2 (same as -1 without overrelaxation factors), -3 (DIF3D module is bypassed), -4 (same as -2, but with leakage results derived from the balance equation with zero residual), or some number greater than 0 that simply sets the maximum number of DIF3D outer iterations. The default value is 30 total iterations. This case will evaluate the 4 negative options as well as ensuring 10 total iterations are obeyed.

Option -4 was verified to skip the DIF3D iteration and skip the inner iteration optimization strategy edits as well as the outer iteration summary (i.e., DIF3D did not solve the diffusion equation). However, this option did not use the residual neutron balance to derive the leakage results; instead these leakage terms were the same as in the base case, including the non-zero residual.

Option -3 was verified to not execute the DIF3D module, instead only processing the geometry and zone information from the A.NIP3 and A.HMG4C blocks.

Option -2 produced the same output as option -4 except for the balance edits, which were the same in Option -2 as the base case.

Option -1 computed the acceleration factors, performed one iteration, and edited the results.

Finally, a value of +10 performed exactly as expected, yielding 10 total iterations before quitting.

#### 3.4.5.4 Card 03 Option 9 Perturbations

Card 03 Option 9 sets the number of upscatter iterations per outer iteration. The default is 5. This case will verify that 20 is also obeyed. This can be verified in the input echo, by observing the “Ups” column of the DIF3D iteration history, and in the total time for each outer iteration where the iteration time should increase by a factor of 4. It should be noted that the 20 requested iterations was changed by DIF3D to an odd number, with a corresponding warning to alert the user. Note that this behavior was not stated in the A.DIF3D listing. Factoring in the 21 iterations, the correct number of upscatter iterations was observed. The time per iteration did increase, but as it increased from ‘0.0’ to ‘0.1’, we do not have enough information to decipher the actual impact. The eigenvalue for this case matched to all reported digits and fluxes matched with an RMS error on the order of  $10^{-9}$ , indicating that the default number of upscatter iterations was sufficient.

#### 3.4.5.5 Card 03 Option 10 Perturbations

Card 03 Option 10 sets a flag that instructs DIF3D to either perform the estimated number of inner iterations for each group (option 0), or to avoid the last pass of the inner iterations in groups whose number of iterations are less than some non-user-facing threshold. The default value is not specified by the A.DIF3D listing. This parameter has no effect on DIF3D-VARIANT. This was verified to be true. Card 3 Option 11 Perturbations

#### 3.4.5.6 Card 3 Option 11 Perturbations

Card 03 Option 11 sets a flag that instructs DIF3D to either not perform acceleration of the optimum over-relaxation factor calculation (option 0, default), or apply asymptotic source extrapolation of the power iterations during the spectral radius calculation (option 1). This parameter has no effect on DIF3D-VARIANT. This was verified to be true. Card 3 Option 12 Perturbations

#### 3.4.5.7 Card 03 Option 12

Card 03 Option 12 sets the number of iterations when determining the optimum over-relaxation factors. A positive integer is supplied and a value of 50 is strongly recommended. In this case a value of 2 was applied instead. This parameter has no effect on DIF3D-VARIANT. This was verified to be true. Card 5 Option 2 Perturbations

#### 3.4.5.8 Card 05 Option 2

Card 05 Option 2 provides the floating point eigenvalue convergence criterion. The default is a value of  $10^{-7}$ . This case will apply a value of  $10^{-4}$ . To ensure the eigenvalue convergence is limiting, the pointwise and average fission source convergence tolerances were set to 0.01. Therefore we should expect that increasing the eigenvalue convergence (compared to the base case) should reduce the total number of iterations such that the fission source convergence is limiting.



February 13, 2020

---

This was indeed observed, as the case with a  $10^{-4}$  eigenvalue convergence criterion converged in 39 iterations instead of the base case's 131 iterations. Further, this was achieved when the eigenvalue dropped below  $10^{-4}$ ; the fission source measures had already passed 0.01.

#### 3.4.5.9 Card 05 Option 3 Perturbations

Card 05 Option 3 provides the floating point pointwise fission source convergence criterion. The default is a value of  $10^{-5}$ . This perturbation case will apply a value of  $10^{-4}$ . Like the previous case, the other convergence parameters were set so the pointwise fission source convergence criterion was limiting. Specifically, this means that the eigenvalue and average fission source criterion were 0.01 while the pointwise fission source criterion was  $10^{-4}$ . In this case, the iterations should complete when the fission source criterion is met.

This was indeed observed, as the case with a  $10^{-4}$  pointwise fission source convergence criterion converged in 67 iterations instead of the base case's 131 iterations. Further, this convergence was achieved when the pointwise fission source was converged to less than  $10^{-4}$ , the provided value.

#### 3.4.5.10 Card 05 Option 4 Perturbations

Card 05 Option 4 provides the floating point average fission source convergence criterion. The default is a value of  $10^{-5}$ . This perturbation case will apply a value of  $10^{-4}$ . Since the default case reaches the eigenvalue convergence after the fission source is converged to the stated value, then the parameters were also set that the average fission source convergence criterion was limiting. Specifically, this means that the eigenvalue and pointwise fission source criterion were 0.01 while the average fission source criterion was  $10^{-4}$ . In this case, we should see the iterations end when the fission source criterion is met.

This was indeed observed, as the case with a  $10^{-4}$  average fission source convergence criterion converged in 61 iterations instead of the base case's 131 iterations. Further, this convergence was achieved when the rel. sum error of the fission source was converged to less than  $10^{-4}$ , the provided value.

#### 3.4.5.11 Card 12 Option 5 Perturbations

Card 12 Option 5 sets the number of XY-Plane partial current sweeps per group, per outer iteration. Positive integers are accepted; the default is 0, meaning the code will decide. In the base case, the code decided to use 2 radial inner iterations for each group. Therefore the perturbed case will increase this by a factor of 1000, to 2000 radial inner iterations per group. This should be observable by the edit stating this value, as well as seeing the increase in time per outer iteration. The value of 2000 was chosen so that the runtime impact was noticeable. This runtime impact was observed to some extent as the time per iteration increased from 0.0 seconds to 0.2 seconds. The statement of the number of inners had too many digits for printing, and thus only asterisks were displayed. The eigenvalues matched to all reported values and the fluxes differed with an RMS on the order of  $10^{-12}$ .

#### 3.4.5.12 Card 12 Option 6 Perturbations

Card 12 Option 6 sets the number of axial partial current sweeps per group, per outer iteration. Positive integers are accepted; the default is 0, meaning the code will decide. In the base case, the code decided to use 2 axial inner iterations for each group. Therefore the perturbed case will increase this by a factor of 10, to 20 axial inner iterations per group. This should be observable by the edit stating this value, as well as seeing the increase in time per outer iteration. This runtime impact was indeed observed as the time per iteration increased from 0.0 seconds to 0.1 seconds. The eigenvalues matched to all reported values and the fluxes differed with an RMS on the order of  $10^{-8}$ .

#### 3.4.5.13 Card 12 Option 11 Perturbations

Card 12 Option 1 sets a flag denoting if the omega transformation acceleration option is applied (option 0, default) or not (option 1). If used, then the number of inner iterations per group, as decided by the code, should be “significantly reduced”. Since the number of inners per group is already 2 for each group, it is unlikely that this option will have any effect. It was applied and it was found to not change the number of axial inner sweeps, however the omega and gamma parameters printed before the iteration histories were modified with omega having values of 0 for each group and gamma having values of 1 for each group. Some of the last significant digits in the fission and eigenvalue errors were changed, indicating that the convergence is affected by this parameter. The eigenvalues matched to all reported values and the fluxes differed with an RMS on the order of  $10^{-10}$ . This omega acceleration is known to yield inconsistent results compared to the solution without omega acceleration as documented in Section 7.5 of [4]. Therefore no further work is necessary.

#### 3.4.5.14 Restart Calculation

A restart computation can be performed with three approaches in DIF3D: (1) the binary DIF3D and NHFLUX files from the previous computation are provided via the “BLOCK=OLD” input block; (2) a restart is performed with the NHFLUX (or NHFLUX if DIF3D-VARIANT) file and a combination of A.DIF3D Type 06 and possibly 07 cards; or (3) DIF3D is executed and then restarted with tighter convergence criterion (or number of iterations) from within the same input. This sub-section will test these approaches using a restart from the default case that terminated itself after 30 iterations.

The first approach was performed with the BLOCK=OLD NHFLUX and DIF3D files, and a single card in the A.DIF3D input that set the maximum number of iterations to 2,000 instead of the 30 of the previous computation (and thus in the DIF3D binary file). After running this in DIF3D, it is expected that (1) DIF3D’s user input specifications echo would the changes to the number of iterations, state that this is a restart, and include the  $k_{\text{eff}}$  from the restart NHFLUX file (2) the initial  $k_{\text{eff}}$  from the 1<sup>st</sup> iteration of the new calculation should differ from the original calculation’s first guess, (3) the outer iterations should continue until the new calculation’s convergence criteria are met, and (4) the final eigenvalue and reported fluxes should match to on the order of the convergence criterion. All of these were observed, indicating the binary file-based restart was successful.

February 13, 2020

---

The second approach was also performed with only the BLOCK=OLD NHFLUX file and the Type 06 card. The A.DIF3D input was modified to include the  $k_{\text{eff}}$  and dominance ratio from the 30 iteration calculation, and the restart flag set to 1 (indicating a restart should be performed). The restart case also had the number of iterations set to 2,000. After running this in DIF3D, it is expected that 1) DIF3D's user input specifications echo would the changes to the number of iterations, state that this is a restart, and include the initial  $k_{\text{eff}}$  2) the initial  $k_{\text{eff}}$  from the 1<sup>st</sup> iteration of the new calculation should differ from the original calculation's first guess, 3) the outer iterations should continue until the new calculation's convergence criteria are met, and (4) the final eigenvalue and reported fluxes should match to on the order of the convergence criterion. All of these were observed, indicating the restart was successful.

The third approach (restarting within same input file) was performed by executing the original DIF3D case to 30 iterations, using the DIF3D and NHFLUX files which were just generated with modifications for an increase number of iterations, and re-executing DIF3D. Similar behavior should be observed with this case compared to the original. This was confirmed, indicating this restart methodology was successful.

Further, these methods output files and convergence histories matched to within the convergence criterion, indicating they effectively perform the same function within DIF3D.

#### 3.4.6 *Solution Edit Verification*

DIF3D prints a balance of the solution results in the form of neutron balance edits, power edits, flux edits, zone-averaged flux edits, and region-averaged flux edits. In addition to these are the writing of the SFEDIT, RZFLUX, and PWDINT interface files. All of these are controlled by options 6 through 11 of the A.DIF3D module's Type 04 card. This section will verify that these options are correctly obeyed. This section will also verify the correctness of the neutron balance tables, as these are the only tables that are not verified elsewhere.

The verification that the edit toggles can be performed with any model. The verification of the correctness of the neutron balances requires a model that utilizes multiple regions, one or more areas, and has cross sections with more than one group. Further, as the individual parameters will be calculated independent from DIF3D, a small model is desirable.

To that end, the four composition cross sections used in the Model Building section of this verification effort (defined in Table 23 and Table 26) will be applied with a 2-ring, 10cm pitch, and 10 cm tall triangular-Z model. The lower 5 cm of the core has REG1 in the central position and REG2 in the 2<sup>nd</sup> ring. The upper 5 cm has REG3 in the central position and REG4 in the outer ring. A sixth-core symmetry model with reflective boundary conditions applied on all sides was used. Finally, AREA1 is defined as all four regions while AREA2 is only REG1. The A.NIP3 input (aside from the composition definitions) is provided in Figure 140.

```

UNFORM=A.NIP3
01  HEXZ - EDITS
02 0 3 40000000 40000000 40000000
40000000 0 3 3 3
03 124
04 3 3 3 3 3 3
09 Z 1 5.0 1 10.
29 10. 2
30 REG1 1 1 1 0. 5.
30 REG2 2 1 6 0. 5.
30 REG3 2 1 6 5. 10.
30 REG4 1 1 1 5. 10.
07 AREA1 REG1 REG2 REG3 REG4
07 AREA2 REG1

```

**Figure 140. Hexagonal-Z Diffusion Edit Table Model**

To verify that the edit toggles were correct, the same A.DIF3D Type 04 cards used in Section 3.1.11 and provided in Table 84 were applied. Again, the first four do not print the binary interface files while the last two do. The first should print none of the edits of interest. The second prints all edits to standard and auxiliary output. The third prints only to auxiliary output. The fourth to only standard output. The final two cases print the surface fast flux and power density to the SFEDIT file in mesh cell order and then in region order. Each of these six tasks was verified to ensure the output was produced as intended; no deficiencies were noted.

The next task is to verify the correctness of the PWDINT file. This was performed by comparing these files, after conversion to ASCII with the afore-mentioned CCCC\_convert utility, to the power density values provided in the already-verified DIF3D ASCII edits.

Similarly, the RZFLUX files were verified consistent with the already verified flux edit tables as well as by comparing the neutron loss terms to those provided in the standard output (and verified later in this section). This was performed by evaluating the binary files using a custom Python program quite similar to the RTFLUX reading interface. Similar to the other solution edit verification cases, the total neutron losses and absorption values in this file were zero, despite the problem containing losses and absorption. All other terms, including the zone-averaged fluxes were as expected.

It was then verified that the SFEDIT files were printed, and that the case 5 SFEDIT file is different from the case 6 SFEDIT file by comparing the MD5 hashes of each file. The accuracy of the contents of these files, however, was not verified as part of this work.

The final task to be performed in this section is the verification of the correctness of the neutron balance tables. DIF3D outputs these quantities in one table per group, and a final table containing the information integrated over all energy groups. All of these terms that are not leakage or buckling were confirmed to match independent calculations and are thus verified. Further, the area edits were confirmed to match expectations for all reaction and leakage types (AREA1 matches the region TOTALS row, and AREA2 matches the REG1 row).

The group-wise net leakage, group-wise total buckling, group-integrated net leakage, and group-wise total buckling were then verified to in fact be simple sums of their constituent parts. This was found to be true. Since the buckling in each of the cardinal directions is related to the leakage, ( $L_i = B_i D_i^2$ ) with knowledge of the diffusion coefficient, we can verify that the reported

February 13, 2020

leakage does in fact produce the reported buckling. This was done for each group and direction and it was found that DIF3D is properly representing this function.

The diffusion equivalent of this verification computed the leakage terms directly from one region to another. However, with the transport solver (and especially in hexagonal geometry) this process is more involved and increases the risk of mistakes in the verification process. Instead, this transport solver verification case will simplify the process and identify the group-integrated net leakage that produces the DIF3D-reported eigenvalue, using independently generated (though previously verified) absorption rates and fission source rates. This required net leakage will then be compared to what DIF3D reports. Since it is also required that the group-wise, direction-dependent leakages match, this method has to be implemented on a model wherein the group-wise, direction-dependent leakages were the sole contributor to the net leakage. This method thereby verifies both (as well as ensuring the remaining leakages are zero as expected).

To create such a model, the model described earlier and shown in Figure 140 was replaced with a 2-ring model filled with only regions filled with COMP3. The background material was also assigned the COMP3 region to minimize any interference of the background regions on our solution domain. Additionally a leakage boundary was applied to one of the surfaces. Further, a group-wise albedo was supplied with the A.NIP3 Type 05 card such that only one of the two groups on this surface was a leakage boundary, and the other was treated as purely reflecting. An example of this for the right X-boundary is provided in Figure 141. In this way, the net neutron leakage was isolated to a single group and single surface at a time. DIF3D was then run for this model, the fluxes and eigenvalue collected and used to back-calculate the leakage that produces that eigenvalue. This process was repeated for each of the surfaces and each of the groups. Each and every case showed that the DIF3D and reference group-wise, direction-wise leakages matched. Therefore these balance tables are verified.

```

UNFORM=A.NIP3
01  HEXZ - EDITS
02 0 3 40000000 40000000 40000000 40000000 0 3 3 3
03 124
04 7 4 4 3 3 3
05 XU 1.E10 1
05 XU 0. 2
09 Z 1 5. 1 10.
29 10. 2
30 REG3 1 1 1 0. 5.
30 REG3 2 1 6 0. 5.
30 REG3 1 1 1 5. 10.
30 REG3 2 1 6 5. 10.
31 REG3

```

**Figure 141. Hexagonal-Z Transport Neutron Leakage Edit Table Model**

While not truly necessary since the same code in DIF3D produces the balances regardless of the actual hexagonal-Z geometry type, this same process for verifying the correctness of the balance table values was also performed in third- and full-core geometries. The same conclusions were found in third-core geometry with nothing of note. For full-core, a leakage boundary on the upper X and/or upper Y boundaries cannot be successfully set with group-wise albedo coefficients; when trying to do so as shown in Figure 142, the net effect is that the reflective boundary is applied to both groups. The effect of this on verification is that the full-core geometry verification of the group-wise planar leakages were zero. This issue did not affect

February 13, 2020

third- and sixth-core geometries as group-wise albedos were successfully set. This is an issue that could be remedied by future revisions to DIF3D.

```

UNFORM=A.NIP3
01  HEXZ - EDITS
02 0 3 40000000 40000000 40000000 40000000 0 3 3
03 120
04 4 4 4 4 3 3
05 XL 0.
05 YL 0.
05 YU 0.
05 XU 1.E10 1
05 XU 0. 2
09 Z 1 5. 1 10.
29 10. 2
30 REG3 1 1 1 0. 5.
30 REG3 2 1 6 0. 5.
30 REG3 1 1 1 5. 10.
30 REG3 2 1 6 5. 10.

```

**Figure 142. Full-Core Hexagonal-Z Transport Neutron Leakage with Group-Wise Albedos**

### 3.4.7 Integral Verification

The purpose of this task is to provide a final check for the reasonability of DIF3D solutions for more realistic problems. To do this, the 4<sup>th</sup> series of models of the Takeda and Ikeda benchmark set [18] was used including the provided four-group cross sections. The full-core geometry for this case is shown in Figure 143. These models have three configurations termed “Rods-In”, “Rods-Half”, and “Rods-Out.” In each case, six hexagonal positions are modified (only one is depicted due to symmetry) to simulate a control rod change. It is worth noting that the axial definitions of the control rod geometry are considerably simplified for the purposes of simplifying the benchmark model. The next section will describe the convergence of the most challenging of these problems, the Rods-In case. The data for the other cases is provided, but not discussed for brevity in Sections 3.4.7.2 and 3.4.7.3 for the Rods-Half and Rods-Out cases, respectively.

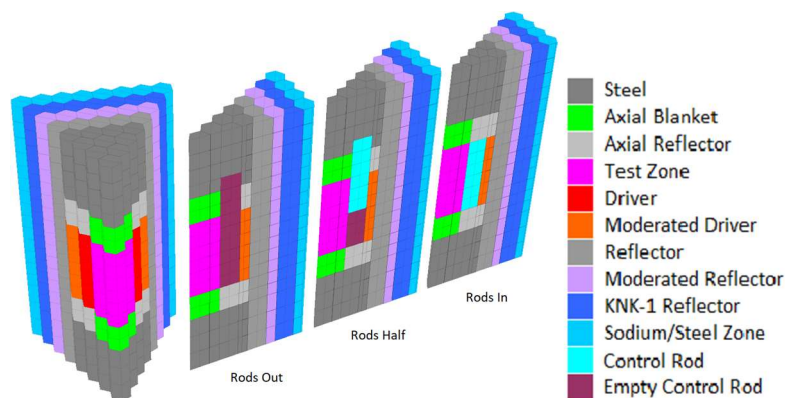


**Figure 143. Takeda Benchmark Model Series 4**



February 13, 2020

### 3.4.7.1 Rods-In Case

#### 3.4.7.1.1 Reference MCNP Results

The Monte Carlo solutions published with the benchmark contained 50 to 60 pcm of statistical uncertainty for the reported eigenvalue; these were computed with less than three million histories due to computational limitations of the time. This uncertainty was considered too large for this work and therefore MCNP6.2 was used to recreate the reference solutions. In this case, the goal is to show that the DIF3D results are converging to the MCNP6.2-based reference solution.

The MCNP reference solution was generated here with one million histories per batch, 100 inactive batches, and 16,000 active batches for a total of 16 billion active histories. The resultant value of  $k_{\text{eff}}$  predicted by MCNP was  $0.88105 \pm 0.00001$ . The relative errors for all tally bins are less than 0.4% and are distributed as is shown in Figure 144.

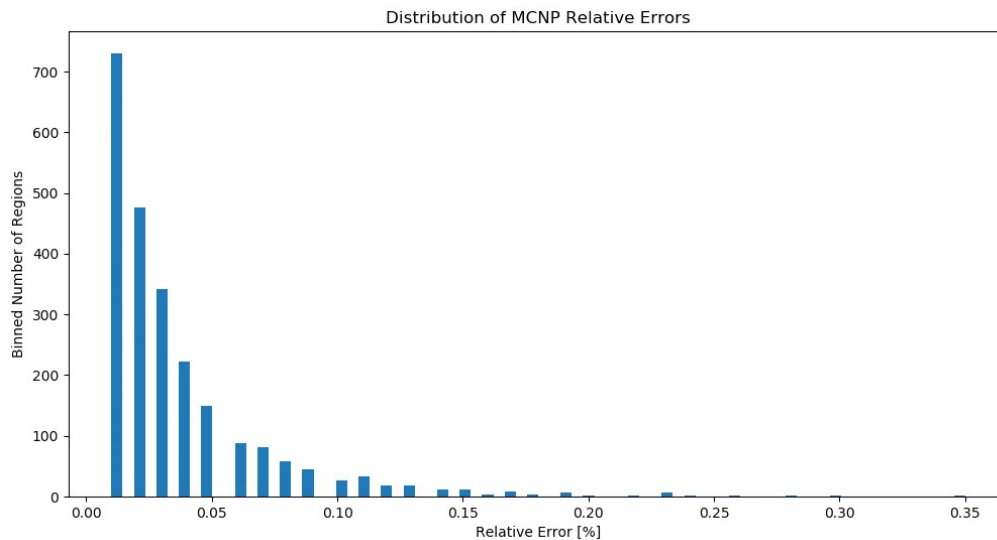


**Figure 144. MCNP Relative Error Distribution for Rods-In Case**

#### 3.4.7.1.2 DIF3D Results

The DIF3D-VARIANT solver was used to solve the same reactor using the same multigroup cross sections as analyzed by MCNP. Since an exact analytical match is not expected, this verification focuses on ensuring that the DIF3D solution converges to the MCNP solution as the spatial and angular orders are increased.

The DIF3D “Rods In” eigenvalue errors are provided in Table 153. This table is organized similar to the previous case with the flux, leakage, and source spatial approximations in the columns and the angular (flux and leakage) represented with the rows. The missing values in the table are a result of the DIF3D-VARIANT code requiring more memory than DIF3D can allocate and thus the code did not execute.

The spatial flux order (8-3-5, 10-3-5, and 12-3-5) reduces the eigenvalue error by a few tens of pcm in some cases. The spatial leakage approximation (10-3-5, 10-4-5, and 10-5-5) is slightly

February 13, 2020

closer to convergence with less than a 5 pcm change between the 10-4-5 and 10-5-5 cases. Combined, this type of behavior indicates that additional spatial flux and leakage refinement may be useful, if it could be performed.

The last aspect of refinement to consider is angular refinement. The two 13<sup>th</sup> angular order cases that completed show a few pcm change compared to the equivalent P<sub>11</sub> cases. Therefore it is possible that increasing the angular order to 15 and above may be worth another several pcm. Overall, these results are sufficiently accurate given the inability to further refine the space-angle approximations.

**Table 153. Takeda 4, Rods-In, Eigenvalue Errors [pcm]**

<b>Flux</b>	<b>6<sup>th</sup></b>	<b>7<sup>th</sup></b>	<b>8<sup>th</sup></b>	<b>8<sup>th</sup></b>	<b>10<sup>th</sup></b>	<b>12<sup>th</sup></b>	<b>10<sup>th</sup></b>	<b>10<sup>th</sup></b>
<b>Leakage</b>	<b>1<sup>st</sup></b>	<b>2<sup>nd</sup></b>	<b>3<sup>rd</sup></b>	<b>3<sup>rd</sup></b>	<b>3<sup>rd</sup></b>	<b>3<sup>rd</sup></b>	<b>4<sup>th</sup></b>	<b>5<sup>th</sup></b>
<b>Source</b>	<b>4<sup>th</sup></b>	<b>7<sup>th</sup></b>	<b>8<sup>th</sup></b>	<b>5<sup>th</sup></b>	<b>5<sup>th</sup></b>	<b>5<sup>th</sup></b>	<b>5<sup>th</sup></b>	<b>5<sup>th</sup></b>
<b>P<sub>1</sub></b>	-2697	-2716	-2717	-2717	-2717	-2717	-2718	-2717
<b>P<sub>3</sub></b>	-145	-307	-317	-317	-314	-313	-318	-319
<b>P<sub>5</sub></b>	195	-79	-96	-95	-87	-85	-94	-97
<b>P<sub>7</sub></b>	312	-21	-46	-46	-32	-28	-43	-48
<b>P<sub>9</sub></b>	353	0	-29	-28	-11	-	-	-
<b>P<sub>11</sub></b>	370	9	-21	-20	-	-	-	-
<b>P<sub>13</sub></b>	380	13	-	-	-	-	-	-
<b>P<sub>15</sub></b>	383	-	-	-	-	-	-	-

The peak flux and flux root-mean-squared-errors followed similar trends to the eigenvalue errors shown in Table 153 and are repeated in Table 154 and Table 155 below.



February 13, 2020

Table 154. Takeda 4, Rods-In, Peak Flux Errors [%]

Flux	6 <sup>th</sup>	7 <sup>th</sup>	8 <sup>th</sup>	8 <sup>th</sup>	10 <sup>th</sup>	12 <sup>th</sup>	10 <sup>th</sup>	10 <sup>th</sup>
Leakage	1 <sup>st</sup>	2 <sup>nd</sup>	3 <sup>rd</sup>	3 <sup>rd</sup>	3 <sup>rd</sup>	3 <sup>rd</sup>	4 <sup>th</sup>	5 <sup>th</sup>
Source	4 <sup>th</sup>	7 <sup>th</sup>	8 <sup>th</sup>	5 <sup>th</sup>	5 <sup>th</sup>	5 <sup>th</sup>	5 <sup>th</sup>	5 <sup>th</sup>
<b>Group 1</b>								
P <sub>1</sub>	6.25	6.23	6.23	6.23	6.23	6.23	6.23	6.22
P <sub>3</sub>	0.03	-0.29	-0.29	-0.29	-0.28	-0.28	-0.29	-0.29
P <sub>5</sub>	0.25	-0.17	-0.17	-0.17	-0.15	-0.15	-0.17	-0.17
P <sub>7</sub>	0.44	-0.09	-0.08	-0.08	-0.05	-0.05	-0.08	-0.08
P <sub>9</sub>	0.51	-0.05	-0.05	-0.06	-0.03	-	-	-
P <sub>11</sub>	0.55	-0.03	-0.05	-0.06	-	-	-	-
P <sub>13</sub>	0.59	-0.03	-	-	-	-	-	-
P <sub>15</sub>	0.6	-	-	-	-	-	-	-
<b>Group 2</b>								
P <sub>1</sub>	5.79	5.78	5.78	5.78	5.78	5.78	5.78	5.77
P <sub>3</sub>	0.08	-0.13	-0.13	-0.13	-0.12	-0.12	-0.13	-0.13
P <sub>5</sub>	0.18	-0.09	-0.08	-0.09	-0.08	-0.07	-0.09	-0.09
P <sub>7</sub>	0.27	-0.06	-0.05	-0.05	-0.03	-0.03	-0.05	-0.05
P <sub>9</sub>	0.3	-0.04	-0.04	-0.04	-0.02	-	-	-
P <sub>11</sub>	0.31	-0.03	-0.03	-0.04	-	-	-	-
P <sub>13</sub>	0.32	-0.03	-	-	-	-	-	-
P <sub>15</sub>	0.33	-	-	-	-	-	-	-
<b>Group 3</b>								
P <sub>1</sub>	1.44	1.43	1.43	1.43	1.43	1.43	1.43	1.43
P <sub>3</sub>	-0.11	0.06	0.07	0.07	0.06	0.05	0.07	0.07
P <sub>5</sub>	-0.18	0.01	0.01	0.01	0	-0.01	0.01	0.01
P <sub>7</sub>	-0.19	0.01	0.01	0.01	-0.01	-0.02	0	0.01
P <sub>9</sub>	-0.19	0.01	0.01	0.01	-0.01	-	-	-
P <sub>11</sub>	-0.19	0.01	0.01	0.02	-	-	-	-
P <sub>13</sub>	-0.19	0.01	-	-	-	-	-	-
P <sub>15</sub>	-0.19	-	-	-	-	-	-	-
<b>Group 4</b>								
P <sub>1</sub>	-4.95	-4.9	-4.98	-4.98	-4.9	-4.9	-4.99	-4.99
P <sub>3</sub>	-0.08	-0.2	-0.23	-0.23	-0.2	-0.2	-0.23	-0.23
P <sub>5</sub>	0.23	0	-0.06	-0.06	-0.07	-0.07	-0.06	-0.07
P <sub>7</sub>	0.33	0.01	-0.03	-0.03	-0.03	-0.03	-0.03	-0.03
P <sub>9</sub>	0.37	0.03	-0.01	-0.01	-0.02	-	-	-
P <sub>11</sub>	0.38	0.03	0	0	-	-	-	-
P <sub>13</sub>	0.38	0.04	-	-	-	-	-	-
P <sub>15</sub>	0.39	-	-	-	-	-	-	-

Table 155. Takeda 4, Rods-In, Root-Mean-Squared Flux Errors

Flux	6 <sup>th</sup>	7 <sup>th</sup>	8 <sup>th</sup>	8 <sup>th</sup>	10 <sup>th</sup>	12 <sup>th</sup>	10 <sup>th</sup>	10 <sup>th</sup>
Leakage	1 <sup>st</sup>	2 <sup>nd</sup>	3 <sup>rd</sup>	3 <sup>rd</sup>	3 <sup>rd</sup>	3 <sup>rd</sup>	4 <sup>th</sup>	5 <sup>th</sup>
Source	4 <sup>th</sup>	7 <sup>th</sup>	8 <sup>th</sup>	5 <sup>th</sup>	5 <sup>th</sup>	5 <sup>th</sup>	5 <sup>th</sup>	5 <sup>th</sup>
<b>Group 1</b>								
P <sub>1</sub>	5.51E-05	5.52E-05	5.52E-05	5.52E-05	5.52E-05	5.52E-05	5.52E-05	5.52E-05
P <sub>3</sub>	5.40E-06	7.74E-06	7.82E-06	7.82E-06	7.81E-06	7.81E-06	7.83E-06	7.85E-06
P <sub>5</sub>	3.42E-06	2.39E-06	2.58E-06	2.59E-06	2.52E-06	2.49E-06	2.59E-06	2.62E-06
P <sub>7</sub>	6.52E-06	7.79E-07	1.15E-06	1.15E-06	9.95E-07	9.45E-07	1.14E-06	1.21E-06
P <sub>9</sub>	7.70E-06	3.10E-07	6.54E-07	6.66E-07	4.62E-07	-	-	-
P <sub>11</sub>	8.27E-06	3.75E-07	4.65E-07	4.88E-07	-	-	-	-
P <sub>13</sub>	8.64E-06	4.72E-07	-	-	-	-	-	-
P <sub>15</sub>	8.75E-06	-	-	-	-	-	-	-
<b>Group 2</b>								
P <sub>1</sub>	3.19E-05	3.19E-05	3.19E-05	3.19E-05	3.19E-05	3.19E-05	3.19E-05	3.19E-05
P <sub>3</sub>	9.00E-07	2.00E-06	2.05E-06	2.05E-06	2.04E-06	2.04E-06	2.06E-06	2.07E-06
P <sub>5</sub>	2.29E-06	5.38E-07	6.17E-07	6.23E-07	5.74E-07	5.55E-07	6.18E-07	6.44E-07
P <sub>7</sub>	3.16E-06	2.42E-07	3.14E-07	3.21E-07	2.32E-07	2.06E-07	3.07E-07	3.42E-07
P <sub>9</sub>	3.47E-06	1.91E-07	2.21E-07	2.36E-07	1.43E-07	-	-	-
P <sub>11</sub>	3.60E-06	1.87E-07	1.90E-07	2.11E-07	-	-	-	-
P <sub>13</sub>	3.68E-06	1.93E-07	-	-	-	-	-	-
P <sub>15</sub>	3.70E-06	-	-	-	-	-	-	-
<b>Group 3</b>								
P <sub>1</sub>	7.55E-06	7.59E-06	7.59E-06	7.59E-06	7.59E-06	7.59E-06	7.59E-06	7.59E-06
P <sub>3</sub>	4.24E-07	4.22E-07	4.52E-07	4.52E-07	4.52E-07	4.52E-07	4.53E-07	4.56E-07
P <sub>5</sub>	8.93E-07	1.27E-07	1.61E-07	1.60E-07	1.53E-07	1.48E-07	1.59E-07	1.67E-07
P <sub>7</sub>	1.08E-06	7.26E-08	9.50E-08	9.45E-08	8.36E-08	7.82E-08	9.23E-08	1.02E-07
P <sub>9</sub>	1.14E-06	6.69E-08	7.38E-08	7.37E-08	6.25E-08	-	-	-
P <sub>11</sub>	1.16E-06	6.74E-08	6.58E-08	6.64E-08	-	-	-	-
P <sub>13</sub>	1.17E-06	6.93E-08	-	-	-	-	-	-
P <sub>15</sub>	1.18E-06	-	-	-	-	-	-	-
<b>Group 4</b>								
P <sub>1</sub>	8.36E-06	8.40E-06	8.40E-06	8.40E-06	8.40E-06	8.40E-06	8.40E-06	8.40E-06
P <sub>3</sub>	2.83E-07	4.05E-07	4.37E-07	4.38E-07	4.41E-07	4.42E-07	4.45E-07	4.46E-07
P <sub>5</sub>	6.05E-07	9.07E-08	1.30E-07	1.29E-07	1.21E-07	1.19E-07	1.32E-07	1.40E-07
P <sub>7</sub>	7.65E-07	4.89E-08	7.26E-08	7.31E-08	5.77E-08	5.49E-08	7.03E-08	8.10E-08
P <sub>9</sub>	8.18E-07	5.78E-08	5.91E-08	5.99E-08	4.21E-08	-	-	-
P <sub>11</sub>	8.38E-07	6.45E-08	5.65E-08	5.78E-08	-	-	-	-
P <sub>13</sub>	8.47E-07	6.88E-08	-	-	-	-	-	-
P <sub>15</sub>	8.51E-07	-	-	-	-	-	-	-

The region-wise flux comparisons for DIF3D and MCNP for the 7-2-7 P<sub>9</sub> case are provided in Figure 145. This case was chosen as it represents a good balance of low errors in the above metrics. This figure provides two plots, each showing the ratio of the DIF3D-to-MCNP group 1 fluxes. The left figure shows this ratio in the bottom axial plane while the right figure provides

February 13, 2020

it for the central plane. The color scheme is such that white is exceedingly close to 1.0, red is above 1, and blue is below 1.

Overall very close agreement is observed for the majority of the regions, with the maximal errors being observed in the outer ring next to the vacuum boundary. These outer ring locations are typically where DIF3D is known to perform the weakest due to the difficulty in representing vacuum boundary conditions with spherical harmonics. The maximum MCNP relative error for these outer ring locations was between 0.1% and 0.3% for the bottom-most plane, and 0.03% to 0.07% for the central axial plane.

The groups 2, 3, and 4 behaviors are shown in Figure 146 through Figure 148, respectively. These lower energy groups exhibit the same general trends as in the first group and thus will not be discussed further.

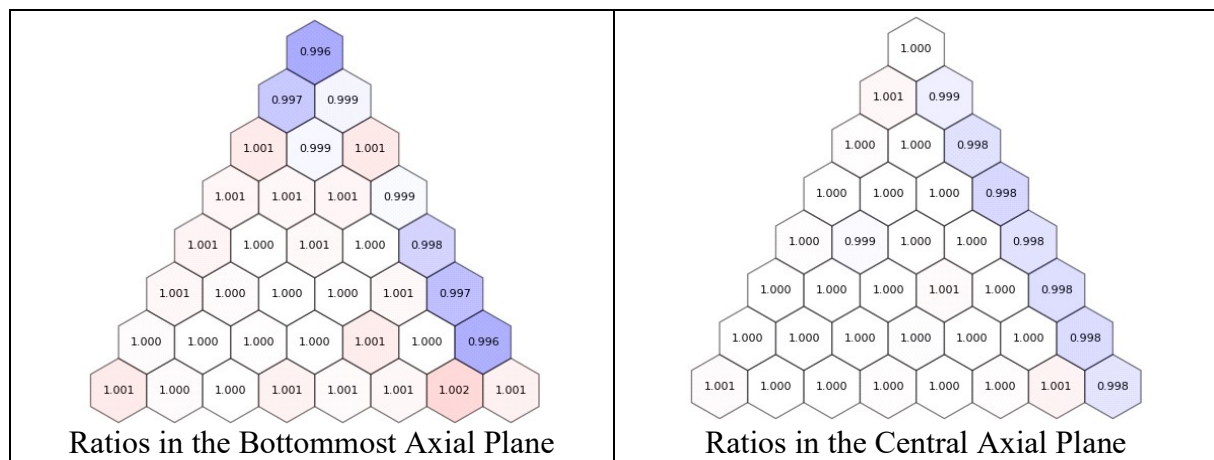


**Figure 145. Ratio of DIF3D to MCNP Fluxes in Group 1**

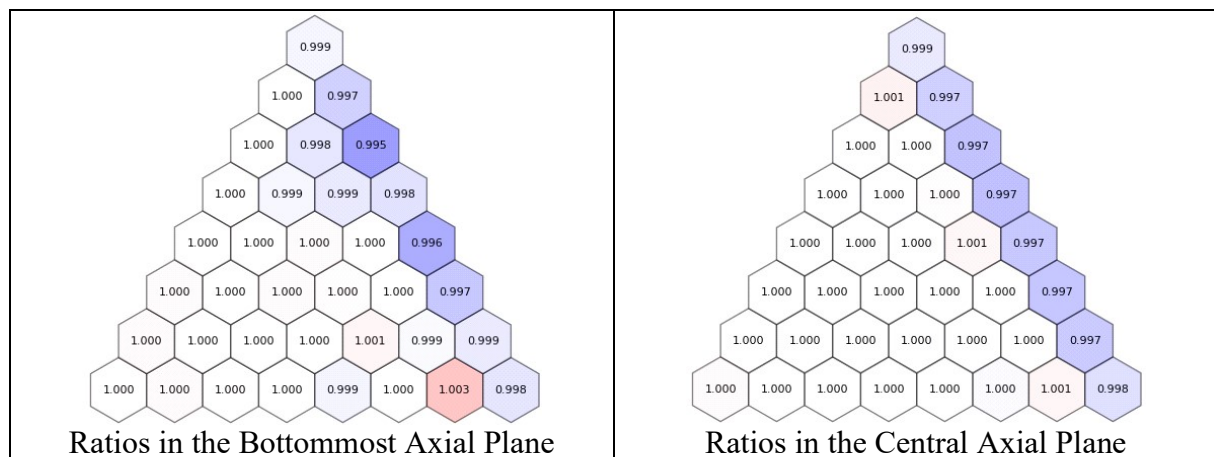
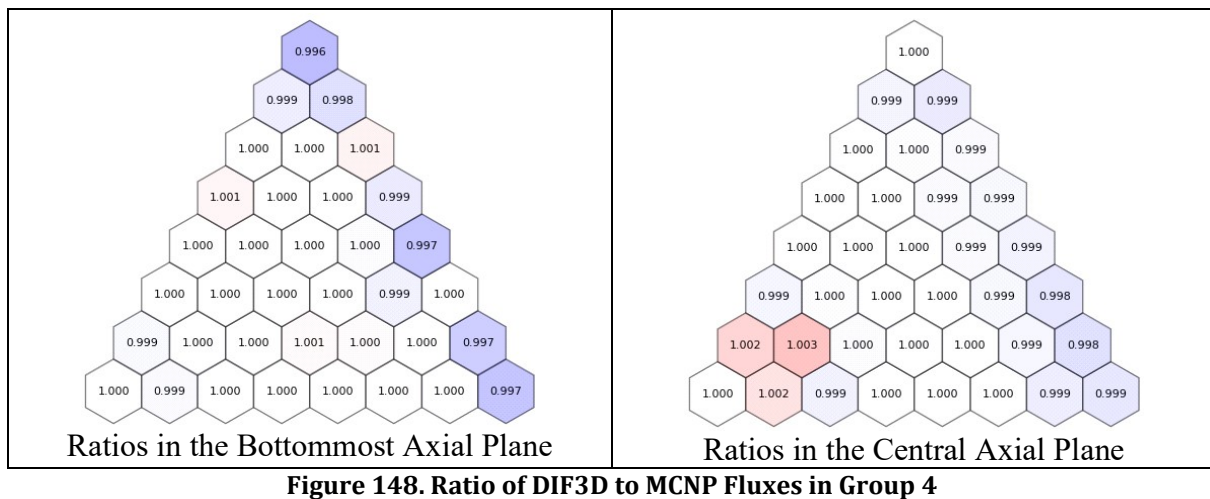
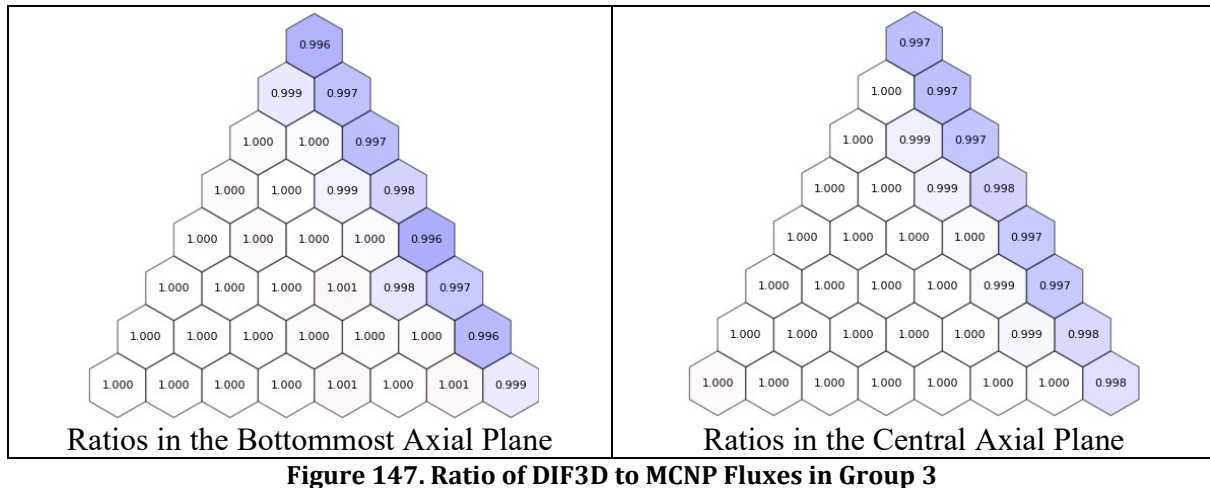


**Figure 146. Ratio of DIF3D to MCNP Fluxes in Group 2**

February 13, 2020



These results, and those provided in Sections 3.4.7.2 and 3.4.7.3, indicate that the DIF3D can closely match the MCNP reference, converging with increasing spatial and angular orders, and therefore can be used to provide confidence in the verification of DIF3D.

### 3.4.7.2 Rods-Half Case

#### 3.4.7.2.1 Reference MCNP Results

The MCNP reference solution was generated here with one million histories per batch, 100 inactive batches, and 16,000 active batches for a total of 16 billion active histories. The resultant value of  $k_{\text{eff}}$  predicted by MCNP was  $0.985211 \pm 0.000005$ . The relative errors for all tally bins are less than around 0.4% and are distributed as is shown in Figure 149.

February 13, 2020

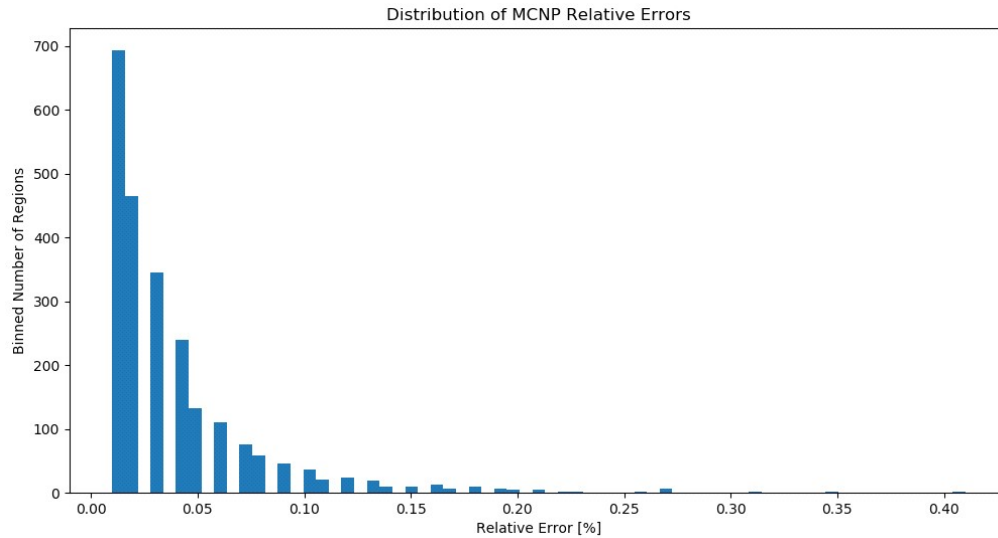


Figure 149. MCNP Relative Error Distribution for Rods-Half Case

#### 3.4.7.2.2 DIF3D Results

The following tables provide the eigenvalue errors, the errors in the peak fluxes, and the root-mean-squared errors of the fluxes on a per-mesh basis. Similar trends are observed to those discussed in Section 3.4.7.1.

Table 156. Takeda 4, Rods-Half, Eigenvalue Errors [pcm]

Flux	6 <sup>th</sup>	7 <sup>th</sup>	8 <sup>th</sup>	8 <sup>th</sup>	10 <sup>th</sup>	12 <sup>th</sup>	10 <sup>th</sup>	10 <sup>th</sup>
Leakage	1 <sup>st</sup>	2 <sup>nd</sup>	3 <sup>rd</sup>	3 <sup>rd</sup>	3 <sup>rd</sup>	3 <sup>rd</sup>	4 <sup>th</sup>	5 <sup>th</sup>
Source	4 <sup>th</sup>	7 <sup>th</sup>	8 <sup>th</sup>	5 <sup>th</sup>	5 <sup>th</sup>	5 <sup>th</sup>	5 <sup>th</sup>	5 <sup>th</sup>
P <sub>1</sub>	-2465	-2487	-2490	-2490	-2489	-2489	-2491	-2490
P <sub>3</sub>	-162	-268	-277	-276	-274	-274	-277	-278
P <sub>5</sub>	105	-77	-92	-91	-86	-84	-92	-93
P <sub>7</sub>	200	-23	-44	-44	-36	-32	-43	-46
P <sub>9</sub>	237	-3	-27	-26	-16	-	-	-
P <sub>11</sub>	253	8	-19	-18	-	-	-	-
P <sub>13</sub>	262	13	-	-	-	-	-	-
P <sub>15</sub>	265	-	-	-	-	-	-	-

Table 157. Takeda 4, Rods-Half, Peak Flux Errors [%]

Flux	6 <sup>th</sup>	7 <sup>th</sup>	8 <sup>th</sup>	8 <sup>th</sup>	10 <sup>th</sup>	12 <sup>th</sup>	10 <sup>th</sup>	10 <sup>th</sup>
Leakage	1 <sup>st</sup>	2 <sup>nd</sup>	3 <sup>rd</sup>	3 <sup>rd</sup>	3 <sup>rd</sup>	3 <sup>rd</sup>	4 <sup>th</sup>	5 <sup>th</sup>
Source	4 <sup>th</sup>	7 <sup>th</sup>	8 <sup>th</sup>	5 <sup>th</sup>	5 <sup>th</sup>	5 <sup>th</sup>	5 <sup>th</sup>	5 <sup>th</sup>
<b>Group 1</b>								
P <sub>1</sub>	5.95	5.98	5.98	5.98	5.97	5.97	5.98	5.98
P <sub>3</sub>	0.17	-0.03	-0.01	-0.01	-0.01	-0.01	-0.01	-0.01
P <sub>5</sub>	0.16	-0.09	-0.07	-0.07	-0.06	-0.06	-0.06	-0.06
P <sub>7</sub>	0.29	-0.05	-0.02	-0.03	-0.02	-0.01	-0.02	-0.02
P <sub>9</sub>	0.33	-0.03	-0.02	-0.02	-0.01	-	-	-
P <sub>11</sub>	0.36	-0.03	-0.01	-0.02	-	-	-	-
P <sub>13</sub>	0.39	-0.03	-	-	-	-	-	-
P <sub>15</sub>	0.39	-	-	-	-	-	-	-
<b>Group 2</b>								
P <sub>1</sub>	5.59	5.63	5.63	5.63	5.63	5.62	5.63	5.63
P <sub>3</sub>	0.24	0.15	0.16	0.16	0.16	0.16	0.16	0.16
P <sub>5</sub>	0.14	0.01	0.03	0.03	0.03	0.03	0.03	0.03
P <sub>7</sub>	0.16	-0.01	0.01	0.01	0.02	0.02	0.02	0.02
P <sub>9</sub>	0.16	-0.02	0.01	0	0.01	-	-	-
P <sub>11</sub>	0.16	-0.03	0.01	0	-	-	-	-
P <sub>13</sub>	0.17	-0.03	-	-	-	-	-	-
P <sub>15</sub>	0.16	-	-	-	-	-	-	-
<b>Group 3</b>								
P <sub>1</sub>	0.99	1	1	1	1	1	1	1
P <sub>3</sub>	-0.1	-0.13	-0.14	-0.1	-0.14	-0.14	-0.15	-0.15
P <sub>5</sub>	0.07	-0.01	-0.03	0	-0.03	-0.03	-0.03	-0.04
P <sub>7</sub>	0.11	0	-0.02	0	-0.01	-0.01	-0.02	-0.02
P <sub>9</sub>	0.12	0.01	-0.02	0	0	-	-	-
P <sub>11</sub>	0.12	0	-0.02	-0.02	-	-	-	-
P <sub>13</sub>	0.12	0	-	-	-	-	-	-
P <sub>15</sub>	0.12	-	-	-	-	-	-	-
<b>Group 4</b>								
P <sub>1</sub>	-2.8	-2.92	-2.91	-2.9	-2.9	-2.91	-2.91	-2.91
P <sub>3</sub>	0	-0.23	-0.26	-0.2	-0.27	-0.27	-0.26	-0.27
P <sub>5</sub>	0.21	-0.04	-0.08	0	-0.08	-0.08	-0.08	-0.09
P <sub>7</sub>	0.31	0	-0.05	0	-0.03	-0.03	-0.04	-0.05
P <sub>9</sub>	0.35	0.01	-0.03	0	-0.02	-	-	-
P <sub>11</sub>	0.36	0.02	-0.02	-0.02	-	-	-	-
P <sub>13</sub>	0.37	0.03	-	-	-	-	-	-
P <sub>15</sub>	0.37	-	-	-	-	-	-	-

Table 158. Takeda 4, Rods-Half, Root-Mean-Squared Flux Errors

Flux	6 <sup>th</sup>	7 <sup>th</sup>	8 <sup>th</sup>	8 <sup>th</sup>	10 <sup>th</sup>	12 <sup>th</sup>	10 <sup>th</sup>	10 <sup>th</sup>
Leakage	1 <sup>st</sup>	2 <sup>nd</sup>	3 <sup>rd</sup>	3 <sup>rd</sup>	3 <sup>rd</sup>	3 <sup>rd</sup>	4 <sup>th</sup>	5 <sup>th</sup>
Source	4 <sup>th</sup>	7 <sup>th</sup>	8 <sup>th</sup>	5 <sup>th</sup>	5 <sup>th</sup>	5 <sup>th</sup>	5 <sup>th</sup>	5 <sup>th</sup>
<b>Group 1</b>								
P <sub>1</sub>	5.23E-05	5.26E-05	5.26E-05	5.26E-05	5.26E-05	5.26E-05	5.26E-05	5.26E-05
P <sub>3</sub>	6.07E-06	7.91E-06	8.01E-06	8.01E-06	8.00E-06	7.99E-06	8.03E-06	8.03E-06
P <sub>5</sub>	3.09E-06	2.53E-06	2.74E-06	2.74E-06	2.69E-06	2.66E-06	2.75E-06	2.77E-06
P <sub>7</sub>	5.84E-06	8.00E-07	1.23E-06	1.23E-06	1.11E-06	1.07E-06	1.24E-06	1.29E-06
P <sub>9</sub>	6.98E-06	2.64E-07	6.74E-07	6.70E-07	5.19E-07	-	-	-
P <sub>11</sub>	7.54E-06	3.64E-07	4.32E-07	4.29E-07	-	-	-	-
P <sub>13</sub>	7.87E-06	4.87E-07	-	-	-	-	-	-
P <sub>15</sub>	7.98E-06	-	-	-	-	-	-	-
<b>Group 2</b>								
P <sub>1</sub>	3.25E-05	3.28E-05	3.28E-05	3.28E-05	3.28E-05	3.28E-05	3.28E-05	3.28E-05
P <sub>3</sub>	1.55E-06	2.42E-06	2.50E-06	2.49E-06	2.47E-06	2.47E-06	2.50E-06	2.51E-06
P <sub>5</sub>	2.15E-06	6.37E-07	7.61E-07	7.53E-07	7.09E-07	6.89E-07	7.63E-07	7.83E-07
P <sub>7</sub>	2.95E-06	2.27E-07	3.66E-07	3.61E-07	2.87E-07	2.66E-07	3.55E-07	3.89E-07
P <sub>9</sub>	3.24E-06	1.43E-07	2.27E-07	2.24E-07	1.51E-07	-	-	-
P <sub>11</sub>	3.37E-06	1.64E-07	1.75E-07	1.70E-07	-	-	-	-
P <sub>13</sub>	3.44E-06	1.90E-07	-	-	-	-	-	-
P <sub>15</sub>	3.46E-06	-	-	-	-	-	-	-
<b>Group 3</b>								
P <sub>1</sub>	7.37E-06	7.49E-06	7.50E-06	7.50E-06	7.50E-06	7.50E-06	7.50E-06	7.50E-06
P <sub>3</sub>	5.35E-07	7.23E-07	7.71E-07	7.71E-07	7.60E-07	7.57E-07	7.79E-07	7.87E-07
P <sub>5</sub>	1.13E-06	1.89E-07	2.61E-07	2.61E-07	2.29E-07	2.19E-07	2.62E-07	2.77E-07
P <sub>7</sub>	1.39E-06	8.41E-08	1.50E-07	1.50E-07	1.03E-07	9.02E-08	1.44E-07	1.66E-07
P <sub>9</sub>	1.47E-06	6.47E-08	1.11E-07	1.11E-07	6.23E-08	-	-	-
P <sub>11</sub>	1.50E-06	6.65E-08	9.47E-08	9.50E-08	-	-	-	-
P <sub>13</sub>	1.51E-06	6.99E-08	-	-	-	-	-	-
P <sub>15</sub>	1.52E-06	-	-	-	-	-	-	-
<b>Group 4</b>								
P <sub>1</sub>	8.69E-06	8.76E-06	8.76E-06	8.76E-06	8.76E-06	8.76E-06	8.77E-06	8.76E-06
P <sub>3</sub>	4.38E-07	5.91E-07	6.35E-07	6.35E-07	6.24E-07	6.22E-07	6.43E-07	6.50E-07
P <sub>5</sub>	7.87E-07	1.49E-07	2.06E-07	2.05E-07	1.74E-07	1.65E-07	2.05E-07	2.19E-07
P <sub>7</sub>	9.66E-07	7.20E-08	1.16E-07	1.17E-07	6.90E-08	5.87E-08	1.07E-07	1.26E-07
P <sub>9</sub>	1.03E-06	6.64E-08	8.86E-08	8.94E-08	4.07E-08	-	-	-
P <sub>11</sub>	1.05E-06	7.37E-08	7.89E-08	7.98E-08	-	-	-	-
P <sub>13</sub>	1.06E-06	7.87E-08	-	-	-	-	-	-
P <sub>15</sub>	1.07E-06	-	-	-	-	-	-	-

The region-wise flux comparisons for DIF3D and MCNP for the 7-2-7 P<sub>9</sub> case are provided in the following figures. This case was chosen as it represents a good balance of low errors in of the above metrics. These figures show the ratio of the DIF3D-to-MCNP for the group 1 through



February 13, 2020

4 fluxes, respectively. The left side of each figure shows this ratio in the bottom axial plane while the right side of the figure provides it for the central plane.

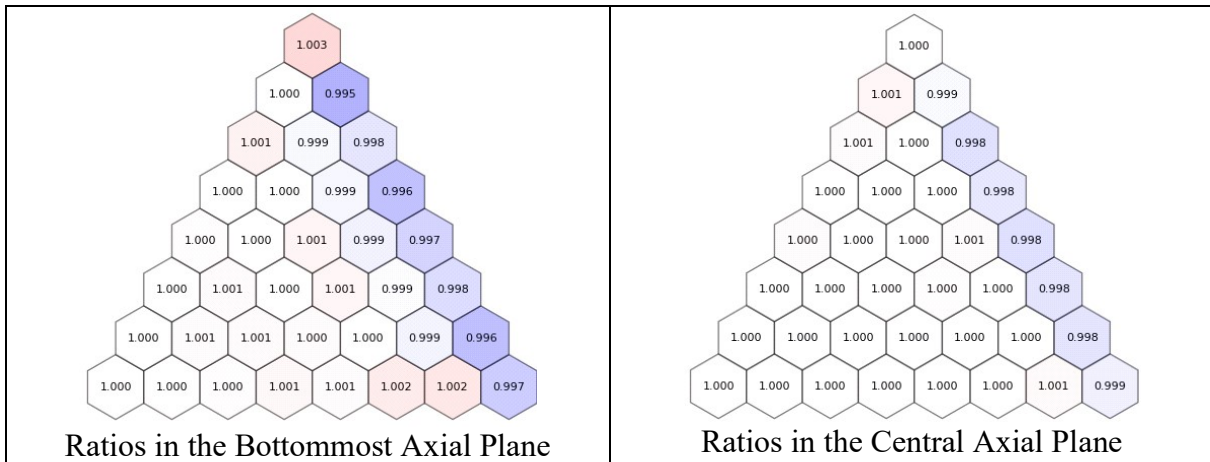


Figure 150. Ratio of DIF3D to MCNP Fluxes in Group 1

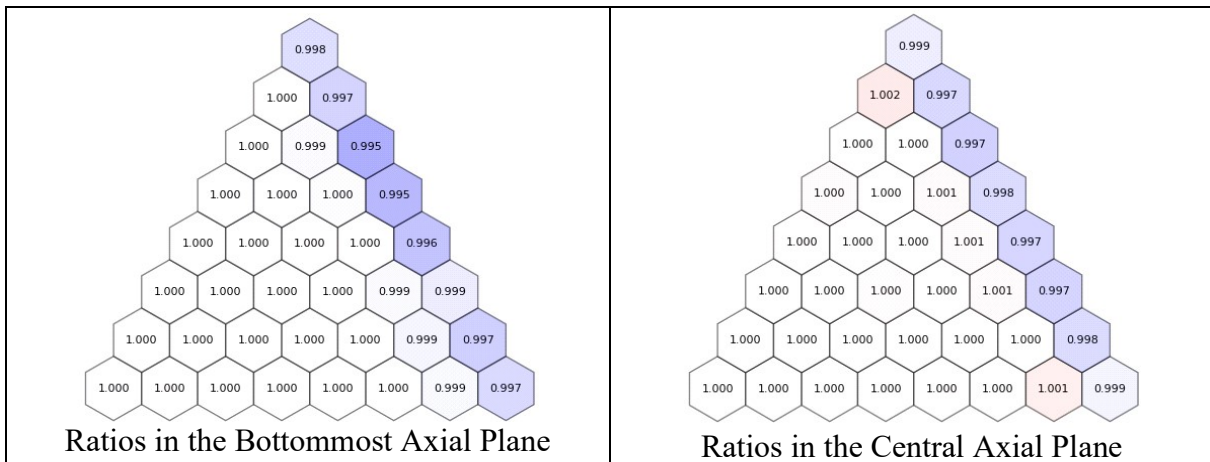


Figure 151. Ratio of DIF3D to MCNP Fluxes in Group 2

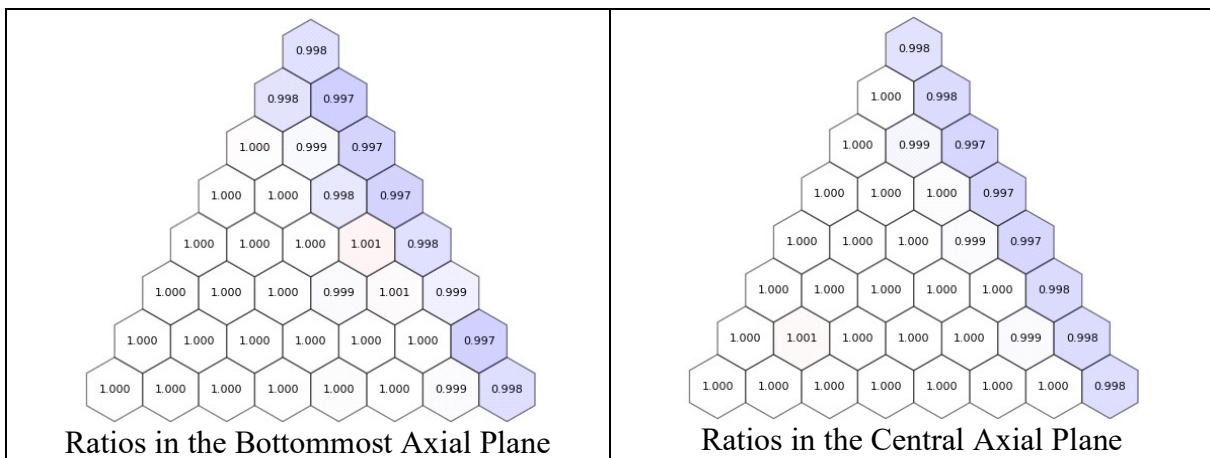


Figure 152. Ratio of DIF3D to MCNP Fluxes in Group 3



February 13, 2020

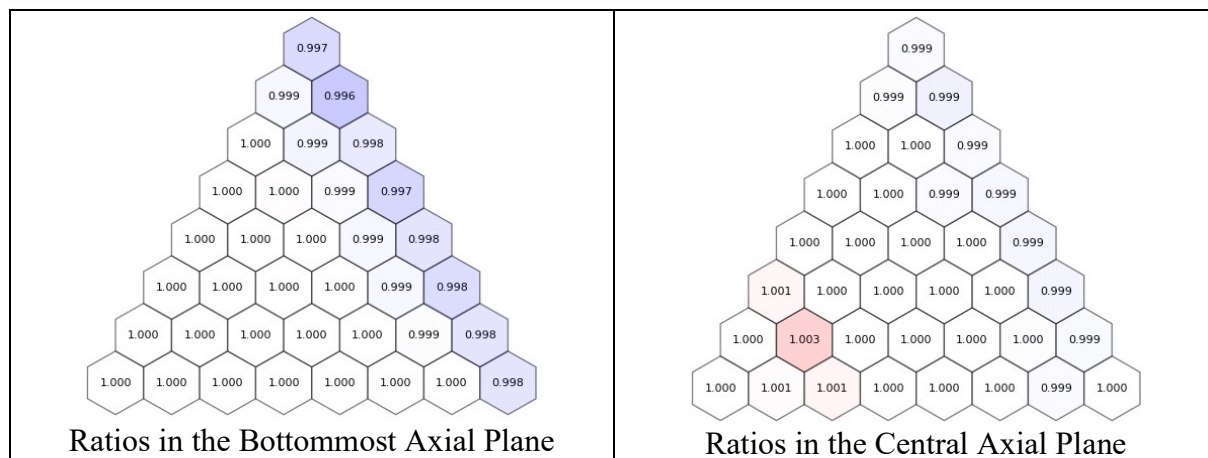


Figure 153. Ratio of DIF3D to MCNP Fluxes in Group 4

### 3.4.7.3 Rods-Out Case

#### 3.4.7.3.1 Reference MCNP Results

The MCNP reference solution was generated here with one million histories per batch, 100 inactive batches, and 16,000 active batches for a total of 16 billion active histories. The resultant value of  $k_{\text{eff}}$  predicted by MCNP was  $1.096650 \pm 0.000005$ . The relative errors for all tally bins are less than 0.4% and are distributed as is shown in Figure 154.

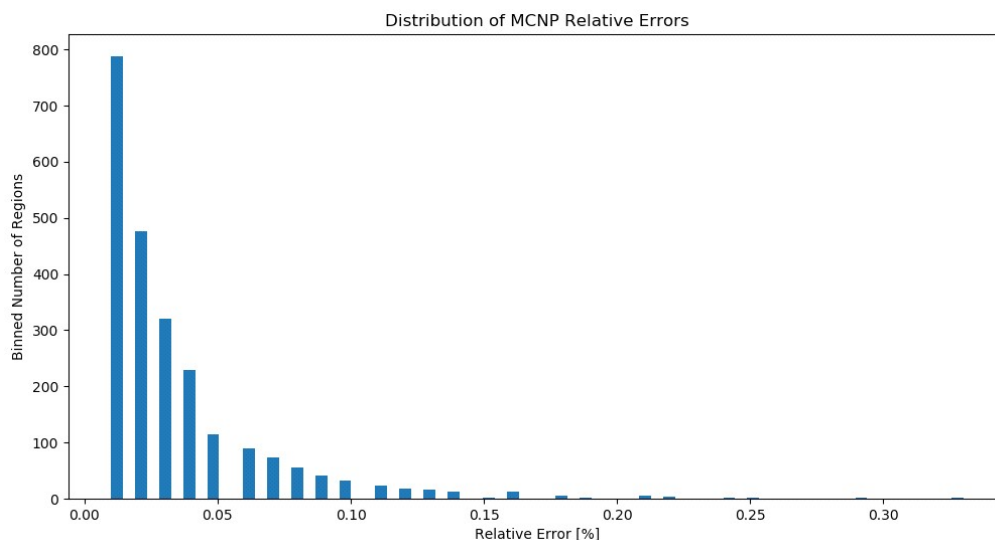


Figure 154. MCNP Relative Error Distribution for Rods-Out Case

#### 3.4.7.3.2 DIF3D Results

The following tables provide the eigenvalue errors, the errors in the peak fluxes, and the root-mean-squared errors of the fluxes on a per-mesh basis. Similar trends are observed to those discussed in Section 3.4.7.1.

February 13, 2020

Table 159. Takeda 4, Rods-Out, Eigenvalue Errors [pcm]

Flux	6 <sup>th</sup>	7 <sup>th</sup>	8 <sup>th</sup>	8 <sup>th</sup>	10 <sup>th</sup>	12 <sup>th</sup>	10 <sup>th</sup>	10 <sup>th</sup>
Leakage	1 <sup>st</sup>	2 <sup>nd</sup>	3 <sup>rd</sup>	3 <sup>rd</sup>	3 <sup>rd</sup>	3 <sup>rd</sup>	4 <sup>th</sup>	5 <sup>th</sup>
Source	4 <sup>th</sup>	7 <sup>th</sup>	8 <sup>th</sup>	5 <sup>th</sup>	5 <sup>th</sup>	5 <sup>th</sup>	5 <sup>th</sup>	5 <sup>th</sup>
P <sub>1</sub>	-2125	-2130	-2131	-2131	-2130	-2130	-2131	-2130
P <sub>3</sub>	-179	-214	-217	-218	-217	-216	-217	-217
P <sub>5</sub>	0	-71	-80	-80	-77	-76	-80	-81
P <sub>7</sub>	68	-26	-40	-40	-35	-33	-40	-41
P <sub>9</sub>	98	-6	-24	-23	-18	-	-	-
P <sub>11</sub>	112	2	-16	-16	-	-	-	-
P <sub>13</sub>	120	7	-	-	-	-	-	-
P <sub>15</sub>	123	-	-	-	-	-	-	-

February 13, 2020

Table 160. Takeda 4, Rods-Out, Peak Flux Errors [%]

Flux	6 <sup>th</sup>	7 <sup>th</sup>	8 <sup>th</sup>	8 <sup>th</sup>	10 <sup>th</sup>	12 <sup>th</sup>	10 <sup>th</sup>	10 <sup>th</sup>
Leakage	1 <sup>st</sup>	2 <sup>nd</sup>	3 <sup>rd</sup>	3 <sup>rd</sup>	3 <sup>rd</sup>	3 <sup>rd</sup>	4 <sup>th</sup>	5 <sup>th</sup>
Source	4 <sup>th</sup>	7 <sup>th</sup>	8 <sup>th</sup>	5 <sup>th</sup>	5 <sup>th</sup>	5 <sup>th</sup>	5 <sup>th</sup>	5 <sup>th</sup>
<b>Group 1</b>								
P <sub>1</sub>	5.62	5.63	5.63	5.63	5.63	5.63	5.63	5.63
P <sub>3</sub>	0.21	0.09	0.1	0.1	0.1	0.1	0.11	0.11
P <sub>5</sub>	0.09	-0.03	-0.01	-0.01	-0.02	-0.02	0	0
P <sub>7</sub>	0.16	-0.03	0.01	0.01	0	0	0.01	0.01
P <sub>9</sub>	0.17	-0.02	0.01	0.01	0	-	-	-
P <sub>11</sub>	0.19	-0.02	0	0	-	-	-	-
P <sub>13</sub>	0.22	-0.03	-	-	-	-	-	-
P <sub>15</sub>	0.22	-	-	-	-	-	-	-
<b>Group 2</b>								
P <sub>1</sub>	5.42	5.45	5.44	5.44	5.44	5.44	5.44	5.44
P <sub>3</sub>	0.3	0.27	0.27	0.28	0.27	0.27	0.28	0.28
P <sub>5</sub>	0.11	0.07	0.09	0.09	0.08	0.07	0.09	0.09
P <sub>7</sub>	0.09	0.02	0.05	0.05	0.04	0.03	0.05	0.06
P <sub>9</sub>	0.07	0	0.03	0.03	0.02	-	-	-
P <sub>11</sub>	0.07	-0.01	0.03	0.03	-	-	-	-
P <sub>13</sub>	0.06	-0.02	-	-	-	-	-	-
P <sub>15</sub>	0.06	-	-	-	-	-	-	-
<b>Group 3</b>								
P <sub>1</sub>	3.01	3.02	3.02	3.02	3.02	3.02	3.02	3.02
P <sub>3</sub>	0.15	0.18	0.19	0.19	0.19	0.19	0.18	0.18
P <sub>5</sub>	0.03	0.05	0.07	0.07	0.07	0.07	0.07	0.07
P <sub>7</sub>	-0.02	0.01	0.03	0.03	0.03	0.03	0.03	0.03
P <sub>9</sub>	-0.06	-0.01	0.02	0.02	0.02	-	-	-
P <sub>11</sub>	-0.07	-0.02	0.01	0.01	-	-	-	-
P <sub>13</sub>	-0.08	-0.02	-	-	-	-	-	-
P <sub>15</sub>	-0.08	-	-	-	-	-	-	-
<b>Group 4</b>								
P <sub>1</sub>	-2.23	2.26	-2.26	-2.26	-2.25	-2.25	-2.26	-2.25
P <sub>3</sub>	-0.04	0.09	-0.13	-0.13	-0.13	-0.13	-0.13	-0.13
P <sub>5</sub>	0.14	0.01	-0.03	-0.03	-0.03	-0.03	-0.03	-0.03
P <sub>7</sub>	0.2	0.03	-0.01	-0.01	-0.01	-0.01	-0.01	-0.02
P <sub>9</sub>	0.22	0.03	-0.01	-0.01	0	-	-	-
P <sub>11</sub>	0.23	0.04	0	-0.01	-	-	-	-
P <sub>13</sub>	0.23	0.04	-	-	-	-	-	-
P <sub>15</sub>	0.23	-	-	-	-	-	-	-

**Table 161. Takeda 4, Rods-Out, Root-Mean-Squared Flux Errors**

Flux	6 <sup>th</sup>	7 <sup>th</sup>	8 <sup>th</sup>	8 <sup>th</sup>	10 <sup>th</sup>	12 <sup>th</sup>	10 <sup>th</sup>	10 <sup>th</sup>
Leakage	1 <sup>st</sup>	2 <sup>nd</sup>	3 <sup>rd</sup>	3 <sup>rd</sup>	3 <sup>rd</sup>	3 <sup>rd</sup>	4 <sup>th</sup>	5 <sup>th</sup>
Source	4 <sup>th</sup>	7 <sup>th</sup>	8 <sup>th</sup>	5 <sup>th</sup>	5 <sup>th</sup>	5 <sup>th</sup>	5 <sup>th</sup>	5 <sup>th</sup>
<b>Group 1</b>								
P <sub>1</sub>	4.59E-05	4.61E-05	4.61E-05	4.61E-05	4.60E-05	4.60E-05	4.61E-05	4.61E-05
P <sub>3</sub>	5.45E-06	6.92E-06	7.01E-06	7.01E-06	6.99E-06	6.98E-06	7.02E-06	7.02E-06
P <sub>5</sub>	1.83E-06	2.32E-06	2.53E-06	2.53E-06	2.47E-06	2.45E-06	2.54E-06	2.56E-06
P <sub>7</sub>	4.30E-06	7.67E-07	1.19E-06	1.18E-06	1.06E-06	1.02E-06	1.20E-06	1.23E-06
P <sub>9</sub>	5.35E-06	2.36E-07	6.59E-07	6.53E-07	4.99E-07	-	-	-
P <sub>11</sub>	5.86E-06	2.88E-07	4.13E-07	4.12E-07	-	-	-	-
P <sub>13</sub>	6.16E-06	3.99E-07	-	-	-	-	-	-
P <sub>15</sub>	6.27E-06	-	-	-	-	-	-	-
<b>Group 2</b>								
P <sub>1</sub>	3.21E-05	3.23E-05	3.23E-05	3.23E-05	3.22E-05	3.22E-05	3.23E-05	3.23E-05
P <sub>3</sub>	2.09E-06	2.58E-06	2.65E-06	2.65E-06	2.62E-06	2.61E-06	2.66E-06	2.66E-06
P <sub>5</sub>	8.45E-07	8.01E-07	9.49E-07	9.46E-07	8.79E-07	8.54E-07	9.59E-07	9.79E-07
P <sub>7</sub>	1.30E-06	3.12E-07	4.93E-07	4.92E-07	3.92E-07	3.64E-07	4.94E-07	5.27E-07
P <sub>9</sub>	1.55E-06	1.37E-07	3.14E-07	3.09E-07	2.05E-07	-	-	-
P <sub>11</sub>	1.68E-06	1.15E-07	2.29E-07	2.30E-07	-	-	-	-
P <sub>13</sub>	1.75E-06	1.37E-07	-	-	-	-	-	-
P <sub>15</sub>	1.78E-06	-	-	-	-	-	-	-
<b>Group 3</b>								
P <sub>1</sub>	6.83E-06	6.86E-06	6.86E-06	6.86E-06	6.86E-06	6.86E-06	6.86E-06	6.86E-06
P <sub>3</sub>	5.60E-07	5.98E-07	6.15E-07	6.15E-07	6.11E-07	6.09E-07	6.19E-07	6.21E-07
P <sub>5</sub>	5.26E-07	1.89E-07	2.32E-07	2.31E-07	2.20E-07	2.14E-07	2.37E-07	2.44E-07
P <sub>7</sub>	5.98E-07	8.14E-08	1.29E-07	1.28E-07	1.10E-07	1.04E-07	1.32E-07	1.43E-07
P <sub>9</sub>	6.20E-07	4.80E-08	8.88E-08	8.75E-08	6.89E-08	-	-	-
P <sub>11</sub>	6.31E-07	4.21E-08	7.00E-08	6.93E-08	-	-	-	-
P <sub>13</sub>	6.34E-07	4.39E-08	-	-	-	-	-	-
P <sub>15</sub>	6.36E-07	-	-	-	-	-	-	-
<b>Group 4</b>								
P <sub>1</sub>	7.44E-06	7.49E-06	7.48E-06	7.48E-06	7.48E-06	7.48E-06	7.49E-06	7.49E-06
P <sub>3</sub>	4.53E-07	4.80E-07	5.11E-07	5.12E-07	5.03E-07	5.00E-07	5.16E-07	5.21E-07
P <sub>5</sub>	6.20E-07	1.43E-07	1.85E-07	1.85E-07	1.63E-07	1.57E-07	1.88E-07	1.96E-07
P <sub>7</sub>	7.28E-07	6.73E-08	1.04E-07	1.05E-07	7.44E-08	6.64E-08	1.03E-07	1.15E-07
P <sub>9</sub>	7.67E-07	5.24E-08	7.53E-08	7.55E-08	4.52E-08	-	-	-
P <sub>11</sub>	7.82E-07	5.18E-08	6.31E-08	6.37E-08	-	-	-	-
P <sub>13</sub>	7.89E-07	5.43E-08	-	-	-	-	-	-
P <sub>15</sub>	7.92E-07	-	-	-	-	-	-	-

The region-wise flux comparisons for DIF3D and MCNP for the 7-2-7 P<sub>11</sub> case are provided in the following figures. This case was chosen as it represents a good balance of low errors in of the above metrics. These figures show the ratio of the DIF3D-to-MCNP for the group 1 through

February 13, 2020

4 fluxes, respectively. The left side of each figure shows this ratio in the bottom axial plane while the right side of the figure provides it for the central plane.

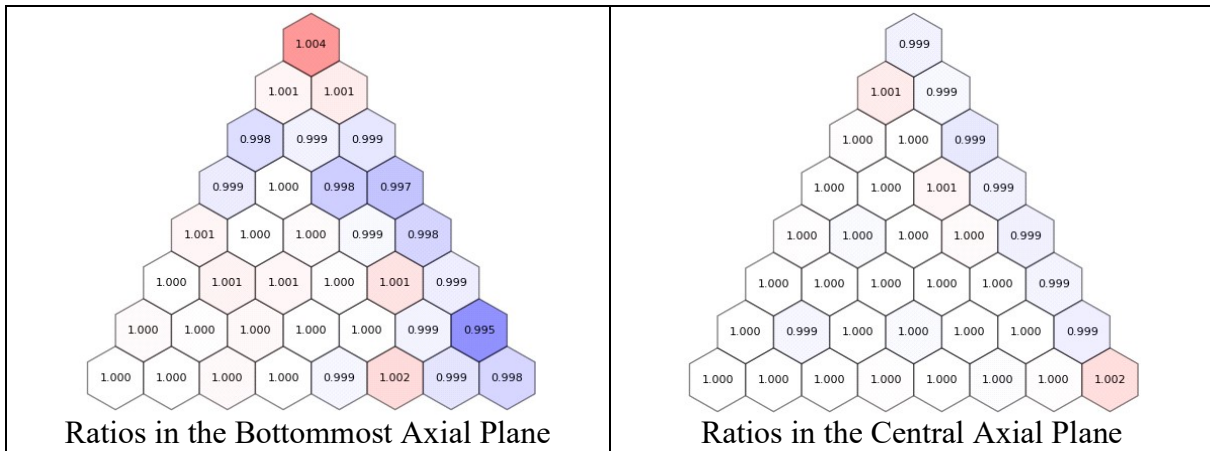


Figure 155. Ratio of DIF3D to MCNP Fluxes in Group 1

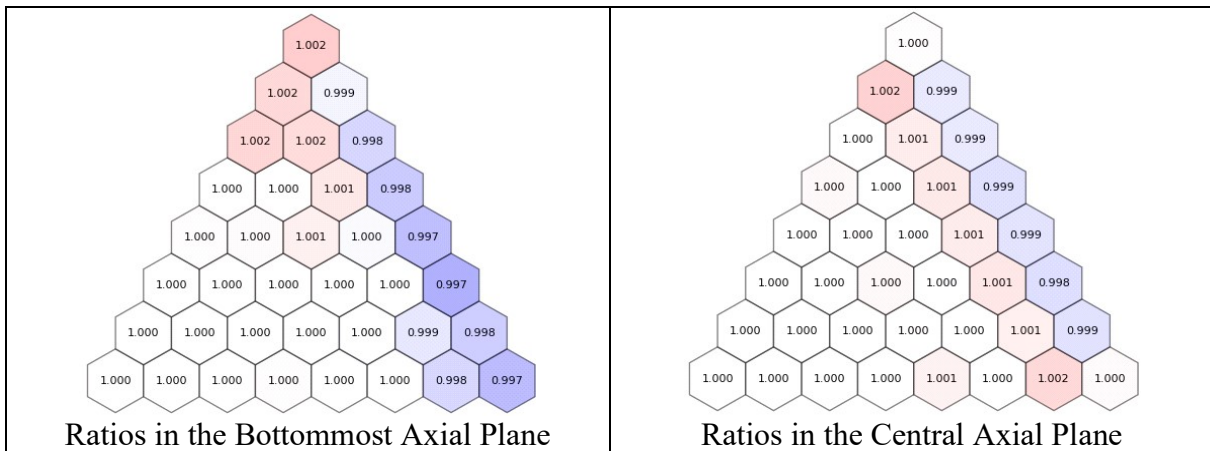


Figure 156. Ratio of DIF3D to MCNP Fluxes in Group 2

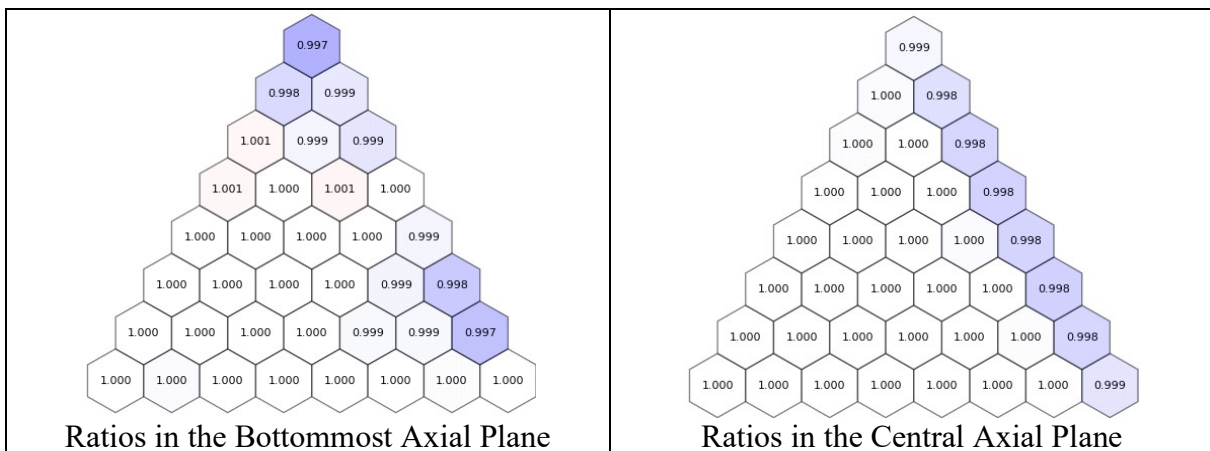


Figure 157. Ratio of DIF3D to MCNP Fluxes in Group 3

February 13, 2020

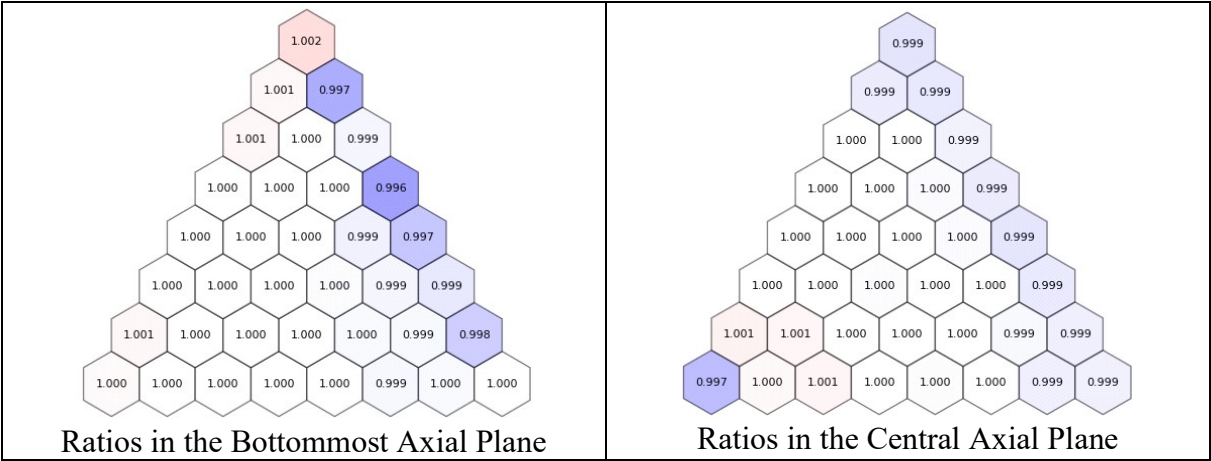


Figure 158. Ratio of DIF3D to MCNP Fluxes in Group 4

## 4 Monte Carlo Verification

This section presents the verification of the MCNP6.2 capabilities relied on to create the reference solutions for the verification of the DIF3D transport capability.

As stated elsewhere, MCNP6.2 as utilized as the Monte Carlo solver of choice for DIF3D verification. This selection was made due to the high likelihood that no issues will be uncovered during this MCNP verification due to the prevalence of the code and its previous versions.

In this section, MCNP refers specifically to version 6.2; this is the version that was used to create all DIF3D reference solutions as well as used in this MCNP verification. Specifically, the MCNP executable was compiled on the ANL Kookie cluster using the GNU Compiler Collection C and Fortran compilers (gcc and gfortran) version 4.8.0 20150623 (Red Hat 4.8.5-39). The MCNP executable was compiled with support for OpenMP threading as was a plotting capability. In short, the following command was used to compile MCNP6.2, in the correct location: ‘make build CONFIG="plot omp gcc gfortran" -j 8’. Note that MPI support was not included in this executable as it was not necessary.

### 4.1 MCNP6.2 Capabilities to Verify

As stated elsewhere in this report, all MCNP computations were done using models that were generated from DIF3D models converted to MCNP models and multigroup cross section libraries via an automated script. This script specifically exercised the following features in defining a model and extracting information from it:

1. Cell Definitions:
  - a. Cells defined in the standard style with the volume, universe, and importance specified as a keyword parameter in the relevant cell card instead of with a volume, universe, or importance data card.
  - b. In XYZ geometry, 0-importance cells (i.e., problem boundaries) are defined via standard surface operators of the 6 external surfaces as would normally be done for simple models.
  - c. Hexagonal-Z geometries defined the 0-importance region with the complement operator (#) instead of the union of external surfaces to simplify the code to perform the DIF3D to MCNP conversion.
2. Surface Definitions:
  - a. Only planar surfaces were utilized, specifically:
    - i. Plane parallel to the X-, Y-, and Z-axes (px, py, pz surface types, respectively)
    - ii. Plane defined with three points (p surface type)
  - b. Boundary Conditions:
    - i. Only vacuum and reflective boundaries were applied
      1. Vacuum boundary conditions were applied in the typical way, by setting neutron importance to 0 in a cell or cells that are not part of the model.

2. Reflective boundary conditions were applied with the '\*' symbol before the surface id.
3. Physics Treatments:
  - a. Only neutrons were tracked via the 'mode n' card.
  - b. Forward-multigroup physics were specified with the 'mgopt F G' card where G is the number of groups.
  - c. The L'Ecuyer 63-bit generator number 1 was selected with the 'rand gen=2' card for all cases.
4. Source definitions:
  - a. For eigenvalue problems, the kcode and ksrc cards were exercised
    - i. Only the nsrck (number of histories per cycle), rkk (guess for  $k_{eff}$ ), ikz (inactive cycles), and kct (total cycles) options were used for the kcode card; the rest remained at their default.
      1. The rkk value was either taken from the DIF3D case used to create the MCNP input, or the default of 1.0 was used.
    - ii. The initial sources were defined via the ksrc card. For this, a src point was added at the centroid of each of the fissile cells in the DIF3D model.
  - b. For fixed source problems, the nps and sdef cards were utilized
    - i. The nps card had a single value: the number of histories to simulate; the second option (npsmg) is not relevant and thus was left at its default.
    - ii. The sdef card was used to define a volumetric, isotropic, group-wise source as follows:
      1. The source volume position, shape, and size was defined with uniform probability distributions spanning the relevant X, Y, and Z domains.
        - a. For Hexagonal-Z geometry, the particular cells that contained the fixed source were also defined via the 'cel' keyword on the sdef card so that rejection sampling would be performed on the X, Y, and Z domains and only sources within the hexagon would be accepted.
      2. The isotropic nature is defined by default by MCNP.
      3. The energy distribution of the source was specified with a line (i.e., discrete) distribution at the group midpoint energies and probabilities of interest.
5. Materials
  - a. Materials defined with zaid and fraction defined per the information in the DIF3D model; remaining optional parameters left at their default values for multigroup neutron transport problems.
  - b. All materials used multigroup cross section data in the form of the multigroup ACE files. These were created using the information in the ISOTXS file passed to the 'simple\_ace\_mg.pl' script distributed with MCNP. This script is not explicitly verified, but is implicitly as it was used for the generation of all multigroup ACE files used for DIF3D verification, and this MCNP verification.



- i. Data defined as either isotropic or linearly anisotropic ( $P_1$ ). Linearly anisotropic data is converted to a histogram bin representation with 1,000 bins via the `simple_ace_mg.pl` script.
  - c. All multigroup ACE files were defined with XS<sub>n</sub> cards instead of making an external xsdata file.
- 6. Tallies
  - a. The only tallies utilized were F4-type neutron flux tallies.
  - b. F4 tallies had an energy group structure applied for tallying when more than 1-group exists in the data (i.e., all but the simplest cases in this MCNP verification).
  - c. An F4 tally filter bin exists for each energy group and cell of interest:
    - i. The energy group structure, if relevant (i.e., all cases except the 1-group cases in this section) was defined with the “E4” card.
    - ii. The cell filter bins are simply a list of all cells of interest.

Table 162 provides the MCNP capabilities that are required to be verified in this section as well as identifying which of the selected the problems will be relied upon to verify that capability. The capabilities that are always enabled in every case (e.g., the pseudo-random number generator selection) are the same in all cases are not explicitly specified in the table.

This table shows a total of 11 test problems. The majority of these problems are criticality problems with analytically derived reference solutions in a compendium developed by Sood, et al [17]. This collection includes a total of 75 cases with analytically determined solutions to the eigenvalue form of the neutron transport equation for configurations of multiple geometries (slabs, cylinders, spheres, and multi-region slab-lattices), groups, and scattering treatments. The subset of cases considered for this work are those that are infinite, slab, or multi-region slabs as those are the features that can be represented by the planar geometries considered by this verification work. Additionally, a selection of problems were chosen to provide the model attributes necessary to adequately test the features of Table 162 as well as to ensure a mix of multigroup cases with up- and down-scattering.

The remaining test problems are simple fixed source test problems created chosen to test the fixed source capability used when generating fixed source reference solutions for DIF3D.

Each of the above test problems will be discussed individually in the next section.

Table 162. MCNP Capability Verification List

Capability	Cases									
	Crit. 6	Crit. 31	Crit. 32	Crit. 54	Crit. 64	Crit. 72	Crit. 74	Crit. 75	Fixed Source	Fixed Cell Source
Standard 0-Importance/Vacuum	X		X	X						
0-Importance/Vacuum via Complement										
px surfaces	X	X			X	X	X	X	X	X
py surfaces			X							
pz surfaces				X						
p surfaces defined via 3 points					X					
Reflective px surfaces	X	X			X	X	X	X		
Reflective py surfaces			X							
Reflective pz surfaces				X						
Reflective p surfaces					X					
Criticality (kcode and ksrc)	X	X	X	X	X	X	X	X		
Volumetric sdf without Cell Rejection									X	
Volumetric sdf with Cell Rejection										X
Isotropic Scattering	X	X		X	X		X	X		
Linearly Anisotropic Scattering	X		X			X				
F4 Tallies	X			X		X	X	X	X	X

#### 4.2 MCNP6.2 Verification Cases

This section describes the cases and the verification results for each of the analytical cases provided in Table 162.

##### 4.2.1 Criticality Case 6

This case is problem 6 from [17]. This model is a one-group, isotropic, slab problem with a half-thickness of 2.256751 cm. The analytical solution presented in Sood provides the eigenvalue (1.0) and the flux at four locations within the model.

The MCNP representation of this model utilizes a reflective px surface at 0 cm and a px surface at the right face. The model is subdivided into 50 cells to obtain a spatial flux distribution with

February 13, 2020

cell-wise F4 tallies to compare with the reference fluxes. Since the analytic benchmark suite includes no space-dependent flux distributions for a case with anisotropic scattering, the isotropic multigroup data used for this case were defined using the same equi-probable cosine bin format that would be used with anisotropic scattering. Specifically, two equal-width cosine bins were defined, from -1 to 0, and 0 to 1; this is functionally equivalent to isotropic scattering, though it exercised the same code in MCNP that would be exercised for anisotropic scattering. For this reason, this isotropic problem is identified as testing anisotropic scattering in Table 162. All other isotropic scattering cases used truly isotropic multigroup data (i.e., no angular distribution was provided).

This model was simulated using 100 discarded batches and 1,100 active batches of 2,000,000 histories for a total of 2.2 billion active histories. The resultant eigenvalue for this case was  $1.00001 \pm 0.000015$ . The MCNP flux distribution is provided along with the reference solution in Figure 159. This solution was obtained by normalizing to the peak flux tally bin, similar to the normalization performed in the reference solution. Further, the points used for producing the MCNP curve are the midpoints of the spatial bins, thereby approximating the continuous solution. Note that the MCNP flux distribution plot includes stochastic error bars, however, the uncertainties are so low that they cannot be observed. The reference solution includes a point at the escape boundary; the spatial tally bin structure did not include a point centered on this location but it is clear to see that the tallied flux is directed at this reference point. From this eigenvalue bias and the figure, it is clear that the MCNP solution is faithfully recreating the analytic solution to the neutron transport equation for this case.

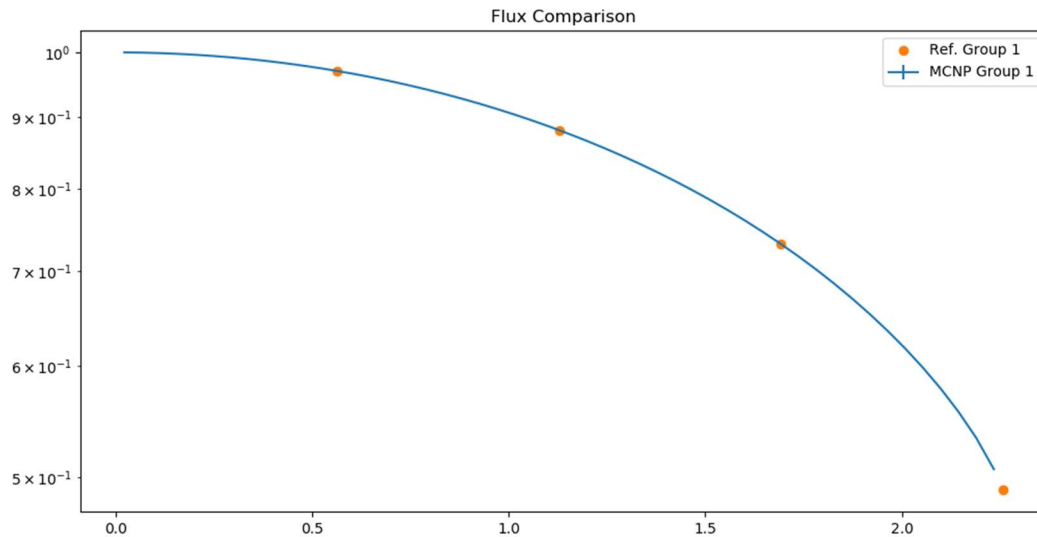


**Figure 159. Criticality Case 6 Flux Distribution**

#### 4.2.1.1 *Perturbations to Criticality Case 6*

As discussed above, this case used the anisotropic scattering description to represent an isotropic problem. To verify that this description is mathematically equivalent to describing isotropic scattering, the above case was repeated with the multigroup ACE file generated with isotropic scattering and thus no equi-probable scattering bins. No statistically significant differences were observed in either the eigenvalue or flux distribution.

#### 4.2.2 Criticality Case 31

This case is problem 31 from [17]. This model is a one-group, linearly anisotropic, infinite homogeneous medium problem. The analytical solution presented in Sood provides the eigenvalue of 2.5. No flux solution is provided since, for an infinite medium problem, none is necessary. The linearly anisotropic nature of this problem has no effect on the analytical solution; it is mainly included in the reference set to contrast with the next problem, Criticality Case 32, which has the same cross sections but a finite width and critical eigenvalue.

The MCNP representation of this model utilizes reflective px surfaces at 0 and 5 cm. This model was simulated using 100 discarded batches and 1,100 active batches of 2,000,000 histories for a total of 2.2 billion active histories.

The resultant eigenvalue for this case was  $2.50000 \pm 0.00000$ , exactly matching the reference. It is clear that the MCNP solution is faithfully recreating the analytic solution to the neutron transport equation for this case.

#### 4.2.3 Criticality Case 32

This case is problem 32 from [17], and it is a critical slab of the same composition used in Criticality Case 31 (one-group, linearly anisotropic). The half-thickness of the slab is 0.77032 cm.

The MCNP representation of this model utilizes a reflective py surface at 0 and a py leakage surface at 0.77032 cm. This model was simulated using 100 discarded batches and 1,100 active batches of 2,000,000 histories for a total of 2.2 billion active histories.

The resultant eigenvalue for this case was  $1.00001 \pm 0.00002$  for an eigenvalue bias compared to the reference of 1 pcm. From this eigenvalue bias it is clear that the MCNP solution is faithfully recreating the analytic solution to the neutron transport equation in this case.

##### 4.2.3.1 Isotropic Perturbation to Criticality Case 32

Since the Case 32 incorporates anisotropic scattering, it should be verified that the solution is measurably impacted by the presence of the  $P_1$  scattering moment. To do this, an isotropic scattering version of this same problem (with cross sections otherwise the same) was created. The eigenvalue for this case was found to increase by more than 3,100 pcm. This indicates that the problem is sensitive to the  $P_1$  moment and thus this problem is adequately sensitive to the presence of anisotropic scattering and thus is an adequate test of anisotropic scattering.

##### 4.2.3.2 Union Boundary Perturbation to Criticality Case 32

Since the Case 32 incorporates a complement-based boundary domain, this was useful to further prove the conjecture that MCNP is correctly handling complement-based problem boundaries. Specifically, the complement used in Case 32 was replaced with the typical union operator. Since the boundary is the boundary and a leakage from this boundary should not affect the random number stream, one should expect that MCNP yield the exact same eigenvalue with and without the complement. This was confirmed as the union-based version of this problem also achieved the same eigenvalue and uncertainty as the complement-based problem. Since

February 13, 2020

this could simply be because of statistical convergence to the correct answer, it was also verified that significantly fewer histories (10,000 total) also yielded the exact same eigenvalue for both cases. This verifies that the usage of union or complement alone does not change the random number stream.

#### 4.2.4 Criticality Case 54

This case is problem 54 from [17]. This model is a two-group, isotropic, slab problem with a half-thickness of 7.566853385 cm. The analytical solution presented in Sood provides the eigenvalue (critical) and the flux at four locations within the model.

The MCNP representation of this model utilizes a reflective pz surface at 0 cm and a pz surface as the opposite face. The model is subdivided into 50 cells to obtain a spatial flux distribution with cell-wise F4 tallies to compare with the reference fluxes.

This model was simulated using 100 discarded batches and 1,100 active batches of 2,000,000 histories for a total of 2.2 billion active histories. The resultant eigenvalue for this case was  $1.00004 \pm 0.00002$  for an eigenvalue bias compared to the reference of 4 pcm. The MCNP flux distributions for each group are provided along with the reference solution in Figure 160. These were obtained by normalizing both groups to the group 1 peak flux tally bin, similar to the normalization performed in the reference solution. Further, the points used for producing the MCNP curve are the midpoints of the spatial bins, thereby approximating the continuous solution. Note that the MCNP flux distribution plot includes stochastic error bars, however, the uncertainties are so low that these bars are not observable. The reference solutions include points at the escape boundary; the spatial tally bin structure did not include a point centered on this location but it is clear to see that the tallied fluxes are directed at these reference points. From this eigenvalue bias and the figure, it is clear that the MCNP solution is faithfully recreating the analytic solution to the neutron transport equation for this case.

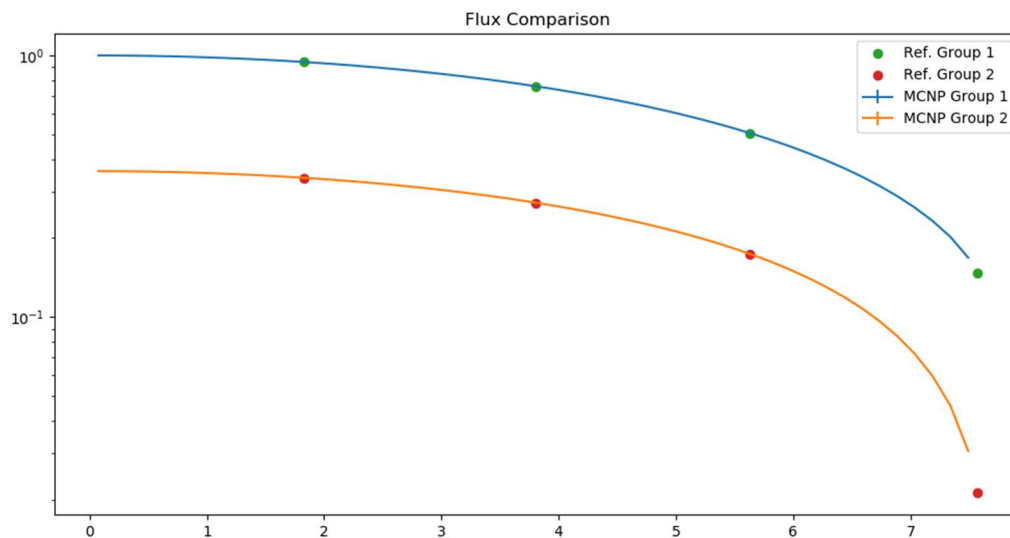


Figure 160. Criticality Case 54 Flux Distributions

February 13, 2020

#### 4.2.5 Criticality Case 64

This case is problem 64 from [17]. This model is a two-group, isotropic, critical infinite-slab lattice model with fissile media surrounded by a moderator. The fissile media is 0.46013547 cm thick with the moderator extending an additional 90.34787455 cm on each side. The analytical solution presented in Sood provides no flux solution.

The MCNP representation of this model utilizes a reflective px surfaces at 0 cm, and general planes defined by three points each for the fuel/moderator interface and the reflective boundary at around 91 cm.

This model was simulated using 100 discarded batches and 1,100 active batches of 2,000,000 histories for a total of 2.2 billion active histories. The resultant eigenvalue for this case was  $0.99999 \pm 0.00001$  for an eigenvalue bias compared to the reference of 1 pcm. It is clear that the MCNP solution is faithfully recreating the analytic solution to the neutron transport equation for this case.

#### 4.2.6 Criticality Case 72

This case is problem 72 from [17]. This model is a two-group, linearly anisotropic, infinite homogeneous medium problem. The analytical solution presented in Sood provides the eigenvalue of 1.000196. The group 1-to-group 2 ratio is provided as 26.823271.

The MCNP representation of this model utilizes reflective px surfaces at 0 and 5 cm. Further, to test the volume normalization, of tallies within MCNP, the model was further subdivided in to two 2.5 cm thick cells. These cells each have equal volume, however, MCNP was erroneously told that one cell had a volume of  $10 \text{ cm}^3$  and the other with a volume of  $1 \text{ cm}^3$ . Since the model is an infinite homogeneous medium, the flux will be spatially flat; therefore setting the volumes in this way allows MCNP's tally volume normalization to be verified by simply observing a factor of 10 (including statistical variation) difference in the two tallies.

This model was simulated using 100 discarded batches and 1,100 active batches of 2,000,000 histories for a total of 2.2 billion active histories. The resultant eigenvalue for this case was  $1.00022 \pm 0.00001$  for an eigenvalue bias of -2.4 pcm. Similarly, the flux tallies are provided in Table 163. These results show that the group ratios are within 0.1% of the reference, given a maximum error of 0.01% in the MCNP fluxes, this is acceptable agreement. Next, it is clear that the Cell 2 flux is 10x larger than the Cell 1 flux; this is consistent with the expectations given the artificial volumes provided. From these results it is clear that the MCNP solution is faithfully recreating the analytic solution to the neutron transport equation for this case.

**Table 163. Criticality Case 72 Fluxes**

	<b>Cell 1 Flux</b>	<b>Cell 2 Flux</b>
<b>Group 1</b>	3.10947E+00	3.10943E+01
<b>Group 2</b>	1.15933E-01	1.15933E+00
<b>Group Ratio</b>	26.821267	26.820922
<b>Ref. Group Ratio</b>	26.823271	26.823271
<b>Group Ratio Error [%]</b>	-0.007%	-0.009%

#### 4.2.7 Criticality Case 74

This case is problem 74 from [17]. This model is a three-group, up-scattering, isotropic, infinite homogeneous medium problem. The analytical solution presented in Sood provides the eigenvalue of 1.6. The group 2-to-group 1 ratio is provided as 0.48 and the group 3-to-group 1 ratio is provided as 0.15.

The MCNP representation of this model utilizes reflective px surfaces at 0 and 5 cm. This model was simulated using 100 discarded batches and 1,100 active batches of 2,000,000 histories for a total of 2.2 billion active histories. The resultant eigenvalue for this case was  $1.60000 \pm 0.000001$ . Similarly, the normalized flux tallies are provided in Table 164. The reported relative uncertainties are less than the four significant digits that MCNP uses to print these results, and therefore MCNP reports only 0s. Therefore they are not included in this table. From these results it is clear that the MCNP solution is faithfully recreating the analytic solution to the neutron transport equation for this case.

**Table 164. Criticality Case 74 Normalized Fluxes**

<b>Groups</b>	<b>Normalized Ref. Flux</b>	<b>Normalized MCNP Flux</b>
<b>1</b>	1.00000	1.00000
<b>2</b>	0.48000	0.48003
<b>3</b>	0.15000	0.15001

#### 4.2.8 Criticality Case 75

This case is problem 75 from [17]. This model is a six-group, up-scattering, isotropic, infinite homogeneous medium problem. The analytical solution presented in Sood provides the eigenvalue of 1.6. The flux vector, normalized to the flux in the 1<sup>st</sup> group is provided as [1.0, 0.48, 0.15, 0.15, 0.48, 1.0].

The MCNP representation of this model utilizes reflective px surfaces at 0 and 5 cm. This model was simulated using 100 discarded batches and 1,100 active batches of 2,000,000 histories for a total of 2.2 billion active histories. The resultant eigenvalue for this case was  $1.60000 \pm 0.000001$ . The normalized flux tallies are provided in Table 165. The reported relative uncertainties are less than the four significant digits that MCNP uses to print these results, and therefore MCNP reports only 0s. Therefore they are not included in this table. From these results it is clear that the MCNP solution is faithfully recreating the analytic solution to the neutron transport equation for this case.



Table 165. Criticality Case 75 Normalized Fluxes

Groups	Normalized Ref. Flux	Normalized MCNP Flux
1	1.00000	1.00000
2	0.48000	0.48002
3	0.15000	0.15000
4	0.15000	0.15001
5	0.48000	0.48004
6	1.00000	1.00005

#### 4.2.9 Fixed Source Case

This fixed source case is meant to exercise MCNP's ability to model a uniform volumetric, multigroup, isotropic fixed source within a defined Cartesian region of space. Since the criticality cases explored above fully encapsulate the verification of MCNP's ability to track and collide neutrons, regardless of the source type, a simple model that tests the ability of MCNP to define a volumetric fixed source is sufficient for our needs.

To that end, one of the simplest fixed source transport problems that can be devised is a mono-energetic, mono-directional beam of particles impinging on a half-space of a purely absorbing media. The scalar flux as a function of distance for such a problem is simply  $\phi(x) = S_0 e^{-\Sigma_a x}$ . Further, since the basic tallies of interest (F4) are histograms in space, this continuous analytical function can be trivially integrated across an arbitrary spatial domain. Doing so will yield the following analytical reference solution:  $\int_{x_{left}}^{x_{right}} \phi(x) dx = \frac{S_0}{\Sigma_a} (e^{-\Sigma_a x_{left}} - e^{-\Sigma_a x_{right}})$ .

To use this problem to verify a uniform volumetric fixed source capability, the problem will be mimicked in the MCNP model by using a thin ( $10^{-6}$  cm) volumetric source immediately to adjacent to the half-space in a void region. This is mathematically equivalent to a plane source but still exercises MCNP's volumetric source definition capability.

The multigroup source definition will be verified by converting this mono-energetic case into a two-group case by way of a two-group source and two-group purely absorbing cross sections. In other words, a multigroup source with no scattering still has the solution provided above for each group.

Next, this problem requires the use of a mono-directional source. Avoiding a mono-directional source will either add an intrinsic error to the MCNP solution or complicate the simple analytical reference solution shown above. Instead of doing this, an isotropic source will be used in the MCNP model, but an additional verification case (the Fixed Isotropic Source Case) will also be developed and discussed to show that MCNP can create an isotropic source.

Given the above approach, a 20 cm slab with vacuum boundaries was generated in MCNP. The group 1 source was set to a normalized probability of 0.6 and group 2 to 0.4. These in effect become the values of  $S_{0,1}$  and  $S_{0,2}$ . The macroscopic absorption cross sections were set to 0.5 1/cm for group 1 and 1.0 1/cm for group 2. The MCNP model discretized the 20 cm slab into



February 13, 2020

40 equal-volume tally regions, each with a thickness of 0.5 cm. This was simulated with 0.5 billion histories to yield the flux distributions plotted in Figure 161.

In this figure, the reference integrals for each bin are compared to the respective MCNP tally results for each group. The X-values used in these plots are the midpoints of the bin. The reference group 1 and MCNP group 1 fluxes overlap such that the reference group 1 line is not visible. The MCNP group 2 results match exactly with the reference group 2 until the group 2 flux drops to a value below  $10^{-7}$ . This is expected behavior in Monte Carlo problems in cases when the number of tally scores are too few to adequately sample the true solution. For example, the right most group 2 bin only received one of the 0.5 billion initial neutrons.

In addition to these results, the MCNP print table 110 was used to verify that the source points sampled were being tallied within the spatial domain of interest. This case therefore verifies that the volumetric source definition was accurately implemented in MCNP and accurately used when creating reference solutions for DIF3D verification.

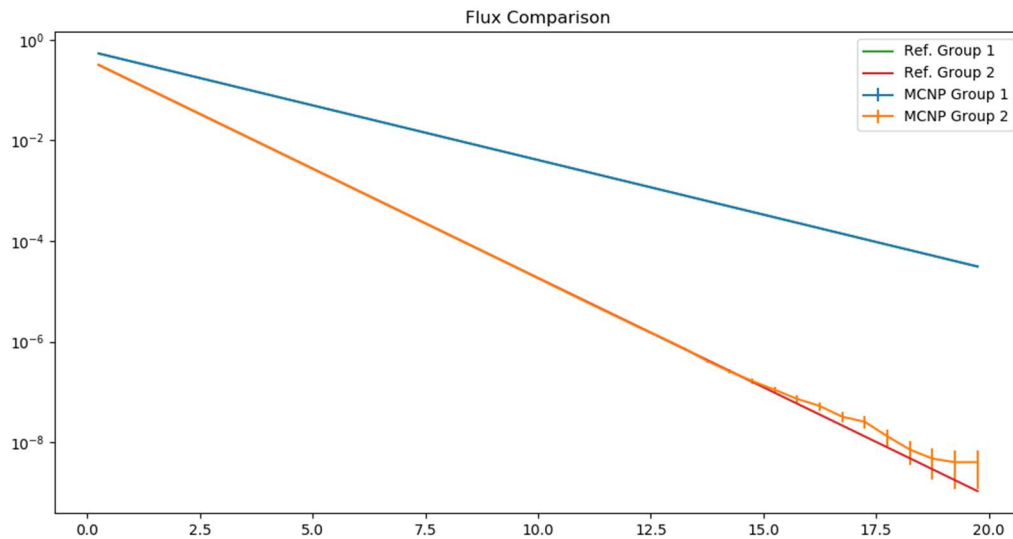


**Figure 161. Fixed Source Case Flux Distributions**

#### 4.2.10 Fixed Cell Source Case

When using MCNP to create reference solutions for hexagonal fixed source problems, a Cartesian bounding box was defined around each cell, and MCNP's sdf card's "cel" keyword was used to define a specific cell within that bounding box that rejection sampling should be performed. This is done to result in a fixed source that is uniformly generated within that cell of arbitrary shape. This problem modifies the previous Fixed Source verification case by utilizing the same cell rejection sampling methodology.

Specifically, the uniform source was defined to be between  $-1.1 \times 10^{-6}$  and 0 but equally distributed between two planar cells between  $-10^{-6}$  and  $-0.5 \times 10^{-6}$ . The use of two cells is consistent with the way that the hexagonal fixed source volumes were defined when the MCNP solution was relied upon for DIF3D verification. Otherwise, the same source strengths, cross sections, tallying regions, and number of histories were used in this problem as in the previous.

February 13, 2020

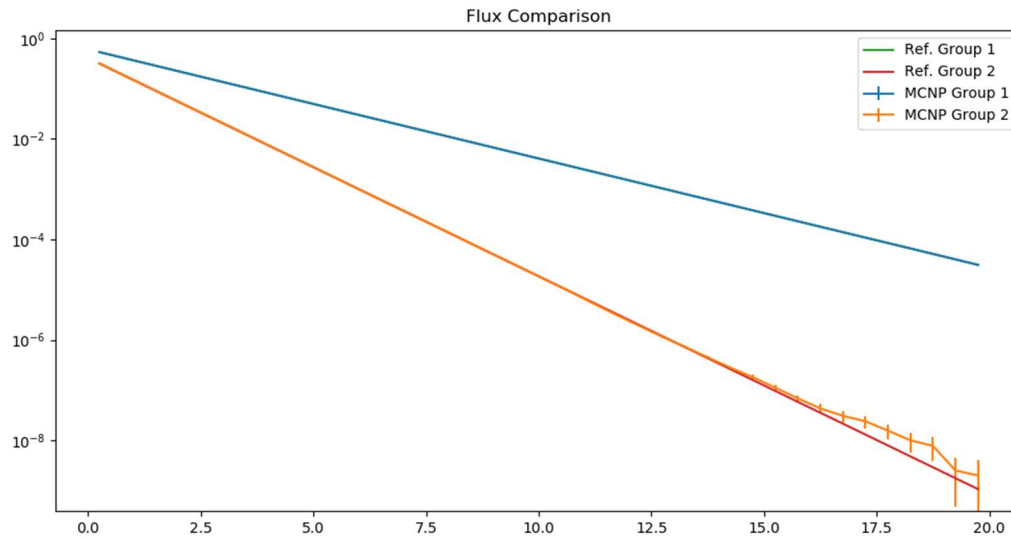


**Figure 162. Fixed Cell Source Case Flux Distributions**

This case produced the flux distributions plotted in Figure 162. This figure shows similar performance to that discussed previously. Again note that the reference and MCNP group 1 fluxes overlap such that the reference solution is not visible. In addition to these results, the MCNP print table 110 was used to verify that the source points sampled were being tallied within the two cells of interest and not outside. This case therefore verifies that the volumetric source definition with the cell rejection technique was accurately implemented in MCNP and accurately used when creating reference solutions for DIF3D verification.

#### 4.2.11 Fixed Isotropic Source Case

The above cases required a mono-directional source defined in MCNP. To verify that an isotropic source is correctly defined, a “point” source (a very small volumetric source) was defined at the center of a 10 cm cube. F4 tallies were then created to measure the flux on all six faces of the 5 cm cube. Specifically this was performed by adding a cell on the outside of each face of the cube that was 0.001 cm thick. The cross sections and group-wise source for this case were the same as in the original problem, though their values are irrelevant.

With this model, a source defined in the +X direction should direct all its neutrons to the right-most face. Similarly, an isotropic source will yield the same flux on each of the six faces of the cube. The resultant fluxes are shown in Table 166 below. The mono-directional fluxes have uncertainties of less than 0.02%. The isotropic flux uncertainties are less than 0.8%. These uncertainties are less than the differences between each of the six faces in the isotropic case, implying that they are stochastically equivalent. The isotropic source definition is therefore verified.

February 13, 2020

Table 166. Fixed Isotropic Source Case Fluxes

Direction	Mono-Directional (+X)		Isotropic	
	Group 1	Group 2	Group 1	Group 2
<b>-X</b>	0.00E+00	0.00E+00	2.64E-05	3.94E-06
<b>+X</b>	1.72E-04	3.28E-05	2.64E-05	3.93E-06
<b>-Y</b>	0.00E+00	0.00E+00	2.64E-05	3.93E-06
<b>+Y</b>	0.00E+00	0.00E+00	2.64E-05	3.94E-06
<b>-Z</b>	0.00E+00	0.00E+00	2.64E-05	3.94E-06
<b>+Z</b>	0.00E+00	0.00E+00	2.64E-05	3.94E-06

## 5 Conclusion

This work details the verification of DIF3D features necessary to support hexagonal-Z fast reactor design work, including the ability to define a model, solve the correct system, and edit results to screen/text files or binary files. This work required verification of the forward and adjoint forms of the fixed source, inhomogeneous fixed source, and k-eigenvalue forms of the transport and diffusion equation as implemented specifically for 3D hexagonal geometries in DIF3D. Further, since the DIF3D validation basis requires modeling in 3D Cartesian geometry, these geometries were also incorporated into the verification effort. Since analytic solutions of the neutron diffusion and transport equations are either limited in scope or not possible, this verification required multiple tiers of problems unique to each solver and geometry type, each testing features independent and complementary arguments for why this separate testing of functionalities is acceptable. This separate testing was also supplemented with a high-level integral check of each the diffusion and transport capabilities and applicable geometries.

The following is a compilation of the issues identified herein. The sections identified in the following list are the first instance of this report where the issue was uncovered.

1. GEODST Output, Section 3.1.1.2.2.2
  - a. The definition of the NZCL variable (number of zone classifications) in the GEODST file is unclear; this has no effect on this verification.
2. NDXSRF Output, Section 3.1.1.2.2.2.2
  - a. The nuclide classification value in the NDXSRF file differs from that provided in the NDXSRF listing. Specifically, an “undefined” isotope classification is given a value of 0 instead of the listing’s specification to use a value greater than 7. The effect of this will be analyzed with downstream use cases, e.g., the REBUS verification.
3. NDXSRF Isotope Classification, Section 3.1.1.2.9
  - a. This section highlights that erroneous isotope classifications in the ISOTXS File do not raise an error. Further, when erroneous isotope classifications are used, the edits of these classifications take on non-sensical values (such as “INELASTIC” as an isotope classification). This indicates the usage of enumerated constants or format statement identifiers for which it may be possible to have a runtime error for certain isotope classifications. This issue would only be uncovered by erroneous input and thus is outside the scope of this work, but is noted as it was identified herein.
4. COMPXS Output, Section 3.1.1.2.2.2.4
  - a. The COMPXS file listing does not discuss the presence of the XSCADP array (down-scattering anisotropic scattering cross sections). This array was inferred due to symmetry with the  $P_0$  arrays, the presence of anisotropic up-scattering and self-scattering arrays, and the values that remained in the file that were not described.

## 5. LABELS Output, Section 3.1.1.2.2.2.5

- a. The LABELS specification description of the LINTAX variable (original number of fine mesh intervals in the axial dimension) is unclear and could use clarification. When inspecting the relevant source code (src\_G4CH4C/gnip4c.f), it was identified that the function that populates the LINTAX variable (wrrods) is not called unless a moveable control device is specified. This description should therefore be modified to state that it only applies if a moveable control device is specified.
- b. The following relates to the output produced by the CCCC\_convert.x program used to convert LABELS to ASCII:
  - i. The ASCII file outputted by CCCC\_convert.x raises an error in modern graphical text editors stating that not all characters “are representable in hexadecimal” and thus they need to be viewed with UTF-8 formatting. This seems to be isolated to the Hollerith user identification value on line 1, which is displayed as “^@^@^@^@^@^@^@^@” on older editors such as VIM and Nano.
  - ii. The file identification card on line 1 should begin with “ 0V LABELS” versus “ 1D LABELS”
  - iii. The 1D record on line 2 is not part of the standard
  - iv. The 2D record beginning on line 3 should be a 1D record
  - v. The 3D record beginning on line 6 should be a 2D record
  - vi. The 3D record beginning on line 8 should be a continuation of the line 6 2D record.

## 6. Auxiliary Output, Sections 3.1.1.2.2.1, 3.2.1.2.1.2, 3.3.1.2.1.2, and 3.4.1.2.1.2

- a. The auxiliary output is printing “EDIT OF (NONFISSIONABLE COMPOSITION)” instead of “EDIT OF (NONFISSIONABLE COMPOSITION COMP1)” (as found in the standard output) for the composition edit table headers. This may be indicative of a memory access error that should be investigated.

## 7. GNIP4C Edit Master Control, Section 3.1.1.2.10.6

- a. The third option of the Type 02 card of the A.NIP3 input block accepts values of 0, 1, 2, or 3. These options write no edits, write only to standard output, only to auxiliary out, or to both output streams, respectively. When the edits are turned off, it is noted that the reactor region map is still edited from the GNIP4C module, regardless of the output type.
- b. The ninth option of the Type 02 card of the A.NIP3 input block accepts values of 0, 1, 2, or 3. These options write no cross section processing edits, write these only to standard output, only to auxiliary out, or to both output streams, respectively. This option was found to be ignored as the edits are always written to both outputs.

8. GNIP4C Region/Mesh and Zone/Mesh Interval Plots, Sections 3.2.1.2.3.2 and 3.2.1.2.3.3
  - a. The tenth and eleventh options of the Type 02 card of the A.NIP3 input block accepts values of 0, 1, 2, or 3. Per the listing, these options control whether or not a region/mesh and zone/mesh interval plot is printed, and whether it is done so in standard and/or auxiliary outputs. This was found to not be regarded as the maps are always printed to both outputs. This error only affected the processing of triangular-Z geometries and hexagonal-Z geometries.
9. HMG4C Module ISOTXS Edits, Section 3.1.1.2.6
  - a. The ISOTXS edits for ISOTXS files with all scattering moments in the same 7D record did not print the higher order scattering matrices, despite their presence. This does not affect the solution accuracy.
10. HMG4C Module COMPXS Edits, Section 3.1.1.2.10.2
  - a. The fourth option of the Type 02 card in the HMG4C module does not respect options that print COMPXS edit output to one of standard or auxiliary outputs: if the user wants this information printed to one output, it will be in both locations. If the user does not wish for the output to be printed, it will be suppressed in both edits. The same behavior was behaved for Supplied COMPXS Edits as discussed in 3.1.1.2.10.5.
11. DIF3D Module COMPXS Edit Error, Section 3.1.1.2.2
  - a. When an (n,2n) scattering matrix is specified in the ISOTXS file without an associated (n,2n) principal cross section, DIF3D incorrectly prints the COMPXS diagonal-entries of the scattering matrix. This was only observed with the DIF3D-FD solver. The results were not observed to impact the solution, as verified with an infinite-homogeneous eigenvalue computation using an afflicted COMPXS set.
12. DIF3D Module Min. Plane-Block Size, Section 3.1.10.1
  - a. The A.DIF3D listing states that the 5<sup>th</sup> option of the Type 03 card's default value is 4500. However, this work identified that the default is actually 10,000.
13. DIF3D Module Variational Nodal Options Output, Section 3.3.1.2.1.1
  - a. The DIF3D edit of the problem description for DIF3D-VARIANT on an XYZ geometry includes a flag for whether or not 45 degree symmetry was applied. The possible values are listed as 0 or 1 (no or yes). However, in the Section's case, DIF3D outputs a value of -1, which would be illegal per this definition. This should be clarified.
14. DIF3D Module Number of Upscatter Iterations, Section 3.3.5.4
  - a. DIF3D allows the user to set the number of upscatter iterations with A.DIF3D's Type 03 card, Option 9. For DIF3D-VARIANT computations, this value is forced to be an odd number by the code, and a warning is raised stating that one additional iteration was added (if an even number provided). This is inconsequential but could be stated for increased clarity in the A.DIF3D listing.

15. DIF3D Power Peaking Calculation, Section 3.1.7
  - a. It was identified that the algorithm used to evaluate the peak fast flux in DIF3D-VARIANT can be quite unreliable due to the polynomial order used and the location of the peak within the mesh. While it is not clear whether this issue impacts current design activities, it is a trivial matter for the core designer to use the EvaluateFlux routine to check the DIF3D output tables as demonstrated on this problem.
16. RZFLUX Balance Information, Section 3.1.11
  - a. The RZFLUX file contains parameters for the total neutron losses, absorptions, surface leakages, buckling losses, black absorber losses, and control rod absorptions. The total neutron losses and total neutron absorption values were identified to be 0 despite having non-zero values in the verified DIF3D edits.
17. DIF3D Edits of Median Energy of Fission, Absorption, and the Flux, Section 3.1.11
  - a. This work identified that minimum energies of 0 eV in an input ISOTXS file are converted internally by DIF3D to a value of  $1.382882 \times 10^{-5}$  eV for lethargy-related computations. This is not a bug, but is not identified anywhere and so is stated here.
18. DIF3D Leakage Determination, Section 3.3.5.3
  - a. The sixth option of the A.DIF3D module's Type 03 card provides an option to derive leakage results from the balance equation (i.e., any neutron balance residual is considered as leakage) instead of from the neutron current. This is option -4. DIF3D-VARIANT, in both 3D Cartesian and Hexagonal-Z geometries, ignored this option and instead computed the leakages from the neutron currents. This does not affect DIF3D-FD.
19. DIF3D-VARIANT Full-Core Hexagonal-Z Group-wise Albedos, Section 3.4.6
  - a. For full-core Hexagonal-Z DIF3D-VARIANT models, a leakage boundary on the upper X and/or upper Y boundaries cannot be successfully set with group-wise albedo coefficients. This was outside the scope of verification as identified in [6]. However, when trying to do so as shown in Figure 142, the net effect is that the reflective boundary is applied to both groups. This issue did not affect third- and sixth-core geometries as group-wise albedos were successfully set.

None of the above are debilitating or impactful to fast reactor design analysis and do not affect the verification of this software. Further, many are simply items that the user should be aware of. The authors will create issue-tracking system tickets for these items, if not already addressed, in the DIF3D issue tracking system.

Therefore, in conclusion, DIF3D is considered verified for the purposes identified in [6]. This verification is specific to DIF3D version 11.0, release 3012 (more specifically, the executable named `dif3d_v11.0_r3012_d2019_03_14_512GB.x` installed on the KOOKIE cluster within the Nuclear Science and Engineering Division at Argonne National Laboratory).



## 6 References

- [1] K. L. Derstine, "DIF3D: A Code to Solve One-, Two-, and Three-Dimensional Finite-Difference Diffusion Theory Problems," ANL-82-64, Argonne National Laboratory (1984).
- [2] R. D. Lawrence, "The DIF3D Nodal Neutronics Option for Two- and Three-Dimensional Diffusion Theory Calculations in Hexagonal Geometry," ANL-83-1, Argonne National Laboratory, March 1983.
- [3] Palmiotti, G., Lewis, E. E., Carrico, C. B., "VARIANT: VARIational Anisotropic Nodal Transport for Multidimensional Cartesian and Hexagonal Geometry Calculation," Argonne National Laboratory ANL-95/40, 1995.
- [4] M. A. Smith, E. E. Lewis, E. R. Shemon, "DIF3D-VARIANT 11.0, A Decade of Updates," ANL/NE-14/1 (2014).
- [5] L. C. Just, H. Henryson II, A. S. Kennedy, S. D. Sparck, B. J. Toppel and P. M. Walker, "The System Aspects and Interface Data Sets of the Argonne Reactor Computation (ARC) System," ANL-7711, Argonne National Laboratory (1971).
- [6] M. A. Smith, A. G. Nelson, and F. Heidet, Argonne National Laboratory, unpublished information (2019).
- [7] K. Salari, P. Knupp, "Code Verification by the Method of Manufactured Solutions," SAND2000-1444, Sandia National Laboratory (2000).
- [8] R. D. O'Dell, "Standard Interface Files and Procedures for Reactor Physics Codes, Version IV", UC-32, Los Alamos Scientific Laboratory (1977).
- [9] C. H. Lee and W. S. Yang, "MC2-3: Multigroup Cross Section Generation Code for Fast Reactor Analysis," Argonne National Laboratory, ANL/NE-11-41 Rev.2 (2013).
- [10] R. D. Lawrence, "Progress in Nodal Methods for the Solution of the Neutron Diffusion and Transport Equations," Prog. Nucl. Energy, 17, 271 (1986).
- [11] M. Makai and C. Maeder, "A Fast Nodal Neutron Diffusion Method for Cartesian Geometry", Nuclear Science and Engineering, 84, 390 (1983).
- [12] ANL, "Benchmark Problem Book", Report ANL-7416, Supplement 2, Argonne National Laboratory, Argonne, IL, 1977.
- [13] Y. A. Chao, and Y. A. Shatilla, "Conformal Mapping and Hexagonal Nodal Methods – II: Implementation in the ANC-H Code", Nucl. Sci. Eng., **121**(2), 210-225 (1995).
- [14] J. Lee, and N. Z. Cho, "AFEN Method and its Solution of the Hexagonal Three-Dimensional VVER-1000 Benchmark Problem," Progress in Nuclear Energy, **48**(8), 880-890 (2006).
- [15] C.J. Werner, et al., "MCNP6.2 Release Notes", LA-UR-18-20808, Los Alamos National Laboratory (2018).
- [16] F. B. Brown, "New Tools to Prepare ACE Cross-section Files for MCNP Analytic Test Problems", LA-UR-16-24290, Los Alamos National Laboratory (2018).
- [17] A. Sood, R. A. Forster, D. K. Parsons, "Analytical Benchmark Test Set for Criticality Code Verification", Prog. Nucl. Energy, 42, 55-106 (2003).
- [18] T. Takeda, H. Ikeda, "3D Neutron Transport Benchmarks", Report NEACRP-L-330, OECD/NEA Committee on Reactor Physics (1991).
- [19] B. D. Ganapol, "Analytical Benchmarks for Nuclear Engineering Applications", Report NEA/DB/DOC(2008)1, NEA (2008).





## **Nuclear Science and Engineering Division**

Argonne National Laboratory

9700 South Cass Avenue, Bldg. 208

Argonne, IL 60439-4842

[www.anl.gov](http://www.anl.gov)



Argonne National Laboratory is a U.S. Department of Energy  
laboratory managed by UChicago Argonne, LLC